

Criteria 3

Research, Innovations and Extension

Key Indicator 3.3

Research Publication and Awards

3.3.1 Number of research papers published per teacher in the Journals notified on UGC website during the last five years



Rajarshi Shahu
College of Pharmacy

Journey Towards Academic Excellence

3.3.1 Number of research papers published per teacher in the Journals notified on UGC website during the last five years

2019-2020

Sr. No.	Title of paper	Name of the author/s	Department of the teacher	Name of journal	Impact Factor	Page No. with Link
1	An effort to tailor the solid dispersion loaded surface-modified, microporous-cryogel formulation of acitretin for the treatment of psoriasis.	Prakash Kendre, Nikita Borawake, Shirish Jain, Somnath Vibhute, Ajinkya Pote	Pharmaceutics	Materials Technology https://doi.org/10.1080/10667857.2020.1868210 (Taylor & Francis, Impact Factor: 3.846)	3.297	<u>01</u>
2	An effort to tailor the solid dispersion loaded surface-modified, microporous-cryogel formulation of acitretin for the treatment of psoriasis.	Prakash Kendre, Nikita Borawake, Shirish Jain , Somnath Vibhute, Ajinkya Pote	Pharmaceutics	Materials Technology https://doi.org/10.1080/10667857.2020.1868210 (Taylor & Francis, Impact Factor: 3.846)	3.297	<u>12</u>
3	An effort to tailor the solid dispersion loaded, surface-modified, microporous-cryogel formulation of acitretin for the treatment of psoriasis.	Prakash Kendre, Nikita Borawake, Shirish Jain, Somnath Vibhute, Ajinkya Pote	Pharmaceutics	Materials Technology https://doi.org/10.1080/10667857.2020.1868210 (Taylor & Francis, Impact Factor: 3.846)	3.297	<u>23</u>
4	An effort to augment solubility and efficiency of the oral bosentan-bucco-adhesive drug delivery system using graft copolymer as the carrier.	Prakash N. Kendre, Pravin D. Chaudhari, Shirish P. Jain, Somnath K. Vibhute	Pharmaceutics	Polymer Bulletin volume 78, pages 5851–5871 (2021) (Springer Nature; Impact Factor: 2.870)	2.843	<u>34</u>
5	An effort to augment solubility and efficiency of the oral bosentan-bucco-adhesive drug delivery system using graft copolymer as the carrier.	Prakash N. Kendre, Pravin D. Chaudhari, Shirish P. Jain , Somnath K. Vibhute	Pharmaceutics	Polymer Bulletin volume 78, pages 5851–5871 (2021) (Springer Nature; Impact Factor: 2.870)	2.843	<u>57</u>

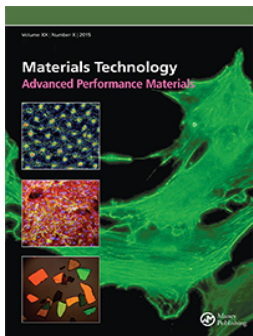
Sr. No.	Title of paper	Name of the author/s	Department of the teacher	Name of journal	Impact Factor	Page No. with Link
6	An effort to augment solubility and efficiency of the oral bosentan-bucco-adhesive drug delivery system using graft copolymer as the carrier.	Prakash N. Kendre, Pravin D. Chaudhari, Shirish P. Jain, Somnath K. Vibhute	Pharmaceutics	Polymer Bulletin volume 78, pages5851–5871 (2021)(Springer Nature; Impact Factor: 2.870)	2.843	<u>80</u>
7	Design, fabrication, and characterization of graft copolymer assisted ocular insert: a state of art in reducing post-operative pain. Drug Development and Industrial Pharmacy	Prakash N. Kendre , Pooja D. Kadam, Shirish P. Jain, Somnath K. Vibhute & Ajinkya K. Pote	Pharmaceutics	Drug Development and Industrial Pharmacy, 2020, 46, 1988-1999 (Taylor & Francis: Impact Factor: 3.225)	3.225	<u>103</u>
8	Design, fabrication, and characterization of graft copolymer assisted ocular insert: a state of art in reducing post-operative pain. Drug Development and Industrial Pharmacy	Prakash N. Kendre, Pooja D. Kadam, Shirish P. Jain , Somnath K. Vibhute & Ajinkya K. Pote	Pharmaceutics	Drug Development and Industrial Pharmacy, 2020, 46, 1988-1999 (Taylor & Francis: Impact Factor: 3.225)	3.225	<u>116</u>
9	Design, fabrication, and characterization of graft copolymer assisted ocular insert: a state of art in reducing post-operative pain. Drug Development and Industrial Pharmacy	Prakash N. Kendre, Pooja D. Kadam, Shirish P. Jain, Somnath K. Vibhute & Ajinkya K. Pote	Pharmaceutics	Drug Development and Industrial Pharmacy, 2020, 46, 1988-1999 (Taylor & Francis: Impact Factor: 3.225)	3.225	<u>129</u>
10	A facile approach to fabrication and characterization of novel herbal microemulsion-based UV shielding cream	R. D. Bhalke, S. S. Kulkarni, P. N. Kendre , V. V. Pande and M. A. Giri	Pharmaceutics	Futur J Pharm Sci (2020) 6:76	0	<u>142</u>
11	A facile approach to fabrication and characterization of novel herbal microemulsion-based UV shielding cream	R. D. Bhalke, S. S. Kulkarni, P. N. Kendre, V. V. Pande and M. A. Giri	Pharmaceutics	Futur J Pharm Sci (2020) 6:76	0	<u>152</u>

Sr. No.	Title of paper	Name of the author/s	Department of the teacher	Name of journal	Impact Factor	Page No. with Link
12	Evaluation of the diuretic activity of ethanolic and aqueous extracts of tabernaemontana divaricata in rats	Chanchal Raj*, Shailesh Kewatkar , A. Balasubramaniam, Ashish Jain, Prakash Turiya, Sandeep Dhull, Nadeem Sayyed	Pharmacognosy	Journal of Seybold Report, 2020, 15, 10, 460	0	<u>162</u>
13	Anti-inflammatory, Anti-oxidant and Anti-microbial properties of Polyherbal formulation in Acne Treatment	Rakesh S. Shivatare, Shailesh M. Kewatkar , Priya Lohakare, Nitin Bhutale, Ramesh Musale, Durga Choudhary, Gayatri Ganu, Dheeraj H. Nagore	Pharmacognosy	Int. J. Pharm. Sci. Rev. Res., 62(1), 2020, 73-77	0	<u>178</u>
14	Isolation, Identification and Characterization of Ximenynic Acid with Anti-Aging Activity from Santalum Album	Rakesh S Shivatare, Ramesh Musale, Priya Lohakare, Dipika Patil, Durga Choudhary, Gayatri Ganu, Dheeraj H Nagore, Shailesh M Kewatkar	Pharmacognosy	International Journal of research in pharmaceutical sciences, 2020,14, 1, 9	0	<u>183</u>
15	In vitro Antioxidant Activity and Stability Indicating High-performance Thin-layer Chromatographic Method for Ximenynic Acid in Santalum album Seed Extract	Rakesh S. Shivatare, Ramesh Musale, Priya Lohakare, Dipika Patil, Durga Choudhary, Gayatri Ganu, Dheeraj H. Nagore, Sohan Chitlange, Shailesh M. kewatkar	Pharmacognosy	Asian Journal of Pharmaceutics Jan-Mar 2020 • 14 (1)	0	<u>189</u>
16	In Vivo And In Vitro Investigations Of Pharmacological Potentials Of Cassia Obtusifolia Plant	Kewatkar S. M* , Paithankar V. V, Bhujbal S. S, Jain S. P., Nagore D. H.	Pharmacognosy	Asian J Pharm Clin Res, Vol 13, Issue 3, 2020, 87-94	0	<u>197</u>
17	Discovery of Naturally Occurring Flavonoids as Human Cytochrome P450 (CYP3A4) Inhibitors with the Aid of Computational Chemistry	Sharuk L. Khan , Gajanan M. Sonwane, Falak A. Siddiqui, Shirish P. Jain, Mayura A. Kale, Vijay S. Borkar	Pharmaceutical Chemistry	Indo Global Journal of Pharmaceutical Sciences, 2020; 10(4): 58-69	0	<u>205</u>

Sr. No.	Title of paper	Name of the author/s	Department of the teacher	Name of journal	Impact Factor	Page No. with Link
18	Discovery of Naturally Occurring Flavonoids as Human Cytochrome P450 (CYP3A4) Inhibitors with the Aid of Computational Chemistry	Sharuk L. Khan, Gajanan M. Sonwane , Falak A. Siddiqui, Shirish P. Jain, Mayura A. Kale, Vijay S. Borkar	Pharmaceutical Chemistry	Indo Global Journal of Pharmaceutical Sciences, 2020; 10(4): 58-69	0	<u>217</u>
19	Discovery of Naturally Occurring Flavonoids as Human Cytochrome P450 (CYP3A4) Inhibitors with the Aid of Computational Chemistry	Sharuk L. Khan, Gajanan M. Sonwane, Falak A. Siddiqui, Shirish P. Jain , Mayura A. Kale, Vijay S. Borkar	Pharmaceutical Chemistry	Indo Global Journal of Pharmaceutical Sciences, 2020; 10(4): 58-69	0	<u>229</u>
20	Discovery of Naturally Occurring Flavonoids as Human Cytochrome P450 (CYP3A4) Inhibitors with the Aid of Computational Chemistry	Sharuk L. Khan, Gajanan M. Sonwane, Falak A. Siddiqui, Shirish P. Jain, Mayura A. Kale, Vijay S. Borkar	Pharmaceutical Chemistry	Indo Global Journal of Pharmaceutical Sciences, 2020; 10(4): 58-69	0	<u>241</u>
21	Variants in NIPAL4 and ALOXE3 cause autosomal recessive congenital ichthyosis in Pakistani families	Abida Akbar, Muneeba Bint-E-Farrakh, Andrew H Crosby, Asma Gul, Gaurav V Harlalka	Pharmacology	Congenit Anom (Kyoto) 2020;1-2.	1.474	<u>253</u>
22	Supramolecular complexes of phospholipids and β -cyclodextrin with bioactive β -carotene: A comparative physico-chemical and functional evaluation	D. R. Telange , S. Gujar, A. M. Pethe	Pharmaceutics	Indian Journal of Pharmaceutical Education and Research, 2020, 54, 2, S221-S228	0	<u>255</u>
23	Antiparkinsonian and Antioxidant Effects of Hydroalcoholic Extract of Camellia sinensis, Asparagus racemosus, Mucuna pruriens and their Combination	Mahendra Ashok Giri , Rasika Dnyandeo Bhalke, K Vanitha Prakash, Sanjay Bhaskar Kasture	Pharmacology	Int. J. Pharm. Investigation 2020;10(4):569-574	0	<u>265</u>

Sr. No.	Title of paper	Name of the author/s	Department of the teacher	Name of journal	Impact Factor	Page No. with Link
24	Evaluation Of Camellia sinensis, Withania somnifera and their Combination for Antioxidant and Antiparkinsonian Effect	MA Giri , RD Bhalke, K Vanitha Prakash, SB Kasture	Pharmacology	J. Pharm. Sci. & Res. Vol. 12(8), 2020, 1093-1099	0	271
25	Design & Development of Curcumin Loaded Zinc Oxide Nanoparticles Decorated Mesoporous Silica Liquid Stitches: A Proof of Concept in Animals	Ajinkya Kailas Pote, Vishal Vijay Pande, Vipul Pralhadbhai Patel, Mahendra Ashok Giri , Rasika D Bhalke and Aniket Uttam Pund	Pharmacology	MATERIALS TECHNOLOGY https://doi.org/10.1080/10667857.2020.1863557	3.297	272
26	B-Sitosterol: Isolation from Muntingia Calabura Linn. Bark Extract, Structural Elucidation, and Molecular Docking Studies As Potential Inhibitor Of Sars-Cov-2 Mpro (Covid-19)	Rakesh N Chaudhari, Sharuk L.Khan , Ravindra S Chaudhary, Shirish P Jain, Falak A Siddiqui	Pharmaceutical Chemistry & Quality Assurance	Asian J Pharm Clin Res, Vol 13, Issue 5, 2020, 204-209	0	287
27	B-Sitosterol: Isolation from Muntingia Calabura Linn. Bark Extract, Structural Elucidation, and Molecular Docking Studies As Potential Inhibitor Of Sars-Cov-2 Mpro (Covid-19)	Rakesh N Chaudhari, Sharuk L.Khan, Ravindra S Chaudhary, Shirish P Jain , Falak A Siddiqui	Pharmaceutical Chemistry & Quality Assurance	Asian J Pharm Clin Res, Vol 13, Issue 5, 2020, 204-209	0	293
28	Pharmacological Activity Investigation of Alkaline Water – A Review	Gajanan Sonwane , Sujat Bhagat, Vijay Borkar, Shirish Jain , Sharuk khan , Mayura Kale	Pharmaceutical Chemistry & Quality Assurance	Int. J. Pharm. Sci. Rev. Res., 64(1), September - October 2020; Article No. 17, Pages: 88-91	0	299

Sr. No.	Title of paper	Name of the author/s	Department of the teacher	Name of journal	Impact Factor	Page No. with Link
29	Pharmacological Activity Investigation of Alkaline Water – A Review	Gajanan Sonwane, Sujat Bhagat, Vijay Borkar , Shirish Jain, Sharuk khan, Mayura Kale	Pharmaceutical Chemistry & Quality Assurance	Int. J. Pharm. Sci. Rev. Res., 64(1), September - October 2020; Article No. 17, Pages: 88-91	0	303
30	Pharmacological Activity Investigation of Alkaline Water – A Review	Gajanan Sonwane, Sujat Bhagat, Vijay Borkar, Shirish Jain , Sharuk khan, Mayura Kale	Pharmaceutical Chemistry & Quality Assurance	Int. J. Pharm. Sci. Rev. Res., 64(1), September - October 2020; Article No. 17, Pages: 88-91	0	307
31	Pharmacological Activity Investigation of Alkaline Water – A Review	Gajanan Sonwane, Sujat Bhagat, Vijay Borkar, Shirish Jain, Sharuk khan , Mayura Kale	Pharmaceutical Chemistry & Quality Assurance	Int. J. Pharm. Sci. Rev. Res., 64(1), September - October 2020; Article No. 17, Pages: 88-91	0	311
32	Synthesis of 2,5-disubstituted-1,3,4-thiadiazole derivatives from (2S)-3-(benzyloxy)-2-[(tert-butoxycarbonyl) amino] propanoic acid and evaluation of anti-microbial activity	Amit A. Pund , Shweta S. Saboo, Gajanan M. Sonawane , Amol C. Dukale, and Baban K. Magare	Pharmaceutical Chemistry & Quality Assurance	Synthetic Communications, 2020, 50, 3854-3864	1.937	315
33	Pharmacognostical Standardization of Ailanthus excelsa leaves and Randia dumetorum fruit along with Antioxidant activity and free Radical Scavenging capacity of its fractions	Vivek Paithankar, Shailesh M. Kewatkar , Trupti A. Nimburkar, Supriya S. Deshpande	Pharmacognosy	International Journal of research in pharmaceutical sciences, 2020, 11 (SPL4), 1213-1221	0	327



An effort to tailor the solid dispersion loaded, surface-modified, microporous-cryogel formulation of acitretin for the treatment of psoriasis

Prakash N. Kendre , Nikita Borawake , Shirish P Jain , Somnath K. Vibhute & Ajinkya K. Pote

To cite this article: Prakash N. Kendre , Nikita Borawake , Shirish P Jain , Somnath K. Vibhute & Ajinkya K. Pote (2020): An effort to tailor the solid dispersion loaded, surface-modified, microporous-cryogel formulation of acitretin for the treatment of psoriasis, Materials Technology, DOI: [10.1080/10667857.2020.1868210](https://doi.org/10.1080/10667857.2020.1868210)

To link to this article: <https://doi.org/10.1080/10667857.2020.1868210>



Published online: 28 Dec 2020.



Submit your article to this journal [↗](#)



Article views: 6



View related articles [↗](#)



View Crossmark data [↗](#)



An effort to tailor the solid dispersion loaded, surface-modified, microporous-cryogel formulation of acitretin for the treatment of psoriasis

Prakash N. Kendre^a, Nikita Borawake^b, Shirish P Jain^a, Somnath K. Vibhute^a and Ajinkya K. Pote^a

^aDepartment of Pharmaceutics, Rajarshi Shahu College of Pharmacy, Buldana, India; ^bSanjivani College of Pharmaceutical Education and Research, Kopergaon, India

ABSTRACT

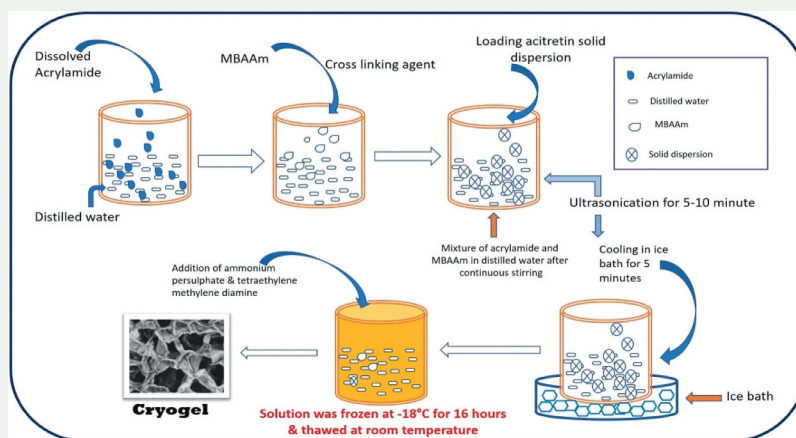
Acitretin is the drug of choice for the treatment of psoriasis, but due to its poor solubility, the development of oral and topical formulations of acitretin has been restricted. The aim of the present investigation was to enhance the solubility of acitretin. Solid dispersions of acitretin were prepared using a lipidic solubilizer, Gelucire[®] 44/14. These solid dispersions were characterized through FT-IR, DSC, XRD, drug content and solubility studies. The most solubilized dispersion was loaded on an N, N-methylenebisacrylamide microporous cryogel. Physical parameters of the solubilized drug such as the porosity, rheological behaviour, surface properties, appearance, drug content and diffusion behaviour were studied. It was concluded that the solubilized form of acitretin, loaded on a surface-modified cryogel, is the best option for the treatment of psoriasis. The hydration of the skin was excellent, and the permeability of the acitretin into the skin was better.

ARTICLE HISTORY

Received 27 November 2020
Accepted 17 December 2020

KEYWORDS

Acitretin; Gelucire[®] 44/14; N, N-methylenebisacrylamide; solid dispersion; cryogel; microporous



Introduction

Most of the drugs available today have greater potential in the management of various diseases, but certain properties of these drugs have restricted the development of different dosage forms. With recent advancements in the field of science and technology and in the manufacture of modified excipients with excellent features, it is possible to overcome these hurdles in the development of newer dosage forms.

Psoriasis is a condition in which skin cells build up and form scales, rashes and itchy, dry patches that are very uncomfortable to the patients physically as well as socially [1]. There are many problems associated with psoriasis, including inflammation, redness of the skin, sharply demarcated papules and rounded plaques. Regular hydration of the skin is required to avoid

serious skin damage [2]. Many drugs are used to treat psoriasis and the symptoms associated with it. These drugs include methotrexate, cyclosporine and acitretin. Treatment with topical steroids for prolonged periods may be dangerous. This may suppress the body's immune system. Drugs such as methotrexate may be hepatotoxic and may impair kidney function [3].

Acitretin is the drug of choice for the treatment of psoriasis, but due to its poor solubility (0.0729 mg/L), its use and the development of oral formulations have been restricted [4]. Hence, the development of topical formulations is the need of the hour. Acitretin is a retinoid, a form of vitamin A. It is used in the treatment of psoriasis because of its role in epithelial cell growth, sebum production and collagen synthesis [5].

CONTACT Prakash N. Kendre ✉ prakashkendre@gmail.com ✉ Rajarshi Shahu College of Pharmacy, At Post-Malviher, District Buldana-443001, Maharashtra, India

This article has been republished with minor changes. These changes do not impact the academic content of the article.

© 2020 Informa UK Limited, trading as Taylor & Francis Group

Cryogels are supermacroporous hydrophilic gels produced using the cryotropic gelation technique. Cryogels have interconnected pores whose size ranges from microns to several hundred microns. Cryogels can be formulated at sub-zero temperatures using various monomers. The process of polymerisation is carried out in the presence of a frozen monomer solution. The monomer is present in the interstices between the crystals of ice. The pores of cryogels can permit the entry of solutes freely. Cryogels are very flexible. Their permeability is good, and their mechanical strength is excellent.

In this study, a solubilised form of acitretin was embedded in the micropores of a cryogel. Cryogels can hold huge amounts of water. Thus, they keep the skin hydrated during the treatment of psoriasis, which is their main advantage over other topical formulations. The drug would diffuse slowly through the pores of the gel continuously for long periods of time.

Materials and methods

Materials

Acitretin was received as a gift sample from Glenmark Pharmaceuticals, Sinner, Nashik, India. Gelucire® 44/14 was obtained as a gift sample from Gattefosse India Pvt. Ltd., Mumbai. Acrylamide, N, N-methylenebisacrylamide (MBAAm), ammonium persulphate (APS), Tetramethylethyldiamine N, N, N', N'-tetramethylethylenediamine (TEMED) and other materials were purchased from Loba Chemie, Mumbai. All the other chemicals and reagents used in the study were of analytical grade.

Methods

The work was divided in two parts as preparation and evaluation of solid dispersion and preparation and evaluation of solid dispersion loaded cryogel.

Preparation of solid dispersion (fusion method)

On the basis of the results of a solubility study, acitretin and Gelucire 44/14 were accurately mixed in the ratios 1:1, 1:2, 1:3, 1:4, 1:5 and 1:6 (formulation batches SD1 to SD6, respectively). Gelucire 44/14 was melted in a porcelain dish on a heating mantle at 50°C under continuous stirring, and the drug was dispersed into the melted Gelucire 44/14. The resultant dispersion was cooled at room temperature to form a solid mass. This dried solid mass was pass through a fine screen to obtain particles of uniform size. The material was packed in an airtight container in which it was kept till it was processed further.

Fourier transform infrared (FT-IR) spectroscopy

FT-IR spectroscopy was used to confirm the identity of the acitretin. The drug and KBr (ratio of 1:100) were mixed and ground gently using a mortar and pestle. A pellet was made using the pellet press method. This yielded a translucent pellet. This pellet was placed in the sample holder of an FT-IR 8400 spectrometer (Shimadzu, Japan) at R.C. Patel College of Pharmacy, Shirpur, India. The instrument was run, and the FT-IR spectra of the acitretin were obtained. In the same way, physical blends of the drug and other excipients were also analysed to test their compatibility and suitability for the final formulation.

Differential scanning calorimetry (DSC)

Differential scanning calorimetric measurements were performed using a DSC-60 (Shimadzu) thermal analyser. Samples weighing about 5 mg were placed in aluminium hermetically sealed pans and scanned at a heating rate of 10°C/minute over a temperature range of 0–300°C with nitrogen as an effluent gas. The thermal properties of pure acitretin and its physical mixtures with the excipients were determined. This testing was done at the Department of Plastic and Polymer Engineering, Aurangabad.

X-ray diffractometry (XRD)

Small-angle XRD measurements were made to determine the structural ordering of the samples studied. The measurements were carried out using a D8 ADVANCE powder diffractometer. The drug sample was smeared over a low-back ground sample holder (amorphous silica holder) and fixed on the sample stage in a goniometer. The instrument was set in a B-B geometry. The current and voltage is set at 40 mV and 35 mA, and data were collected. This testing was carried out at the Sophisticated Test and Instrumentation Centre, Kochi University, Kerala.

Solubility study

The solubility of the acitretin in various solvents such as distilled water, phosphate buffers (pH 6.8 and 7.4) and 0.1 N HCl were determined using the shaking flask method. An excess amount of drug was taken in a 50-ml conical flask containing 10 ml of solvent. Solvents with different concentrations (1–5%) of Gelucire® 44/14 were used. The mixture was shaken at 37°C for 48 hours at 75 rpm using an orbital shaking incubator (Dolphin™). The resultant solutions were filtered through Whatman filter paper (0.45 µm). The filtered solutions were diluted and examined for UV absorbance at 353 nm.

Characterisation of solid dispersion

The prepared solid dispersion of acitretin was analysed in FT-IR, DSC, XRD, solubility, drug content and dissolution studies.

Scanning electron microscopy (SEM). The surface morphology of the solid dispersion was studied using a high-resolution scanning electron microscope. The dried samples were covered with double-sided sticking tape and placed on aluminium stubs. They were sealed and coated with gold ions (200 °Å) under low pressure for 5 minutes using a sputtering device.

Determination of drug content. Ten milligrams of the solid dispersion were dissolved in a volumetric flask containing tetrahydrofuran, and the volume was made up with tetrahydrofuran to 10 ml. Then ultrasonication was performed to dissolve the drug rapidly in the tetrahydrofuran. The resultant solution was filtered through 0.45 µm filter media, and the drug content was determined using a UV-spectrophotometer at a wavelength of 353 nm [6].

Entrapment efficiency (EE). The solid dispersion samples were dissolved completely in the tetrahydrofuran, and the solution was filtered through 0.45 µm filter media to determine the amount of drug entrapped in the Gelucire carrier. A UV-spectrophotometer was used, with the wavelength set at 353 nm. The percentage entrapment efficiency was calculated using the following equation [7]:

$$\% \text{Entrapment Efficiency (EE)} = \frac{\text{Entrapped drug}}{\text{Entrapped drug} + \text{Freed drug}} \times 100 \dots (1)$$

In vitro dissolution study. All the solid dispersion formulations (SD1 to SD6) were subjected to an *in vitro* dissolution study using a USP Type-II dissolution test apparatus (Electrolab, India). Phosphate buffer saline (pH 7.4) was used as the dissolution medium. The temperature was 37°C ± 0.5°C, and the speed was 100 rpm [6]. The samples were withdrawn after 15, 30, 45, 60, 75 and 90 minutes and analysed using a UV-spectrophotometer at a wavelength of 353 nm. The plain drug was also subjected to a dissolution study similarly for comparison with the solid dispersions. The samples were measured in triplicate for better accuracy.

Preparation of cryogel

A cryogel was prepared using the step-wise process presented in Figure 1. All the formulations were designated as CRG1 to CRG4. The concentrations of the acrylamide, MBAAm, APS and TEMED are presented in Table 1. The same amount of acitretin solid dispersion was used in all the trial batches. The resultant mixtures were frozen and maintained at -18°C for 16 hours. They were thawed at room temperature (25°C) over 12 hours. The freezing-and-thawing process was repeated thrice [8,9].

The prepared cryogel was characterised through FT-IR, DSC, XRD, drug content, entrapment efficiency, surface morphology, porosity, rheological behaviour, *in vitro* dissolution testing and stability studies. The methods used in the FT-IR, DSC and XRD analyses were the same as those described previously.

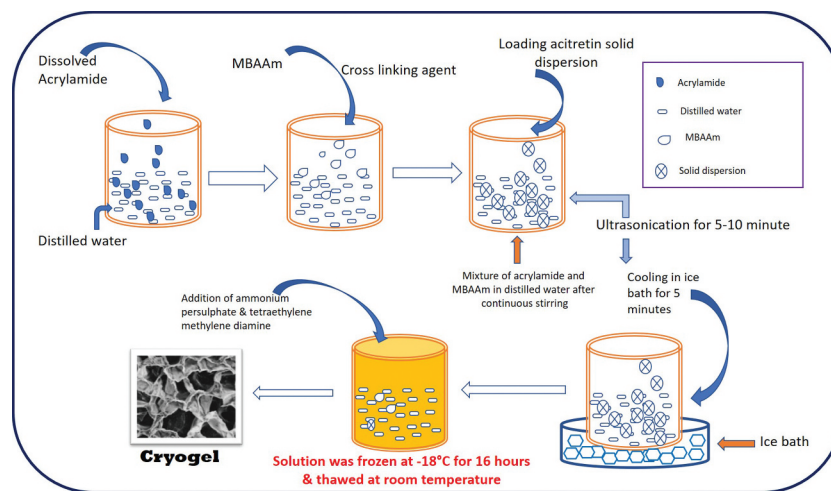


Figure 1. Cryogel preparation method with diagrammatic re-presentation.

Table 1. Composition of cryogel formulation.

Batch	Acrylamide (gm)	Deionised water (ml)	*MBAAm (gm)	Solid dispersion (gm)	*APS (gm)	*TEMED (µl)
CRG1	0.765	20	0.110	1	0.02	25
CRG2	0.765	20	0.120	1	0.02	50
CRG3	0.765	20	0.130	1	0.02	75
CRG4	0.765	20	0.140	1	0.02	100

*MBAAm: N, N' Methylene bis acrylamide; APS: Ammonium per-sulphate; TEMED: N, N, N', N'-tetramethyl ethylenediamine.

Characterisation of solid dispersion-loaded cryogel
Microscopic analysis using CX23 Olympus microscope. The surface morphology of the prepared cryogel was studied using a high-resolution scanning electron microscope. The changes produced in the surface texture by the freeze–thaw process was observed. The dried samples were covered with double-sided sticking tape and were placed on aluminium stubs. They were sealed and coated with gold ions under low pressure for 5 minutes using a sputtering device.

Mercury porosimetry study. The pore size, particle size distribution and surface area were determined using the mercury porosimeter technique. A Pascal 440 porosimeter, which has a dilatometer, a pressure source and a monitoring device, was used. The sample mass was 0.132 g, the mercury height was 41.683 mm, and the weight of the dilatometer, the mercury and the sample were 236.462 g. After correction this weight was 236.543 g, and the capillary mercury height was 0.683 mm. The dilatometer consists of a sample holder and a calibrated stem. The volume of the mercury that enters the pores was measured using a mercury penetrometer (an electrical capacitance dilatometer). This test was carried out at the Sophisticated Instrumentation Centre for Applied Research and Testing (SICART), Gujarat, India.

Rheological behaviour of cryogel. A Brookfield RST-CC digital rheometer was used to determine the rheology and viscosity of the formulations. The viscosity was measured as 12 MP in four blocks (UID140).

Swelling index of cryogel. This study was conducted to find out the swelling capacity of the dried form of the cryogel. The cryogel samples were dried to constant mass, and the mass of each dried sample was noted. The dried samples were placed in deionised water (swelling medium) at room temperature for 4 hours. Then the excess water was removed carefully, and the surface was cleaned slowly without squeezing. The samples were weighed again to calculate the swelling index. The swelling index was calculated using Equation (2) [10–12]:

$$\text{Swelling index} = [(W_s - W_0)/W_0] \times 100 \quad (2)$$

Where, W_0 and W_s are the weights of cryogels before and after swelling, respectively.

Determination of drug content. The drug content was determined by dissolving 10 mg of cryogel in a volumetric flask containing tetrahydrofuran, and the volume was made up with tetrahydrofuran to 10 ml. Then ultrasonication was performed to dissolve the drug rapidly in tetrahydrofuran. The resultant

solution was then filtered through 0.45 μm filter media, and the drug content was determined using a UV-spectrophotometer at a wavelength of 353 nm [7].

Entrapment efficiency (EE). The cryogel sample was washed with deionised water slowly to remove the untrapped drug adhering to the surface. Then the cryogel was completely dissolved in the tetrahydrofuran, and the solution was filtered through 0.45 μm filter media. The amount of entrapped drug was determined using a UV-spectrophotometer at a wavelength of 353 nm. The entrapment efficiency was calculated using Equation (1) as discussed in Section 2.2.6.3 (Characterisation of solid dispersion) [7].

In vitro diffusion study. All the cryogel formulations (CRG1 to CRG4) were subjected to an *in vitro* diffusion study using a Franz diffusion cell. The donor compartment and receiver compartment of the apparatus were separated by a cellulose acetate membrane (mol. wt. 10000–12000 Da, Himedia). The membrane was directly in contact with the phosphate buffer saline (pH 7.4, dissolution medium) in the receiver compartment. It was stirred continuously using small magnetic beads at the bottom to keep the distribution of the released drug uniform. An accurately weighed amount of cryogel (1 g) was placed on the cellulose acetate membrane of the donor compartment. The temperature of dissolution medium was maintained at $37^\circ\text{C} \pm 0.5^\circ\text{C}$. Samples were withdrawn at 1-hour intervals for the next 22 hours. Most of the drug was released into the dissolution medium in this period. Fresh dissolution medium was added after each withdrawal to maintain the sink condition throughout the study. The removed samples were analysed for cumulative percent drug release. A UV-spectrophotometer with the wavelength at 353 nm was used. The flux was determined using the known surface area (20 cm^2) of the cellulose acetate membrane. The samples were measured in triplicate so that the accuracy of the results would be better.

Results and discussion

Evaluation of solid dispersion

The present research study was conducted in two phases, with the formulation and development of solid dispersions of the poorly soluble acitretin using a lipodic solubilizer, i.e. Gelucire® 44/14 being in the initial phase. This study was conducted to enhance the solubility of acitretin and make it more suitable and convenient for preparing a topical cryogel preparation for the treatment of psoriasis.

The FT-IR study showed that there were C–H stretching vibrations in the 3100–3000 cm^{-1} region

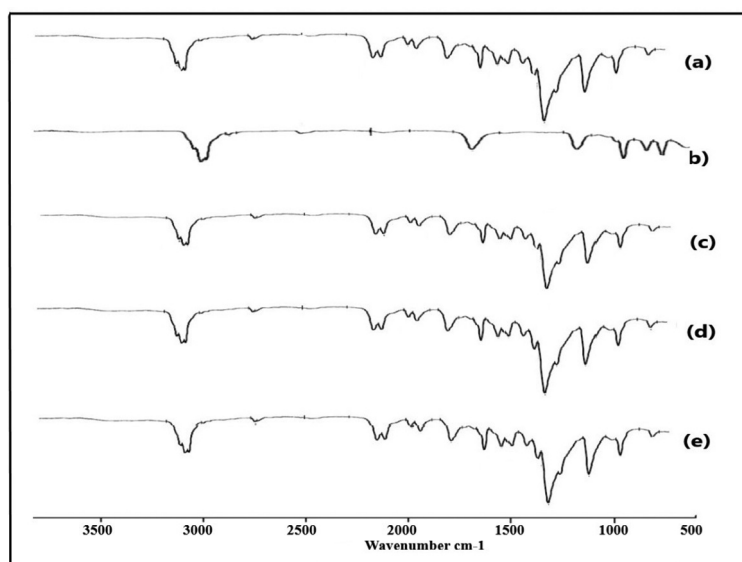


Figure 2. FT-IR spectra: Acitretin (a); Gelucire® 44/14 (b); Physical mixture of acitretin and Gelucire® 44/14 (c); Acitretin solid dispersion (d); Solid dispersion loaded cryogel (e).

(Figure 2). This is the characteristic region for identification of acitretin. Another useful region (1300–1000 cm^{-1}) had C–H plane bending frequencies. The actual peaks appeared at 1257 cm^{-1} , 1154 cm^{-1} , 1125 cm^{-1} and 1024 cm^{-1} . Stretching of the C = O of carboxylic acids appeared in the 1740–1660 cm^{-1} region, exactly as in ketones. C–C stretching was observed in the 1650–1200 cm^{-1} region, which indicated the presence of the phenyl group. The actual peaks were observed at 1707 cm^{-1} , 1578 cm^{-1} , 1473 cm^{-1} , 1442 cm^{-1} and 1257 cm^{-1} . Another important region (2990–2950 cm^{-1}) had the characteristic two asymmetric and one symmetric stretching vibration of the CH_3 group. The actual peaks appeared at 2947 cm^{-1} and 2912 cm^{-1} [13].

The spectral regions of the physical blends of the drug and Gelucire® 44/14 were similar to those of the cryogel formulation. These observations indicate that there was no interaction between the acitretin and Gelucire® 44/14. This study has given the green signal with regard to the suitability of the components for preparing a cryogel formulation.

Another analytical investigation was very useful for identifying the drug as well as confirming entrapment of the drug in the Gelucire® 44/14 matrix. The drug and drug-loaded samples were subjected to DSC analysis. The heat flow related with transitions in materials is measured as a function of the temperature in DSC. It gives information about physical and chemical changes that are involved in endothermic/exothermic processes. It also confirms whether form of a substance is amorphous or crystalline after heat is applied.

The thermograms of acitretin (Figure 3) show the onset of peaks at 226.35°C. There is a major endothermic peak at 227.66°C and an end set at 230.51°C.

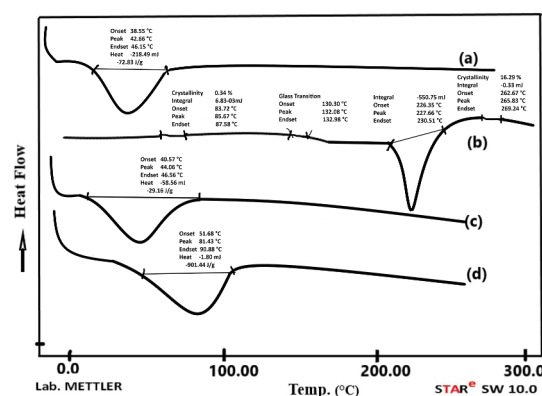


Figure 3. Differential Calorimetry Study: Gelucire® 44/14 (a); Acitretin (b); Acitretin solid dispersion (c); Solid dispersion loaded cryogel (d).

These are the characteristic peaks in the identification of acitretin [7]. A glass transition peak was observed at 132.98°C. The thermograms of Gelucire® 44/14 show a major endothermic peak with the onset at 38.55°C, the midpoint at 42.66°C and the end point at 46.15°C. These are characteristic peaks of Gelucire® 44/14. With the physical blend of acitretin and Gelucire®, there was a slight, insignificant shifting of the peak. The major endothermic peak shifted slightly, from 42.66°C to 44.06°C. The solid dispersion of acitretin was also analysed for thermal changes, if any. No peaks of acitretin were detected, and the same endothermic peaks characteristic of only Gelucire® 44/14 were observed at 44.06°C. This may confirm the complete entrapment of acitretin inside the Gelucire® 44/14 matrix, and may indicate that acitretin was converted to the amorphous form. It was interesting to observe major changes in the thermograms of the solid

dispersion-loaded cryogel formulation. There were no major peaks (at 269.24°C) of acitretin and only a small endothermic peak, slight shifting, from 87.58°C to 81.42°C, indicating that the acitretin was amorphous. This may be due to loading of the solid dispersion in the depth of the micron-sized pores of the cryogel formulation. This confirmed the complete loading and entrapment of acitretin [14,15].

The XRD study clearly indicated that pure acitretin was present in the crystalline form. There were sharp peaks of the 2θ value at 11.780°, 12.282° and 25.780°, with intensities of 4326, 4037 and 4693, respectively (Figure 4). The XRD data of the cryogel showed a very flat peak with 2θ values of 14.256°, 16.094°, 23.214° and 24.706°, with reduced intensities of 607, 796, 2366 and 2536, respectively. This confirmed that the crystalline acitretin was converted to a less crystalline form due to entrapment in the Gelucire® 44/14 and to the amorphous form due to entrapment in the pores of the microporous cryogel formulation. First two peaks of 2θ 4.45 and 9.10 were observed, these peaks may be appeared due to cryogel formation.

The solubility study was conducted to verify if the solubility of the acitretin was enhanced in the presence of the lipidic solubilizer, Gelucire® 44/14, which has a higher

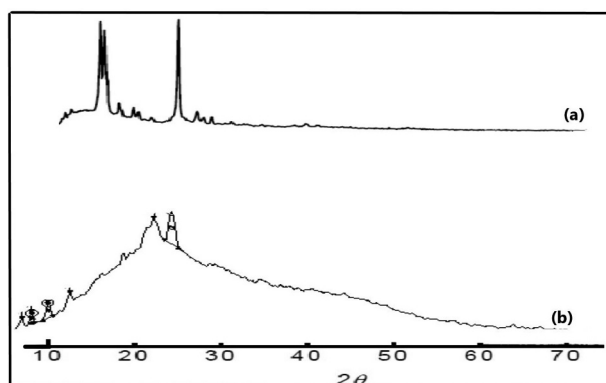


Figure 4. X-ray diffraction study: Acitretin (a); Solid dispersion loaded cryogel (b).

HLB (hydrophilic lipophilic balance) value, 14. Before the solubility study was conducted, the maximum concentration of Gelucire® 44/14 required for preparing a solid dispersion was determined by conducting trials with various levels of Gelucire® 44/14 (1–5%). On the basis of this study, solid dispersions were prepared using acitretin: Gelucire® 44/14 various ratios from 1:1 to 1:6 (batches SD1 to SD6). It was observed that the solubility increased with increasing concentration of Gelucire® 44/14. The highest solubilities were 1.2082 mg/ml, 3.437 mg/ml, 3.1362 mg/ml and 3.7012 mg/ml in distilled water, phosphate buffer (pH 6.8), phosphate buffer (pH 7.4) and 0.1 N HCl, respectively. Enhancement of solubility due to the presence of Gelucire® 44/14 was observed. Gelucire® 44/14 has solubilising properties (higher HLB value of 14) [16]. All the observations of the solubility study are shown in Figure 5.

The *in vitro* dissolution study of the solid dispersion was conducted in a phosphate buffer solution (pH 7.4). Batch SD6 showed the maximum drug release ($98.21 \pm 1.24\%$), whereas the lowest drug release ($63.28 \pm 1.55\%$) was observed with batch SD1 after 90 minutes. The increased drug release was observed with the batches containing higher levels of Gelucire 44/14. This drug release behaviour was due to the solubilising property of Gelucire® 44/14. As discussed in the solubility study section, the solubility of the solid dispersion was increased manifold, and highest solubility was that of batch SD6 (acitretin:Gelucire ratio 44/14). The drug release profiles of the acitretin solid dispersion formulations are presented in Figure 6.

Evaluation of cryogel formulation

The void spaces in the material are called as porosity and it is the fraction of the volume of voids over the total surface area. It gives an idea about the interconnected pores and pore size distribution. The porosity is a very important property as the drug diffuses through the pores. The acitretin cryogel was subjected to

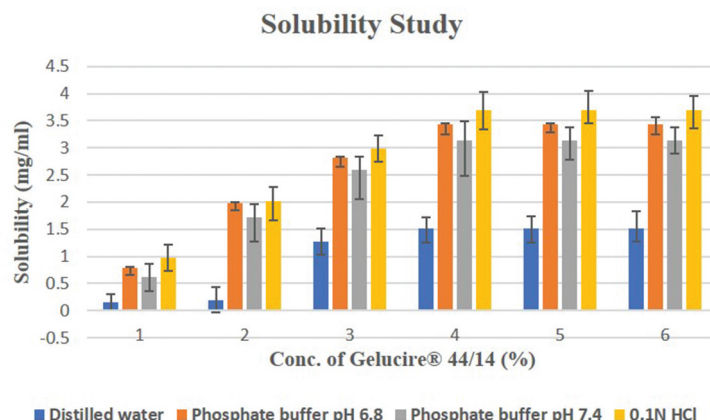


Figure 5. Solubility study of acitretin in the presence of Gelucire® 44/14 in different solvents.

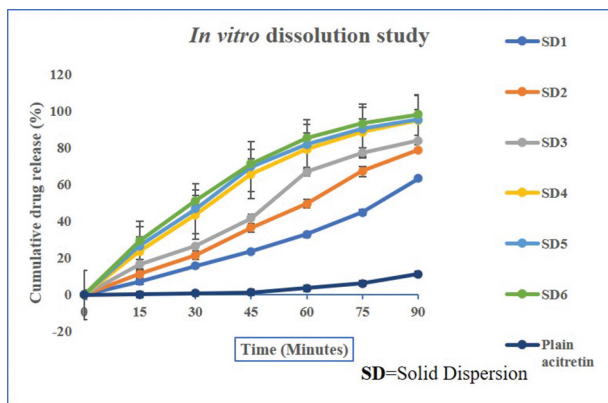


Figure 6. In vitro drug release profiles of acitretin solid dispersion.

mercury intrusion porosimetry for pore structure analysis, which also gives an idea about various other parameters related to porosity. This analysis confirmed the porous nature of the prepared cryogel. The average pore diameter was found to be $0.11 \mu\text{m}$, and the total porosity was 78.89% per gram weight of cryogel. The total specific surface area was found to be $4.152 \text{ m}^2/\text{g}$ weight of cryogel. The total cumulative volume occupied was found to be $0.0795 \text{ cm}^3/\text{g}$ weight of cryogel. The total bulk density and apparent density were found to be $0.9925 \text{ g}/\text{cm}^3$ and $1.0775 \text{ g}/\text{cm}^3$, respectively. The pores were found to be interconnected to each other, with a few dead pores. The solubilised form of acitretin was embedded in the pores.

The surface morphology of the solid dispersions was studied using scanning electron microscopic analysis at different resolutions. The surface texture of the solid dispersion was found to be smooth, and the average particle size was $250 \mu\text{m}$. The smooth surface was possibly due to the presence of Gelucire® 44/14, which is lipidic in nature. The drug, acitretin, was completely covered with this lipidic Gelucire® 44/14 carrier. This smooth surface enhances the flow properties of the solid dispersion, which are essential for designing and developing any pharmaceutical product. The images obtained using scanning electron microscopy are presented in Figure 7.

A microscopic study conducted in the laboratory using a CX23 Olympus microscope confirmed the porous structure of the cryogel. It had distinct pores are interconnected to form a porous network. The scanning electron microscopic (SEM) images are shown in Figure 8.

The viscosity of the cryogel was found to be 40.306 Pa s at set temperature condition. The viscosity values indicate that the final formulation did not exhibit good spreadability. The cryogel appears like a firm gel with a porous structure as described in the foregoing. The viscosity was observed to increase as the temperature increased up to 1400°C but subsequently it decreases with decreasing the temperature condition. So, the viscosity of the cryogel depends on the temperature at certain shear rate values. The type of rheograms are referred to as scissored as structure

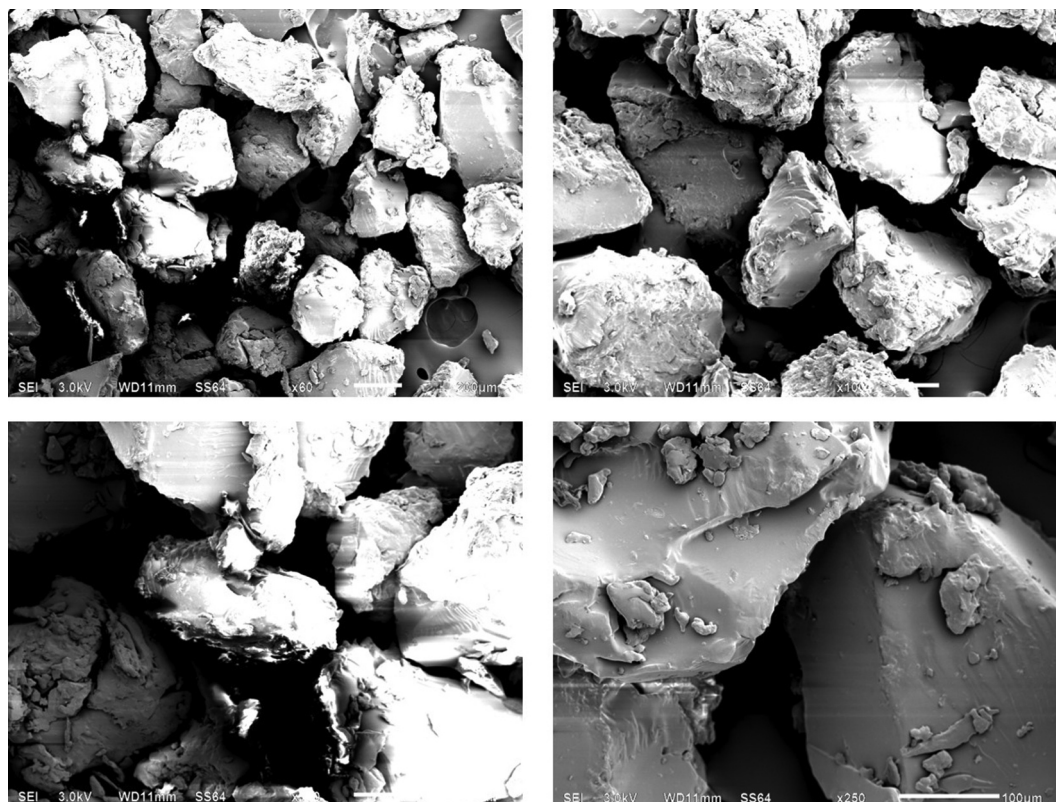


Figure 7. Scanning electron microscopy study of acitretin solid dispersion at various resolution.

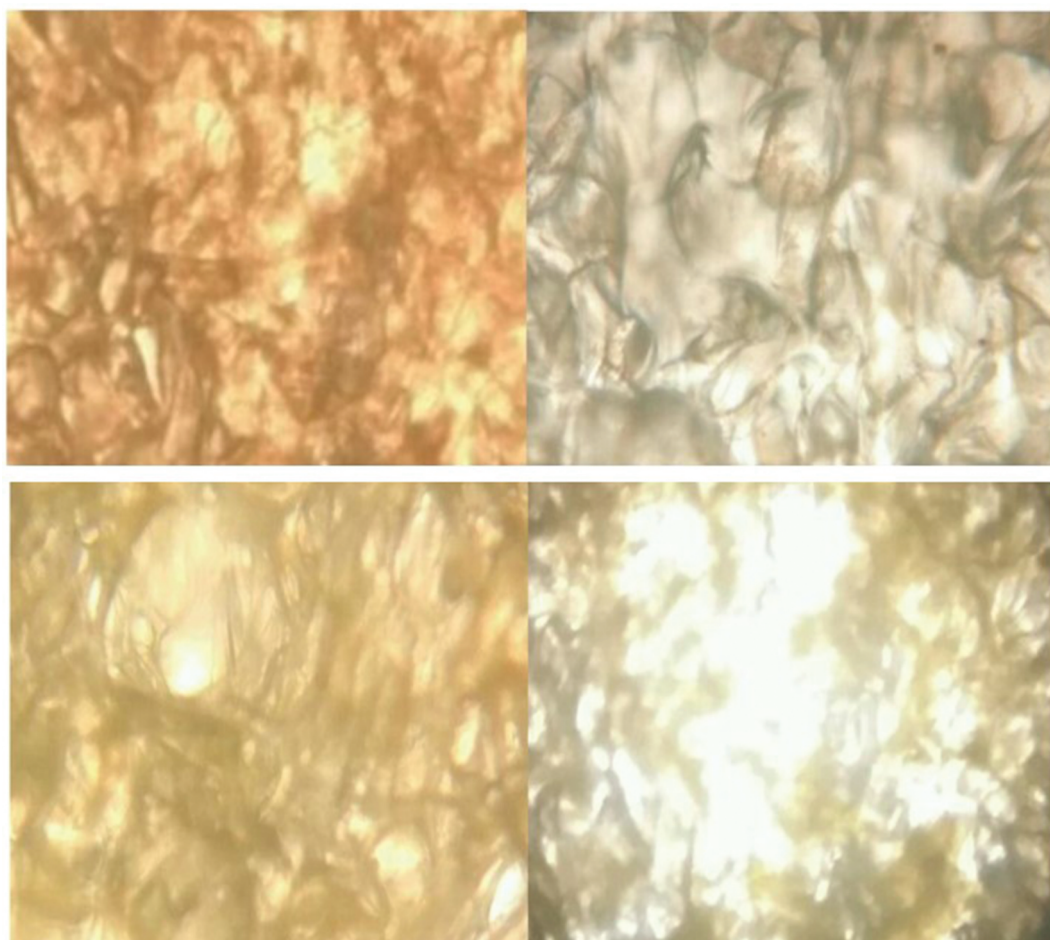


Figure 8. Various images showing cryogel surface using digital microscope.

breaking occurs in the up curve, while the fluid is nearly Newtonian on the down curve. Here the dominant gel-like structure prevents flows at low shear rates, but the viscosity decreases at higher shear rates because the structure is destroyed. This phenomenon is the opposite of thixotropy, and hence it is called anti-thixotropy or rheopexy. It is reversible viscosity which increases with the shear rate, and this occurs when the maximum shear rate is relatively low.

The pH of the all the cryogel formulation batches was found to be in the range 6.66–6.80, which was assumed to be safe to apply on skin [17].

A drug entrapment efficiency study was conducted to determine the amount of drug present in the polymer carrier. This amount depends on the capacity of the carrier material to entrap the drug completely. Batch SD6, which had more Gelucire 44/14 (carrier material) had the maximum entrapment efficiency ($96.44 \pm 1.25\%$). The entrapment efficiency of batch SD1, with less carrier material, was lower ($85.38 \pm 1.12\%$). The results of the entrapment efficiency study are presented in Table 2.

A drug content study helps to determine the presence of the drug in the carrier material and it allows the accurate dose in the form of a solid dispersion to be measured for further product development. The

Table 2. Evaluation of solid dispersion for entrapment efficiency and drug content study.

Batch No.	*Entrapment Efficiency (%)	*Drug Content (%)
SD1	85.38 ± 1.12	78.31 ± 1.55
SD2	88.58 ± 1.04	81.20 ± 1.24
SD3	90.28 ± 1.25	83.88 ± 1.22
SD4	93.25 ± 1.33	82.25 ± 1.78
SD5	94.28 ± 1.58	86.57 ± 1.58
SD6	96.44 ± 1.25	88.88 ± 1.12

*All the experiments were conducted triplicate \pm SD; (n = 3).

maximum drug content was found to be $88.88 \pm 1.12\%$ (SD6), and the minimum drug content of $78.31 \pm 1.55\%$ was observed that of batch SD1. The results of the drug content study are presented in Table 2.

Like the solid dispersions, the cryogel formulation batches were subjected to drug content and entrapment efficiency studies. All the cryogel batches (CRG1 to CRG4) had entrapment efficiency values in the range from $43.25 \pm 0.47\%$ to $53.24 \pm 1.87\%$. The results of the drug entrapment efficiency study of the cryogel formulations are presented in Table 3.

A diffusion study was conducted on the solid dispersion-loaded cryogel formulations (CRG1 to CRG4) using the dialysis bag diffusion method. The drug release profiles are shown in Figure 9. The least drug

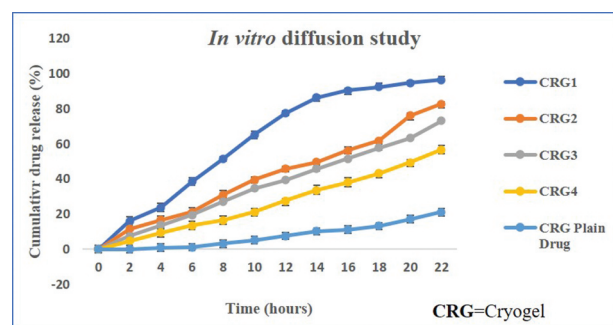
Table 3. Evaluation solid dispersion loaded acitretin cryogel for physicochemical parameters.

Batch No.	*Entrapment Efficiency (%)	*pH	*Flux ($\mu\text{g}/\text{cm}^2/\text{h}$)	*Swelling Index (%)
CRG1	43.25 \pm 0.47	6.78 \pm 0.40	7.28 \pm 1.25	78.28 \pm 1.14
CRG2	47.55 \pm 1.24	6.60 \pm 0.20	5.88 \pm 1.47	89.45 \pm 1.57
CRG3	49.47 \pm 1.25	6.66 \pm 0.45	5.22 \pm 1.33	93.48 \pm 1.53
CRG4	53.24 \pm 1.87	6.80 \pm 0.70	5.68 \pm 1.22	96.11 \pm 1.23

*All the experiments were conducted triplicate \pm SD; (n = 3).

release ($56.78 \pm 1.02\%$) was that of formulation CRG4, and the highest drug release ($96.58 \pm 1.35\%$) was that of formulation CRG1 at the end of the 22-hour study. The drug releases of the remaining formulations, CG2 and CRG3, were $82.87 \pm 1.78\%$ and $73.28 \pm 1.36\%$, respectively, at the end of the diffusion study. Overall observation of *in vitro* diffusion study indicated that the decreasing trend of drug release was due to the increased in the concentration levels of TEMED and MBAAM with fixed amount of acitretin solid dispersion and acrylamide polymer. TEMED and MBAAM were both involved in the process of cryo-gelation. Increased levels of these materials boost the interconnectivity of the pores as well as the cross-linking and elastic properties of the formulation. These physical properties also influence the drug permeability and thereby decrease the rate of drug release from the porous structure [18].

The swelling study is the important study in the design and development of a cryogel formulation. The swelling describes the fractional increase in the weight of the cryogel due to filling of pores with a solvent (e.g. water). In the swelling process, the pores are filled when water is absorbed. Another step involved in the swelling is the diffusion of the solvent (water) into the polymer wall. As discussed in the foregoing (*in vitro* diffusion study), the swelling property was found to be enhanced at higher concentrations of both TEMED and MBAAM in the formulation. The formulation CRG4 showed the highest swelling index ($96.11 \pm 1.23\%$), whereas the lowest swelling index was that of the formulation CRG1. The results of the swelling study are presented in Table 3. The swelling phenomenon had a positive

**Figure 9.** In vitro diffusion study of solid dispersion loaded cryogel formulation.

impact on the drug release property. The drug release increased as the swelling index of the formulation decreased and vice versa. This was again due to the cryogelation effect and the TEMED and MBAAM levels, which had played a very important role. High levels of TEMED and MBAAM increase the interconnectivity of the pores and crosslinking, as a result of which the density of the polymer wall increases. This increase in the density of polymer wall affects the swelling property. The swelling tends to take more time, and this delays the release of the drug [19,20].

Conclusions

Technological advancements have improved the physical and chemical properties of polymeric materials. These modified properties allow the development of many formulations of better efficacy and quality. In this, study an attempt was made to develop a cryogel formulation for acitretin, the drug of choice for the treatment of psoriasis. The prepared cryogel formulation had improved physical and mechanical properties. Cryogel formulations with appropriate levels of polymeric components were prepared using solubility-enhanced solid dispersions of acitretin. Gelucire 44/14 had enhanced the solubility, allowed loading of the acitretin into the surface pores of the cryogel formulation with increased surface area and comfort for application. The cryogel, with a microporous structure, had better permeation properties compared with conventional hydrogels. So, it was concluded that cryogel formulations are a better choice as a delivery platform for drugs such as acitretin in the treatment of skin disorders.

Authors' contributions

Prakash Kendre: Conceptualization, Methodology **Nikita Borawake.:** Data curation, Writing- Original draft preparation. **Shirish Jain:** Visualization, Investigation. **Prakash Kendre:** Supervision. **Somnath Vibhute:** Software, Validation. **Ajinkya Pote:** Writing- Reviewing and Editing.

Acknowledgments

The authors are very thankful to Glenmark Pharmaceuticals, Sinner, Nashik, India for providing Tramadol HCl. They are also grateful to Gattefosse India Pvt. Ltd., Mumbai for providing the gift sample of Gelucire® 44/14. I would like to mention the support of the Principal, Sanjivani College of Pharmaceutical Education and Research, Kopergaon and Rajarshi Shahu College of Pharmacy, Buldana for providing facilities to conduct this research study. Finally, the authors extend thanks to all those whose cooperation helped complete this work successfully.

Consent of publication

Not applicable.

Code of availability

Not applicable.

Data availability statement

Author(s) doesn't allow to disclose the data.

Disclosure statement

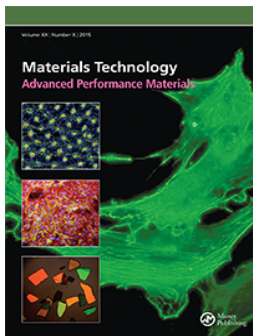
Author(s) declares no conflict of interest.

Funding

This research is not funded or supported by any funding agencies

References

- [1] Kaur I, Handa S, Kumar B. Natural history of psoriasis: A study from the indian subcontinent. *J Dermatol.* **1997**;24:230–234.
- [2] Christophers E. Psoriasis - Epidemiology and clinical spectrum. *Clin Exp Dermatol.* **2001**;26:314–320.
- [3] Krueger G, Koo J, Lebwohl M, et al. The impact of psoriasis on quality of life results of a 1998 national psoriasis foundation patient-membership survey. 2001. Available from: <https://jamanetwork.com/>. Accessed on December 20, 2019.
- [4] Hsia E, Johnston MJ, Houlden RJ, et al. Effects of topically applied acitretin in reconstructed human epidermis and the rhino mouse. *J Invest Dermatol.* **2008**;128:125–130.
- [5] Allen JG, Bloxham DP. The pharmacology and pharmacokinetics of the retinoids. *Pharmacol Ther.* **1989**;40:1–27.
- [6] Agrawal V, Gupta V, Ramteke S, et al. Preparation and evaluation of tubular micelles of pluronic lecithin organogel for transdermal delivery of sumatriptan. *AAPS PharmSciTech.* **2010**;11:1718–1725.
- [7] Agrawal Y, Petkar KC, Sawant KK. Development, evaluation and clinical studies of Acitretin loaded nanostructured lipid carriers for topical treatment of psoriasis. *Int J Pharm.* **2010**;401:93–102.
- [8] Wright E, Andrews G, McCoy C, et al. The effect of dilute solution properties on poly(vinyl alcohol) films. *J Mech Behav Biomed Mater.* **2013**;28:222–231. [cited 2020 Aug 3]. Available from: <https://pure.qub.ac.uk/en/publications/the-effect-of-dilute-solution-properties-on-polyvinyl-alcohol-fil>
- [9] Pazos V, Mongrain R, Tardif JC. Polyvinyl alcohol cryogel: optimizing the parameters of cryogenic treatment using hyperelastic models. *J Mech Behav Biomed Mater.* **2009**;2:542–549.
- [10] Caló E, Barros J, Ballamy L, et al. Poly(vinyl alcohol)-Gantrez® AN cryogels for wound care applications. *RSC Adv.* **2016**;6:105487–105494.
- [11] Zou X, Deng P, Zhou C, et al. Preparation of a novel antibacterial chitosan-poly(ethylene glycol) cryogel/silver nanoparticles composites. *J Biomater Sci Polym Ed.* **2017**;28:1324–1337.
- [12] Kim I, Lee SS, Bae S, et al. Heparin functionalized injectable cryogel with rapid shape-recovery property for neovascularization. *Biomacromolecules.* **2018**;19:2257–2269.
- [13] Swarnalatha N, Gunasekaran S, Muthu SRP. Indian journal of science experimental and theoretical investigations of spectroscopic properties of acitretin. *Indian J Sci.* **2017**;14:44–62.
- [14] Harivardhan Reddy L, Murthy RSR. Etoposide-loaded nanoparticles made from glyceride lipids: formulation, characterization, in vitro drug release, and stability evaluation. *AAPS PharmSciTech.* **2005**;6:E158.
- [15] Sarmiento B, Ferreira D, Veiga F, et al. Characterization of insulin-loaded alginate nanoparticles produced by ionotropic pre-gelation through DSC and FTIR studies. *Carbohydr Polym.* **2006**;66:1–7.
- [16] Kendre PN, Chaudhari PD. Design and optimization of oral bioadhesive nanocurcumin delivery using novel hydrophilic carrier for cancer treatment: an alternative to parenteral chemotherapy. *Indian Drugs.* **2016**;53:24–36.
- [17] Worth AP, Cronin MTD. The use of pH measurements to predict the potential of chemicals to cause acute dermal and ocular toxicity. *Toxicology.* **2001**;169:119–131.
- [18] Memic A, Colombani T, Eggermont LJ, et al. Latest advances in cryogel technology for biomedical applications. *Adv Ther.* **2019**;2:1800114.
- [19] Bencherif SA, Sands RW, Bhatta D, et al. Injectable preformed scaffolds with shape-memory properties. *Proc Natl Acad Sci U S A.* **2012**;109:19590–19595.
- [20] Shih TY, Blacklow SO, Li AW, et al. Injectable, tough alginate cryogels as cancer vaccines. *Adv Healthc Mater.* **2018**;7:1701469.



An effort to tailor the solid dispersion loaded, surface-modified, microporous-cryogel formulation of acitretin for the treatment of psoriasis

Prakash N. Kendre , Nikita Borawake , Shirish P Jain , Somnath K. Vibhute & Ajinkya K. Pote

To cite this article: Prakash N. Kendre , Nikita Borawake , Shirish P Jain , Somnath K. Vibhute & Ajinkya K. Pote (2020): An effort to tailor the solid dispersion loaded, surface-modified, microporous-cryogel formulation of acitretin for the treatment of psoriasis, Materials Technology, DOI: [10.1080/10667857.2020.1868210](https://doi.org/10.1080/10667857.2020.1868210)

To link to this article: <https://doi.org/10.1080/10667857.2020.1868210>



Published online: 28 Dec 2020.



Submit your article to this journal [↗](#)



Article views: 6



View related articles [↗](#)



View Crossmark data [↗](#)



An effort to tailor the solid dispersion loaded, surface-modified, microporous-cryogel formulation of acitretin for the treatment of psoriasis

Prakash N. Kendre^a, Nikita Borawake^b, Shirish P Jain^a, Somnath K. Vibhute^a and Ajinkya K. Pote^a

^aDepartment of Pharmaceutics, Rajarshi Shahu College of Pharmacy, Buldana, India; ^bSanjivani College of Pharmaceutical Education and Research, Kopergaon, India

ABSTRACT

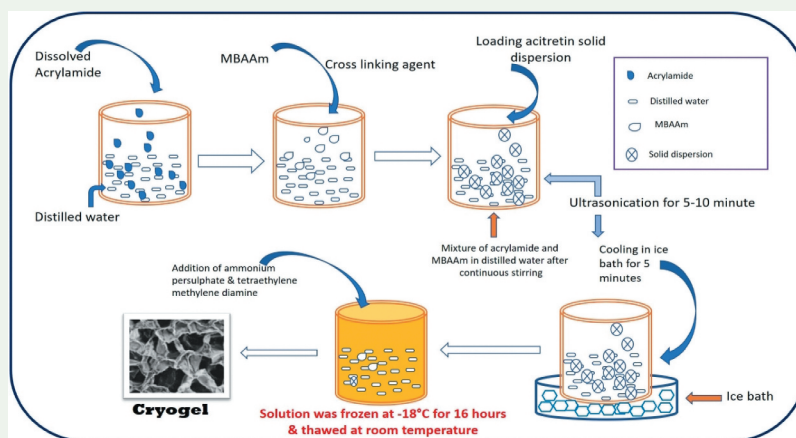
Acitretin is the drug of choice for the treatment of psoriasis, but due to its poor solubility, the development of oral and topical formulations of acitretin has been restricted. The aim of the present investigation was to enhance the solubility of acitretin. Solid dispersions of acitretin were prepared using a lipodic solubilizer, Gelucire[®] 44/14. These solid dispersions were characterized through FT-IR, DSC, XRD, drug content and solubility studies. The most solubilized dispersion was loaded on an N, N-methylenebisacrylamide microporous cryogel. Physical parameters of the solubilized drug such as the porosity, rheological behaviour, surface properties, appearance, drug content and diffusion behaviour were studied. It was concluded that the solubilized form of acitretin, loaded on a surface-modified cryogel, is the best option for the treatment of psoriasis. The hydration of the skin was excellent, and the permeability of the acitretin into the skin was better.

ARTICLE HISTORY

Received 27 November 2020
Accepted 17 December 2020

KEYWORDS

Acitretin; Gelucire[®] 44/14; N, N-methylenebisacrylamide; solid dispersion; cryogel; microporous



Introduction

Most of the drugs available today have greater potential in the management of various diseases, but certain properties of these drugs have restricted the development of different dosage forms. With recent advancements in the field of science and technology and in the manufacture of modified excipients with excellent features, it is possible to overcome these hurdles in the development of newer dosage forms.

Psoriasis is a condition in which skin cells build up and form scales, rashes and itchy, dry patches that are very uncomfortable to the patients physically as well as socially [1]. There are many problems associated with psoriasis, including inflammation, redness of the skin, sharply demarcated papules and rounded plaques. Regular hydration of the skin is required to avoid

serious skin damage [2]. Many drugs are used to treat psoriasis and the symptoms associated with it. These drugs include methotrexate, cyclosporine and acitretin. Treatment with topical steroids for prolonged periods may be dangerous. This may suppress the body's immune system. Drugs such as methotrexate may be hepatotoxic and may impair kidney function [3].

Acitretin is the drug of choice for the treatment of psoriasis, but due to its poor solubility (0.0729 mg/L), its use and the development of oral formulations have been restricted [4]. Hence, the development of topical formulations is the need of the hour. Acitretin is a retinoid, a form of vitamin A. It is used in the treatment of psoriasis because of its role in epithelial cell growth, sebum production and collagen synthesis [5].

CONTACT Prakash N. Kendre ✉ prakashkendre@gmail.com 📧 Rajarshi Shahu College of Pharmacy, At Post-Malviher, District Buldana-443001, Maharashtra, India

This article has been republished with minor changes. These changes do not impact the academic content of the article.

© 2020 Informa UK Limited, trading as Taylor & Francis Group

Cryogels are supermacroporous hydrophilic gels produced using the cryotropic gelation technique. Cryogels have interconnected pores whose size ranges from microns to several hundred microns. Cryogels can be formulated at sub-zero temperatures using various monomers. The process of polymerisation is carried out in the presence of a frozen monomer solution. The monomer is present in the interstices between the crystals of ice. The pores of cryogels can permit the entry of solutes freely. Cryogels are very flexible. Their permeability is good, and their mechanical strength is excellent.

In this study, a solubilised form of acitretin was embedded in the micropores of a cryogel. Cryogels can hold huge amounts of water. Thus, they keep the skin hydrated during the treatment of psoriasis, which is their main advantage over other topical formulations. The drug would diffuse slowly through the pores of the gel continuously for long periods of time.

Materials and methods

Materials

Acitretin was received as a gift sample from Glenmark Pharmaceuticals, Sinner, Nashik, India. Gelucire® 44/14 was obtained as a gift sample from Gattefosse India Pvt. Ltd., Mumbai. Acrylamide, N, N-methylenebisacrylamide (MBAAm), ammonium persulphate (APS), Tetramethylethyldiamine N, N, N', N'-tetramethylethylenediamine (TEMED) and other materials were purchased from Loba Chemie, Mumbai. All the other chemicals and reagents used in the study were of analytical grade.

Methods

The work was divided in two parts as preparation and evaluation of solid dispersion and preparation and evaluation of solid dispersion loaded cryogel.

Preparation of solid dispersion (fusion method)

On the basis of the results of a solubility study, acitretin and Gelucire 44/14 were accurately mixed in the ratios 1:1, 1:2, 1:3, 1:4, 1:5 and 1:6 (formulation batches SD1 to SD6, respectively). Gelucire 44/14 was melted in a porcelain dish on a heating mantle at 50°C under continuous stirring, and the drug was dispersed into the melted Gelucire 44/14. The resultant dispersion was cooled at room temperature to form a solid mass. This dried solid mass was pass through a fine screen to obtain particles of uniform size. The material was packed in an airtight container in which it was kept till it was processed further.

Fourier transform infrared (FT-IR) spectroscopy

FT-IR spectroscopy was used to confirm the identity of the acitretin. The drug and KBr (ratio of 1:100) were mixed and ground gently using a mortar and pestle. A pellet was made using the pellet press method. This yielded a translucent pellet. This pellet was placed in the sample holder of an FT-IR 8400 spectrometer (Shimadzu, Japan) at R.C. Patel College of Pharmacy, Shirpur, India. The instrument was run, and the FT-IR spectra of the acitretin were obtained. In the same way, physical blends of the drug and other excipients were also analysed to test their compatibility and suitability for the final formulation.

Differential scanning calorimetry (DSC)

Differential scanning calorimetric measurements were performed using a DSC-60 (Shimadzu) thermal analyser. Samples weighing about 5 mg were placed in aluminium hermetically sealed pans and scanned at a heating rate of 10°C/minute over a temperature range of 0–300°C with nitrogen as an effluent gas. The thermal properties of pure acitretin and its physical mixtures with the excipients were determined. This testing was done at the Department of Plastic and Polymer Engineering, Aurangabad.

X-ray diffractometry (XRD)

Small-angle XRD measurements were made to determine the structural ordering of the samples studied. The measurements were carried out using a D8 ADVANCE powder diffractometer. The drug sample was smeared over a low-back ground sample holder (amorphous silica holder) and fixed on the sample stage in a goniometer. The instrument was set in a B-B geometry. The current and voltage is set at 40 mV and 35 mA, and data were collected. This testing was carried out at the Sophisticated Test and Instrumentation Centre, Kochi University, Kerala.

Solubility study

The solubility of the acitretin in various solvents such as distilled water, phosphate buffers (pH 6.8 and 7.4) and 0.1 N HCl were determined using the shaking flask method. An excess amount of drug was taken in a 50-ml conical flask containing 10 ml of solvent. Solvents with different concentrations (1–5%) of Gelucire® 44/14 were used. The mixture was shaken at 37°C for 48 hours at 75 rpm using an orbital shaking incubator (Dolphin™). The resultant solutions were filtered through Whatman filter paper (0.45 µm). The filtered solutions were diluted and examined for UV absorbance at 353 nm.

Characterisation of solid dispersion

The prepared solid dispersion of acitretin was analysed in FT-IR, DSC, XRD, solubility, drug content and dissolution studies.

Scanning electron microscopy (SEM). The surface morphology of the solid dispersion was studied using a high-resolution scanning electron microscope. The dried samples were covered with double-sided sticking tape and placed on aluminium stubs. They were sealed and coated with gold ions (200 °A) under low pressure for 5 minutes using a sputtering device.

Determination of drug content. Ten milligrams of the solid dispersion were dissolved in a volumetric flask containing tetrahydrofuran, and the volume was made up with tetrahydrofuran to 10 ml. Then ultrasonication was performed to dissolve the drug rapidly in the tetrahydrofuran. The resultant solution was filtered through 0.45 µm filter media, and the drug content was determined using a UV-spectrophotometer at a wavelength of 353 nm [6].

Entrapment efficiency (EE). The solid dispersion samples were dissolved completely in the tetrahydrofuran, and the solution was filtered through 0.45 µm filter media to determine the amount of drug entrapped in the Gelucire carrier. A UV-spectrophotometer was used, with the wavelength set at 353 nm. The percentage entrapment efficiency was calculated using the following equation [7]:

$$\% \text{Entrapment Efficiency (EE)} = \frac{\text{Entrapped drug}}{\text{Entrapped drug} + \text{Freed drug}} \times 100 \dots (1)$$

In vitro dissolution study. All the solid dispersion formulations (SD1 to SD6) were subjected to an *in vitro* dissolution study using a USP Type-II dissolution test apparatus (Electrolab, India). Phosphate buffer saline (pH 7.4) was used as the dissolution medium. The temperature was 37°C ± 0.5°C, and the speed was 100 rpm [6]. The samples were withdrawn after 15, 30, 45, 60, 75 and 90 minutes and analysed using a UV-spectrophotometer at a wavelength of 353 nm. The plain drug was also subjected to a dissolution study similarly for comparison with the solid dispersions. The samples were measured in triplicate for better accuracy.

Preparation of cryogel

A cryogel was prepared using the step-wise process presented in Figure 1. All the formulations were designated as CRG1 to CRG4. The concentrations of the acrylamide, MBAAm, APS and TEMED are presented in Table 1. The same amount of acitretin solid dispersion was used in all the trial batches. The resultant mixtures were frozen and maintained at -18°C for 16 hours. They were thawed at room temperature (25°C) over 12 hours. The freezing-and-thawing process was repeated thrice [8,9].

The prepared cryogel was characterised through FT-IR, DSC, XRD, drug content, entrapment efficiency, surface morphology, porosity, rheological behaviour, *in vitro* dissolution testing and stability studies. The methods used in the FT-IR, DSC and XRD analyses were the same as those described previously.

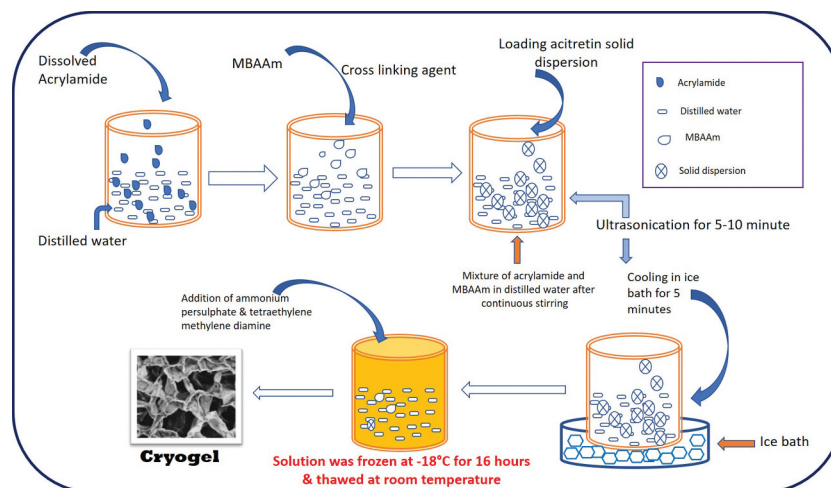


Figure 1. Cryogel preparation method with diagrammatic re-presentation.

Table 1. Composition of cryogel formulation.

Batch	Acrylamide (gm)	Deionised water (ml)	*MBAAm (gm)	Solid dispersion (gm)	*APS (gm)	*TEMED (µl)
CRG1	0.765	20	0.110	1	0.02	25
CRG2	0.765	20	0.120	1	0.02	50
CRG3	0.765	20	0.130	1	0.02	75
CRG4	0.765	20	0.140	1	0.02	100

*MBAAm: N, N' Methylene bis acrylamide; APS: Ammonium per-sulphate; TEMED: N, N, N', N'-tetramethyl ethylenediamine.

Characterisation of solid dispersion-loaded cryogel
Microscopic analysis using CX23 Olympus microscope. The surface morphology of the prepared cryogel was studied using a high-resolution scanning electron microscope. The changes produced in the surface texture by the freeze–thaw process was observed. The dried samples were covered with double-sided sticking tape and were placed on aluminium stubs. They were sealed and coated with gold ions under low pressure for 5 minutes using a sputtering device.

Mercury porosimetry study. The pore size, particle size distribution and surface area were determined using the mercury porosimeter technique. A Pascal 440 porosimeter, which has a dilatometer, a pressure source and a monitoring device, was used. The sample mass was 0.132 g, the mercury height was 41.683 mm, and the weight of the dilatometer, the mercury and the sample were 236.462 g. After correction this weight was 236.543 g, and the capillary mercury height was 0.683 mm. The dilatometer consists of a sample holder and a calibrated stem. The volume of the mercury that enters the pores was measured using a mercury penetrometer (an electrical capacitance dilatometer). This test was carried out at the Sophisticated Instrumentation Centre for Applied Research and Testing (SICART), Gujarat, India.

Rheological behaviour of cryogel. A Brookfield RST-CC digital rheometer was used to determine the rheology and viscosity of the formulations. The viscosity was measured as 12 MP in four blocks (UID140).

Swelling index of cryogel. This study was conducted to find out the swelling capacity of the dried form of the cryogel. The cryogel samples were dried to constant mass, and the mass of each dried sample was noted. The dried samples were placed in deionised water (swelling medium) at room temperature for 4 hours. Then the excess water was removed carefully, and the surface was cleaned slowly without squeezing. The samples were weighed again to calculate the swelling index. The swelling index was calculated using Equation (2) [10–12]:

$$\text{Swelling index} = [(W_s - W_0)/W_0] \times 100 \quad (2)$$

Where, W_0 and W_s are the weights of cryogels before and after swelling, respectively.

Determination of drug content. The drug content was determined by dissolving 10 mg of cryogel in a volumetric flask containing tetrahydrofuran, and the volume was made up with tetrahydrofuran to 10 ml. Then ultrasonication was performed to dissolve the drug rapidly in tetrahydrofuran. The resultant

solution was then filtered through 0.45 μm filter media, and the drug content was determined using a UV-spectrophotometer at a wavelength of 353 nm [7].

Entrapment efficiency (EE). The cryogel sample was washed with deionised water slowly to remove the untrapped drug adhering to the surface. Then the cryogel was completely dissolved in the tetrahydrofuran, and the solution was filtered through 0.45 μm filter media. The amount of entrapped drug was determined using a UV-spectrophotometer at a wavelength of 353 nm. The entrapment efficiency was calculated using Equation (1) as discussed in Section 2.2.6.3 (Characterisation of solid dispersion) [7].

In vitro diffusion study. All the cryogel formulations (CRG1 to CRG4) were subjected to an *in vitro* diffusion study using a Franz diffusion cell. The donor compartment and receiver compartment of the apparatus were separated by a cellulose acetate membrane (mol. wt. 10000–12000 Da, Himedia). The membrane was directly in contact with the phosphate buffer saline (pH 7.4, dissolution medium) in the receiver compartment. It was stirred continuously using small magnetic beads at the bottom to keep the distribution of the released drug uniform. An accurately weighed amount of cryogel (1 g) was placed on the cellulose acetate membrane of the donor compartment. The temperature of dissolution medium was maintained at $37^\circ\text{C} \pm 0.5^\circ\text{C}$. Samples were withdrawn at 1-hour intervals for the next 22 hours. Most of the drug was released into the dissolution medium in this period. Fresh dissolution medium was added after each withdrawal to maintain the sink condition throughout the study. The removed samples were analysed for cumulative percent drug release. A UV-spectrophotometer with the wavelength at 353 nm was used. The flux was determined using the known surface area (20 cm^2) of the cellulose acetate membrane. The samples were measured in triplicate so that the accuracy of the results would be better.

Results and discussion

Evaluation of solid dispersion

The present research study was conducted in two phases, with the formulation and development of solid dispersions of the poorly soluble acitretin using a lipodic solubilizer, i.e. Gelucire® 44/14 being in the initial phase. This study was conducted to enhance the solubility of acitretin and make it more suitable and convenient for preparing a topical cryogel preparation for the treatment of psoriasis.

The FT-IR study showed that there were C–H stretching vibrations in the 3100–3000 cm^{-1} region

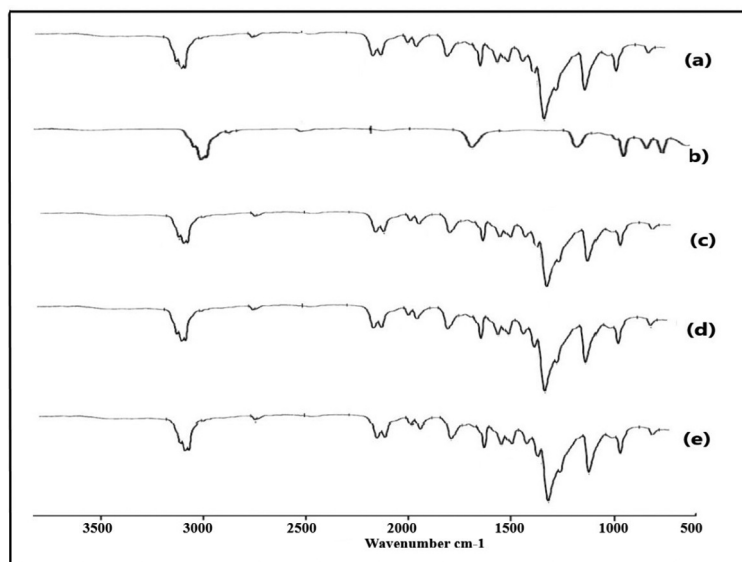


Figure 2. FT-IR spectra: Acitretin (a); Gelucire® 44/14 (b); Physical mixture of acitretin and Gelucire® 44/14 (c); Acitretin solid dispersion (d); Solid dispersion loaded cryogel (e).

(Figure 2). This is the characteristic region for identification of acitretin. Another useful region ($1300\text{--}1000\text{ cm}^{-1}$) had C–H plane bending frequencies. The actual peaks appeared at 1257 cm^{-1} , 1154 cm^{-1} , 1125 cm^{-1} and 1024 cm^{-1} . Stretching of the C = O of carboxylic acids appeared in the $1740\text{--}1660\text{ cm}^{-1}$ region, exactly as in ketones. C–C stretching was observed in the $1650\text{--}1200\text{ cm}^{-1}$ region, which indicated the presence of the phenyl group. The actual peaks were observed at 1707 cm^{-1} , 1578 cm^{-1} , 1473 cm^{-1} , 1442 cm^{-1} and 1257 cm^{-1} . Another important region ($2990\text{--}2950\text{ cm}^{-1}$) had the characteristic two asymmetric and one symmetric stretching vibration of the CH_3 group. The actual peaks appeared at 2947 cm^{-1} and 2912 cm^{-1} [13].

The spectral regions of the physical blends of the drug and Gelucire® 44/14 were similar to those of the cryogel formulation. These observations indicate that there was no interaction between the acitretin and Gelucire® 44/14. This study has given the green signal with regard to the suitability of the components for preparing a cryogel formulation.

Another analytical investigation was very useful for identifying the drug as well as confirming entrapment of the drug in the Gelucire® 44/14 matrix. The drug and drug-loaded samples were subjected to DSC analysis. The heat flow related with transitions in materials is measured as a function of the temperature in DSC. It gives information about physical and chemical changes that are involved in endothermic/exothermic processes. It also confirms whether form of a substance is amorphous or crystalline after heat is applied.

The thermograms of acitretin (Figure 3) show the onset of peaks at 226.35°C . There is a major endothermic peak at 227.66°C and an end set at 230.51°C .

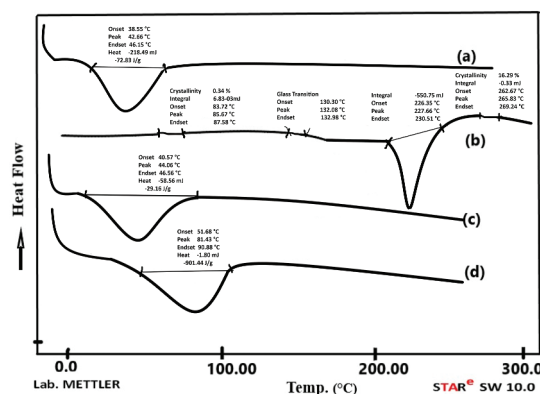


Figure 3. Differential Calorimetry Study: Gelucire® 44/14 (a); Acitretin (b); Acitretin solid dispersion (c); Solid dispersion loaded cryogel (d).

These are the characteristic peaks in the identification of acitretin [7]. A glass transition peak was observed at 132.98°C . The thermograms of Gelucire® 44/14 show a major endothermic peak with the onset at 38.55°C , the midpoint at 42.66°C and the end point at 46.15°C . These are characteristic peaks of Gelucire® 44/14. With the physical blend of acitretin and Gelucire®, there was a slight, insignificant shifting of the peak. The major endothermic peak shifted slightly, from 42.66°C to 44.06°C . The solid dispersion of acitretin was also analysed for thermal changes, if any. No peaks of acitretin were detected, and the same endothermic peaks characteristic of only Gelucire® 44/14 were observed at 44.06°C . This may confirm the complete entrapment of acitretin inside the Gelucire® 44/14 matrix, and may indicate that acitretin was converted to the amorphous form. It was interesting to observe major changes in the thermograms of the solid

dispersion-loaded cryogel formulation. There were no major peaks (at 269.24°C) of acitretin and only a small endothermic peak, slight shifting, from 87.58°C to 81.42°C, indicating that the acitretin was amorphous. This may be due to loading of the solid dispersion in the depth of the micron-sized pores of the cryogel formulation. This confirmed the complete loading and entrapment of acitretin [14,15].

The XRD study clearly indicated that pure acitretin was present in the crystalline form. There were sharp peaks of the 2θ value at 11.780°, 12.282° and 25.780°, with intensities of 4326, 4037 and 4693, respectively (Figure 4). The XRD data of the cryogel showed a very flat peak with 2θ values of 14.256°, 16.094°, 23.214° and 24.706°, with reduced intensities of 607, 796, 2366 and 2536, respectively. This confirmed that the crystalline acitretin was converted to a less crystalline form due to entrapment in the Gelucire® 44/14 and to the amorphous form due to entrapment in the pores of the microporous cryogel formulation. First two peaks of 2θ 4.45 and 9.10 were observed, these peaks may be appeared due to cryogel formation.

The solubility study was conducted to verify if the solubility of the acitretin was enhanced in the presence of the lipidic solubilizer, Gelucire® 44/14, which has a higher

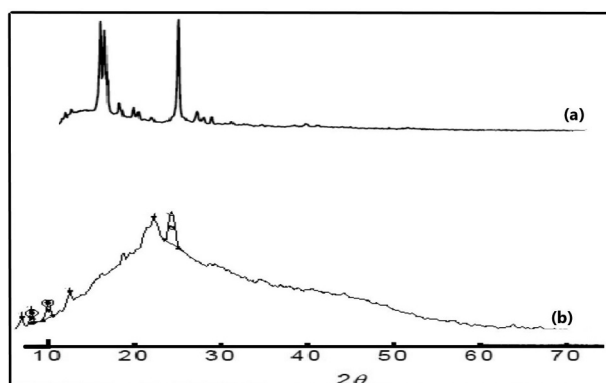


Figure 4. X-ray diffraction study: Acitretin (a); Solid dispersion loaded cryogel (b).

HLB (hydrophilic lipophilic balance) value, 14. Before the solubility study was conducted, the maximum concentration of Gelucire® 44/14 required for preparing a solid dispersion was determined by conducting trials with various levels of Gelucire® 44/14 (1–5%). On the basis of this study, solid dispersions were prepared using acitretin: Gelucire® 44/14 various ratios from 1:1 to 1:6 (batches SD1 to SD6). It was observed that the solubility increased with increasing concentration of Gelucire® 44/14. The highest solubilities were 1.2082 mg/ml, 3.437 mg/ml, 3.1362 mg/ml and 3.7012 mg/ml in distilled water, phosphate buffer (pH 6.8), phosphate buffer (pH 7.4) and 0.1 N HCl, respectively. Enhancement of solubility due to the presence of Gelucire® 44/14 was observed. Gelucire® 44/14 has solubilising properties (higher HLB value of 14) [16]. All the observations of the solubility study are shown in Figure 5.

The *in vitro* dissolution study of the solid dispersion was conducted in a phosphate buffer solution (pH 7.4). Batch SD6 showed the maximum drug release ($98.21 \pm 1.24\%$), whereas the lowest drug release ($63.28 \pm 1.55\%$) was observed with batch SD1 after 90 minutes. The increased drug release was observed with the batches containing higher levels of Gelucire 44/14. This drug release behaviour was due to the solubilising property of Gelucire® 44/14. As discussed in the solubility study section, the solubility of the solid dispersion was increased manifold, and highest solubility was that of batch SD6 (acitretin:Gelucire ratio 44/14). The drug release profiles of the acitretin solid dispersion formulations are presented in Figure 6.

Evaluation of cryogel formulation

The void spaces in the material are called as porosity and it is the fraction of the volume of voids over the total surface area. It gives an idea about the interconnected pores and pore size distribution. The porosity is a very important property as the drug diffuses through the pores. The acitretin cryogel was subjected to

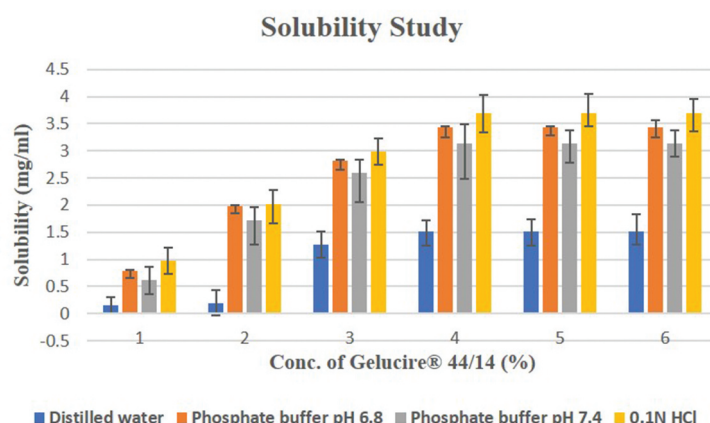


Figure 5. Solubility study of acitretin in the presence of Gelucire® 44/14 in different solvents.

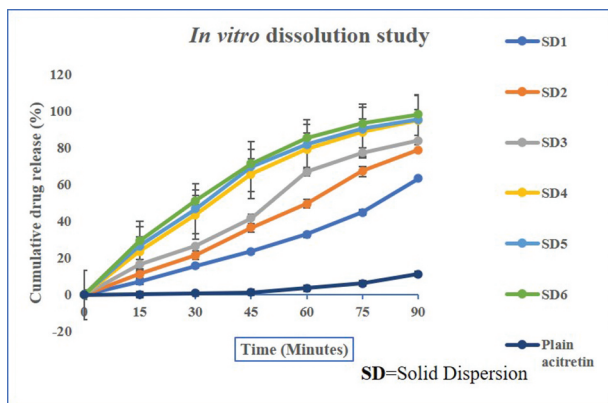


Figure 6. In vitro drug release profiles of acitretin solid dispersion.

mercury intrusion porosimetry for pore structure analysis, which also gives an idea about various other parameters related to porosity. This analysis confirmed the porous nature of the prepared cryogel. The average pore diameter was found to be $0.11 \mu\text{m}$, and the total porosity was 78.89% per gram weight of cryogel. The total specific surface area was found to be $4.152 \text{ m}^2/\text{g}$ weight of cryogel. The total cumulative volume occupied was found to be $0.0795 \text{ cm}^3/\text{g}$ weight of cryogel. The total bulk density and apparent density were found to be $0.9925 \text{ g}/\text{cm}^3$ and $1.0775 \text{ g}/\text{cm}^3$, respectively. The pores were found to be interconnected to each other, with a few dead pores. The solubilised form of acitretin was embedded in the pores.

The surface morphology of the solid dispersions was studied using scanning electron microscopic analysis at different resolutions. The surface texture of the solid dispersion was found to be smooth, and the average particle size was $250 \mu\text{m}$. The smooth surface was possibly due to the presence of Gelucire® 44/14, which is lipidic in nature. The drug, acitretin, was completely covered with this lipidic Gelucire® 44/14 carrier. This smooth surface enhances the flow properties of the solid dispersion, which are essential for designing and developing any pharmaceutical product. The images obtained using scanning electron microscopy are presented in Figure 7.

A microscopic study conducted in the laboratory using a CX23 Olympus microscope confirmed the porous structure of the cryogel. It had distinct pores are interconnected to form a porous network. The scanning electron microscopic (SEM) images are shown in Figure 8.

The viscosity of the cryogel was found to be 40.306 Pa s at set temperature condition. The viscosity values indicate that the final formulation did not exhibit good spreadability. The cryogel appears like a firm gel with a porous structure as described in the foregoing. The viscosity was observed to increase as the temperature increased up to 1400°C but subsequently it decreases with decreasing the temperature condition. So, the viscosity of the cryogel depends on the temperature at certain shear rate values. The type of rheograms are referred to as scissored as structure

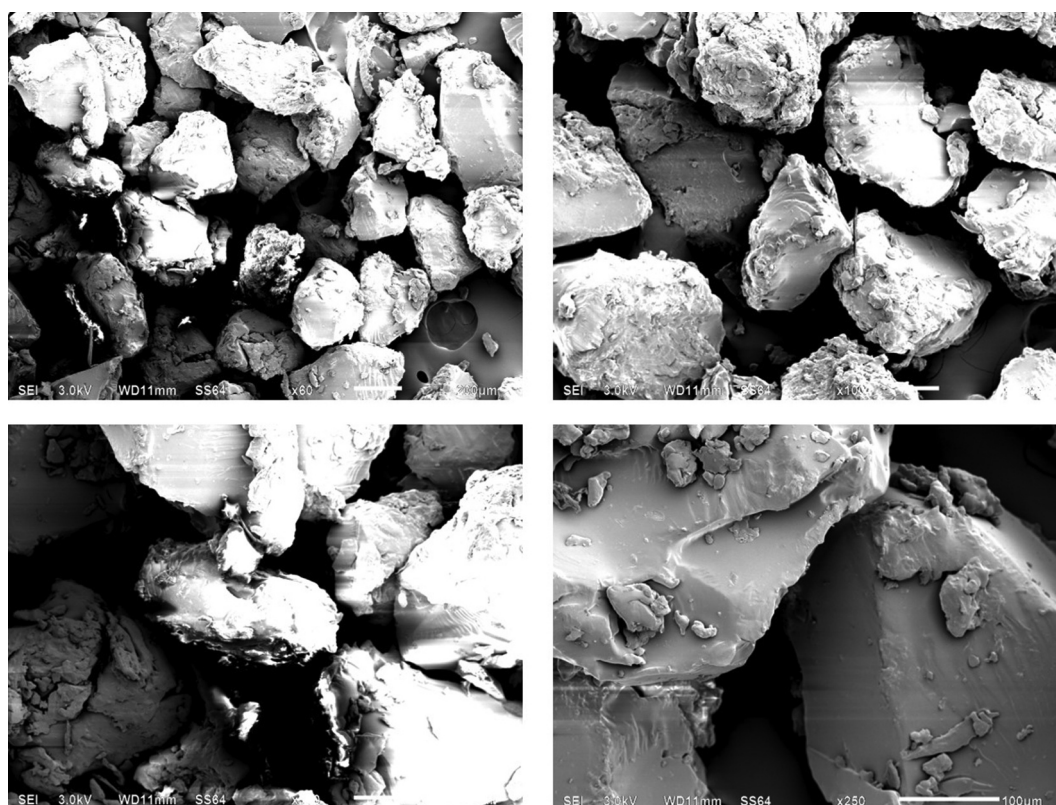


Figure 7. Scanning electron microscopy study of acitretin solid dispersion at various resolution.

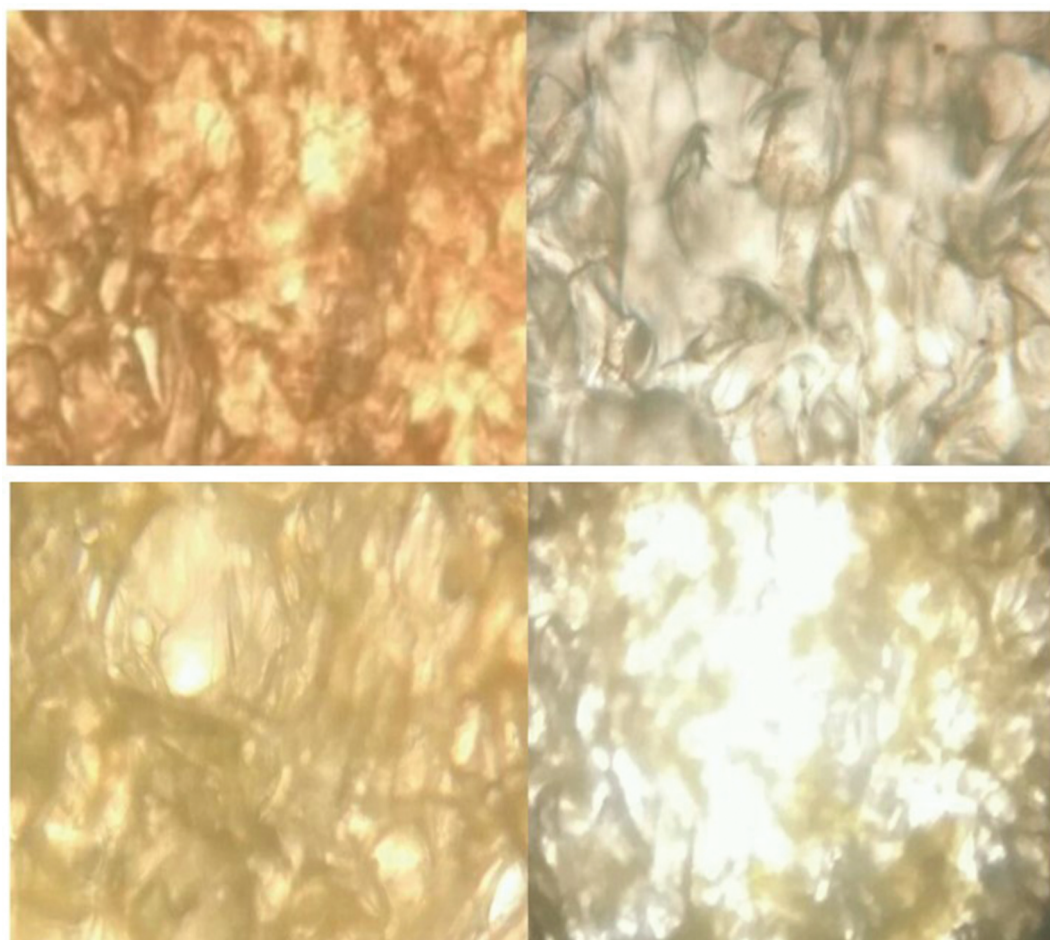


Figure 8. Various images showing cryogel surface using digital microscope.

breaking occurs in the up curve, while the fluid is nearly Newtonian on the down curve. Here the dominant gel-like structure prevents flows at low shear rates, but the viscosity decreases at higher shear rates because the structure is destroyed. This phenomenon is the opposite of thixotropy, and hence it is called anti-thixotropy or rheopexy. It is reversible viscosity which increases with the shear rate, and this occurs when the maximum shear rate is relatively low.

The pH of the all the cryogel formulation batches was found to be in the range 6.66–6.80, which was assumed to be safe to apply on skin [17].

A drug entrapment efficiency study was conducted to determine the amount of drug present in the polymer carrier. This amount depends on the capacity of the carrier material to entrap the drug completely. Batch SD6, which had more Gelucire 44/14 (carrier material) had the maximum entrapment efficiency ($96.44 \pm 1.25\%$). The entrapment efficiency of batch SD1, with less carrier material, was lower ($85.38 \pm 1.12\%$). The results of the entrapment efficiency study are presented in Table 2.

A drug content study helps to determine the presence of the drug in the carrier material and it allows the accurate dose in the form of a solid dispersion to be measured for further product development. The

Table 2. Evaluation of solid dispersion for entrapment efficiency and drug content study.

Batch No.	*Entrapment Efficiency (%)	*Drug Content (%)
SD1	85.38 ± 1.12	78.31 ± 1.55
SD2	88.58 ± 1.04	81.20 ± 1.24
SD3	90.28 ± 1.25	83.88 ± 1.22
SD4	93.25 ± 1.33	82.25 ± 1.78
SD5	94.28 ± 1.58	86.57 ± 1.58
SD6	96.44 ± 1.25	88.88 ± 1.12

*All the experiments were conducted triplicate \pm SD; (n = 3).

maximum drug content was found to be $88.88 \pm 1.12\%$ (SD6), and the minimum drug content of $78.31 \pm 1.55\%$ was observed that of batch SD1. The results of the drug content study are presented in Table 2.

Like the solid dispersions, the cryogel formulation batches were subjected to drug content and entrapment efficiency studies. All the cryogel batches (CRG1 to CRG4) had entrapment efficiency values in the range from $43.25 \pm 0.47\%$ to $53.24 \pm 1.87\%$. The results of the drug entrapment efficiency study of the cryogel formulations are presented in Table 3.

A diffusion study was conducted on the solid dispersion-loaded cryogel formulations (CRG1 to CRG4) using the dialysis bag diffusion method. The drug release profiles are shown in Figure 9. The least drug

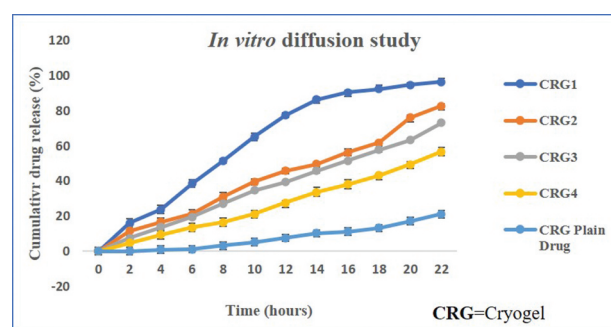
Table 3. Evaluation solid dispersion loaded acitretin cryogel for physicochemical parameters.

Batch No.	*Entrapment Efficiency (%)	*pH	*Flux ($\mu\text{g}/\text{cm}^2/\text{h}$)	*Swelling Index (%)
CRG1	43.25 \pm 0.47	6.78 \pm 0.40	7.28 \pm 1.25	78.28 \pm 1.14
CRG2	47.55 \pm 1.24	6.60 \pm 0.20	5.88 \pm 1.47	89.45 \pm 1.57
CRG3	49.47 \pm 1.25	6.66 \pm 0.45	5.22 \pm 1.33	93.48 \pm 1.53
CRG4	53.24 \pm 1.87	6.80 \pm 0.70	5.68 \pm 1.22	96.11 \pm 1.23

*All the experiments were conducted triplicate \pm SD; (n = 3).

release ($56.78 \pm 1.02\%$) was that of formulation CRG4, and the highest drug release ($96.58 \pm 1.35\%$) was that of formulation CRG1 at the end of the 22-hour study. The drug releases of the remaining formulations, CG2 and CRG3, were $82.87 \pm 1.78\%$ and $73.28 \pm 1.36\%$, respectively, at the end of the diffusion study. Overall observation of *in vitro* diffusion study indicated that the decreasing trend of drug release was due to the increased in the concentration levels of TEMED and MBAAM with fixed amount of acitretin solid dispersion and acrylamide polymer. TEMED and MBAAM were both involved in the process of cryo-gelation. Increased levels of these materials boost the interconnectivity of the pores as well as the cross-linking and elastic properties of the formulation. These physical properties also influence the drug permeability and thereby decrease the rate of drug release from the porous structure [18].

The swelling study is the important study in the design and development of a cryogel formulation. The swelling describes the fractional increase in the weight of the cryogel due to filling of pores with a solvent (e.g. water). In the swelling process, the pores are filled when water is absorbed. Another step involved in the swelling is the diffusion of the solvent (water) into the polymer wall. As discussed in the foregoing (*in vitro* diffusion study), the swelling property was found to be enhanced at higher concentrations of both TEMED and MBAAM in the formulation. The formulation CRG4 showed the highest swelling index ($96.11 \pm 1.23\%$), whereas the lowest swelling index was that of the formulation CRG1. The results of the swelling study are presented in Table 3. The swelling phenomenon had a positive

**Figure 9.** In vitro diffusion study of solid dispersion loaded cryogel formulation.

impact on the drug release property. The drug release increased as the swelling index of the formulation decreased and vice versa. This was again due to the cryogelation effect and the TEMED and MBAAM levels, which had played a very important role. High levels of TEMED and MBAAM increase the interconnectivity of the pores and crosslinking, as a result of which the density of the polymer wall increases. This increase in the density of polymer wall affects the swelling property. The swelling tends to take more time, and this delays the release of the drug [19,20].

Conclusions

Technological advancements have improved the physical and chemical properties of polymeric materials. These modified properties allow the development of many formulations of better efficacy and quality. In this, study an attempt was made to develop a cryogel formulation for acitretin, the drug of choice for the treatment of psoriasis. The prepared cryogel formulation had improved physical and mechanical properties. Cryogel formulations with appropriate levels of polymeric components were prepared using solubility-enhanced solid dispersions of acitretin. Gelucire 44/14 had enhanced the solubility, allowed loading of the acitretin into the surface pores of the cryogel formulation with increased surface area and comfort for application. The cryogel, with a microporous structure, had better permeation properties compared with conventional hydrogels. So, it was concluded that cryogel formulations are a better choice as a delivery platform for drugs such as acitretin in the treatment of skin disorders.

Authors' contributions

Prakash Kendre: Conceptualization, Methodology **Nikita Borawake.:** Data curation, Writing- Original draft preparation. **Shirish Jain:** Visualization, Investigation. **Prakash Kendre:** Supervision. **Somnath Vibhute:** Software, Validation. **Ajinkya Pote:** Writing- Reviewing and Editing.

Acknowledgments

The authors are very thankful to Glenmark Pharmaceuticals, Sinner, Nashik, India for providing Tramadol HCl. They are also grateful to Gattefosse India Pvt. Ltd., Mumbai for providing the gift sample of Gelucire[®] 44/14. I would like to mention the support of the Principal, Sanjivani College of Pharmaceutical Education and Research, Kopergaon and Rajarshi Shahu College of Pharmacy, Buldana for providing facilities to conduct this research study. Finally, the authors extend thanks to all those whose cooperation helped complete this work successfully.

Consent of publication

Not applicable.

Code of availability

Not applicable.

Data availability statement

Author(s) doesn't allow to disclose the data.

Disclosure statement

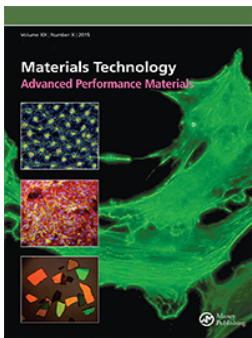
Author(s) declares no conflict of interest.

Funding

This research is not funded or supported by any funding agencies

References

- [1] Kaur I, Handa S, Kumar B. Natural history of psoriasis: A study from the indian subcontinent. *J Dermatol.* **1997**;24:230–234.
- [2] Christophers E. Psoriasis - Epidemiology and clinical spectrum. *Clin Exp Dermatol.* **2001**;26:314–320.
- [3] Krueger G, Koo J, Lebwohl M, et al. The impact of psoriasis on quality of life results of a 1998 national psoriasis foundation patient-membership survey. 2001. Available from: <https://jamanetwork.com/>. Accessed on December 20, 2019.
- [4] Hsia E, Johnston MJ, Houlden RJ, et al. Effects of topically applied acitretin in reconstructed human epidermis and the rhino mouse. *J Invest Dermatol.* **2008**;128:125–130.
- [5] Allen JG, Bloxham DP. The pharmacology and pharmacokinetics of the retinoids. *Pharmacol Ther.* **1989**;40:1–27.
- [6] Agrawal V, Gupta V, Ramteke S, et al. Preparation and evaluation of tubular micelles of pluronic lecithin organogel for transdermal delivery of sumatriptan. *AAPS PharmSciTech.* **2010**;11:1718–1725.
- [7] Agrawal Y, Petkar KC, Sawant KK. Development, evaluation and clinical studies of Acitretin loaded nanostructured lipid carriers for topical treatment of psoriasis. *Int J Pharm.* **2010**;401:93–102.
- [8] Wright E, Andrews G, McCoy C, et al. The effect of dilute solution properties on poly(vinyl alcohol) films. *J Mech Behav Biomed Mater.* **2013**;28:222–231. [cited 2020 Aug 3]. Available from: <https://pure.qub.ac.uk/en/publications/the-effect-of-dilute-solution-properties-on-polyvinyl-alcohol-fil>
- [9] Pazos V, Mongrain R, Tardif JC. Polyvinyl alcohol cryogel: optimizing the parameters of cryogenic treatment using hyperelastic models. *J Mech Behav Biomed Mater.* **2009**;2:542–549.
- [10] Caló E, Barros J, Ballamy L, et al. Poly(vinyl alcohol)-Gantrez® AN cryogels for wound care applications. *RSC Adv.* **2016**;6:105487–105494.
- [11] Zou X, Deng P, Zhou C, et al. Preparation of a novel antibacterial chitosan-poly(ethylene glycol) cryogel/silver nanoparticles composites. *J Biomater Sci Polym Ed.* **2017**;28:1324–1337.
- [12] Kim I, Lee SS, Bae S, et al. Heparin functionalized injectable cryogel with rapid shape-recovery property for neovascularization. *Biomacromolecules.* **2018**;19:2257–2269.
- [13] Swarnalatha N, Gunasekaran S, Muthu SRP. Indian journal of science experimental and theoretical investigations of spectroscopic properties of acitretin. *Indian J Sci.* **2017**;14:44–62.
- [14] Harivardhan Reddy L, Murthy RSR. Etoposide-loaded nanoparticles made from glyceride lipids: formulation, characterization, in vitro drug release, and stability evaluation. *AAPS PharmSciTech.* **2005**;6:E158.
- [15] Sarmiento B, Ferreira D, Veiga F, et al. Characterization of insulin-loaded alginate nanoparticles produced by ionotropic pre-gelation through DSC and FTIR studies. *Carbohydr Polym.* **2006**;66:1–7.
- [16] Kendre PN, Chaudhari PD. Design and optimization of oral bioadhesive nanocurcumin delivery using novel hydrophilic carrier for cancer treatment: an alternative to parenteral chemotherapy. *Indian Drugs.* **2016**;53:24–36.
- [17] Worth AP, Cronin MTD. The use of pH measurements to predict the potential of chemicals to cause acute dermal and ocular toxicity. *Toxicology.* **2001**;169:119–131.
- [18] Memic A, Colombani T, Eggermont LJ, et al. Latest advances in cryogel technology for biomedical applications. *Adv Ther.* **2019**;2:1800114.
- [19] Bencherif SA, Sands RW, Bhatta D, et al. Injectable preformed scaffolds with shape-memory properties. *Proc Natl Acad Sci U S A.* **2012**;109:19590–19595.
- [20] Shih TY, Blacklow SO, Li AW, et al. Injectable, tough alginate cryogels as cancer vaccines. *Adv Healthc Mater.* **2018**;7:1701469.



An effort to tailor the solid dispersion loaded, surface-modified, microporous-cryogel formulation of acitretin for the treatment of psoriasis

Prakash N. Kendre , Nikita Borawake , Shirish P Jain , Somnath K. Vibhute & Ajinkya K. Pote

To cite this article: Prakash N. Kendre , Nikita Borawake , Shirish P Jain , Somnath K. Vibhute & Ajinkya K. Pote (2020): An effort to tailor the solid dispersion loaded, surface-modified, microporous-cryogel formulation of acitretin for the treatment of psoriasis, Materials Technology, DOI: [10.1080/10667857.2020.1868210](https://doi.org/10.1080/10667857.2020.1868210)

To link to this article: <https://doi.org/10.1080/10667857.2020.1868210>



Published online: 28 Dec 2020.



Submit your article to this journal [↗](#)



Article views: 6



View related articles [↗](#)



View Crossmark data [↗](#)



An effort to tailor the solid dispersion loaded, surface-modified, microporous-cryogel formulation of acitretin for the treatment of psoriasis

Prakash N. Kendre^a, Nikita Borawake^b, Shirish P Jain^a, Somnath K. Vibhute^a and Ajinkya K. Pote^a

^aDepartment of Pharmaceutics, Rajarshi Shahu College of Pharmacy, Buldana, India; ^bSanjivani College of Pharmaceutical Education and Research, Kopergaon, India

ABSTRACT

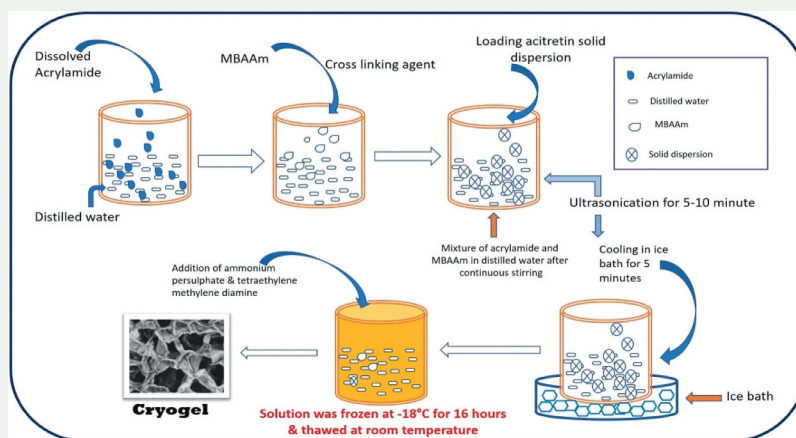
Acitretin is the drug of choice for the treatment of psoriasis, but due to its poor solubility, the development of oral and topical formulations of acitretin has been restricted. The aim of the present investigation was to enhance the solubility of acitretin. Solid dispersions of acitretin were prepared using a lipidic solubilizer, Gelucire[®] 44/14. These solid dispersions were characterized through FT-IR, DSC, XRD, drug content and solubility studies. The most solubilized dispersion was loaded on an N, N-methylenebisacrylamide microporous cryogel. Physical parameters of the solubilized drug such as the porosity, rheological behaviour, surface properties, appearance, drug content and diffusion behaviour were studied. It was concluded that the solubilized form of acitretin, loaded on a surface-modified cryogel, is the best option for the treatment of psoriasis. The hydration of the skin was excellent, and the permeability of the acitretin into the skin was better.

ARTICLE HISTORY

Received 27 November 2020
Accepted 17 December 2020

KEYWORDS

Acitretin; Gelucire[®] 44/14; N, N-methylenebisacrylamide; solid dispersion; cryogel; microporous



Introduction

Most of the drugs available today have greater potential in the management of various diseases, but certain properties of these drugs have restricted the development of different dosage forms. With recent advancements in the field of science and technology and in the manufacture of modified excipients with excellent features, it is possible to overcome these hurdles in the development of newer dosage forms.

Psoriasis is a condition in which skin cells build up and form scales, rashes and itchy, dry patches that are very uncomfortable to the patients physically as well as socially [1]. There are many problems associated with psoriasis, including inflammation, redness of the skin, sharply demarcated papules and rounded plaques. Regular hydration of the skin is required to avoid

serious skin damage [2]. Many drugs are used to treat psoriasis and the symptoms associated with it. These drugs include methotrexate, cyclosporine and acitretin. Treatment with topical steroids for prolonged periods may be dangerous. This may suppress the body's immune system. Drugs such as methotrexate may be hepatotoxic and may impair kidney function [3].

Acitretin is the drug of choice for the treatment of psoriasis, but due to its poor solubility (0.0729 mg/L), its use and the development of oral formulations have been restricted [4]. Hence, the development of topical formulations is the need of the hour. Acitretin is a retinoid, a form of vitamin A. It is used in the treatment of psoriasis because of its role in epithelial cell growth, sebum production and collagen synthesis [5].

CONTACT Prakash N. Kendre ✉ prakashkendre@gmail.com ✉ Rajarshi Shahu College of Pharmacy, At Post-Malviher, District Buldana-443001, Maharashtra, India

This article has been republished with minor changes. These changes do not impact the academic content of the article.

© 2020 Informa UK Limited, trading as Taylor & Francis Group

Cryogels are supermacroporous hydrophilic gels produced using the cryotropic gelation technique. Cryogels have interconnected pores whose size ranges from microns to several hundred microns. Cryogels can be formulated at sub-zero temperatures using various monomers. The process of polymerisation is carried out in the presence of a frozen monomer solution. The monomer is present in the interstices between the crystals of ice. The pores of cryogels can permit the entry of solutes freely. Cryogels are very flexible. Their permeability is good, and their mechanical strength is excellent.

In this study, a solubilised form of acitretin was embedded in the micropores of a cryogel. Cryogels can hold huge amounts of water. Thus, they keep the skin hydrated during the treatment of psoriasis, which is their main advantage over other topical formulations. The drug would diffuse slowly through the pores of the gel continuously for long periods of time.

Materials and methods

Materials

Acitretin was received as a gift sample from Glenmark Pharmaceuticals, Sinner, Nashik, India. Gelucire® 44/14 was obtained as a gift sample from Gattefosse India Pvt. Ltd., Mumbai. Acrylamide, N, N-methylenebisacrylamide (MBAAm), ammonium persulphate (APS), Tetramethylethyldiamine N, N, N', N'-tetramethylethylenediamine (TEMED) and other materials were purchased from Loba Chemie, Mumbai. All the other chemicals and reagents used in the study were of analytical grade.

Methods

The work was divided in two parts as preparation and evaluation of solid dispersion and preparation and evaluation of solid dispersion loaded cryogel.

Preparation of solid dispersion (fusion method)

On the basis of the results of a solubility study, acitretin and Gelucire 44/14 were accurately mixed in the ratios 1:1, 1:2, 1:3, 1:4, 1:5 and 1:6 (formulation batches SD1 to SD6, respectively). Gelucire 44/14 was melted in a porcelain dish on a heating mantle at 50°C under continuous stirring, and the drug was dispersed into the melted Gelucire 44/14. The resultant dispersion was cooled at room temperature to form a solid mass. This dried solid mass was pass through a fine screen to obtain particles of uniform size. The material was packed in an airtight container in which it was kept till it was processed further.

Fourier transform infrared (FT-IR) spectroscopy

FT-IR spectroscopy was used to confirm the identity of the acitretin. The drug and KBr (ratio of 1:100) were mixed and ground gently using a mortar and pestle. A pellet was made using the pellet press method. This yielded a translucent pellet. This pellet was placed in the sample holder of an FT-IR 8400 spectrometer (Shimadzu, Japan) at R.C. Patel College of Pharmacy, Shirpur, India. The instrument was run, and the FT-IR spectra of the acitretin were obtained. In the same way, physical blends of the drug and other excipients were also analysed to test their compatibility and suitability for the final formulation.

Differential scanning calorimetry (DSC)

Differential scanning calorimetric measurements were performed using a DSC-60 (Shimadzu) thermal analyser. Samples weighing about 5 mg were placed in aluminium hermetically sealed pans and scanned at a heating rate of 10°C/minute over a temperature range of 0–300°C with nitrogen as an effluent gas. The thermal properties of pure acitretin and its physical mixtures with the excipients were determined. This testing was done at the Department of Plastic and Polymer Engineering, Aurangabad.

X-ray diffractometry (XRD)

Small-angle XRD measurements were made to determine the structural ordering of the samples studied. The measurements were carried out using a D8 ADVANCE powder diffractometer. The drug sample was smeared over a low-back ground sample holder (amorphous silica holder) and fixed on the sample stage in a goniometer. The instrument was set in a B-B geometry. The current and voltage is set at 40 mV and 35 mA, and data were collected. This testing was carried out at the Sophisticated Test and Instrumentation Centre, Kochi University, Kerala.

Solubility study

The solubility of the acitretin in various solvents such as distilled water, phosphate buffers (pH 6.8 and 7.4) and 0.1 N HCl were determined using the shaking flask method. An excess amount of drug was taken in a 50-ml conical flask containing 10 ml of solvent. Solvents with different concentrations (1–5%) of Gelucire® 44/14 were used. The mixture was shaken at 37°C for 48 hours at 75 rpm using an orbital shaking incubator (Dolphin™). The resultant solutions were filtered through Whatman filter paper (0.45 µm). The filtered solutions were diluted and examined for UV absorbance at 353 nm.

Characterisation of solid dispersion

The prepared solid dispersion of acitretin was analysed in FT-IR, DSC, XRD, solubility, drug content and dissolution studies.

Scanning electron microscopy (SEM). The surface morphology of the solid dispersion was studied using a high-resolution scanning electron microscope. The dried samples were covered with double-sided sticking tape and placed on aluminium stubs. They were sealed and coated with gold ions (200 °Å) under low pressure for 5 minutes using a sputtering device.

Determination of drug content. Ten milligrams of the solid dispersion were dissolved in a volumetric flask containing tetrahydrofuran, and the volume was made up with tetrahydrofuran to 10 ml. Then ultrasonication was performed to dissolve the drug rapidly in the tetrahydrofuran. The resultant solution was filtered through 0.45 µm filter media, and the drug content was determined using a UV-spectrophotometer at a wavelength of 353 nm [6].

Entrapment efficiency (EE). The solid dispersion samples were dissolved completely in the tetrahydrofuran, and the solution was filtered through 0.45 µm filter media to determine the amount of drug entrapped in the Gelucire carrier. A UV-spectrophotometer was used, with the wavelength set at 353 nm. The percentage entrapment efficiency was calculated using the following equation [7]:

$$\% \text{Entrapment Efficiency (EE)} = \frac{\text{Entrapped drug}}{\text{Entrapped drug} + \text{Freed drug}} \times 100 \dots \quad (1)$$

In vitro dissolution study. All the solid dispersion formulations (SD1 to SD6) were subjected to an *in vitro* dissolution study using a USP Type-II dissolution test apparatus (Electrolab, India). Phosphate buffer saline (pH 7.4) was used as the dissolution medium. The temperature was 37°C ± 0.5°C, and the speed was 100 rpm [6]. The samples were withdrawn after 15, 30, 45, 60, 75 and 90 minutes and analysed using a UV-spectrophotometer at a wavelength of 353 nm. The plain drug was also subjected to a dissolution study similarly for comparison with the solid dispersions. The samples were measured in triplicate for better accuracy.

Preparation of cryogel

A cryogel was prepared using the step-wise process presented in Figure 1. All the formulations were designated as CRG1 to CRG4. The concentrations of the acrylamide, MBAAm, APS and TEMED are presented in Table 1. The same amount of acitretin solid dispersion was used in all the trial batches. The resultant mixtures were frozen and maintained at -18°C for 16 hours. They were thawed at room temperature (25°C) over 12 hours. The freezing-and-thawing process was repeated thrice [8,9].

The prepared cryogel was characterised through FT-IR, DSC, XRD, drug content, entrapment efficiency, surface morphology, porosity, rheological behaviour, *in vitro* dissolution testing and stability studies. The methods used in the FT-IR, DSC and XRD analyses were the same as those described previously.

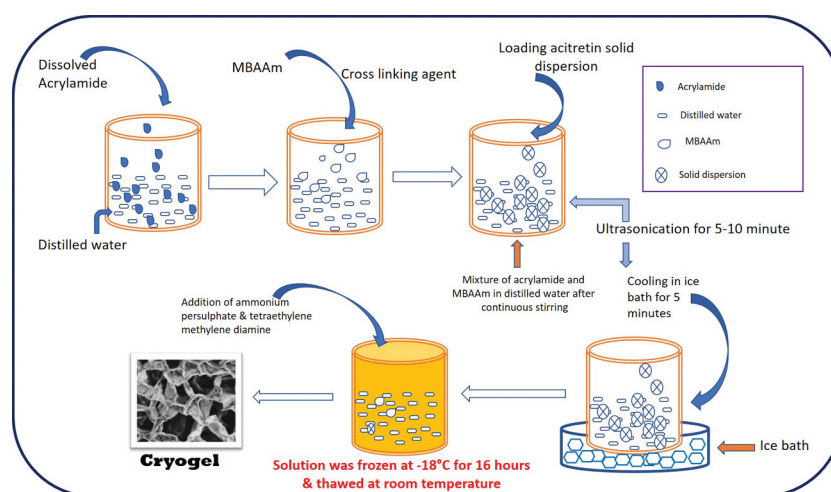


Figure 1. Cryogel preparation method with diagrammatic re-presentation.

Table 1. Composition of cryogel formulation.

Batch	Acrylamide (gm)	Deionised water (ml)	*MBAAm (gm)	Solid dispersion (gm)	*APS (gm)	*TEMED (µl)
CRG1	0.765	20	0.110	1	0.02	25
CRG2	0.765	20	0.120	1	0.02	50
CRG3	0.765	20	0.130	1	0.02	75
CRG4	0.765	20	0.140	1	0.02	100

*MBAAm: N, N' Methylene bis acrylamide; APS: Ammonium per-sulphate; TEMED: N, N, N', N'-tetramethyl ethylenediamine.

Characterisation of solid dispersion-loaded cryogel
Microscopic analysis using CX23 Olympus microscope. The surface morphology of the prepared cryogel was studied using a high-resolution scanning electron microscope. The changes produced in the surface texture by the freeze–thaw process was observed. The dried samples were covered with double-sided sticking tape and were placed on aluminium stubs. They were sealed and coated with gold ions under low pressure for 5 minutes using a sputtering device.

Mercury porosimetry study. The pore size, particle size distribution and surface area were determined using the mercury porosimeter technique. A Pascal 440 porosimeter, which has a dilatometer, a pressure source and a monitoring device, was used. The sample mass was 0.132 g, the mercury height was 41.683 mm, and the weight of the dilatometer, the mercury and the sample were 236.462 g. After correction this weight was 236.543 g, and the capillary mercury height was 0.683 mm. The dilatometer consists of a sample holder and a calibrated stem. The volume of the mercury that enters the pores was measured using a mercury penetrometer (an electrical capacitance dilatometer). This test was carried out at the Sophisticated Instrumentation Centre for Applied Research and Testing (SICART), Gujarat, India.

Rheological behaviour of cryogel. A Brookfield RST-CC digital rheometer was used to determine the rheology and viscosity of the formulations. The viscosity was measured as 12 MP in four blocks (UID140).

Swelling index of cryogel. This study was conducted to find out the swelling capacity of the dried form of the cryogel. The cryogel samples were dried to constant mass, and the mass of each dried sample was noted. The dried samples were placed in deionised water (swelling medium) at room temperature for 4 hours. Then the excess water was removed carefully, and the surface was cleaned slowly without squeezing. The samples were weighed again to calculate the swelling index. The swelling index was calculated using Equation (2) [10–12]:

$$\text{Swelling index} = [(W_s - W_0)/W_0] \times 100 \quad (2)$$

Where, W_0 and W_s are the weights of cryogels before and after swelling, respectively.

Determination of drug content. The drug content was determined by dissolving 10 mg of cryogel in a volumetric flask containing tetrahydrofuran, and the volume was made up with tetrahydrofuran to 10 ml. Then ultrasonication was performed to dissolve the drug rapidly in tetrahydrofuran. The resultant

solution was then filtered through 0.45 μm filter media, and the drug content was determined using a UV-spectrophotometer at a wavelength of 353 nm [7].

Entrapment efficiency (EE). The cryogel sample was washed with deionised water slowly to remove the untrapped drug adhering to the surface. Then the cryogel was completely dissolved in the tetrahydrofuran, and the solution was filtered through 0.45 μm filter media. The amount of entrapped drug was determined using a UV-spectrophotometer at a wavelength of 353 nm. The entrapment efficiency was calculated using Equation (1) as discussed in Section 2.2.6.3 (Characterisation of solid dispersion) [7].

In vitro diffusion study. All the cryogel formulations (CRG1 to CRG4) were subjected to an *in vitro* diffusion study using a Franz diffusion cell. The donor compartment and receiver compartment of the apparatus were separated by a cellulose acetate membrane (mol. wt. 10000–12000 Da, Himedia). The membrane was directly in contact with the phosphate buffer saline (pH 7.4, dissolution medium) in the receiver compartment. It was stirred continuously using small magnetic beads at the bottom to keep the distribution of the released drug uniform. An accurately weighed amount of cryogel (1 g) was placed on the cellulose acetate membrane of the donor compartment. The temperature of dissolution medium was maintained at $37^\circ\text{C} \pm 0.5^\circ\text{C}$. Samples were withdrawn at 1-hour intervals for the next 22 hours. Most of the drug was released into the dissolution medium in this period. Fresh dissolution medium was added after each withdrawal to maintain the sink condition throughout the study. The removed samples were analysed for cumulative percent drug release. A UV-spectrophotometer with the wavelength at 353 nm was used. The flux was determined using the known surface area (20 cm^2) of the cellulose acetate membrane. The samples were measured in triplicate so that the accuracy of the results would be better.

Results and discussion

Evaluation of solid dispersion

The present research study was conducted in two phases, with the formulation and development of solid dispersions of the poorly soluble acitretin using a lipodic solubilizer, i.e. Gelucire® 44/14 being in the initial phase. This study was conducted to enhance the solubility of acitretin and make it more suitable and convenient for preparing a topical cryogel preparation for the treatment of psoriasis.

The FT-IR study showed that there were C–H stretching vibrations in the 3100–3000 cm^{-1} region

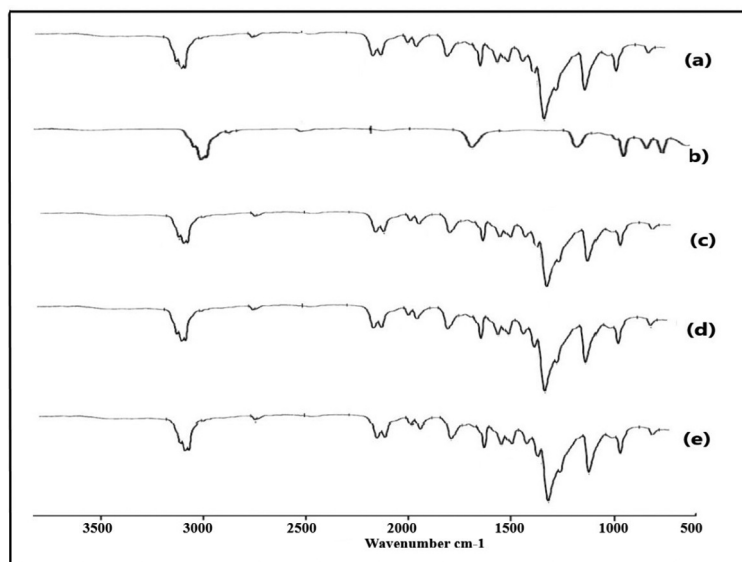


Figure 2. FT-IR spectra: Acitretin (a); Gelucire® 44/14 (b); Physical mixture of acitretin and Gelucire® 44/14 (c); Acitretin solid dispersion (d); Solid dispersion loaded cryogel (e).

(Figure 2). This is the characteristic region for identification of acitretin. Another useful region ($1300\text{--}1000\text{ cm}^{-1}$) had C–H plane bending frequencies. The actual peaks appeared at 1257 cm^{-1} , 1154 cm^{-1} , 1125 cm^{-1} and 1024 cm^{-1} . Stretching of the C = O of carboxylic acids appeared in the $1740\text{--}1660\text{ cm}^{-1}$ region, exactly as in ketones. C–C stretching was observed in the $1650\text{--}1200\text{ cm}^{-1}$ region, which indicated the presence of the phenyl group. The actual peaks were observed at 1707 cm^{-1} , 1578 cm^{-1} , 1473 cm^{-1} , 1442 cm^{-1} and 1257 cm^{-1} . Another important region ($2990\text{--}2950\text{ cm}^{-1}$) had the characteristic two asymmetric and one symmetric stretching vibration of the CH_3 group. The actual peaks appeared at 2947 cm^{-1} and 2912 cm^{-1} [13].

The spectral regions of the physical blends of the drug and Gelucire® 44/14 were similar to those of the cryogel formulation. These observations indicate that there was no interaction between the acitretin and Gelucire® 44/14. This study has given the green signal with regard to the suitability of the components for preparing a cryogel formulation.

Another analytical investigation was very useful for identifying the drug as well as confirming entrapment of the drug in the Gelucire® 44/14 matrix. The drug and drug-loaded samples were subjected to DSC analysis. The heat flow related with transitions in materials is measured as a function of the temperature in DSC. It gives information about physical and chemical changes that are involved in endothermic/exothermic processes. It also confirms whether form of a substance is amorphous or crystalline after heat is applied.

The thermograms of acitretin (Figure 3) show the onset of peaks at 226.35°C . There is a major endothermic peak at 227.66°C and an end set at 230.51°C .

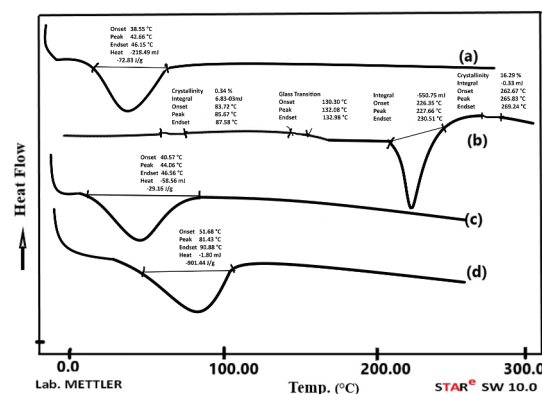


Figure 3. Differential Calorimetry Study: Gelucire® 44/14 (a); Acitretin (b); Acitretin solid dispersion (c); Solid dispersion loaded cryogel (d).

These are the characteristic peaks in the identification of acitretin [7]. A glass transition peak was observed at 132.98°C . The thermograms of Gelucire® 44/14 show a major endothermic peak with the onset at 38.55°C , the midpoint at 42.66°C and the end point at 46.15°C . These are characteristic peaks of Gelucire® 44/14. With the physical blend of acitretin and Gelucire®, there was a slight, insignificant shifting of the peak. The major endothermic peak shifted slightly, from 42.66°C to 44.06°C . The solid dispersion of acitretin was also analysed for thermal changes, if any. No peaks of acitretin were detected, and the same endothermic peaks characteristic of only Gelucire® 44/14 were observed at 44.06°C . This may confirm the complete entrapment of acitretin inside the Gelucire® 44/14 matrix, and may indicate that acitretin was converted to the amorphous form. It was interesting to observe major changes in the thermograms of the solid

dispersion-loaded cryogel formulation. There were no major peaks (at 269.24°C) of acitretin and only a small endothermic peak, slight shifting, from 87.58°C to 81.42°C, indicating that the acitretin was amorphous. This may be due to loading of the solid dispersion in the depth of the micron-sized pores of the cryogel formulation. This confirmed the complete loading and entrapment of acitretin [14,15].

The XRD study clearly indicated that pure acitretin was present in the crystalline form. There were sharp peaks of the 2θ value at 11.780°, 12.282° and 25.780°, with intensities of 4326, 4037 and 4693, respectively (Figure 4). The XRD data of the cryogel showed a very flat peak with 2θ values of 14.256°, 16.094°, 23.214° and 24.706°, with reduced intensities of 607, 796, 2366 and 2536, respectively. This confirmed that the crystalline acitretin was converted to a less crystalline form due to entrapment in the Gelucire® 44/14 and to the amorphous form due to entrapment in the pores of the microporous cryogel formulation. First two peaks of 2θ 4.45 and 9.10 were observed, these peaks may be appeared due to cryogel formation.

The solubility study was conducted to verify if the solubility of the acitretin was enhanced in the presence of the lipidic solubilizer, Gelucire® 44/14, which has a higher

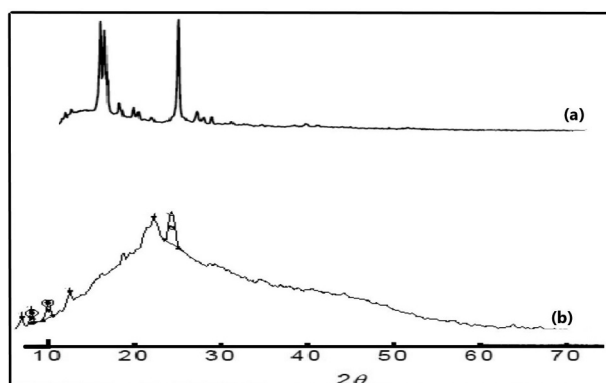


Figure 4. X-ray diffraction study: Acitretin (a); Solid dispersion loaded cryogel (b).

HLB (hydrophilic lipophilic balance) value, 14. Before the solubility study was conducted, the maximum concentration of Gelucire® 44/14 required for preparing a solid dispersion was determined by conducting trials with various levels of Gelucire® 44/14 (1–5%). On the basis of this study, solid dispersions were prepared using acitretin: Gelucire® 44/14 various ratios from 1:1 to 1:6 (batches SD1 to SD6). It was observed that the solubility increased with increasing concentration of Gelucire® 44/14. The highest solubilities were 1.2082 mg/ml, 3.437 mg/ml, 3.1362 mg/ml and 3.7012 mg/ml in distilled water, phosphate buffer (pH 6.8), phosphate buffer (pH 7.4) and 0.1 N HCl, respectively. Enhancement of solubility due to the presence of Gelucire® 44/14 was observed. Gelucire® 44/14 has solubilising properties (higher HLB value of 14) [16]. All the observations of the solubility study are shown in Figure 5.

The *in vitro* dissolution study of the solid dispersion was conducted in a phosphate buffer solution (pH 7.4). Batch SD6 showed the maximum drug release ($98.21 \pm 1.24\%$), whereas the lowest drug release ($63.28 \pm 1.55\%$) was observed with batch SD1 after 90 minutes. The increased drug release was observed with the batches containing higher levels of Gelucire 44/14. This drug release behaviour was due to the solubilising property of Gelucire® 44/14. As discussed in the solubility study section, the solubility of the solid dispersion was increased manifold, and highest solubility was that of batch SD6 (acitretin:Gelucire ratio 44/14). The drug release profiles of the acitretin solid dispersion formulations are presented in Figure 6.

Evaluation of cryogel formulation

The void spaces in the material are called as porosity and it is the fraction of the volume of voids over the total surface area. It gives an idea about the interconnected pores and pore size distribution. The porosity is a very important property as the drug diffuses through the pores. The acitretin cryogel was subjected to

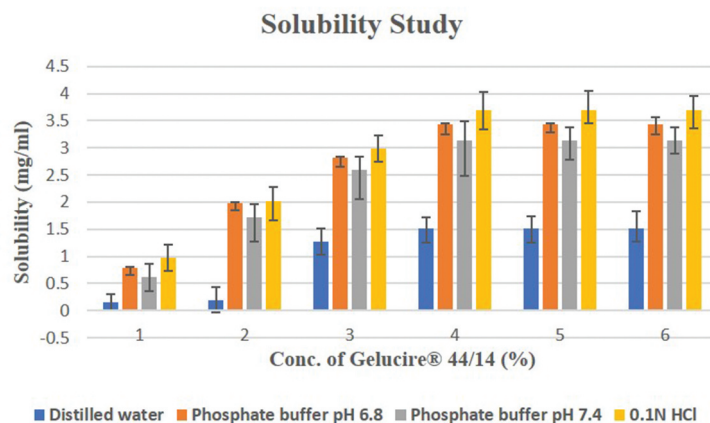


Figure 5. Solubility study of acitretin in the presence of Gelucire® 44/14 in different solvents.

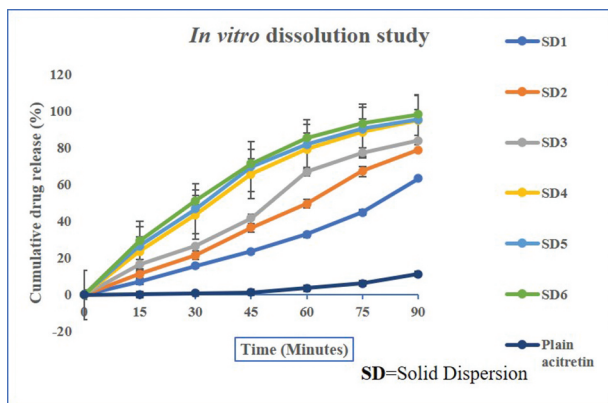


Figure 6. In vitro drug release profiles of acitretin solid dispersion.

mercury intrusion porosimetry for pore structure analysis, which also gives an idea about various other parameters related to porosity. This analysis confirmed the porous nature of the prepared cryogel. The average pore diameter was found to be $0.11 \mu\text{m}$, and the total porosity was 78.89% per gram weight of cryogel. The total specific surface area was found to be $4.152 \text{ m}^2/\text{g}$ weight of cryogel. The total cumulative volume occupied was found to be $0.0795 \text{ cm}^3/\text{g}$ weight of cryogel. The total bulk density and apparent density were found to be $0.9925 \text{ g}/\text{cm}^3$ and $1.0775 \text{ g}/\text{cm}^3$, respectively. The pores were found to be interconnected to each other, with a few dead pores. The solubilised form of acitretin was embedded in the pores.

The surface morphology of the solid dispersions was studied using scanning electron microscopic analysis at different resolutions. The surface texture of the solid dispersion was found to be smooth, and the average particle size was $250 \mu\text{m}$. The smooth surface was possibly due to the presence of Gelucire® 44/14, which is lipidic in nature. The drug, acitretin, was completely covered with this lipidic Gelucire® 44/14 carrier. This smooth surface enhances the flow properties of the solid dispersion, which are essential for designing and developing any pharmaceutical product. The images obtained using scanning electron microscopy are presented in Figure 7.

A microscopic study conducted in the laboratory using a CX23 Olympus microscope confirmed the porous structure of the cryogel. It had distinct pores are interconnected to form a porous network. The scanning electron microscopic (SEM) images are shown in Figure 8.

The viscosity of the cryogel was found to be 40.306 Pa s at set temperature condition. The viscosity values indicate that the final formulation did not exhibit good spreadability. The cryogel appears like a firm gel with a porous structure as described in the foregoing. The viscosity was observed to increase as the temperature increased up to 1400°C but subsequently it decreases with decreasing the temperature condition. So, the viscosity of the cryogel depends on the temperature at certain shear rate values. The type of rheograms are referred to as scissored as structure

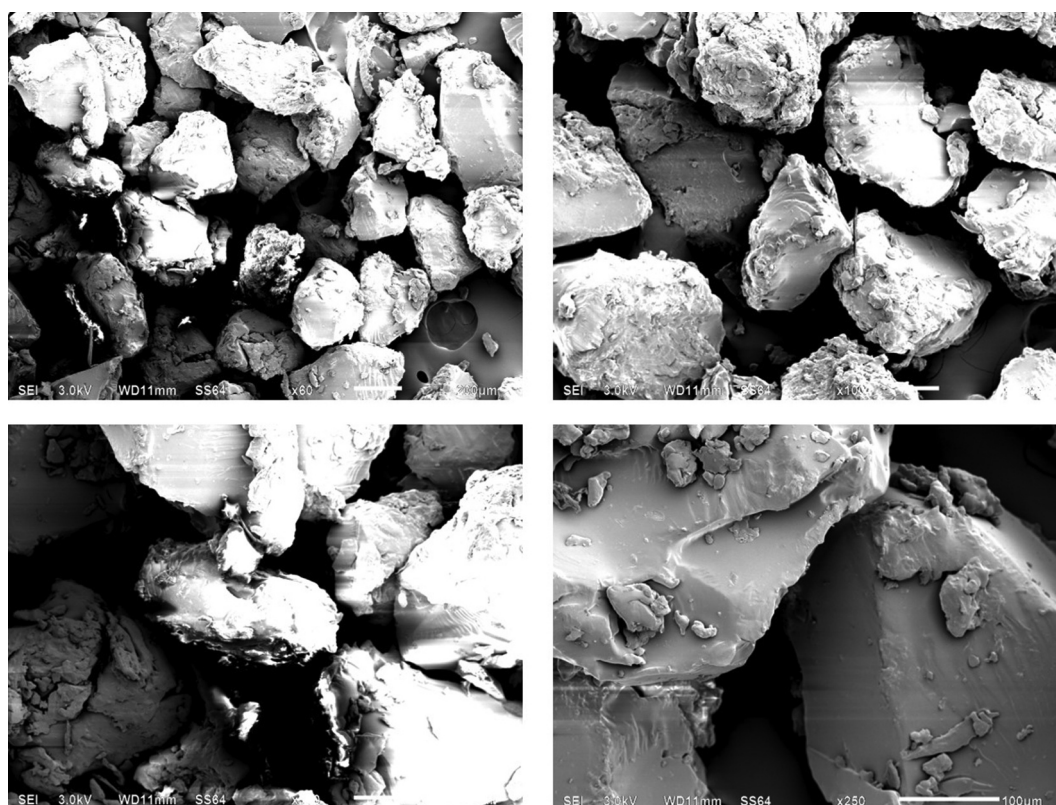


Figure 7. Scanning electron microscopy study of acitretin solid dispersion at various resolution.

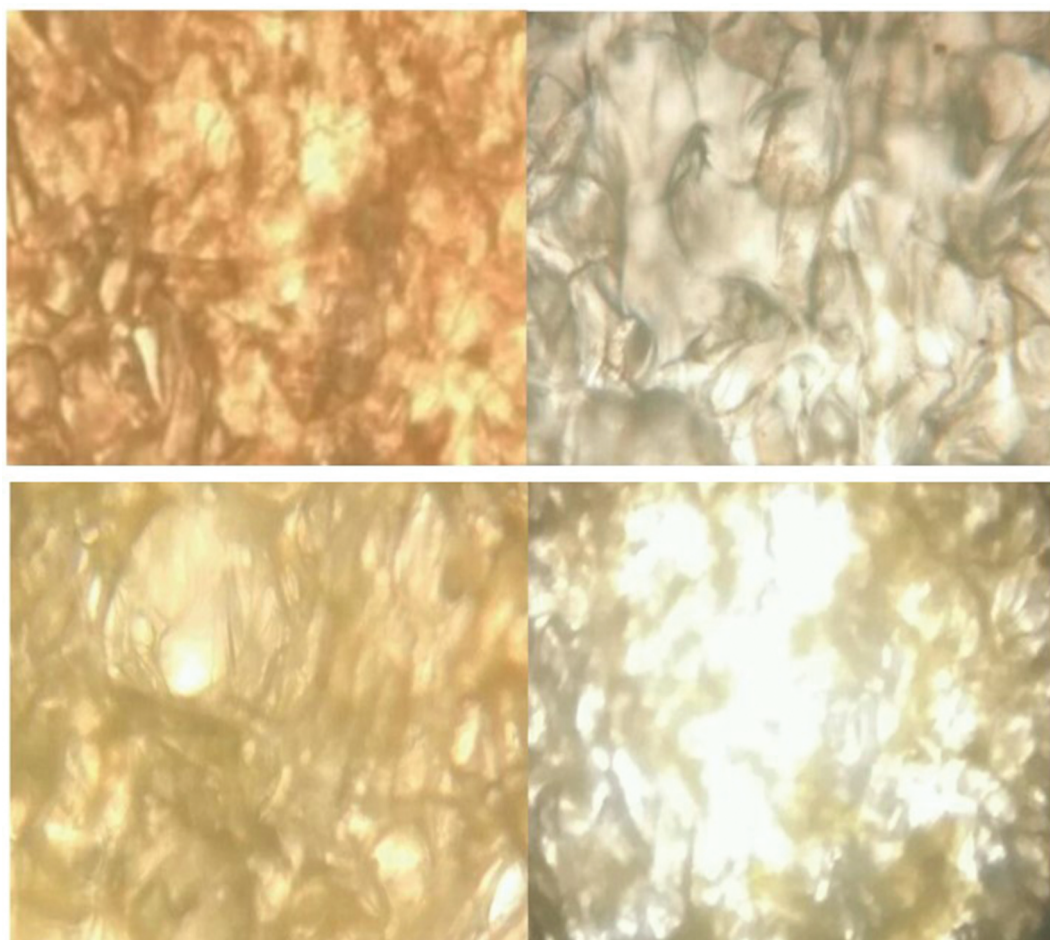


Figure 8. Various images showing cryogel surface using digital microscope.

breaking occurs in the up curve, while the fluid is nearly Newtonian on the down curve. Here the dominant gel-like structure prevents flows at low shear rates, but the viscosity decreases at higher shear rates because the structure is destroyed. This phenomenon is the opposite of thixotropy, and hence it is called anti-thixotropy or rheopexy. It is reversible viscosity which increases with the shear rate, and this occurs when the maximum shear rate is relatively low.

The pH of the all the cryogel formulation batches was found to be in the range 6.66–6.80, which was assumed to be safe to apply on skin [17].

A drug entrapment efficiency study was conducted to determine the amount of drug present in the polymer carrier. This amount depends on the capacity of the carrier material to entrap the drug completely. Batch SD6, which had more Gelucire 44/14 (carrier material) had the maximum entrapment efficiency ($96.44 \pm 1.25\%$). The entrapment efficiency of batch SD1, with less carrier material, was lower ($85.38 \pm 1.12\%$). The results of the entrapment efficiency study are presented in Table 2.

A drug content study helps to determine the presence of the drug in the carrier material and it allows the accurate dose in the form of a solid dispersion to be measured for further product development. The

Table 2. Evaluation of solid dispersion for entrapment efficiency and drug content study.

Batch No.	*Entrapment Efficiency (%)	*Drug Content (%)
SD1	85.38 ± 1.12	78.31 ± 1.55
SD2	88.58 ± 1.04	81.20 ± 1.24
SD3	90.28 ± 1.25	83.88 ± 1.22
SD4	93.25 ± 1.33	82.25 ± 1.78
SD5	94.28 ± 1.58	86.57 ± 1.58
SD6	96.44 ± 1.25	88.88 ± 1.12

*All the experiments were conducted triplicate \pm SD; (n = 3).

maximum drug content was found to be $88.88 \pm 1.12\%$ (SD6), and the minimum drug content of $78.31 \pm 1.55\%$ was observed that of batch SD1. The results of the drug content study are presented in Table 2.

Like the solid dispersions, the cryogel formulation batches were subjected to drug content and entrapment efficiency studies. All the cryogel batches (CRG1 to CRG4) had entrapment efficiency values in the range from $43.25 \pm 0.47\%$ to $53.24 \pm 1.87\%$. The results of the drug entrapment efficiency study of the cryogel formulations are presented in Table 3.

A diffusion study was conducted on the solid dispersion-loaded cryogel formulations (CRG1 to CRG4) using the dialysis bag diffusion method. The drug release profiles are shown in Figure 9. The least drug

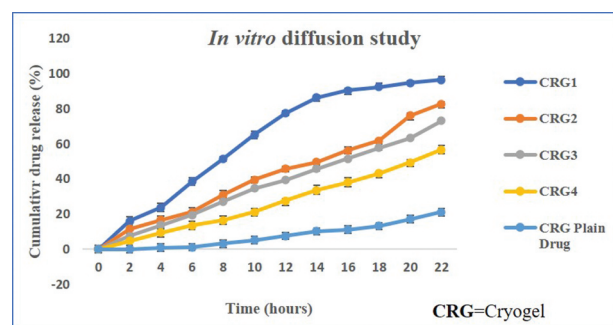
Table 3. Evaluation solid dispersion loaded acitretin cryogel for physicochemical parameters.

Batch No.	*Entrapment Efficiency (%)	*pH	*Flux ($\mu\text{g}/\text{cm}^2/\text{h}$)	*Swelling Index (%)
CRG1	43.25 \pm 0.47	6.78 \pm 0.40	7.28 \pm 1.25	78.28 \pm 1.14
CRG2	47.55 \pm 1.24	6.60 \pm 0.20	5.88 \pm 1.47	89.45 \pm 1.57
CRG3	49.47 \pm 1.25	6.66 \pm 0.45	5.22 \pm 1.33	93.48 \pm 1.53
CRG4	53.24 \pm 1.87	6.80 \pm 0.70	5.68 \pm 1.22	96.11 \pm 1.23

*All the experiments were conducted triplicate \pm SD; (n = 3).

release ($56.78 \pm 1.02\%$) was that of formulation CRG4, and the highest drug release ($96.58 \pm 1.35\%$) was that of formulation CRG1 at the end of the 22-hour study. The drug releases of the remaining formulations, CG2 and CRG3, were $82.87 \pm 1.78\%$ and $73.28 \pm 1.36\%$, respectively, at the end of the diffusion study. Overall observation of *in vitro* diffusion study indicated that the decreasing trend of drug release was due to the increased in the concentration levels of TEMED and MBAAM with fixed amount of acitretin solid dispersion and acrylamide polymer. TEMED and MBAAM were both involved in the process of cryo-gelation. Increased levels of these materials boost the interconnectivity of the pores as well as the cross-linking and elastic properties of the formulation. These physical properties also influence the drug permeability and thereby decrease the rate of drug release from the porous structure [18].

The swelling study is the important study in the design and development of a cryogel formulation. The swelling describes the fractional increase in the weight of the cryogel due to filling of pores with a solvent (e.g. water). In the swelling process, the pores are filled when water is absorbed. Another step involved in the swelling is the diffusion of the solvent (water) into the polymer wall. As discussed in the foregoing (*in vitro* diffusion study), the swelling property was found to be enhanced at higher concentrations of both TEMED and MBAAM in the formulation. The formulation CRG4 showed the highest swelling index ($96.11 \pm 1.23\%$), whereas the lowest swelling index was that of the formulation CRG1. The results of the swelling study are presented in Table 3. The swelling phenomenon had a positive

**Figure 9.** In vitro diffusion study of solid dispersion loaded cryogel formulation.

impact on the drug release property. The drug release increased as the swelling index of the formulation decreased and vice versa. This was again due to the cryogelation effect and the TEMED and MBAAM levels, which had played a very important role. High levels of TEMED and MBAAM increase the interconnectivity of the pores and crosslinking, as a result of which the density of the polymer wall increases. This increase in the density of polymer wall affects the swelling property. The swelling tends to take more time, and this delays the release of the drug [19,20].

Conclusions

Technological advancements have improved the physical and chemical properties of polymeric materials. These modified properties allow the development of many formulations of better efficacy and quality. In this, study an attempt was made to develop a cryogel formulation for acitretin, the drug of choice for the treatment of psoriasis. The prepared cryogel formulation had improved physical and mechanical properties. Cryogel formulations with appropriate levels of polymeric components were prepared using solubility-enhanced solid dispersions of acitretin. Gelucire 44/14 had enhanced the solubility, allowed loading of the acitretin into the surface pores of the cryogel formulation with increased surface area and comfort for application. The cryogel, with a microporous structure, had better permeation properties compared with conventional hydrogels. So, it was concluded that cryogel formulations are a better choice as a delivery platform for drugs such as acitretin in the treatment of skin disorders.

Authors' contributions

Prakash Kendre: Conceptualization, Methodology **Nikita Borawake.:** Data curation, Writing- Original draft preparation. **Shirish Jain:** Visualization, Investigation. **Prakash Kendre:** Supervision. **Somnath Vibhute:** Software, Validation. **Ajinkya Pote:** Writing- Reviewing and Editing.

Acknowledgments

The authors are very thankful to Glenmark Pharmaceuticals, Sinner, Nashik, India for providing Tramadol HCl. They are also grateful to Gattefosse India Pvt. Ltd., Mumbai for providing the gift sample of Gelucire® 44/14. I would like to mention the support of the Principal, Sanjivani College of Pharmaceutical Education and Research, Kopergaon and Rajarshi Shahu College of Pharmacy, Buldana for providing facilities to conduct this research study. Finally, the authors extend thanks to all those whose cooperation helped complete this work successfully.

Consent of publication

Not applicable.

Code of availability

Not applicable.

Data availability statement

Author(s) doesn't allow to disclose the data.

Disclosure statement

Author(s) declares no conflict of interest.

Funding

This research is not funded or supported by any funding agencies

References

- [1] Kaur I, Handa S, Kumar B. Natural history of psoriasis: A study from the indian subcontinent. *J Dermatol.* **1997**;24:230–234.
- [2] Christophers E. Psoriasis - Epidemiology and clinical spectrum. *Clin Exp Dermatol.* **2001**;26:314–320.
- [3] Krueger G, Koo J, Lebwohl M, et al. The impact of psoriasis on quality of life results of a 1998 national psoriasis foundation patient-membership survey. 2001. Available from: <https://jamanetwork.com/>. Accessed on December 20, 2019.
- [4] Hsia E, Johnston MJ, Houlden RJ, et al. Effects of topically applied acitretin in reconstructed human epidermis and the rhino mouse. *J Invest Dermatol.* **2008**;128:125–130.
- [5] Allen JG, Bloxham DP. The pharmacology and pharmacokinetics of the retinoids. *Pharmacol Ther.* **1989**;40:1–27.
- [6] Agrawal V, Gupta V, Ramteke S, et al. Preparation and evaluation of tubular micelles of pluronic lecithin organogel for transdermal delivery of sumatriptan. *AAPS PharmSciTech.* **2010**;11:1718–1725.
- [7] Agrawal Y, Petkar KC, Sawant KK. Development, evaluation and clinical studies of Acitretin loaded nanostructured lipid carriers for topical treatment of psoriasis. *Int J Pharm.* **2010**;401:93–102.
- [8] Wright E, Andrews G, McCoy C, et al. The effect of dilute solution properties on poly(vinyl alcohol) films. *J Mech Behav Biomed Mater.* **2013**;28:222–231. [cited 2020 Aug 3]. Available from: <https://pure.qub.ac.uk/en/publications/the-effect-of-dilute-solution-properties-on-polyvinyl-alcohol-fil>
- [9] Pazos V, Mongrain R, Tardif JC. Polyvinyl alcohol cryogel: optimizing the parameters of cryogenic treatment using hyperelastic models. *J Mech Behav Biomed Mater.* **2009**;2:542–549.
- [10] Caló E, Barros J, Ballamy L, et al. Poly(vinyl alcohol)-Gantrez® AN cryogels for wound care applications. *RSC Adv.* **2016**;6:105487–105494.
- [11] Zou X, Deng P, Zhou C, et al. Preparation of a novel antibacterial chitosan-poly(ethylene glycol) cryogel/silver nanoparticles composites. *J Biomater Sci Polym Ed.* **2017**;28:1324–1337.
- [12] Kim I, Lee SS, Bae S, et al. Heparin functionalized injectable cryogel with rapid shape-recovery property for neovascularization. *Biomacromolecules.* **2018**;19:2257–2269.
- [13] Swarnalatha N, Gunasekaran S, Muthu SRP. Indian journal of science experimental and theoretical investigations of spectroscopic properties of acitretin. *Indian J Sci.* **2017**;14:44–62.
- [14] Harivardhan Reddy L, Murthy RSR. Etoposide-loaded nanoparticles made from glyceride lipids: formulation, characterization, in vitro drug release, and stability evaluation. *AAPS PharmSciTech.* **2005**;6:E158.
- [15] Sarmiento B, Ferreira D, Veiga F, et al. Characterization of insulin-loaded alginate nanoparticles produced by ionotropic pre-gelation through DSC and FTIR studies. *Carbohydr Polym.* **2006**;66:1–7.
- [16] Kendre PN, Chaudhari PD. Design and optimization of oral bioadhesive nanocurcumin delivery using novel hydrophilic carrier for cancer treatment: an alternative to parenteral chemotherapy. *Indian Drugs.* **2016**;53:24–36.
- [17] Worth AP, Cronin MTD. The use of pH measurements to predict the potential of chemicals to cause acute dermal and ocular toxicity. *Toxicology.* **2001**;169:119–131.
- [18] Memic A, Colombani T, Eggermont LJ, et al. Latest advances in cryogel technology for biomedical applications. *Adv Ther.* **2019**;2:1800114.
- [19] Bencherif SA, Sands RW, Bhatta D, et al. Injectable preformed scaffolds with shape-memory properties. *Proc Natl Acad Sci U S A.* **2012**;109:19590–19595.
- [20] Shih TY, Blacklow SO, Li AW, et al. Injectable, tough alginate cryogels as cancer vaccines. *Adv Healthc Mater.* **2018**;7:1701469.

An effort to augment solubility and efficiency of the oral bosentan-bucco-adhesive drug delivery system using graft co-polymer as the carrier

**Prakash N. Kendre, Pravin
D. Chaudhari, Shirish P. Jain & Somnath
K. Vibhute**

Polymer Bulletin

ISSN 0170-0839

Polym. Bull.

DOI 10.1007/s00289-020-03412-z



Your article is protected by copyright and all rights are held exclusively by Springer-Verlag GmbH Germany, part of Springer Nature. This e-offprint is for personal use only and shall not be self-archived in electronic repositories. If you wish to self-archive your article, please use the accepted manuscript version for posting on your own website. You may further deposit the accepted manuscript version in any repository, provided it is only made publicly available 12 months after official publication or later and provided acknowledgement is given to the original source of publication and a link is inserted to the published article on Springer's website. The link must be accompanied by the following text: "The final publication is available at link.springer.com".



An effort to augment solubility and efficiency of the oral bosentan-bucco-adhesive drug delivery system using graft co-polymer as the carrier

Prakash N. Kendre¹ · Pravin D. Chaudhari² · Shirish P. Jain¹ · Somnath K. Vibhute¹

Received: 25 January 2020 / Revised: 11 July 2020 / Accepted: 6 October 2020
© Springer-Verlag GmbH Germany, part of Springer Nature 2020

Abstract

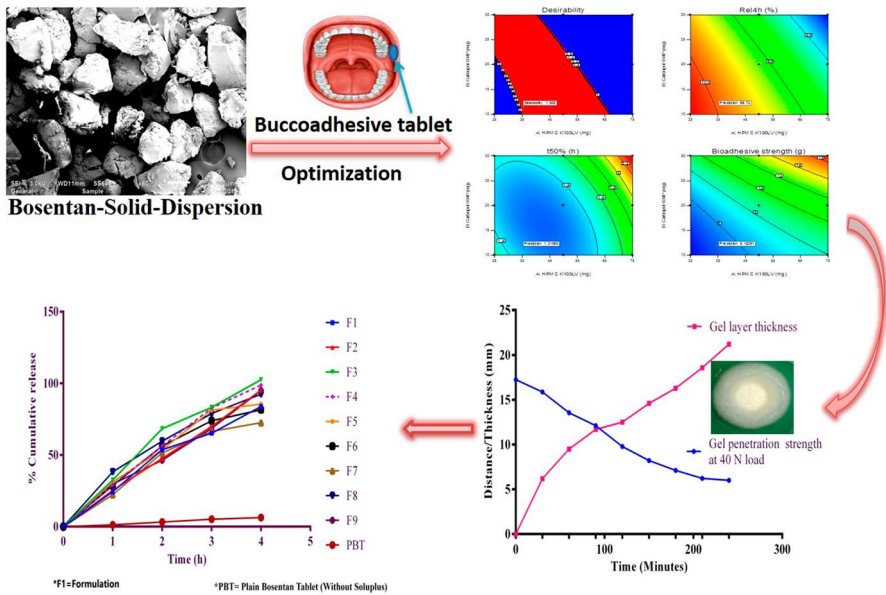
Although there are rapid developments in molecular science and synthetic chemistry for investigation of many essential drug molecules, poor solubility and bioavailability issues are major constraint in the design of more efficient formulations. This research study focuses on the enhancement of solubility and development of the bucco-adhesive drug delivery system of bosentan using Soluplus® (polyvinyl-caprolactam-polyvinyl-acetate-polyethylene glycol graft co-polymer) as a carrier. A 3²-factorial design was implemented to develop bucco-adhesive tablets using hydroxypropyl methyl cellulose (HPMC) K100 LV (X_1) and Carbopol 934 P (X_2) as independent variables at various levels whereas $t_{50\%}$ (Y_1) (time required to release 50% of drug), Rel_{4h} (Y_2) (percentage of the drug release in 4 h) and bio-adhesive strength (Y_3) were considered as set response parameters. The positive effect of the surface response quadratic model demonstrated the change in the already set dependent variables of $t_{50\%}$, Rel_{4h} and bio-adhesive strength. The FT-IR study confirmed the suitability of all the components used in the design of formulation. DSC and XRD study have confirmed the encapsulation of bosentan in the Soluplus® carrier and amorphous form of bosentan, respectively. Overall, 6.832-fold increase in solubility was observed for bosentan-solid dispersion. High-water uptake and swelling of bucco-adhesive tablets (containing bosentan-solid dispersion) was observed due to presence of the highly hydrophilic-Soluplus®. Rel_{4h} was found to be $97.86 \pm 0.57\%$ for optimized formulation (F4) and was decreased with increasing polymer content. The values of $t_{50\%}$ were found to be enhanced from 1.11 to 2.32 h at the lower to higher levels of both the polymers respectively.

✉ Prakash N. Kendre
prakashkendre@gmail.com

¹ Rajarshi Shahu College of Pharmacy, Buldana, Maharashtra 443 001, India

² Modern College of Pharmacy, Nigdi, Pune, India

Graphic abstract



Keywords Bosentan · Solid dispersion · Bucco-adhesive tablet · 32-factorial design · soluplus® · HPMC K100 LV and carbopol 934 P

Introduction

Sometimes inherent characteristics of drug molecules pose the major hurdle in the design and development of formulation. The poor aqueous solubility of the drug compounds is one of the major issues involved during the dosage form development stage [1]. Suitable solubility enhancement techniques can address this poor solubility issue satisfactorily. Bosentan, a dual endothelial receptor antagonist used in the treatment of pulmonary arterial hypertension (PAH). But its poor aqueous solubility makes it out of place to develop the efficient drug delivery system. The present study is an attempt to enhance the solubility of bosentan to develop efficient buccal adhesive drug delivery system. As the buccal route of administration is effective to avoid the first pass hepatic metabolism of the drug, an effective drug delivery system can be designed with maximum drug utilization in the buccal mucosal cavity [2, 3]. This is the most suitable, convenient and easily accessible site for drug delivery. The exposure of drug to the systemic circulation through the internal jugular vein, bypasses the hepatic first-pass metabolism leading to high bioavailability. The buccal route enjoys excellent patient compliance owing to ease of self-administration [4]. The solid dispersion of bosentan was prepared using an amphiphilic graft copolymer, Soluplus® (polyvinyl caprolactam–polyvinyl acetate–polyethylene glycol

graft co-polymer) specially designed and manufactured by BASF Corporation to enhance the solubility of poorly soluble drugs like bosentan. Due to its bifunctional behaviour, it can serve as an excellent matrix to dissolve drugs in aqueous media [5–7]. Initially, bosentan-solid dispersion was prepared successfully followed by the formulation of the bucco-adhesive tablet by optimization technique using central composite designs (CCD) for two factors at three levels [8].

Materials and methods

Materials

Bosentan was received as a gift sample from Dr. Reddy's Laboratories Pvt. Ltd., Hyderabad, India. Soluplus® was provided as a gift sample by BASF Corporation, Mumbai, Maharashtra, India. Polymers, HPMC K4M, HPMC K100M, HPMC K100 M LV, Carbopol 971P and Carbopol 934P were obtained as gift samples from Colorcon Asia Pvt. Ltd., Goa, India. All other excipients and reagents used were of analytical grade and obtained from reputed suppliers in India.

Methods

Preparation of bosentan-solid dispersion

A bosentan-solid dispersion was prepared by solvent evaporation technique. Soluplus® was dissolved completely in ethanol. Bosentan was added slowly to the clear ethanolic drug solution with the continuous stirring till the uniform distribution of bosentan. The ratio of bosentan to Soluplus® was maintained at 1:1, 1:2, 1:3, 1:4 and 1:5 and coded as BSD1, BSD2, BSD3, BSD4 and BSD5, respectively. The ethanol was evaporated completely and resultant mass was dried and grinded to obtain a free-flowing powder, which was passed through a 100 µm sieve. The dried solid dispersion was kept in a desiccator until further use and testing [9].

Fourier transform infrared spectroscopy (FT-IR) study

The interaction between drug and excipients was studied using an FTIR spectrophotometer (Shimadzu, Japan). Spectra were recorded in the range 4000–400 cm⁻¹. All the samples were prepared using the KBr pellet technique, and the spectra were recorded at a resolution of 0.15 cm⁻¹ and a scanning speed of 20 scan/s.

Differential scanning calorimetric study (DSC) study

Differential scanning calorimetric (DSC) measurement was performed by a (DSC-60 Shimadzu) thermal analyser. The samples of about 5 mg were hermetically placed in the aluminium-sealed pans and scanned at heating rate of 10 °C/min over

a temperature range of 0–300 °C by using nitrogen gas as effluent gas. The thermal properties of the pure bosentan and bosentan-solid dispersion were characterized.

X-ray diffraction (XRD) study

The XRD spectra/patterns were recorded (Philips PW3710 analytical X-ray diffractometer at Diya Lab, Mumbai, India) the pure drug and solid dispersion formulation for confirmation of change of basic form of drug (crystalline or amorphous) after formulating in the final dosage form.

Phase solubility study

The Phase solubility study was conducted to predict the effect and trend of Soluplus® to enhance solubility and dissolution of bosentan. Shaking flask method was used to conduct the phase solubility study. An excess amount of the bosentan was added to the solutions at the concentration range of 5%, 10%, 15%, 25%, and 30% w/v Soluplus®. The samples were shaken for 72 h in the mechanical flask shaker at 37 ± 2 °C. The concentration of the bosentan in the solution after equilibration for 72 h was determined using UV spectrophotometer (1650 PC, Shimadzu, Japan) at 272 nm [7].

In order to ensure the favourable concentration of the Soluplus® for solubilization of bosentan, ΔG_{tr}° value was calculated using the following equation:

$$\Delta G_{tr}^{\circ} = 2.303RT \log (S_o/S_s) \quad (1)$$

where, S_o/S_s is the ratio of molar solubility of the bosentan before and after entrapment with Soluplus®. R and T are constant of gas (8.31 JK^{-1}) and temperature (in degree Kelvin) respectively [9].

Solubility study of bosentan-solid dispersion

Prepared solid dispersions (BSD1 to BSD5) were subjected to the solubility study using same method mentioned under the above section of the phase solubility study. Enhancement in the solubility of bosentan-solid dispersion after equilibration for 72 h was determined using the UV spectrophotometer (1650 PC, Shimadzu, Japan) at 272 nm [5].

Preparation of bucco-adhesive tablets

Formulation batch of the solid dispersion with maximum solubility was selected for the further development of the bucco-adhesive tablets using 3^2 -factorial design. Polymers HPMC K4M, HPMC K100LV, HPMC K100M and Carbopol 934P were used to develop bucco-adhesive tablets. Avicel PH102 was used as a diluent in all the formulations. Initially, preliminary batches were performed to select a suitable polymer with the selected range of levels to obtain expected results.

Selection of suitable experimental design

The response surface methodology (RSM) is an effective method for optimizing the bio-adhesive matrix tablet formulation. All factors at all combinations can be studied effectively using a central composite design (CCD). This approach is used most frequently to establish the effects of the individual variables and interactions with very little experimentation [10, 11]. Another advantage of this design is that it allows a quadratic surface response to be established, which is otherwise difficult with a factorial design at two levels. In this study, a CCD for two factors, namely, HPMC K100LV and Carbopol 934P, at three levels with a value of $\alpha=1$, i.e., a 3^2 -factorial, was chosen for the optimization of the bucco-adhesive matrix tablets. This computer-aided study was conducted using Design-Expert® software version 9.0.6.2 (Stat-Ease Inc., Minneapolis, MN, 55,143).

On the basis of the observations from preliminary trials, a combination of the HPMC K100 LV (X_1) and Carbopol 934P (X_2) were selected as independent factors for the optimization of bucco-adhesive matrix tablets. The composition for the development of preliminary batches of the bucco-adhesive tablets is given in Table 1. Dependent variables, $t_{50\%}(Y_1)$, time required to release 50% of drug; $Rel_{4h}(Y_2)$, percentage of the drug release in 4 h and bio-adhesive strength (Y_3) were selected to optimize the final bucco-adhesive tablet formulation using a computer-aided factorial design. The tablets were compressed using the direct compression technique in a single rotary multiple punch machine (Kambert Pvt. Ltd., Ahmedabad, India). Finally, tablets with flat surface with uniform size of 12 mm diameter were compressed as per the compositions of 3^2 factorial design which is mentioned in Table 2.

Evaluation of physical parameters and assay study

All the buccal adhesive tablets were evaluated for physical parameters like weight variation, friability, hardness, thickness and diameter. Ten tablets of each batch were crushed in a mortar to obtain powdered form. Powdered tablets equivalent to 100 mg of pure drug were weighed and transferred to 250-mL volumetric flasks containing methanol. Each flask was sonicated and the contents filtered through 0.45 μ Whatman filter paper. The absorbances were measured at 272 nm using UV-visible spectrophotometer to calculate bosentan content.

Table 1 Composition of bio-adhesive tablets containing bosentan-solid dispersion

Sr. no	Ingredients	Concentration (mg)
1	Bosentan-solid dispersion (BSD) (Equivalent to 62.5 mg of Bosentan)	371.32
2	HPMC K100 LV	25–75
3	Carbopol 934P	10–30
4	Avicel PH 102	Q.S
5	Magnesium stearate	2.5
6	Aerosil (Colloidal silicon dioxide)	2.5

Table 2 Formulation batches as per two-factor, three-level central composite design (CCD) layout translation of coded levels in actual units

Trial no	Formulation code	Coded factor level (mg)	
		X1: HPMC K 100 LV	X2: Carbapol 934 P
1	F1	50	30
2	F2	75	30
3	F3	25	20
4	F4	50	10
5	F5	75	10
6	F6	25	30
7	F7	25	10
8	F8	50	20
9	F9	75	20
Independent variable	Coded levels		
	High (+1)	Medium (0)	Low (-1)
X1: HPMC K 100 LV (mg)	70	50	30
X2: Carbapol 934 P (mg)	30	20	10

In vitro dissolution study

Initially, a dissolution study was conducted for the bosentan-solid dispersion using USP-II dissolution test apparatus (paddle type). Phosphate buffer (pH 6.8), 900 mL was used as the dissolution medium at 37 ± 0.5 °C and 50 rpm. Aliquot samples were withdrawn at the intervals of every 15 min for 2 h, filtered through 0.45 μ Whatman filter paper and absorbances were measured at 272 nm using the UV spectrophotometer [7]. All the sample of dissolution study were analysed in triplicate as mean \pm SD, $n = 3$.

Similarly, the dissolution study was conducted for all the bucco-adhesive tablet formulations prepared according to the 3^2 factorial design. As the anatomy and physiology of buccal cavity differs from the stomach where it consists of very small volume of saliva with very short residence time, this dissolution study includes modified dissolution test apparatus which was described by Hughes et al. [12]. This apparatus consists of single, stirred, continuous flow-through filtration cell which includes a dip tube, specially designed to remove finely divided solid particles. The composition of saliva solution was used as described by Hughes et al. To analyse the dissolved drug, filtered solution was removed continuously. The volume of saliva was maintained up to 10 ml in the cell which was pumped at the rate of 6 ml/min. This facilitates the residence time for saliva solution of approximately 100 s and gives almost complete removal in 8 min. All the sample of dissolution study were analysed in triplicate as mean \pm SD; $n = 3$.

Measurement of bio-adhesive strength Goat mucosa procured from the slaughter's house was used as the model membrane to study the bio-adhesive strength of the tablets. The mucosal membrane was isolated by removing the underlying con-

nective tissue. It was washed with a phosphate buffer (pH 6.8). The apparatus was specially designed for measuring adhesive strength as prescribed in the literature. It was built using a double-beam physical balance [11, 12]. The force required to detach a tablet from the surface of the mucosal membrane was measured in triplicate ($n = 3$) as the mean \pm SD and this force was treated as the bio-adhesive strength.

Determination of swelling and study of gel-forming behaviour The swelling behaviour of the soaked tablets was evaluated over a period of 4 h to check uptake of water. Tablets were weighed accurately and placed in 5 mL of a phosphate buffer (pH 6.8) solution. Tablets were reweighed after every 30 min over the 4-h period and excess of water was removed carefully using filter paper. The swelling index (weight gain) was calculated using the following Eq. (2):

$$\text{Swelling index} = \frac{\text{Wet weight of tablet} - \text{original weight of tablet}}{\text{Original weight of tablet}} \times 100 \quad (2)$$

Similarly, the gel-forming behaviour of the tablets was studied over a period of 4 h. The optimized tablets were soaked in a phosphate buffer (pH 6.8) and the thickness of the gel layer as well as the gel penetration strength was measured. The gel penetration strength under a fixed load of 40 N was determined using a Brookfield CT-3 Texture Analyzer, Brookfield Engineering Ltd. [15, 16].

Mathematical modelling of the drug release data In vitro dissolution study data was analysed using the PCP Disso Software package which has provisions for volume correction, dilution factor adjustment, time interval settings, drug loss due to sampling, etc. The software helped to calculate the amount of drug dissolved as a percent release, rate of drug release and log fraction released at varied time intervals. The kinetic constant (k), the diffusion release exponent (n) and the contributions of Fickian diffusion and polymer relaxation in a swollen matrix were also determined. On the basis of this phenomenological analysis, the type of drug release [Fickian, Non-Fickian (anomalous) or zero-order] was predicted. Time taken for 50% drug release, i.e. $t_{50\%}$ was also calculated in this study. The data were analysed to check best-fit model using different equations [17–20].

Optimization of analysed data For optimization, the response variables considered were the amount of drug released in 4 h $\text{Rel}_{4\text{h}}$ (Y_1), time required to release 50% of drug) $t_{50\%}$ (Y_2) and the bio-adhesive strength (Y_3).

The PCP Disso software was used to calculate the amount of drug released and the kinetic constants. Design-Expert 9.01 software (Stat-Ease, USA) was used to fit a full second-order polynomial equation with added interaction terms to correlate the studied responses $\text{Rel}_{4\text{h}}$ (Y_1), $t_{50\%}$ (Y_2) and bio-adhesive strength (Y_3) with the variables to be examined. All the polynomial regression results were represented as three-dimensional coloured response surfaces and contour graphs. The optimum formulations were confirmed in two stages. First, a feasible space was located; and second, an exhaustive grid search was conducted to predict the possible solutions.

Validation of response surface methodology (RSM) To validate the response surface, few formulations were selected as check points. The tablets were formulated (as described in earlier section of bucco-adhesive tablet preparation) using the optimal composition and evaluated for physical properties, content, dissolution and adhesive strength. The predicted and observed responses were compared, residual graphs plotted and the percent error estimated from the observed responses. Correlation plots were also constructed separately for all the formulations.

Results and discussion

Pre-formulation study

Before design and development of the bucco-adhesive tablets, various analytical tests like FTIR, DSC and XRD were performed to check the suitability of the components for the final formulation.

FTIR spectra of pure bosentan showed major peaks at 3620.15 cm^{-1} , 3369.75 cm^{-1} representing N–H stretching; C–H stretching at 2960.83 cm^{-1} , 2924.18 cm^{-1} , 2758.30 cm^{-1} ; C=O stretching at 1707.06 cm^{-1} ; S=O stretching at 1558.54 cm^{-1} ; N–H out of plane at 1454.38 cm^{-1} ; C–H bend at 1342.50 cm^{-1} , 1251.84 cm^{-1} ; C–N stretching at 1170.83 cm^{-1} , 1112.96 cm^{-1} and N–H, O–H bending at 1020.38 cm^{-1} , 844.85 cm^{-1} . The presence of these spectra is the characteristic for identification of bosentan. The solid dispersion formulation also showed the same type spectra indicating that there was no interaction among the bosentan and Soluplus®. The FT-IR spectra are shown in Fig. 1.

The DSC study was also conducted to check thermal behaviour of the pure bosentan, Soluplus, solid dispersion and physical blend containing the HPMC K100 LV, Carbopol and solid dispersion. The bosentan has shown sharp major endothermic peak at $97.99\text{ }^{\circ}\text{C}$ and short endothermic peak at $116.72\text{ }^{\circ}\text{C}$. The Soluplus® has shown the endothermic peak at $77.43\text{ }^{\circ}\text{C}$. The resultant solid dispersion has shown only the endothermic peak of Soluplus® at $85.26\text{ }^{\circ}\text{C}$ with slightly variation as compared to original peak and showing no change in the glass transition peak. The absence of all thermal peaks of drug in the solid dispersion indicates complete encapsulation of drug in the matrix of Soluplus®. All the observed thermal peaks of plain drug and physical blend containing the HPMC K100 LV, Carbopol and solid dispersion are highlighted in Fig. 2.

The XRD data showed that the sharp highly intense peaks at 2θ values of 15.29° , 16.57° , 18.52° , 22.56° , 20.16° and 77.58° and intensity of 1505.13, 789.25, 754.88, 653.25, 461.25, 402.25, respectively, whereas solid dispersion showed flat peaks showing major peak at 496.35 and other peaks at less than 200. Complete entrapment of bosentan in the Soluplus® carrier is confirmed by the presence of flat peaks. The results of the XRD data are highlighted in Fig. 3.

The phase solubility study was conducted to check the effect and trend of Soluplus® on the solubility and dissolution of the bosentan which is poorly water-soluble drug having maximum solubility of 0.00904 mg/ml only. In the present study, solid dispersion formulation was prepared to increase the solubility of

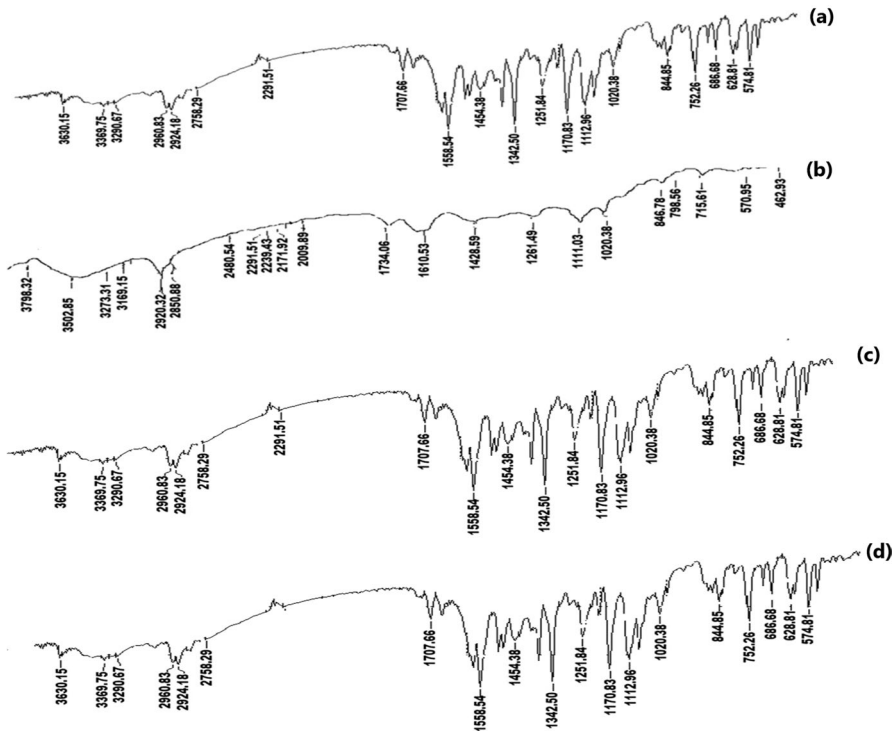


Fig. 1 FT-IR study: Bosentan (a); Soluplus® (b); Bosentan-solid dispersion (c); Physical blend of HPMC K100M LV, Carbopol 934P and Solid dispersion (d)

bosentan. It was found that at 5% concentration of Soluplus®, the water solubility of bosentan increases more than five times. This was mainly due to the micelle solubilisation effect of Soluplus®. The values of Gibb's free energy related with water solubility of bosentan in the presence of Soluplus® are shown in Table 3. More negative values of Gibb's free energy show the higher solubilisation effect which was observed in this at higher concentration of Soluplus®.

For solubility of bosentan-solid dispersion in phosphate buffer (pH 6.8), the significant differences were found as shown in Table 3. The solubility of bosentan was found to be proportional to the concentration of Soluplus®. Maximum solubility of 0.0658 ± 0.021 mg/ml was observed for solid dispersion at 1:5 ratio of bosentan to Soluplus®. Overall, 6.832-fold increase in solubility was observed for solid dispersion as compared to the pure bosentan (plain bosentan) which showed 0.00963 mg/ml of solubility in water [21].

During dissolution study of bosentan-solid dispersion, maximum drug dissolution was observed in two hours, showing $98.78 \pm 1.02\%$ release at highest concentration level of Soluplus® (5%) whereas least release of $88.58 \pm 1.12\%$ was observed at lowest level of Soluplus® (1%). From this study, it is confirmed that the dissolution increases at higher concentration of Soluplus® which is due to the

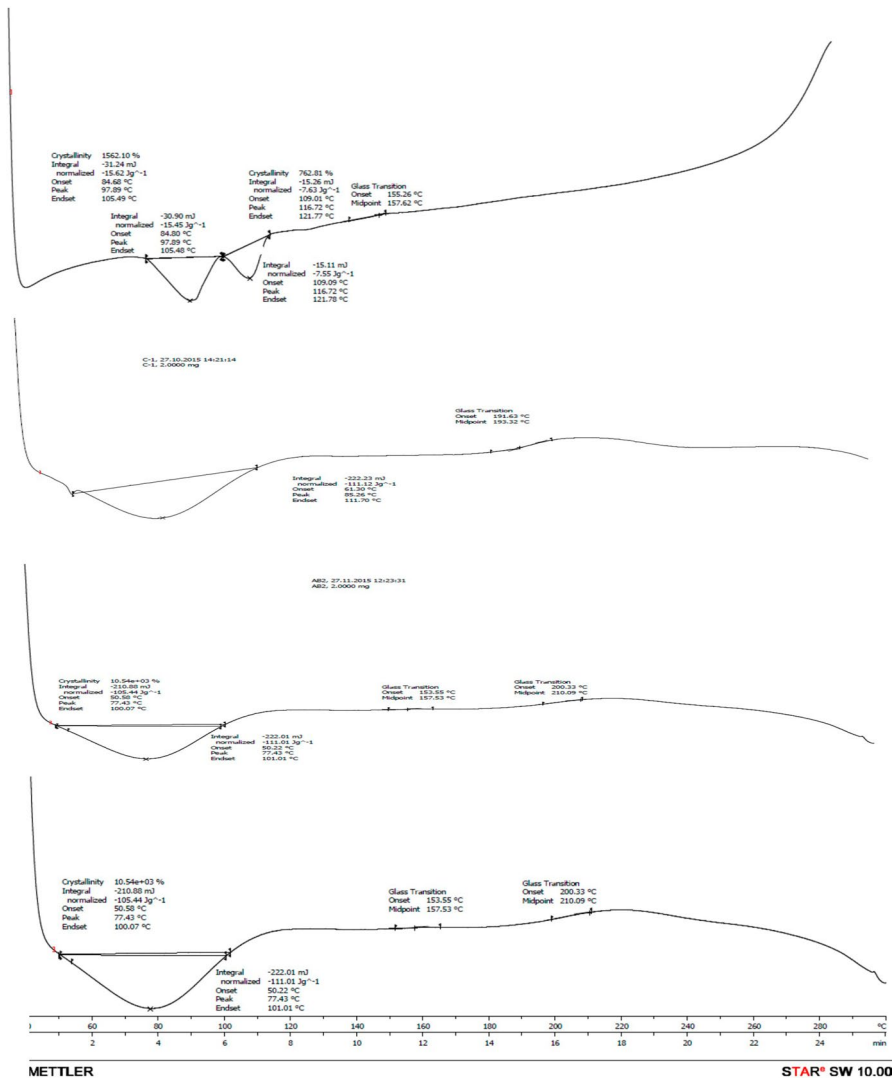


Fig. 2 DSC study: Bosentan (a); Soluplus® (b); Bosentan-solid dispersion (c); Physical blend of HPMC K100M LV, Carbopol 934P and solid dispersion (d)

solubilising and amphiphilic nature of the Soluplus® to dissolve the bosentan in aqueous medium [21]. The drug release profile is shown in Fig. 4.

Pre-optimization considerations and bosentan-solid dispersion-loaded-bucco-adhesive tablets

Many research studies have established reliable values for the bio-adhesive parameters of certain polymers, and these can be screened for use as the bio-adhesive

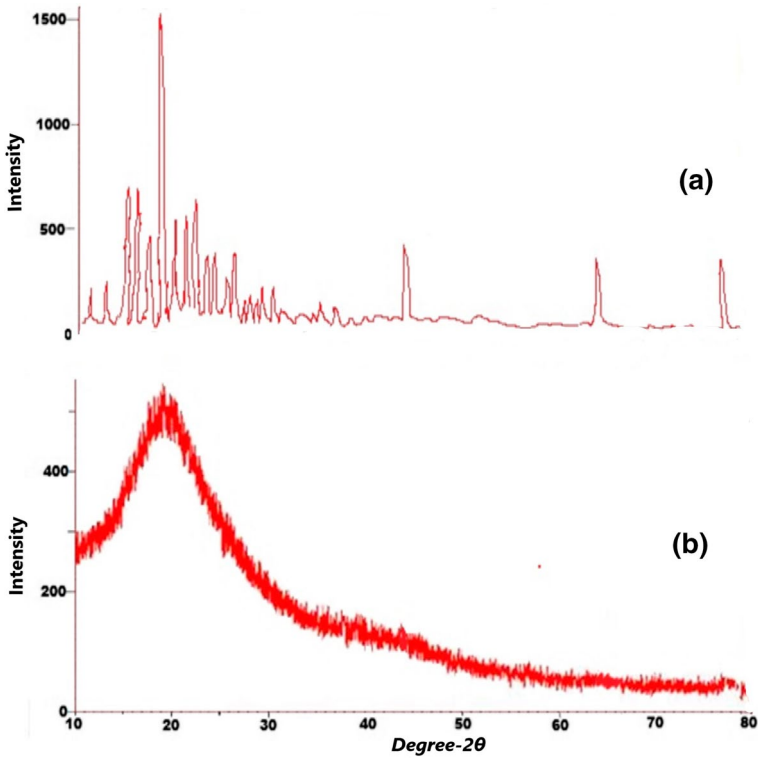


Fig. 3 XRD study: Bosentan (a); Bosentan-solid dispersion (b)

Table 3 Results of phase solubility study and solubility study of solid dispersion

Phase solubility study		Solubility study of solid dispersion	
Conc. of Soluplus® (%)	ΔG°_{tr}	Ratio of Bosentan: Soluplus®	Solubility (mg/ml) Bosentan-Solid Dispersion (BSD)
1	1954.93	1:1	0.0213 ± 0.006
2	1658.25	1:2	0.0321 ± 0.0055
3	-268.58	1:3	0.0405 ± 0.0050
4	-689.64	1:4	0.0515 ± 0.004
5	-1025.25	1:5	0.0658 ± 0.0021
		Observed solubility of plain bosentan = 0.00963 mg/ml	

material. These include Carbopol 934P, sodium carboxymethyl cellulose (highest adhesive force) and other polymers such as poly (methyl vinyl ether-co-maleic anhydride), tragacanth and sodium alginate [22]. The bio-adhesive potential of HPMC has also been investigated by various scientists [23–25].

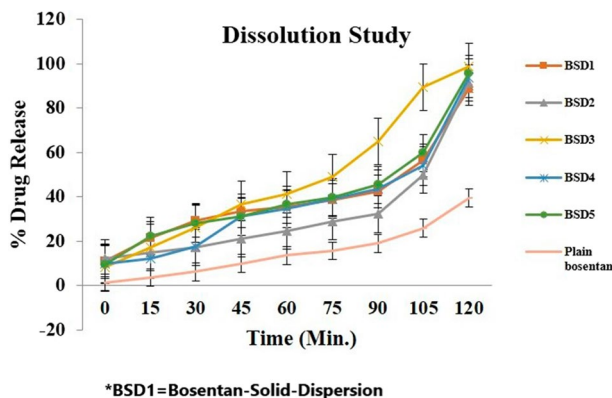


Fig. 4 In vitro dissolution study of bosentan-solid dispersion in phosphate buffer, pH 6.8

Various polymers, including two grades of Carbopol 934P and Carbopol 971P (CP 934P and CP 971P), hydroxypropyl methylcellulose (HPMC K4M, HPMC K100LV) and sodium carboxymethylcellulose (sodium CMC) were selected for the selection of optimized formulation batch depending upon their excellent bio-adhesive strength, release rate-controlling property, non-irritancy, non-toxicity, stability and compatibility with drugs. HPMC and Carbopol are known to have excellent bio-adhesive and drug release rate properties [25, 26].

Initially, drug release parameters of the five polymers were studied by formulating them into matrix tablet forms (drug-to-polymer ratio 1:1) to check the effect of polymer type on the drug-release properties.

The initial dissolution study revealed that the tablets were vulnerable to fragmentation. Hence, in the subsequent investigations, the quantity of polymer in the tablets was increased (drug-to-polymer ratio 1:4). The increased drug-to-polymer ratio yielded excellent results, and hence this ratio was chosen for further work.

As inadequate hydration leads to the dose dumping problem, HPMC K100LV, which shows rapid hydration, was selected for further studies. The use of higher-viscosity grades of HPMC resulted in lower levels of drug release at sub-therapeutic levels. As reported previously, Carbopols have excellent extended drug release and bio-adhesion properties [27, 28]. Hence, on the basis of the preliminary findings, Carbopol 934P was chosen as it is a promising bio-adhesion-regulating polymer. Considering the performances of HPMC K100LV and Carbopol 934P, a combination of these polymers was selected for formulation development [29–32]. The use of combinations of Carbopol and HPMC has been reported extensively in the scientific literature [33–35]. It has been reported that, the use of water-insoluble fillers in large amounts can markedly decrease the release rates of drugs [36]. Hence, the use of fillers, such as microcrystalline cellulose, lactose anhydrous or di-calcium phosphate can help to achieve controlled release.

Microcrystalline cellulose (Avicel PH 102) was selected as a diluent, and colloidal silicon dioxide and magnesium stearate were selected for improving the flow properties of the materials during compression.

Evaluation of physical parameters

The evaluation of the compressed matrices suggests that all the physical parameters were practically within the acceptable limits according to the Pharmacopoeia standards. The tablet weight varied between 546 and 555 mg, thickness between 3.42 and 3.54 mm, and hardness between 5.2 and 6.5 kg/cm². The bosentan content varied between 93.48% and 99.15%, and the friability ranged between 0.15% and 0.55%. All the observed values are presented in Table 4.

Effect of polymer combination on in vitro drug release

The response surface methodology (RSM) is an effective tool for optimizing the bio-adhesive matrix tablet formulation. All factors at all combinations can be studied effectively using a central composite design (CCD). This approach is used most frequently to establish the effects of individual variables and interactions with very little experimentation [10, 11].

All the formulations showed surface erosion, diffusion and polymer relaxation mechanisms. For matrix systems, a value of the exponent ' n ' of 0.45 indicates that the drug release is diffusion controlled, and a value of 0.89 indicates that the drug release is swelling controlled. Values of ' n ' between 0.45 and 0.89 can be considered to indicate both phenomena (anomalous transport). If the release is controlled by more than one process, such as by both diffusion and erosion, then the value of ' n ' will fall in a different range, with contributions from both phenomena [17–20]. Surface erosion was observed due to the adhesive property of the polymers [36]. The values of the exponent n varied between 0.4412 and 0.5964 shown in Table 5, indicates Non-Fickian release behaviour. The exponent n increases with increasing HPMC and Carbopol levels shows linear relationship. These observations seem to be in agreement with the results of Nokhodchi et al. [37]. The viscosity of the HPMC and Carbopol blend increased due to reduced hydration (in this case, due to increase in the concentration and combination of both the polymer, pores on the surface of tablet blocks quickly which prevents further

Table 4 Evaluation physical parameters of buccal bio-adhesive tablets

Formula-tion code	Weight (mg)	Hardness (kg/cm ²)	Diameter (mm)	Thickness (mm)	Friability (%)	Drug content (%)
F1	553 ± 1.27	5.4 ± 0.22	12 ± 0.01	3.52 ± 0.04	0.15 ± 0.01	98.45 ± 1.01
F2	554 ± 1.45	6.5 ± 0.15	12 ± 0.03	3.44 ± 0.01	0.55 ± 0.02	94.45 ± 1.03
F3	546 ± 1.87	5.8 ± 0.21	12 ± 0.01	3.44 ± 0.02	0.47 ± 0.01	95.47 ± 1.31
F4	553 ± 1.42	5.3 ± 0.61	12 ± 0.05	3.42 ± 0.01	0.18 ± 0.01	99.15 ± 1.09
F5	555 ± 1.25	5.5 ± 0.44	12 ± 0.01	3.53 ± 0.01	0.55 ± 0.02	98.88 ± 1.23
F6	554 ± 1.58	6.4 ± 0.18	12 ± 0.03	3.54 ± 0.01	0.45 ± 0.03	95.89 ± 1.31
F7	546 ± 1.58	6.3 ± 0.55	12 ± 0.04	3.52 ± 0.09	0.48 ± 0.02	95.17 ± 1.21
F8	553 ± 2.18	6.1 ± 0.47	12 ± 0.02	3.50 ± 0.01	0.52 ± 0.03	93.48 ± 1.36
F9	550 ± 1.28	5.2 ± 0.77	12 ± 0.02	3.52 ± 0.01	0.16 ± 0.01	96.78 ± 1.33

*All the values are calculated as ± SD; $n = 3$

Optimization of formulation

Mathematical relationships were developed for the response variables studied. These are presented in Eqs. (3), (4) and (5). Under analysis of variance (ANOVA), all the equations were found to be statistically significant ($p < 0.001$).

$$Rel_{4h}(Y_1) = 91.75 - 9.92X_1 - 5.08X_2 - 2.09X_1X_2 - 1.14X_1^2 - 1.14X_2^2 \quad (3)$$

$$t_{50\%}(Y_2) = 1.30 + 0.29X_1 + 0.17X_2 + 0.19X_1X_2 + 0.34X_1^2 + 0.13X_2^2 \quad (4)$$

$$\text{Bio-adhesive strength } (Y_3) = 8.71 + 2.83X_1 + 3.50X_2 + 0.92X_1X_2 - 0.25X_1^2 + 1.08X_2^2 \quad (5)$$

The standard error of the implemented design is represented in the contour plot and response surface plot shown in Fig. 6. ANOVA of the response surface model statistics for the responses of Rel_{4h} suggested a linear model, showing a p value of < 0.0001 , an adjusted R^2 value of 0.9465 and a predicted R -squared value of 0.8836.

The contour and response surface plots have shown the effects of the two polymers (HPMC K100LV and Carbopol 934P) on the drug release for 4 h (Rel_{4h} , Y_1) study. The drug release decreases at higher levels, whereas it increases at lower levels of HPMC and Carbopol (in this case batch F2 and F7 respectively).

ANOVA of the response surface model statistics related to the responses of $t_{50\%}$ suggested a linear model with a p value of < 0.0001 , an adjusted R -squared value of 0.3213 and a predicted R -squared value of -0.1052 .

The contour and response surface plots show the effects of the two polymers on the time required for release of 50% of the drug ($t_{50\%}$, Y_2). Here also time required for 50% of drug release increases with increased levels of both the polymers, Fig. 7.

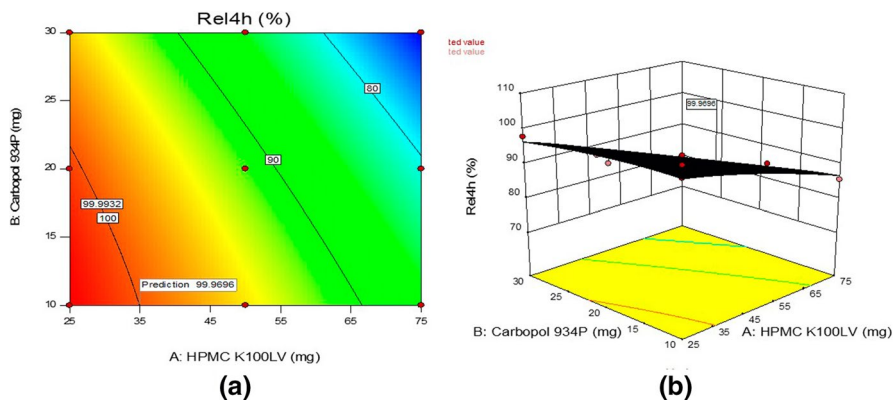


Fig. 6 Evaluation of set response parameter Rel_{4h} (Y_1) in the form of Contour plot (a) and Surface response plot (b)

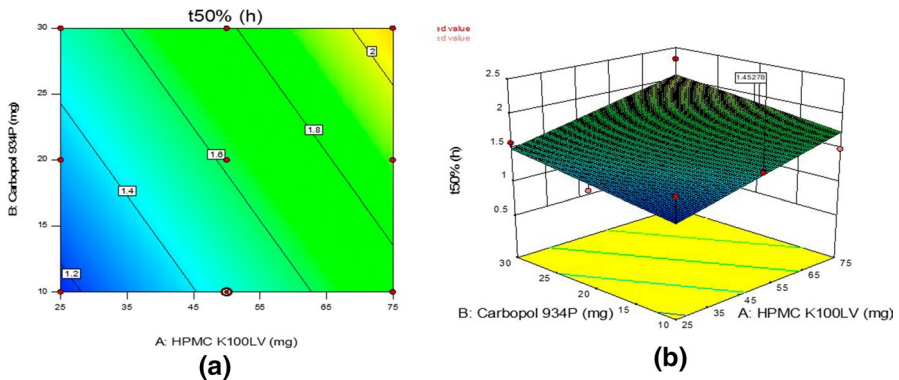


Fig. 7 Evaluation of set response parameter $t_{50\%}$ (Y_2) in the form of Contour plot (a) and Surface response plot (b)

ANOVA of the response surface model statistics related to the responses of the bio-adhesive strength (Y_3) suggests a linear model, with a p value of < 0.0001 , an adjusted R -squared value of 0.8343 and a predicted R -squared value of 0.6936.

The contour and response surface plots show the effects of the two polymers on the bio-adhesive strength (Y_3) of the tablets. Bio-adhesive strength increases with increased levels of both the polymers with major contribution of Carbopol which has higher bio-adhesion property [22].

The contour, response surface plots showing the effects of these two polymers on bio-adhesive strength (Y_3) for all the nine batches as per factorial design are highlighted in Fig. 8.

Values for all the response parameters Rel_{4h} , $t_{50\%}$ and the bio-adhesive strength predicted by the software were closely in agreement with the values obtained for experimentally designed formulations. The Formulation F4 has shown very closed values for all the response parameters and hence considered as optimized

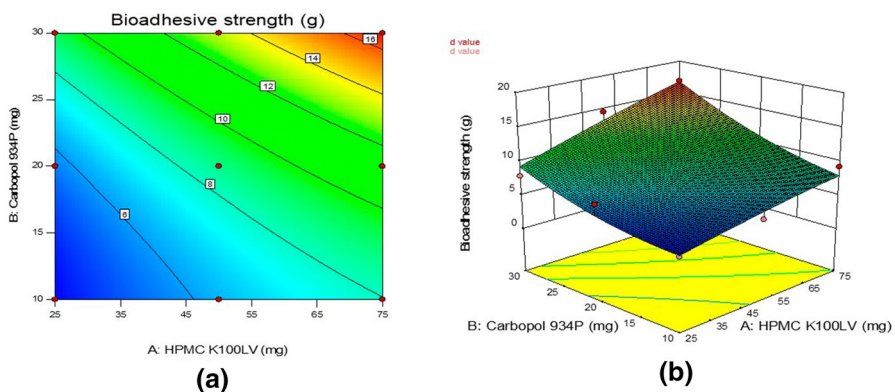


Fig. 8 Evaluation of set response parameter bio-adhesive strength (Y_3) in the form of Contour plot (a) and Surface response plot (b)

formulation in this case. Figure 9 shows overlay plot and plot of predicted Versus actual values for all the set response parameters (Y_1, Y_2 and Y_3).

Effect of Soluplus® on tablet swelling and gel penetration study

A swelling study was conducted for optimized bucco-adhesive tablet formulation (F4) over a period of 4 h as depicted in Fig. 10a. The bucco-adhesive tablet formulation with plain bositentan was also evaluated for this study (shown in dotted line, Fig. 4). The swelling was faster in tablets with higher concentrations of HPMC K100LV and was much greater than tablet formulation containing plain bositentan. This may be again due to the presence of Soluplus® in optimized tablet (F4) which is more hydrophilic in nature and immediately solubilises in the presence of dissolution medium, supporting the swelling of polymers. Although the amount of the polymers used were same to that of optimized tablet formulation. The maximum swelling was attained in the first 2 h, after which the polymer started eroding slowly in the dissolution medium. The high-water uptake may be due to quick hydration of

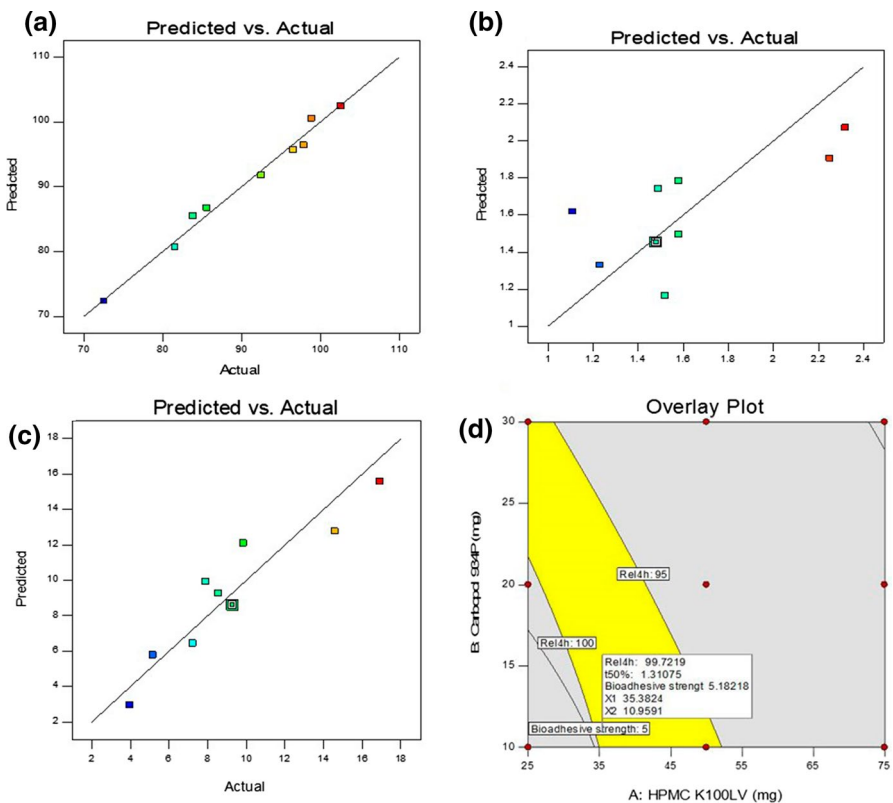


Fig. 9 Effect of HPMC K100M LV and Carbopol 934P on Rel_{4h} (Y_1), $t_{50\%}$ (Y_2) and bio-adhesive strength (Y_3) in the form of predicted Versus actual responses (a) and Overlay plot (b)

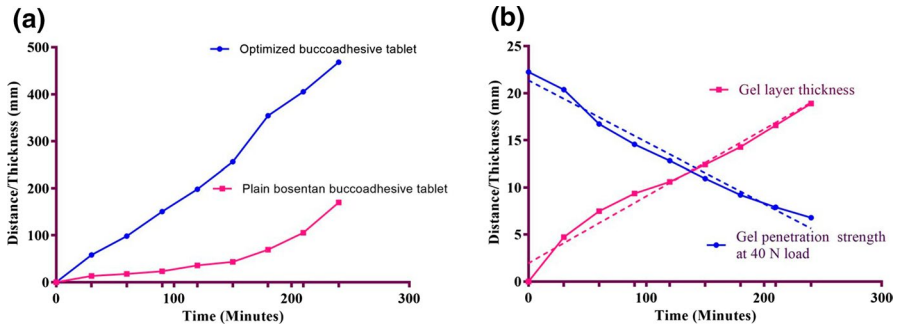


Fig. 10 Swelling index (a) and gel forming behaviour study (b) of optimized bucco-adhesive tablet formulation (F4) and plain bosentan tablet (without Soluplus®)

HPMC K100LV as the swelling rate of the tablets increases with increasing concentration of HPMC K100 LV in the tablets [39, 40].

The gel layer thickness of the optimized formulation F4 increased over the 4-h study. A gel penetration study was conducted similarly, to determine the maximum gel strength of the tablets after swelling in a dissolution medium. It was observed that at a fixed load (40 N in this case); the strength of the gel was higher at the beginning but decreases as time passes. This may be due to the fact that the gel becomes less viscous with time due to the accumulation of the aqueous medium. The presence of Soluplus® enabled the bosentan to solubilise quickly which further was entrapped in the viscous gel layer for prolonged release over the 4-h period of time. Formulation with plain bosentan had much higher gel strength but less gel layer thickness as compared to the optimized formulation (F4, containing Soluplus®). The results of the gel layer thickness study and the gel penetration study are shown in Fig. 10b.

Stability study of optimized bucco-adhesive tablet formulation

No significant changes were observed in the tablet friability, drug content and adhesive strength of the optimized bio-adhesive tablets after 6 months. A slight increase in hardness was observed due to an uptake of water by the hydrophilic components (HPMC K 100LV and Carbopol 934P) in the tablet at a relative humidity of 75%. No significant changes were noted for the properties of the bio-adhesive tablets in the stability study. All the observations of the study are highlighted in Table 6.

Conclusion

Bosentan is one of the important lives saving drugs used in the management of Pulmonary Arterial Hypertension (PAH). In the present study, efforts were made to enhance the solubility of the bosentan and develop bucco-adhesive tablets. From this study, it was concluded that the bucco-adhesive tablet formulation containing

Table 6 Evaluation physical parameters of buccal bio-adhesive tablets after stability study

Formulation code	*Weight (mg)	*Hardness (kg/cm ²)	*Diameter (mm)	*Thickness (mm)	Friability (%)	Drug content (%)
F1	562.00 ± 1.21	5.50 ± 0.45	12 ± 0.02	3.56 ± 0.03	0.11	97.99
F2	564.14 ± 1.54	6.79 ± 0.13	12 ± 0.03	3.57 ± 0.022	0.12	95.55
F3	547.00 ± 1.68	6.10 ± 0.12	12 ± 0.02	3.48 ± 0.03	0.16	96.58
F4	555.54 ± 1.25	5.50 ± 0.48	12 ± 0.02	3.52 ± 0.02	0.13	98.24
F5	558.10 ± 1.11	5.80 ± 0.63	12 ± 0.02	3.58 ± 0.02	0.17	99.87
F6	559.85 ± 1.48	6.70 ± 0.47	12 ± 0.03	3.59 ± 0.02	0.22	96.68
F7	554.12 ± 1.35	6.80 ± 0.57	12 ± 0.04	3.56 ± 0.05	0.35	94.57
F8	543.45 ± 2.78	6.50 ± 0.95	12 ± 0.02	3.52 ± 0.03	0.27	92.46
F9	560.85 ± 1.56	5.45 ± 0.58	12 ± 0.01	3.56 ± 0.01	0.12	95.94

* All the values are calculated as ±SD; n = 3

bosentan-solid dispersion may be better option to avoid first-pass-hepatic-metabolism and acid-degradation of the drug in gastrointestinal tract with enhanced solubility and efficient delivery in the oral mucosal region.

Acknowledgements The authors are very thankful to Dr. Reddy's Laboratories Pvt. Ltd., Hyderabad, India for providing a gift sample of bosentan. They are also thankful to Colorcon Asia Ltd., India for providing a sample of HPMC. The authors are happy to acknowledge BASF Corporation Ltd., India for providing a gift sample of Soluplus®. Authors are grateful to Mr. Anant Ketkar, Mr. Vinay Patil and Dr. A. R. Paradkar, Poona College of Pharmacy, Pune for providing the assistance of PCP Disso Software. They are also thankful to the Management and the Principal, Rajarshi Shahu College of Pharmacy, Buldana, India for their consistent support and motivation.

Compliance with ethical standards

Conflict of interest The authors declare that they have no conflict of interest.

References

1. Lipinski CA, Lombardo F, Dominy BW (2002) Poor aqueous solubility-an industry wide problem in drug discovery. *Am Pharm Rev* 5(3):82–85
2. Tiwari BD, Shikare OM, Sontakke AM (2014) Bioequivalence study: an overview. *JPharm Sci Innv* 3(5):421–425
3. Vargas M, Bustamante C, Villarraga EA (2015) Fed and fasting bioequivalence study for two formulations of bosentan 125 mg tablets in healthy Colombian people. *J BioequivAvailab* 7:210–215. <https://doi.org/10.4172/jbb.1000242>
4. Voorspoels J, Remon JP, Eechaute W et al (1996) Buccal absorption of testosterone and its esters using a bioadhesive tablet in dogs. *Pharm Res* 13:1228–1232
5. Sandeep Patnaik LA, Avinash Chunduri M, Akilesh Sai et al (2016) Enhanced dissolution characteristics of piroxicam-Soluplus® nanosuspensions. *J Exp Nanosci* 11(12):916–929. <https://doi.org/10.1080/17458080.2016.1178402>
6. Kendre PN, Chaudhari PD (2017) Effect of polyvinyl caprolactam-polyvinyl acetate-polyethylene glycol graft copolymer on bioadhesion and release rate property of eplerenone pellets. *Drug Dev Ind Pharm* 43(5):751–761
7. Karathanos V, Mourtzinis I, Yannakopoulou K (2007) Study of the solubility, antioxidant activity and structure of inclusion complex of vanillin with cyclodextrin. *Food Chem* 101:652–658
8. Kendre PN, Chaudhari PD (2017) Effect of amphiphilic graft co-polymer-carrier on physical stability of bosentan nanocomposite: assessment of solubility, dissolution and bioavailability. *Eur J Pharm Biopharm.* <https://doi.org/10.1016/j.ejpb.2017.06.024>
9. Van den Mooter G, Augustijns P, Bleton N et al (1998) Physico-chemical characterization of solid dispersions of temazepam with polyethylene glycol 6000 and PVP K30. *Int J Pharm* 164:67–80
10. Ahuja N, Katare OP, Singh B (2007) Studies on dissolution enhancement and mathematical modeling of drug release of a poorly water-soluble drug using water-soluble carriers. *Eur J Pharm Biopharm* 65:26–38
11. Doornbos CA, Haan PD (1995) Optimization techniques in formulation and processing. In: Swarbrick J, Boylan JC (eds) *Encyclopaedia of pharmaceutical technology*. Marcel Dekker, New York, pp 77–160
12. Hughes L, Gehris A (2002) A new method of characterizing buccal dissolution of drugs: Rohm and Haas Research laboratory spring house. PA, USA
13. Singh B, Ahuja N (2002) Development of controlled-release buccoadhesive hydrophilic matrices of diltiazem hydrochloride: optimization of bioadhesion, dissolution and diffusion parameters. *Drug Dev Ind Pharm* 28:433–444
14. Yang L, Johnson B, Fassih R (1998) Determination of continuous changes in the gel layer thickness of poly (ethylene oxide) and HPMC tablets undergoing hydration: a texture analysis study. *Pharm Res* 15:1902–1906
15. Swain S, Behera A, Dinda SC et al (2014) Formulation design, optimization and pharmacodynamic evaluation of sustained release mucoadhesive microcapsules of venlafaxine HCl. *Indian J Pharm Sci* 76(4):354–363

16. Giovagnoli SP, Balsi MR, Schoubben LP et al (2008) Physicochemical characterization and release mechanism of a novel prednisone biodegradable microspheres formulation. *J Pharm Sci* 97(1):303–317
17. Gupta PK, Robinson JR (1992) Oral controlled-release delivery. In: Kydonieus A (ed) *Treatise on controlled drug delivery*. Marcel Dekker, New Jersey, pp 255–310
18. Grassi M, Grassi G (2005) Mathematical modelling and controlled drug delivery: matrix systems. *Current Drug Deliv* 1:97–116
19. Dash S, Murthy PN, Nath L et al (2010) Kinetic modelling on drug release from controlled drug delivery systems. *Acta Poloniae Pharmaceutica* 67(3):217–223
20. Smart JD, Kellaway IW, Worthington HEC (1984) An in vitro investigation of mucosa-adhesive materials for use in controlled drug delivery. *J Pharm Pharmacol* 36:295–299
21. Lian X, Dong J, Zhang J et al (2014) Soluplus® based 9-nitrocamptothecin solid dispersion for peroral administration: preparation, characterization, in vitro and in vivo evaluation. *Int J Pharm* 477:399–407
22. Mortazavi SA, Smart JD (1995) An investigation of some factors influencing the in vitro assessment of mucoadhesion. *Int J Pharm* 116:223–230
23. Ranga Rao KV, Buri P (1989) A novel in situ method to test polymer and coated microspheres for bioadhesion. *Int J Pharm* 52:265–270
24. Nafee NA, Ismail FA, Boraie NA et al (2004) Mucoadhesive delivery systems. Evaluation of mucoadhesive polymers for buccal tablet formulation. *Drug Dev Ind Pharm* 30(9):985–993
25. Li S, Lin S, Daggy BP et al (2003) Effect of HPMC and Carbopol on the release and floating properties of gastric floating drug delivery system using factorial design. *Int J Pharm* 253:13–22
26. Vasir JK, Tambwekar K, Garg S (2003) Bioadhesive microspheres as a controlled drug delivery system. *Int J Pharm* 255(1–2):13–32
27. Andrews GP, Laverty TP, Jones DS (2009) Mucoadhesive polymeric platforms for controlled drug delivery. *Eur J Pharm Biopharm* 71:505–518
28. Nur AO, Zhang JS (2000) Recent progress in sustained/controlled oral delivery of captopril: an overview. *Int J Pharm* 194:139–146
29. Vjera G, Davide G, Andrews N (2005) Comparison of mucoadhesive properties of various polymers. *Adv Drug Deliv Rev* 57:1713–1723
30. Prudat-Christiaens C, Arnaud P, Allain P et al (1996) Aminophylline bio adhesive tablets attempted by wet granulation. *Int J Pharm* 141:109–116
31. Agarwal V, Mishra B (1999) Design development and biopharmaceutical properties of buccoadhesive compacts of pentazocin. *Drug Dev Ind Pharm* 25:701–709
32. Chitnis VS, Malshe VS, Lalla JK (1991) Bioadhesive polymers-synthesis, evaluation and application in controlled release tablets. *Drug Dev Ind Pharm* 17:879–892
33. Furlanetto S, Cirri M, Maestrelli F et al (2006) Study of formulation variables influencing the drug release rate from matrix tablets by experimental design. *Eur J Pharm Biopharm* 62:77–84
34. Prajapati ST, Patel LD, Patel DM (2008) Gastric floating matrix tablets: design and optimization using combination of polymers. *Acta Pharm* 58(2):221–229. <https://doi.org/10.2478/v10007-008-0006-3>
35. Doelker E (1987) Water-swollen derivatives in pharmacy. In: Peppas NA (ed) *Hydrogels in medicine and pharmacy*. CRS Press Inc., Florida, pp 115–160
36. Von Burkersroda F, Schedl L, Gopferich A (2002) Why degradable polymers undergo surface erosion or bulk erosion. *Biomaterials* 23(21):4221–4231
37. Nokhodchi A, Farid DJ, Najafi M et al (1997) Studies on controlled release formulation of diclofenac sodium. *Drug Dev Ind Pharm* 23:1019–1022
38. Perez-Marcos FB, Armstrong JL (1994) Release of propranolol hydrochloride from matrix tablets containing hydroxyl propyl methyl cellulose K4M and Carbopol 974. *Int J Pharm* 111:251–259
39. Colombo P, Bettini R, Santi P et al (2000) Swellable matrices for controlled drug delivery: gel-layer behaviour, mechanisms and optimal performance. *Pharm Sci Tech Today* 3(6):198–204
40. Siepmann J, Kranz H, Bodmeier R et al (1999) HPMC-matrices for controlled drug delivery: a new model combining diffusion, swelling, and dissolution mechanisms and predicting the release kinetics. *Pharm Res* 16(11):1748–1756

An effort to augment solubility and efficiency of the oral bosentan-bucco-adhesive drug delivery system using graft co-polymer as the carrier

**Prakash N. Kendre, Pravin
D. Chaudhari, Shirish P. Jain & Somnath
K. Vibhute**

Polymer Bulletin

ISSN 0170-0839

Polym. Bull.

DOI 10.1007/s00289-020-03412-z



Your article is protected by copyright and all rights are held exclusively by Springer-Verlag GmbH Germany, part of Springer Nature. This e-offprint is for personal use only and shall not be self-archived in electronic repositories. If you wish to self-archive your article, please use the accepted manuscript version for posting on your own website. You may further deposit the accepted manuscript version in any repository, provided it is only made publicly available 12 months after official publication or later and provided acknowledgement is given to the original source of publication and a link is inserted to the published article on Springer's website. The link must be accompanied by the following text: "The final publication is available at link.springer.com".



An effort to augment solubility and efficiency of the oral bosentan-bucco-adhesive drug delivery system using graft co-polymer as the carrier

Prakash N. Kendre¹ · Pravin D. Chaudhari² · Shirish P. Jain¹ · Somnath K. Vibhute¹

Received: 25 January 2020 / Revised: 11 July 2020 / Accepted: 6 October 2020
© Springer-Verlag GmbH Germany, part of Springer Nature 2020

Abstract

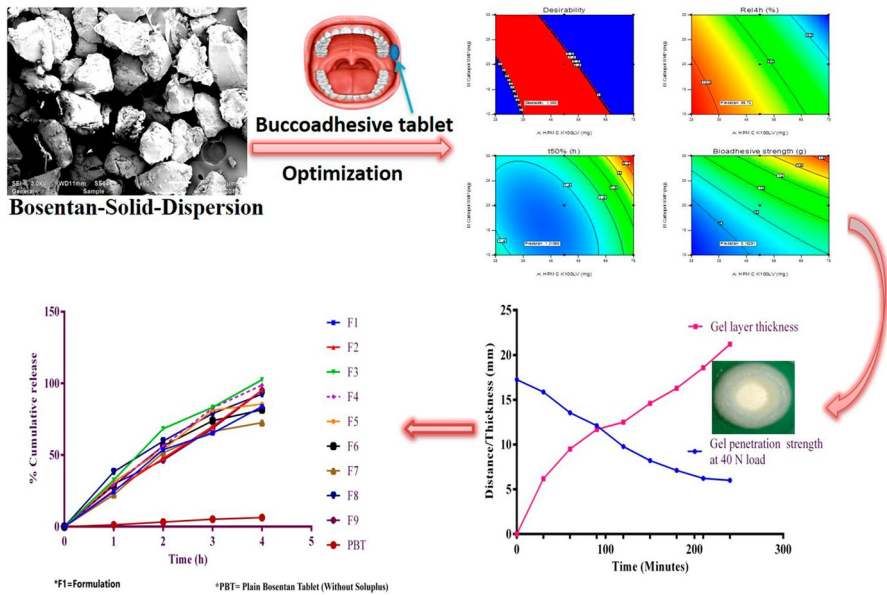
Although there are rapid developments in molecular science and synthetic chemistry for investigation of many essential drug molecules, poor solubility and bioavailability issues are major constraint in the design of more efficient formulations. This research study focuses on the enhancement of solubility and development of the bucco-adhesive drug delivery system of bosentan using Soluplus® (polyvinyl-caprolactam-polyvinyl-acetate-polyethylene glycol graft co-polymer) as a carrier. A 3²-factorial design was implemented to develop bucco-adhesive tablets using hydroxypropyl methyl cellulose (HPMC) K100 LV (X_1) and Carbopol 934 P (X_2) as independent variables at various levels whereas $t_{50\%}$ (Y_1) (time required to release 50% of drug), Rel_{4h} (Y_2) (percentage of the drug release in 4 h) and bio-adhesive strength (Y_3) were considered as set response parameters. The positive effect of the surface response quadratic model demonstrated the change in the already set dependent variables of $t_{50\%}$, Rel_{4h} and bio-adhesive strength. The FT-IR study confirmed the suitability of all the components used in the design of formulation. DSC and XRD study have confirmed the encapsulation of bosentan in the Soluplus® carrier and amorphous form of bosentan, respectively. Overall, 6.832-fold increase in solubility was observed for bosentan-solid dispersion. High-water uptake and swelling of bucco-adhesive tablets (containing bosentan-solid dispersion) was observed due to presence of the highly hydrophilic-Soluplus®. Rel_{4h} was found to be $97.86 \pm 0.57\%$ for optimized formulation (F4) and was decreased with increasing polymer content. The values of $t_{50\%}$ were found to be enhanced from 1.11 to 2.32 h at the lower to higher levels of both the polymers respectively.

✉ Prakash N. Kendre
prakashkendre@gmail.com

¹ Rajarshi Shahu College of Pharmacy, Buldana, Maharashtra 443 001, India

² Modern College of Pharmacy, Nigdi, Pune, India

Graphic abstract



Keywords Bosentan · Solid dispersion · Bucco-adhesive tablet · 32-factorial design · soluplus® · HPMC K100 LV and carbopol 934 P

Introduction

Sometimes inherent characteristics of drug molecules pose the major hurdle in the design and development of formulation. The poor aqueous solubility of the drug compounds is one of the major issues involved during the dosage form development stage [1]. Suitable solubility enhancement techniques can address this poor solubility issue satisfactorily. Bosentan, a dual endothelial receptor antagonist used in the treatment of pulmonary arterial hypertension (PAH). But its poor aqueous solubility makes it out of place to develop the efficient drug delivery system. The present study is an attempt to enhance the solubility of bosentan to develop efficient buccal adhesive drug delivery system. As the buccal route of administration is effective to avoid the first pass hepatic metabolism of the drug, an effective drug delivery system can be designed with maximum drug utilization in the buccal mucosal cavity [2, 3]. This is the most suitable, convenient and easily accessible site for drug delivery. The exposure of drug to the systemic circulation through the internal jugular vein, bypasses the hepatic first-pass metabolism leading to high bioavailability. The buccal route enjoys excellent patient compliance owing to ease of self-administration [4]. The solid dispersion of bosentan was prepared using an amphiphilic graft copolymer, Soluplus® (polyvinyl caprolactam–polyvinyl acetate–polyethylene glycol

graft co-polymer) specially designed and manufactured by BASF Corporation to enhance the solubility of poorly soluble drugs like bosentan. Due to its bifunctional behaviour, it can serve as an excellent matrix to dissolve drugs in aqueous media [5–7]. Initially, bosentan-solid dispersion was prepared successfully followed by the formulation of the bucco-adhesive tablet by optimization technique using central composite designs (CCD) for two factors at three levels [8].

Materials and methods

Materials

Bosentan was received as a gift sample from Dr. Reddy's Laboratories Pvt. Ltd., Hyderabad, India. Soluplus® was provided as a gift sample by BASF Corporation, Mumbai, Maharashtra, India. Polymers, HPMC K4M, HPMC K100M, HPMC K100 M LV, Carbopol 971P and Carbopol 934P were obtained as gift samples from Colorcon Asia Pvt. Ltd., Goa, India. All other excipients and reagents used were of analytical grade and obtained from reputed suppliers in India.

Methods

Preparation of bosentan-solid dispersion

A bosentan-solid dispersion was prepared by solvent evaporation technique. Soluplus® was dissolved completely in ethanol. Bosentan was added slowly to the clear ethanolic drug solution with the continuous stirring till the uniform distribution of bosentan. The ratio of bosentan to Soluplus® was maintained at 1:1, 1:2, 1:3, 1:4 and 1:5 and coded as BSD1, BSD2, BSD3, BSD4 and BSD5, respectively. The ethanol was evaporated completely and resultant mass was dried and grinded to obtain a free-flowing powder, which was passed through a 100 μm sieve. The dried solid dispersion was kept in a desiccator until further use and testing [9].

Fourier transform infrared spectroscopy (FT-IR) study

The interaction between drug and excipients was studied using an FTIR spectrophotometer (Shimadzu, Japan). Spectra were recorded in the range 4000–400 cm^{-1} . All the samples were prepared using the KBr pellet technique, and the spectra were recorded at a resolution of 0.15 cm^{-1} and a scanning speed of 20 scan/s.

Differential scanning calorimetric study (DSC) study

Differential scanning calorimetric (DSC) measurement was performed by a (DSC-60 Shimadzu) thermal analyser. The samples of about 5 mg were hermetically placed in the aluminium-sealed pans and scanned at heating rate of 10 $^{\circ}\text{C}/\text{min}$ over

a temperature range of 0–300 °C by using nitrogen gas as effluent gas. The thermal properties of the pure bosentan and bosentan-solid dispersion were characterized.

X-ray diffraction (XRD) study

The XRD spectra/patterns were recorded (Philips PW3710 analytical X-ray diffractometer at Diya Lab, Mumbai, India) the pure drug and solid dispersion formulation for confirmation of change of basic form of drug (crystalline or amorphous) after formulating in the final dosage form.

Phase solubility study

The Phase solubility study was conducted to predict the effect and trend of Soluplus® to enhance solubility and dissolution of bosentan. Shaking flask method was used to conduct the phase solubility study. An excess amount of the bosentan was added to the solutions at the concentration range of 5%, 10%, 15%, 25%, and 30% w/v Soluplus®. The samples were shaken for 72 h in the mechanical flask shaker at 37 ± 2 °C. The concentration of the bosentan in the solution after equilibration for 72 h was determined using UV spectrophotometer (1650 PC, Shimadzu, Japan) at 272 nm [7].

In order to ensure the favourable concentration of the Soluplus® for solubilization of bosentan, ΔG_{tr}° value was calculated using the following equation:

$$\Delta G_{tr}^{\circ} = 2.303RT \log (S_o/S_s) \quad (1)$$

where, S_o/S_s is the ratio of molar solubility of the bosentan before and after entrapment with Soluplus®. R and T are constant of gas (8.31 JK^{-1}) and temperature (in degree Kelvin) respectively [9].

Solubility study of bosentan-solid dispersion

Prepared solid dispersions (BSD1 to BSD5) were subjected to the solubility study using same method mentioned under the above section of the phase solubility study. Enhancement in the solubility of bosentan-solid dispersion after equilibration for 72 h was determined using the UV spectrophotometer (1650 PC, Shimadzu, Japan) at 272 nm [5].

Preparation of bucco-adhesive tablets

Formulation batch of the solid dispersion with maximum solubility was selected for the further development of the bucco-adhesive tablets using 3^2 -factorial design. Polymers HPMC K4M, HPMC K100LV, HPMC K100M and Carbopol 934P were used to develop bucco-adhesive tablets. Avicel PH102 was used as a diluent in all the formulations. Initially, preliminary batches were performed to select a suitable polymer with the selected range of levels to obtain expected results.

Selection of suitable experimental design

The response surface methodology (RSM) is an effective method for optimizing the bio-adhesive matrix tablet formulation. All factors at all combinations can be studied effectively using a central composite design (CCD). This approach is used most frequently to establish the effects of the individual variables and interactions with very little experimentation [10, 11]. Another advantage of this design is that it allows a quadratic surface response to be established, which is otherwise difficult with a factorial design at two levels. In this study, a CCD for two factors, namely, HPMC K100LV and Carbopol 934P, at three levels with a value of $\alpha=1$, i.e., a 3^2 -factorial, was chosen for the optimization of the bucco-adhesive matrix tablets. This computer-aided study was conducted using Design-Expert® software version 9.0.6.2 (Stat-Ease Inc., Minneapolis, MN, 55,143).

On the basis of the observations from preliminary trials, a combination of the HPMC K100 LV (X_1) and Carbopol 934P (X_2) were selected as independent factors for the optimization of bucco-adhesive matrix tablets. The composition for the development of preliminary batches of the bucco-adhesive tablets is given in Table 1. Dependent variables, $t_{50\%}(Y_1)$, time required to release 50% of drug; $Rel_{4h}(Y_2)$, percentage of the drug release in 4 h and bio-adhesive strength (Y_3) were selected to optimize the final bucco-adhesive tablet formulation using a computer-aided factorial design. The tablets were compressed using the direct compression technique in a single rotary multiple punch machine (Kambert Pvt. Ltd., Ahmedabad, India). Finally, tablets with flat surface with uniform size of 12 mm diameter were compressed as per the compositions of 3^2 factorial design which is mentioned in Table 2.

Evaluation of physical parameters and assay study

All the buccal adhesive tablets were evaluated for physical parameters like weight variation, friability, hardness, thickness and diameter. Ten tablets of each batch were crushed in a mortar to obtain powdered form. Powdered tablets equivalent to 100 mg of pure drug were weighed and transferred to 250-mL volumetric flasks containing methanol. Each flask was sonicated and the contents filtered through 0.45 μ Whatman filter paper. The absorbances were measured at 272 nm using UV-visible spectrophotometer to calculate bosentan content.

Table 1 Composition of bio-adhesive tablets containing bosentan-solid dispersion

Sr. no	Ingredients	Concentration (mg)
1	Bosentan-solid dispersion (BSD) (Equivalent to 62.5 mg of Bosentan)	371.32
2	HPMC K100 LV	25–75
3	Carbopol 934P	10–30
4	Avicel PH 102	Q.S
5	Magnesium stearate	2.5
6	Aerosil (Colloidal silicon dioxide)	2.5

Table 2 Formulation batches as per two-factor, three-level central composite design (CCD) layout translation of coded levels in actual units

Trial no	Formulation code	Coded factor level (mg)	
		X1: HPMC K 100 LV	X2: Carbapol 934 P
1	F1	50	30
2	F2	75	30
3	F3	25	20
4	F4	50	10
5	F5	75	10
6	F6	25	30
7	F7	25	10
8	F8	50	20
9	F9	75	20
Independent variable	Coded levels		
	High (+1)	Medium (0)	Low (-1)
X1: HPMC K 100 LV (mg)	70	50	30
X2: Carbapol 934 P (mg)	30	20	10

In vitro dissolution study

Initially, a dissolution study was conducted for the bosentan-solid dispersion using USP-II dissolution test apparatus (paddle type). Phosphate buffer (pH 6.8), 900 mL was used as the dissolution medium at 37 ± 0.5 °C and 50 rpm. Aliquot samples were withdrawn at the intervals of every 15 min for 2 h, filtered through 0.45 μ Whatman filter paper and absorbances were measured at 272 nm using the UV spectrophotometer [7]. All the sample of dissolution study were analysed in triplicate as mean \pm SD, $n = 3$.

Similarly, the dissolution study was conducted for all the bucco-adhesive tablet formulations prepared according to the 3^2 factorial design. As the anatomy and physiology of buccal cavity differs from the stomach where it consists of very small volume of saliva with very short residence time, this dissolution study includes modified dissolution test apparatus which was described by Hughes et al. [12]. This apparatus consists of single, stirred, continuous flow-through filtration cell which includes a dip tube, specially designed to remove finely divided solid particles. The composition of saliva solution was used as described by Hughes et al. To analyse the dissolved drug, filtered solution was removed continuously. The volume of saliva was maintained up to 10 ml in the cell which was pumped at the rate of 6 ml/min. This facilitates the residence time for saliva solution of approximately 100 s and gives almost complete removal in 8 min. All the sample of dissolution study were analysed in triplicate as mean \pm SD; $n = 3$.

Measurement of bio-adhesive strength Goat mucosa procured from the slaughter's house was used as the model membrane to study the bio-adhesive strength of the tablets. The mucosal membrane was isolated by removing the underlying con-

nective tissue. It was washed with a phosphate buffer (pH 6.8). The apparatus was specially designed for measuring adhesive strength as prescribed in the literature. It was built using a double-beam physical balance [11, 12]. The force required to detach a tablet from the surface of the mucosal membrane was measured in triplicate ($n = 3$) as the mean \pm SD and this force was treated as the bio-adhesive strength.

Determination of swelling and study of gel-forming behaviour The swelling behaviour of the soaked tablets was evaluated over a period of 4 h to check uptake of water. Tablets were weighed accurately and placed in 5 mL of a phosphate buffer (pH 6.8) solution. Tablets were reweighed after every 30 min over the 4-h period and excess of water was removed carefully using filter paper. The swelling index (weight gain) was calculated using the following Eq. (2):

$$\text{Swelling index} = \frac{\text{Wet weight of tablet} - \text{original weight of tablet}}{\text{Original weight of tablet}} \times 100 \quad (2)$$

Similarly, the gel-forming behaviour of the tablets was studied over a period of 4 h. The optimized tablets were soaked in a phosphate buffer (pH 6.8) and the thickness of the gel layer as well as the gel penetration strength was measured. The gel penetration strength under a fixed load of 40 N was determined using a Brookfield CT-3 Texture Analyzer, Brookfield Engineering Ltd. [15, 16].

Mathematical modelling of the drug release data In vitro dissolution study data was analysed using the PCP Disso Software package which has provisions for volume correction, dilution factor adjustment, time interval settings, drug loss due to sampling, etc. The software helped to calculate the amount of drug dissolved as a percent release, rate of drug release and log fraction released at varied time intervals. The kinetic constant (k), the diffusion release exponent (n) and the contributions of Fickian diffusion and polymer relaxation in a swollen matrix were also determined. On the basis of this phenomenological analysis, the type of drug release [Fickian, Non-Fickian (anomalous) or zero-order] was predicted. Time taken for 50% drug release, i.e. $t_{50\%}$ was also calculated in this study. The data were analysed to check best-fit model using different equations [17–20].

Optimization of analysed data For optimization, the response variables considered were the amount of drug released in 4 h $\text{Rel}_{4\text{h}}$ (Y_1), time required to release 50% of drug) $t_{50\%}$ (Y_2) and the bio-adhesive strength (Y_3).

The PCP Disso software was used to calculate the amount of drug released and the kinetic constants. Design-Expert 9.01 software (Stat-Ease, USA) was used to fit a full second-order polynomial equation with added interaction terms to correlate the studied responses $\text{Rel}_{4\text{h}}$ (Y_1), $t_{50\%}$ (Y_2) and bio-adhesive strength (Y_3) with the variables to be examined. All the polynomial regression results were represented as three-dimensional coloured response surfaces and contour graphs. The optimum formulations were confirmed in two stages. First, a feasible space was located; and second, an exhaustive grid search was conducted to predict the possible solutions.

Validation of response surface methodology (RSM) To validate the response surface, few formulations were selected as check points. The tablets were formulated (as described in earlier section of bucco-adhesive tablet preparation) using the optimal composition and evaluated for physical properties, content, dissolution and adhesive strength. The predicted and observed responses were compared, residual graphs plotted and the percent error estimated from the observed responses. Correlation plots were also constructed separately for all the formulations.

Results and discussion

Pre-formulation study

Before design and development of the bucco-adhesive tablets, various analytical tests like FTIR, DSC and XRD were performed to check the suitability of the components for the final formulation.

FTIR spectra of pure bosentan showed major peaks at 3620.15 cm^{-1} , 3369.75 cm^{-1} representing N–H stretching; C–H stretching at 2960.83 cm^{-1} , 2924.18 cm^{-1} , 2758.30 cm^{-1} ; C=O stretching at 1707.06 cm^{-1} ; S=O stretching at 1558.54 cm^{-1} ; N–H out of plane at 1454.38 cm^{-1} ; C–H bend at 1342.50 cm^{-1} , 1251.84 cm^{-1} ; C–N stretching at 1170.83 cm^{-1} , 1112.96 cm^{-1} and N–H, O–H bending at 1020.38 cm^{-1} , 844.85 cm^{-1} . The presence of these spectra is the characteristic for identification of bosentan. The solid dispersion formulation also showed the same type spectra indicating that there was no interaction among the bosentan and Soluplus®. The FT-IR spectra are shown in Fig. 1.

The DSC study was also conducted to check thermal behaviour of the pure bosentan, Soluplus, solid dispersion and physical blend containing the HPMC K100 LV, Carbopol and solid dispersion. The bosentan has shown sharp major endothermic peak at $97.99\text{ }^{\circ}\text{C}$ and short endothermic peak at $116.72\text{ }^{\circ}\text{C}$. The Soluplus® has shown the endothermic peak at $77.43\text{ }^{\circ}\text{C}$. The resultant solid dispersion has shown only the endothermic peak of Soluplus® at $85.26\text{ }^{\circ}\text{C}$ with slightly variation as compared to original peak and showing no change in the glass transition peak. The absence of all thermal peaks of drug in the solid dispersion indicates complete encapsulation of drug in the matrix of Soluplus®. All the observed thermal peaks of plain drug and physical blend containing the HPMC K100 LV, Carbopol and solid dispersion are highlighted in Fig. 2.

The XRD data showed that the sharp highly intense peaks at 2θ values of 15.29° , 16.57° , 18.52° , 22.56° , 20.16° and 77.58° and intensity of 1505.13, 789.25, 754.88, 653.25, 461.25, 402.25, respectively, whereas solid dispersion showed flat peaks showing major peak at 496.35 and other peaks at less than 200. Complete entrapment of bosentan in the Soluplus® carrier is confirmed by the presence of flat peaks. The results of the XRD data are highlighted in Fig. 3.

The phase solubility study was conducted to check the effect and trend of Soluplus® on the solubility and dissolution of the bosentan which is poorly water-soluble drug having maximum solubility of 0.00904 mg/ml only. In the present study, solid dispersion formulation was prepared to increase the solubility of

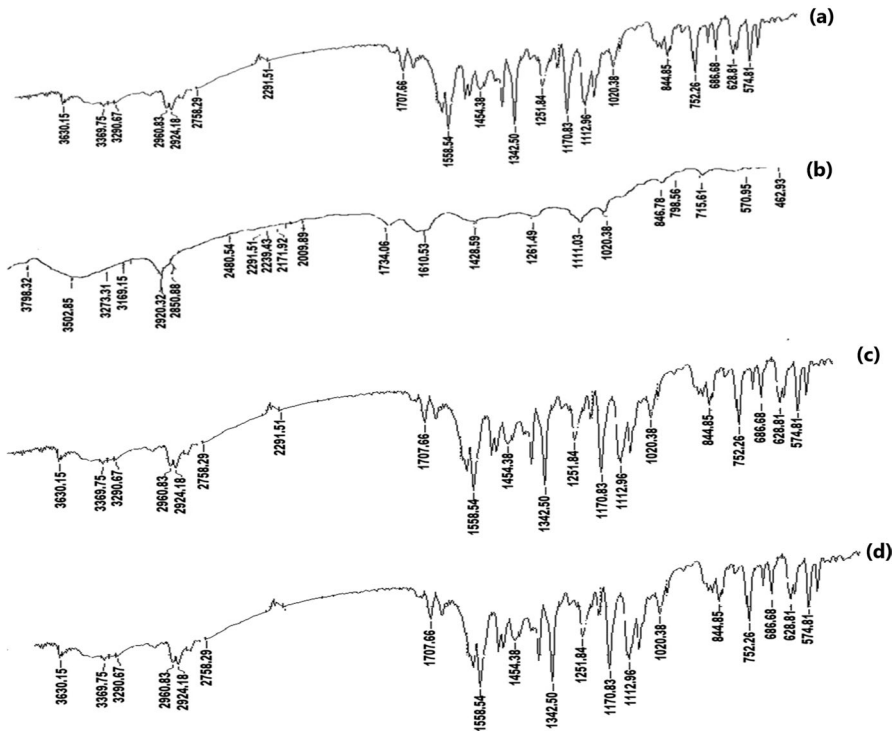


Fig. 1 FT-IR study: Bosentan (a); Soluplus® (b); Bosentan-solid dispersion (c); Physical blend of HPMC K100M LV, Carbopol 934P and Solid dispersion (d)

bosentan. It was found that at 5% concentration of Soluplus®, the water solubility of bosentan increases more than five times. This was mainly due to the micelle solubilisation effect of Soluplus®. The values of Gibb's free energy related with water solubility of bosentan in the presence of Soluplus® are shown in Table 3. More negative values of Gibb's free energy show the higher solubilisation effect which was observed in this at higher concentration of Soluplus®.

For solubility of bosentan-solid dispersion in phosphate buffer (pH 6.8), the significant differences were found as shown in Table 3. The solubility of bosentan was found to be proportional to the concentration of Soluplus®. Maximum solubility of 0.0658 ± 0.021 mg/ml was observed for solid dispersion at 1:5 ratio of bosentan to Soluplus®. Overall, 6.832-fold increase in solubility was observed for solid dispersion as compared to the pure bosentan (plain bosentan) which showed 0.00963 mg/ml of solubility in water [21].

During dissolution study of bosentan-solid dispersion, maximum drug dissolution was observed in two hours, showing $98.78 \pm 1.02\%$ release at highest concentration level of Soluplus® (5%) whereas least release of $88.58 \pm 1.12\%$ was observed at lowest level of Soluplus® (1%). From this study, it is confirmed that the dissolution increases at higher concentration of Soluplus® which is due to the

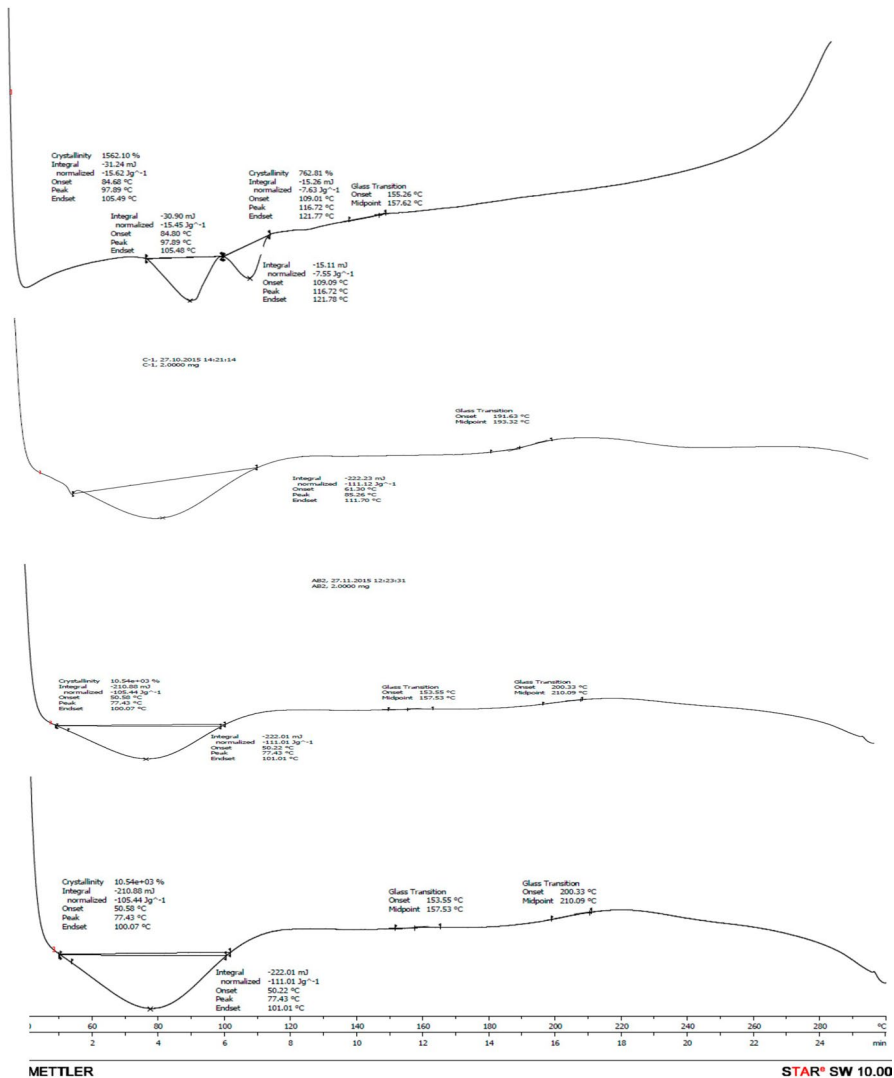


Fig. 2 DSC study: Bosentan (a); Soluplus® (b); Bosentan-solid dispersion (c); Physical blend of HPMC K100M LV, Carbopol 934P and solid dispersion (d)

solubilising and amphiphilic nature of the Soluplus® to dissolve the bosentan in aqueous medium [21]. The drug release profile is shown in Fig. 4.

Pre-optimization considerations and bosentan-solid dispersion-loaded-bucco-adhesive tablets

Many research studies have established reliable values for the bio-adhesive parameters of certain polymers, and these can be screened for use as the bio-adhesive

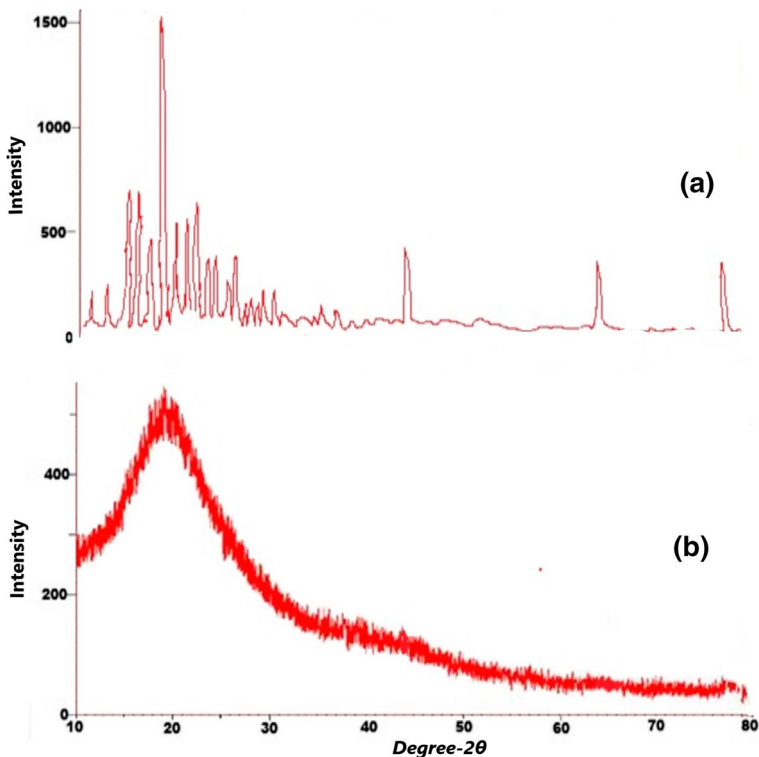


Fig. 3 XRD study: Bosentan (a); Bosentan-solid dispersion (b)

Table 3 Results of phase solubility study and solubility study of solid dispersion

Phase solubility study		Solubility study of solid dispersion	
Conc. of Soluplus® (%)	ΔG°_{tr}	Ratio of Bosentan: Soluplus®	Solubility (mg/ml) Bosentan-Solid Dispersion (BSD)
1	1954.93	1:1	0.0213 ± 0.006
2	1658.25	1:2	0.0321 ± 0.0055
3	-268.58	1:3	0.0405 ± 0.0050
4	-689.64	1:4	0.0515 ± 0.004
5	-1025.25	1:5	0.0658 ± 0.0021
		Observed solubility of plain bosentan = 0.00963 mg/ml	

material. These include Carbopol 934P, sodium carboxymethyl cellulose (highest adhesive force) and other polymers such as poly (methyl vinyl ether-co-maleic anhydride), tragacanth and sodium alginate [22]. The bio-adhesive potential of HPMC has also been investigated by various scientists [23–25].

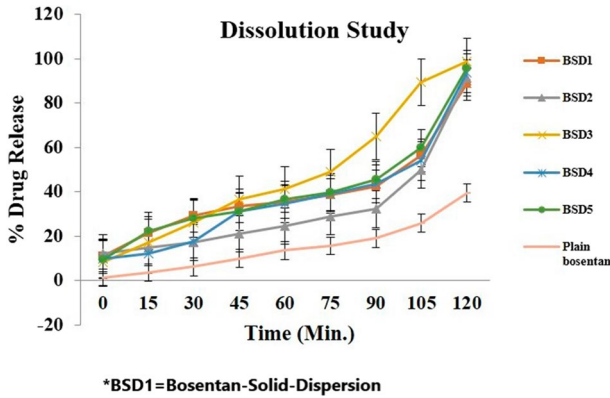


Fig. 4 In vitro dissolution study of bosentan-solid dispersion in phosphate buffer, pH 6.8

Various polymers, including two grades of Carbopol 934P and Carbopol 971P (CP 934P and CP 971P), hydroxypropyl methylcellulose (HPMC K4M, HPMC K100LV) and sodium carboxymethylcellulose (sodium CMC) were selected for the selection of optimized formulation batch depending upon their excellent bio-adhesive strength, release rate-controlling property, non-irritancy, non-toxicity, stability and compatibility with drugs. HPMC and Carbopol are known to have excellent bio-adhesive and drug release rate properties [25, 26].

Initially, drug release parameters of the five polymers were studied by formulating them into matrix tablet forms (drug-to-polymer ratio 1:1) to check the effect of polymer type on the drug-release properties.

The initial dissolution study revealed that the tablets were vulnerable to fragmentation. Hence, in the subsequent investigations, the quantity of polymer in the tablets was increased (drug-to-polymer ratio 1:4). The increased drug-to-polymer ratio yielded excellent results, and hence this ratio was chosen for further work.

As inadequate hydration leads to the dose dumping problem, HPMC K100LV, which shows rapid hydration, was selected for further studies. The use of higher-viscosity grades of HPMC resulted in lower levels of drug release at sub-therapeutic levels. As reported previously, Carbopols have excellent extended drug release and bio-adhesion properties [27, 28]. Hence, on the basis of the preliminary findings, Carbopol 934P was chosen as it is a promising bio-adhesion-regulating polymer. Considering the performances of HPMC K100LV and Carbopol 934P, a combination of these polymers was selected for formulation development [29–32]. The use of combinations of Carbopol and HPMC has been reported extensively in the scientific literature [33–35]. It has been reported that, the use of water-insoluble fillers in large amounts can markedly decrease the release rates of drugs [36]. Hence, the use of fillers, such as microcrystalline cellulose, lactose anhydrous or di-calcium phosphate can help to achieve controlled release.

Microcrystalline cellulose (Avicel PH 102) was selected as a diluent, and colloidal silicon dioxide and magnesium stearate were selected for improving the flow properties of the materials during compression.

Evaluation of physical parameters

The evaluation of the compressed matrices suggests that all the physical parameters were practically within the acceptable limits according to the Pharmacopoeia standards. The tablet weight varied between 546 and 555 mg, thickness between 3.42 and 3.54 mm, and hardness between 5.2 and 6.5 kg/cm². The bosentan content varied between 93.48% and 99.15%, and the friability ranged between 0.15% and 0.55%. All the observed values are presented in Table 4.

Effect of polymer combination on in vitro drug release

The response surface methodology (RSM) is an effective tool for optimizing the bio-adhesive matrix tablet formulation. All factors at all combinations can be studied effectively using a central composite design (CCD). This approach is used most frequently to establish the effects of individual variables and interactions with very little experimentation [10, 11].

All the formulations showed surface erosion, diffusion and polymer relaxation mechanisms. For matrix systems, a value of the exponent '*n*' of 0.45 indicates that the drug release is diffusion controlled, and a value of 0.89 indicates that the drug release is swelling controlled. Values of '*n*' between 0.45 and 0.89 can be considered to indicate both phenomena (anomalous transport). If the release is controlled by more than one process, such as by both diffusion and erosion, then the value of '*n*' will fall in a different range, with contributions from both phenomena [17–20]. Surface erosion was observed due to the adhesive property of the polymers [36]. The values of the exponent *n* varied between 0.4412 and 0.5964 shown in Table 5, indicates Non-Fickian release behaviour. The exponent *n* increases with increasing HPMC and Carbopol levels shows linear relationship. These observations seem to be in agreement with the results of Nokhodchi et al. [37]. The viscosity of the HPMC and Carbopol blend increased due to reduced hydration (in this case, due to increase in the concentration and combination of both the polymer, pores on the surface of tablet blocks quickly which prevents further

Table 4 Evaluation physical parameters of buccal bio-adhesive tablets

Formula- tion code	Weight (mg)	Hardness (kg/ cm ²)	Diameter (mm)	Thickness (mm)	Friability (%)	Drug content (%)
F1	553 ± 1.27	5.4 ± 0.22	12 ± 0.01	3.52 ± 0.04	0.15 ± 0.01	98.45 ± 1.01
F2	554 ± 1.45	6.5 ± 0.15	12 ± 0.03	3.44 ± 0.01	0.55 ± 0.02	94.45 ± 1.03
F3	546 ± 1.87	5.8 ± 0.21	12 ± 0.01	3.44 ± 0.02	0.47 ± 0.01	95.47 ± 1.31
F4	553 ± 1.42	5.3 ± 0.61	12 ± 0.05	3.42 ± 0.01	0.18 ± 0.01	99.15 ± 1.09
F5	555 ± 1.25	5.5 ± 0.44	12 ± 0.01	3.53 ± 0.01	0.55 ± 0.02	98.88 ± 1.23
F6	554 ± 1.58	6.4 ± 0.18	12 ± 0.03	3.54 ± 0.01	0.45 ± 0.03	95.89 ± 1.31
F7	546 ± 1.58	6.3 ± 0.55	12 ± 0.04	3.52 ± 0.09	0.48 ± 0.02	95.17 ± 1.21
F8	553 ± 2.18	6.1 ± 0.47	12 ± 0.02	3.50 ± 0.01	0.52 ± 0.03	93.48 ± 1.36
F9	550 ± 1.28	5.2 ± 0.77	12 ± 0.02	3.52 ± 0.01	0.16 ± 0.01	96.78 ± 1.33

*All the values are calculated as ± SD; *n* = 3

Optimization of formulation

Mathematical relationships were developed for the response variables studied. These are presented in Eqs. (3), (4) and (5). Under analysis of variance (ANOVA), all the equations were found to be statistically significant ($p < 0.001$).

$$Rel_{4h}(Y_1) = 91.75 - 9.92X_1 - 5.08X_2 - 2.09X_1X_2 - 1.14X_1^2 - 1.14X_2^2 \quad (3)$$

$$t_{50\%}(Y_2) = 1.30 + 0.29X_1 + 0.17X_2 + 0.19X_1X_2 + 0.34X_1^2 + 0.13X_2^2 \quad (4)$$

$$\text{Bio-adhesive strength } (Y_3) = 8.71 + 2.83X_1 + 3.50X_2 + 0.92X_1X_2 - 0.25X_1^2 + 1.08X_2^2 \quad (5)$$

The standard error of the implemented design is represented in the contour plot and response surface plot shown in Fig. 6. ANOVA of the response surface model statistics for the responses of Rel_{4h} suggested a linear model, showing a p value of < 0.0001 , an adjusted R^2 value of 0.9465 and a predicted R -squared value of 0.8836.

The contour and response surface plots have shown the effects of the two polymers (HPMC K100LV and Carbopol 934P) on the drug release for 4 h (Rel_{4h} , Y_1) study. The drug release decreases at higher levels, whereas it increases at lower levels of HPMC and Carbopol (in this case batch F2 and F7 respectively).

ANOVA of the response surface model statistics related to the responses of $t_{50\%}$ suggested a linear model with a p value of < 0.0001 , an adjusted R -squared value of 0.3213 and a predicted R -squared value of -0.1052 .

The contour and response surface plots show the effects of the two polymers on the time required for release of 50% of the drug ($t_{50\%}$, Y_2). Here also time required for 50% of drug release increases with increased levels of both the polymers, Fig. 7.

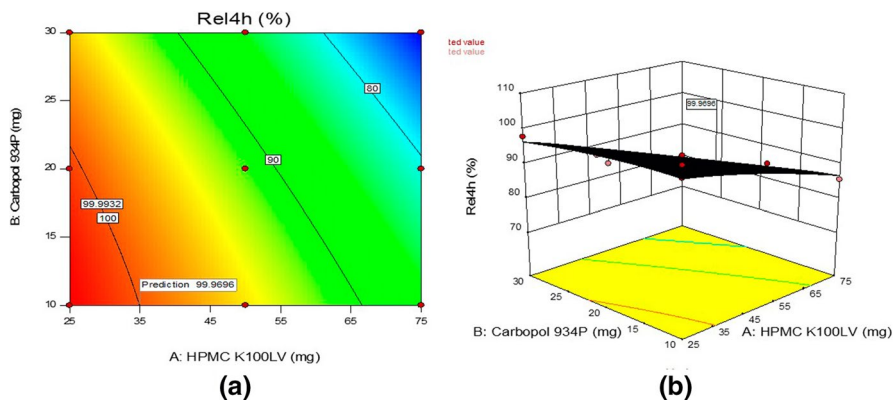


Fig. 6 Evaluation of set response parameter Rel_{4h} (Y_1) in the form of Contour plot (a) and Surface response plot (b)

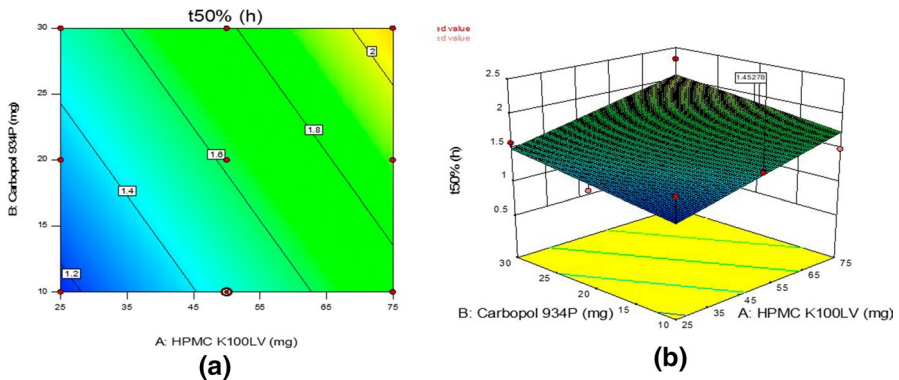


Fig. 7 Evaluation of set response parameter $t_{50\%}$ (Y_2) in the form of Contour plot (a) and Surface response plot (b)

ANOVA of the response surface model statistics related to the responses of the bio-adhesive strength (Y_3) suggests a linear model, with a p value of < 0.0001 , an adjusted R -squared value of 0.8343 and a predicted R -squared value of 0.6936.

The contour and response surface plots show the effects of the two polymers on the bio-adhesive strength (Y_3) of the tablets. Bio-adhesive strength increases with increased levels of both the polymers with major contribution of Carbopol which has higher bio-adhesion property [22].

The contour, response surface plots showing the effects of these two polymers on bio-adhesive strength (Y_3) for all the nine batches as per factorial design are highlighted in Fig. 8.

Values for all the response parameters Rel_{4h} , $t_{50\%}$ and the bio-adhesive strength predicted by the software were closely in agreement with the values obtained for experimentally designed formulations. The Formulation F4 has shown very closed values for all the response parameters and hence considered as optimized

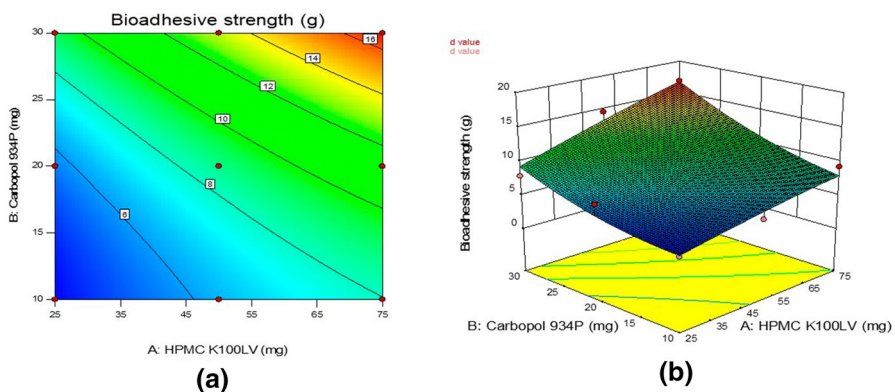


Fig. 8 Evaluation of set response parameter bio-adhesive strength (Y_3) in the form of Contour plot (a) and Surface response plot (b)

formulation in this case. Figure 9 shows overlay plot and plot of predicted Versus actual values for all the set response parameters (Y_1, Y_2 and Y_3).

Effect of Soluplus® on tablet swelling and gel penetration study

A swelling study was conducted for optimized bucco-adhesive tablet formulation (F4) over a period of 4 h as depicted in Fig. 10a. The bucco-adhesive tablet formulation with plain bositentan was also evaluated for this study (shown in dotted line, Fig. 4). The swelling was faster in tablets with higher concentrations of HPMC K100LV and was much greater than tablet formulation containing plain bositentan. This may be again due to the presence of Soluplus® in optimized tablet (F4) which is more hydrophilic in nature and immediately solubilises in the presence of dissolution medium, supporting the swelling of polymers. Although the amount of the polymers used were same to that of optimized tablet formulation. The maximum swelling was attained in the first 2 h, after which the polymer started eroding slowly in the dissolution medium. The high-water uptake may be due to quick hydration of

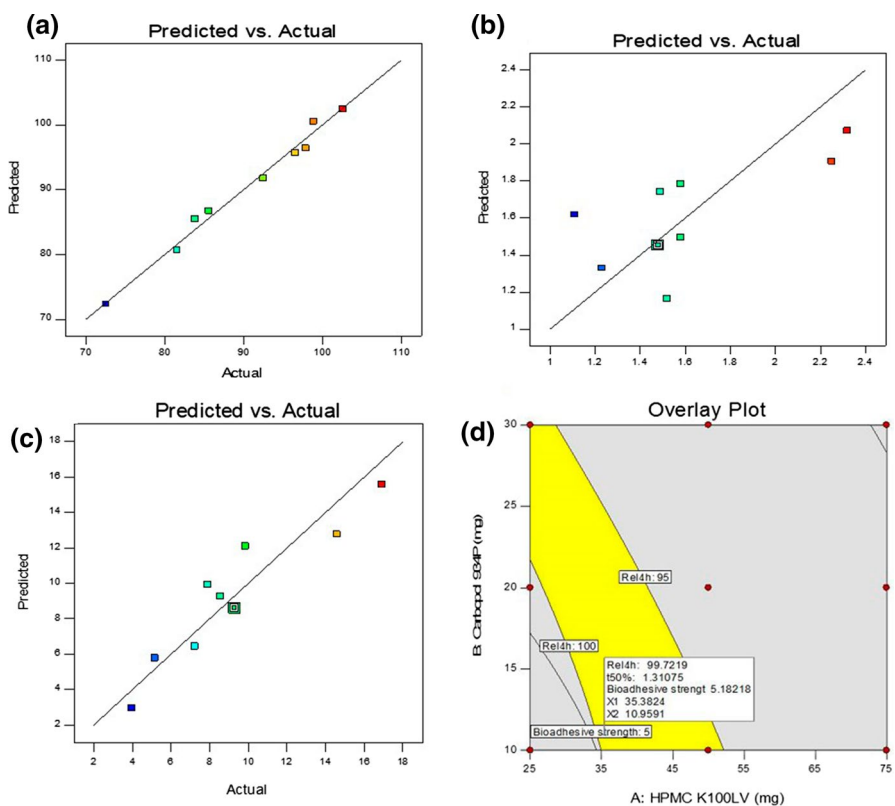


Fig. 9 Effect of HPMC K100M LV and Carbopol 934P on Rel_{4h} (Y_1), $t_{50\%}$ (Y_2) and bio-adhesive strength (Y_3) in the form of predicted Versus actual responses (a) and Overlay plot (b)

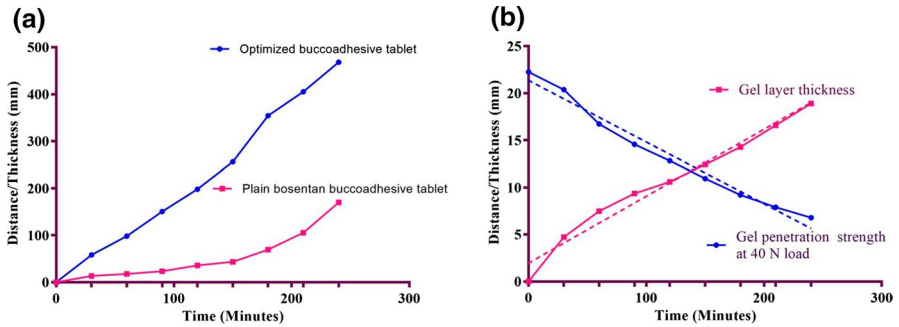


Fig. 10 Swelling index (a) and gel forming behaviour study (b) of optimized bucco-adhesive tablet formulation (F4) and plain bosentan tablet (without Soluplus®)

HPMC K100LV as the swelling rate of the tablets increases with increasing concentration of HPMC K100 LV in the tablets [39, 40].

The gel layer thickness of the optimized formulation F4 increased over the 4-h study. A gel penetration study was conducted similarly, to determine the maximum gel strength of the tablets after swelling in a dissolution medium. It was observed that at a fixed load (40 N in this case); the strength of the gel was higher at the beginning but decreases as time passes. This may be due to the fact that the gel becomes less viscous with time due to the accumulation of the aqueous medium. The presence of Soluplus® enabled the bosentan to solubilise quickly which further was entrapped in the viscous gel layer for prolonged release over the 4-h period of time. Formulation with plain bosentan had much higher gel strength but less gel layer thickness as compared to the optimized formulation (F4, containing Soluplus®). The results of the gel layer thickness study and the gel penetration study are shown in Fig. 10b.

Stability study of optimized bucco-adhesive tablet formulation

No significant changes were observed in the tablet friability, drug content and adhesive strength of the optimized bio-adhesive tablets after 6 months. A slight increase in hardness was observed due to an uptake of water by the hydrophilic components (HPMC K 100LV and Carbopol 934P) in the tablet at a relative humidity of 75%. No significant changes were noted for the properties of the bio-adhesive tablets in the stability study. All the observations of the study are highlighted in Table 6.

Conclusion

Bosentan is one of the important lives saving drugs used in the management of Pulmonary Arterial Hypertension (PAH). In the present study, efforts were made to enhance the solubility of the bosentan and develop bucco-adhesive tablets. From this study, it was concluded that the bucco-adhesive tablet formulation containing

Table 6 Evaluation physical parameters of buccal bio-adhesive tablets after stability study

Formulation code	*Weight (mg)	*Hardness (kg/cm ²)	*Diameter (mm)	*Thickness (mm)	Friability (%)	Drug content (%)
F1	562.00 ± 1.21	5.50 ± 0.45	12 ± 0.02	3.56 ± 0.03	0.11	97.99
F2	564.14 ± 1.54	6.79 ± 0.13	12 ± 0.03	3.57 ± 0.022	0.12	95.55
F3	547.00 ± 1.68	6.10 ± 0.12	12 ± 0.02	3.48 ± 0.03	0.16	96.58
F4	555.54 ± 1.25	5.50 ± 0.48	12 ± 0.02	3.52 ± 0.02	0.13	98.24
F5	558.10 ± 1.11	5.80 ± 0.63	12 ± 0.02	3.58 ± 0.02	0.17	99.87
F6	559.85 ± 1.48	6.70 ± 0.47	12 ± 0.03	3.59 ± 0.02	0.22	96.68
F7	554.12 ± 1.35	6.80 ± 0.57	12 ± 0.04	3.56 ± 0.05	0.35	94.57
F8	543.45 ± 2.78	6.50 ± 0.95	12 ± 0.02	3.52 ± 0.03	0.27	92.46
F9	560.85 ± 1.56	5.45 ± 0.58	12 ± 0.01	3.56 ± 0.01	0.12	95.94

* All the values are calculated as ±SD; n = 3

bosentan-solid dispersion may be better option to avoid first-pass-hepatic-metabolism and acid-degradation of the drug in gastrointestinal tract with enhanced solubility and efficient delivery in the oral mucosal region.

Acknowledgements The authors are very thankful to Dr. Reddy's Laboratories Pvt. Ltd., Hyderabad, India for providing a gift sample of bosentan. They are also thankful to Colorcon Asia Ltd., India for providing a sample of HPMC. The authors are happy to acknowledge BASF Corporation Ltd., India for providing a gift sample of Soluplus®. Authors are grateful to Mr. Anant Ketkar, Mr. Vinay Patil and Dr. A. R. Paradkar, Poona College of Pharmacy, Pune for providing the assistance of PCP Disso Software. They are also thankful to the Management and the Principal, Rajarshi Shahu College of Pharmacy, Buldana, India for their consistent support and motivation.

Compliance with ethical standards

Conflict of interest The authors declare that they have no conflict of interest.

References

1. Lipinski CA, Lombardo F, Dominy BW (2002) Poor aqueous solubility-an industry wide problem in drug discovery. *Am Pharm Rev* 5(3):82–85
2. Tiwari BD, Shikare OM, Sontakke AM (2014) Bioequivalence study: an overview. *JPharm Sci Innv* 3(5):421–425
3. Vargas M, Bustamante C, Villarraga EA (2015) Fed and fasting bioequivalence study for two formulations of bosentan 125 mg tablets in healthy Colombian people. *J BioequivAvailab* 7:210–215. <https://doi.org/10.4172/jbb.1000242>
4. Voorspoels J, Remon JP, Eechaute W et al (1996) Buccal absorption of testosterone and its esters using a bioadhesive tablet in dogs. *Pharm Res* 13:1228–1232
5. Sandeep Patnaik LA, Avinash Chunduri M, Akilesh Sai et al (2016) Enhanced dissolution characteristics of piroxicam-Soluplus® nanosuspensions. *J Exp Nanosci* 11(12):916–929. <https://doi.org/10.1080/17458080.2016.1178402>
6. Kendre PN, Chaudhari PD (2017) Effect of polyvinyl caprolactam-polyvinyl acetate-polyethylene glycol graft copolymer on bioadhesion and release rate property of eplerenone pellets. *Drug Dev Ind Pharm* 43(5):751–761
7. Karathanos V, Mourtzinos I, Yannakopoulou K (2007) Study of the solubility, antioxidant activity and structure of inclusion complex of vanillin with cyclodextrin. *Food Chem* 101:652–658
8. Kendre PN, Chaudhari PD (2017) Effect of amphiphilic graft co-polymer-carrier on physical stability of bosentan nanocomposite: assessment of solubility, dissolution and bioavailability. *Eur J Pharm Biopharm.* <https://doi.org/10.1016/j.ejpb.2017.06.024>
9. Van den Mooter G, Augustijns P, Bleton N et al (1998) Physico-chemical characterization of solid dispersions of temazepam with polyethylene glycol 6000 and PVP K30. *Int J Pharm* 164:67–80
10. Ahuja N, Katare OP, Singh B (2007) Studies on dissolution enhancement and mathematical modeling of drug release of a poorly water-soluble drug using water-soluble carriers. *Eur J Pharm Biopharm* 65:26–38
11. Doornbos CA, Haan PD (1995) Optimization techniques in formulation and processing. In: Swarbrick J, Boylan JC (eds) *Encyclopaedia of pharmaceutical technology*. Marcel Dekker, New York, pp 77–160
12. Hughes L, Gehris A (2002) A new method of characterizing buccal dissolution of drugs: Rohm and Haas Research laboratory spring house. PA, USA
13. Singh B, Ahuja N (2002) Development of controlled-release buccoadhesive hydrophilic matrices of diltiazem hydrochloride: optimization of bioadhesion, dissolution and diffusion parameters. *Drug Dev Ind Pharm* 28:433–444
14. Yang L, Johnson B, Fassih R (1998) Determination of continuous changes in the gel layer thickness of poly (ethylene oxide) and HPMC tablets undergoing hydration: a texture analysis study. *Pharm Res* 15:1902–1906
15. Swain S, Behera A, Dinda SC et al (2014) Formulation design, optimization and pharmacodynamic evaluation of sustained release mucoadhesive microcapsules of venlafaxine HCl. *Indian J Pharm Sci* 76(4):354–363

16. Giovagnoli SP, Balsi MR, Schoubben LP et al (2008) Physicochemical characterization and release mechanism of a novel prednisone biodegradable microspheres formulation. *J Pharm Sci* 97(1):303–317
17. Gupta PK, Robinson JR (1992) Oral controlled-release delivery. In: Kydonieus A (ed) *Treatise on controlled drug delivery*. Marcel Dekker, New Jersey, pp 255–310
18. Grassi M, Grassi G (2005) Mathematical modelling and controlled drug delivery: matrix systems. *Current Drug Deliv* 1:97–116
19. Dash S, Murthy PN, Nath L et al (2010) Kinetic modelling on drug release from controlled drug delivery systems. *Acta Poloniae Pharmaceutica* 67(3):217–223
20. Smart JD, Kellaway IW, Worthington HEC (1984) An in vitro investigation of mucosa-adhesive materials for use in controlled drug delivery. *J Pharm Pharmacol* 36:295–299
21. Lian X, Dong J, Zhang J et al (2014) Soluplus® based 9-nitrocamptothecin solid dispersion for peroral administration: preparation, characterization, in vitro and in vivo evaluation. *Int J Pharm* 477:399–407
22. Mortazavi SA, Smart JD (1995) An investigation of some factors influencing the in vitro assessment of mucoadhesion. *Int J Pharm* 116:223–230
23. Ranga Rao KV, Buri P (1989) A novel in situ method to test polymer and coated microspheres for bioadhesion. *Int J Pharm* 52:265–270
24. Nafee NA, Ismail FA, Boraie NA et al (2004) Mucoadhesive delivery systems. Evaluation of mucoadhesive polymers for buccal tablet formulation. *Drug Dev Ind Pharm* 30(9):985–993
25. Li S, Lin S, Daggy BP et al (2003) Effect of HPMC and Carbopol on the release and floating properties of gastric floating drug delivery system using factorial design. *Int J Pharm* 253:13–22
26. Vasir JK, Tambwekar K, Garg S (2003) Bioadhesive microspheres as a controlled drug delivery system. *Int J Pharm* 255(1–2):13–32
27. Andrews GP, Laverty TP, Jones DS (2009) Mucoadhesive polymeric platforms for controlled drug delivery. *Eur J Pharm Biopharm* 71:505–518
28. Nur AO, Zhang JS (2000) Recent progress in sustained/controlled oral delivery of captopril: an overview. *Int J Pharm* 194:139–146
29. Vjera G, Davide G, Andrews N (2005) Comparison of mucoadhesive properties of various polymers. *Adv Drug Deliv Rev* 57:1713–1723
30. Prudat-Christiaens C, Arnaud P, Allain P et al (1996) Aminophylline bio adhesive tablets attempted by wet granulation. *Int J Pharm* 141:109–116
31. Agarwal V, Mishra B (1999) Design development and biopharmaceutical properties of buccoadhesive compacts of pentazocin. *Drug Dev Ind Pharm* 25:701–709
32. Chitnis VS, Malshe VS, Lalla JK (1991) Bioadhesive polymers-synthesis, evaluation and application in controlled release tablets. *Drug Dev Ind Pharm* 17:879–892
33. Furlanetto S, Cirri M, Maestrelli F et al (2006) Study of formulation variables influencing the drug release rate from matrix tablets by experimental design. *Eur J Pharm Biopharm* 62:77–84
34. Prajapati ST, Patel LD, Patel DM (2008) Gastric floating matrix tablets: design and optimization using combination of polymers. *Acta Pharm* 58(2):221–229. <https://doi.org/10.2478/v10007-008-0006-3>
35. Doelker E (1987) Water-swollen derivatives in pharmacy. In: Peppas NA (ed) *Hydrogels in medicine and pharmacy*. CRS Press Inc., Florida, pp 115–160
36. Von Burkersroda F, Schedl L, Gopferich A (2002) Why degradable polymers undergo surface erosion or bulk erosion. *Biomaterials* 23(21):4221–4231
37. Nokhodchi A, Farid DJ, Najafi M et al (1997) Studies on controlled release formulation of diclofenac sodium. *Drug Dev Ind Pharm* 23:1019–1022
38. Perez-Marcos FB, Armstrong JL (1994) Release of propranolol hydrochloride from matrix tablets containing hydroxyl propyl methyl cellulose K4M and Carbopol 974. *Int J Pharm* 111:251–259
39. Colombo P, Bettini R, Santi P et al (2000) Swellable matrices for controlled drug delivery: gel-layer behaviour, mechanisms and optimal performance. *Pharm Sci Tech Today* 3(6):198–204
40. Siepmann J, Kranz H, Bodmeier R et al (1999) HPMC-matrices for controlled drug delivery: a new model combining diffusion, swelling, and dissolution mechanisms and predicting the release kinetics. *Pharm Res* 16(11):1748–1756

An effort to augment solubility and efficiency of the oral bosentan-bucco-adhesive drug delivery system using graft co-polymer as the carrier

**Prakash N. Kendre, Pravin
D. Chaudhari, Shirish P. Jain & Somnath
K. Vibhute**

Polymer Bulletin

ISSN 0170-0839

Polym. Bull.

DOI 10.1007/s00289-020-03412-z



Your article is protected by copyright and all rights are held exclusively by Springer-Verlag GmbH Germany, part of Springer Nature. This e-offprint is for personal use only and shall not be self-archived in electronic repositories. If you wish to self-archive your article, please use the accepted manuscript version for posting on your own website. You may further deposit the accepted manuscript version in any repository, provided it is only made publicly available 12 months after official publication or later and provided acknowledgement is given to the original source of publication and a link is inserted to the published article on Springer's website. The link must be accompanied by the following text: "The final publication is available at link.springer.com".



An effort to augment solubility and efficiency of the oral bosentan-bucco-adhesive drug delivery system using graft co-polymer as the carrier

Prakash N. Kendre¹ · Pravin D. Chaudhari² · Shirish P. Jain¹ · Somnath K. Vibhute¹

Received: 25 January 2020 / Revised: 11 July 2020 / Accepted: 6 October 2020
© Springer-Verlag GmbH Germany, part of Springer Nature 2020

Abstract

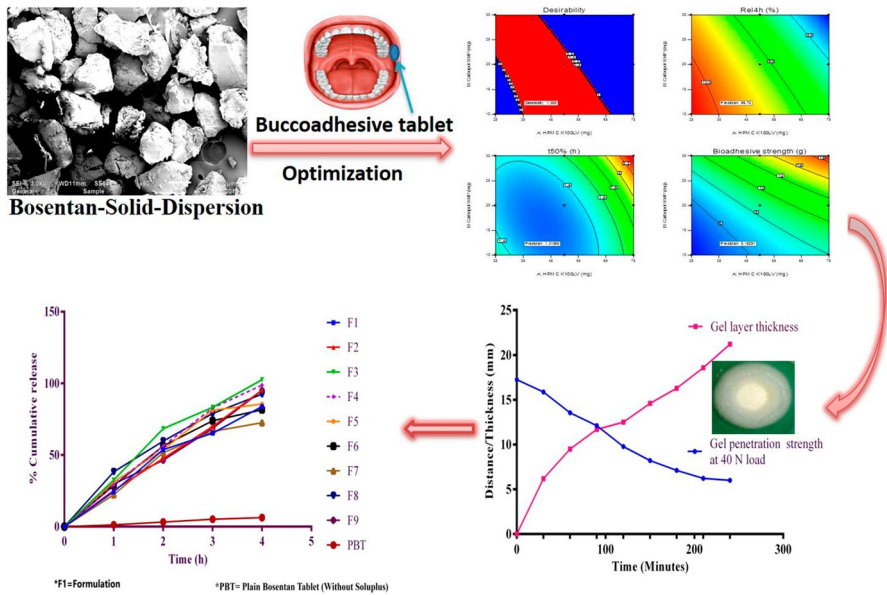
Although there are rapid developments in molecular science and synthetic chemistry for investigation of many essential drug molecules, poor solubility and bioavailability issues are major constraint in the design of more efficient formulations. This research study focuses on the enhancement of solubility and development of the bucco-adhesive drug delivery system of bosentan using Soluplus® (polyvinyl-caprolactam-polyvinyl-acetate-polyethylene glycol graft co-polymer) as a carrier. A 3²-factorial design was implemented to develop bucco-adhesive tablets using hydroxypropyl methyl cellulose (HPMC) K100 LV (X_1) and Carbopol 934 P (X_2) as independent variables at various levels whereas $t_{50\%}$ (Y_1) (time required to release 50% of drug), Rel_{4h} (Y_2) (percentage of the drug release in 4 h) and bio-adhesive strength (Y_3) were considered as set response parameters. The positive effect of the surface response quadratic model demonstrated the change in the already set dependent variables of $t_{50\%}$, Rel_{4h} and bio-adhesive strength. The FT-IR study confirmed the suitability of all the components used in the design of formulation. DSC and XRD study have confirmed the encapsulation of bosentan in the Soluplus® carrier and amorphous form of bosentan, respectively. Overall, 6.832-fold increase in solubility was observed for bosentan-solid dispersion. High-water uptake and swelling of bucco-adhesive tablets (containing bosentan-solid dispersion) was observed due to presence of the highly hydrophilic-Soluplus®. Rel_{4h} was found to be $97.86 \pm 0.57\%$ for optimized formulation (F4) and was decreased with increasing polymer content. The values of $t_{50\%}$ were found to be enhanced from 1.11 to 2.32 h at the lower to higher levels of both the polymers respectively.

✉ Prakash N. Kendre
prakashkendre@gmail.com

¹ Rajarshi Shahu College of Pharmacy, Buldana, Maharashtra 443 001, India

² Modern College of Pharmacy, Nigdi, Pune, India

Graphic abstract



Keywords Bosentan · Solid dispersion · Bucco-adhesive tablet · 32-factorial design · soluplus® · HPMC K100 LV and carbopol 934 P

Introduction

Sometimes inherent characteristics of drug molecules pose the major hurdle in the design and development of formulation. The poor aqueous solubility of the drug compounds is one of the major issues involved during the dosage form development stage [1]. Suitable solubility enhancement techniques can address this poor solubility issue satisfactorily. Bosentan, a dual endothelial receptor antagonist used in the treatment of pulmonary arterial hypertension (PAH). But its poor aqueous solubility makes it out of place to develop the efficient drug delivery system. The present study is an attempt to enhance the solubility of bosentan to develop efficient buccal adhesive drug delivery system. As the buccal route of administration is effective to avoid the first pass hepatic metabolism of the drug, an effective drug delivery system can be designed with maximum drug utilization in the buccal mucosal cavity [2, 3]. This is the most suitable, convenient and easily accessible site for drug delivery. The exposure of drug to the systemic circulation through the internal jugular vein, bypasses the hepatic first-pass metabolism leading to high bioavailability. The buccal route enjoys excellent patient compliance owing to ease of self-administration [4]. The solid dispersion of bosentan was prepared using an amphiphilic graft copolymer, Soluplus® (polyvinyl caprolactam–polyvinyl acetate–polyethylene glycol

graft co-polymer) specially designed and manufactured by BASF Corporation to enhance the solubility of poorly soluble drugs like bosentan. Due to its bifunctional behaviour, it can serve as an excellent matrix to dissolve drugs in aqueous media [5–7]. Initially, bosentan-solid dispersion was prepared successfully followed by the formulation of the bucco-adhesive tablet by optimization technique using central composite designs (CCD) for two factors at three levels [8].

Materials and methods

Materials

Bosentan was received as a gift sample from Dr. Reddy's Laboratories Pvt. Ltd., Hyderabad, India. Soluplus® was provided as a gift sample by BASF Corporation, Mumbai, Maharashtra, India. Polymers, HPMC K4M, HPMC K100M, HPMC K100 M LV, Carbopol 971P and Carbopol 934P were obtained as gift samples from Colorcon Asia Pvt. Ltd., Goa, India. All other excipients and reagents used were of analytical grade and obtained from reputed suppliers in India.

Methods

Preparation of bosentan-solid dispersion

A bosentan-solid dispersion was prepared by solvent evaporation technique. Soluplus® was dissolved completely in ethanol. Bosentan was added slowly to the clear ethanolic drug solution with the continuous stirring till the uniform distribution of bosentan. The ratio of bosentan to Soluplus® was maintained at 1:1, 1:2, 1:3, 1:4 and 1:5 and coded as BSD1, BSD2, BSD3, BSD4 and BSD5, respectively. The ethanol was evaporated completely and resultant mass was dried and grinded to obtain a free-flowing powder, which was passed through a 100 μm sieve. The dried solid dispersion was kept in a desiccator until further use and testing [9].

Fourier transform infrared spectroscopy (FT-IR) study

The interaction between drug and excipients was studied using an FTIR spectrophotometer (Shimadzu, Japan). Spectra were recorded in the range 4000–400 cm^{-1} . All the samples were prepared using the KBr pellet technique, and the spectra were recorded at a resolution of 0.15 cm^{-1} and a scanning speed of 20 scan/s.

Differential scanning calorimetric study (DSC) study

Differential scanning calorimetric (DSC) measurement was performed by a (DSC-60 Shimadzu) thermal analyser. The samples of about 5 mg were hermetically placed in the aluminium-sealed pans and scanned at heating rate of 10 $^{\circ}\text{C}/\text{min}$ over

a temperature range of 0–300 °C by using nitrogen gas as effluent gas. The thermal properties of the pure bosentan and bosentan-solid dispersion were characterized.

X-ray diffraction (XRD) study

The XRD spectra/patterns were recorded (Philips PW3710 analytical X-ray diffractometer at Diya Lab, Mumbai, India) the pure drug and solid dispersion formulation for confirmation of change of basic form of drug (crystalline or amorphous) after formulating in the final dosage form.

Phase solubility study

The Phase solubility study was conducted to predict the effect and trend of Soluplus® to enhance solubility and dissolution of bosentan. Shaking flask method was used to conduct the phase solubility study. An excess amount of the bosentan was added to the solutions at the concentration range of 5%, 10%, 15%, 25%, and 30% w/v Soluplus®. The samples were shaken for 72 h in the mechanical flask shaker at 37 ± 2 °C. The concentration of the bosentan in the solution after equilibration for 72 h was determined using UV spectrophotometer (1650 PC, Shimadzu, Japan) at 272 nm [7].

In order to ensure the favourable concentration of the Soluplus® for solubilization of bosentan, ΔG_{tr}° value was calculated using the following equation:

$$\Delta G_{tr}^{\circ} = 2.303RT \log (S_o/S_s) \quad (1)$$

where, S_o/S_s is the ratio of molar solubility of the bosentan before and after entrapment with Soluplus®. R and T are constant of gas (8.31 JK^{-1}) and temperature (in degree Kelvin) respectively [9].

Solubility study of bosentan-solid dispersion

Prepared solid dispersions (BSD1 to BSD5) were subjected to the solubility study using same method mentioned under the above section of the phase solubility study. Enhancement in the solubility of bosentan-solid dispersion after equilibration for 72 h was determined using the UV spectrophotometer (1650 PC, Shimadzu, Japan) at 272 nm [5].

Preparation of bucco-adhesive tablets

Formulation batch of the solid dispersion with maximum solubility was selected for the further development of the bucco-adhesive tablets using 3^2 -factorial design. Polymers HPMC K4M, HPMC K100LV, HPMC K100M and Carbopol 934P were used to develop bucco-adhesive tablets. Avicel PH102 was used as a diluent in all the formulations. Initially, preliminary batches were performed to select a suitable polymer with the selected range of levels to obtain expected results.

Selection of suitable experimental design

The response surface methodology (RSM) is an effective method for optimizing the bio-adhesive matrix tablet formulation. All factors at all combinations can be studied effectively using a central composite design (CCD). This approach is used most frequently to establish the effects of the individual variables and interactions with very little experimentation [10, 11]. Another advantage of this design is that it allows a quadratic surface response to be established, which is otherwise difficult with a factorial design at two levels. In this study, a CCD for two factors, namely, HPMC K100LV and Carbopol 934P, at three levels with a value of $\alpha=1$, i.e., a 3^2 -factorial, was chosen for the optimization of the bucco-adhesive matrix tablets. This computer-aided study was conducted using Design-Expert® software version 9.0.6.2 (Stat-Ease Inc., Minneapolis, MN, 55,143).

On the basis of the observations from preliminary trials, a combination of the HPMC K100 LV (X_1) and Carbopol 934P (X_2) were selected as independent factors for the optimization of bucco-adhesive matrix tablets. The composition for the development of preliminary batches of the bucco-adhesive tablets is given in Table 1. Dependent variables, $t_{50\%}(Y_1)$, time required to release 50% of drug; $Rel_{4h}(Y_2)$, percentage of the drug release in 4 h and bio-adhesive strength (Y_3) were selected to optimize the final bucco-adhesive tablet formulation using a computer-aided factorial design. The tablets were compressed using the direct compression technique in a single rotary multiple punch machine (Kambert Pvt. Ltd., Ahmedabad, India). Finally, tablets with flat surface with uniform size of 12 mm diameter were compressed as per the compositions of 3^2 factorial design which is mentioned in Table 2.

Evaluation of physical parameters and assay study

All the buccal adhesive tablets were evaluated for physical parameters like weight variation, friability, hardness, thickness and diameter. Ten tablets of each batch were crushed in a mortar to obtain powdered form. Powdered tablets equivalent to 100 mg of pure drug were weighed and transferred to 250-mL volumetric flasks containing methanol. Each flask was sonicated and the contents filtered through 0.45 μ Whatman filter paper. The absorbances were measured at 272 nm using UV-visible spectrophotometer to calculate bosentan content.

Table 1 Composition of bio-adhesive tablets containing bosentan-solid dispersion

Sr. no	Ingredients	Concentration (mg)
1	Bosentan-solid dispersion (BSD) (Equivalent to 62.5 mg of Bosentan)	371.32
2	HPMC K100 LV	25–75
3	Carbopol 934P	10–30
4	Avicel PH 102	Q.S
5	Magnesium stearate	2.5
6	Aerosil (Colloidal silicon dioxide)	2.5

Table 2 Formulation batches as per two-factor, three-level central composite design (CCD) layout translation of coded levels in actual units

Trial no	Formulation code	Coded factor level (mg)	
		X1: HPMC K 100 LV	X2: Carbapol 934 P
1	F1	50	30
2	F2	75	30
3	F3	25	20
4	F4	50	10
5	F5	75	10
6	F6	25	30
7	F7	25	10
8	F8	50	20
9	F9	75	20
Independent variable	Coded levels		
	High (+1)	Medium (0)	Low (-1)
X1: HPMC K 100 LV (mg)	70	50	30
X2: Carbapol 934 P (mg)	30	20	10

In vitro dissolution study

Initially, a dissolution study was conducted for the bosentan-solid dispersion using USP-II dissolution test apparatus (paddle type). Phosphate buffer (pH 6.8), 900 mL was used as the dissolution medium at 37 ± 0.5 °C and 50 rpm. Aliquot samples were withdrawn at the intervals of every 15 min for 2 h, filtered through 0.45 μ Whatman filter paper and absorbances were measured at 272 nm using the UV spectrophotometer [7]. All the sample of dissolution study were analysed in triplicate as mean \pm SD, $n = 3$.

Similarly, the dissolution study was conducted for all the bucco-adhesive tablet formulations prepared according to the 3^2 factorial design. As the anatomy and physiology of buccal cavity differs from the stomach where it consists of very small volume of saliva with very short residence time, this dissolution study includes modified dissolution test apparatus which was described by Hughes et al. [12]. This apparatus consists of single, stirred, continuous flow-through filtration cell which includes a dip tube, specially designed to remove finely divided solid particles. The composition of saliva solution was used as described by Hughes et al. To analyse the dissolved drug, filtered solution was removed continuously. The volume of saliva was maintained up to 10 ml in the cell which was pumped at the rate of 6 ml/min. This facilitates the residence time for saliva solution of approximately 100 s and gives almost complete removal in 8 min. All the sample of dissolution study were analysed in triplicate as mean \pm SD; $n = 3$.

Measurement of bio-adhesive strength Goat mucosa procured from the slaughter's house was used as the model membrane to study the bio-adhesive strength of the tablets. The mucosal membrane was isolated by removing the underlying con-

nective tissue. It was washed with a phosphate buffer (pH 6.8). The apparatus was specially designed for measuring adhesive strength as prescribed in the literature. It was built using a double-beam physical balance [11, 12]. The force required to detach a tablet from the surface of the mucosal membrane was measured in triplicate ($n = 3$) as the mean \pm SD and this force was treated as the bio-adhesive strength.

Determination of swelling and study of gel-forming behaviour The swelling behaviour of the soaked tablets was evaluated over a period of 4 h to check uptake of water. Tablets were weighed accurately and placed in 5 mL of a phosphate buffer (pH 6.8) solution. Tablets were reweighed after every 30 min over the 4-h period and excess of water was removed carefully using filter paper. The swelling index (weight gain) was calculated using the following Eq. (2):

$$\text{Swelling index} = \frac{\text{Wet weight of tablet} - \text{original weight of tablet}}{\text{Original weight of tablet}} \times 100 \quad (2)$$

Similarly, the gel-forming behaviour of the tablets was studied over a period of 4 h. The optimized tablets were soaked in a phosphate buffer (pH 6.8) and the thickness of the gel layer as well as the gel penetration strength was measured. The gel penetration strength under a fixed load of 40 N was determined using a Brookfield CT-3 Texture Analyzer, Brookfield Engineering Ltd. [15, 16].

Mathematical modelling of the drug release data In vitro dissolution study data was analysed using the PCP Disso Software package which has provisions for volume correction, dilution factor adjustment, time interval settings, drug loss due to sampling, etc. The software helped to calculate the amount of drug dissolved as a percent release, rate of drug release and log fraction released at varied time intervals. The kinetic constant (k), the diffusion release exponent (n) and the contributions of Fickian diffusion and polymer relaxation in a swollen matrix were also determined. On the basis of this phenomenological analysis, the type of drug release [Fickian, Non-Fickian (anomalous) or zero-order] was predicted. Time taken for 50% drug release, i.e. $t_{50\%}$ was also calculated in this study. The data were analysed to check best-fit model using different equations [17–20].

Optimization of analysed data For optimization, the response variables considered were the amount of drug released in 4 h $\text{Rel}_{4\text{h}}$ (Y_1), time required to release 50% of drug) $t_{50\%}$ (Y_2) and the bio-adhesive strength (Y_3).

The PCP Disso software was used to calculate the amount of drug released and the kinetic constants. Design-Expert 9.01 software (Stat-Ease, USA) was used to fit a full second-order polynomial equation with added interaction terms to correlate the studied responses $\text{Rel}_{4\text{h}}$ (Y_1), $t_{50\%}$ (Y_2) and bio-adhesive strength (Y_3) with the variables to be examined. All the polynomial regression results were represented as three-dimensional coloured response surfaces and contour graphs. The optimum formulations were confirmed in two stages. First, a feasible space was located; and second, an exhaustive grid search was conducted to predict the possible solutions.

Validation of response surface methodology (RSM) To validate the response surface, few formulations were selected as check points. The tablets were formulated (as described in earlier section of bucco-adhesive tablet preparation) using the optimal composition and evaluated for physical properties, content, dissolution and adhesive strength. The predicted and observed responses were compared, residual graphs plotted and the percent error estimated from the observed responses. Correlation plots were also constructed separately for all the formulations.

Results and discussion

Pre-formulation study

Before design and development of the bucco-adhesive tablets, various analytical tests like FTIR, DSC and XRD were performed to check the suitability of the components for the final formulation.

FTIR spectra of pure bosentan showed major peaks at 3620.15 cm^{-1} , 3369.75 cm^{-1} representing N–H stretching; C–H stretching at 2960.83 cm^{-1} , 2924.18 cm^{-1} , 2758.30 cm^{-1} ; C=O stretching at 1707.06 cm^{-1} ; S=O stretching at 1558.54 cm^{-1} ; N–H out of plane at 1454.38 cm^{-1} ; C–H bend at 1342.50 cm^{-1} , 1251.84 cm^{-1} ; C–N stretching at 1170.83 cm^{-1} , 1112.96 cm^{-1} and N–H, O–H bending at 1020.38 cm^{-1} , 844.85 cm^{-1} . The presence of these spectra is the characteristic for identification of bosentan. The solid dispersion formulation also showed the same type spectra indicating that there was no interaction among the bosentan and Soluplus®. The FT-IR spectra are shown in Fig. 1.

The DSC study was also conducted to check thermal behaviour of the pure bosentan, Soluplus, solid dispersion and physical blend containing the HPMC K100 LV, Carbopol and solid dispersion. The bosentan has shown sharp major endothermic peak at $97.99\text{ }^{\circ}\text{C}$ and short endothermic peak at $116.72\text{ }^{\circ}\text{C}$. The Soluplus® has shown the endothermic peak at $77.43\text{ }^{\circ}\text{C}$. The resultant solid dispersion has shown only the endothermic peak of Soluplus® at $85.26\text{ }^{\circ}\text{C}$ with slightly variation as compared to original peak and showing no change in the glass transition peak. The absence of all thermal peaks of drug in the solid dispersion indicates complete encapsulation of drug in the matrix of Soluplus®. All the observed thermal peaks of plain drug and physical blend containing the HPMC K100 LV, Carbopol and solid dispersion are highlighted in Fig. 2.

The XRD data showed that the sharp highly intense peaks at 2θ values of 15.29° , 16.57° , 18.52° , 22.56° , 20.16° and 77.58° and intensity of 1505.13, 789.25, 754.88, 653.25, 461.25, 402.25, respectively, whereas solid dispersion showed flat peaks showing major peak at 496.35 and other peaks at less than 200. Complete entrapment of bosentan in the Soluplus® carrier is confirmed by the presence of flat peaks. The results of the XRD data are highlighted in Fig. 3.

The phase solubility study was conducted to check the effect and trend of Soluplus® on the solubility and dissolution of the bosentan which is poorly water-soluble drug having maximum solubility of 0.00904 mg/ml only. In the present study, solid dispersion formulation was prepared to increase the solubility of

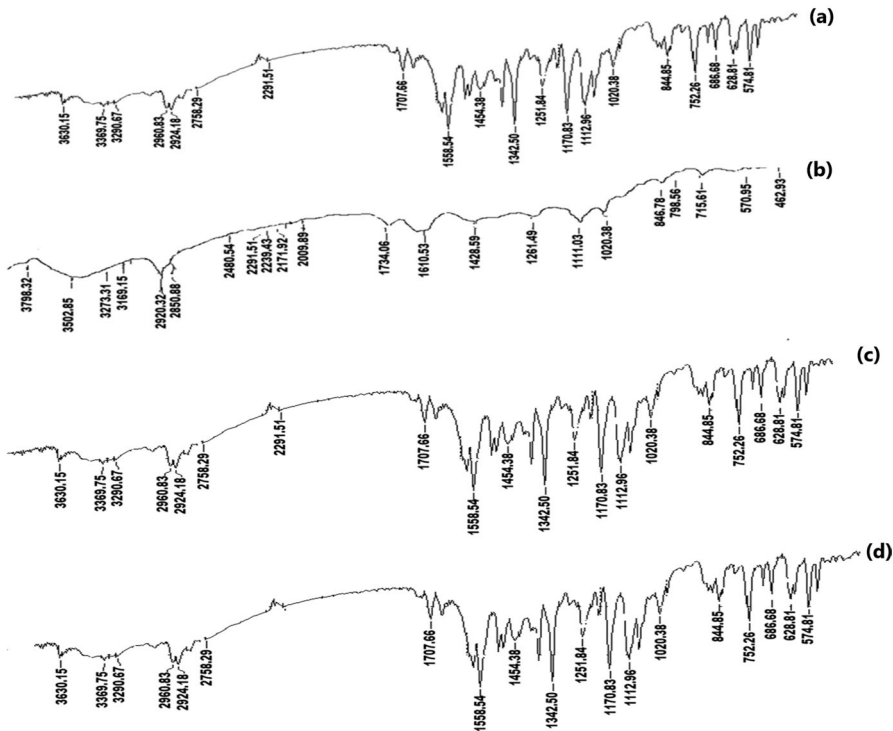


Fig. 1 FT-IR study: Bosentan (a); Soluplus® (b); Bosentan-solid dispersion (c); Physical blend of HPMC K100M LV, Carbopol 934P and Solid dispersion (d)

bosentan. It was found that at 5% concentration of Soluplus®, the water solubility of bosentan increases more than five times. This was mainly due to the micelle solubilisation effect of Soluplus®. The values of Gibb's free energy related with water solubility of bosentan in the presence of Soluplus® are shown in Table 3. More negative values of Gibb's free energy show the higher solubilisation effect which was observed in this at higher concentration of Soluplus®.

For solubility of bosentan-solid dispersion in phosphate buffer (pH 6.8), the significant differences were found as shown in Table 3. The solubility of bosentan was found to be proportional to the concentration of Soluplus®. Maximum solubility of 0.0658 ± 0.021 mg/ml was observed for solid dispersion at 1:5 ratio of bosentan to Soluplus®. Overall, 6.832-fold increase in solubility was observed for solid dispersion as compared to the pure bosentan (plain bosentan) which showed 0.00963 mg/ml of solubility in water [21].

During dissolution study of bosentan-solid dispersion, maximum drug dissolution was observed in two hours, showing $98.78 \pm 1.02\%$ release at highest concentration level of Soluplus® (5%) whereas least release of $88.58 \pm 1.12\%$ was observed at lowest level of Soluplus® (1%). From this study, it is confirmed that the dissolution increases at higher concentration of Soluplus® which is due to the

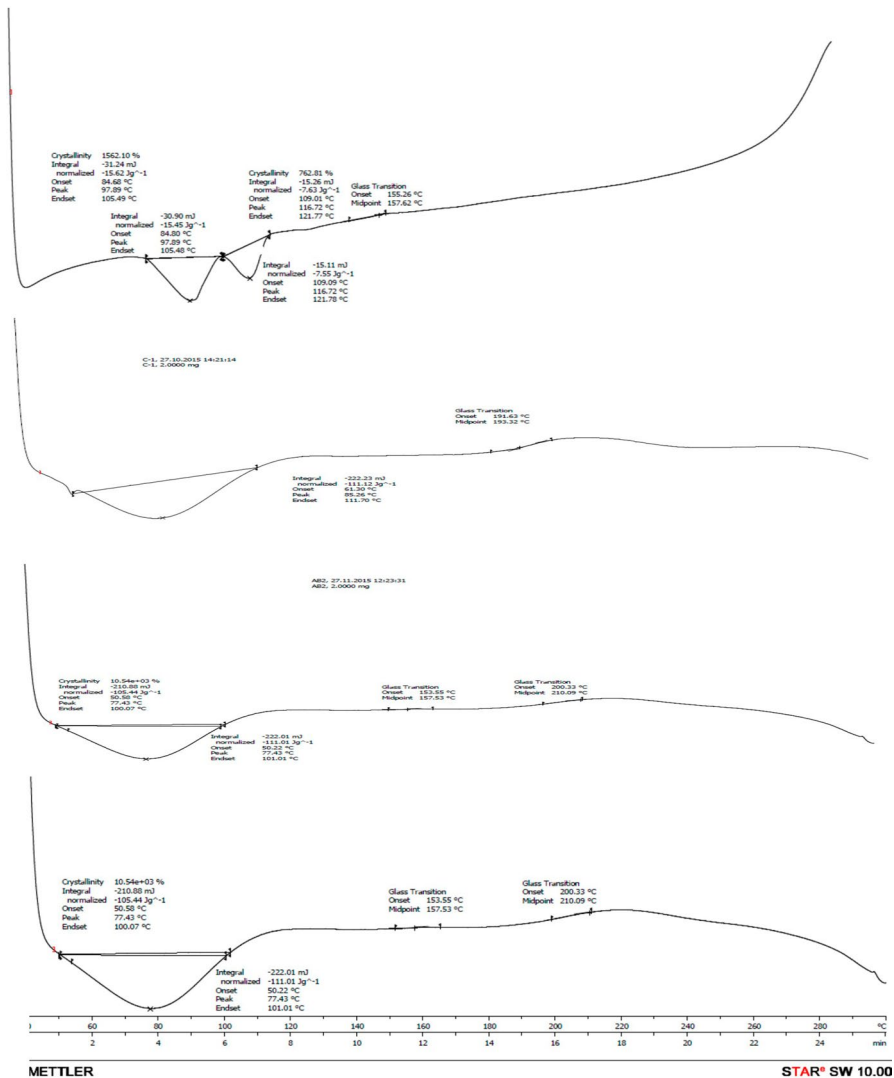


Fig. 2 DSC study: Bosentan (a); Soluplus® (b); Bosentan-solid dispersion (c); Physical blend of HPMC K100M LV, Carbopol 934P and solid dispersion (d)

solubilising and amphiphilic nature of the Soluplus® to dissolve the bosentan in aqueous medium [21]. The drug release profile is shown in Fig. 4.

Pre-optimization considerations and bosentan-solid dispersion-loaded-bucco-adhesive tablets

Many research studies have established reliable values for the bio-adhesive parameters of certain polymers, and these can be screened for use as the bio-adhesive

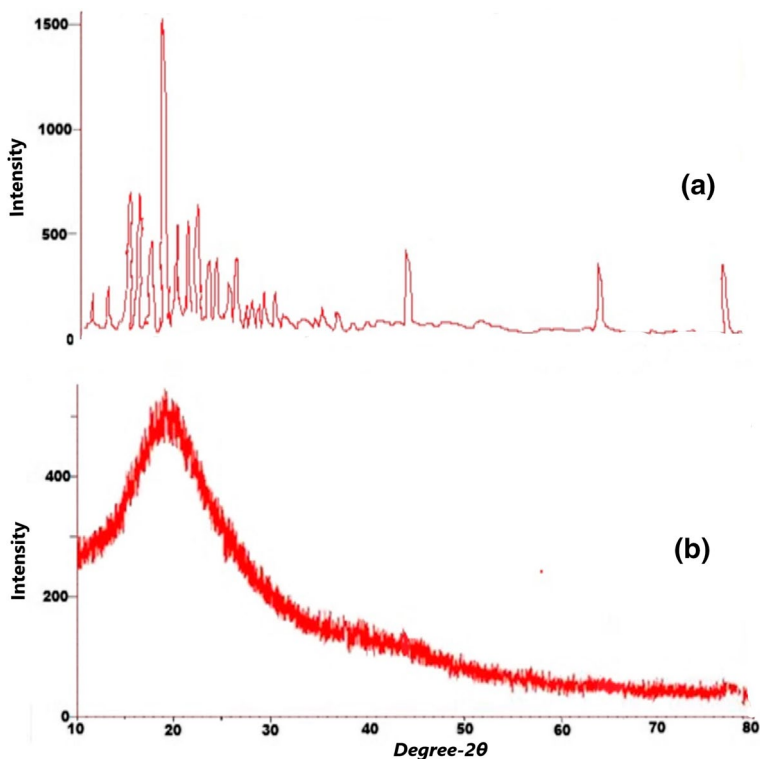


Fig. 3 XRD study: Bosentan (a); Bosentan-solid dispersion (b)

Table 3 Results of phase solubility study and solubility study of solid dispersion

Phase solubility study		Solubility study of solid dispersion	
Conc. of Soluplus® (%)	ΔG°_{tr}	Ratio of Bosentan: Soluplus®	Solubility (mg/ml) Bosentan-Solid Dispersion (BSD)
1	1954.93	1:1	0.0213 ± 0.006
2	1658.25	1:2	0.0321 ± 0.0055
3	-268.58	1:3	0.0405 ± 0.0050
4	-689.64	1:4	0.0515 ± 0.004
5	-1025.25	1:5	0.0658 ± 0.0021
		Observed solubility of plain bosentan = 0.00963 mg/ml	

material. These include Carbopol 934P, sodium carboxymethyl cellulose (highest adhesive force) and other polymers such as poly (methyl vinyl ether-co-maleic anhydride), tragacanth and sodium alginate [22]. The bio-adhesive potential of HPMC has also been investigated by various scientists [23–25].

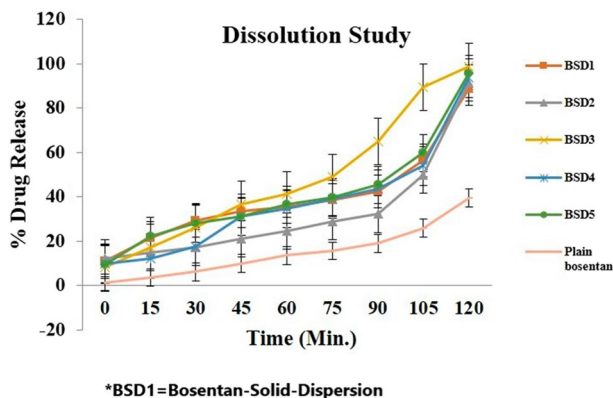


Fig. 4 In vitro dissolution study of bosentan-solid dispersion in phosphate buffer, pH 6.8

Various polymers, including two grades of Carbopol 934P and Carbopol 971P (CP 934P and CP 971P), hydroxypropyl methylcellulose (HPMC K4M, HPMC K100LV) and sodium carboxymethylcellulose (sodium CMC) were selected for the selection of optimized formulation batch depending upon their excellent bio-adhesive strength, release rate-controlling property, non-irritancy, non-toxicity, stability and compatibility with drugs. HPMC and Carbopol are known to have excellent bio-adhesive and drug release rate properties [25, 26].

Initially, drug release parameters of the five polymers were studied by formulating them into matrix tablet forms (drug-to-polymer ratio 1:1) to check the effect of polymer type on the drug-release properties.

The initial dissolution study revealed that the tablets were vulnerable to fragmentation. Hence, in the subsequent investigations, the quantity of polymer in the tablets was increased (drug-to-polymer ratio 1:4). The increased drug-to-polymer ratio yielded excellent results, and hence this ratio was chosen for further work.

As inadequate hydration leads to the dose dumping problem, HPMC K100LV, which shows rapid hydration, was selected for further studies. The use of higher-viscosity grades of HPMC resulted in lower levels of drug release at sub-therapeutic levels. As reported previously, Carbopols have excellent extended drug release and bio-adhesion properties [27, 28]. Hence, on the basis of the preliminary findings, Carbopol 934P was chosen as it is a promising bio-adhesion-regulating polymer. Considering the performances of HPMC K100LV and Carbopol 934P, a combination of these polymers was selected for formulation development [29–32]. The use of combinations of Carbopol and HPMC has been reported extensively in the scientific literature [33–35]. It has been reported that, the use of water-insoluble fillers in large amounts can markedly decrease the release rates of drugs [36]. Hence, the use of fillers, such as microcrystalline cellulose, lactose anhydrous or di-calcium phosphate can help to achieve controlled release.

Microcrystalline cellulose (Avicel PH 102) was selected as a diluent, and colloidal silicon dioxide and magnesium stearate were selected for improving the flow properties of the materials during compression.

Evaluation of physical parameters

The evaluation of the compressed matrices suggests that all the physical parameters were practically within the acceptable limits according to the Pharmacopoeia standards. The tablet weight varied between 546 and 555 mg, thickness between 3.42 and 3.54 mm, and hardness between 5.2 and 6.5 kg/cm². The bosentan content varied between 93.48% and 99.15%, and the friability ranged between 0.15% and 0.55%. All the observed values are presented in Table 4.

Effect of polymer combination on in vitro drug release

The response surface methodology (RSM) is an effective tool for optimizing the bio-adhesive matrix tablet formulation. All factors at all combinations can be studied effectively using a central composite design (CCD). This approach is used most frequently to establish the effects of individual variables and interactions with very little experimentation [10, 11].

All the formulations showed surface erosion, diffusion and polymer relaxation mechanisms. For matrix systems, a value of the exponent ' n ' of 0.45 indicates that the drug release is diffusion controlled, and a value of 0.89 indicates that the drug release is swelling controlled. Values of ' n ' between 0.45 and 0.89 can be considered to indicate both phenomena (anomalous transport). If the release is controlled by more than one process, such as by both diffusion and erosion, then the value of ' n ' will fall in a different range, with contributions from both phenomena [17–20]. Surface erosion was observed due to the adhesive property of the polymers [36]. The values of the exponent n varied between 0.4412 and 0.5964 shown in Table 5, indicates Non-Fickian release behaviour. The exponent n increases with increasing HPMC and Carbopol levels shows linear relationship. These observations seem to be in agreement with the results of Nokhodchi et al. [37]. The viscosity of the HPMC and Carbopol blend increased due to reduced hydration (in this case, due to increase in the concentration and combination of both the polymer, pores on the surface of tablet blocks quickly which prevents further

Table 4 Evaluation physical parameters of buccal bio-adhesive tablets

Formula-tion code	Weight (mg)	Hardness (kg/cm ²)	Diameter (mm)	Thickness (mm)	Friability (%)	Drug content (%)
F1	553 ± 1.27	5.4 ± 0.22	12 ± 0.01	3.52 ± 0.04	0.15 ± 0.01	98.45 ± 1.01
F2	554 ± 1.45	6.5 ± 0.15	12 ± 0.03	3.44 ± 0.01	0.55 ± 0.02	94.45 ± 1.03
F3	546 ± 1.87	5.8 ± 0.21	12 ± 0.01	3.44 ± 0.02	0.47 ± 0.01	95.47 ± 1.31
F4	553 ± 1.42	5.3 ± 0.61	12 ± 0.05	3.42 ± 0.01	0.18 ± 0.01	99.15 ± 1.09
F5	555 ± 1.25	5.5 ± 0.44	12 ± 0.01	3.53 ± 0.01	0.55 ± 0.02	98.88 ± 1.23
F6	554 ± 1.58	6.4 ± 0.18	12 ± 0.03	3.54 ± 0.01	0.45 ± 0.03	95.89 ± 1.31
F7	546 ± 1.58	6.3 ± 0.55	12 ± 0.04	3.52 ± 0.09	0.48 ± 0.02	95.17 ± 1.21
F8	553 ± 2.18	6.1 ± 0.47	12 ± 0.02	3.50 ± 0.01	0.52 ± 0.03	93.48 ± 1.36
F9	550 ± 1.28	5.2 ± 0.77	12 ± 0.02	3.52 ± 0.01	0.16 ± 0.01	96.78 ± 1.33

*All the values are calculated as ± SD; $n = 3$

Optimization of formulation

Mathematical relationships were developed for the response variables studied. These are presented in Eqs. (3), (4) and (5). Under analysis of variance (ANOVA), all the equations were found to be statistically significant ($p < 0.001$).

$$Rel_{4h}(Y_1) = 91.75 - 9.92X_1 - 5.08X_2 - 2.09X_1X_2 - 1.14X_1^2 - 1.14X_2^2 \quad (3)$$

$$t_{50\%}(Y_2) = 1.30 + 0.29X_1 + 0.17X_2 + 0.19X_1X_2 + 0.34X_1^2 + 0.13X_2^2 \quad (4)$$

$$\text{Bio-adhesive strength } (Y_3) = 8.71 + 2.83X_1 + 3.50X_2 + 0.92X_1X_2 - 0.25X_1^2 + 1.08X_2^2 \quad (5)$$

The standard error of the implemented design is represented in the contour plot and response surface plot shown in Fig. 6. ANOVA of the response surface model statistics for the responses of Rel_{4h} suggested a linear model, showing a p value of < 0.0001 , an adjusted R^2 value of 0.9465 and a predicted R -squared value of 0.8836.

The contour and response surface plots have shown the effects of the two polymers (HPMC K100LV and Carbopol 934P) on the drug release for 4 h (Rel_{4h} , Y_1) study. The drug release decreases at higher levels, whereas it increases at lower levels of HPMC and Carbopol (in this case batch F2 and F7 respectively).

ANOVA of the response surface model statistics related to the responses of $t_{50\%}$ suggested a linear model with a p value of < 0.0001 , an adjusted R -squared value of 0.3213 and a predicted R -squared value of -0.1052 .

The contour and response surface plots show the effects of the two polymers on the time required for release of 50% of the drug ($t_{50\%}$, Y_2). Here also time required for 50% of drug release increases with increased levels of both the polymers, Fig. 7.

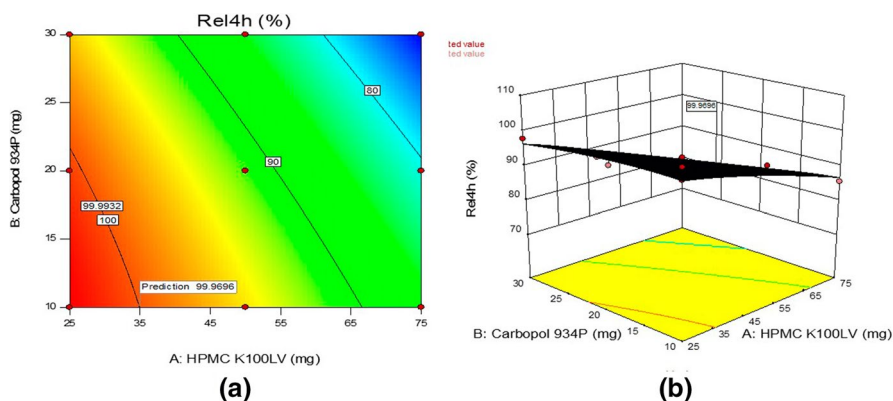


Fig. 6 Evaluation of set response parameter Rel_{4h} (Y_1) in the form of Contour plot (a) and Surface response plot (b)

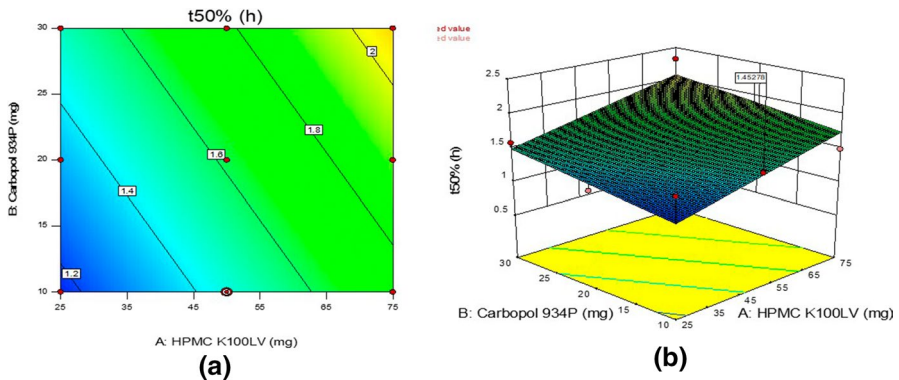


Fig. 7 Evaluation of set response parameter $t_{50\%}$ (Y_2) in the form of Contour plot (a) and Surface response plot (b)

ANOVA of the response surface model statistics related to the responses of the bio-adhesive strength (Y_3) suggests a linear model, with a p value of < 0.0001 , an adjusted R -squared value of 0.8343 and a predicted R -squared value of 0.6936.

The contour and response surface plots show the effects of the two polymers on the bio-adhesive strength (Y_3) of the tablets. Bio-adhesive strength increases with increased levels of both the polymers with major contribution of Carbopol which has higher bio-adhesion property [22].

The contour, response surface plots showing the effects of these two polymers on bio-adhesive strength (Y_3) for all the nine batches as per factorial design are highlighted in Fig. 8.

Values for all the response parameters Rel_{4h} , $t_{50\%}$ and the bio-adhesive strength predicted by the software were closely in agreement with the values obtained for experimentally designed formulations. The Formulation F4 has shown very closed values for all the response parameters and hence considered as optimized

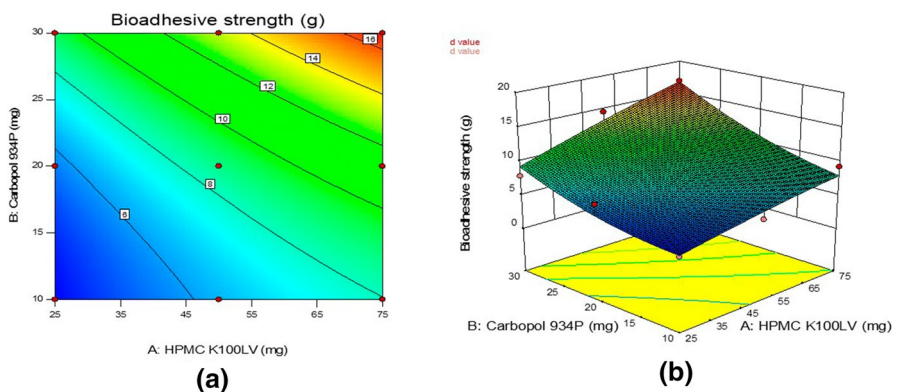


Fig. 8 Evaluation of set response parameter bio-adhesive strength (Y_3) in the form of Contour plot (a) and Surface response plot (b)

formulation in this case. Figure 9 shows overlay plot and plot of predicted Versus actual values for all the set response parameters (Y_1, Y_2 and Y_3).

Effect of Soluplus® on tablet swelling and gel penetration study

A swelling study was conducted for optimized bucco-adhesive tablet formulation (F4) over a period of 4 h as depicted in Fig. 10a. The bucco-adhesive tablet formulation with plain bositentan was also evaluated for this study (shown in dotted line, Fig. 4). The swelling was faster in tablets with higher concentrations of HPMC K100LV and was much greater than tablet formulation containing plain bositentan. This may be again due to the presence of Soluplus® in optimized tablet (F4) which is more hydrophilic in nature and immediately solubilises in the presence of dissolution medium, supporting the swelling of polymers. Although the amount of the polymers used were same to that of optimized tablet formulation. The maximum swelling was attained in the first 2 h, after which the polymer started eroding slowly in the dissolution medium. The high-water uptake may be due to quick hydration of

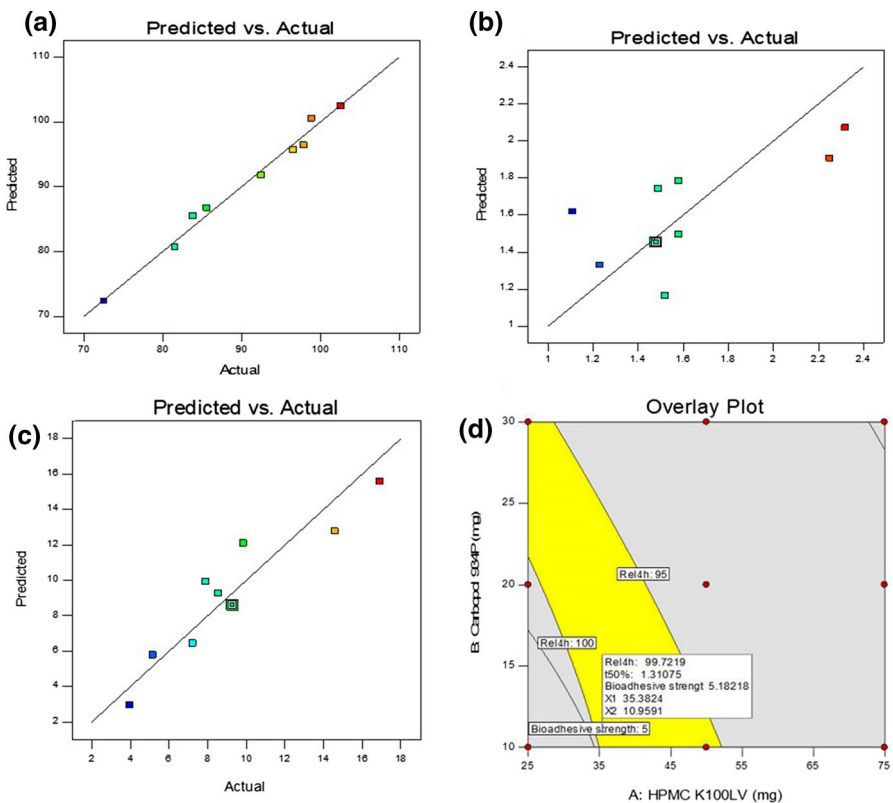


Fig. 9 Effect of HPMC K100M LV and Carbopol 934P on Rel_{4h} (Y_1), $t_{50\%}$ (Y_2) and bio-adhesive strength (Y_3) in the form of predicted Versus actual responses (a) and Overlay plot (b)

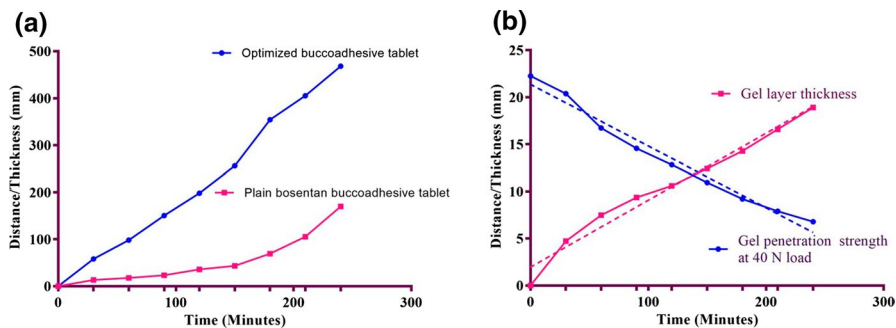


Fig. 10 Swelling index (a) and gel forming behaviour study (b) of optimized bucco-adhesive tablet formulation (F4) and plain bosentan tablet (without Soluplus®)

HPMC K100LV as the swelling rate of the tablets increases with increasing concentration of HPMC K100 LV in the tablets [39, 40].

The gel layer thickness of the optimized formulation F4 increased over the 4-h study. A gel penetration study was conducted similarly, to determine the maximum gel strength of the tablets after swelling in a dissolution medium. It was observed that at a fixed load (40 N in this case); the strength of the gel was higher at the beginning but decreases as time passes. This may be due to the fact that the gel becomes less viscous with time due to the accumulation of the aqueous medium. The presence of Soluplus® enabled the bosentan to solubilise quickly which further was entrapped in the viscous gel layer for prolonged release over the 4-h period of time. Formulation with plain bosentan had much higher gel strength but less gel layer thickness as compared to the optimized formulation (F4, containing Soluplus®). The results of the gel layer thickness study and the gel penetration study are shown in Fig. 10b.

Stability study of optimized bucco-adhesive tablet formulation

No significant changes were observed in the tablet friability, drug content and adhesive strength of the optimized bio-adhesive tablets after 6 months. A slight increase in hardness was observed due to an uptake of water by the hydrophilic components (HPMC K 100LV and Carbopol 934P) in the tablet at a relative humidity of 75%. No significant changes were noted for the properties of the bio-adhesive tablets in the stability study. All the observations of the study are highlighted in Table 6.

Conclusion

Bosentan is one of the important lives saving drugs used in the management of Pulmonary Arterial Hypertension (PAH). In the present study, efforts were made to enhance the solubility of the bosentan and develop bucco-adhesive tablets. From this study, it was concluded that the bucco-adhesive tablet formulation containing

Table 6 Evaluation physical parameters of buccal bio-adhesive tablets after stability study

Formulation code	*Weight (mg)	*Hardness (kg/cm ²)	*Diameter (mm)	*Thickness (mm)	Friability (%)	Drug content (%)
F1	562.00 ± 1.21	5.50 ± 0.45	12 ± 0.02	3.56 ± 0.03	0.11	97.99
F2	564.14 ± 1.54	6.79 ± 0.13	12 ± 0.03	3.57 ± 0.022	0.12	95.55
F3	547.00 ± 1.68	6.10 ± 0.12	12 ± 0.02	3.48 ± 0.03	0.16	96.58
F4	555.54 ± 1.25	5.50 ± 0.48	12 ± 0.02	3.52 ± 0.02	0.13	98.24
F5	558.10 ± 1.11	5.80 ± 0.63	12 ± 0.02	3.58 ± 0.02	0.17	99.87
F6	559.85 ± 1.48	6.70 ± 0.47	12 ± 0.03	3.59 ± 0.02	0.22	96.68
F7	554.12 ± 1.35	6.80 ± 0.57	12 ± 0.04	3.56 ± 0.05	0.35	94.57
F8	543.45 ± 2.78	6.50 ± 0.95	12 ± 0.02	3.52 ± 0.03	0.27	92.46
F9	560.85 ± 1.56	5.45 ± 0.58	12 ± 0.01	3.56 ± 0.01	0.12	95.94

* All the values are calculated as ±SD; n = 3

bosentan-solid dispersion may be better option to avoid first-pass-hepatic-metabolism and acid-degradation of the drug in gastrointestinal tract with enhanced solubility and efficient delivery in the oral mucosal region.

Acknowledgements The authors are very thankful to Dr. Reddy's Laboratories Pvt. Ltd., Hyderabad, India for providing a gift sample of bosentan. They are also thankful to Colorcon Asia Ltd., India for providing a sample of HPMC. The authors are happy to acknowledge BASF Corporation Ltd., India for providing a gift sample of Soluplus®. Authors are grateful to Mr. Anant Ketkar, Mr. Vinay Patil and Dr. A. R. Paradkar, Poona College of Pharmacy, Pune for providing the assistance of PCP Disso Software. They are also thankful to the Management and the Principal, Rajarshi Shahu College of Pharmacy, Buldana, India for their consistent support and motivation.

Compliance with ethical standards

Conflict of interest The authors declare that they have no conflict of interest.

References

1. Lipinski CA, Lombardo F, Dominy BW (2002) Poor aqueous solubility-an industry wide problem in drug discovery. *Am Pharm Rev* 5(3):82–85
2. Tiwari BD, Shikare OM, Sontakke AM (2014) Bioequivalence study: an overview. *JPharm Sci Innv* 3(5):421–425
3. Vargas M, Bustamante C, Villarraga EA (2015) Fed and fasting bioequivalence study for two formulations of bosentan 125 mg tablets in healthy Colombian people. *J BioequivAvailab* 7:210–215. <https://doi.org/10.4172/jbb.1000242>
4. Voorspoels J, Remon JP, Eechaute W et al (1996) Buccal absorption of testosterone and its esters using a bioadhesive tablet in dogs. *Pharm Res* 13:1228–1232
5. Sandeep Patnaik LA, Avinash Chunduri M, Akilesh Sai et al (2016) Enhanced dissolution characteristics of piroxicam-Soluplus® nanosuspensions. *J Exp Nanosci* 11(12):916–929. <https://doi.org/10.1080/17458080.2016.1178402>
6. Kendre PN, Chaudhari PD (2017) Effect of polyvinyl caprolactam-polyvinyl acetate-polyethylene glycol graft copolymer on bioadhesion and release rate property of eplerenone pellets. *Drug Dev Ind Pharm* 43(5):751–761
7. Karathanos V, Mourtzinos I, Yannakopoulou K (2007) Study of the solubility, antioxidant activity and structure of inclusion complex of vanillin with cyclodextrin. *Food Chem* 101:652–658
8. Kendre PN, Chaudhari PD (2017) Effect of amphiphilic graft co-polymer-carrier on physical stability of bosentan nanocomposite: assessment of solubility, dissolution and bioavailability. *Eur J Pharm Biopharm.* <https://doi.org/10.1016/j.ejpb.2017.06.024>
9. Van den Mooter G, Augustijns P, Bleton N et al (1998) Physico-chemical characterization of solid dispersions of temazepam with polyethylene glycol 6000 and PVP K30. *Int J Pharm* 164:67–80
10. Ahuja N, Katare OP, Singh B (2007) Studies on dissolution enhancement and mathematical modeling of drug release of a poorly water-soluble drug using water-soluble carriers. *Eur J Pharm Biopharm* 65:26–38
11. Doornbos CA, Haan PD (1995) Optimization techniques in formulation and processing. In: Swarbrick J, Boylan JC (eds) *Encyclopaedia of pharmaceutical technology*. Marcel Dekker, New York, pp 77–160
12. Hughes L, Gehris A (2002) A new method of characterizing buccal dissolution of drugs: Rohm and Haas Research laboratory spring house. PA, USA
13. Singh B, Ahuja N (2002) Development of controlled-release buccoadhesive hydrophilic matrices of diltiazem hydrochloride: optimization of bioadhesion, dissolution and diffusion parameters. *Drug Dev Ind Pharm* 28:433–444
14. Yang L, Johnson B, Fassih R (1998) Determination of continuous changes in the gel layer thickness of poly (ethylene oxide) and HPMC tablets undergoing hydration: a texture analysis study. *Pharm Res* 15:1902–1906
15. Swain S, Behera A, Dinda SC et al (2014) Formulation design, optimization and pharmacodynamic evaluation of sustained release mucoadhesive microcapsules of venlafaxine HCl. *Indian J Pharm Sci* 76(4):354–363

16. Giovagnoli SP, Balsi MR, Schoubben LP et al (2008) Physicochemical characterization and release mechanism of a novel prednisone biodegradable microspheres formulation. *J Pharm Sci* 97(1):303–317
17. Gupta PK, Robinson JR (1992) Oral controlled-release delivery. In: Kydonieus A (ed) *Treatise on controlled drug delivery*. Marcel Dekker, New Jersey, pp 255–310
18. Grassi M, Grassi G (2005) Mathematical modelling and controlled drug delivery: matrix systems. *Current Drug Deliv* 1:97–116
19. Dash S, Murthy PN, Nath L et al (2010) Kinetic modelling on drug release from controlled drug delivery systems. *Acta Poloniae Pharmaceutica* 67(3):217–223
20. Smart JD, Kellaway IW, Worthington HEC (1984) An in vitro investigation of mucosa-adhesive materials for use in controlled drug delivery. *J Pharm Pharmacol* 36:295–299
21. Lian X, Dong J, Zhang J et al (2014) Soluplus® based 9-nitrocamptothecin solid dispersion for peroral administration: preparation, characterization, in vitro and in vivo evaluation. *Int J Pharm* 477:399–407
22. Mortazavi SA, Smart JD (1995) An investigation of some factors influencing the in vitro assessment of mucoadhesion. *Int J Pharm* 116:223–230
23. Ranga Rao KV, Buri P (1989) A novel in situ method to test polymer and coated microspheres for bioadhesion. *Int J Pharm* 52:265–270
24. Nafee NA, Ismail FA, Boraie NA et al (2004) Mucoadhesive delivery systems. Evaluation of mucoadhesive polymers for buccal tablet formulation. *Drug Dev Ind Pharm* 30(9):985–993
25. Li S, Lin S, Daggy BP et al (2003) Effect of HPMC and Carbopol on the release and floating properties of gastric floating drug delivery system using factorial design. *Int J Pharm* 253:13–22
26. Vasir JK, Tambwekar K, Garg S (2003) Bioadhesive microspheres as a controlled drug delivery system. *Int J Pharm* 255(1–2):13–32
27. Andrews GP, Laverty TP, Jones DS (2009) Mucoadhesive polymeric platforms for controlled drug delivery. *Eur J Pharm Biopharm* 71:505–518
28. Nur AO, Zhang JS (2000) Recent progress in sustained/controlled oral delivery of captopril: an overview. *Int J Pharm* 194:139–146
29. Vjera G, Davide G, Andrews N (2005) Comparison of mucoadhesive properties of various polymers. *Adv Drug Deliv Rev* 57:1713–1723
30. Prudat-Christiaens C, Arnaud P, Allain P et al (1996) Aminophylline bio adhesive tablets attempted by wet granulation. *Int J Pharm* 141:109–116
31. Agarwal V, Mishra B (1999) Design development and biopharmaceutical properties of buccoadhesive compacts of pentazocin. *Drug Dev Ind Pharm* 25:701–709
32. Chitnis VS, Malshe VS, Lalla JK (1991) Bioadhesive polymers-synthesis, evaluation and application in controlled release tablets. *Drug Dev Ind Pharm* 17:879–892
33. Furlanetto S, Cirri M, Maestrelli F et al (2006) Study of formulation variables influencing the drug release rate from matrix tablets by experimental design. *Eur J Pharm Biopharm* 62:77–84
34. Prajapati ST, Patel LD, Patel DM (2008) Gastric floating matrix tablets: design and optimization using combination of polymers. *Acta Pharm* 58(2):221–229. <https://doi.org/10.2478/v10007-008-0006-3>
35. Doelker E (1987) Water-swollen derivatives in pharmacy. In: Peppas NA (ed) *Hydrogels in medicine and pharmacy*. CRS Press Inc., Florida, pp 115–160
36. Von Burkersroda F, Schedl L, Gopferich A (2002) Why degradable polymers undergo surface erosion or bulk erosion. *Biomaterials* 23(21):4221–4231
37. Nokhodchi A, Farid DJ, Najafi M et al (1997) Studies on controlled release formulation of diclofenac sodium. *Drug Dev Ind Pharm* 23:1019–1022
38. Perez-Marcos FB, Armstrong JL (1994) Release of propranolol hydrochloride from matrix tablets containing hydroxyl propyl methyl cellulose K4M and Carbopol 974. *Int J Pharm* 111:251–259
39. Colombo P, Bettini R, Santi P et al (2000) Swellable matrices for controlled drug delivery: gel-layer behaviour, mechanisms and optimal performance. *Pharm Sci Tech Today* 3(6):198–204
40. Siepmann J, Kranz H, Bodmeier R et al (1999) HPMC-matrices for controlled drug delivery: a new model combining diffusion, swelling, and dissolution mechanisms and predicting the release kinetics. *Pharm Res* 16(11):1748–1756



Design, fabrication, and characterization of graft co-polymer assisted ocular insert: a state of art in reducing post-operative pain

Prakash N. Kendre , Pooja D. Kadam , Shirish P. Jain , Somnath K. Vibhute & Ajinkya K. Pote

To cite this article: Prakash N. Kendre , Pooja D. Kadam , Shirish P. Jain , Somnath K. Vibhute & Ajinkya K. Pote (2020): Design, fabrication, and characterization of graft co-polymer assisted ocular insert: a state of art in reducing post-operative pain, Drug Development and Industrial Pharmacy, DOI: [10.1080/03639045.2020.1833908](https://doi.org/10.1080/03639045.2020.1833908)

To link to this article: <https://doi.org/10.1080/03639045.2020.1833908>



Published online: 15 Oct 2020.



Submit your article to this journal [↗](#)



Article views: 5



View related articles [↗](#)



View Crossmark data [↗](#)

RESEARCH ARTICLE



Design, fabrication, and characterization of graft co-polymer assisted ocular insert: a state of art in reducing post-operative pain

Prakash N. Kendre^a, Pooja D. Kadam^b, Shirish P. Jain^c, Somnath K. Vibhute^a and Ajinkya K. Pote^a

^aDepartment of Pharmaceutics, Rajarshi Shahu College of Pharmacy, Buldana, India; ^bDepartment of Pharmaceutics, Sanjivani College of Pharmaceutical Education & Research, Kopargaon, India; ^cRajarshi Shahu College of Pharmacy, Buldana, India

ABSTRACT

Purpose: Targeted delivery of drugs at appropriate concentrations to ocular tissues is required to avoid wastage. Hence, advanced systems that maximize the release of poorly soluble drugs and deliver them at ocular sites must be designed.

Methods: In this study, Soluplus[®] (polyvinyl caprolactam–polyvinyl acetate–polyethylene glycol–graft copolymer) was selected as a solubilizer as well as film former for preparing ocular inserts and polyethylene glycol 400 (PEG-400) as a plasticizer. On the basis of an initial phase solubility study, the maximum concentration of Soluplus[®] possible was used for developing the inserts. An optimized formulation was obtained using a 3²-factorial design. Two factors at three levels were used to design the ocular inserts. Soluplus[®] (X_1) and the plasticizer, PEG-400 (X_2), were set as the independent variables at various levels, and the Rel_{4h} (drug release in 4 h, Y_1) and tensile strength (Y_2) were set as the dependent variables. A pre-formulation study was conducted to select suitable materials.

Results: Various physico-chemical parameters of the optimized formulation, including the tensile strength and folding endurance, were studied using FT-IR, DSC, XRD, and SEM. An *in vitro* dissolution study was conducted to determine the amount of drug released. There was no redness, swelling, or watering of the rabbit eye.

Conclusion: It was concluded that the ocular inserts of the poorly soluble nepafenac developed using a graft-co-polymer enhanced the solubility and utilization of the drug for a prolonged period.

ARTICLE HISTORY

Received 5 May 2020
Revised 22 August 2020
Accepted 1 October 2020

KEYWORDS

Ocular insert; ophthalmic drug delivery; Nepafenac; graft-co-polymer; Soluplus[®]

Introduction

In designing a formulation, the issues of absorption, distribution, metabolism, and elimination must be considered. When it comes to the delivery of pharmaceuticals, the eye offers unique opportunities and challenges. Though the absorption by this route is incompetent, there are few side effects with conventional ocular dosage forms. Most ocular formulations such as eye drops and suspensions are used to administer active drugs topically on the tissues around the ocular cavity. These dosage forms are easy to administer but suffer from inherent drawbacks. Ocular drug delivery is generally used to treat eye diseases. But problem of rapid and extensive elimination of conventional eye drops from the eye have been noticed here which lead to extensive loss of drug. Less amount of drug penetrates the corneal layer and reaches the internal tissue of eye. Drug loss occurs at lachrymal drainage and then drug dilution by tears. Hence, ocular bioavailability is reduced which leads to unwanted toxicity and side effect. Eye is a portal for drug delivery which is generally used for local therapy instead of systemic therapy. Due to high blood concentration of drug, there is risk of eye damage which can be overcome by local therapy [1,2]. Traditional topical formulations are highly concentrated, and corneal drug absorption with these formulations is low. There are ocular and systemic side effects because the pre-corneal residence time of eye drops is low [3]. Frequent administration of concentrated solutions is required to achieve the therapeutic effect. This results in the short residence of high drug

concentrations in the tear film, followed by long periods of under-dosing [4–6]. This leads to poor patient compliance. Several approaches have been adopted to overcome these issues. The use of various ophthalmic vehicles, such as suspensions, ointments, inserts, and aqueous gels, has been investigated to extend the ocular residence time of topically applied medications [7–9].

Sterile preparations with a solid or semisolid consistency, and of sizes and shapes designed for ophthalmic application, are generally known as ophthalmic inserts. These inserts are placed in the lower fornix and, sometimes, on the cornea or in the upper fornix. An ophthalmic insert is a polymeric vehicle consisting of the drug and is mainly used for topical therapy [10]. Increased ocular residence, the possibility of releasing drugs at a slow and constant rate, accurate dosing, exclusion of preservatives and increased shelf life are the prime advantages offered by ophthalmic inserts over conventional dosage forms [8–16]. Many of the such topical eye inserts are designed using polymeric components offering continuous release of drug without loss due to drainage and reducing the frequent administration [17].

The reduction of systemic absorption, which occurs freely with eye drops, is achieved with the use of these devices. Patient compliance is improved because of the lower frequency of administration and lower incidence of side effects [18–20]. The difficult problem of limited precorneal drug residence time is overcome by the use of ocular inserts [21,22]. The prime objective of using ophthalmic inserts is to increase the time of contact between the

preparation and the conjunctival tissue to ensure sustained release appropriate for topical or systemic treatment. Ophthalmic inserts consist of polymeric supports with or without drugs, the latter being incorporated as dispersions or solutions in the polymeric supports [23].

There are many polymers and film forming materials used in the design and development of ophthalmic inserts or oral dissolving films. Choice of selection of such materials is based on their physico-chemical properties and compatibility with the drug to be used for delivery. Many synthetically modified polymers and materials are available and many of the researchers have used for the development of various drug delivery systems. Polymers like: polyvinyl alcohol, polyamides, polysulfonates, cellulose acetates hydroxypropyl methyl cellulose, and modified graft-co-polymers like: Soluplus[®] (polyvinyl caprolactam–polyvinyl acetate–polyethylene glycol–graft copolymer), polyethylene oxide acrylates, polyvinyl alcohol-g-poly (oxyethylene methacrylate) PVA-g-POEM, Kollicoat[®] IR, Kollicoat[®] VA64, etc.

Soluplus[®] (polyvinyl caprolactam–polyvinyl acetate–polyethylene glycol–graft copolymer) is one of the graft-copolymers used by many researchers for the development of various drug delivery systems. It is an amphiphilic graft-copolymer which enables the enhancement of solubility and bioavailability of poor soluble drugs. Soluplus[®] can be processed as solid solutions using hot-melt-extrusion or other techniques [24–28].

However, considering the constraints of eye physiology, very few anti-inflammatory drugs show suitability to formulate the appropriate drug delivery system for the management of ocular inflammations [29].

Nepafenac is a non-steroidal anti-inflammatory prodrug (NSAID) that is usually sold as prescription eye drops. It is used to treat the pain and inflammation associated with cataract surgery [30]. It has several advantages over other ophthalmic NSAIDs. First, it has a unique prodrug structure. Prodrugs are the inactive forms of drugs that get converted into active forms after metabolic conversion in the body [29]. Nepafenac rapidly penetrates the cornea. After nepafenac penetrates the cornea, it is deaminated by intraocular hydrolases to amfenac [(2-amino-3-benzoyl phenyl) acetate], a potent inhibitor of COX-1 and COX-2 [31].

The aim of the present study was to enhance the solubility of nepafenac using the novel polymer Soluplus[®] and to formulate and evaluate nepafenac ocular inserts using a 3²-factorial design.

Materials and methods

Materials

Soluplus[®] (polyvinyl caprolactam–polyvinyl acetate–polyethylene glycol–graft copolymer) was obtained from BASF (Mumbai, India). Polyethylene glycol 400 (PEG-400) and dichloromethane were procured from Loba Chemie (Mumbai, India). All the materials used in this study were of analytical grade.

Methods

Preparation of nepafenac ocular insert

Ocular inserts of nepafenac were prepared using the solvent casting method. Soluplus[®] (polyvinyl caprolactam–polyvinyl acetate–polyethylene glycol–graft copolymer) was used as a solubility enhancer and film former, PEG-400 was used as a plasticizer to produce inserts of uniform strength, and dichloromethane was used as a solvent. Two factors at three levels were used to design the ocular inserts. Soluplus[®] (X_1) and the plasticizer, PEG-400 (X_2),

Table 1. Concentration levels and its translation of components used in the design of ocular formulation.

Independent variable	Levels		
	High (+1)	Medium (0)	Low (–1)
X_1 : Soluplus [®] (% w/w)	70	50	30
X_2 : PEG-400 (% w/v)	30	20	10

Measurable responses: Y_1 =Rel_{4h} (%); Y_2 =tensile strength (N/cm²).

Table 2. Composition of ocular insert batches as per 3²-factorial design.

Batch no.	Soluplus [®] (X_1) (% w/w)	PEG-400 (X_2) (%w/v)
F1	50	30
F2	50	20
F3	30	30
F4	30	10
F5	70	20
F6	70	30
F7	50	10
F8	70	10
F9	30	20

were considered as independent variables at various levels, and the drug release 4 h (Y_1) and tensile strength (Y_2) were considered as dependent variables (Table 1).

The concentration of nepafenac was maintained constant (1% w/w) in all the formulations. The compositions of the ocular inserts of the nine runs of the 3²-factorial design are listed in Table 2.

The required amount of Soluplus[®] was dissolved in a beaker in the required quantity of dichloromethane and stirred until it was completely dissolved. Polyethylene glycol 400 was added to the solution with stirring. A weighed amount of drug was added to this solution, which was stirred for 2 h to obtain a uniform dispersion. The polymer solution was finally sonicated to eliminate air bubbles. The casting solution was mixed and poured on a clean glass of film former (VJ Instruments, Karanja Lad, India) using a spreader. The spreader produces uniform films. The dichloromethane is evaporated by adjusting its temperature controller knob. The dried thin films thus obtained were cut to the required size (5 × 5 mm²) using a sharp cutter and ruler. They were wrapped in aluminum foil and stored in an airtight container (desiccator) [32,33].

Pre-formulation study

Solubility study. A solubility study was conducted to predict the maximum concentration of Soluplus[®] that will increase the solubility of nepafenac. The shaking flask method was used to determine the solubility. An excess amount of nepafenac was added to aqueous solutions of Soluplus[®]. Solutions with Soluplus[®] were prepared at concentrations of 5%, 10%, 15%, 25%, 45%, and 65% (w/w). Nepafenac powder was added to glass flasks containing Soluplus[®] with concentration levels as mentioned above. The samples were shaken for 24 h in a mechanical shaker. The concentrations of the nepafenac in the solutions were determined after equilibration for 24 h. A UV-spectrophotometer (1650 PC, Shimadzu, Kyoto, Japan) was used at 328 nm [34].

Fourier transform infrared (FT-IR) spectroscopy. The interaction between the nepafenac, Soluplus[®] and nepafenac ocular inserts was studied using an FT-IR spectrophotometer (Shimadzu, Kyoto, Japan). Spectra were recorded in the range 4000–400 cm^{–1}. All the samples were prepared using the KBr pellet technique, and

the spectra were recorded at a resolution of 0.15 cm^{-1} and a scanning speed of 20 scans s^{-1} [35,36].

Differential scanning calorimetric study. Differential scanning calorimetric (DSC) measurements were made using a thermal analyzer (DSC-60, Shimadzu, Kyoto, Japan). Samples of about 5 mg weight were hermetically placed in aluminum sealed pans and scanned at a heating rate of $10^\circ\text{C min}^{-1}$ over a temperature range of $0\text{--}300^\circ\text{C}$ with using nitrogen gas as an effluent gas. The thermal properties of pure nepafenac and the nepafenac ocular insert were determined [37].

Evaluation and characterization of nepafenac ocular films

Physical examination. The color and transparency of the nepafenac ocular inserts were inspected visually and other physical parameters were also evaluated using advanced tools and technologies to check the physical stability of the final formulation.

Determination of pH. The pH of the ocular inserts was determined using a digital pH meter (PICO + pH meter, Lab India, Mumbai, India). One-gram samples were added to 100 ml of distilled water each and stored for 2 h. The pH of the ocular inserts was calculated in triplicate, and the average value was calculated [38–40].

Thickness of films. The film thickness was measured using digital Vernier calipers or a micrometer screw gauge at different points, and the mean value was calculated [4,41,42].

Uniformity of weight. Three ocular inserts were cut from different parts of the film. They were individually weighed using a calibrated digital balance. The mean value was calculated. The standard deviation was calculated from the mean value [43].

Drug content uniformity. Inserts were cut from different places of the cast films. Each insert was placed in a vial containing 5 ml of pH 7.4 phosphate buffer and shaken to extract the drug from the film. One milliliter of the resulting solution was taken and diluted. The solution was analyzed using a spectrophotometer. Phosphate buffer (pH 7.4) was used as the blank [44].

Percentage moisture absorption. A percentage moisture absorption test was performed to determine the physical stability or integrity of the ocular inserts. Ocular inserts were weighed and placed in desiccators containing 100 ml of a saturated solution of aluminum chloride at 79.5% RH. After 72 h, the ocular inserts were removed and reweighed. The percentage moisture absorption was calculated using the following equation [45–47]:

$$\% \text{ Moisture absorption} = \frac{\text{[final weight} - \text{initial weight]}}{\text{initial weight}} \times 100 \quad (1)$$

Folding endurance. The folding endurance of ocular inserts/films was determined by folding them many times at the same place till a crack appeared (in this case it was folded 200 times). The number of folds required to produce the crack was counted. The folding endurance test was repeated with more sets of ocular inserts [48].

Tensile strength. The tensile strength is one of the significant mechanical properties determining the physical integrity of a film.

It is calculated as the applied load (force) at rupture divided by the cross-sectional area of a strip. A CT3 texture analyzer with a 30-g load cell was used. Film strips were held between two clamps placed 80 mm apart. Then, the strips were stretched by the top clamp at a rate of 3 mm/s, and the force at which the films broke were measured. The tensile strength was calculated using the following equation [49,50]:

$$\text{Tensile strength} \left(\frac{\text{N}}{\text{cm}^2} \right) = \frac{\text{breaking load}}{\text{cross sectional area of the sample}} \quad (2)$$

Percentage elongation. The percentage elongation at breaking was calculated according to the following equation [49,50]:

$$\% \text{ Elongation at break} = \left\{ \frac{\text{Change in length (mm)}}{\text{original length (mm)}} \right\} \times 100 \quad (3)$$

Scanning electron microscopy (SEM). A beam of electron produced by an electron gun goes through two condenser lenses, a scan coil and an objective lens to finally interact with a sample in SEM. In the sample, the electrons lose energy due to scattering and absorption. The morphology of the nepafenac ocular inserts was studied using a JSM 5400 scanning electron microscope (Diya Labs, Mumbai, India) with an acceleration voltage of 30 kV. The samples were coated with gold prior to imaging [51].

In vitro drug release study. The prepared ocular inserts were subjected to the *in vitro* drug release study using vial method. In this method, the ocular inserts (1 cm^2 size) were placed into the 25 ml capacity vials containing 10 ml of phosphate buffer solution, pH 7.4 (as pH of lacrimal fluid is 7.4). These vials were placed on the hot plate maintaining the temperature of $37^\circ\text{C} \pm 0.5^\circ\text{C}$ with continuous stirring using magnetic beads at the bottom of the vial, the care was taken to maintain the minimum speed of shaking as like blinking of eyes. The 1 ml sample was withdrawn at the interval 30 min and at the same time it was replaced with fresh 1 ml of the dissolution media to maintain the sink condition. Withdrawn sample were filtered through the Whatman paper and analyzed for drug release study using UV-spectrophotometer at 238 nm. All the results were noted in triplicate for better accuracy [4].

Data validation and optimization. Desirability approached was implemented to generate and validate the mathematical models. Various feasibility and search grid methods were implemented to establish the composition of the optimized formulation. The optimized formulation was developed and evaluated for all the obtained responses (Y_1 and Y_2). Finally, the experimental values were compared with the predicted values in order using mathematical models [52,53].

The data relating to the targeted parameters were analyzed using one-way analysis of variance (ANOVA) in Design-Expert-Software 12.0 version (Stat-Ease Inc., Minneapolis, MN). Individual parameters were analyzed using polynomial equation:

$$Y = \beta_0 + \beta_1 X_1 + \beta_2 X_2 + \beta_3 X_1 X_2 + \beta_4 X_1^2 + \beta_5 X_2^2 \quad (4)$$

where Y is the measured response, β_0 is the intercept, and β_1 to β_5 are the regression coefficients. X_1 and X_2 are the main effects, $X_1 X_2$ is the interaction term between X_1 and X_2 , and X_1^2 and X_2^2 are the quadratic terms of the independent variables. Using multiple linear regression analysis (MLRA) and ANOVA, polynomial models containing only substantial terms were produced ($p < .05$) for every

response. All the resultant models and data were used to construct three-dimensional diagrams to represent response *Y* as a function of *X*. Contour plots were generated to represent the effect of all the independent variables on each response.

Stability studies. The selected formulations were stored at 25 °C/60%RH and 40 °C/75%RH for 2 months and evaluated for their physical appearance, drug content, and drug–excipient compatibility at specific periods of time [44].

Sterility testing. Sterility testing is carried out to detect the presence of viable forms of microorganisms. The testing was performed using fluid thioglycolate medium and soybean casein digest medium, as per the Indian Pharmacopoeia. The formulations were sterilized separately under UV radiation for 30 min. The irradiated formulations were tested under aseptic conditions for viable forms of bacteria, fungi, and yeast in both the media prescribed by the Indian Pharmacopoeia [54–59].

Ocular irritancy test. The sterilized ocular inserts were used in an eye irritancy test. The Draize technique, which has been designed for testing ocular irritation of ophthalmic products, was used. Clearance for handling the experimental animals was obtained from the Institutional Animal Ethical Committee (IAEC) constituted for the purpose. The ocular inserts were placed into the lower cul-de-sac, and observations of the various parameters were made 1 h, 24 h, 48 h, 72 h, and 1 week after administration. Three male rabbits weighing between 1.5 and 2 kg were used in the study. The sterile formulation was administered twice a day for a period of seven days. The rabbits were observed periodically for redness, swelling, and watering of the eyes [60–63].

Results and discussion

As described in above-mentioned section of methods, the thin films were formed using the solvent casting method and a film former. The composition of the films was according to the 3²-factorial design (Table 2). The thin films obtained were transparent, flexible, and smooth in appearance.

Preliminary batches were produced to finalize the specific ranges of concentrations of Soluplus[®] and the plasticizer (PEG-400). Flexible, transparent, and smooth-surfaced thin films were obtained. There was better release of nepafenac in the ocular region. At higher concentration levels of Soluplus[®] and PEG-400, the films obtained were very sticky, thick, and somewhat tacky. At lower concentrations of both Soluplus[®] and the plasticizer, the films were very brittle and could not be removed easily from the glass surface after drying. Hence, on the basis of this preliminary study, the final concentrations of Soluplus[®] and PEG-400 were 30–70% and 10–30%, respectively. Nine possible combinations were obtained from the 3²-factorial design (Table 2). After batches of all the formulations were prepared, the films obtained were evaluated for various physical and chemical properties. These are discussed in a later section.

Pre-formulation study

Before finalizing the optimized formulations and characterizing them, a preliminary study was conducted on the compatibility of all the components used in the design of the ocular films. Physical blends of the drug and other components were subjected to FT-IR, DSC, and XRD analysis. The results of the study conducted to

check the suitability of the materials used are presented in the following sections.

FT-IR study

Compatibility of the drug and other components used is essential for preparing a final formulation. Nepafenac and Soluplus[®] were subjected to FT-IR analysis. Major peaks of nepafenac spectra consisting of N–H stretch at 3440; C=O stretch (carboxylic acid group) at 1676; C–O (ester group) at 1194; C–H stretch (aromatic group) 2877; C–H bending (aromatic group); C–Br stretch at 753. No extra peaks were found in the spectrum of the drug and excipients blend, indicating an absence of interactions or the instability of ocular insert formulation. FT-IR spectra of pure nepafenac and blend of nepafenac and Soluplus[®] is presented in Figure 1.

Differential scanning calorimetry

Nepafenac, Soluplus[®] and their blend were subjected to DSC analysis. In the DSC thermogram of nepafenac, a sharp endothermic peak was found at 184.93 °C, corresponding to the melting and reported decomposition at 183.54–186.4 °C.

Soluplus[®] showed an endothermic peak at 63.66 °C. The DSC thermograph of the drug–Soluplus[®] mixture showed an endothermic peak at the melting point of Soluplus[®] (62.93 °C). This shows that nepafenac is completely entrapped within Soluplus[®]. This indicates that there is no interaction between nepafenac and Soluplus[®]. The DSC thermograms are presented in Figure 2.

Solubility study

There was significant increase in solubility of nepafenac at 45% concentration level of Soluplus[®], beyond this level, there was no significant increase in solubility. It is observed that the presence of Soluplus[®] increases the solubility of nepafenac almost more than 200 times compared with the plain drug [64–66]. From this study, it was clear that the concentration of Soluplus[®] should not be less than 45% for maximum solubility of nepafenac (Figure 3). But another aspect in the design of ocular inserts is to keep all the physical and chemical properties so that the final formulation is stable and improved. Hence, the concentration level of Soluplus[®] was maintained between 30% and 70% for the development of ocular insert formulations, as mentioned in Table 1.

Evaluation and characterization of ocular inserts of nepafenac

As per the 3²-factorial design, all the nine formulations were prepared using different concentrations of Soluplus[®] and PEG-400. Various physical and chemical properties such as weight, thickness, tensile strength, percent elongation, folding endurance, percent moisture absorption, surface pH, and drug content of these formulations were evaluated (Table 3). The average weight of these inserts (10 × 10 mm²) was in the range from 8.38 ± 0.01 mg to 22.44 ± 0.02 mg. Batch F4 has the minimum weight (8.38 ± 0.01 mg), and batch F6 has the maximum weight (22.44 ± 0.02 mg). The variation in the weight was observed due to the fact that batch F4 has lower concentrations of both Soluplus[®] and PEG-400, whereas batch F6 has higher levels of both Soluplus[®] and PEG-400. In all the formulations, the concentration of the drug was maintained at the same level. Overall, from all the observations, it is clear that as the concentration levels of both Soluplus[®] and PEG-400 increase, the weight of the insert/film

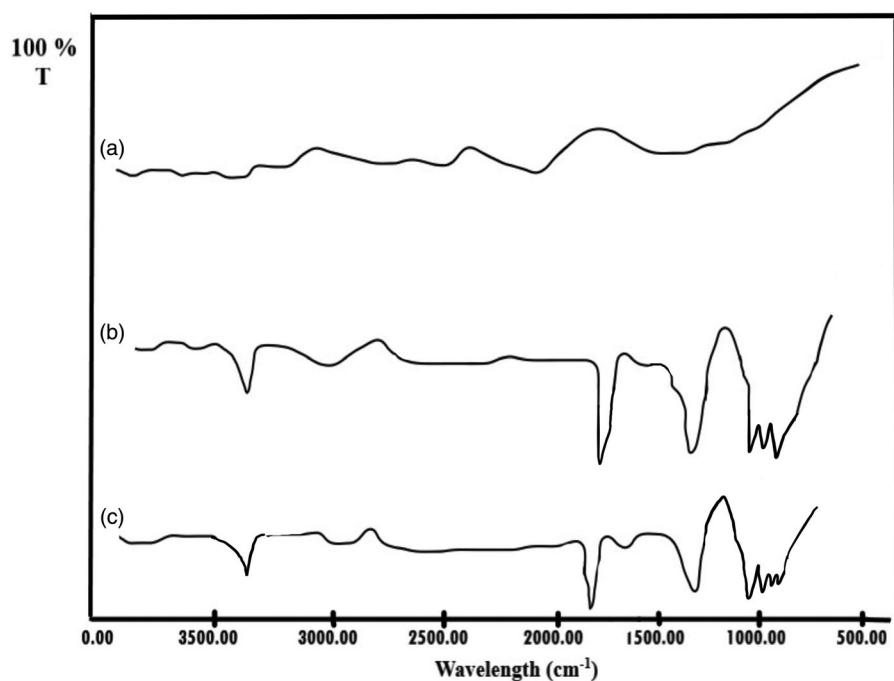


Figure 1. FT-IR spectra of: Soluplus® (a); Nepafenac (b); blend of nepafenac and Soluplus® (c).

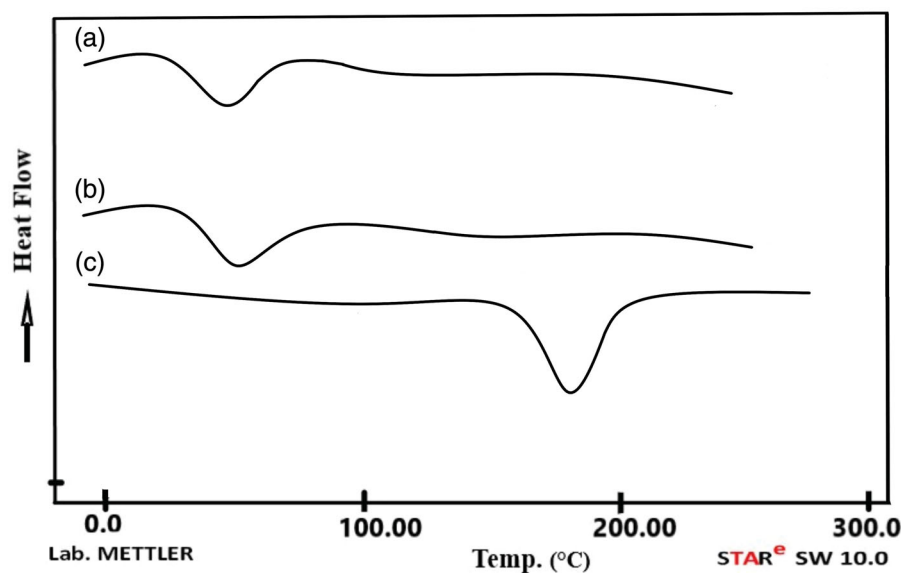


Figure 2. DSC thermogram of: Soluplus® (a); blend of nepafenac and Soluplus® (b); Nepafenac (c).

also increases. There were similar observations about the thickness, tensile strength, percent elongation, and moisture absorption, the highest values of these parameters among all the nine formulations prepared as per the 3^2 -factorial design were $289.25 \pm 1.25 \mu\text{m}$, $7.58 \pm 1.78 \text{ N/m}^2$, $96.28 \pm 1.25\%$, and $8.56 \pm 1.47\%$, respectively. In the similar way, the lowest values were $123.5 \pm 1.45 \mu\text{m}$, $2.55 \pm 1.27 \text{ N/m}^2$, $52.0 \pm 1.2\%$, and $3.25 \pm 2.35\%$, respectively.

All the results considered were the average of three values for each parameter. But the final decision was based on another important dependent variable $\text{Rel}_{4\text{hr}}$, which was also

discussed subsequently. Other physical parameters such as the surface pH was found to be in the range of 7.4–7.8 whereas folding endurance was found to be varied from a low value of 127 to values >223 . Here also, the concentrations of both Soluplus® and PEG-400 played an important role. The effect was directly proportional to the concentration levels of the two materials although the same amount of drug was present in all the formulations. The folding endurance increased with the concentration levels. The drug content in all the nine formulations was found to be satisfactory (above 90%). It was in the range from $95.43 \pm 1.8\%$ to $98.99 \pm 1.25\%$ (Table 4).

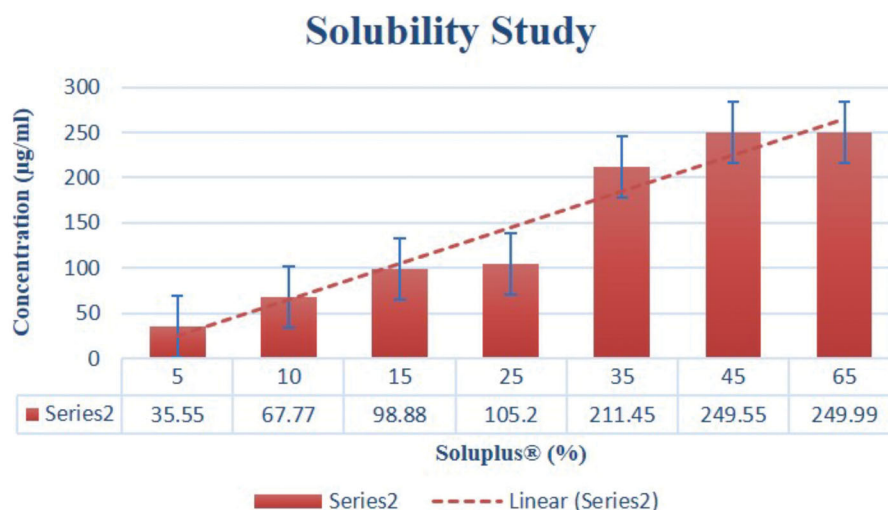


Figure 3. Solubility study of Nepafenac in the presence of Soluplus® as solubilizer.

Table 3. Evaluation of physical and chemical properties of nepafenac ocular insert.

Batch	Weight (mg)	Thickness (µm)	% Drug content	Tensile strength (N/m ²)	% elongation	% Moisture absorption
F1	18.3 ± 0.01	213.33 ± 1.654	98.23 ± 1.5	5.55 ± 1.02	92.99 ± 1.2	6.98 ± 1.25
F2	16.7 ± 0.012	198.65 ± 2.453	98.99 ± 1.25	4.54 ± 1.55	90.99 ± 1.78	5.60 ± 2.25
F3	11.8 ± 0.02	158.76 ± 3.564	95.43 ± 2.24	5.95 ± 2.01	74.00 ± 1.01	4.65 ± 1.58
F4	8.38 ± 0.24	123.5 ± 1.45	96.45 ± 1.88	2.55 ± 1.27	52.0 ± 1.28	3.25 ± 2.35
F5	17.8 ± 0.06	208.32 ± 1.55	95.89 ± 1.2	5.01 ± 1.87	94.0 ± 1.88	7.80 ± 1.25
F6	22.44 ± 0.02	289.25 ± 1.25	98.258 ± 1.25	7.58 ± 1.78	96.28 ± 1.25	8.56 ± 1.47
F7	17.58 ± 0.05	211.25 ± 2.25	96.45 ± 1.55	3.25 ± 1.01	88.25 ± 2.25	5.4 ± 1.54
F8	18.58 ± 0.25	221.3 ± 1.25	97.54 ± 1.25	4.55 ± 1.28	91.25 ± 1.02	6.89 ± 2.25
F9	9.5 ± 0.432	134.201 ± 2.64	97.55 ± 1.54	5.58 ± 1.78	78.29 ± 1.67	4.58 ± 1.77

All the observations were taken in triplicate as ± SD ($n = 3$).

Table 4. Summary of *in vitro* drug release data as per with mathematical model fitting as per 3²-factorial design.

Batch	Zero order		First order		Higuchi model	
	K_0	R^2	$K1$ (h ⁻¹)	R^2	KH (h ⁻¹)	R^2
F1	1.48 ± 0.058	0.9988 ± 0.014	0.03 ± 0.01	0.9934 ± 0.04	8.69 ± 0.34	0.9433 ± 0.014
F2	1.25 ± 0.145	0.9752 ± 0.055	0.015 ± 0.01	0.9635 ± 0.014	7.69 ± 0.38	0.9655 ± 0.05
F3	2.38 ± 0.065	0.9556 ± 0.055	0.045 ± 0.02	0.9567 ± 0.01	7.25 ± 0.45	0.8936 ± 0.025
F4	1.28 ± 0.048	0.9438 ± 0.045	0.025 ± 0.01	0.9433 ± 0.05	6.55 ± 0.24	0.9633 ± 0.025
F5	1.25 ± 0.068	0.9755 ± 0.014	0.035 ± 0.03	0.9855 ± 0.014	11.55 ± 0.36	0.9523 ± 0.025
F6	1.54 ± 0.055	0.9775 ± 0.023	0.025 ± 0.02	0.9624 ± 0.016	13.52 ± 0.35	0.9733 ± 0.02
F7	2.28 ± 0.024	0.9466 ± 0.014	0.042 ± 0.03	0.9725 ± 0.016	19.25 ± 0.34	0.9833 ± 0.055
F8	3.25 ± 0.047	0.8622 ± 0.035	0.044 ± 0.05	0.9815 ± 0.019	18.55 ± 0.56	0.9688 ± 0.025
F9	1.85 ± 0.036	0.9625 ± 0.014	0.055 ± 0.03	0.9725 ± 0.045	18.65 ± 0.65	0.9833 ± 0.02

All the observations were taken in triplicate as ± SD ($n = 3$).

Scanning electron microscopy

The morphology of the nepafenac ocular inserts prepared was characterized by SEM analysis. The SEM images revealed that the inserts have a uniform surface with small pores and drug may release from this surface. The ocular inserts had a clear appearance with smooth surface and texture, SEM images are shown in Figure 4.

In vitro drug release study

An *in vitro* drug release study of the nepafenac ocular inserts was carried out. The release profile obtained is shown in Figure 5. It was observed that the release of the drug from the inserts of all the nine formulations in 4 h was in the range from 66.55% to 95.25%. The drug release of formulation F3 was very low (66.55%), whereas that of formulation F6 was the highest (95.25%). The low drug release from formulation F3 was due to the fact that the formulation contains higher levels of plasticizer

compared with the concentration of Soluplus®, which retards the release from the insert. Formulation F6, in contrast, contains lower levels of the plasticizer compared with Soluplus®. Overall, the same trend was observed with the remaining formulations due to the different levels of the two components. Soluplus® is the polymer of choice for playing the roles of both film former and solubilizer. Hence, the formulations containing higher levels of Soluplus® had the maximum drug release. Further, the drug release was also influenced by presence of pores at the film surface, the permeation capacity of film surface and the diffusivity and solubility of the drug in the presence of Soluplus®. Hence, the role of Soluplus® was found to be very important in improving the solubility of nepafenac. The solubility of nepafenac increased (more than 200 times) as described in section 'Solubility study'. This phenomenon played a major role in the release of the drug, along with the role of the supportive plasticizer (PEG-400), which gave the inserts sufficient strength for continuous release up to 4 h [64–66].

In Vitro Drug Release Study

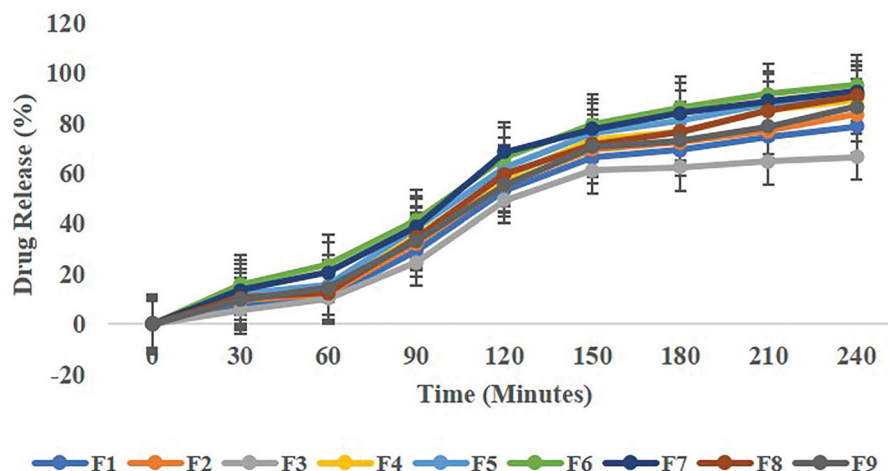


Figure 4. In vitro drug release study of all the nine formulations as per 3²-factorial design.

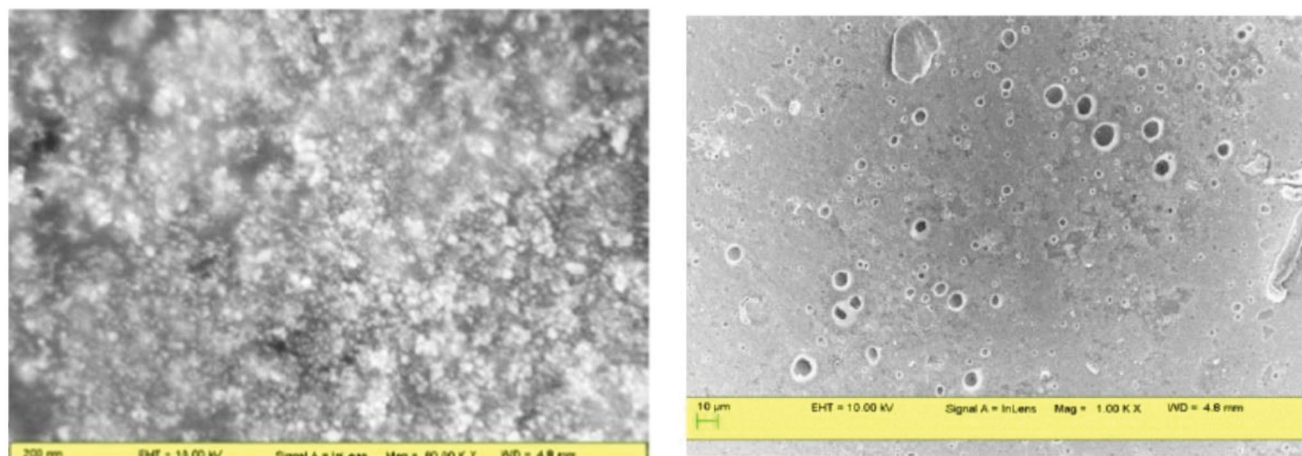


Figure 5. Scanning electron microscopic (SEM) images of optimized ocular insert at different resolutions.

Table 5. Summary of ANOVA for response parameters as per 3²-factorial design.

Response	F Value	Prob>F	Predicted R ²	Adjusted R ²	% CV
Rel 4h (Y ₁)	13.85	0.05	98.24	99.51	1.58
Tensile strength (Y ₂)	23.31	0.05	97.36	98.54	2.36

Regression equations best models:

$$Y_1 = 86.07X_1 + 5.87X_2 - 5.36X_1X_2;$$

$$Y_2 = 4.54X_1 - 0.700X_2 + 0.0925X_1X_2 + 0.756X_1^2 - 0.138X_2^2.$$

The *in vitro* drug release data of the nine formulations fitted the zero-order equation well, but the best-fit model was the first-order equation. The results of ANOVA and mathematical models were generated by regression analysis and fits of all the models are shown in Table 5.

If there are many insignificant model terms (not counting those required to support hierarchy), model reduction may improve the model, but in the case of both responses Y₁ and Y₂, all the model terms (X₁, X₂ and X₁:X₂) are significant. In the case of response Y₁ (Rel_{4h}), the model F-value of 13.85 implies that the model is significant. There is only a 0.74% chance that an F-value this large could occur due to noise. *p* Values less than .0500 (in this case *p* = .0074) indicate model terms that are significant. The predicted R² value of 0.9824 is in reasonable agreement with the adjusted R² value of 0.9951 in the case of the response parameter of Y₁ (Rel_{4h}). Adequate precision measures the signal to noise ratio. A

signal-to-noise ratio greater than 4 is desirable. In this case, the ratio is 12.887, indicating an adequate signal. This model can be used to navigate the design space. The 2FI model generated for Rel_{4h} indicated that the Soluplus[®] (X₁) concentration had a positive influence on Y₁. As the concentration of Soluplus[®] increases, the release of nepafenac also increases. In addition to the main effects, the interaction term, X₁:X₂ (Soluplus[®]: PEG-400), had a significant negative influence on Y₁. As the concentration of Soluplus[®] increases, the release of nepafenac also increases, but at higher concentrations of X₂ along with X₁ has a negative influence on Rel_{4h}. Here, the release of the drug decreases as the concentration of X₂ increases. This was due to the retardant effect of PEG-400 as it increases the plasticity the insert.

In the case of response Y₂ (tensile strength), the F-value of 23.31 implies that the model is significant. There is only a 0.15% chance that an F-value this large could occur due to noise. *p* Values less than .0500 (in this case *p* = .0015) indicate that the model terms are significant. The predicted R² of 0.9736 is in reasonable agreement with the adjusted R² of 0.9854 in the case of the response parameter of Y₂ (tensile strength). Adequate precision measures the signal to noise ratio. A ratio greater than 4 is desirable. In this case, the ratio of 9.887 indicates an adequate signal. This model can be used to navigate the design space. The quadratic model generated for Y₂ indicated that the Soluplus[®] (X₁)

Table 6. Response parameters as per 3^2 factorial design.

Formulation Batch	Independent variable X_1 : Soluplus® (%)	Independent variable X_2 : PEG-400 (%)	Y_1	Y_2
			Rel _{4h} ^a (%)	Tensile strength ^a (N/cm ²)
F1	50	30	78.66 ± 1.25	5.55 ± 1.02
F2	50	20	83.55 ± 1.02	4.54 ± 1.55
F3	30	30	66.55 ± 2.03	5.95 ± 2.01
F4	30	10	89.25 ± 1.14	2.55 ± 1.27
F5	70	20	91.44 ± 1.58	5.01 ± 1.87
F6	70	30	95.25 ± 1.36	7.58 ± 1.78
F7	50	10	92.5 ± 1.75	3.25 ± 1.01
F8	70	10	90.88 ± 1.34	4.55 ± 1.28
F9	30	20	86.54 ± 1.78	5.58 ± 1.78

^aAll the observations were taken in triplicate as ± SD ($n = 3$).

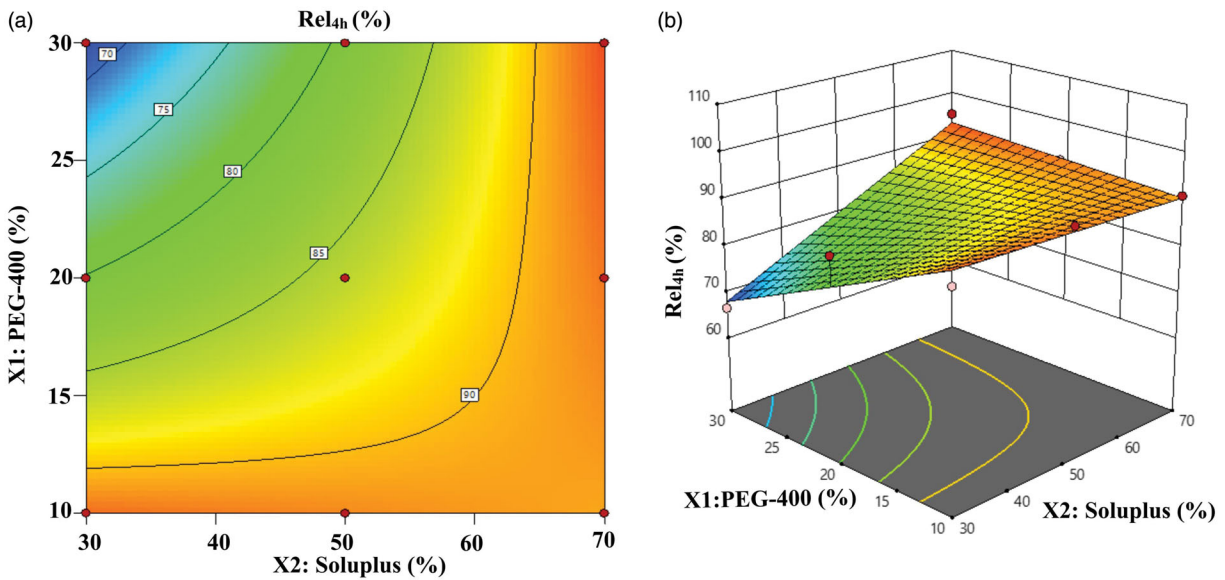


Figure 6. Contour and 3D surface response graph: (a, b) for Rel_{4h} response parameter, respectively.

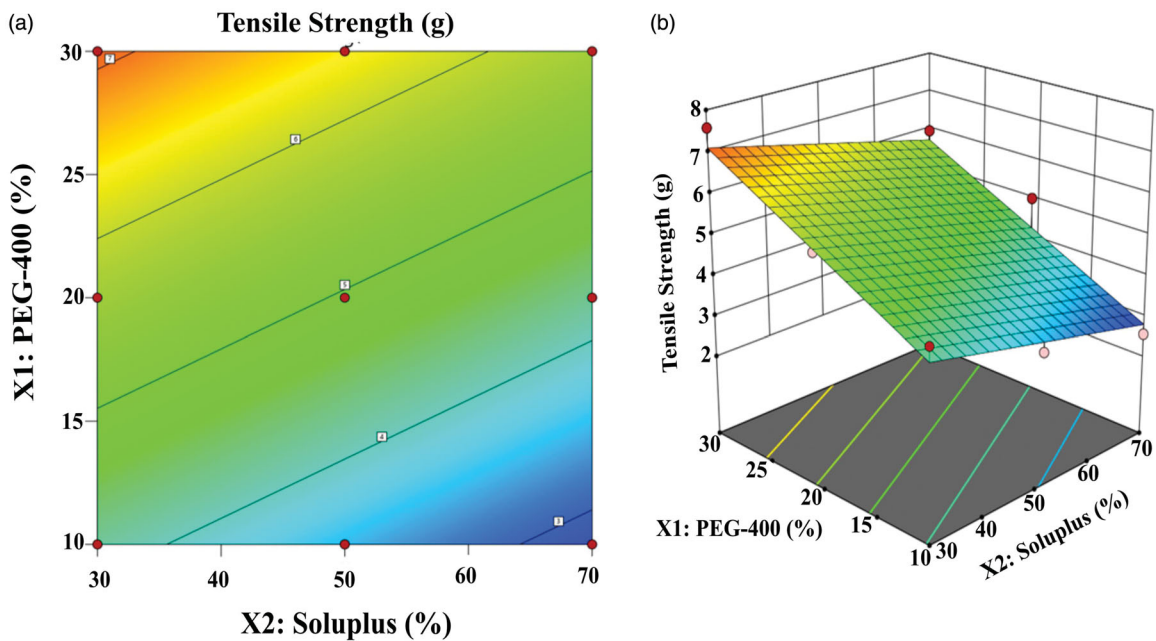


Figure 7. Contour and 3D surface response graph: (a, b) for tensile strength response parameter, respectively.

concentration had a negative influence on Y_2 . As the concentration of Soluplus® increased, the tensile strength of the insert decreased, whereas with higher concentrations of PEG-400 (X_2),

the tensile strength increases. This is due to the plasticizer effect of PEG-400. In addition to the main effects, the interaction term $X_1 \times X_2$ (Soluplus®: PEG-400) had a significant negative influence on

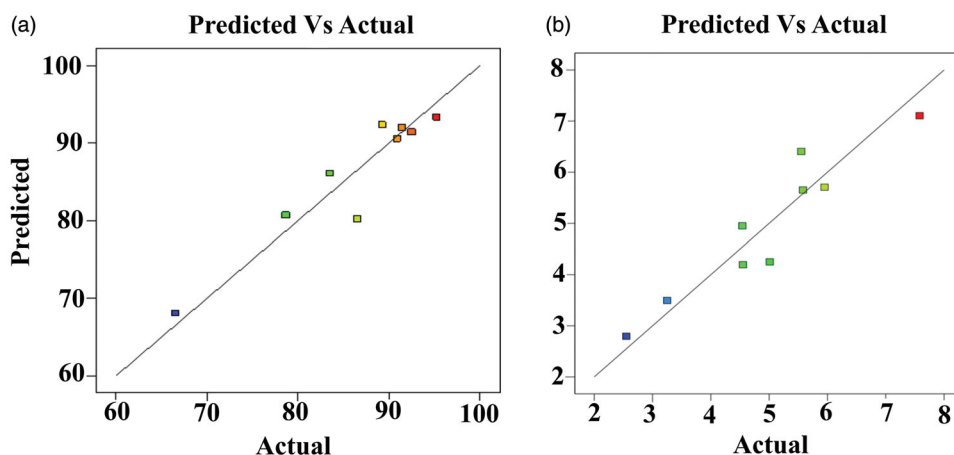


Figure 8. The relation between predicted vs. actual experimental values for both the response variables Rel4h (Y₁) (a) and tensile strength (Y₂) (b).

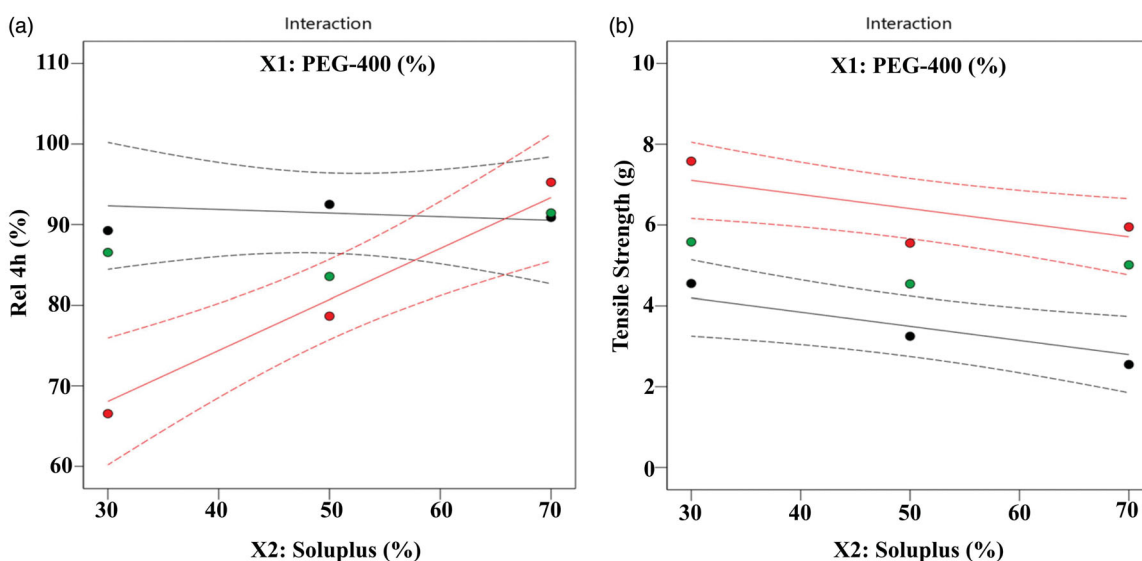


Figure 9. Response plots (a, b) showing the combined effect of due to interaction of X₁:X₂ on both response parameter Rel4h (Y₁) (a) and tensile strength (Y₂) (b).

Y₂ ($p=0.0143$). As the concentration of PEG-400 increases, the tensile strength also increases, but at higher concentrations of X₂ along with X₁ has a negative influence on the tensile strength. Here, it decreases as the concentration of X₁ increases. The results of the response parameters Rel_{4h} (Y₁) and tensile strength (Y₂) are shown in Table 6.

The effects of all the independent factors are presented in the form of contour plots and three-dimensional surface response plots (Figures 6 and 7).

The relation between the predicted and actual experimental values for both the response variables Y₁ and Y₂ is shown graphically in Figure 8. The combined effect due to interaction (X₁:X₂) on the response parameters Y₁ and Y₂ is shown in Figure 9. Overlay plot for both responses (Y₁ and Y₂) is highlighted in Figure 10.

The main aim of the present study was to develop an ocular insert which released the nepafenac in 4 h (Rel_{4h}) and had better tensile strength for continuous drug release.

Stability study

The selected formulations were tested for 3 months at storage conditions of 25°C and 40°C at 60% RH (relative humidity) and 75% RH, and they were analyzed for their drug content. The

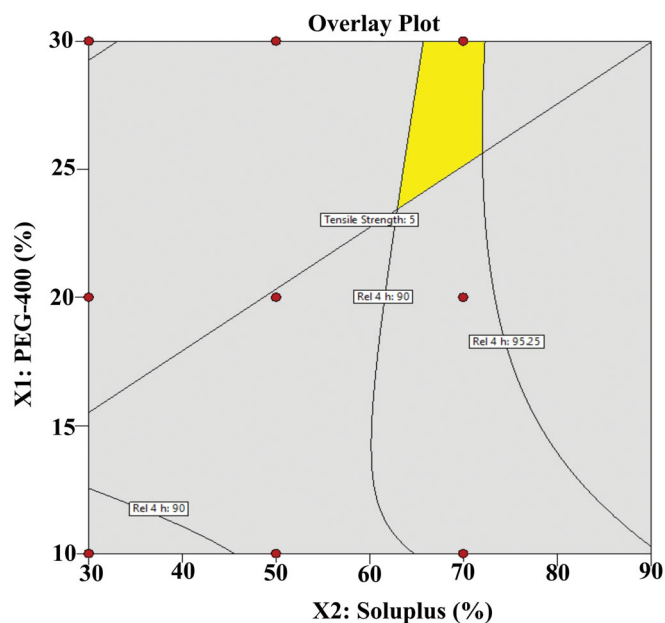


Figure 10. Overlay plot for both response parameter Rel4h (Y₁) and tensile strength (Y₂).

Table 7. Evaluation of optimized ocular insert after stability study.

Batch	Weight (mg)	Thickness (μm)	% Drug content	Tensile strength (N/m^2)	% elongation
F1	19.6 \pm 0.03	222.90 \pm 1.28	97.33 \pm 1.25	4.80 \pm 1.15	98.33 \pm 1.26
F2	18.9 \pm 0.032	202.78 \pm 2.25	96.80 \pm 1.55	5.54 \pm 1.78	91.25 \pm 1.54
F3	13.1 \pm 0.22	162.54 \pm 2.35	94.83 \pm 2.94	6.10 \pm 2.14	76.58 \pm 1.45
F4	10.25 \pm 0.21	126.4 \pm 1.35	95.85 \pm 1.25	3.25 \pm 1.47	60.10 \pm 1.78
F5	19.4 \pm 0.23	210.87 \pm 1.67	95.25 \pm 1.22	5.22 \pm 1.54	96.55 \pm 1.45
F6	25.12 \pm 0.12	292.95 \pm 1.90	97.568 \pm 1.85	7.24 \pm 1.52	98.57 \pm 1.65
F7	19.98 \pm 0.15	213.14 \pm 2.45	95.88 \pm 1.65	3.58 \pm 1.23	90.95 \pm 2.75
F8	19.68 \pm 0.25	223.31 \pm 1.02	95.74 \pm 1.85	3.75 \pm 1.81	92.65 \pm 1.32
F9	11.9 \pm 0.36	135.21 \pm 2.25	95.75 \pm 1.89	5.88 \pm 1.64	80.47 \pm 1.27

All the observations were taken in triplicate as \pm SD ($n = 3$).

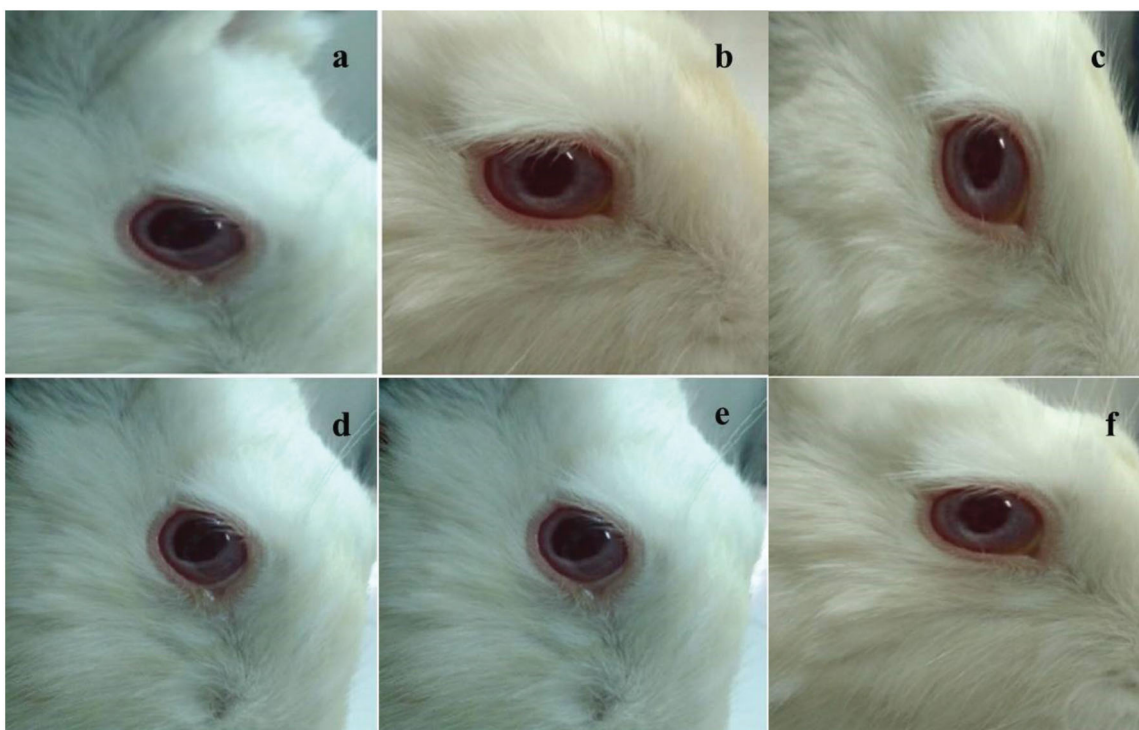


Figure 11. Ocular irritancy test for optimized ocular insert on rabbit eye at every interval for one-week period.

residual drug content of the selected formulations was found to be within the permissible limits. The formulations showed satisfactory physical stability at 25 °C and 40 °C at 60% RH and 75% RH, respectively, and no significant changes were observed after stability study. The physical appearance did not change considerably. The results of stability study are highlighted in Table 7.

Sterility testing

All the sterile inserts complied with the test for sterility with a positive control and a negative control test conducted as per the procedure of the Indian Pharmacopeia. The formulations did not show any microbial growth, which suggests that the inserts were sterile.

Ocular irritancy test

The sterilized formulations were placed into the lower cul-de-sac, and the various criteria were observed at 1 h, 12 h, 24 h, 48 h, 72 h, and 1 week after administration. No redness, swelling, or watering of the rabbit eye was observed. This indicates that the inserts did not produce ocular irritancy and toxicity (Figure 11).

Conclusion

The aim of the present study was to develop an ocular insert/film of the poorly water-soluble nepafenac using a 3²-factorial design. The response parameters Rel_{4h} and tensile strength were set as the dependent variables. The goal was set by considering the constraints of the variations in the concentration levels of the film former (Soluplus[®]) and the plasticizer (PEG-400). Using the feasibility and grid search methods, an insert with a drug release greater than 90% after 4 h and with better physical stability and strength was obtained successfully. All the physico-chemical parameters were found to be excellent for delivering nepafenac in a continuous manner for 4 h. It is concluded that an optimized insert/film of the poorly water-soluble nepafenac can be formulated using the novel graft-co-polymer at appropriate concentrations of the plasticizer, PEG-400, by reducing the dosing frequency. The effect is prolonged and the patient compliance is better.

Acknowledgements

Authors are very thankful to the BASF Corporation, Mumbai, India and grateful to Micro Labs, Hosur, India. Authors are also thankful to the Management and Principal of the College to provide other

chemicals and supporting resources to complete this research work successfully.

Disclosure statement

No potential conflict of interest was reported by the author(s).

Data availability statement

Author/s hereby declares that the raw/processed data required to reproduce these findings cannot be shared at this time due to legal or ethical reasons.

References

- [1] Sreenivas SA, Hiremath SP, Godbole AM. Ofloxacin ocular inserts: design, formulation and evaluation. *Iran J Pharm Res.* 2006;5(2):159–162.
- [2] Chien YW. *Ocular drug delivery and delivery systems; novel drug delivery systems.* 2nd ed. New York: Marcel Dekker; 1996. p. 269–270.
- [3] Ara T, Sharma S, Bhandari A. Preparation and evaluation of ocular inserts of diclofenac sodium for controlled drug delivery. *Der Pharm.* 2014;6(6):93–99.
- [4] Jafariazar Z, Jamalnia N, Ghorbani-Bidkorbeh F, et al. Design and evaluation of ocular controlled delivery system for diclofenac sodium. *Iran J Pharm Res.* 2015;14:23–31.
- [5] Lee VH, Robinson JR Jr. Topical ocular drug delivery: recent developments and future challenges. *J Ocul Pharmacol Ther.* 1986;2:67–108.
- [6] Hermans K, Van den Plas D, Kerimova S, et al. Development and characterization of mucoadhesive chitosan films for ocular delivery of cyclosporine A. *Int J Pharm.* 2014;472:10–19.
- [7] Sultana Y, Aqil M, Ali A. Ocular inserts for controlled delivery of pefloxacin mesylate: preparation and evaluation. *Acta Pharm.* 2005;55:305–314.
- [8] Baranowski P, Karolewicz B, Gajda M, et al. Ophthalmic drug dosage forms: characterization and research methods. *Science.* 2014;2014:1–14.
- [9] Atram S, Bobade N. Current trends towards an ocular drug delivery system: review. *Int J Pharm Pharm Sci.* 2013;3(1):28–34.
- [10] Karthikeyan D, Bhowmick M, Pandey V, et al. The concept of ocular inserts as drug delivery systems: an overview. *Asian J Pharm.* 2008;2:192–193.
- [11] Attia M, Kassem M, Safwat S. In-vivo performance of 3H-dexamethasone ophthalmic film delivery systems in the rabbit eye. *Int J Pharm.* 1988;47:21–30.
- [12] Kumar S, Nagori B. Ocular insert: dosage form for sustain ophthalmic drug delivery. *J Farm Klin Indones.* 2012;1(2):61–73.
- [13] Bade M, Gawali V. Ocular inserts: a rate controlled drug delivery system – a review. *IJPE.* 2012;2(1):49–63.
- [14] Rajput G, Sharma S. Review on ophthalmic inserts. *Int J Pharma Prof Res.* 2013;4(3):912–920.
- [15] Barath S, Hiremath S. Ocular delivery system of pefloxacin mesylate. *Pharmazie.* 1999;54:55–58.
- [16] Hume LR, Lee HK, Benedetti L, et al. Ocular sustained delivery of prednisolone using hyaluronic acid benzyl ester films. *Int J Pharm.* 1994;111:295–298.
- [17] Rathore K, Nema R. An insight into ophthalmic drug delivery system. *Int J Pharm Sci Drug Res.* 2009;1:1–5.
- [18] Grass G, Cobby J, Makoid M. Ocular delivery of pilocarpine from erodible matrices. *J Pharm Sci.* 1984;73:618–621.
- [19] Maichuk Y. Ophthalmic drug inserts. *Invest Ophthalmol Vis Sci.* 1975;14:87–90.
- [20] Ozawa H, Hosaka S, Kunitomo T, et al. Ocular inserts for controlled release of antibiotics. *Biomaterials.* 1983;4:170–174.
- [21] Kumari A, Sharma P, Garg V. Ocular insert: advancement in therapy of eye diseases. *J Adv Pharm Technol Res.* 2010;1(3):291–296.
- [22] Saettone MF, Salminen L. Ocular inserts for topical delivery. *Adv Drug Deliv Rev.* 1995;16:95–106.
- [23] Sampath Kumar K, Bhowmik D. Ocular inserts: a novel controlled drug delivery system. *Pharma Innov J.* 2013;1(12):1–16.
- [24] Michael L, Collnot E-M, Djuric D, et al. Soluplus[®] as an effective absorption enhancer of poorly soluble drugs in vitro and in vivo. *Eur J Pharm Sci.* 2012;45:336–343.
- [25] Shamma R, Elkasabgy Design of freeze-dried Soluplus/polyvinyl alcohol-based film for the oral delivery of an insoluble drug for the pediatric use. *Drug Deliv.* 2016;23(2):489–499.
- [26] Dian L, Yu E, Chen X, et al. Enhancing oral bioavailability of quercetin using novel soluplus polymeric micelles. *Nanoscale Res Lett.* 2014;9:684.
- [27] Shamma RN, Basha M. Soluplus[®]: a novel polymeric solubilizer for optimization of carvedilol solid dispersion: formulation design and effect of method of preparation. *Powder Technol.* 2013;237:406–414.
- [28] Kim DH, Park MS, Choi Y, et al. Synthesis of PVA-g-POEM graft copolymers and their use in highly permeable thin composite membranes. *Chem Eng J.* 2018;346:739–747.
- [29] Available from: <https://www.drugbank.ca/drugs/db06802>
- [30] Ahuja M, Dhake AS, Sharma SK, et al. Topical ocular delivery of NSAIDs. *AAPS J.* 2008;10(2):229–241.
- [31] Lane S. Nepafenac: a unique nonsteroidal prodrug. *Int Ophthalmol Clin.* 2006;46(4):13–20.
- [32] Khurana G, Arora S, Pawar P. Ocular insert for sustained delivery of gatifloxacin sesquihydrate: preparation and evaluations. *Int Pharm Investig.* 2012;2(2):70–77.
- [33] Agrawal A, Jadhav L. Ocular drug delivery system and role of ocular inserts in eye disorder treatment: a review. *Asian J Pharm Technol Innov.* 2016;4(21):45–54.
- [34] Karathanos VT, Mourtzinos I, Yannakopoulou K, et al. Study of the solubility, antioxidant activity and structure of inclusion complex of vanillin with cyclodextrin. *Food Chem.* 2007;101:652–658.
- [35] Aburahma M, Mahmoud A. Biodegradable ocular inserts for sustained delivery of brimonidine tartarate: preparation and in-vitro/in-vivo evaluation. *AAPS PharmSciTech.* 2011;12(4):1335–1347.
- [36] Dave V, Paliwal S, Yadav S. Formulation and evaluation of controlled delivery of aceclofenac through ocular insert. *Turk J Pharm Sci.* 2013;10(2):205–220.
- [37] Mathurm M, Gilhotra RM. Glycerogelatin-based ocular inserts of aceclofenac: physicochemical, drug release studies and efficacy against prostaglandin E2-induced ocular inflammation. *Drug Deliv.* 2011;18(1):54–64.
- [38] Pandey A, Mali P. Design and in-vitro characterization of levobunolol hydrochloride ocuserts with special reference to glaucoma treatment. *Indian J Pharm Educ Res.* 2012;46(3):265–269.

- [39] Pandey P, Panwar A. Design and evaluation of ocular inserts for controlled drug delivery of acyclovir. *Int J Pharm Biol Arch*. 2011;2(4):1106–1110.
- [40] Nappinnai M. Fluconazole ocular inserts: formulation and in-vitro evaluation. *J Pharm Sci Res*. 2010;2(6):344–350.
- [41] Rajasekaran A, Sivakumar V. Design and evaluation of polymeric controlled release natamycin ocular inserts. *Kathmandu Univ J Sci Eng Technol*. 2010;6(1):108–115.
- [42] Gandhi P, Rathod H, Patel S. A review on: ocular inserts a novel drug delivery system. *Asian J Pharm Res Dev*. 2013;1(1):40–48.
- [43] Kaul S, Kumar G, Kothiyal P. An insight into ocular insert. *Int J Pharm Sci Res*. 2015;3:1–7.
- [44] Gorle A, Gattani S. Development and evaluation of ocular drug delivery system. *Pharm Dev Technol*. 2010;15(1):46–52.
- [45] Damodharan N, Soundrapandian C. Ophthalmic inserts of piroxicam: development and in-vitro drug release studies. *Asian J Chem*. 2008;20(5):3447–3454.
- [46] Ashture A, Kankudte A. Formulation and evaluation of controlled release ocular inserts of betaxolol hydrochloride; IOSR. *J Pharm*. 2012;2(5):34–38.
- [47] Kothawade S, Deshpande S, Lunkad A. Formulation and in-vitro characterization of ketorolac tromethamine ophthalmic inserts. *Res J Pharm Dosage Forms Tech*. 2013;5(6):1–3.
- [48] Ramkanth S, Chetty C. Design and evaluation of diclofenac sodium ocusert. *Int J PharmTech Res*. 2009;1(4):1219–1223.
- [49] Patel D. In-vitro and in-vivo evaluation of ocular inserts of ofloxacin. *DARU*. 2007;15(3):138–145.
- [50] Shafie M, Rady M. In-vitro and in-vivo evaluation of timolol maleate ocular inserts using different polymers. *J Clin Exp Ophthalmol*. 2012;3(8):1–9.
- [51] Franca J, Foureaux G. Bimatoprost-loaded ocular inserts as sustained release drug delivery systems for glaucoma treatment: in vitro and in vivo evaluation. *PLoS One*. 2014;9:1–14.
- [52] Paterakis PG, Korakianiti ES, Dallas PP, et al. Evaluation and simultaneous optimization of some pellet's characteristics using 3² factorial design and the desirability function. *Int J Pharm*. 2002;248:51–60.
- [53] Sanchez-Lafuente C, Furlanetto S, Fernandez-Arevalo M, et al. Didanosine extended-release matrix tablets: optimization of formulation variables using statistical experimental design. *Int J Pharm*. 2002;237:107–118.
- [54] Gadhave M, Pawar S. Formulation and evaluation of moxifloxacin ocusert. *Int J Pharm Clin Res*. 2016;8(12):1610–1615.
- [55] Gevariya H, Dharamsi A, Girhepunje K, et al. Once a day ocular inserts for sustained delivery of levofloxacin: design, formulation and evaluation. *Asian J Pharm*. 2009;3:314–318.
- [56] Morsi N, Ghorab D, Refai H, et al. Nanodispersion-loaded mucoadhesive polymeric inserts for prolonged treatment of post-operative ocular inflammation. *J Microencapsul*. 2017;34(3):280–292.
- [57] Mirzaeeia S, Alizadehc M. Design and evaluation of soluble ocular insert for controlled release of chloramphenicol. *J Rep Pharm Sci*. 2017;6(2):123–133.
- [58] Indian Pharmacopoeia. Ministry of Health and Family Welfare. Government of India. Vol. 2. New Delhi: Controller of Publication; 1996. p. 117–147.
- [59] Mundada A, Shrikhande B. Design and evaluation of soluble ocular drug insert for controlled release of ciprofloxacin hydrochloride. *Drug Dev Ind Pharm*. 2006;32:443–448.
- [60] Potu A, Reddy V. Design and evaluation of ocular inserts for controlled drug delivery of ketorolac tromethamine. *World J Pharm Res*. 2014;3(4):722–734.
- [61] Gorle A, Gattani S. Design and evaluation of polymeric ocular drug delivery system. *Chem Pharm Bull*. 2009;57(9):914–919.
- [62] Sankar V, Chandrasekaran A. Design and evaluation of diclofenac sodium ocular inserts. *Acta Pharm Sci*. 2006;48:5–10.
- [63] Michael H, Mostafa H, Mehdi J, et al. Draize rabbit eye test compatibility with eye irritation threshold in humans: a quantitative structural-activity relationship analysis. *Toxicol Sci*. 2003;76:384–391.
- [64] Kendre PN, Chaudhari PD. Effect of amphiphilic graft copolymer-carrier on physical stability of bosentan nanocomposite: assessment of solubility, dissolution and bioavailability. *Eur J Pharm Biopharm*. 2018;126:177–186.
- [65] Kendre PN, Chaudhari PD. Effect of polyvinyl caprolactam-polyvinyl acetate-polyethylene glycol graft copolymer on bioadhesion and release rate property of eplerenone pellets. *Drug Dev Ind Pharm*. 2017;43(5):751–761.
- [66] Kendre P, Chaudhari PD. Design and optimization of oral bioadhesive nanocurcumin delivery using novel hydrophilic carrier for cancer treatment: an alternative to parenteral chemotherapy. *Indian Drugs*. 2016;53:24–36.



Design, fabrication, and characterization of graft co-polymer assisted ocular insert: a state of art in reducing post-operative pain

Prakash N. Kendre , Pooja D. Kadam , Shirish P. Jain , Somnath K. Vibhute & Ajinkya K. Pote

To cite this article: Prakash N. Kendre , Pooja D. Kadam , Shirish P. Jain , Somnath K. Vibhute & Ajinkya K. Pote (2020): Design, fabrication, and characterization of graft co-polymer assisted ocular insert: a state of art in reducing post-operative pain, Drug Development and Industrial Pharmacy, DOI: [10.1080/03639045.2020.1833908](https://doi.org/10.1080/03639045.2020.1833908)

To link to this article: <https://doi.org/10.1080/03639045.2020.1833908>



Published online: 15 Oct 2020.



Submit your article to this journal [↗](#)



Article views: 5



View related articles [↗](#)



View Crossmark data [↗](#)

RESEARCH ARTICLE



Design, fabrication, and characterization of graft co-polymer assisted ocular insert: a state of art in reducing post-operative pain

Prakash N. Kendre^a, Pooja D. Kadam^b, Shirish P. Jain^c, Somnath K. Vibhute^a and Ajinkya K. Pote^a

^aDepartment of Pharmaceutics, Rajarshi Shahu College of Pharmacy, Buldana, India; ^bDepartment of Pharmaceutics, Sanjivani College of Pharmaceutical Education & Research, Kopargaon, India; ^cRajarshi Shahu College of Pharmacy, Buldana, India

ABSTRACT

Purpose: Targeted delivery of drugs at appropriate concentrations to ocular tissues is required to avoid wastage. Hence, advanced systems that maximize the release of poorly soluble drugs and deliver them at ocular sites must be designed.

Methods: In this study, Soluplus[®] (polyvinyl caprolactam–polyvinyl acetate–polyethylene glycol–graft copolymer) was selected as a solubilizer as well as film former for preparing ocular inserts and polyethylene glycol 400 (PEG-400) as a plasticizer. On the basis of an initial phase solubility study, the maximum concentration of Soluplus[®] possible was used for developing the inserts. An optimized formulation was obtained using a 3²-factorial design. Two factors at three levels were used to design the ocular inserts. Soluplus[®] (X_1) and the plasticizer, PEG-400 (X_2), were set as the independent variables at various levels, and the Rel_{4h} (drug release in 4 h, Y_1) and tensile strength (Y_2) were set as the dependent variables. A pre-formulation study was conducted to select suitable materials.

Results: Various physico-chemical parameters of the optimized formulation, including the tensile strength and folding endurance, were studied using FT-IR, DSC, XRD, and SEM. An *in vitro* dissolution study was conducted to determine the amount of drug released. There was no redness, swelling, or watering of the rabbit eye.

Conclusion: It was concluded that the ocular inserts of the poorly soluble nepafenac developed using a graft-co-polymer enhanced the solubility and utilization of the drug for a prolonged period.

ARTICLE HISTORY

Received 5 May 2020
Revised 22 August 2020
Accepted 1 October 2020

KEYWORDS

Ocular insert; ophthalmic drug delivery; Nepafenac; graft-co-polymer; Soluplus[®]

Introduction

In designing a formulation, the issues of absorption, distribution, metabolism, and elimination must be considered. When it comes to the delivery of pharmaceuticals, the eye offers unique opportunities and challenges. Though the absorption by this route is incompetent, there are few side effects with conventional ocular dosage forms. Most ocular formulations such as eye drops and suspensions are used to administer active drugs topically on the tissues around the ocular cavity. These dosage forms are easy to administer but suffer from inherent drawbacks. Ocular drug delivery is generally used to treat eye diseases. But problem of rapid and extensive elimination of conventional eye drops from the eye have been noticed here which lead to extensive loss of drug. Less amount of drug penetrates the corneal layer and reaches the internal tissue of eye. Drug loss occurs at lachrymal drainage and then drug dilution by tears. Hence, ocular bioavailability is reduced which leads to unwanted toxicity and side effect. Eye is a portal for drug delivery which is generally used for local therapy instead of systemic therapy. Due to high blood concentration of drug, there is risk of eye damage which can be overcome by local therapy [1,2]. Traditional topical formulations are highly concentrated, and corneal drug absorption with these formulations is low. There are ocular and systemic side effects because the pre-corneal residence time of eye drops is low [3]. Frequent administration of concentrated solutions is required to achieve the therapeutic effect. This results in the short residence of high drug

concentrations in the tear film, followed by long periods of under-dosing [4–6]. This leads to poor patient compliance. Several approaches have been adopted to overcome these issues. The use of various ophthalmic vehicles, such as suspensions, ointments, inserts, and aqueous gels, has been investigated to extend the ocular residence time of topically applied medications [7–9].

Sterile preparations with a solid or semisolid consistency, and of sizes and shapes designed for ophthalmic application, are generally known as ophthalmic inserts. These inserts are placed in the lower fornix and, sometimes, on the cornea or in the upper fornix. An ophthalmic insert is a polymeric vehicle consisting of the drug and is mainly used for topical therapy [10]. Increased ocular residence, the possibility of releasing drugs at a slow and constant rate, accurate dosing, exclusion of preservatives and increased shelf life are the prime advantages offered by ophthalmic inserts over conventional dosage forms [8–16]. Many of the such topical eye inserts are designed using polymeric components offering continuous release of drug without loss due to drainage and reducing the frequent administration [17].

The reduction of systemic absorption, which occurs freely with eye drops, is achieved with the use of these devices. Patient compliance is improved because of the lower frequency of administration and lower incidence of side effects [18–20]. The difficult problem of limited precorneal drug residence time is overcome by the use of ocular inserts [21,22]. The prime objective of using ophthalmic inserts is to increase the time of contact between the

preparation and the conjunctival tissue to ensure sustained release appropriate for topical or systemic treatment. Ophthalmic inserts consist of polymeric supports with or without drugs, the latter being incorporated as dispersions or solutions in the polymeric supports [23].

There are many polymers and film forming materials used in the design and development of ophthalmic inserts or oral dissolving films. Choice of selection of such materials is based on their physico-chemical properties and compatibility with the drug to be used for delivery. Many synthetically modified polymers and materials are available and many of the researchers have used for the development of various drug delivery systems. Polymers like: polyvinyl alcohol, polyamides, polysulfonates, cellulose acetates hydroxypropyl methyl cellulose, and modified graft-co-polymers like: Soluplus[®] (polyvinyl caprolactam–polyvinyl acetate–polyethylene glycol–graft copolymer), polyethylene oxide acrylates, polyvinyl alcohol-g-poly (oxyethylene methacrylate) PVA-g-POEM, Kollicoat[®] IR, Kollicoat[®] VA64, etc.

Soluplus[®] (polyvinyl caprolactam–polyvinyl acetate–polyethylene glycol–graft copolymer) is one of the graft-copolymers used by many researchers for the development of various drug delivery systems. It is an amphiphilic graft-copolymer which enables the enhancement of solubility and bioavailability of poor soluble drugs. Soluplus[®] can be processed as solid solutions using hot-melt-extrusion or other techniques [24–28].

However, considering the constraints of eye physiology, very few anti-inflammatory drugs show suitability to formulate the appropriate drug delivery system for the management of ocular inflammations [29].

Nepafenac is a non-steroidal anti-inflammatory prodrug (NSAID) that is usually sold as prescription eye drops. It is used to treat the pain and inflammation associated with cataract surgery [30]. It has several advantages over other ophthalmic NSAIDs. First, it has a unique prodrug structure. Prodrugs are the inactive forms of drugs that get converted into active forms after metabolic conversion in the body [29]. Nepafenac rapidly penetrates the cornea. After nepafenac penetrates the cornea, it is deaminated by intraocular hydrolases to amfenac [(2-amino-3-benzoyl phenyl) acetate], a potent inhibitor of COX-1 and COX-2 [31].

The aim of the present study was to enhance the solubility of nepafenac using the novel polymer Soluplus[®] and to formulate and evaluate nepafenac ocular inserts using a 3²-factorial design.

Materials and methods

Materials

Soluplus[®] (polyvinyl caprolactam–polyvinyl acetate–polyethylene glycol–graft copolymer) was obtained from BASF (Mumbai, India). Polyethylene glycol 400 (PEG-400) and dichloromethane were procured from Loba Chemie (Mumbai, India). All the materials used in this study were of analytical grade.

Methods

Preparation of nepafenac ocular insert

Ocular inserts of nepafenac were prepared using the solvent casting method. Soluplus[®] (polyvinyl caprolactam–polyvinyl acetate–polyethylene glycol–graft copolymer) was used as a solubility enhancer and film former, PEG-400 was used as a plasticizer to produce inserts of uniform strength, and dichloromethane was used as a solvent. Two factors at three levels were used to design the ocular inserts. Soluplus[®] (X_1) and the plasticizer, PEG-400 (X_2),

Table 1. Concentration levels and its translation of components used in the design of ocular formulation.

Independent variable	Levels		
	High (+1)	Medium (0)	Low (–1)
X_1 : Soluplus [®] (% w/w)	70	50	30
X_2 : PEG-400 (% w/v)	30	20	10

Measurable responses: Y_1 =Rel_{4h} (%); Y_2 =tensile strength (N/cm²).

Table 2. Composition of ocular insert batches as per 3²-factorial design.

Batch no.	Soluplus [®] (X_1) (% w/w)	PEG-400 (X_2) (%w/v)
F1	50	30
F2	50	20
F3	30	30
F4	30	10
F5	70	20
F6	70	30
F7	50	10
F8	70	10
F9	30	20

were considered as independent variables at various levels, and the drug release 4 h (Y_1) and tensile strength (Y_2) were considered as dependent variables (Table 1).

The concentration of nepafenac was maintained constant (1% w/w) in all the formulations. The compositions of the ocular inserts of the nine runs of the 3²-factorial design are listed in Table 2.

The required amount of Soluplus[®] was dissolved in a beaker in the required quantity of dichloromethane and stirred until it was completely dissolved. Polyethylene glycol 400 was added to the solution with stirring. A weighed amount of drug was added to this solution, which was stirred for 2 h to obtain a uniform dispersion. The polymer solution was finally sonicated to eliminate air bubbles. The casting solution was mixed and poured on a clean glass of film former (VJ Instruments, Karanja Lad, India) using a spreader. The spreader produces uniform films. The dichloromethane is evaporated by adjusting its temperature controller knob. The dried thin films thus obtained were cut to the required size (5 × 5 mm²) using a sharp cutter and ruler. They were wrapped in aluminum foil and stored in an airtight container (desiccator) [32,33].

Pre-formulation study

Solubility study. A solubility study was conducted to predict the maximum concentration of Soluplus[®] that will increase the solubility of nepafenac. The shaking flask method was used to determine the solubility. An excess amount of nepafenac was added to aqueous solutions of Soluplus[®]. Solutions with Soluplus[®] were prepared at concentrations of 5%, 10%, 15%, 25%, 45%, and 65% (w/w). Nepafenac powder was added to glass flasks containing Soluplus[®] with concentration levels as mentioned above. The samples were shaken for 24 h in a mechanical shaker. The concentrations of the nepafenac in the solutions were determined after equilibration for 24 h. A UV-spectrophotometer (1650 PC, Shimadzu, Kyoto, Japan) was used at 328 nm [34].

Fourier transform infrared (FT-IR) spectroscopy. The interaction between the nepafenac, Soluplus[®] and nepafenac ocular inserts was studied using an FT-IR spectrophotometer (Shimadzu, Kyoto, Japan). Spectra were recorded in the range 4000–400 cm^{–1}. All the samples were prepared using the KBr pellet technique, and

the spectra were recorded at a resolution of 0.15 cm^{-1} and a scanning speed of 20 scans s^{-1} [35,36].

Differential scanning calorimetric study. Differential scanning calorimetric (DSC) measurements were made using a thermal analyzer (DSC-60, Shimadzu, Kyoto, Japan). Samples of about 5 mg weight were hermetically placed in aluminum sealed pans and scanned at a heating rate of $10^\circ\text{C min}^{-1}$ over a temperature range of $0\text{--}300^\circ\text{C}$ with using nitrogen gas as an effluent gas. The thermal properties of pure nepafenac and the nepafenac ocular insert were determined [37].

Evaluation and characterization of nepafenac ocular films

Physical examination. The color and transparency of the nepafenac ocular inserts were inspected visually and other physical parameters were also evaluated using advanced tools and technologies to check the physical stability of the final formulation.

Determination of pH. The pH of the ocular inserts was determined using a digital pH meter (PICO + pH meter, Lab India, Mumbai, India). One-gram samples were added to 100 ml of distilled water each and stored for 2 h. The pH of the ocular inserts was calculated in triplicate, and the average value was calculated [38–40].

Thickness of films. The film thickness was measured using digital Vernier calipers or a micrometer screw gauge at different points, and the mean value was calculated [4,41,42].

Uniformity of weight. Three ocular inserts were cut from different parts of the film. They were individually weighed using a calibrated digital balance. The mean value was calculated. The standard deviation was calculated from the mean value [43].

Drug content uniformity. Inserts were cut from different places of the cast films. Each insert was placed in a vial containing 5 ml of pH 7.4 phosphate buffer and shaken to extract the drug from the film. One milliliter of the resulting solution was taken and diluted. The solution was analyzed using a spectrophotometer. Phosphate buffer (pH 7.4) was used as the blank [44].

Percentage moisture absorption. A percentage moisture absorption test was performed to determine the physical stability or integrity of the ocular inserts. Ocular inserts were weighed and placed in desiccators containing 100 ml of a saturated solution of aluminum chloride at 79.5% RH. After 72 h, the ocular inserts were removed and reweighed. The percentage moisture absorption was calculated using the following equation [45–47]:

$$\% \text{ Moisture absorption} = \frac{\text{[final weight} - \text{initial weight]}}{\text{initial weight}} \times 100 \quad (1)$$

Folding endurance. The folding endurance of ocular inserts/films was determined by folding them many times at the same place till a crack appeared (in this case it was folded 200 times). The number of folds required to produce the crack was counted. The folding endurance test was repeated with more sets of ocular inserts [48].

Tensile strength. The tensile strength is one of the significant mechanical properties determining the physical integrity of a film.

It is calculated as the applied load (force) at rupture divided by the cross-sectional area of a strip. A CT3 texture analyzer with a 30-g load cell was used. Film strips were held between two clamps placed 80 mm apart. Then, the strips were stretched by the top clamp at a rate of 3 mm/s, and the force at which the films broke were measured. The tensile strength was calculated using the following equation [49,50]:

$$\text{Tensile strength} \left(\frac{\text{N}}{\text{cm}^2} \right) = \frac{\text{breaking load}}{\text{cross sectional area of the sample}} \quad (2)$$

Percentage elongation. The percentage elongation at breaking was calculated according to the following equation [49,50]:

$$\% \text{ Elongation at break} = \left\{ \frac{\text{Change in length (mm)}}{\text{original length (mm)}} \right\} \times 100 \quad (3)$$

Scanning electron microscopy (SEM). A beam of electron produced by an electron gun goes through two condenser lenses, a scan coil and an objective lens to finally interact with a sample in SEM. In the sample, the electrons lose energy due to scattering and absorption. The morphology of the nepafenac ocular inserts was studied using a JSM 5400 scanning electron microscope (Diya Labs, Mumbai, India) with an acceleration voltage of 30 kV. The samples were coated with gold prior to imaging [51].

In vitro drug release study. The prepared ocular inserts were subjected to the *in vitro* drug release study using vial method. In this method, the ocular inserts (1 cm^2 size) were placed into the 25 ml capacity vials containing 10 ml of phosphate buffer solution, pH 7.4 (as pH of lacrimal fluid is 7.4). These vials were placed on the hot plate maintaining the temperature of $37^\circ\text{C} \pm 0.5^\circ\text{C}$ with continuous stirring using magnetic beads at the bottom of the vial, the care was taken to maintain the minimum speed of shaking as like blinking of eyes. The 1 ml sample was withdrawn at the interval 30 min and at the same time it was replaced with fresh 1 ml of the dissolution media to maintain the sink condition. Withdrawn sample were filtered through the Whatman paper and analyzed for drug release study using UV-spectrophotometer at 238 nm. All the results were noted in triplicate for better accuracy [4].

Data validation and optimization. Desirability approached was implemented to generate and validate the mathematical models. Various feasibility and search grid methods were implemented to establish the composition of the optimized formulation. The optimized formulation was developed and evaluated for all the obtained responses (Y_1 and Y_2). Finally, the experimental values were compared with the predicted values in order using mathematical models [52,53].

The data relating to the targeted parameters were analyzed using one-way analysis of variance (ANOVA) in Design-Expert-Software 12.0 version (Stat-Ease Inc., Minneapolis, MN). Individual parameters were analyzed using polynomial equation:

$$Y = \beta_0 + \beta_1 X_1 + \beta_2 X_2 + \beta_3 X_1 X_2 + \beta_4 X_1^2 + \beta_5 X_2^2 \quad (4)$$

where Y is the measured response, β_0 is the intercept, and β_1 to β_5 are the regression coefficients. X_1 and X_2 are the main effects, $X_1 X_2$ is the interaction term between X_1 and X_2 , and X_1^2 and X_2^2 are the quadratic terms of the independent variables. Using multiple linear regression analysis (MLRA) and ANOVA, polynomial models containing only substantial terms were produced ($p < .05$) for every

response. All the resultant models and data were used to construct three-dimensional diagrams to represent response *Y* as a function of *X*. Contour plots were generated to represent the effect of all the independent variables on each response.

Stability studies. The selected formulations were stored at 25 °C/60%RH and 40 °C/75%RH for 2 months and evaluated for their physical appearance, drug content, and drug–excipient compatibility at specific periods of time [44].

Sterility testing. Sterility testing is carried out to detect the presence of viable forms of microorganisms. The testing was performed using fluid thioglycolate medium and soybean casein digest medium, as per the Indian Pharmacopoeia. The formulations were sterilized separately under UV radiation for 30 min. The irradiated formulations were tested under aseptic conditions for viable forms of bacteria, fungi, and yeast in both the media prescribed by the Indian Pharmacopoeia [54–59].

Ocular irritancy test. The sterilized ocular inserts were used in an eye irritancy test. The Draize technique, which has been designed for testing ocular irritation of ophthalmic products, was used. Clearance for handling the experimental animals was obtained from the Institutional Animal Ethical Committee (IAEC) constituted for the purpose. The ocular inserts were placed into the lower cul-de-sac, and observations of the various parameters were made 1 h, 24 h, 48 h, 72 h, and 1 week after administration. Three male rabbits weighing between 1.5 and 2 kg were used in the study. The sterile formulation was administered twice a day for a period of seven days. The rabbits were observed periodically for redness, swelling, and watering of the eyes [60–63].

Results and discussion

As described in above-mentioned section of methods, the thin films were formed using the solvent casting method and a film former. The composition of the films was according to the 3²-factorial design (Table 2). The thin films obtained were transparent, flexible, and smooth in appearance.

Preliminary batches were produced to finalize the specific ranges of concentrations of Soluplus[®] and the plasticizer (PEG-400). Flexible, transparent, and smooth-surfaced thin films were obtained. There was better release of nepafenac in the ocular region. At higher concentration levels of Soluplus[®] and PEG-400, the films obtained were very sticky, thick, and somewhat tacky. At lower concentrations of both Soluplus[®] and the plasticizer, the films were very brittle and could not be removed easily from the glass surface after drying. Hence, on the basis of this preliminary study, the final concentrations of Soluplus[®] and PEG-400 were 30–70% and 10–30%, respectively. Nine possible combinations were obtained from the 3²-factorial design (Table 2). After batches of all the formulations were prepared, the films obtained were evaluated for various physical and chemical properties. These are discussed in a later section.

Pre-formulation study

Before finalizing the optimized formulations and characterizing them, a preliminary study was conducted on the compatibility of all the components used in the design of the ocular films. Physical blends of the drug and other components were subjected to FT-IR, DSC, and XRD analysis. The results of the study conducted to

check the suitability of the materials used are presented in the following sections.

FT-IR study

Compatibility of the drug and other components used is essential for preparing a final formulation. Nepafenac and Soluplus[®] were subjected to FT-IR analysis. Major peaks of nepafenac spectra consisting of N–H stretch at 3440; C=O stretch (carboxylic acid group) at 1676; C–O (ester group) at 1194; C–H stretch (aromatic group) 2877; C–H bending (aromatic group); C–Br stretch at 753. No extra peaks were found in the spectrum of the drug and excipients blend, indicating an absence of interactions or the instability of ocular insert formulation. FT-IR spectra of pure nepafenac and blend of nepafenac and Soluplus[®] is presented in Figure 1.

Differential scanning calorimetry

Nepafenac, Soluplus[®] and their blend were subjected to DSC analysis. In the DSC thermogram of nepafenac, a sharp endothermic peak was found at 184.93 °C, corresponding to the melting and reported decomposition at 183.54–186.4 °C.

Soluplus[®] showed an endothermic peak at 63.66 °C. The DSC thermograph of the drug–Soluplus[®] mixture showed an endothermic peak at the melting point of Soluplus[®] (62.93 °C). This shows that nepafenac is completely entrapped within Soluplus[®]. This indicates that there is no interaction between nepafenac and Soluplus[®]. The DSC thermograms are presented in Figure 2.

Solubility study

There was significant increase in solubility of nepafenac at 45% concentration level of Soluplus[®], beyond this level, there was no significant increase in solubility. It is observed that the presence of Soluplus[®] increases the solubility of nepafenac almost more than 200 times compared with the plain drug [64–66]. From this study, it was clear that the concentration of Soluplus[®] should not be less than 45% for maximum solubility of nepafenac (Figure 3). But another aspect in the design of ocular inserts is to keep all the physical and chemical properties so that the final formulation is stable and improved. Hence, the concentration level of Soluplus[®] was maintained between 30% and 70% for the development of ocular insert formulations, as mentioned in Table 1.

Evaluation and characterization of ocular inserts of nepafenac

As per the 3²-factorial design, all the nine formulations were prepared using different concentrations of Soluplus[®] and PEG-400. Various physical and chemical properties such as weight, thickness, tensile strength, percent elongation, folding endurance, percent moisture absorption, surface pH, and drug content of these formulations were evaluated (Table 3). The average weight of these inserts (10 × 10 mm²) was in the range from 8.38 ± 0.01 mg to 22.44 ± 0.02 mg. Batch F4 has the minimum weight (8.38 ± 0.01 mg), and batch F6 has the maximum weight (22.44 ± 0.02 mg). The variation in the weight was observed due to the fact that batch F4 has lower concentrations of both Soluplus[®] and PEG-400, whereas batch F6 has higher levels of both Soluplus[®] and PEG-400. In all the formulations, the concentration of the drug was maintained at the same level. Overall, from all the observations, it is clear that as the concentration levels of both Soluplus[®] and PEG-400 increase, the weight of the insert/film

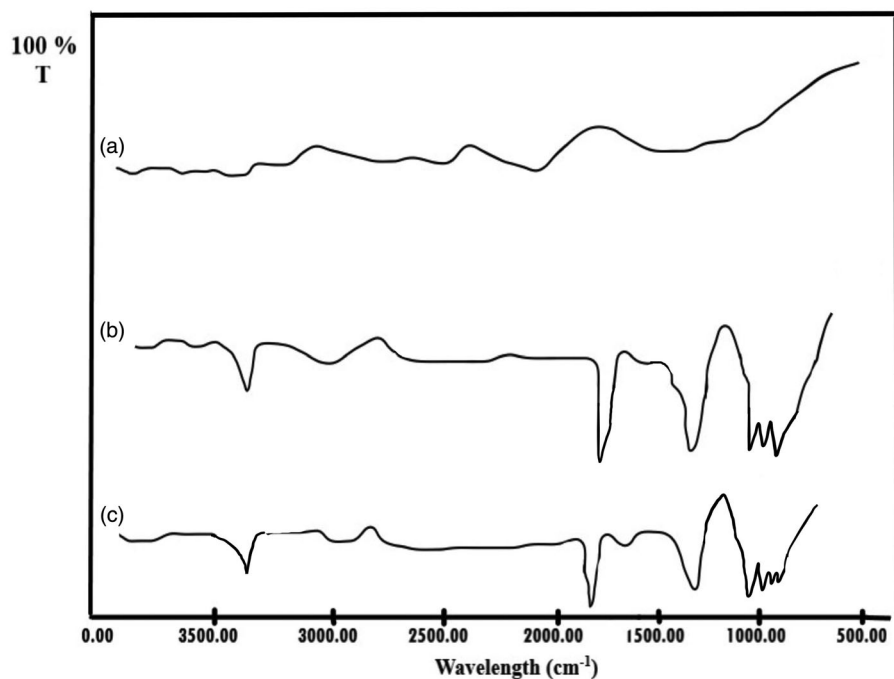


Figure 1. FT-IR spectra of: Soluplus® (a); Nepafenac (b); blend of nepafenac and Soluplus® (c).

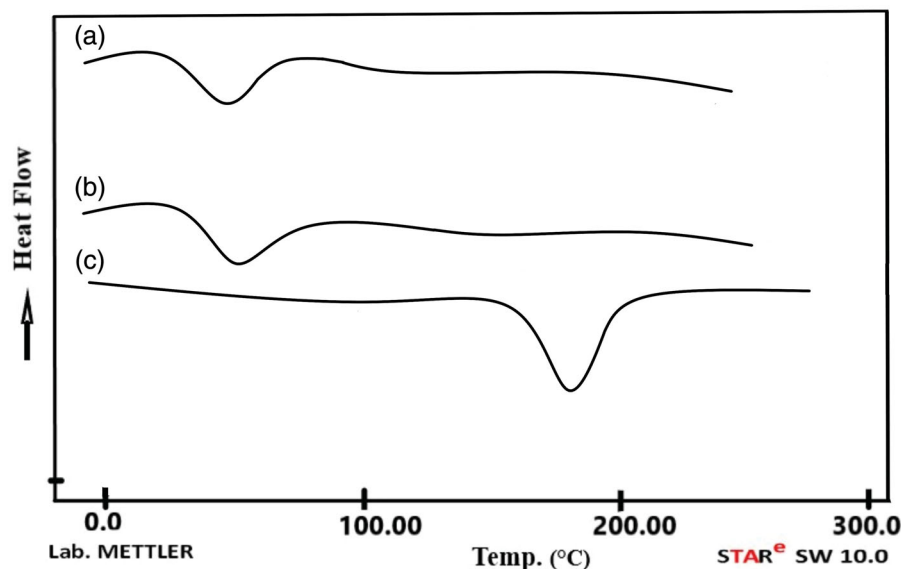


Figure 2. DSC thermogram of: Soluplus® (a); blend of nepafenac and Soluplus® (b); Nepafenac (c).

also increases. There were similar observations about the thickness, tensile strength, percent elongation, and moisture absorption, the highest values of these parameters among all the nine formulations prepared as per the 3^2 -factorial design were $289.25 \pm 1.25 \mu\text{m}$, $7.58 \pm 1.78 \text{ N/m}^2$, $96.28 \pm 1.25\%$, and $8.56 \pm 1.47\%$, respectively. In the similar way, the lowest values were $123.5 \pm 1.45 \mu\text{m}$, $2.55 \pm 1.27 \text{ N/m}^2$, $52.0 \pm 1.2\%$, and $3.25 \pm 2.35\%$, respectively.

All the results considered were the average of three values for each parameter. But the final decision was based on another important dependent variable $\text{Rel}_{4\text{hr}}$, which was also

discussed subsequently. Other physical parameters such as the surface pH was found to be in the range of 7.4–7.8 whereas folding endurance was found to be varied from a low value of 127 to values >223 . Here also, the concentrations of both Soluplus® and PEG-400 played an important role. The effect was directly proportional to the concentration levels of the two materials although the same amount of drug was present in all the formulations. The folding endurance increased with the concentration levels. The drug content in all the nine formulations was found to be satisfactory (above 90%). It was in the range from $95.43 \pm 1.8\%$ to $98.99 \pm 1.25\%$ (Table 4).

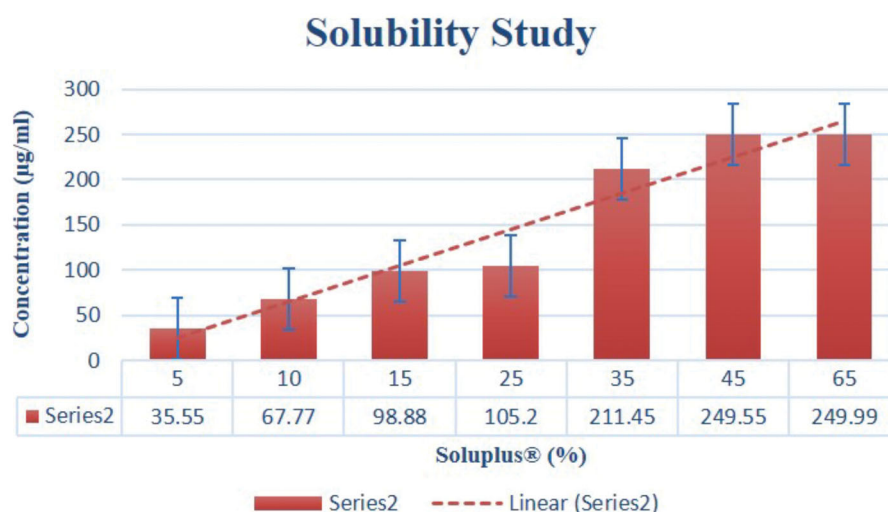


Figure 3. Solubility study of Nepafenac in the presence of Soluplus® as solubilizer.

Table 3. Evaluation of physical and chemical properties of nepafenac ocular insert.

Batch	Weight (mg)	Thickness (µm)	% Drug content	Tensile strength (N/m ²)	% elongation	% Moisture absorption
F1	18.3 ± 0.01	213.33 ± 1.654	98.23 ± 1.5	5.55 ± 1.02	92.99 ± 1.2	6.98 ± 1.25
F2	16.7 ± 0.012	198.65 ± 2.453	98.99 ± 1.25	4.54 ± 1.55	90.99 ± 1.78	5.60 ± 2.25
F3	11.8 ± 0.02	158.76 ± 3.564	95.43 ± 2.24	5.95 ± 2.01	74.00 ± 1.01	4.65 ± 1.58
F4	8.38 ± 0.24	123.5 ± 1.45	96.45 ± 1.88	2.55 ± 1.27	52.0 ± 1.28	3.25 ± 2.35
F5	17.8 ± 0.06	208.32 ± 1.55	95.89 ± 1.2	5.01 ± 1.87	94.0 ± 1.88	7.80 ± 1.25
F6	22.44 ± 0.02	289.25 ± 1.25	98.258 ± 1.25	7.58 ± 1.78	96.28 ± 1.25	8.56 ± 1.47
F7	17.58 ± 0.05	211.25 ± 2.25	96.45 ± 1.55	3.25 ± 1.01	88.25 ± 2.25	5.4 ± 1.54
F8	18.58 ± 0.25	221.3 ± 1.25	97.54 ± 1.25	4.55 ± 1.28	91.25 ± 1.02	6.89 ± 2.25
F9	9.5 ± 0.432	134.201 ± 2.64	97.55 ± 1.54	5.58 ± 1.78	78.29 ± 1.67	4.58 ± 1.77

All the observations were taken in triplicate as ± SD ($n = 3$).

Table 4. Summary of *in vitro* drug release data as per with mathematical model fitting as per 3²-factorial design.

Batch	Zero order		First order		Higuchi model	
	K_0	R^2	$K1$ (h ⁻¹)	R^2	KH (h ⁻¹)	R^2
F1	1.48 ± 0.058	0.9988 ± 0.014	0.03 ± 0.01	0.9934 ± 0.04	8.69 ± 0.34	0.9433 ± 0.014
F2	1.25 ± 0.145	0.9752 ± 0.055	0.015 ± 0.01	0.9635 ± 0.014	7.69 ± 0.38	0.9655 ± 0.05
F3	2.38 ± 0.065	0.9556 ± 0.055	0.045 ± 0.02	0.9567 ± 0.01	7.25 ± 0.45	0.8936 ± 0.025
F4	1.28 ± 0.048	0.9438 ± 0.045	0.025 ± 0.01	0.9433 ± 0.05	6.55 ± 0.24	0.9633 ± 0.025
F5	1.25 ± 0.068	0.9755 ± 0.014	0.035 ± 0.03	0.9855 ± 0.014	11.55 ± 0.36	0.9523 ± 0.025
F6	1.54 ± 0.055	0.9775 ± 0.023	0.025 ± 0.02	0.9624 ± 0.016	13.52 ± 0.35	0.9733 ± 0.02
F7	2.28 ± 0.024	0.9466 ± 0.014	0.042 ± 0.03	0.9725 ± 0.016	19.25 ± 0.34	0.9833 ± 0.055
F8	3.25 ± 0.047	0.8622 ± 0.035	0.044 ± 0.05	0.9815 ± 0.019	18.55 ± 0.56	0.9688 ± 0.025
F9	1.85 ± 0.036	0.9625 ± 0.014	0.055 ± 0.03	0.9725 ± 0.045	18.65 ± 0.65	0.9833 ± 0.02

All the observations were taken in triplicate as ± SD ($n = 3$).

Scanning electron microscopy

The morphology of the nepafenac ocular inserts prepared was characterized by SEM analysis. The SEM images revealed that the inserts have a uniform surface with small pores and drug may release from this surface. The ocular inserts had a clear appearance with smooth surface and texture, SEM images are shown in Figure 4.

In vitro drug release study

An *in vitro* drug release study of the nepafenac ocular inserts was carried out. The release profile obtained is shown in Figure 5. It was observed that the release of the drug from the inserts of all the nine formulations in 4 h was in the range from 66.55% to 95.25%. The drug release of formulation F3 was very low (66.55%), whereas that of formulation F6 was the highest (95.25%). The low drug release from formulation F3 was due to the fact that the formulation contains higher levels of plasticizer

compared with the concentration of Soluplus®, which retards the release from the insert. Formulation F6, in contrast, contains lower levels of the plasticizer compared with Soluplus®. Overall, the same trend was observed with the remaining formulations due to the different levels of the two components. Soluplus® is the polymer of choice for playing the roles of both film former and solubilizer. Hence, the formulations containing higher levels of Soluplus® had the maximum drug release. Further, the drug release was also influenced by presence of pores at the film surface, the permeation capacity of film surface and the diffusivity and solubility of the drug in the presence of Soluplus®. Hence, the role of Soluplus® was found to be very important in improving the solubility of nepafenac. The solubility of nepafenac increased (more than 200 times) as described in section 'Solubility study'. This phenomenon played a major role in the release of the drug, along with the role of the supportive plasticizer (PEG-400), which gave the inserts sufficient strength for continuous release up to 4 h [64–66].

In Vitro Drug Release Study

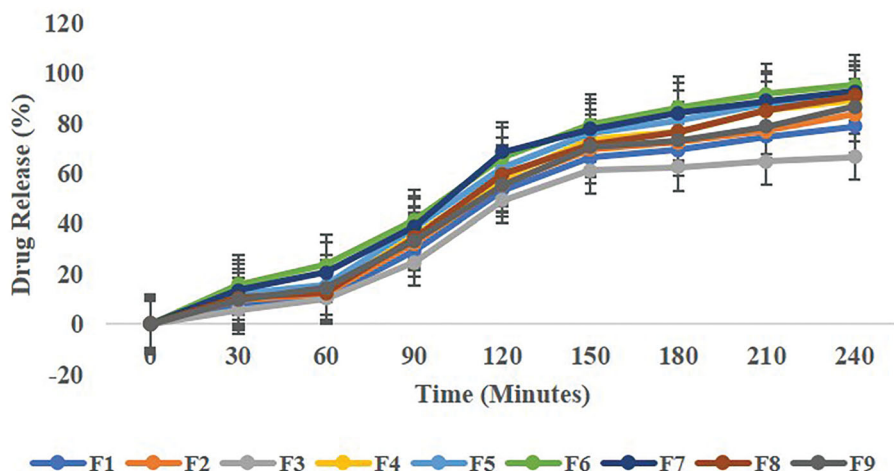


Figure 4. In vitro drug release study of all the nine formulations as per 3²-factorial design.

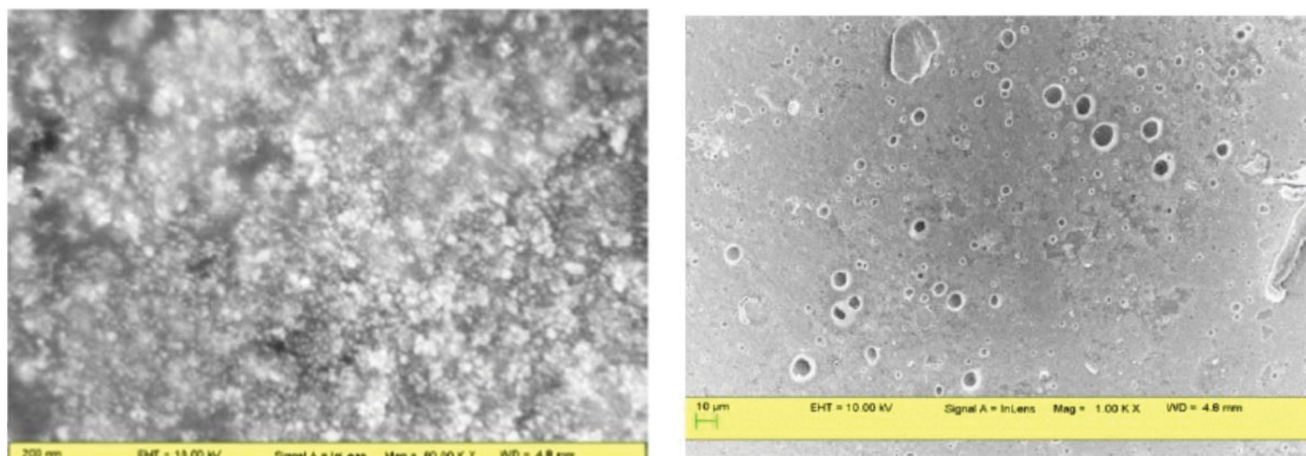


Figure 5. Scanning electron microscopic (SEM) images of optimized ocular insert at different resolutions.

Table 5. Summary of ANOVA for response parameters as per 3²-factorial design.

Response	F Value	Prob>F	Predicted R ²	Adjusted R ²	% CV
Rel 4h (Y ₁)	13.85	0.05	98.24	99.51	1.58
Tensile strength (Y ₂)	23.31	0.05	97.36	98.54	2.36

Regression equations best models:

$$Y_1 = 86.07X_1 + 5.87X_2 - 5.36X_1X_2;$$

$$Y_2 = 4.54X_1 - 0.700X_2 + 0.0925X_1X_2 + 0.756X_1^2 - 0.138X_2^2.$$

The *in vitro* drug release data of the nine formulations fitted the zero-order equation well, but the best-fit model was the first-order equation. The results of ANOVA and mathematical models were generated by regression analysis and fits of all the models are shown in Table 5.

If there are many insignificant model terms (not counting those required to support hierarchy), model reduction may improve the model, but in the case of both responses Y₁ and Y₂, all the model terms (X₁, X₂ and X₁:X₂) are significant. In the case of response Y₁ (Rel_{4h}), the model F-value of 13.85 implies that the model is significant. There is only a 0.74% chance that an F-value this large could occur due to noise. *p* Values less than .0500 (in this case *p* = .0074) indicate model terms that are significant. The predicted R² value of 0.9824 is in reasonable agreement with the adjusted R² value of 0.9951 in the case of the response parameter of Y₁ (Rel_{4h}). Adequate precision measures the signal to noise ratio. A

signal-to-noise ratio greater than 4 is desirable. In this case, the ratio is 12.887, indicating an adequate signal. This model can be used to navigate the design space. The 2FI model generated for Rel_{4h} indicated that the Soluplus[®] (X₁) concentration had a positive influence on Y₁. As the concentration of Soluplus[®] increases, the release of nepafenac also increases. In addition to the main effects, the interaction term, X₁:X₂ (Soluplus[®]: PEG-400), had a significant negative influence on Y₁. As the concentration of Soluplus[®] increases, the release of nepafenac also increases, but at higher concentrations of X₂ along with X₁ has a negative influence on Rel_{4h}. Here, the release of the drug decreases as the concentration of X₂ increases. This was due to the retardant effect of PEG-400 as it increases the plasticity the insert.

In the case of response Y₂ (tensile strength), the F-value of 23.31 implies that the model is significant. There is only a 0.15% chance that an F-value this large could occur due to noise. *p* Values less than .0500 (in this case *p* = .0015) indicate that the model terms are significant. The predicted R² of 0.9736 is in reasonable agreement with the adjusted R² of 0.9854 in the case of the response parameter of Y₂ (tensile strength). Adequate precision measures the signal to noise ratio. A ratio greater than 4 is desirable. In this case, the ratio of 9.887 indicates an adequate signal. This model can be used to navigate the design space. The quadratic model generated for Y₂ indicated that the Soluplus[®] (X₁)

Table 6. Response parameters as per 3^2 factorial design.

Formulation Batch	Independent variable X_1 : Soluplus® (%)	Independent variable X_2 : PEG-400 (%)	Y_1	Y_2
			Rel _{4h} ^a (%)	Tensile strength ^a (N/cm ²)
F1	50	30	78.66 ± 1.25	5.55 ± 1.02
F2	50	20	83.55 ± 1.02	4.54 ± 1.55
F3	30	30	66.55 ± 2.03	5.95 ± 2.01
F4	30	10	89.25 ± 1.14	2.55 ± 1.27
F5	70	20	91.44 ± 1.58	5.01 ± 1.87
F6	70	30	95.25 ± 1.36	7.58 ± 1.78
F7	50	10	92.5 ± 1.75	3.25 ± 1.01
F8	70	10	90.88 ± 1.34	4.55 ± 1.28
F9	30	20	86.54 ± 1.78	5.58 ± 1.78

^aAll the observations were taken in triplicate as ± SD ($n = 3$).

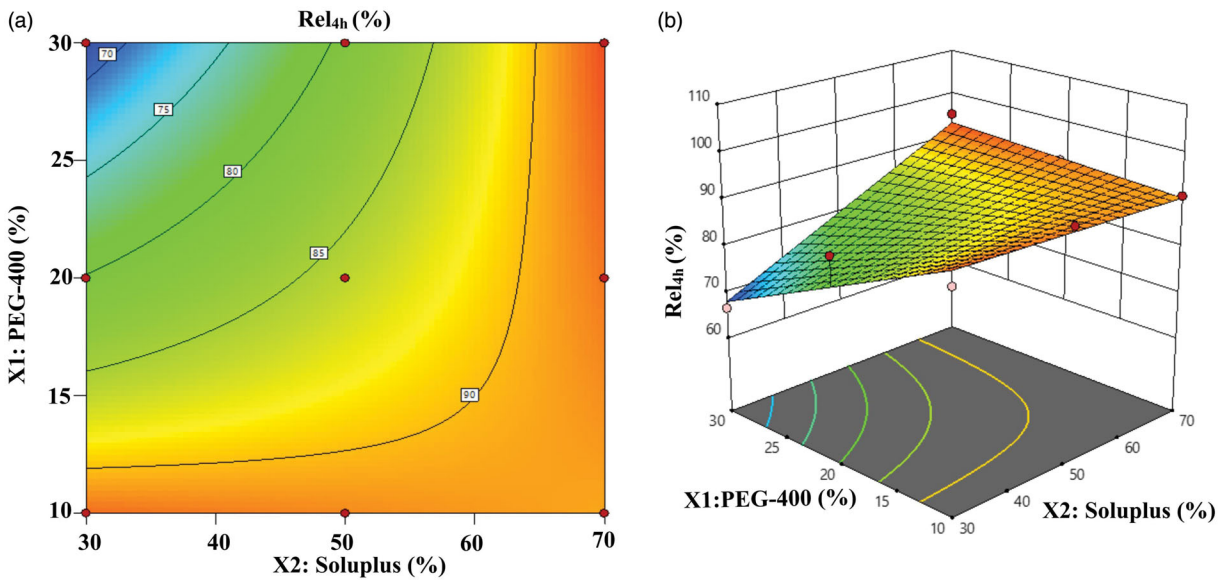


Figure 6. Contour and 3D surface response graph: (a, b) for Rel_{4h} response parameter, respectively.

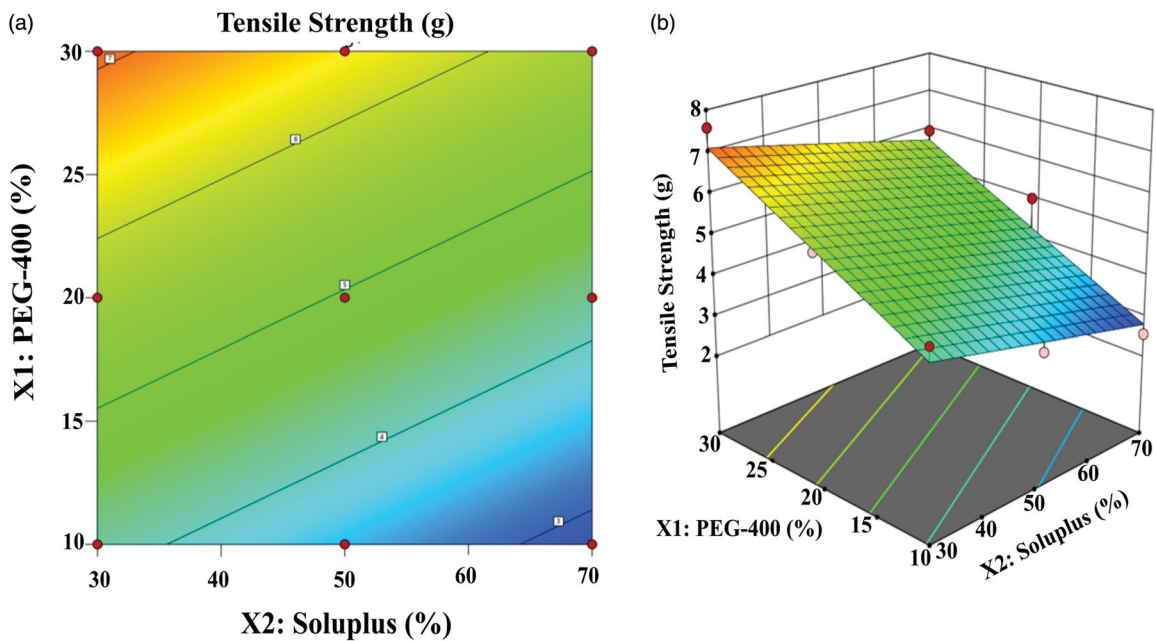


Figure 7. Contour and 3D surface response graph: (a, b) for tensile strength response parameter, respectively.

concentration had a negative influence on Y_2 . As the concentration of Soluplus® increased, the tensile strength of the insert decreased, whereas with higher concentrations of PEG-400 (X_2),

the tensile strength increases. This is due to the plasticizer effect of PEG-400. In addition to the main effects, the interaction term $X_1 \cdot X_2$ (Soluplus®: PEG-400) had a significant negative influence on

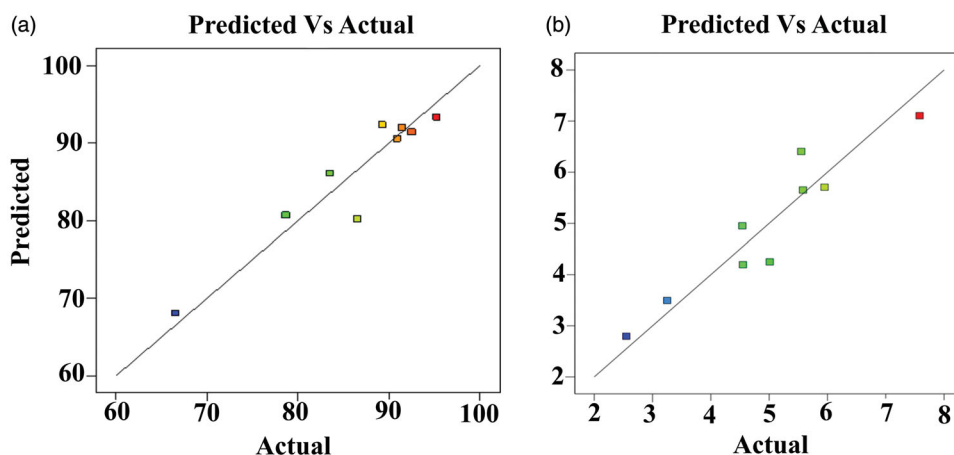


Figure 8. The relation between predicted vs. actual experimental values for both the response variables Rel4h (Y₁) (a) and tensile strength (Y₂) (b).

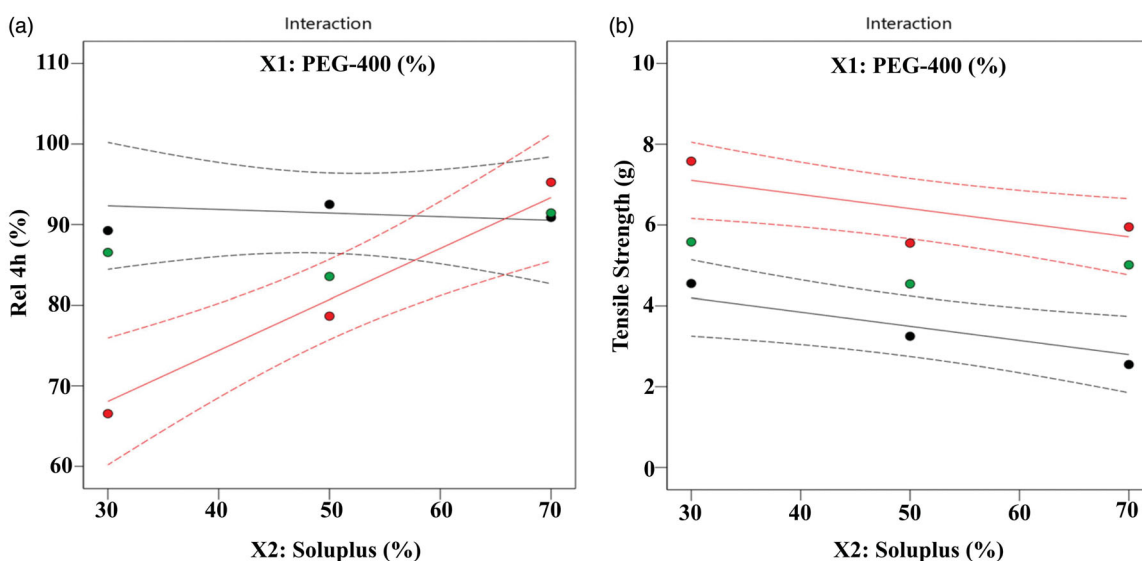


Figure 9. Response plots (a, b) showing the combined effect of due to interaction of X₁:X₂ on both response parameter Rel4h (Y₁) (a) and tensile strength (Y₂) (b).

Y₂ (p=.0143). As the concentration of PEG-400 increases, the tensile strength also increases, but at higher concentrations of X₂ along with X₁ has a negative influence on the tensile strength. Here, it decreases as the concentration of X₁ increases. The results of the response parameters Rel_{4h} (Y₁) and tensile strength (Y₂) are shown in Table 6.

The effects of all the independent factors are presented in the form of contour plots and three-dimensional surface response plots (Figures 6 and 7).

The relation between the predicted and actual experimental values for both the response variables Y₁ and Y₂ is shown graphically in Figure 8. The combined effect due to interaction (X₁:X₂) on the response parameters Y₁ and Y₂ is shown in Figure 9. Overlay plot for both responses (Y₁ and Y₂) is highlighted in Figure 10.

The main aim of the present study was to develop an ocular insert which released the nepafenac in 4 h (Rel_{4h}) and had better tensile strength for continuous drug release.

Stability study

The selected formulations were tested for 3 months at storage conditions of 25°C and 40°C at 60% RH (relative humidity) and 75% RH, and they were analyzed for their drug content. The

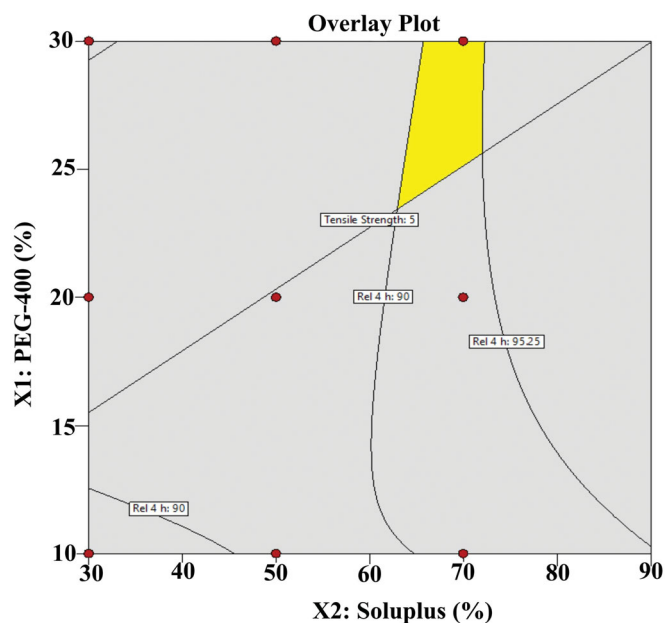


Figure 10. Overlay plot for both response parameter Rel4h (Y₁) and tensile strength (Y₂). 125

Table 7. Evaluation of optimized ocular insert after stability study.

Batch	Weight (mg)	Thickness (μm)	% Drug content	Tensile strength (N/m^2)	% elongation
F1	19.6 \pm 0.03	222.90 \pm 1.28	97.33 \pm 1.25	4.80 \pm 1.15	98.33 \pm 1.26
F2	18.9 \pm 0.032	202.78 \pm 2.25	96.80 \pm 1.55	5.54 \pm 1.78	91.25 \pm 1.54
F3	13.1 \pm 0.22	162.54 \pm 2.35	94.83 \pm 2.94	6.10 \pm 2.14	76.58 \pm 1.45
F4	10.25 \pm 0.21	126.4 \pm 1.35	95.85 \pm 1.25	3.25 \pm 1.47	60.10 \pm 1.78
F5	19.4 \pm 0.23	210.87 \pm 1.67	95.25 \pm 1.22	5.22 \pm 1.54	96.55 \pm 1.45
F6	25.12 \pm 0.12	292.95 \pm 1.90	97.568 \pm 1.85	7.24 \pm 1.52	98.57 \pm 1.65
F7	19.98 \pm 0.15	213.14 \pm 2.45	95.88 \pm 1.65	3.58 \pm 1.23	90.95 \pm 2.75
F8	19.68 \pm 0.25	223.31 \pm 1.02	95.74 \pm 1.85	3.75 \pm 1.81	92.65 \pm 1.32
F9	11.9 \pm 0.36	135.21 \pm 2.25	95.75 \pm 1.89	5.88 \pm 1.64	80.47 \pm 1.27

All the observations were taken in triplicate as \pm SD ($n = 3$).

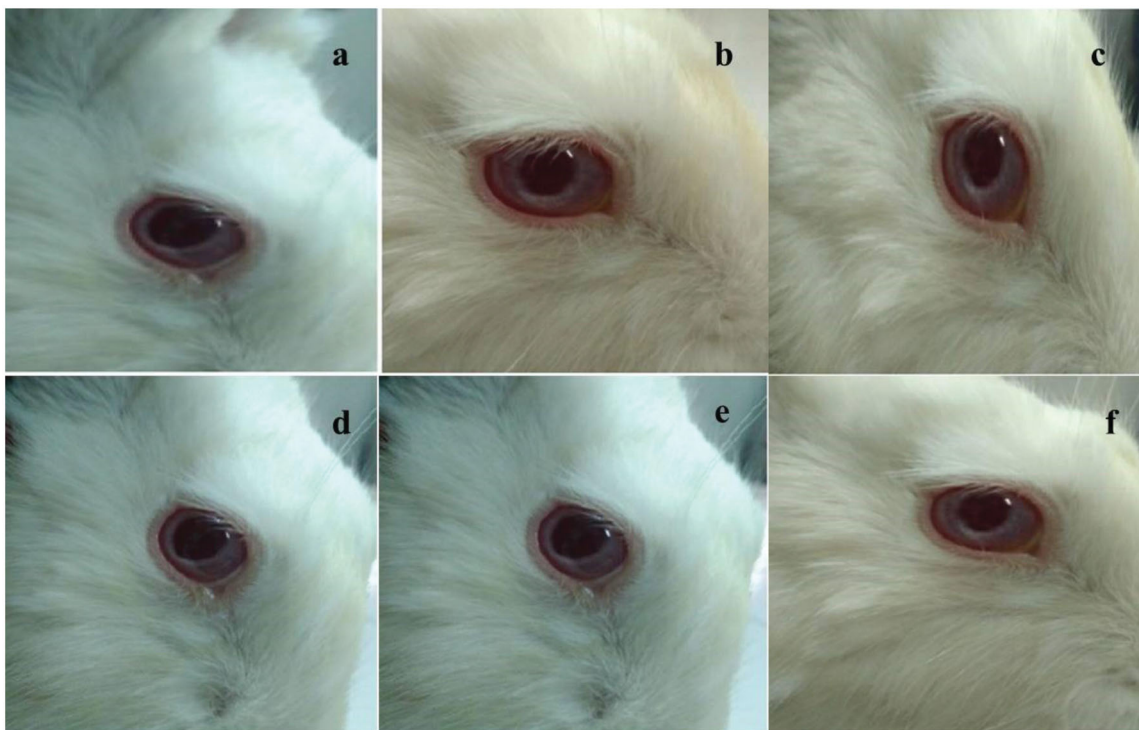


Figure 11. Ocular irritancy test for optimized ocular insert on rabbit eye at every interval for one-week period.

residual drug content of the selected formulations was found to be within the permissible limits. The formulations showed satisfactory physical stability at 25°C and 40°C at 60% RH and 75% RH, respectively, and no significant changes were observed after stability study. The physical appearance did not change considerably. The results of stability study are highlighted in Table 7.

Sterility testing

All the sterile inserts complied with the test for sterility with a positive control and a negative control test conducted as per the procedure of the Indian Pharmacopeia. The formulations did not show any microbial growth, which suggests that the inserts were sterile.

Ocular irritancy test

The sterilized formulations were placed into the lower cul-de-sac, and the various criteria were observed at 1 h, 12 h, 24 h, 48 h, 72 h, and 1 week after administration. No redness, swelling, or watering of the rabbit eye was observed. This indicates that the inserts did not produce ocular irritancy and toxicity (Figure 11).

Conclusion

The aim of the present study was to develop an ocular insert/film of the poorly water-soluble nepafenac using a 3²-factorial design. The response parameters Rel_{4h} and tensile strength were set as the dependent variables. The goal was set by considering the constraints of the variations in the concentration levels of the film former (Soluplus®) and the plasticizer (PEG-400). Using the feasibility and grid search methods, an insert with a drug release greater than 90% after 4 h and with better physical stability and strength was obtained successfully. All the physico-chemical parameters were found to be excellent for delivering nepafenac in a continuous manner for 4 h. It is concluded that an optimized insert/film of the poorly water-soluble nepafenac can be formulated using the novel graft-co-polymer at appropriate concentrations of the plasticizer, PEG-400, by reducing the dosing frequency. The effect is prolonged and the patient compliance is better.

Acknowledgements

Authors are very thankful to the BASF Corporation, Mumbai, India and grateful to Micro Labs, Hosur, India. Authors are also thankful to the Management and Principal of the College to provide other

chemicals and supporting resources to complete this research work successfully.

Disclosure statement

No potential conflict of interest was reported by the author(s).

Data availability statement

Author/s hereby declares that the raw/processed data required to reproduce these findings cannot be shared at this time due to legal or ethical reasons.

References

- [1] Sreenivas SA, Hiremath SP, Godbole AM. Ofloxacin ocular inserts: design, formulation and evaluation. *Iran J Pharm Res.* 2006;5(2):159–162.
- [2] Chien YW. *Ocular drug delivery and delivery systems; novel drug delivery systems.* 2nd ed. New York: Marcel Dekker; 1996. p. 269–270.
- [3] Ara T, Sharma S, Bhandari A. Preparation and evaluation of ocular inserts of diclofenac sodium for controlled drug delivery. *Der Pharm.* 2014;6(6):93–99.
- [4] Jafariazar Z, Jamalnia N, Ghorbani-Bidkorbeh F, et al. Design and evaluation of ocular controlled delivery system for diclofenac sodium. *Iran J Pharm Res.* 2015;14:23–31.
- [5] Lee VH, Robinson JR Jr. Topical ocular drug delivery: recent developments and future challenges. *J Ocul Pharmacol Ther.* 1986;2:67–108.
- [6] Hermans K, Van den Plas D, Kerimova S, et al. Development and characterization of mucoadhesive chitosan films for ocular delivery of cyclosporine A. *Int J Pharm.* 2014; 472:10–19.
- [7] Sultana Y, Aqil M, Ali A. Ocular inserts for controlled delivery of pefloxacin mesylate: preparation and evaluation. *Acta Pharm.* 2005;55:305–314.
- [8] Baranowski P, Karolewicz B, Gajda M, et al. Ophthalmic drug dosage forms: characterization and research methods. *Science.* 2014;2014:1–14.
- [9] Atram S, Bobade N. Current trends towards an ocular drug delivery system: review. *Int J Pharm Pharm Sci.* 2013;3(1): 28–34.
- [10] Karthikeyan D, Bhowmick M, Pandey V, et al. The concept of ocular inserts as drug delivery systems: an overview. *Asian J Pharm.* 2008;2:192–193.
- [11] Attia M, Kassem M, Safwat S. In-vivo performance of 3H-dexamethasone ophthalmic film delivery systems in the rabbit eye. *Int J Pharm.* 1988;47:21–30.
- [12] Kumar S, Nagori B. Ocular insert: dosage form for sustain ophthalmic drug delivery. *J Farm Klin Indones.* 2012;1(2): 61–73.
- [13] Bade M, Gawali V. Ocular inserts: a rate controlled drug delivery system – a review. *IJPE.* 2012;2(1):49–63.
- [14] Rajput G, Sharma S. Review on ophthalmic inserts. *Int J Pharma Prof Res.* 2013;4(3):912–920.
- [15] Barath S, Hiremath S. Ocular delivery system of pefloxacin mesylate. *Pharmazie.* 1999;54:55–58.
- [16] Hume LR, Lee HK, Benedetti L, et al. Ocular sustained delivery of prednisolone using hyaluronic acid benzyl ester films. *Int J Pharm.* 1994;111:295–298.
- [17] Rathore K, Nema R. An insight into ophthalmic drug delivery system. *Int J Pharm Sci Drug Res.* 2009;1:1–5.
- [18] Grass G, Cobby J, Makoid M. Ocular delivery of pilocarpine from erodible matrices. *J Pharm Sci.* 1984;73:618–621.
- [19] Maichuk Y. Ophthalmic drug inserts. *Invest Ophthalmol Vis Sci.* 1975;14:87–90.
- [20] Ozawa H, Hosaka S, Kunitomo T, et al. Ocular inserts for controlled release of antibiotics. *Biomaterials.* 1983;4: 170–174.
- [21] Kumari A, Sharma P, Garg V. Ocular insert: advancement in therapy of eye diseases. *J Adv Pharm Technol Res.* 2010; 1(3):291–296.
- [22] Saettone MF, Salminen L. Ocular inserts for topical delivery. *Adv Drug Deliv Rev.* 1995;16:95–106.
- [23] Sampath Kumar K, Bhowmik D. Ocular inserts: a novel controlled drug delivery system. *Pharma Innov J.* 2013;1(12): 1–16.
- [24] Michael L, Collnot E-M, Djuric D, et al. Soluplus[®] as an effective absorption enhancer of poorly soluble drugs in vitro and in vivo. *Eur J Pharm Sci.* 2012;45:336–343.
- [25] Shamma R, Elkasabgy Design of freeze-dried Soluplus/polyvinyl alcohol-based film for the oral delivery of an insoluble drug for the pediatric use. *Drug Deliv.* 2016;23(2):489–499.
- [26] Dian L, Yu E, Chen X, et al. Enhancing oral bioavailability of quercetin using novel soluplus polymeric micelles. *Nanoscale Res Lett.* 2014;9:684.
- [27] Shamma RN, Basha M. Soluplus[®]: a novel polymeric solubilizer for optimization of carvedilol solid dispersion: formulation design and effect of method of preparation. *Powder Technol.* 2013;237:406–414.
- [28] Kim DH, Park MS, Choi Y, et al. Synthesis of PVA-g-POEM graft copolymers and their use in highly permeable thin composite membranes. *Chem Eng J.* 2018;346:739–747.
- [29] Available from: <https://www.drugbank.ca/drugs/db06802>
- [30] Ahuja M, Dhake AS, Sharma SK, et al. Topical ocular delivery of NSAIDs. *AAPS J.* 2008;10(2):229–241.
- [31] Lane S. Nepafenac: a unique nonsteroidal prodrug. *Int Ophthalmol Clin.* 2006;46(4):13–20.
- [32] Khurana G, Arora S, Pawar P. Ocular insert for sustained delivery of gatifloxacin sesquihydrate: preparation and evaluations. *Int Pharm Investig.* 2012;2(2):70–77.
- [33] Agrawal A, Jadhav L. Ocular drug delivery system and role of ocular inserts in eye disorder treatment: a review. *Asian J Pharm Technol Innov.* 2016;4(21):45–54.
- [34] Karathanos VT, Mourtzinis I, Yannakopoulou K, et al. Study of the solubility, antioxidant activity and structure of inclusion complex of vanillin with cyclodextrin. *Food Chem.* 2007;101:652–658.
- [35] Aburahma M, Mahmoud A. Biodegradable ocular inserts for sustained delivery of brimonidine tartarate: preparation and in-vitro/in-vivo evaluation. *AAPS PharmSciTech.* 2011;12(4): 1335–1347.
- [36] Dave V, Paliwal S, Yadav S. Formulation and evaluation of controlled delivery of aceclofenac through ocular insert. *Turk J Pharm Sci.* 2013;10(2):205–220.
- [37] Mathurm M, Gilhotra RM. Glycerogelatin-based ocular inserts of aceclofenac: physicochemical, drug release studies and efficacy against prostaglandin E2-induced ocular inflammation. *Drug Deliv.* 2011;18(1):54–64.
- [38] Pandey A, Mali P. Design and in-vitro characterization of levobunolol hydrochloride ocuserts with special reference to glaucoma treatment. *Indian J Pharm Educ Res.* 2012; 46(3):265–269.

- [39] Pandey P, Panwar A. Design and evaluation of ocular inserts for controlled drug delivery of acyclovir. *Int J Pharm Biol Arch*. 2011;2(4):1106–1110.
- [40] Nappinnai M. Fluconazole ocular inserts: formulation and in-vitro evaluation. *J Pharm Sci Res*. 2010;2(6):344–350.
- [41] Rajasekaran A, Sivakumar V. Design and evaluation of polymeric controlled release natamycin ocular inserts. *Kathmandu Univ J Sci Eng Technol*. 2010;6(1):108–115.
- [42] Gandhi P, Rathod H, Patel S. A review on: ocular inserts a novel drug delivery system. *Asian J Pharm Res Dev*. 2013;1(1):40–48.
- [43] Kaul S, Kumar G, Kothiyal P. An insight into ocular insert. *Int J Pharm Sci Res*. 2015;3:1–7.
- [44] Gorle A, Gattani S. Development and evaluation of ocular drug delivery system. *Pharm Dev Technol*. 2010;15(1):46–52.
- [45] Damodharan N, Soundrapandian C. Ophthalmic inserts of piroxicam: development and in-vitro drug release studies. *Asian J Chem*. 2008;20(5):3447–3454.
- [46] Ashture A, Kankudte A. Formulation and evaluation of controlled release ocular inserts of betaxolol hydrochloride; IOSR. *J Pharm*. 2012;2(5):34–38.
- [47] Kothawade S, Deshpande S, Lunkad A. Formulation and in-vitro characterization of ketorolac tromethamine ophthalmic inserts. *Res J Pharm Dosage Forms Tech*. 2013;5(6):1–3.
- [48] Ramkanth S, Chetty C. Design and evaluation of diclofenac sodium ocusert. *Int J PharmTech Res*. 2009;1(4):1219–1223.
- [49] Patel D. In-vitro and in-vivo evaluation of ocular inserts of ofloxacin. *DARU*. 2007;15(3):138–145.
- [50] Shafie M, Rady M. In-vitro and in-vivo evaluation of timolol maleate ocular inserts using different polymers. *J Clin Exp Ophthalmol*. 2012;3(8):1–9.
- [51] Franca J, Foureaux G. Bimatoprost-loaded ocular inserts as sustained release drug delivery systems for glaucoma treatment: in vitro and in vivo evaluation. *PLoS One*. 2014;9:1–14.
- [52] Paterakis PG, Korakianiti ES, Dallas PP, et al. Evaluation and simultaneous optimization of some pellet's characteristics using 3² factorial design and the desirability function. *Int J Pharm*. 2002;248:51–60.
- [53] Sanchez-Lafuente C, Furlanetto S, Fernandez-Arevalo M, et al. Didanosine extended-release matrix tablets: optimization of formulation variables using statistical experimental design. *Int J Pharm*. 2002;237:107–118.
- [54] Gadhave M, Pawar S. Formulation and evaluation of moxifloxacin ocusert. *Int J Pharm Clin Res*. 2016;8(12):1610–1615.
- [55] Gevariya H, Dharamsi A, Girhepunje K, et al. Once a day ocular inserts for sustained delivery of levofloxacin: design, formulation and evaluation. *Asian J Pharm*. 2009;3:314–318.
- [56] Morsi N, Ghorab D, Refai H, et al. Nanodispersion-loaded mucoadhesive polymeric inserts for prolonged treatment of post-operative ocular inflammation. *J Microencapsul*. 2017;34(3):280–292.
- [57] Mirzaeeia S, Alizadehc M. Design and evaluation of soluble ocular insert for controlled release of chloramphenicol. *J Rep Pharm Sci*. 2017;6(2):123–133.
- [58] Indian Pharmacopoeia. Ministry of Health and Family Welfare. Government of India. Vol. 2. New Delhi: Controller of Publication; 1996. p. 117–147.
- [59] Mundada A, Shrikhande B. Design and evaluation of soluble ocular drug insert for controlled release of ciprofloxacin hydrochloride. *Drug Dev Ind Pharm*. 2006;32:443–448.
- [60] Potu A, Reddy V. Design and evaluation of ocular inserts for controlled drug delivery of ketorolac tromethamine. *World J Pharm Res*. 2014;3(4):722–734.
- [61] Gorle A, Gattani S. Design and evaluation of polymeric ocular drug delivery system. *Chem Pharm Bull*. 2009;57(9):914–919.
- [62] Sankar V, Chandrasekaran A. Design and evaluation of diclofenac sodium ocular inserts. *Acta Pharm Sci*. 2006;48:5–10.
- [63] Michael H, Mostafa H, Mehdi J, et al. Draize rabbit eye test compatibility with eye irritation threshold in humans: a quantitative structural-activity relationship analysis. *Toxicol Sci*. 2003;76:384–391.
- [64] Kendre PN, Chaudhari PD. Effect of amphiphilic graft copolymer-carrier on physical stability of bosentan nanocomposite: assessment of solubility, dissolution and bioavailability. *Eur J Pharm Biopharm*. 2018;126:177–186.
- [65] Kendre PN, Chaudhari PD. Effect of polyvinyl caprolactam-polyvinyl acetate-polyethylene glycol graft copolymer on bioadhesion and release rate property of eplerenone pellets. *Drug Dev Ind Pharm*. 2017;43(5):751–761.
- [66] Kendre P, Chaudhari PD. Design and optimization of oral bioadhesive nanocurcumin delivery using novel hydrophilic carrier for cancer treatment: an alternative to parenteral chemotherapy. *Indian Drugs*. 2016;53:24–36.



Design, fabrication, and characterization of graft co-polymer assisted ocular insert: a state of art in reducing post-operative pain

Prakash N. Kendre , Pooja D. Kadam , Shirish P. Jain , Somnath K. Vibhute & Ajinkya K. Pote

To cite this article: Prakash N. Kendre , Pooja D. Kadam , Shirish P. Jain , Somnath K. Vibhute & Ajinkya K. Pote (2020): Design, fabrication, and characterization of graft co-polymer assisted ocular insert: a state of art in reducing post-operative pain, Drug Development and Industrial Pharmacy, DOI: [10.1080/03639045.2020.1833908](https://doi.org/10.1080/03639045.2020.1833908)

To link to this article: <https://doi.org/10.1080/03639045.2020.1833908>



Published online: 15 Oct 2020.



Submit your article to this journal [↗](#)



Article views: 5



View related articles [↗](#)



View Crossmark data [↗](#)

RESEARCH ARTICLE



Design, fabrication, and characterization of graft co-polymer assisted ocular insert: a state of art in reducing post-operative pain

Prakash N. Kendre^a, Pooja D. Kadam^b, Shirish P. Jain^c, Somnath K. Vibhute^a and Ajinkya K. Pote^a

^aDepartment of Pharmaceutics, Rajarshi Shahu College of Pharmacy, Buldana, India; ^bDepartment of Pharmaceutics, Sanjivani College of Pharmaceutical Education & Research, Kopargaon, India; ^cRajarshi Shahu College of Pharmacy, Buldana, India

ABSTRACT

Purpose: Targeted delivery of drugs at appropriate concentrations to ocular tissues is required to avoid wastage. Hence, advanced systems that maximize the release of poorly soluble drugs and deliver them at ocular sites must be designed.

Methods: In this study, Soluplus[®] (polyvinyl caprolactam–polyvinyl acetate–polyethylene glycol–graft copolymer) was selected as a solubilizer as well as film former for preparing ocular inserts and polyethylene glycol 400 (PEG-400) as a plasticizer. On the basis of an initial phase solubility study, the maximum concentration of Soluplus[®] possible was used for developing the inserts. An optimized formulation was obtained using a 3²-factorial design. Two factors at three levels were used to design the ocular inserts. Soluplus[®] (X_1) and the plasticizer, PEG-400 (X_2), were set as the independent variables at various levels, and the Rel_{4h} (drug release in 4 h, Y_1) and tensile strength (Y_2) were set as the dependent variables. A pre-formulation study was conducted to select suitable materials.

Results: Various physico-chemical parameters of the optimized formulation, including the tensile strength and folding endurance, were studied using FT-IR, DSC, XRD, and SEM. An *in vitro* dissolution study was conducted to determine the amount of drug released. There was no redness, swelling, or watering of the rabbit eye.

Conclusion: It was concluded that the ocular inserts of the poorly soluble nepafenac developed using a graft-co-polymer enhanced the solubility and utilization of the drug for a prolonged period.

ARTICLE HISTORY

Received 5 May 2020
Revised 22 August 2020
Accepted 1 October 2020

KEYWORDS

Ocular insert; ophthalmic drug delivery; Nepafenac; graft-co-polymer; Soluplus[®]

Introduction

In designing a formulation, the issues of absorption, distribution, metabolism, and elimination must be considered. When it comes to the delivery of pharmaceuticals, the eye offers unique opportunities and challenges. Though the absorption by this route is incompetent, there are few side effects with conventional ocular dosage forms. Most ocular formulations such as eye drops and suspensions are used to administer active drugs topically on the tissues around the ocular cavity. These dosage forms are easy to administer but suffer from inherent drawbacks. Ocular drug delivery is generally used to treat eye diseases. But problem of rapid and extensive elimination of conventional eye drops from the eye have been noticed here which lead to extensive loss of drug. Less amount of drug penetrates the corneal layer and reaches the internal tissue of eye. Drug loss occurs at lachrymal drainage and then drug dilution by tears. Hence, ocular bioavailability is reduced which leads to unwanted toxicity and side effect. Eye is a portal for drug delivery which is generally used for local therapy instead of systemic therapy. Due to high blood concentration of drug, there is risk of eye damage which can be overcome by local therapy [1,2]. Traditional topical formulations are highly concentrated, and corneal drug absorption with these formulations is low. There are ocular and systemic side effects because the pre-corneal residence time of eye drops is low [3]. Frequent administration of concentrated solutions is required to achieve the therapeutic effect. This results in the short residence of high drug

concentrations in the tear film, followed by long periods of under-dosing [4–6]. This leads to poor patient compliance. Several approaches have been adopted to overcome these issues. The use of various ophthalmic vehicles, such as suspensions, ointments, inserts, and aqueous gels, has been investigated to extend the ocular residence time of topically applied medications [7–9].

Sterile preparations with a solid or semisolid consistency, and of sizes and shapes designed for ophthalmic application, are generally known as ophthalmic inserts. These inserts are placed in the lower fornix and, sometimes, on the cornea or in the upper fornix. An ophthalmic insert is a polymeric vehicle consisting of the drug and is mainly used for topical therapy [10]. Increased ocular residence, the possibility of releasing drugs at a slow and constant rate, accurate dosing, exclusion of preservatives and increased shelf life are the prime advantages offered by ophthalmic inserts over conventional dosage forms [8–16]. Many of the such topical eye inserts are designed using polymeric components offering continuous release of drug without loss due to drainage and reducing the frequent administration [17].

The reduction of systemic absorption, which occurs freely with eye drops, is achieved with the use of these devices. Patient compliance is improved because of the lower frequency of administration and lower incidence of side effects [18–20]. The difficult problem of limited precorneal drug residence time is overcome by the use of ocular inserts [21,22]. The prime objective of using ophthalmic inserts is to increase the time of contact between the

preparation and the conjunctival tissue to ensure sustained release appropriate for topical or systemic treatment. Ophthalmic inserts consist of polymeric supports with or without drugs, the latter being incorporated as dispersions or solutions in the polymeric supports [23].

There are many polymers and film forming materials used in the design and development of ophthalmic inserts or oral dissolving films. Choice of selection of such materials is based on their physico-chemical properties and compatibility with the drug to be used for delivery. Many synthetically modified polymers and materials are available and many of the researchers have used for the development of various drug delivery systems. Polymers like: polyvinyl alcohol, polyamides, polysulfonates, cellulose acetates hydroxypropyl methyl cellulose, and modified graft-co-polymers like: Soluplus[®] (polyvinyl caprolactam–polyvinyl acetate–polyethylene glycol–graft copolymer), polyethylene oxide acrylates, polyvinyl alcohol-g-poly (oxyethylene methacrylate) PVA-g-POEM, Kollicoat[®] IR, Kollicoat[®] VA64, etc.

Soluplus[®] (polyvinyl caprolactam–polyvinyl acetate–polyethylene glycol–graft copolymer) is one of the graft-copolymers used by many researchers for the development of various drug delivery systems. It is an amphiphilic graft-copolymer which enables the enhancement of solubility and bioavailability of poor soluble drugs. Soluplus[®] can be processed as solid solutions using hot-melt-extrusion or other techniques [24–28].

However, considering the constraints of eye physiology, very few anti-inflammatory drugs show suitability to formulate the appropriate drug delivery system for the management of ocular inflammations [29].

Nepafenac is a non-steroidal anti-inflammatory prodrug (NSAID) that is usually sold as prescription eye drops. It is used to treat the pain and inflammation associated with cataract surgery [30]. It has several advantages over other ophthalmic NSAIDs. First, it has a unique prodrug structure. Prodrugs are the inactive forms of drugs that get converted into active forms after metabolic conversion in the body [29]. Nepafenac rapidly penetrates the cornea. After nepafenac penetrates the cornea, it is deaminated by intraocular hydrolases to amfenac [(2-amino-3-benzoyl phenyl) acetate], a potent inhibitor of COX-1 and COX-2 [31].

The aim of the present study was to enhance the solubility of nepafenac using the novel polymer Soluplus[®] and to formulate and evaluate nepafenac ocular inserts using a 3²-factorial design.

Materials and methods

Materials

Soluplus[®] (polyvinyl caprolactam–polyvinyl acetate–polyethylene glycol–graft copolymer) was obtained from BASF (Mumbai, India). Polyethylene glycol 400 (PEG-400) and dichloromethane were procured from Loba Chemie (Mumbai, India). All the materials used in this study were of analytical grade.

Methods

Preparation of nepafenac ocular insert

Ocular inserts of nepafenac were prepared using the solvent casting method. Soluplus[®] (polyvinyl caprolactam–polyvinyl acetate–polyethylene glycol–graft copolymer) was used as a solubility enhancer and film former, PEG-400 was used as a plasticizer to produce inserts of uniform strength, and dichloromethane was used as a solvent. Two factors at three levels were used to design the ocular inserts. Soluplus[®] (X_1) and the plasticizer, PEG-400 (X_2),

Table 1. Concentration levels and its translation of components used in the design of ocular formulation.

Independent variable	Levels		
	High (+1)	Medium (0)	Low (–1)
X_1 : Soluplus [®] (% w/w)	70	50	30
X_2 : PEG-400 (% w/v)	30	20	10

Measurable responses: Y_1 =Rel_{4h} (%); Y_2 =tensile strength (N/cm²).

Table 2. Composition of ocular insert batches as per 3²-factorial design.

Batch no.	Soluplus [®] (X_1) (% w/w)	PEG-400 (X_2) (%w/v)
F1	50	30
F2	50	20
F3	30	30
F4	30	10
F5	70	20
F6	70	30
F7	50	10
F8	70	10
F9	30	20

were considered as independent variables at various levels, and the drug release 4 h (Y_1) and tensile strength (Y_2) were considered as dependent variables (Table 1).

The concentration of nepafenac was maintained constant (1% w/w) in all the formulations. The compositions of the ocular inserts of the nine runs of the 3²-factorial design are listed in Table 2.

The required amount of Soluplus[®] was dissolved in a beaker in the required quantity of dichloromethane and stirred until it was completely dissolved. Polyethylene glycol 400 was added to the solution with stirring. A weighed amount of drug was added to this solution, which was stirred for 2 h to obtain a uniform dispersion. The polymer solution was finally sonicated to eliminate air bubbles. The casting solution was mixed and poured on a clean glass of film former (VJ Instruments, Karanja Lad, India) using a spreader. The spreader produces uniform films. The dichloromethane is evaporated by adjusting its temperature controller knob. The dried thin films thus obtained were cut to the required size (5 × 5 mm²) using a sharp cutter and ruler. They were wrapped in aluminum foil and stored in an airtight container (desiccator) [32,33].

Pre-formulation study

Solubility study. A solubility study was conducted to predict the maximum concentration of Soluplus[®] that will increase the solubility of nepafenac. The shaking flask method was used to determine the solubility. An excess amount of nepafenac was added to aqueous solutions of Soluplus[®]. Solutions with Soluplus[®] were prepared at concentrations of 5%, 10%, 15%, 25%, 45%, and 65% (w/w). Nepafenac powder was added to glass flasks containing Soluplus[®] with concentration levels as mentioned above. The samples were shaken for 24 h in a mechanical shaker. The concentrations of the nepafenac in the solutions were determined after equilibration for 24 h. A UV-spectrophotometer (1650 PC, Shimadzu, Kyoto, Japan) was used at 328 nm [34].

Fourier transform infrared (FT-IR) spectroscopy. The interaction between the nepafenac, Soluplus[®] and nepafenac ocular inserts was studied using an FT-IR spectrophotometer (Shimadzu, Kyoto, Japan). Spectra were recorded in the range 4000–400 cm^{–1}. All the samples were prepared using the KBr pellet technique, and

the spectra were recorded at a resolution of 0.15 cm^{-1} and a scanning speed of 20 scans s^{-1} [35,36].

Differential scanning calorimetric study. Differential scanning calorimetric (DSC) measurements were made using a thermal analyzer (DSC-60, Shimadzu, Kyoto, Japan). Samples of about 5 mg weight were hermetically placed in aluminum sealed pans and scanned at a heating rate of $10^\circ\text{C min}^{-1}$ over a temperature range of $0\text{--}300^\circ\text{C}$ with using nitrogen gas as an effluent gas. The thermal properties of pure nepafenac and the nepafenac ocular insert were determined [37].

Evaluation and characterization of nepafenac ocular films

Physical examination. The color and transparency of the nepafenac ocular inserts were inspected visually and other physical parameters were also evaluated using advanced tools and technologies to check the physical stability of the final formulation.

Determination of pH. The pH of the ocular inserts was determined using a digital pH meter (PICO + pH meter, Lab India, Mumbai, India). One-gram samples were added to 100 ml of distilled water each and stored for 2 h. The pH of the ocular inserts was calculated in triplicate, and the average value was calculated [38–40].

Thickness of films. The film thickness was measured using digital Vernier calipers or a micrometer screw gauge at different points, and the mean value was calculated [4,41,42].

Uniformity of weight. Three ocular inserts were cut from different parts of the film. They were individually weighed using a calibrated digital balance. The mean value was calculated. The standard deviation was calculated from the mean value [43].

Drug content uniformity. Inserts were cut from different places of the cast films. Each insert was placed in a vial containing 5 ml of pH 7.4 phosphate buffer and shaken to extract the drug from the film. One milliliter of the resulting solution was taken and diluted. The solution was analyzed using a spectrophotometer. Phosphate buffer (pH 7.4) was used as the blank [44].

Percentage moisture absorption. A percentage moisture absorption test was performed to determine the physical stability or integrity of the ocular inserts. Ocular inserts were weighed and placed in desiccators containing 100 ml of a saturated solution of aluminum chloride at 79.5% RH. After 72 h, the ocular inserts were removed and reweighed. The percentage moisture absorption was calculated using the following equation [45–47]:

$$\% \text{ Moisture absorption} = \frac{\text{[final weight} - \text{initial weight]}}{\text{initial weight}} \times 100 \quad (1)$$

Folding endurance. The folding endurance of ocular inserts/films was determined by folding them many times at the same place till a crack appeared (in this case it was folded 200 times). The number of folds required to produce the crack was counted. The folding endurance test was repeated with more sets of ocular inserts [48].

Tensile strength. The tensile strength is one of the significant mechanical properties determining the physical integrity of a film.

It is calculated as the applied load (force) at rupture divided by the cross-sectional area of a strip. A CT3 texture analyzer with a 30-g load cell was used. Film strips were held between two clamps placed 80 mm apart. Then, the strips were stretched by the top clamp at a rate of 3 mm/s, and the force at which the films broke were measured. The tensile strength was calculated using the following equation [49,50]:

$$\text{Tensile strength} \left(\frac{\text{N}}{\text{cm}^2} \right) = \frac{\text{breaking load}}{\text{cross sectional area of the sample}} \quad (2)$$

Percentage elongation. The percentage elongation at breaking was calculated according to the following equation [49,50]:

$$\% \text{ Elongation at break} = \left\{ \frac{\text{Change in length (mm)}}{\text{original length (mm)}} \right\} \times 100 \quad (3)$$

Scanning electron microscopy (SEM). A beam of electron produced by an electron gun goes through two condenser lenses, a scan coil and an objective lens to finally interact with a sample in SEM. In the sample, the electrons lose energy due to scattering and absorption. The morphology of the nepafenac ocular inserts was studied using a JSM 5400 scanning electron microscope (Diya Labs, Mumbai, India) with an acceleration voltage of 30 kV. The samples were coated with gold prior to imaging [51].

In vitro drug release study. The prepared ocular inserts were subjected to the *in vitro* drug release study using vial method. In this method, the ocular inserts (1 cm^2 size) were placed into the 25 ml capacity vials containing 10 ml of phosphate buffer solution, pH 7.4 (as pH of lacrimal fluid is 7.4). These vials were placed on the hot plate maintaining the temperature of $37^\circ\text{C} \pm 0.5^\circ\text{C}$ with continuous stirring using magnetic beads at the bottom of the vial, the care was taken to maintain the minimum speed of shaking as like blinking of eyes. The 1 ml sample was withdrawn at the interval 30 min and at the same time it was replaced with fresh 1 ml of the dissolution media to maintain the sink condition. Withdrawn sample were filtered through the Whatman paper and analyzed for drug release study using UV-spectrophotometer at 238 nm. All the results were noted in triplicate for better accuracy [4].

Data validation and optimization. Desirability approached was implemented to generate and validate the mathematical models. Various feasibility and search grid methods were implemented to establish the composition of the optimized formulation. The optimized formulation was developed and evaluated for all the obtained responses (Y_1 and Y_2). Finally, the experimental values were compared with the predicted values in order using mathematical models [52,53].

The data relating to the targeted parameters were analyzed using one-way analysis of variance (ANOVA) in Design-Expert-Software 12.0 version (Stat-Ease Inc., Minneapolis, MN). Individual parameters were analyzed using polynomial equation:

$$Y = \beta_0 + \beta_1 X_1 + \beta_2 X_2 + \beta_3 X_1 X_2 + \beta_4 X_1^2 + \beta_5 X_2^2 \quad (4)$$

where Y is the measured response, β_0 is the intercept, and β_1 to β_5 are the regression coefficients. X_1 and X_2 are the main effects, $X_1 X_2$ is the interaction term between X_1 and X_2 , and X_1^2 and X_2^2 are the quadratic terms of the independent variables. Using multiple linear regression analysis (MLRA) and ANOVA, polynomial models containing only substantial terms were produced ($p < .05$) for every

response. All the resultant models and data were used to construct three-dimensional diagrams to represent response Y as a function of X . Contour plots were generated to represent the effect of all the independent variables on each response.

Stability studies. The selected formulations were stored at 25 °C/60%RH and 40 °C/75%RH for 2 months and evaluated for their physical appearance, drug content, and drug–excipient compatibility at specific periods of time [44].

Sterility testing. Sterility testing is carried out to detect the presence of viable forms of microorganisms. The testing was performed using fluid thioglycolate medium and soybean casein digest medium, as per the Indian Pharmacopoeia. The formulations were sterilized separately under UV radiation for 30 min. The irradiated formulations were tested under aseptic conditions for viable forms of bacteria, fungi, and yeast in both the media prescribed by the Indian Pharmacopoeia [54–59].

Ocular irritancy test. The sterilized ocular inserts were used in an eye irritancy test. The Draize technique, which has been designed for testing ocular irritation of ophthalmic products, was used. Clearance for handling the experimental animals was obtained from the Institutional Animal Ethical Committee (IAEC) constituted for the purpose. The ocular inserts were placed into the lower cul-de-sac, and observations of the various parameters were made 1 h, 24 h, 48 h, 72 h, and 1 week after administration. Three male rabbits weighing between 1.5 and 2 kg were used in the study. The sterile formulation was administered twice a day for a period of seven days. The rabbits were observed periodically for redness, swelling, and watering of the eyes [60–63].

Results and discussion

As described in above-mentioned section of methods, the thin films were formed using the solvent casting method and a film former. The composition of the films was according to the 3²-factorial design (Table 2). The thin films obtained were transparent, flexible, and smooth in appearance.

Preliminary batches were produced to finalize the specific ranges of concentrations of Soluplus[®] and the plasticizer (PEG-400). Flexible, transparent, and smooth-surfaced thin films were obtained. There was better release of nepafenac in the ocular region. At higher concentration levels of Soluplus[®] and PEG-400, the films obtained were very sticky, thick, and somewhat tacky. At lower concentrations of both Soluplus[®] and the plasticizer, the films were very brittle and could not be removed easily from the glass surface after drying. Hence, on the basis of this preliminary study, the final concentrations of Soluplus[®] and PEG-400 were 30–70% and 10–30%, respectively. Nine possible combinations were obtained from the 3²-factorial design (Table 2). After batches of all the formulations were prepared, the films obtained were evaluated for various physical and chemical properties. These are discussed in a later section.

Pre-formulation study

Before finalizing the optimized formulations and characterizing them, a preliminary study was conducted on the compatibility of all the components used in the design of the ocular films. Physical blends of the drug and other components were subjected to FT-IR, DSC, and XRD analysis. The results of the study conducted to

check the suitability of the materials used are presented in the following sections.

FT-IR study

Compatibility of the drug and other components used is essential for preparing a final formulation. Nepafenac and Soluplus[®] were subjected to FT-IR analysis. Major peaks of nepafenac spectra consisting of N–H stretch at 3440; C=O stretch (carboxylic acid group) at 1676; C–O (ester group) at 1194; C–H stretch (aromatic group) 2877; C–H bending (aromatic group); C–Br stretch at 753. No extra peaks were found in the spectrum of the drug and excipients blend, indicating an absence of interactions or the instability of ocular insert formulation. FT-IR spectra of pure nepafenac and blend of nepafenac and Soluplus[®] is presented in Figure 1.

Differential scanning calorimetry

Nepafenac, Soluplus[®] and their blend were subjected to DSC analysis. In the DSC thermogram of nepafenac, a sharp endothermic peak was found at 184.93 °C, corresponding to the melting and reported decomposition at 183.54–186.4 °C.

Soluplus[®] showed an endothermic peak at 63.66 °C. The DSC thermograph of the drug–Soluplus[®] mixture showed an endothermic peak at the melting point of Soluplus[®] (62.93 °C). This shows that nepafenac is completely entrapped within Soluplus[®]. This indicates that there is no interaction between nepafenac and Soluplus[®]. The DSC thermograms are presented in Figure 2.

Solubility study

There was significant increase in solubility of nepafenac at 45% concentration level of Soluplus[®], beyond this level, there was no significant increase in solubility. It is observed that the presence of Soluplus[®] increases the solubility of nepafenac almost more than 200 times compared with the plain drug [64–66]. From this study, it was clear that the concentration of Soluplus[®] should not be less than 45% for maximum solubility of nepafenac (Figure 3). But another aspect in the design of ocular inserts is to keep all the physical and chemical properties so that the final formulation is stable and improved. Hence, the concentration level of Soluplus[®] was maintained between 30% and 70% for the development of ocular insert formulations, as mentioned in Table 1.

Evaluation and characterization of ocular inserts of nepafenac

As per the 3²-factorial design, all the nine formulations were prepared using different concentrations of Soluplus[®] and PEG-400. Various physical and chemical properties such as weight, thickness, tensile strength, percent elongation, folding endurance, percent moisture absorption, surface pH, and drug content of these formulations were evaluated (Table 3). The average weight of these inserts (10 × 10 mm²) was in the range from 8.38 ± 0.01 mg to 22.44 ± 0.02 mg. Batch F4 has the minimum weight (8.38 ± 0.01 mg), and batch F6 has the maximum weight (22.44 ± 0.02 mg). The variation in the weight was observed due to the fact that batch F4 has lower concentrations of both Soluplus[®] and PEG-400, whereas batch F6 has higher levels of both Soluplus[®] and PEG-400. In all the formulations, the concentration of the drug was maintained at the same level. Overall, from all the observations, it is clear that as the concentration levels of both Soluplus[®] and PEG-400 increase, the weight of the insert/film

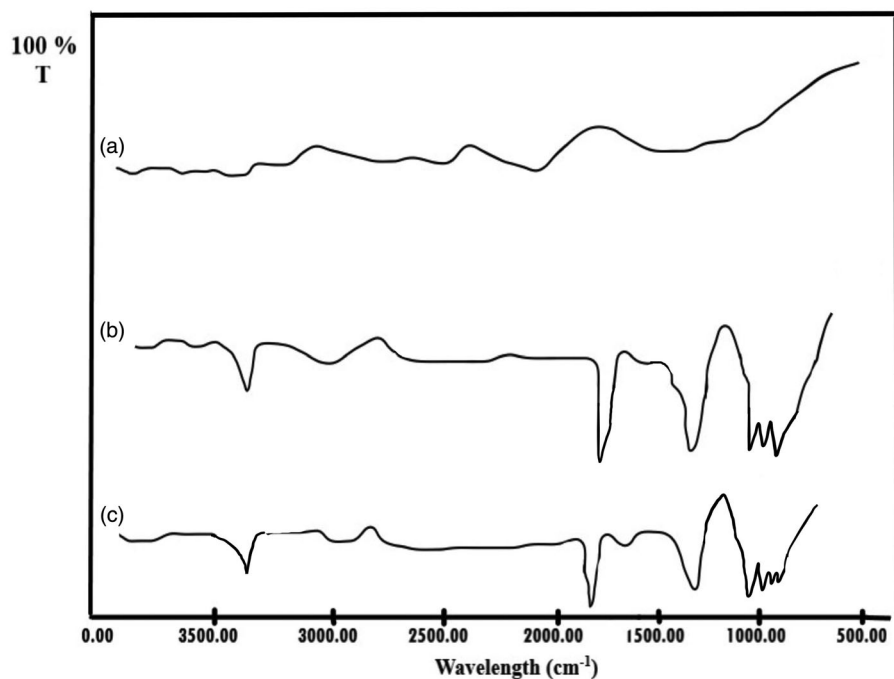


Figure 1. FT-IR spectra of: Soluplus® (a); Nepafenac (b); blend of nepafenac and Soluplus® (c).

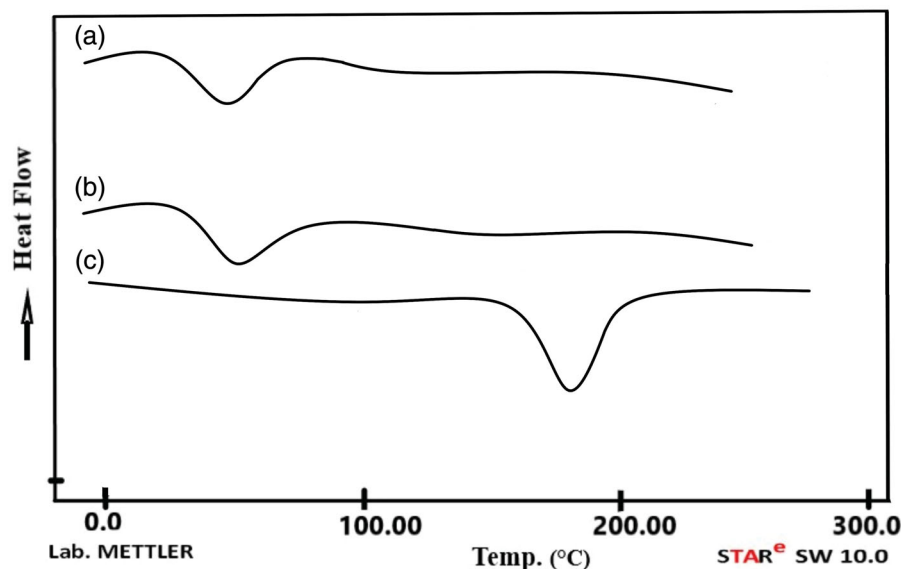


Figure 2. DSC thermogram of: Soluplus® (a); blend of nepafenac and Soluplus® (b); Nepafenac (c).

also increases. There were similar observations about the thickness, tensile strength, percent elongation, and moisture absorption, the highest values of these parameters among all the nine formulations prepared as per the 3^2 -factorial design were $289.25 \pm 1.25 \mu\text{m}$, $7.58 \pm 1.78 \text{ N/m}^2$, $96.28 \pm 1.25\%$, and $8.56 \pm 1.47\%$, respectively. In the similar way, the lowest values were $123.5 \pm 1.45 \mu\text{m}$, $2.55 \pm 1.27 \text{ N/m}^2$, $52.0 \pm 1.2\%$, and $3.25 \pm 2.35\%$, respectively.

All the results considered were the average of three values for each parameter. But the final decision was based on another important dependent variable $\text{Rel}_{4\text{hr}}$, which was also

discussed subsequently. Other physical parameters such as the surface pH was found to be in the range of 7.4–7.8 whereas folding endurance was found to be varied from a low value of 127 to values >223 . Here also, the concentrations of both Soluplus® and PEG-400 played an important role. The effect was directly proportional to the concentration levels of the two materials although the same amount of drug was present in all the formulations. The folding endurance increased with the concentration levels. The drug content in all the nine formulations was found to be satisfactory (above 90%). It was in the range from $95.43 \pm 1.8\%$ to $98.99 \pm 1.25\%$ (Table 4).

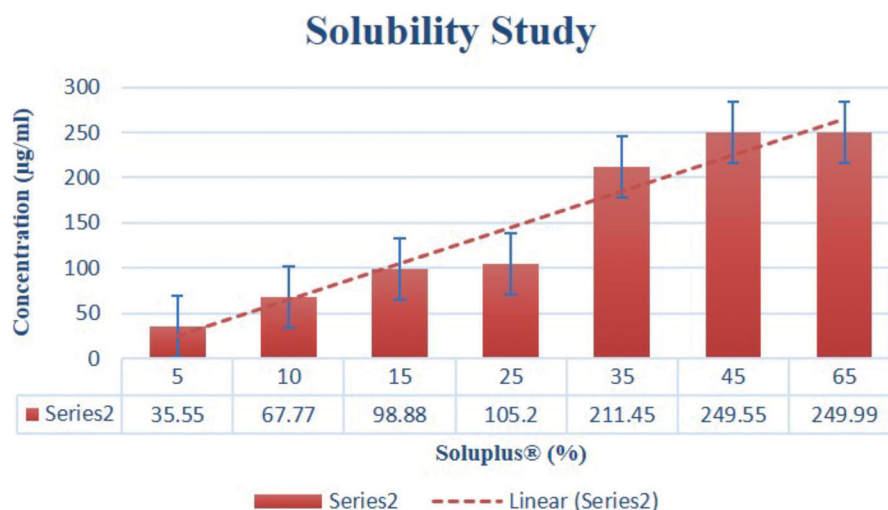


Figure 3. Solubility study of Nepafenac in the presence of Soluplus® as solubilizer.

Table 3. Evaluation of physical and chemical properties of nepafenac ocular insert.

Batch	Weight (mg)	Thickness (µm)	% Drug content	Tensile strength (N/m ²)	% elongation	% Moisture absorption
F1	18.3 ± 0.01	213.33 ± 1.654	98.23 ± 1.5	5.55 ± 1.02	92.99 ± 1.2	6.98 ± 1.25
F2	16.7 ± 0.012	198.65 ± 2.453	98.99 ± 1.25	4.54 ± 1.55	90.99 ± 1.78	5.60 ± 2.25
F3	11.8 ± 0.02	158.76 ± 3.564	95.43 ± 2.24	5.95 ± 2.01	74.00 ± 1.01	4.65 ± 1.58
F4	8.38 ± 0.24	123.5 ± 1.45	96.45 ± 1.88	2.55 ± 1.27	52.0 ± 1.28	3.25 ± 2.35
F5	17.8 ± 0.06	208.32 ± 1.55	95.89 ± 1.2	5.01 ± 1.87	94.0 ± 1.88	7.80 ± 1.25
F6	22.44 ± 0.02	289.25 ± 1.25	98.258 ± 1.25	7.58 ± 1.78	96.28 ± 1.25	8.56 ± 1.47
F7	17.58 ± 0.05	211.25 ± 2.25	96.45 ± 1.55	3.25 ± 1.01	88.25 ± 2.25	5.4 ± 1.54
F8	18.58 ± 0.25	221.3 ± 1.25	97.54 ± 1.25	4.55 ± 1.28	91.25 ± 1.02	6.89 ± 2.25
F9	9.5 ± 0.432	134.201 ± 2.64	97.55 ± 1.54	5.58 ± 1.78	78.29 ± 1.67	4.58 ± 1.77

All the observations were taken in triplicate as ± SD ($n = 3$).

Table 4. Summary of *in vitro* drug release data as per with mathematical model fitting as per 3²-factorial design.

Batch	Zero order		First order		Higuchi model	
	K_0	R^2	$K1$ (h ⁻¹)	R^2	KH (h ⁻¹)	R^2
F1	1.48 ± 0.058	0.9988 ± 0.014	0.03 ± 0.01	0.9934 ± 0.04	8.69 ± 0.34	0.9433 ± 0.014
F2	1.25 ± 0.145	0.9752 ± 0.055	0.015 ± 0.01	0.9635 ± 0.014	7.69 ± 0.38	0.9655 ± 0.05
F3	2.38 ± 0.065	0.9556 ± 0.055	0.045 ± 0.02	0.9567 ± 0.01	7.25 ± 0.45	0.8936 ± 0.025
F4	1.28 ± 0.048	0.9438 ± 0.045	0.025 ± 0.01	0.9433 ± 0.05	6.55 ± 0.24	0.9633 ± 0.025
F5	1.25 ± 0.068	0.9755 ± 0.014	0.035 ± 0.03	0.9855 ± 0.014	11.55 ± 0.36	0.9523 ± 0.025
F6	1.54 ± 0.055	0.9775 ± 0.023	0.025 ± 0.02	0.9624 ± 0.016	13.52 ± 0.35	0.9733 ± 0.02
F7	2.28 ± 0.024	0.9466 ± 0.014	0.042 ± 0.03	0.9725 ± 0.016	19.25 ± 0.34	0.9833 ± 0.055
F8	3.25 ± 0.047	0.8622 ± 0.035	0.044 ± 0.05	0.9815 ± 0.019	18.55 ± 0.56	0.9688 ± 0.025
F9	1.85 ± 0.036	0.9625 ± 0.014	0.055 ± 0.03	0.9725 ± 0.045	18.65 ± 0.65	0.9833 ± 0.02

All the observations were taken in triplicate as ± SD ($n = 3$).

Scanning electron microscopy

The morphology of the nepafenac ocular inserts prepared was characterized by SEM analysis. The SEM images revealed that the inserts have a uniform surface with small pores and drug may release from this surface. The ocular inserts had a clear appearance with smooth surface and texture, SEM images are shown in Figure 4.

In vitro drug release study

An *in vitro* drug release study of the nepafenac ocular inserts was carried out. The release profile obtained is shown in Figure 5. It was observed that the release of the drug from the inserts of all the nine formulations in 4 h was in the range from 66.55% to 95.25%. The drug release of formulation F3 was very low (66.55%), whereas that of formulation F6 was the highest (95.25%). The low drug release from formulation F3 was due to the fact that the formulation contains higher levels of plasticizer

compared with the concentration of Soluplus®, which retards the release from the insert. Formulation F6, in contrast, contains lower levels of the plasticizer compared with Soluplus®. Overall, the same trend was observed with the remaining formulations due to the different levels of the two components. Soluplus® is the polymer of choice for playing the roles of both film former and solubilizer. Hence, the formulations containing higher levels of Soluplus® had the maximum drug release. Further, the drug release was also influenced by presence of pores at the film surface, the permeation capacity of film surface and the diffusivity and solubility of the drug in the presence of Soluplus®. Hence, the role of Soluplus® was found to be very important in improving the solubility of nepafenac. The solubility of nepafenac increased (more than 200 times) as described in section 'Solubility study'. This phenomenon played a major role in the release of the drug, along with the role of the supportive plasticizer (PEG-400), which gave the inserts sufficient strength for continuous release up to 4 h [64–66].

In Vitro Drug Release Study

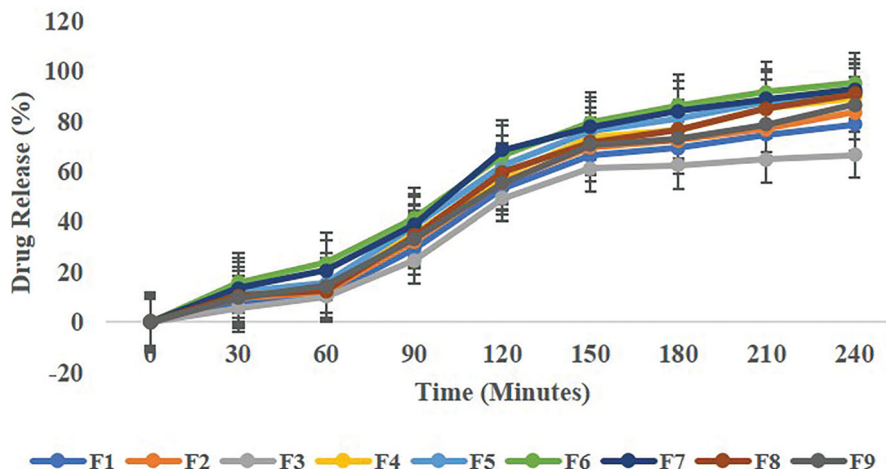


Figure 4. In vitro drug release study of all the nine formulations as per 3²-factorial design.

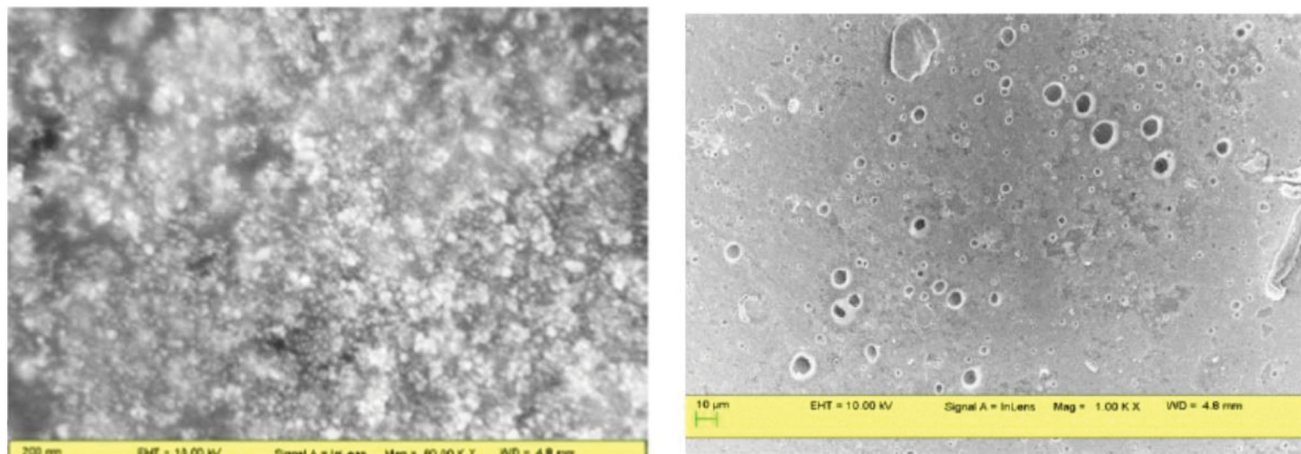


Figure 5. Scanning electron microscopic (SEM) images of optimized ocular insert at different resolutions.

Table 5. Summary of ANOVA for response parameters as per 3²-factorial design.

Response	F Value	Prob>F	Predicted R ²	Adjusted R ²	% CV
Rel 4h (Y ₁)	13.85	0.05	98.24	99.51	1.58
Tensile strength (Y ₂)	23.31	0.05	97.36	98.54	2.36

Regression equations best models:

$$Y_1 = 86.07X_1 + 5.87X_2 - 5.36X_1X_2;$$

$$Y_2 = 4.54X_1 - 0.700X_2 + 0.0925X_1X_2 + 0.756X_1^2 - 0.138X_2^2.$$

The *in vitro* drug release data of the nine formulations fitted the zero-order equation well, but the best-fit model was the first-order equation. The results of ANOVA and mathematical models were generated by regression analysis and fits of all the models are shown in Table 5.

If there are many insignificant model terms (not counting those required to support hierarchy), model reduction may improve the model, but in the case of both responses Y₁ and Y₂, all the model terms (X₁, X₂ and X₁:X₂) are significant. In the case of response Y₁ (Rel_{4h}), the model F-value of 13.85 implies that the model is significant. There is only a 0.74% chance that an F-value this large could occur due to noise. *p* Values less than .0500 (in this case *p*=.0074) indicate model terms that are significant. The predicted R² value of 0.9824 is in reasonable agreement with the adjusted R² value of 0.9951 in the case of the response parameter of Y₁ (Rel_{4h}). Adequate precision measures the signal to noise ratio. A

signal-to-noise ratio greater than 4 is desirable. In this case, the ratio is 12.887, indicating an adequate signal. This model can be used to navigate the design space. The 2FI model generated for Rel_{4h} indicated that the Soluplus[®] (X₁) concentration had a positive influence on Y₁. As the concentration of Soluplus[®] increases, the release of nepafenac also increases. In addition to the main effects, the interaction term, X₁:X₂ (Soluplus[®]: PEG-400), had a significant negative influence on Y₁. As the concentration of Soluplus[®] increases, the release of nepafenac also increases, but at higher concentrations of X₂ along with X₁ has a negative influence on Rel_{4h}. Here, the release of the drug decreases as the concentration of X₂ increases. This was due to the retardant effect of PEG-400 as it increases the plasticity the insert.

In the case of response Y₂ (tensile strength), the F-value of 23.31 implies that the model is significant. There is only a 0.15% chance that an F-value this large could occur due to noise. *p* Values less than .0500 (in this case *p*=.0015) indicate that the model terms are significant. The predicted R² of 0.9736 is in reasonable agreement with the adjusted R² of 0.9854 in the case of the response parameter of Y₂ (tensile strength). Adequate precision measures the signal to noise ratio. A ratio greater than 4 is desirable. In this case, the ratio of 9.887 indicates an adequate signal. This model can be used to navigate the design space. The quadratic model generated for Y₂ indicated that the Soluplus[®] (X₁)

Table 6. Response parameters as per 3^2 factorial design.

Formulation Batch	Independent variable X_1 : Soluplus® (%)	Independent variable X_2 : PEG-400 (%)	Y_1	Y_2
			Rel _{4h} ^a (%)	Tensile strength ^a (N/cm ²)
F1	50	30	78.66 ± 1.25	5.55 ± 1.02
F2	50	20	83.55 ± 1.02	4.54 ± 1.55
F3	30	30	66.55 ± 2.03	5.95 ± 2.01
F4	30	10	89.25 ± 1.14	2.55 ± 1.27
F5	70	20	91.44 ± 1.58	5.01 ± 1.87
F6	70	30	95.25 ± 1.36	7.58 ± 1.78
F7	50	10	92.5 ± 1.75	3.25 ± 1.01
F8	70	10	90.88 ± 1.34	4.55 ± 1.28
F9	30	20	86.54 ± 1.78	5.58 ± 1.78

^aAll the observations were taken in triplicate as ± SD ($n = 3$).

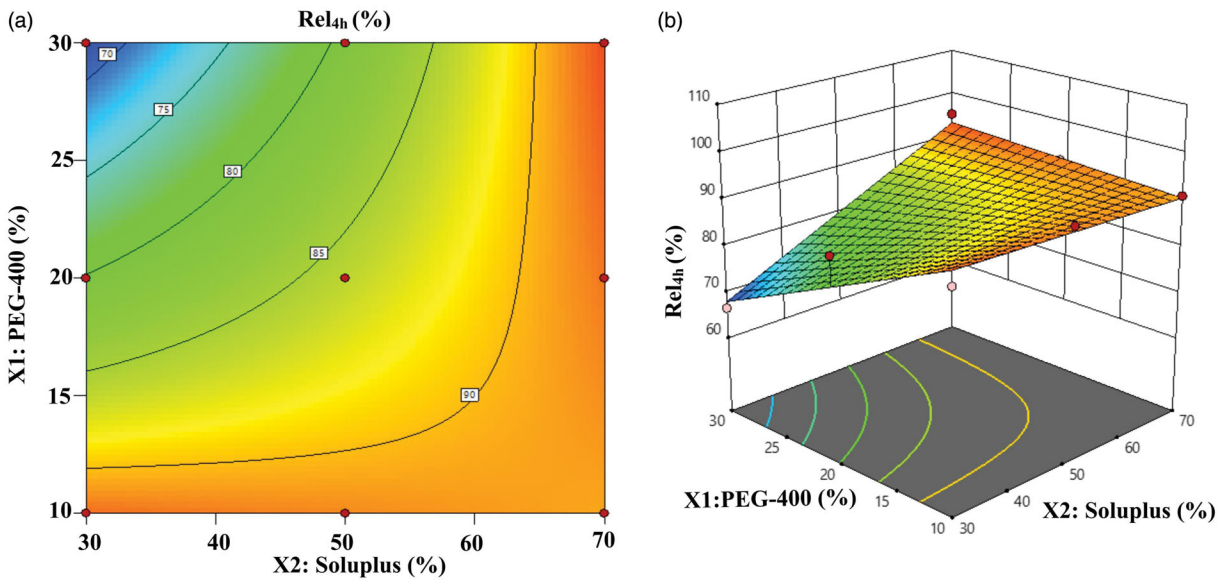


Figure 6. Contour and 3D surface response graph: (a, b) for Rel_{4h} response parameter, respectively.

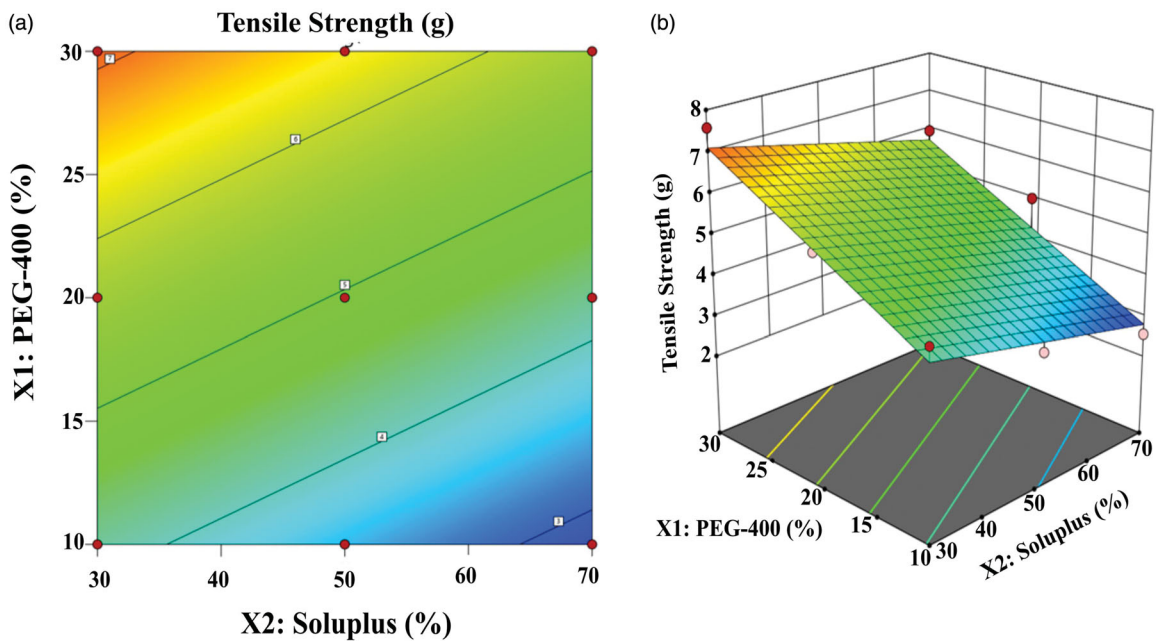


Figure 7. Contour and 3D surface response graph: (a, b) for tensile strength response parameter, respectively.

concentration had a negative influence on Y_2 . As the concentration of Soluplus® increased, the tensile strength of the insert decreased, whereas with higher concentrations of PEG-400 (X_2),

the tensile strength increases. This is due to the plasticizer effect of PEG-400. In addition to the main effects, the interaction term $X_1 \cdot X_2$ (Soluplus®: PEG-400) had a significant negative influence on

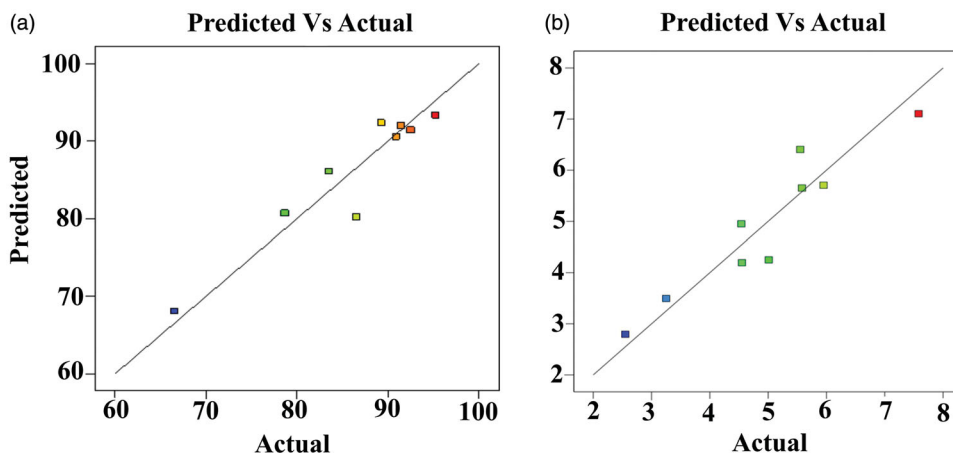


Figure 8. The relation between predicted vs. actual experimental values for both the response variables Rel4h (Y₁) (a) and tensile strength (Y₂) (b).

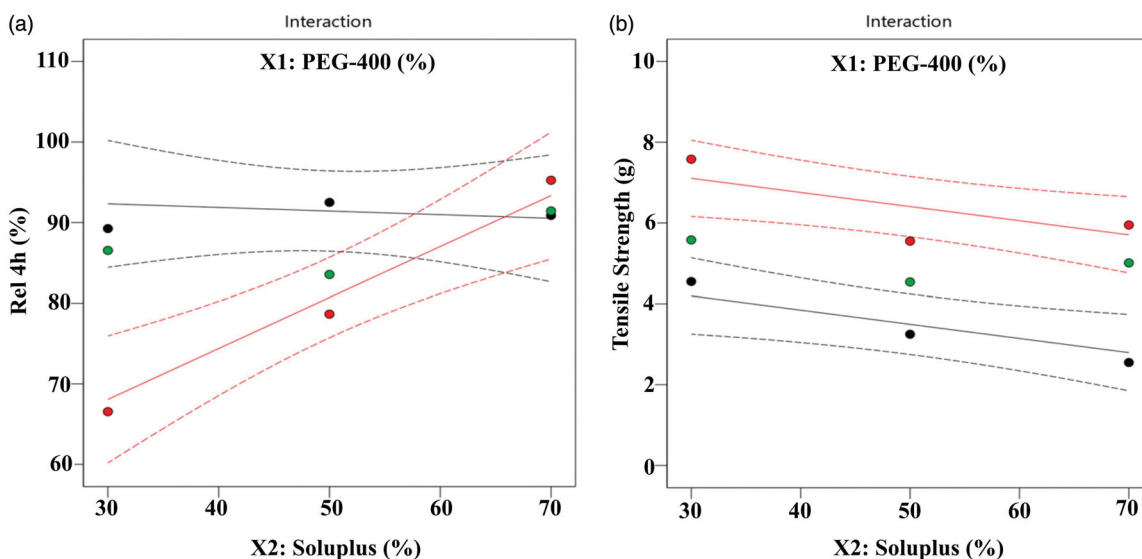


Figure 9. Response plots (a, b) showing the combined effect of due to interaction of X₁:X₂ on both response parameter Rel4h (Y₁) (a) and tensile strength (Y₂) (b).

Y₂ (p=.0143). As the concentration of PEG-400 increases, the tensile strength also increases, but at higher concentrations of X₂ along with X₁ has a negative influence on the tensile strength. Here, it decreases as the concentration of X₁ increases. The results of the response parameters Rel_{4h} (Y₁) and tensile strength (Y₂) are shown in Table 6.

The effects of all the independent factors are presented in the form of contour plots and three-dimensional surface response plots (Figures 6 and 7).

The relation between the predicted and actual experimental values for both the response variables Y₁ and Y₂ is shown graphically in Figure 8. The combined effect due to interaction (X₁:X₂) on the response parameters Y₁ and Y₂ is shown in Figure 9. Overlay plot for both responses (Y₁ and Y₂) is highlighted in Figure 10.

The main aim of the present study was to develop an ocular insert which released the nepafenac in 4 h (Rel_{4h}) and had better tensile strength for continuous drug release.

Stability study

The selected formulations were tested for 3 months at storage conditions of 25°C and 40°C at 60% RH (relative humidity) and 75% RH, and they were analyzed for their drug content. The

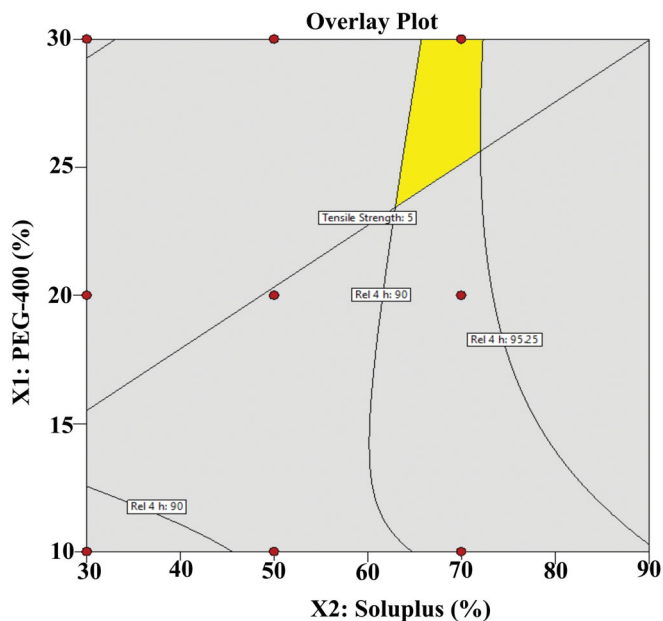


Figure 10. Overlay plot for both response parameter Rel4h (Y₁) and tensile strength (Y₂). 138

Table 7. Evaluation of optimized ocular insert after stability study.

Batch	Weight (mg)	Thickness (μm)	% Drug content	Tensile strength (N/m^2)	% elongation
F1	19.6 \pm 0.03	222.90 \pm 1.28	97.33 \pm 1.25	4.80 \pm 1.15	98.33 \pm 1.26
F2	18.9 \pm 0.032	202.78 \pm 2.25	96.80 \pm 1.55	5.54 \pm 1.78	91.25 \pm 1.54
F3	13.1 \pm 0.22	162.54 \pm 2.35	94.83 \pm 2.94	6.10 \pm 2.14	76.58 \pm 1.45
F4	10.25 \pm 0.21	126.4 \pm 1.35	95.85 \pm 1.25	3.25 \pm 1.47	60.10 \pm 1.78
F5	19.4 \pm 0.23	210.87 \pm 1.67	95.25 \pm 1.22	5.22 \pm 1.54	96.55 \pm 1.45
F6	25.12 \pm 0.12	292.95 \pm 1.90	97.568 \pm 1.85	7.24 \pm 1.52	98.57 \pm 1.65
F7	19.98 \pm 0.15	213.14 \pm 2.45	95.88 \pm 1.65	3.58 \pm 1.23	90.95 \pm 2.75
F8	19.68 \pm 0.25	223.31 \pm 1.02	95.74 \pm 1.85	3.75 \pm 1.81	92.65 \pm 1.32
F9	11.9 \pm 0.36	135.21 \pm 2.25	95.75 \pm 1.89	5.88 \pm 1.64	80.47 \pm 1.27

All the observations were taken in triplicate as \pm SD ($n = 3$).

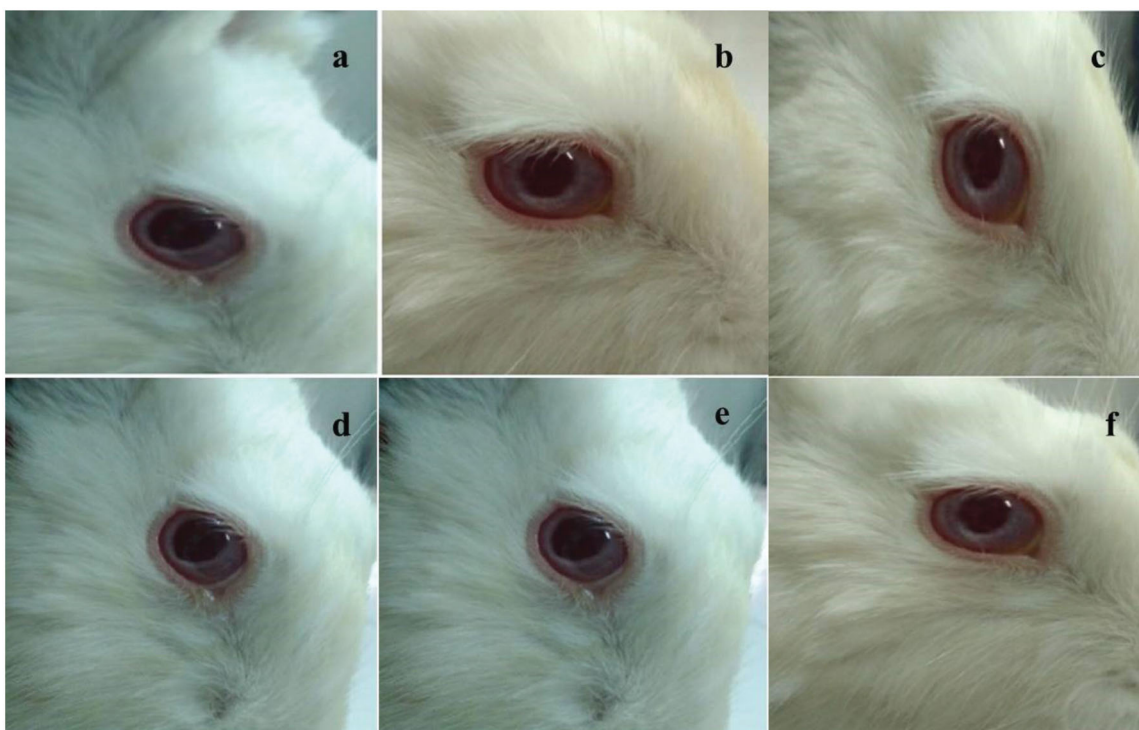


Figure 11. Ocular irritancy test for optimized ocular insert on rabbit eye at every interval for one-week period.

residual drug content of the selected formulations was found to be within the permissible limits. The formulations showed satisfactory physical stability at 25°C and 40°C at 60% RH and 75% RH, respectively, and no significant changes were observed after stability study. The physical appearance did not change considerably. The results of stability study are highlighted in Table 7.

Sterility testing

All the sterile inserts complied with the test for sterility with a positive control and a negative control test conducted as per the procedure of the Indian Pharmacopeia. The formulations did not show any microbial growth, which suggests that the inserts were sterile.

Ocular irritancy test

The sterilized formulations were placed into the lower cul-de-sac, and the various criteria were observed at 1 h, 12 h, 24 h, 48 h, 72 h, and 1 week after administration. No redness, swelling, or watering of the rabbit eye was observed. This indicates that the inserts did not produce ocular irritancy and toxicity (Figure 11).

Conclusion

The aim of the present study was to develop an ocular insert/film of the poorly water-soluble nepafenac using a 3²-factorial design. The response parameters Rel_{4h} and tensile strength were set as the dependent variables. The goal was set by considering the constraints of the variations in the concentration levels of the film former (Soluplus®) and the plasticizer (PEG-400). Using the feasibility and grid search methods, an insert with a drug release greater than 90% after 4 h and with better physical stability and strength was obtained successfully. All the physico-chemical parameters were found to be excellent for delivering nepafenac in a continuous manner for 4 h. It is concluded that an optimized insert/film of the poorly water-soluble nepafenac can be formulated using the novel graft-co-polymer at appropriate concentrations of the plasticizer, PEG-400, by reducing the dosing frequency. The effect is prolonged and the patient compliance is better.

Acknowledgements

Authors are very thankful to the BASF Corporation, Mumbai, India and grateful to Micro Labs, Hosur, India. Authors are also thankful to the Management and Principal of the College to provide other

chemicals and supporting resources to complete this research work successfully.

Disclosure statement

No potential conflict of interest was reported by the author(s).

Data availability statement

Author/s hereby declares that the raw/processed data required to reproduce these findings cannot be shared at this time due to legal or ethical reasons.

References

- [1] Sreenivas SA, Hiremath SP, Godbole AM. Ofloxacin ocular inserts: design, formulation and evaluation. *Iran J Pharm Res.* 2006;5(2):159–162.
- [2] Chien YW. *Ocular drug delivery and delivery systems; novel drug delivery systems.* 2nd ed. New York: Marcel Dekker; 1996. p. 269–270.
- [3] Ara T, Sharma S, Bhandari A. Preparation and evaluation of ocular inserts of diclofenac sodium for controlled drug delivery. *Der Pharm.* 2014;6(6):93–99.
- [4] Jafariazar Z, Jamalnia N, Ghorbani-Bidkorbeh F, et al. Design and evaluation of ocular controlled delivery system for diclofenac sodium. *Iran J Pharm Res.* 2015;14:23–31.
- [5] Lee VH, Robinson JR Jr. Topical ocular drug delivery: recent developments and future challenges. *J Ocul Pharmacol Ther.* 1986;2:67–108.
- [6] Hermans K, Van den Plas D, Kerimova S, et al. Development and characterization of mucoadhesive chitosan films for ocular delivery of cyclosporine A. *Int J Pharm.* 2014; 472:10–19.
- [7] Sultana Y, Aqil M, Ali A. Ocular inserts for controlled delivery of pefloxacin mesylate: preparation and evaluation. *Acta Pharm.* 2005;55:305–314.
- [8] Baranowski P, Karolewicz B, Gajda M, et al. Ophthalmic drug dosage forms: characterization and research methods. *Science.* 2014;2014:1–14.
- [9] Atram S, Bobade N. Current trends towards an ocular drug delivery system: review. *Int J Pharm Pharm Sci.* 2013;3(1): 28–34.
- [10] Karthikeyan D, Bhowmick M, Pandey V, et al. The concept of ocular inserts as drug delivery systems: an overview. *Asian J Pharm.* 2008;2:192–193.
- [11] Attia M, Kassem M, Safwat S. In-vivo performance of 3H-dexamethasone ophthalmic film delivery systems in the rabbit eye. *Int J Pharm.* 1988;47:21–30.
- [12] Kumar S, Nagori B. Ocular insert: dosage form for sustain ophthalmic drug delivery. *J Farm Klin Indones.* 2012;1(2): 61–73.
- [13] Bade M, Gawali V. Ocular inserts: a rate controlled drug delivery system – a review. *IJPE.* 2012;2(1):49–63.
- [14] Rajput G, Sharma S. Review on ophthalmic inserts. *Int J Pharma Prof Res.* 2013;4(3):912–920.
- [15] Barath S, Hiremath S. Ocular delivery system of pefloxacin mesylate. *Pharmazie.* 1999;54:55–58.
- [16] Hume LR, Lee HK, Benedetti L, et al. Ocular sustained delivery of prednisolone using hyaluronic acid benzyl ester films. *Int J Pharm.* 1994;111:295–298.
- [17] Rathore K, Nema R. An insight into ophthalmic drug delivery system. *Int J Pharm Sci Drug Res.* 2009;1:1–5.
- [18] Grass G, Cobby J, Makoid M. Ocular delivery of pilocarpine from erodible matrices. *J Pharm Sci.* 1984;73:618–621.
- [19] Maichuk Y. Ophthalmic drug inserts. *Invest Ophthalmol Vis Sci.* 1975;14:87–90.
- [20] Ozawa H, Hosaka S, Kunitomo T, et al. Ocular inserts for controlled release of antibiotics. *Biomaterials.* 1983;4: 170–174.
- [21] Kumari A, Sharma P, Garg V. Ocular insert: advancement in therapy of eye diseases. *J Adv Pharm Technol Res.* 2010; 1(3):291–296.
- [22] Saettone MF, Salminen L. Ocular inserts for topical delivery. *Adv Drug Deliv Rev.* 1995;16:95–106.
- [23] Sampath Kumar K, Bhowmik D. Ocular inserts: a novel controlled drug delivery system. *Pharma Innov J.* 2013;1(12): 1–16.
- [24] Michael L, Collnot E-M, Djuric D, et al. Soluplus[®] as an effective absorption enhancer of poorly soluble drugs in vitro and in vivo. *Eur J Pharm Sci.* 2012;45:336–343.
- [25] Shamma R, Elkasabgy Design of freeze-dried Soluplus/polyvinyl alcohol-based film for the oral delivery of an insoluble drug for the pediatric use. *Drug Deliv.* 2016;23(2):489–499.
- [26] Dian L, Yu E, Chen X, et al. Enhancing oral bioavailability of quercetin using novel soluplus polymeric micelles. *Nanoscale Res Lett.* 2014;9:684.
- [27] Shamma RN, Basha M. Soluplus[®]: a novel polymeric solubilizer for optimization of carvedilol solid dispersion: formulation design and effect of method of preparation. *Powder Technol.* 2013;237:406–414.
- [28] Kim DH, Park MS, Choi Y, et al. Synthesis of PVA-g-POEM graft copolymers and their use in highly permeable thin composite membranes. *Chem Eng J.* 2018;346:739–747.
- [29] Available from: <https://www.drugbank.ca/drugs/db06802>
- [30] Ahuja M, Dhake AS, Sharma SK, et al. Topical ocular delivery of NSAIDs. *AAPS J.* 2008;10(2):229–241.
- [31] Lane S. Nepafenac: a unique nonsteroidal prodrug. *Int Ophthalmol Clin.* 2006;46(4):13–20.
- [32] Khurana G, Arora S, Pawar P. Ocular insert for sustained delivery of gatifloxacin sesquihydrate: preparation and evaluations. *Int Pharm Investig.* 2012;2(2):70–77.
- [33] Agrawal A, Jadhav L. Ocular drug delivery system and role of ocular inserts in eye disorder treatment: a review. *Asian J Pharm Technol Innov.* 2016;4(21):45–54.
- [34] Karathanos VT, Mourtzinos I, Yannakopoulou K, et al. Study of the solubility, antioxidant activity and structure of inclusion complex of vanillin with cyclodextrin. *Food Chem.* 2007;101:652–658.
- [35] Aburahma M, Mahmoud A. Biodegradable ocular inserts for sustained delivery of brimonidine tartarate: preparation and in-vitro/in-vivo evaluation. *AAPS PharmSciTech.* 2011;12(4): 1335–1347.
- [36] Dave V, Paliwal S, Yadav S. Formulation and evaluation of controlled delivery of aceclofenac through ocular insert. *Turk J Pharm Sci.* 2013;10(2):205–220.
- [37] Mathurm M, Gilhotra RM. Glycerogelatin-based ocular inserts of aceclofenac: physicochemical, drug release studies and efficacy against prostaglandin E2-induced ocular inflammation. *Drug Deliv.* 2011;18(1):54–64.
- [38] Pandey A, Mali P. Design and in-vitro characterization of levobunolol hydrochloride ocuserts with special reference to glaucoma treatment. *Indian J Pharm Educ Res.* 2012; 46(3):265–269.

- [39] Pandey P, Panwar A. Design and evaluation of ocular inserts for controlled drug delivery of acyclovir. *Int J Pharm Biol Arch*. 2011;2(4):1106–1110.
- [40] Nappinnai M. Fluconazole ocular inserts: formulation and in-vitro evaluation. *J Pharm Sci Res*. 2010;2(6):344–350.
- [41] Rajasekaran A, Sivakumar V. Design and evaluation of polymeric controlled release natamycin ocular inserts. *Kathmandu Univ J Sci Eng Technol*. 2010;6(1):108–115.
- [42] Gandhi P, Rathod H, Patel S. A review on: ocular inserts a novel drug delivery system. *Asian J Pharm Res Dev*. 2013;1(1):40–48.
- [43] Kaul S, Kumar G, Kothiyal P. An insight into ocular insert. *Int J Pharm Sci Res*. 2015;3:1–7.
- [44] Gorle A, Gattani S. Development and evaluation of ocular drug delivery system. *Pharm Dev Technol*. 2010;15(1):46–52.
- [45] Damodharan N, Soundrapandian C. Ophthalmic inserts of piroxicam: development and in-vitro drug release studies. *Asian J Chem*. 2008;20(5):3447–3454.
- [46] Ashture A, Kankudte A. Formulation and evaluation of controlled release ocular inserts of betaxolol hydrochloride; IOSR. *J Pharm*. 2012;2(5):34–38.
- [47] Kothawade S, Deshpande S, Lunkad A. Formulation and in-vitro characterization of ketorolac tromethamine ophthalmic inserts. *Res J Pharm Dosage Forms Tech*. 2013;5(6):1–3.
- [48] Ramkanth S, Chetty C. Design and evaluation of diclofenac sodium ocusert. *Int J PharmTech Res*. 2009;1(4):1219–1223.
- [49] Patel D. In-vitro and in-vivo evaluation of ocular inserts of ofloxacin. *DARU*. 2007;15(3):138–145.
- [50] Shafie M, Rady M. In-vitro and in-vivo evaluation of timolol maleate ocular inserts using different polymers. *J Clin Exp Ophthalmol*. 2012;3(8):1–9.
- [51] Franca J, Foureaux G. Bimatoprost-loaded ocular inserts as sustained release drug delivery systems for glaucoma treatment: in vitro and in vivo evaluation. *PLoS One*. 2014;9:1–14.
- [52] Paterakis PG, Korakianiti ES, Dallas PP, et al. Evaluation and simultaneous optimization of some pellet's characteristics using 3² factorial design and the desirability function. *Int J Pharm*. 2002;248:51–60.
- [53] Sanchez-Lafuente C, Furlanetto S, Fernandez-Arevalo M, et al. Didanosine extended-release matrix tablets: optimization of formulation variables using statistical experimental design. *Int J Pharm*. 2002;237:107–118.
- [54] Gadhave M, Pawar S. Formulation and evaluation of moxifloxacin ocusert. *Int J Pharm Clin Res*. 2016;8(12):1610–1615.
- [55] Gevariya H, Dharamsi A, Girhepunje K, et al. Once a day ocular inserts for sustained delivery of levofloxacin: design, formulation and evaluation. *Asian J Pharm*. 2009;3:314–318.
- [56] Morsi N, Ghorab D, Refai H, et al. Nanodispersion-loaded mucoadhesive polymeric inserts for prolonged treatment of post-operative ocular inflammation. *J Microencapsul*. 2017;34(3):280–292.
- [57] Mirzaeeia S, Alizadehc M. Design and evaluation of soluble ocular insert for controlled release of chloramphenicol. *J Rep Pharm Sci*. 2017;6(2):123–133.
- [58] Indian Pharmacopoeia. Ministry of Health and Family Welfare. Government of India. Vol. 2. New Delhi: Controller of Publication; 1996. p. 117–147.
- [59] Mundada A, Shrikhande B. Design and evaluation of soluble ocular drug insert for controlled release of ciprofloxacin hydrochloride. *Drug Dev Ind Pharm*. 2006;32:443–448.
- [60] Potu A, Reddy V. Design and evaluation of ocular inserts for controlled drug delivery of ketorolac tromethamine. *World J Pharm Res*. 2014;3(4):722–734.
- [61] Gorle A, Gattani S. Design and evaluation of polymeric ocular drug delivery system. *Chem Pharm Bull*. 2009;57(9):914–919.
- [62] Sankar V, Chandrasekaran A. Design and evaluation of diclofenac sodium ocular inserts. *Acta Pharm Sci*. 2006;48:5–10.
- [63] Michael H, Mostafa H, Mehdi J, et al. Draize rabbit eye test compatibility with eye irritation threshold in humans: a quantitative structural-activity relationship analysis. *Toxicol Sci*. 2003;76:384–391.
- [64] Kendre PN, Chaudhari PD. Effect of amphiphilic graft copolymer-carrier on physical stability of bosentan nanocomposite: assessment of solubility, dissolution and bioavailability. *Eur J Pharm Biopharm*. 2018;126:177–186.
- [65] Kendre PN, Chaudhari PD. Effect of polyvinyl caprolactam-polyvinyl acetate-polyethylene glycol graft copolymer on bioadhesion and release rate property of eplerenone pellets. *Drug Dev Ind Pharm*. 2017;43(5):751–761.
- [66] Kendre P, Chaudhari PD. Design and optimization of oral bioadhesive nanocurcumin delivery using novel hydrophilic carrier for cancer treatment: an alternative to parenteral chemotherapy. *Indian Drugs*. 2016;53:24–36.

RESEARCH

Open Access



A facile approach to fabrication and characterization of novel herbal microemulsion-based UV shielding cream

R. D. Bhalke¹, S. S. Kulkarni¹, P. N. Kendre², V. V. Pande³ and M. A. Giri^{2*}

Abstract

Background: Since many decades, phytoconstituents are well known for their potential therapeutic benefits but the development of herbal products has been limited due to difficulties like collection, isolation, stability and aqueous solubility of the phytoconstituents. The present study focuses on the development of microemulsion-based sunscreen cream formulation containing therapeutically active phytoconstituents like lycopene, β -carotene and curcumin which are reported for both antioxidant and ultraviolet radiation barrier properties. But the major hurdle in the development of the formulation is poor solubility and stability of these 3 components. Microemulsion preparation helps to enhance the solubility and stability of the final product. Screening of oils, surfactants and cosurfactants were done based on solubility studies followed by the construction of pseudo-ternary phase diagrams, sesame oil, span 80 to tween 80 (surfactant) and isopropyl alcohol (co-surfactant) which were selected to stable microemulsion.

Result: Based on a solubility study of components and pseudo-ternary phase diagrams, surfactant to co-surfactant (Smix) with 2:1 ratio and oil to Smix with 2:8 ratio were selected for preparation of the final microemulsion. Results show an average globule size of 208 nm, conductance 0.935 moh/cm, pH 7.1, zeta potential – 17.5 mV, refractive index 1.002, polydispersibility index 0.342, percent transmittance 90.68% and viscosity 82.45 cps. In a drug content study, the presence of lycopene, β -carotene and curcumin was found to be 87.53, 85.08 and 90.65%, respectively. Finally, microemulsion-based sunscreen cream was prepared and evaluated for various parameters like pH, extrudability, spreadability and drug content study. The sun protection factor (SPF) of microemulsion and cream was found to be 36.32 and 37.65, respectively. The stability study data shows better stability of the final formulation.

Conclusion: Formulation of microemulsion-based sunscreen cream may be a better option in the design and development of herbal phytoconstituents.

Keywords: Microemulsion, Surfactant, Lycopene, Curcumin, β -Carotene, Sunscreen cream

Background

Everyone is very conscious about their health, and nowadays, people are even very sensible about looks and external appearance. In short, the world is fond of cosmetics and skin protection against many harmful environmental effects which are on prime importance. One of the harmful factors is the ultra-violet rays coming

from the sun. This sunburn may darken the skin and severe consequences may lead to skin damage or cancer. Human exposure to harmful ultraviolet (UV) radiations has very dangerous side effects such as skin melanoma, photoaging, skin pigmentation, sunburn and various painful effects. Ultraviolet radiations increase oxidative stress on skin cells by frequent formation of reactive oxygen species (ROS) leading to initiation and promotion of cancer [1].

There are several products available in the market which are sold by many companies and claiming on the

* Correspondence: mahi_jaan83@yahoo.com

²Department of Pharmaceutics, Rajarshi Shahu College of Pharmacy, Sant Gadgebaba Amravati University, Buldhana, India
Full list of author information is available at the end of the article

basis of skin-protection-factor (SPF). These sunscreen products may be lotion, spray, gel and foam applied topically that absorbs or reflects the ultraviolet radiation. Sun protection factor (SPF) is the measure of the fraction of sunburn coming from the sun.

Ideally, these values of SPF represent the measure of time up to which the product protects the skin from harmful effects of ultraviolet (UV) radiation. Although these products are used widely, regulatory aspects are also taken into consideration during design and development.

The sunscreen preparations are designed and developed to apply topically to prevent the entry of ultraviolet rays directly in the skin by absorbing or reflecting from the skin. There are many synthetic components that are used as sun protection like p-aminobenzoic acid (PABA), phenyl benzimidazole sulfonic acid, cinoxate and oxybenzone and inorganic components like titanium dioxide and zinc oxide. Although innumerable numbers of sunscreen products are available in the market, they have several drawbacks. Some physical sunscreen agents make the preparation opaque and may result in whitish appearance of the skin treated topically with them [2–5].

Sunscreens containing synthetic chemicals may cause side effects, such as erythema, oedema and irritation. Herbal sunscreens are eco-friendly with less or no comedogenic effects. Incorporation of antioxidants could provide additional benefit by scavenging free radicals.

There are many phytoconstituents that have great potential to protect the harmful effects of UV radiation. Natural polyphenols and flavonoids are attractive in this respect, due to their potential activity as photoprotectants and antioxidants [6–10].

Tomatoes contain lycopene, which is the most powerful natural antioxidant. Lycopene has a property to improve the skin's ability to reflect back UV radiations and protect skin from its harmful effect, and β -carotene is the carotenoids present in carrot and emphasizes on the UV protective nature because of the antioxidant potential.

Active chemical constituents of turmeric are curcuminoids, which includes curcumin, desmethoxycurcumin and desmethoxycurcumin. There is some important volatile oil such as turmerone and allenton which help to protect skin from free radical damage; it reduces burning sensation of skin and inflammation, improves the texture of the skin and shows potent UV protective action.

These phytoconstituents include quercetin, lycopene, β -carotene, curcumin and other medicinal herbs like *Embilica officinalis*, *Nelumbo nucifera*, *Moringa oleifera* L, and *Terminalia chebula*. These components can be used to develop sunscreen formulations, but due to certain limitations like their solubility and stability issues, they are restricted [11–13].

The present study focuses on the development of microemulsion of phytoconstituents like lycopene, β -

carotene and curcumin. These microemulsion (average globule size of 10–200 μm) are a better option to overcome the issues of solubility and stability of such phytoconstituents. This prepared microemulsion formulation was added to the cream base to develop the final sunscreen formulation with excellent performance of sunburn protection effect.

Microemulsion is isotropic and thermodynamically stable multicomponent fluids composed of water, oil, surfactant and co-surfactant. This unique class of optically clear solutions comprises of the colloidal systems. Microemulsion has transparency, optical isotropy, low viscosity, monophasic, ultra-low interfacial tension, dynamic microstructure and thermodynamic stability. The droplet diameter of microemulsions is generally within the range of 10–200 nm [14].

Pharmaceutical microemulsions contain additional components such as co-surfactant and drugs. The co-surfactant is also amphiphilic with an affinity for both the oil and aqueous phases and partitions to an appreciable extent into the surfactant interfacial monolayer present in the oil-water interface. A wide variety of molecules can function as co-surfactant including non-ionic surfactant, alcohol, alkalotic acids, alkaloids and alkylamines [15–17].

The nanometric size of micelles improved solubilization capacity for lipophilic drug transparency that the property makes the system more suitable for transdermal and topical formulations. Even though microemulsions offer several advantages for topical delivery, it is difficult to stabilize the system because of low viscosity. This problem can be overcome by formulating a microemulsion-based cream [18]. Therefore, the present research work aims at the development of microemulsion containing lycopene, β -carotene and curcumin as an important phytoconstituent possessing both antioxidant and UV radiation protection properties with improved solubility and surface area and stabilization of same by formulating microemulsion-based cream.

Methods

Materials

Crude materials like *Curcuma longa*, *Dacus carota* and *Solanum lycopersicum* are procured from Mahatma Phule Krishi Vidyapeeth, Rahuri, Maharashtra, India. Other supporting materials, tween 80, isopropyl alcohol, sesame oil, glycerine, potassium hydroxide, petroleum jelly, ethanol, chloroform, methanol, dichloromethane and petroleum ether, were procured from Research Fine Chem Pvt. Ltd., Mumbai, India, and were analytical grade.

Methods

Extraction, isolation and pre-formulation study of phytoconstituents

The extraction and isolation of lycopene from *Solanum lycopersicum*, β -carotene from *Dacus carota* and

Table 1 Composition of LCCMBSC

Ingredients	Quantity (g)
Cetostyrl alcohol	0.30
Stearic acid	0.40
Petroleum jelly	0.10
Glycerine	0.40
Potassium hydroxide	0.10
Water	8.5
Methyl paraben	0.02
Polypropyl paraben	0.005
LCCM	1
Rose oil	Q.S

curcumin from *Curcuma longa* were carried out by cold maceration followed by preparative thin-layer chromatography (TLC) [19–21].

Melting point, UV-spectrophotometric analysis and FT-IR spectra have confirmed the identification of the above phytoconstituents.

Solubility study

For the preparation of microemulsion, it is most important to check the solubility of the phytoconstituents in either oil, water or surfactant system. Hence, a solubility study was conducted to select suitable components of the microemulsion system. Initially, various oils (sesame oil, olive oil, coconut oil, castor oil, arachis oil), surfactants (span 80, tween 80, polaxamer 407, IPM) and co-surfactants (isopropyl alcohol, n-butanol, polyethylene glycol-400, amyl alcohol, n-propyl alcohol) were procured and solubility of lycopene, β -carotene and curcumin was checked using the shaking flask method in which excess amount of phytoconstituents was added separately to the oils and surfactants. These mixtures were shaken at 37 °C for 48 h to solubilize the components, and after 48 h, samples were investigated for the amount of phytoconstituents using UV spectrophotometer at 440, 460 and 418 nm, respectively [22–24].

Construction of a pseudo-ternary phase diagram

Based on the solubility study, suitable oils, surfactants and co-surfactants were selected for the preparation of the microemulsion system. For the preparation of a stable microemulsion system, initial batches were prepared with the help of a pseudo-ternary phase diagram. Water titration method was implemented, in which double distilled water was added drop-wise using micro-pipette to previously mix Smix and oils with different ratios (Smix:oils) as 1:1, 2:1, 3:1 and 4:1. Water was added with continuous stirring till turbidity will appear and the amount of added water was noted. Various batches containing Smix:oils at the ratios of 1:1 to 1:9 and 9:1 to 9:8.

Finally, a pseudo-ternary phase diagram was constructed with the help of concentration levels of water, oil and Smix to optimize and finalized the stable microemulsion system. Three-component ternary diagrams with each axis representing an oil phase, Smix and water with fix mass ratio were plotted using CHEMIX school software [14, 25, 26].

Selection of a stable microemulsion system

Finally, stable microemulsion systems were selected based on the maximum microemulsion boundary areas detected in the pseudo-ternary phase diagrams and after evaluation of other physical parameters. After the identification of the microemulsion region in the phase diagram, the microemulsion formulations were selected at desired component ratios. Once this blank microemulsion was prepared, the microemulsion containing phytoconstituents was prepared by mixing them (each 1% w/w) into the surfactant or oils in which they were soluble at a higher amount (based on the results of the solubility study). Finally, a clear and stable microemulsion system (W/O type) was obtained using the appropriate amounts of all the components detected in the pseudo-ternary phase diagrams. The microemulsion system containing phytoconstituents was characterized for various physico-chemical properties like globule size analysis, zeta-potential, viscosity, drug content, pH, transmittance and stability study.

Measurement of globule size and zeta potential

The average globule size and zeta potential of phytoconstituents containing microemulsion was evaluated using Malvern Zetasizer (Nano ZS, 90, UK). A small amount of microemulsion sample (0.1 ml) was diluted to 10 ml of doubled distilled water. This diluted sample was tested for globule size and zeta potential using Malvern Zetasizer. Samples were analysed for globule size and zeta potential in triplicate for better accuracy.

Viscosity determination

Viscosity of the microemulsion formulation and sunscreen formulation was measured by using the Brookfield Viscometer (LVDV-II+pro). Appropriate spindles were chosen to measure the viscosity of both the microemulsion and sunscreen cream. All the operating conditions of rpm and torque were set and samples were kept ready to determine the viscosities. Finally, the viscosities were calculated by the following Eq. (1) [27].

$$\text{Viscosity} = \text{Dial reading} \times \text{Factor. For LV at 6 rpm factor is 1M (1000)} \quad (1)$$

Drug content study

Accurately weighed (5 ml) microemulsion containing 1% w/w of lycopene, β -carotene and curcumin was taken in

25 ml capacity volumetric flask and 10 ml ethanol was added to it. The resultant mixture was stirred for 30 min and finally filtered through Whatman filter paper. These filtrates (1 ml) were diluted with 10 ml ethanol and analysed for content study using UV-visible spectrophotometer at 440, 460 and 418 nm for the determination of lycopene, β-carotene and curcumin respectively [18].

Determination of pH and percent transmittance

The prepared microemulsion system was checked for measurement of pH values using digital pH meter (Lab India). Standard buffer systems of pH 4 and 7 were used to determine the pH of microemulsion. Percent transmittance was measured by diluting the microemulsion 100 times and analysed on UV-visible spectrophotometer against distilled water as blank at 640.2 nm.

Stability study

Microemulsion system was tested for physical stability by centrifuging the small amount of sample at 1250 rpm for 5 h and examined for phase separation and other changes, if any. Further, these microemulsion systems were checked for stability issues at various temperature and humidity conditions for 3 months. The microemulsion was subjected to stability study at 4 ± 2 °C, 30 ± 2 °C and 75 ± 5% relative humidity (RH) and 40 °C ± 2.C/ 75 ± 5% (RH) according to ICH guidelines and evaluated for physical and chemical stability [28].

Preparation of sunscreen formulation

Sunscreen cream is o/w emulsion containing aqueous phase as continuous phase and oil phase as dispersed phase. Water phase is prepared by adding a reported

amount of distilled water. Accurately weighed all water-soluble components such as glycerine, potassium hydroxide and methyl paraben were dissolved in aqueous phase and resultant mixture allowed to heat up to 80 °C. Oil phase was prepared by mixing ceto-stearyl alcohol, stearic acid, propyl paraben and petroleum jelly together with the mentioned amount of MLCC and heated up to 80 °C. Oil phase was added to aqueous phase at 80 °C with slow and constant stirring for 20 min. As a result, homogenized and uniform emulsion-based cream was formed. The accurately weighed microemulsion was added slowly to the above sunscreen base and incorporated uniformly in mortar and pestle [16] (Table 1).

Determination of sun protection factor (SPF)

The sun protection factor of microemulsion and microemulsion-containing sunscreen cream was determined using the UV-spectrophotometric method. In this method, 1 g of sample was weighed accurately and ethanol was added to make 10 ml of the final volume. The resultant mixture was analysed for absorbance at 290–320 nm and SPF was calculated using following Eq. (2) [29, 30]

$$\begin{aligned}
 \text{SPF spectrophotometric} &= \text{CF} \times \text{SPF spectrophotometric} \\
 &= \text{CF} \times \\
 &= \sum_{290}^{320} \text{EE}(\lambda) \text{Abs}(\lambda) \quad (2)
 \end{aligned}$$

where
 CF = Correction factor (10)
 EE = Erythrogenic effect of radiation with wavelength (λ)

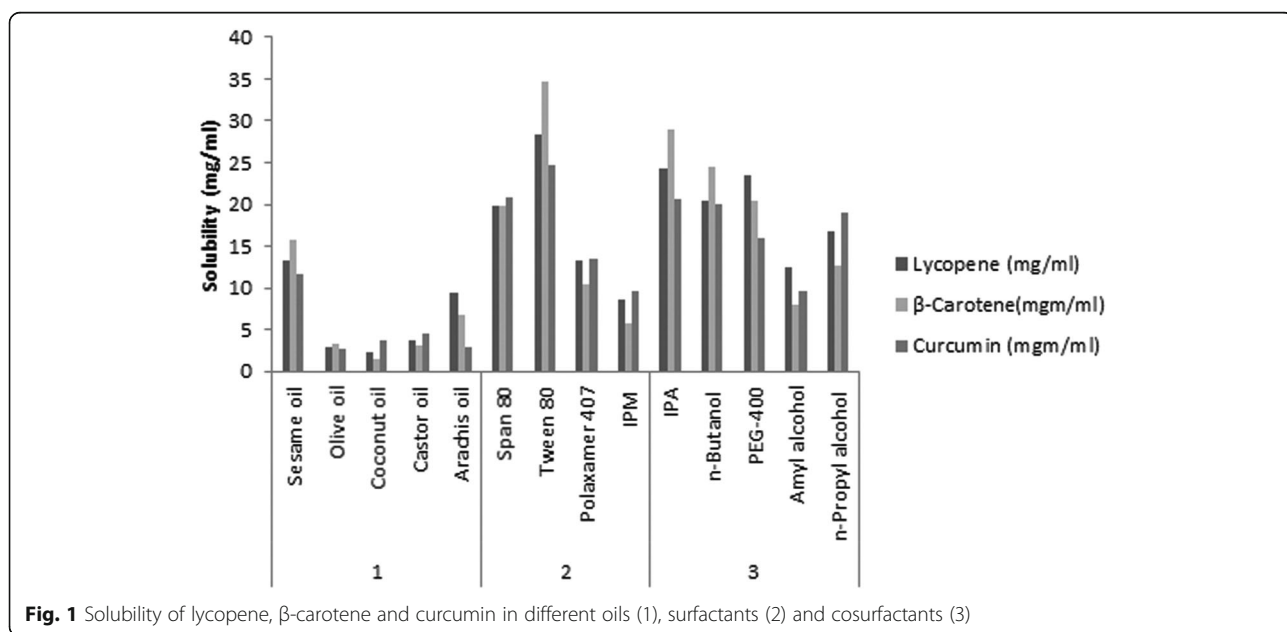


Fig. 1 Solubility of lycopene, β-carotene and curcumin in different oils (1), surfactants (2) and cosurfactants (3)

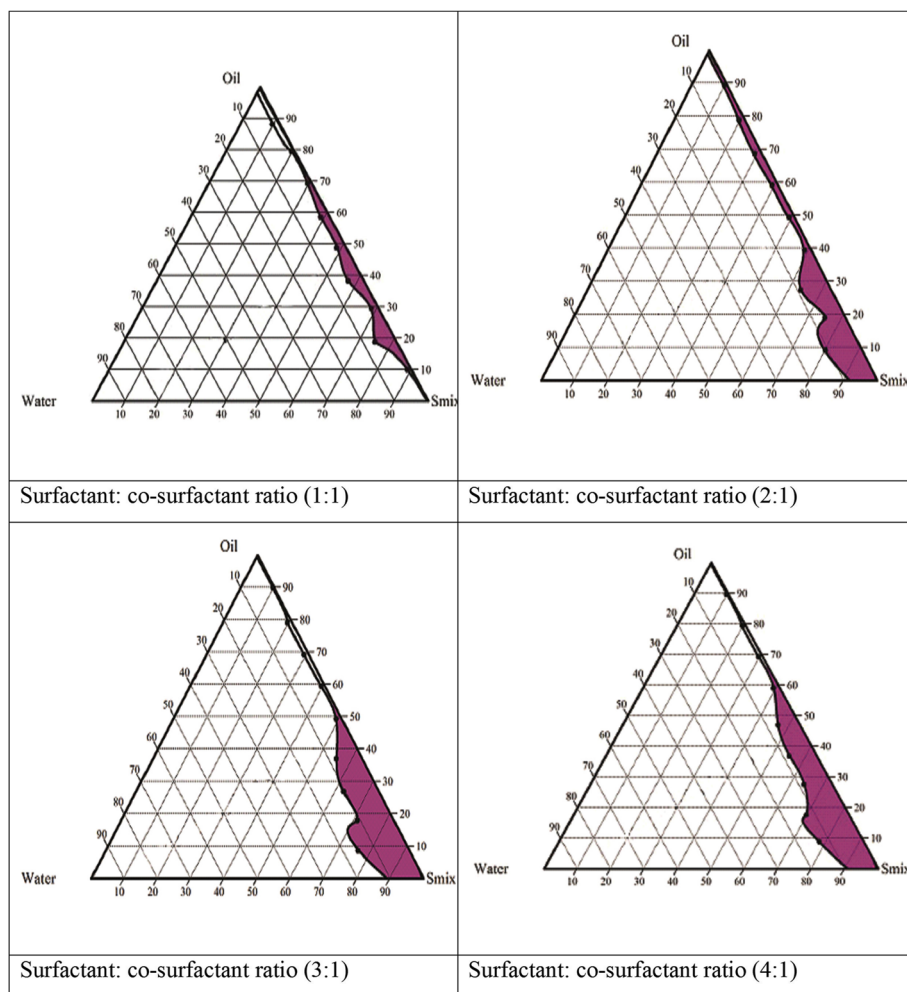


Fig. 2 The pseudo ternary phase diagrams of the oil-surfactant-water system at 1:1, 2:1, 3:1, and 4:1 weight ratio

Abs (λ) = Spectrophotometric absorbance values at wavelength

The value of $EE \times I$ is constant.

Evaluation of sunscreen formulation

The microemulsion-containing sunscreen cream formulation was evaluated for pH, tube extrudability, spreadability, viscosity, drug content and in vitro study using various tools and methods.

Texture characterization and spreadability testing

The prepared sunscreen formulation containing microemulsion was characterized for spreadability using CT-3 texture analyser. A cylindrical analytical probe (12 mm diameter) was inserted within the sample at a specific rate (2 mm/s) and at a definite depth (10 mm) at 25 °C. Readings were taken in triplicate for better accuracy.

Table 2 Various evaluation parameters of an optimized microemulsion system

Observations	Results
Average particle (globule) size	208 nm
Polydispersibility index (PDI)	0.342
Zeta potential	- 17.5 mV
Transmittance	90.68%
Refractive index	1.002 ± 0.03
pH	7.01 ± 0.07
Viscosity	82.45 ± 0.07 cps
Drug content (%)	
(a) Lycopene	87.53%
(b) β -carotene	85.08%
(c) Curcumin	90.65%
SPF	36.32
Conductance	0.935 moh/cm

Table 3 Various evaluation parameters of microemulsion-containing sunscreen cream

Observations	Results
Spreadability	17 ± 5 g cm/s
Extrudability	96.58 ± 0.9%
pH	7.1 ± 0.3
Sun protection factor (SPF)	37.65
Refractive index	1.002 ± 0.03
Viscosity	22,341 ± 3 cps
Drug content (%)	
(a) Lycopene	84.33%
(b) β-carotene	83.88%
(c) Curcumin	88.86%

Extrudability study

This study was conducted to find out the extrudability of sunscreen cream formulation when packaged in the tube container. The sunscreen formulation was filled in the standard collapsible tube, sealed properly using crimping machine and cap was fitted. The filled weight of tube was recorded. The tube was clamped between two glass slides and 500 g weight was placed over the glass slides and then cap was removed slowly. The amount of cream extruded was collected and weighed and compared with the initial filled weight of the tube. Finally, the percentage of cream was calculated and graded.

Skin irritation test

The prepared sunscreen formulation containing microemulsion was tested for the skin irritation. Protocols of the study were approved by Institutional Animal Ethical Committee, and with kind permission of the CPCSEA committee, the work was started using three healthy male rabbits. They were kept carefully following the acclimation period of 7 days to ensure their suitability for study. After an acclimation period, the area on the back of each rabbit was shaved carefully before the experiment. The skin surface of the rabbit on its back was divided into three marked areas; at one patch, there was no formulation and on the other two patches, microemulsion and sunscreen cream formulation was applied (0.5 g of each test formulation was applied on each 3 × 3 cm area). The study was carried out for 48 h, and for every 24 h, the animal was observed for irritancy,

erythema, inflammation and oedema. The score of primary irritation was calculated for each rabbit.

Results

In the initial study, extraction of plant material was carried out and isolation of lycopene, β-carotene and curcumin was obtained from *Solanum lycopersicum*, *Dacus carota* and *Curcuma longa*, respectively, using cold maceration followed by preparative thin-layer chromatography (TLC). Isolated phytoconstituents were tested for identification and quality. Melting point of 184 °C, 171 °C and 181 °C were detected for lycopene, β-carotene and curcumin, respectively, determined by digital melting point apparatus (Veego, model MVP). The melting point was found to be in range and identical to the reported standard melting points. UV-visible spectra and FT-IR spectra confirmed the isolated phytoconstituents based on the various functional groups detected. Maximum absorption spectra (λ_{max}) of lycopene, β-carotene and curcumin were detected at 418, 444 and 460 nm, respectively, after being scanned in UV-visible spectrophotometer in a range from 200 to 800 nm.

Results of globule size analysis showed the average globule size 208 nm (Fig. 1) and conductance of 0.935 moh/cm. The lower value of conductance confirmed the W/O type of emulsion. The microemulsion was tested for pH and average value of 7.1 ± 0.07 was observed. The refractive index is 1.002 ± 0.03. Polydispersibility index (PDI) represents the uniform distribution of globules/particles (> 0.3); the present optimized microemulsion formulation shows an average PDI of 0.342 which has confirmed the uniform distribution of the droplets in the formulation. For better distribution of particles, the zeta potential values of less than - 30.0 mV are generally not considered due to less repulsive forces which may lead to the formation of agglomerates. An average zeta potential value for optimized microemulsion was found to be - 17.5 mV (Fig. 2) which represents the sign of good dispersibility of microemulsion droplets in the continuous phase and less chances of agglomeration with better stability.

In another study of transmittance, the presence micron-sized globules with uniform distribution was observed when the microemulsion was diluted 100 times and showed 90.68% transmittance with clear appearance whereas without diluted microemulsion has shown

Table 4 Skin irritation study data

Test material ^a	Skin reaction ^b	Mean irritation score		
		12 h	24 h	48 h
Sunscreen cream containing microemulsion	Erythema	0	0	0.2
	Oedema	0	0	0

^aTest material was applied on rabbit skin

^bErythema and oedema; the mean irritation score was the summation of each irritation score divided by the number of animals

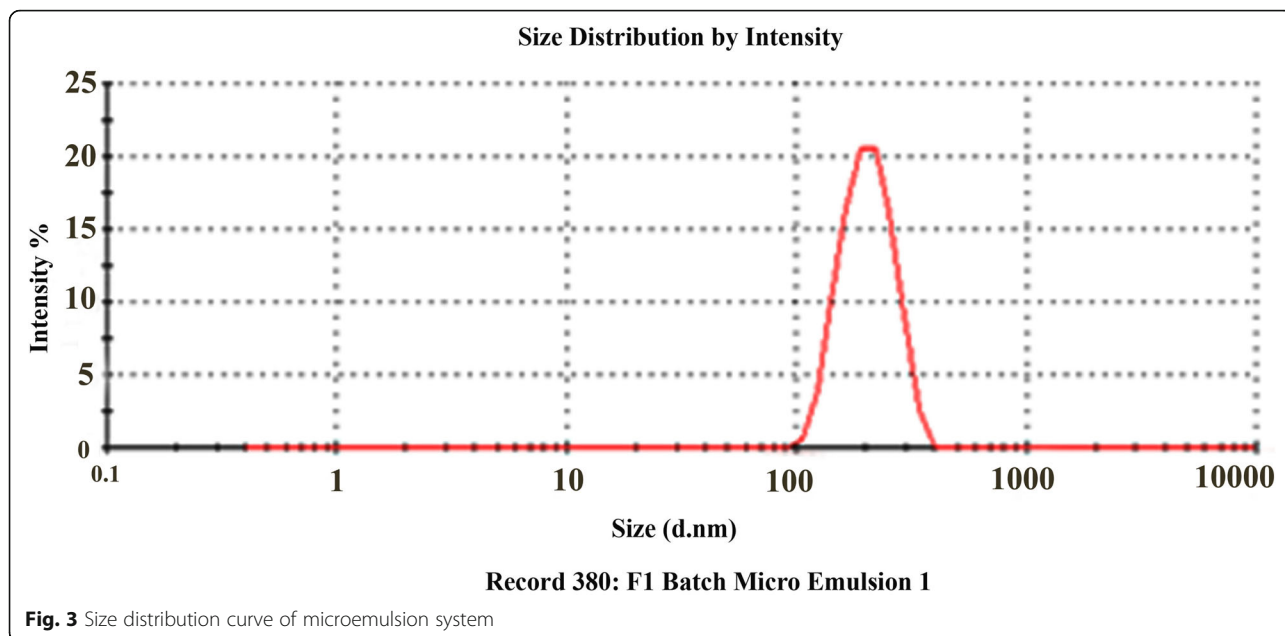


Fig. 3 Size distribution curve of microemulsion system

85.98% transmittance. Further, the sunscreen cream formulation was also evaluated for viscosity, tube extrudability and spreadability. The viscosity of microemulsion was found to be 82.45 ± 0.07 cps, whereas the total content of lycopene, β -carotene and curcumin was found to be 87.53, 85.08 and 90.65%, respectively. The sun protection factor of microemulsion was calculated using Eq. (1) described in the “Methods” section, and it was found to be 36.32. All the results of globule size, PDI, conductance, transmittance, refractive index, pH, viscosity, drug content and sun protection factor (SPF) are presented in Table 2.

The extrudability of the prepared sunscreen cream formulation after packaged into standard tube was found to be $96.58 \pm 0.9\%$.

The viscosity of sunscreen cream at 25 °C was found to be $22,341 \pm 3$ cps which was much higher than the microemulsion preparation. The pH of test sunscreen cream was found to be 7.1 ± 0.3 whereas the percent drug content of lycopene, β -carotene and curcumin was found to be 84.33, 83.88 and 88.86%, respectively (Table 3).

The sun protection factor calculated for the microemulsion-containing sunscreen formulation was found to be 37.65.

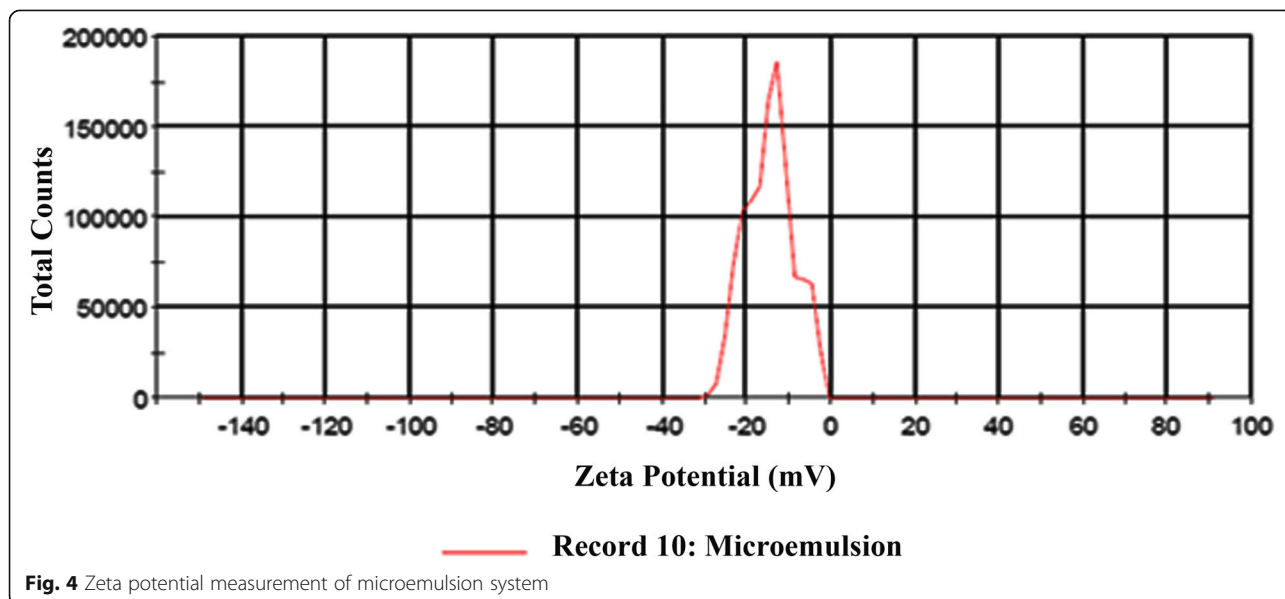
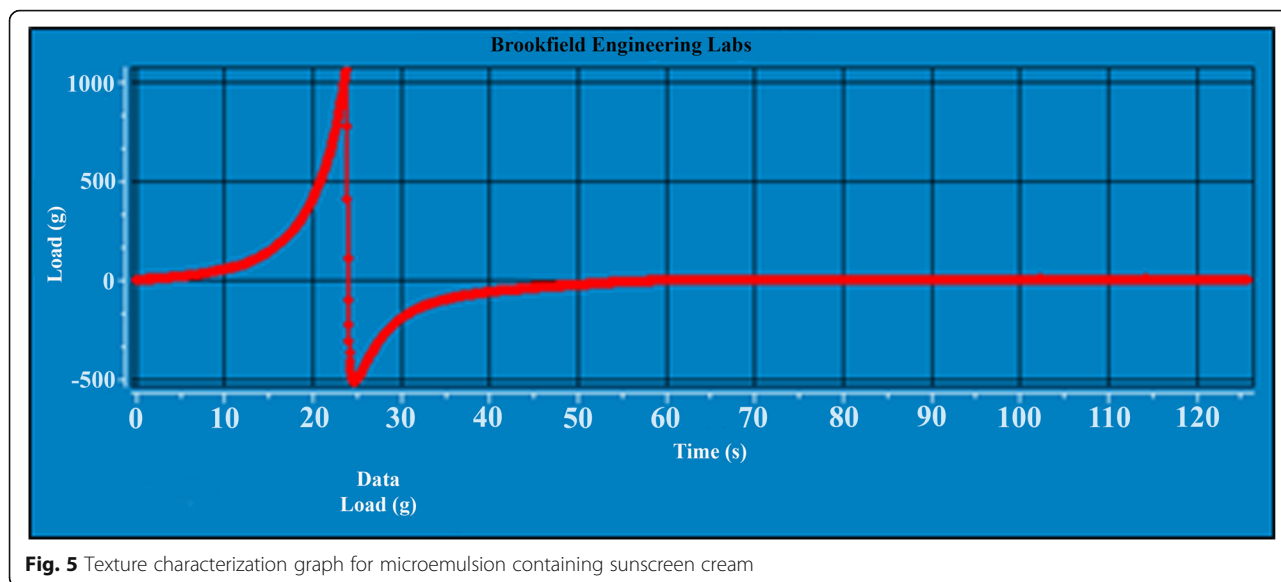


Fig. 4 Zeta potential measurement of microemulsion system

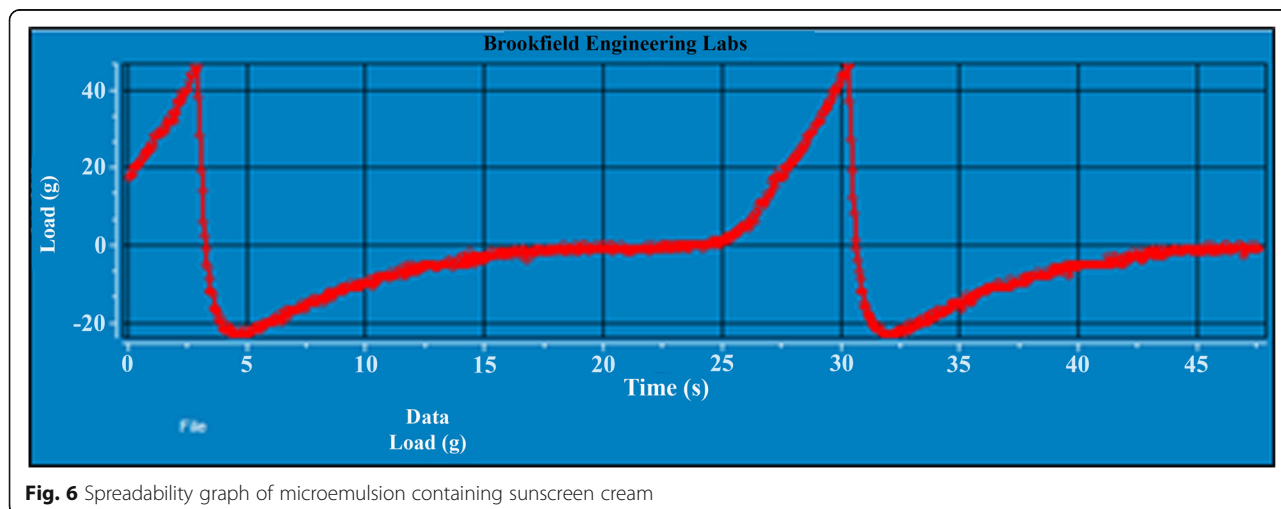


Skin irritancy test was performed to check the irritation of topically applied microemulsion as well as sunscreen cream formulation. The PII (Primary Irritation Index) when no formulation was applied was found to be 0.166; for microemulsion, it was 0.277; and for sunscreen cream, it was found to be 0.222 (Table 4).

Discussion

In the solubility study of lycopene, β-carotene and curcumin, it has been observed that the maximum solubility of these phytoconstituents was found to be in sesame oil, span 80 to tween 80 (1:1) and isopropyl alcohol. Based on these results of this solubility study, sesame oil, span 80 to tween 80 (1:1) and isopropyl alcohol were selected for the preparation of microemulsion. Results of the solubility study are presented in Fig. 3.

From results of the pseudo-ternary phase diagrams, 2:1 ratio of surfactant to co-surfactant and oil to Smix (2:8) was found to be the best for the development of microemulsion since the maximum microemulsion boundary area was observed as shown in Fig. 4. The maximum microemulsion boundary area represents the formation of microemulsion with micron-sized globules at the interface of oil, water and Smix. This area represents clear, transparent and stable microemulsion with no phase separation up to 72 h when kept on standing in the sealed glass container. Finally, these ratios of components were considered to make an optimized microemulsion system, and microemulsion-containing phytoconstituents were formulated successfully. This optimized microemulsion was characterized for various physiochemical parameters for the confirmation of quality.



The spreadability of the prepared sunscreen formulation was studied on the CT-3 texture analyser. The area under positive curve is a measure of energy required to deform the sample to a defined depth grade in order of its stability. Higher peak load and work done indicate lower spreadability. Lower peak load value coupled with a lower work done value indicates that the sample is more spreadable. In the case of sunscreen cream formulation, the texture analysis data represents the spreadability of cream (17 ± 5 g cm/s) as shown in Figs. 5 and 6. The negative peak indicates the work done by the probe which was lower than the positive curve which proves that the test formulation possesses good spreadability.

From the above data, it is concluded that the PII (Primary Irritation Index) of both microemulsion and sunscreen cream in the range of 0.0–0.4 and indicating irritancy was negligible.

Conclusion

Prevention from harmful effects of ultraviolet radiation of the sun is on prime importance to everyone by considering cosmeceutical intension and personal external appearance of the individuals. The use of many available synthetic components such as sun protection may be harmful due to various serious issues as discussed in this manuscript. Considering many beneficial effects of phytoconstituents like antioxidant activity and excellent sun protection effect, the present study has focused on the development of microemulsion-based sunscreen cream formulation with excellent SPF values. From the findings of the present research, it has been concluded that stable microemulsion system containing lycopene, β -carotene and curcumin as an important phytoconstituents possessing both antioxidant and ultraviolet radiation protection properties can be formulated successfully as a sunscreen cream formulation.

Abbreviations

UV: Ultraviolet; ROS: Reactive oxygen species; MPKV: Mahatma Phule Krushi Vidyapith; TLC: Thin-layer chromatography; IR: Infrared; IPM: Isopropyl myristate; IPA: Isopropyl alcohol; PEG: Polyethylene glycol; SPF: Sun protecting factor; CF: Correction factor; RH: Relative humidity; ICH: International Conference on Harmonisation

Acknowledgements

The authors are thankful to the Institute of Sanjivani College of Pharmaceutical Education and Research, Kopergaon, for providing the necessary facilities to carry out our research work in the current format. The authors are very thankful to the Principal and all the supporting members of the institution for providing all the facilities to conduct this research study. The authors are also grateful to the Institutional Animal Ethical Committee (IAEC) for approving the protocol and permission for the animal study. Finally, the authors are thankful to everyone for providing direct or indirect support to conduct this study.

Authors' contributions

RDB has given her contribution for constructing the idea for the manuscript. SSK has given her contribution for collecting the data and material for this

work. PNK has given his contribution for taking responsibility in the construction of the entire part of the manuscript. VVP has given his contribution for making planning as well as organizing and supervising of the course of the article and taking responsibility. MAG has given contribution for guiding the entire team as well as taking effort before submission of the article. All authors have read and approved the final manuscript.

Funding

The research work is of routing major dissertation work of the students, and it is carried through college funding.

Availability of data and materials

All data and materials are available upon request

Ethics approval and consent to participate

Institutional Animal Ethics Committee for Animal Experiments of Sanjivani College of Pharmaceutical Education and Research, Kopergaon, approved the study under the protocol SCPER/CPCSEA/IAEC/2016-17/04 and all experiments were conducted in accordance with guidelines of Committee for the Purpose of Control and Supervision of Experiments on Animals (CPCSEA).

Consent for publication

Not applicable.

Competing interests

The authors declare that they have no competing interests

Author details

¹Department of Pharmacognosy, Sanjivani College of Pharmaceutical Education and Research, Pune University, Kopergaon, India. ²Department of Pharmaceutics, Rajarshi Shahu College of Pharmacy, Sant Gadgebaba Amravati University, Buldhana, India. ³Department of Pharmaceutics, N. N. Saththa College of Pharmacy, BAT University, Ahmednagar, India.

Received: 5 May 2020 Accepted: 12 August 2020

Published online: 05 November 2020

References

- Valachovic E, Zurbenko I (2014) Skin cancer, irradiation, and sunspots: The solar cycle effect. *Biomed Res Int* 11:734–748. <https://doi.org/10.1155/2014/538574>
- Rancan F, Rosan S, Boehm K, Fernández E, Hidalgo ME, Quihot W et al (2002) Protection against UVB irradiation by natural filters extracted from lichens. *J Photochem Photobiol B Biol* 68(2–3):133–139
- Kohlhardt-Floehr C, Boehm F, Troppens S, Lademann J, Truscott TG (2010) Prooxidant and antioxidant behaviour of usnic acid from lichens under UVB-light irradiation - Studies on human cells. *J Photochem Photobiol B Biol* 101(1):97–102
- Millot M, Di Meo F, Tomasi S, Boustie J, Trouillas P (2012) Photoprotective capacities of lichen metabolites: a joint theoretical and experimental study. *J Photochem Photobiol B Biol* 111:17–26
- Lohezic-Le Devehat F, Legouin B, Couteau C, Boustie J, Coiffard L (2013) Lichenic extracts and metabolites as UV filters. *J Photochem Photobiol B Biol* 120:17–28
- Boehm F, Clarke K, Edge R, Fernandez E, Navaratnam S, Quihot W et al (2009) Lichens - Photophysical studies of potential new sunscreens. *J Photochem Photobiol B Biol* 95(1):40–45
- Rojas JL, Diaz-Santos M, Valencia-Islas NA (2015) Metabolites with antioxidant and photo-protective properties from *Usnea roccellina* Motyka, a lichen from Colombian Andes. *UK J Pharm Biosci* 3(4):18
- Baker LA, Marchetti B, Karsili TNV, Stavros VG, Ashfold MNR (2017) Photoprotection: extending lessons learned from studying natural sunscreens to the design of artificial sunscreen constituents. *Chemical Society Reviews*. Royal Society of Chemistry 46:3770–3791
- Radice M, Manfredini S, Ziosi P, Dissette V, Buso P, Fallacara A et al (2016) Herbal extracts, lichens and biomolecules as natural photo-protection alternatives to synthetic UV filters. A systematic review. *FitoTerapia* 114:144–162

10. Cefali LC, Ataide JA, Moriel P, Foglio MA, Mazzola PG (2016) Plant-based active photoprotectants for sunscreens. *Int J Cosmet Sci* 38(4):346–353
11. Saraf S, Kaur C (2010) Phytoconstituents as photoprotective novel cosmetic formulations. *Pharmacognosy Reviews* 4:1–11
12. Offord EA, Gautier JC, Avanti O, Scaletta C, Runge F, Krämer K et al (2002) Photoprotective potential of lycopene, β -carotene, vitamin E, vitamin C and carnosic acid in UVA-irradiated human skin fibroblasts. *Free Radic Biol Med* 32(12):1293–1303
13. Köpcke W, Krutmann J (2008) Protection from sunburn with β -carotene—a meta-analysis. *Photochem Photobiol* 84(2):284 <http://doi.wiley.com/10.1111/j.1751-1097.2007.00253.x>
14. Kawakami K, Yoshikawa T, Hayashi T, Nishihara Y, Masuda K (2002) Microemulsion formulation for enhanced absorption of poorly soluble drugs. II. In vivo study. *J Control Release* 81(1–2):75–82
15. Kogan A, Garti N (2006) Microemulsions as transdermal drug delivery vehicles. Vols. 123–126. *Advances in Colloid and Interface Science* 123–126: 369–385
16. Boonme P (2007) Applications of microemulsions in cosmetics [Internet]. Vol. 6, *Journal of Cosmetic Dermatology*. *J Cosmet Dermatol* 6:223–228
17. Lawrence MJ, Rees GD (2000) Microemulsion-based media as novel drug delivery systems. *Adv Drug Deliv Rev* 45(1):89–121
18. Sabale V, Vora S (2012) Formulation and evaluation of microemulsion-based hydrogel for topical delivery. *Int J Pharm Investig* 2(3):140
19. Kulkarni S, Bhalke R, Pande V, Kendre P, Kulkarni SS (2014) *Indo American Journal of Pharmaceutical Research*. Herbal plants in photo protection and sun screening action: an overview. *Indo Am. J Pharm Res* 4(02):1104–1113
20. Fikselová M, Šilhár S, Mareček J, Frančáková H (2008) Extraction of carrot (*Daucus carota* L.) carotenes under different conditions. *Czech J Food Sci* 26(4):268–274
21. Revathy S, Elumalai S, Benny M, Antony B (2011) Isolation, purification and identification of curcuminoids from turmeric (*Curcuma longa* L.) by column chromatography. *J Exp Sci* 2(7):21–25
22. Kendre PN, Chaudhari PD (2017) Effect of polyvinyl caprolactam–polyvinyl acetate–polyethylene glycol graft copolymer on bioadhesion and release rate property of eplerenone pellets. *Drug Dev Ind Pharm* 43(5):751–761
23. Karathanos VT, Mourtzinou I, Yannakopoulou K, Andrikopoulos NK (2007) Study of the solubility, antioxidant activity and structure of inclusion complex of vanillin with β -cyclodextrin. *Food Chem* 101(2):652–658
24. Kendre PN, Chaudhari PD (2018) Effect of amphiphilic graft co-polymer-carrier on physical stability of bosentan nanocomposite: assessment of solubility, dissolution and bioavailability. *Eur J Pharm Biopharm* 126:177–186
25. Chandra A, Sharma K, Irchhiya R (2009) Microemulsion-based hydrogel formulation for transdermal delivery of dexamethasone. *Asian J Pharm* 3(1):30–36
26. Hussain A, Luckham PF, Tadros TF (1997) Phase behaviour of PH dependent microemulsions at high temperatures and high salinities. *Rev l'Institute Fr du Pet* 52(2):228–231
27. Smaoui S, Ben Hlima H, Ben Chobba I, Kadri A (2017) Development and stability studies of sunscreen cream formulations containing three photoprotective filters. *Arab J Chem*:S1216–S1222. <https://doi.org/10.1016/j.arabjc.2013.02>
28. Derle DV, Sagar BSH, Pimpale R (2006) Microemulsion as a vehicle for transdermal permeation of nimesulide. *Indian J Pharm Sci* 68(5):622–625
29. Nesseem D (2011) Formulation of sunscreens with enhancement sun protection factor response based on solid lipid nanoparticles. *Int J Cosmet Sci* 33(1):70–79
30. Dutra EA, Da Costa E, Oliveira DAG, Kedor-Hackmann ERM, Miritello Santoro MIR (2004) Determination of sun protection factor (SPF) of sunscreens by ultraviolet spectrophotometry. *Rev Bras Ciencias Farm J Pharm Sci* 40(3): 381–385

Publisher's Note

Springer Nature remains neutral with regard to jurisdictional claims in published maps and institutional affiliations.

Submit your manuscript to a SpringerOpen[®] journal and benefit from:

- Convenient online submission
- Rigorous peer review
- Open access: articles freely available online
- High visibility within the field
- Retaining the copyright to your article

Submit your next manuscript at ► springeropen.com

RESEARCH

Open Access



A facile approach to fabrication and characterization of novel herbal microemulsion-based UV shielding cream

R. D. Bhalke¹, S. S. Kulkarni¹, P. N. Kendre², V. V. Pande³ and M. A. Giri^{2*}

Abstract

Background: Since many decades, phytoconstituents are well known for their potential therapeutic benefits but the development of herbal products has been limited due to difficulties like collection, isolation, stability and aqueous solubility of the phytoconstituents. The present study focuses on the development of microemulsion-based sunscreen cream formulation containing therapeutically active phytoconstituents like lycopene, β -carotene and curcumin which are reported for both antioxidant and ultraviolet radiation barrier properties. But the major hurdle in the development of the formulation is poor solubility and stability of these 3 components. Microemulsion preparation helps to enhance the solubility and stability of the final product. Screening of oils, surfactants and cosurfactants were done based on solubility studies followed by the construction of pseudo-ternary phase diagrams, sesame oil, span 80 to tween 80 (surfactant) and isopropyl alcohol (co-surfactant) which were selected to stable microemulsion.

Result: Based on a solubility study of components and pseudo-ternary phase diagrams, surfactant to co-surfactant (Smix) with 2:1 ratio and oil to Smix with 2:8 ratio were selected for preparation of the final microemulsion. Results show an average globule size of 208 nm, conductance 0.935 moh/cm, pH 7.1, zeta potential – 17.5 mV, refractive index 1.002, polydispersibility index 0.342, percent transmittance 90.68% and viscosity 82.45 cps. In a drug content study, the presence of lycopene, β -carotene and curcumin was found to be 87.53, 85.08 and 90.65%, respectively. Finally, microemulsion-based sunscreen cream was prepared and evaluated for various parameters like pH, extrudability, spreadability and drug content study. The sun protection factor (SPF) of microemulsion and cream was found to be 36.32 and 37.65, respectively. The stability study data shows better stability of the final formulation.

Conclusion: Formulation of microemulsion-based sunscreen cream may be a better option in the design and development of herbal phytoconstituents.

Keywords: Microemulsion, Surfactant, Lycopene, Curcumin, β -Carotene, Sunscreen cream

Background

Everyone is very conscious about their health, and nowadays, people are even very sensible about looks and external appearance. In short, the world is fond of cosmetics and skin protection against many harmful environmental effects which are on prime importance. One of the harmful factors is the ultra-violet rays coming

from the sun. This sunburn may darken the skin and severe consequences may lead to skin damage or cancer. Human exposure to harmful ultraviolet (UV) radiations has very dangerous side effects such as skin melanoma, photoaging, skin pigmentation, sunburn and various painful effects. Ultraviolet radiations increase oxidative stress on skin cells by frequent formation of reactive oxygen species (ROS) leading to initiation and promotion of cancer [1].

There are several products available in the market which are sold by many companies and claiming on the

* Correspondence: mahi_jaan83@yahoo.com

²Department of Pharmaceutics, Rajarshi Shahu College of Pharmacy, Sant Gadgebaba Amravati University, Buldhana, India
Full list of author information is available at the end of the article

basis of skin-protection-factor (SPF). These sunscreen products may be lotion, spray, gel and foam applied topically that absorbs or reflects the ultraviolet radiation. Sun protection factor (SPF) is the measure of the fraction of sunburn coming from the sun.

Ideally, these values of SPF represent the measure of time up to which the product protects the skin from harmful effects of ultraviolet (UV) radiation. Although these products are used widely, regulatory aspects are also taken into consideration during design and development.

The sunscreen preparations are designed and developed to apply topically to prevent the entry of ultraviolet rays directly in the skin by absorbing or reflecting from the skin. There are many synthetic components that are used as sun protection like p-aminobenzoic acid (PABA), phenyl benzimidazole sulfonic acid, cinoxate and oxybenzone and inorganic components like titanium dioxide and zinc oxide. Although innumerable numbers of sunscreen products are available in the market, they have several drawbacks. Some physical sunscreen agents make the preparation opaque and may result in whitish appearance of the skin treated topically with them [2–5].

Sunscreens containing synthetic chemicals may cause side effects, such as erythema, oedema and irritation. Herbal sunscreens are eco-friendly with less or no comedogenic effects. Incorporation of antioxidants could provide additional benefit by scavenging free radicals.

There are many phytoconstituents that have great potential to protect the harmful effects of UV radiation. Natural polyphenols and flavonoids are attractive in this respect, due to their potential activity as photoprotectants and antioxidants [6–10].

Tomatoes contain lycopene, which is the most powerful natural antioxidant. Lycopene has a property to improve the skin's ability to reflect back UV radiations and protect skin from its harmful effect, and β -carotene is the carotenoids present in carrot and emphasizes on the UV protective nature because of the antioxidant potential.

Active chemical constituents of turmeric are curcuminoids, which includes curcumin, desmethoxycurcumin and desmethoxycurcumin. There is some important volatile oil such as turmerone and allenton which help to protect skin from free radical damage; it reduces burning sensation of skin and inflammation, improves the texture of the skin and shows potent UV protective action.

These phytoconstituents include quercetin, lycopene, β -carotene, curcumin and other medicinal herbs like *Embilica officinalis*, *Nelumbo nucifera*, *Moringa oleifera* L, and *Terminalia chebula*. These components can be used to develop sunscreen formulations, but due to certain limitations like their solubility and stability issues, they are restricted [11–13].

The present study focuses on the development of microemulsion of phytoconstituents like lycopene, β -

carotene and curcumin. These microemulsion (average globule size of 10–200 μm) are a better option to overcome the issues of solubility and stability of such phytoconstituents. This prepared microemulsion formulation was added to the cream base to develop the final sunscreen formulation with excellent performance of sunburn protection effect.

Microemulsion is isotropic and thermodynamically stable multicomponent fluids composed of water, oil, surfactant and co-surfactant. This unique class of optically clear solutions comprises of the colloidal systems. Microemulsion has transparency, optical isotropy, low viscosity, monophasic, ultra-low interfacial tension, dynamic microstructure and thermodynamic stability. The droplet diameter of microemulsions is generally within the range of 10–200 nm [14].

Pharmaceutical microemulsions contain additional components such as co-surfactant and drugs. The co-surfactant is also amphiphilic with an affinity for both the oil and aqueous phases and partitions to an appreciable extent into the surfactant interfacial monolayer present in the oil-water interface. A wide variety of molecules can function as co-surfactant including non-ionic surfactant, alcohol, alkalotic acids, alkaloids and alkylamines [15–17].

The nanometric size of micelles improved solubilization capacity for lipophilic drug transparency that the property makes the system more suitable for transdermal and topical formulations. Even though microemulsions offer several advantages for topical delivery, it is difficult to stabilize the system because of low viscosity. This problem can be overcome by formulating a microemulsion-based cream [18]. Therefore, the present research work aims at the development of microemulsion containing lycopene, β -carotene and curcumin as an important phytoconstituent possessing both antioxidant and UV radiation protection properties with improved solubility and surface area and stabilization of same by formulating microemulsion-based cream.

Methods

Materials

Crude materials like *Curcuma longa*, *Dacus carota* and *Solanum lycopersicum* are procured from Mahatma Phule Krishi Vidyapeeth, Rahuri, Maharashtra, India. Other supporting materials, tween 80, isopropyl alcohol, sesame oil, glycerine, potassium hydroxide, petroleum jelly, ethanol, chloroform, methanol, dichloromethane and petroleum ether, were procured from Research Fine Chem Pvt. Ltd., Mumbai, India, and were analytical grade.

Methods

Extraction, isolation and pre-formulation study of phytoconstituents

The extraction and isolation of lycopene from *Solanum lycopersicum*, β -carotene from *Dacus carota* and

Table 1 Composition of LCCMBSC

Ingredients	Quantity (g)
Cetostyrl alcohol	0.30
Stearic acid	0.40
Petroleum jelly	0.10
Glycerine	0.40
Potassium hydroxide	0.10
Water	8.5
Methyl paraben	0.02
Polypropyl paraben	0.005
LCCM	1
Rose oil	Q.S

curcumin from *Curcuma longa* were carried out by cold maceration followed by preparative thin-layer chromatography (TLC) [19–21].

Melting point, UV-spectrophotometric analysis and FT-IR spectra have confirmed the identification of the above phytoconstituents.

Solubility study

For the preparation of microemulsion, it is most important to check the solubility of the phytoconstituents in either oil, water or surfactant system. Hence, a solubility study was conducted to select suitable components of the microemulsion system. Initially, various oils (sesame oil, olive oil, coconut oil, castor oil, arachis oil), surfactants (span 80, tween 80, polaxamer 407, IPM) and co-surfactants (isopropyl alcohol, n-butanol, polyethylene glycol-400, amyl alcohol, n-propyl alcohol) were procured and solubility of lycopene, β -carotene and curcumin was checked using the shaking flask method in which excess amount of phytoconstituents was added separately to the oils and surfactants. These mixtures were shaken at 37 °C for 48 h to solubilize the components, and after 48 h, samples were investigated for the amount of phytoconstituents using UV spectrophotometer at 440, 460 and 418 nm, respectively [22–24].

Construction of a pseudo-ternary phase diagram

Based on the solubility study, suitable oils, surfactants and co-surfactants were selected for the preparation of the microemulsion system. For the preparation of a stable microemulsion system, initial batches were prepared with the help of a pseudo-ternary phase diagram. Water titration method was implemented, in which double distilled water was added drop-wise using micro-pipette to previously mix Smix and oils with different ratios (Smix:oils) as 1:1, 2:1, 3:1 and 4:1. Water was added with continuous stirring till turbidity will appear and the amount of added water was noted. Various batches containing Smix:oils at the ratios of 1:1 to 1:9 and 9:1 to 9:8.

Finally, a pseudo-ternary phase diagram was constructed with the help of concentration levels of water, oil and Smix to optimize and finalized the stable microemulsion system. Three-component ternary diagrams with each axis representing an oil phase, Smix and water with fix mass ratio were plotted using CHEMIX school software [14, 25, 26].

Selection of a stable microemulsion system

Finally, stable microemulsion systems were selected based on the maximum microemulsion boundary areas detected in the pseudo-ternary phase diagrams and after evaluation of other physical parameters. After the identification of the microemulsion region in the phase diagram, the microemulsion formulations were selected at desired component ratios. Once this blank microemulsion was prepared, the microemulsion containing phytoconstituents was prepared by mixing them (each 1% w/w) into the surfactant or oils in which they were soluble at a higher amount (based on the results of the solubility study). Finally, a clear and stable microemulsion system (W/O type) was obtained using the appropriate amounts of all the components detected in the pseudo-ternary phase diagrams. The microemulsion system containing phytoconstituents was characterized for various physico-chemical properties like globule size analysis, zeta-potential, viscosity, drug content, pH, transmittance and stability study.

Measurement of globule size and zeta potential

The average globule size and zeta potential of phytoconstituents containing microemulsion was evaluated using Malvern Zetasizer (Nano ZS, 90, UK). A small amount of microemulsion sample (0.1 ml) was diluted to 10 ml of doubled distilled water. This diluted sample was tested for globule size and zeta potential using Malvern Zetasizer. Samples were analysed for globule size and zeta potential in triplicate for better accuracy.

Viscosity determination

Viscosity of the microemulsion formulation and sunscreen formulation was measured by using the Brookfield Viscometer (LVDV-II+pro). Appropriate spindles were chosen to measure the viscosity of both the microemulsion and sunscreen cream. All the operating conditions of rpm and torque were set and samples were kept ready to determine the viscosities. Finally, the viscosities were calculated by the following Eq. (1) [27].

$$\text{Viscosity} = \text{Dial reading} \times \text{Factor. For LV at 6 rpm factor is 1M (1000)} \quad (1)$$

Drug content study

Accurately weighed (5 ml) microemulsion containing 1% w/w of lycopene, β -carotene and curcumin was taken in

25 ml capacity volumetric flask and 10 ml ethanol was added to it. The resultant mixture was stirred for 30 min and finally filtered through Whatman filter paper. These filtrates (1 ml) were diluted with 10 ml ethanol and analysed for content study using UV-visible spectrophotometer at 440, 460 and 418 nm for the determination of lycopene, β-carotene and curcumin respectively [18].

Determination of pH and percent transmittance

The prepared microemulsion system was checked for measurement of pH values using digital pH meter (Lab India). Standard buffer systems of pH 4 and 7 were used to determine the pH of microemulsion. Percent transmittance was measured by diluting the microemulsion 100 times and analysed on UV-visible spectrophotometer against distilled water as blank at 640.2 nm.

Stability study

Microemulsion system was tested for physical stability by centrifuging the small amount of sample at 1250 rpm for 5 h and examined for phase separation and other changes, if any. Further, these microemulsion systems were checked for stability issues at various temperature and humidity conditions for 3 months. The microemulsion was subjected to stability study at 4 ± 2 °C, 30 ± 2 °C and 75 ± 5% relative humidity (RH) and 40 °C ± 2.C/ 75 ± 5% (RH) according to ICH guidelines and evaluated for physical and chemical stability [28].

Preparation of sunscreen formulation

Sunscreen cream is o/w emulsion containing aqueous phase as continuous phase and oil phase as dispersed phase. Water phase is prepared by adding a reported

amount of distilled water. Accurately weighed all water-soluble components such as glycerine, potassium hydroxide and methyl paraben were dissolved in aqueous phase and resultant mixture allowed to heat up to 80 °C. Oil phase was prepared by mixing ceto-stearyl alcohol, stearic acid, propyl paraben and petroleum jelly together with the mentioned amount of MLCC and heated up to 80 °C. Oil phase was added to aqueous phase at 80 °C with slow and constant stirring for 20 min. As a result, homogenized and uniform emulsion-based cream was formed. The accurately weighed microemulsion was added slowly to the above sunscreen base and incorporated uniformly in mortar and pestle [16] (Table 1).

Determination of sun protection factor (SPF)

The sun protection factor of microemulsion and microemulsion-containing sunscreen cream was determined using the UV-spectrophotometric method. In this method, 1 g of sample was weighed accurately and ethanol was added to make 10 ml of the final volume. The resultant mixture was analysed for absorbance at 290–320 nm and SPF was calculated using following Eq. (2) [29, 30]

$$\begin{aligned}
 \text{SPF spectrophotometric} &= CF \times \text{SPF spectrophotometric} \\
 &= CF \times \\
 &= \sum_{290}^{320} EE(\lambda) Abs(\lambda) \quad (2)
 \end{aligned}$$

where
 CF = Correction factor (10)
 EE = Erythrogenic effect of radiation with wavelength (λ)

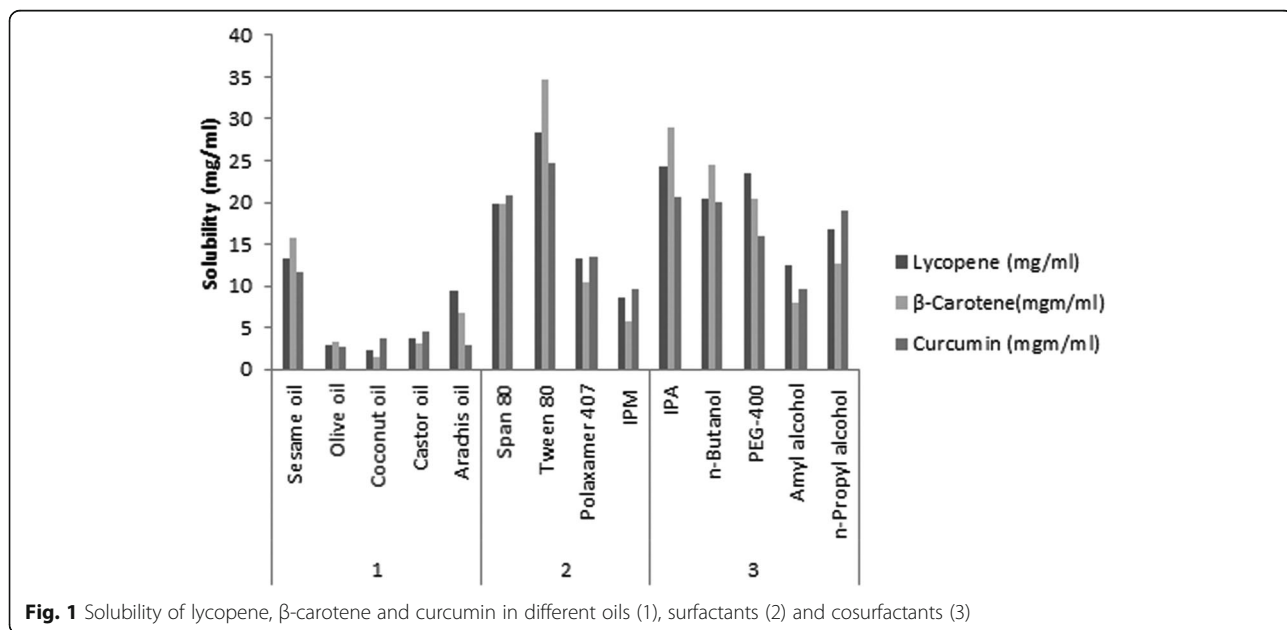


Fig. 1 Solubility of lycopene, β-carotene and curcumin in different oils (1), surfactants (2) and cosurfactants (3)

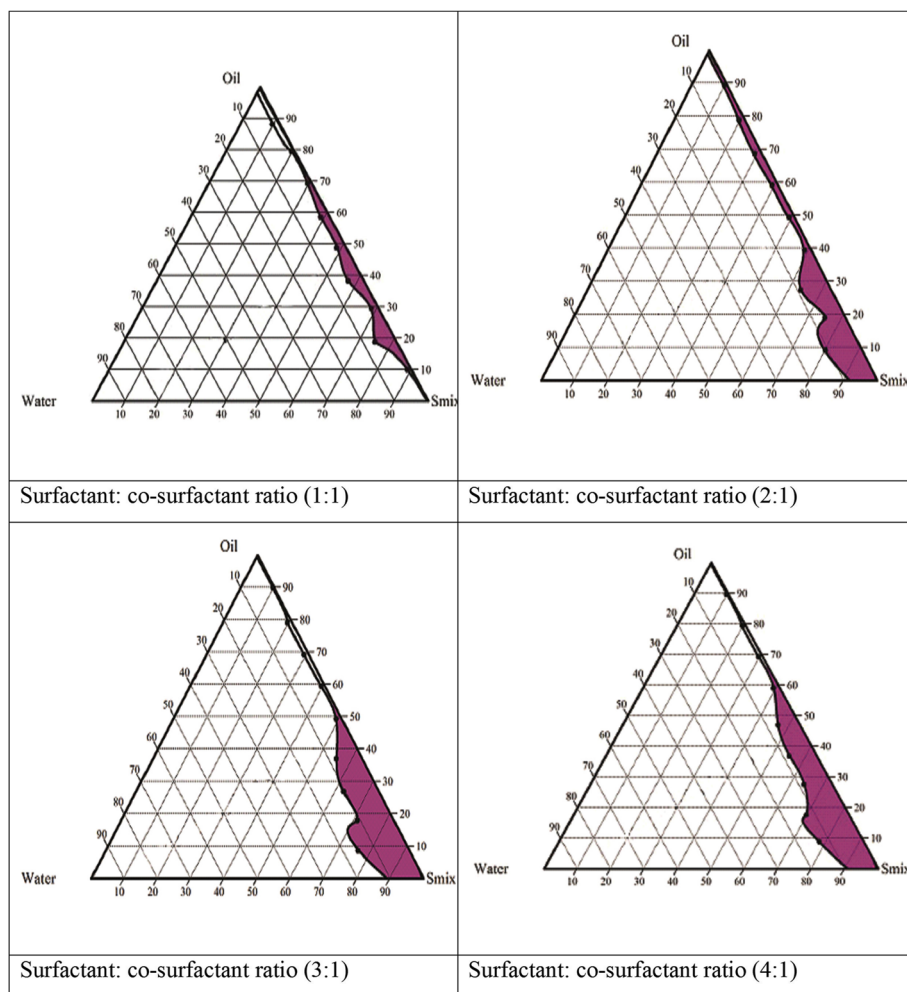


Fig. 2 The pseudo ternary phase diagrams of the oil-surfactant-water system at 1:1, 2:1, 3:1, and 4:1 weight ratio

Abs (λ) = Spectrophotometric absorbance values at wavelength

The value of $EE \times I$ is constant.

Evaluation of sunscreen formulation

The microemulsion-containing sunscreen cream formulation was evaluated for pH, tube extrudability, spreadability, viscosity, drug content and in vitro study using various tools and methods.

Texture characterization and spreadability testing

The prepared sunscreen formulation containing microemulsion was characterized for spreadability using CT-3 texture analyser. A cylindrical analytical probe (12 mm diameter) was inserted within the sample at a specific rate (2 mm/s) and at a definite depth (10 mm) at 25 °C. Readings were taken in triplicate for better accuracy.

Table 2 Various evaluation parameters of an optimized microemulsion system

Observations	Results
Average particle (globule) size	208 nm
Polydispersibility index (PDI)	0.342
Zeta potential	- 17.5 mV
Transmittance	90.68%
Refractive index	1.002 ± 0.03
pH	7.01 ± 0.07
Viscosity	82.45 ± 0.07 cps
Drug content (%)	
(a) Lycopene	87.53%
(b) β-carotene	85.08%
(c) Curcumin	90.65%
SPF	36.32
Conductance	0.935 moh/cm

Table 3 Various evaluation parameters of microemulsion-containing sunscreen cream

Observations	Results
Spreadability	17 ± 5 g cm/s
Extrudability	96.58 ± 0.9%
pH	7.1 ± 0.3
Sun protection factor (SPF)	37.65
Refractive index	1.002 ± 0.03
Viscosity	22,341 ± 3 cps
Drug content (%)	
(a) Lycopene	84.33%
(b) β-carotene	83.88%
(c) Curcumin	88.86%

Extrudability study

This study was conducted to find out the extrudability of sunscreen cream formulation when packaged in the tube container. The sunscreen formulation was filled in the standard collapsible tube, sealed properly using crimping machine and cap was fitted. The filled weight of tube was recorded. The tube was clamped between two glass slides and 500 g weight was placed over the glass slides and then cap was removed slowly. The amount of cream extruded was collected and weighed and compared with the initial filled weight of the tube. Finally, the percentage of cream was calculated and graded.

Skin irritation test

The prepared sunscreen formulation containing microemulsion was tested for the skin irritation. Protocols of the study were approved by Institutional Animal Ethical Committee, and with kind permission of the CPCSEA committee, the work was started using three healthy male rabbits. They were kept carefully following the acclimation period of 7 days to ensure their suitability for study. After an acclimation period, the area on the back of each rabbit was shaved carefully before the experiment. The skin surface of the rabbit on its back was divided into three marked areas; at one patch, there was no formulation and on the other two patches, microemulsion and sunscreen cream formulation was applied (0.5 g of each test formulation was applied on each 3 × 3 cm area). The study was carried out for 48 h, and for every 24 h, the animal was observed for irritancy,

erythema, inflammation and oedema. The score of primary irritation was calculated for each rabbit.

Results

In the initial study, extraction of plant material was carried out and isolation of lycopene, β-carotene and curcumin was obtained from *Solanum lycopersicum*, *Dacus carota* and *Curcuma longa*, respectively, using cold maceration followed by preparative thin-layer chromatography (TLC). Isolated phytoconstituents were tested for identification and quality. Melting point of 184 °C, 171 °C and 181 °C were detected for lycopene, β-carotene and curcumin, respectively, determined by digital melting point apparatus (Veego, model MVP). The melting point was found to be in range and identical to the reported standard melting points. UV-visible spectra and FT-IR spectra confirmed the isolated phytoconstituents based on the various functional groups detected. Maximum absorption spectra (λ_{max}) of lycopene, β-carotene and curcumin were detected at 418, 444 and 460 nm, respectively, after being scanned in UV-visible spectrophotometer in a range from 200 to 800 nm.

Results of globule size analysis showed the average globule size 208 nm (Fig. 1) and conductance of 0.935 moh/cm. The lower value of conductance confirmed the W/O type of emulsion. The microemulsion was tested for pH and average value of 7.1 ± 0.07 was observed. The refractive index is 1.002 ± 0.03. Polydispersibility index (PDI) represents the uniform distribution of globules/particles (> 0.3); the present optimized microemulsion formulation shows an average PDI of 0.342 which has confirmed the uniform distribution of the droplets in the formulation. For better distribution of particles, the zeta potential values of less than - 30.0 mV are generally not considered due to less repulsive forces which may lead to the formation of agglomerates. An average zeta potential value for optimized microemulsion was found to be - 17.5 mV (Fig. 2) which represents the sign of good dispersibility of microemulsion droplets in the continuous phase and less chances of agglomeration with better stability.

In another study of transmittance, the presence micron-sized globules with uniform distribution was observed when the microemulsion was diluted 100 times and showed 90.68% transmittance with clear appearance whereas without diluted microemulsion has shown

Table 4 Skin irritation study data

Test material ^a	Skin reaction ^b	Mean irritation score		
		12 h	24 h	48 h
Sunscreen cream containing microemulsion	Erythema	0	0	0.2
	Oedema	0	0	0

^aTest material was applied on rabbit skin

^bErythema and oedema; the mean irritation score was the summation of each irritation score divided by the number of animals

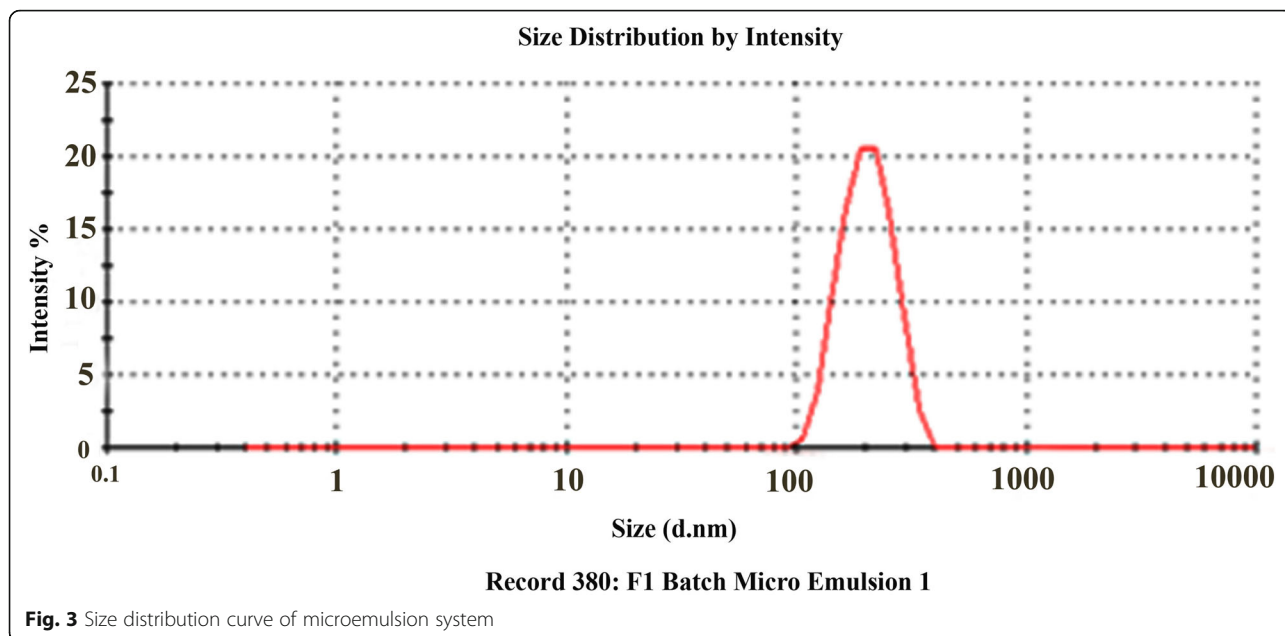


Fig. 3 Size distribution curve of microemulsion system

85.98% transmittance. Further, the sunscreen cream formulation was also evaluated for viscosity, tube extrudability and spreadability. The viscosity of microemulsion was found to be 82.45 ± 0.07 cps, whereas the total content of lycopene, β -carotene and curcumin was found to be 87.53, 85.08 and 90.65%, respectively. The sun protection factor of microemulsion was calculated using Eq. (1) described in the “Methods” section, and it was found to be 36.32. All the results of globule size, PDI, conductance, transmittance, refractive index, pH, viscosity, drug content and sun protection factor (SPF) are presented in Table 2.

The extrudability of the prepared sunscreen cream formulation after packaged into standard tube was found to be $96.58 \pm 0.9\%$.

The viscosity of sunscreen cream at 25 °C was found to be $22,341 \pm 3$ cps which was much higher than the microemulsion preparation. The pH of test sunscreen cream was found to be 7.1 ± 0.3 whereas the percent drug content of lycopene, β -carotene and curcumin was found to be 84.33, 83.88 and 88.86%, respectively (Table 3).

The sun protection factor calculated for the microemulsion-containing sunscreen formulation was found to be 37.65.

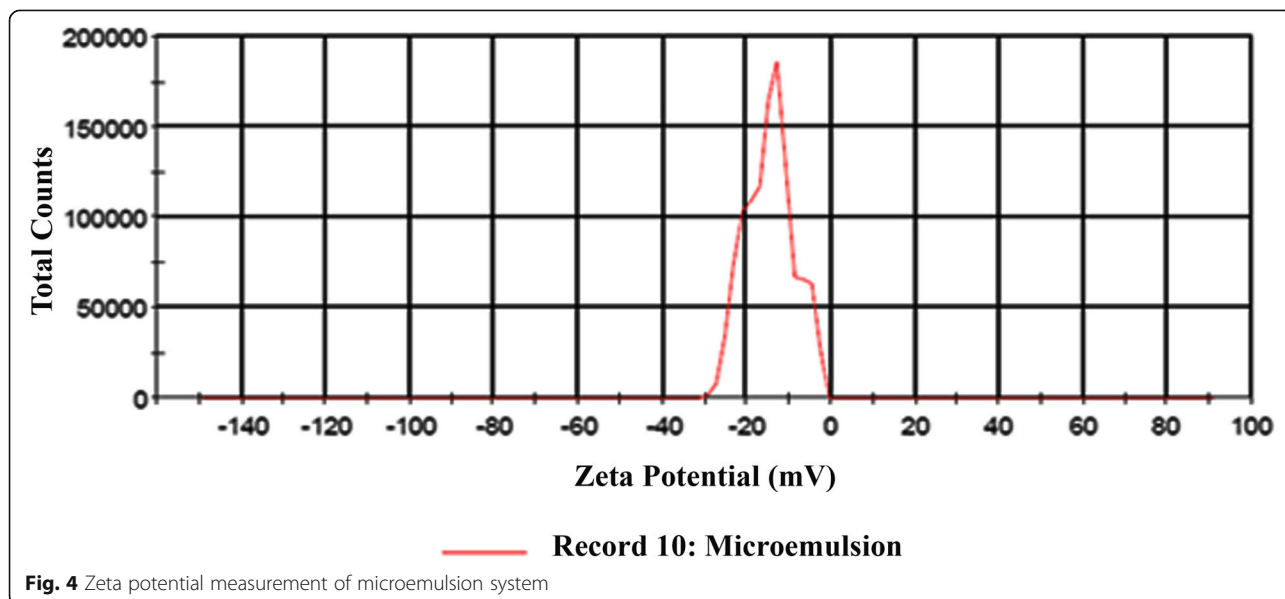
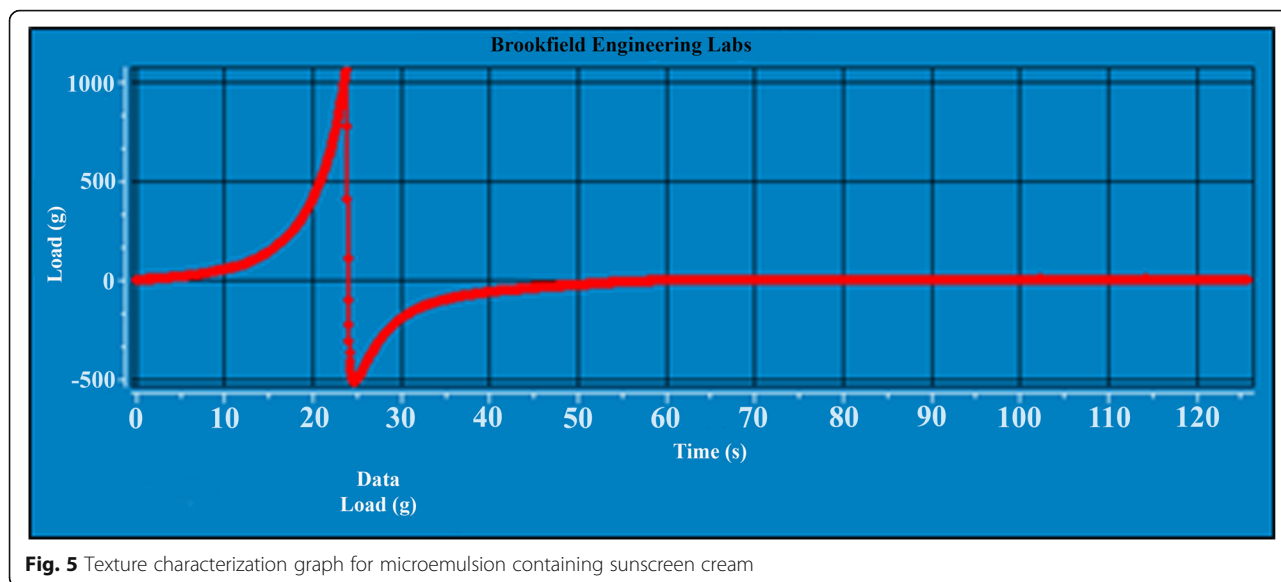


Fig. 4 Zeta potential measurement of microemulsion system

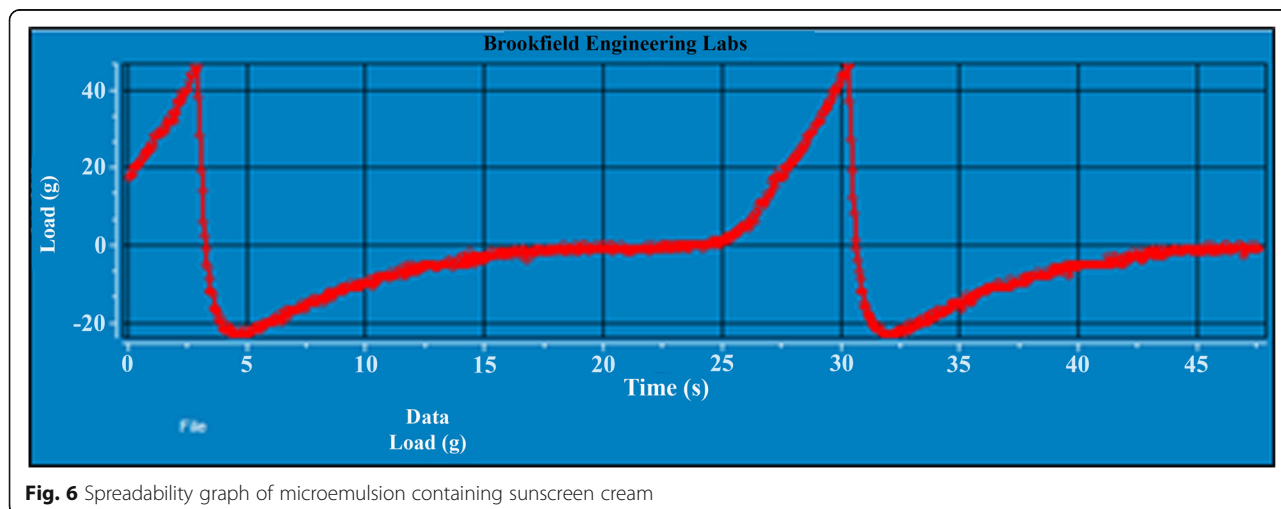


Skin irritancy test was performed to check the irritation of topically applied microemulsion as well as sunscreen cream formulation. The PII (Primary Irritation Index) when no formulation was applied was found to be 0.166; for microemulsion, it was 0.277; and for sunscreen cream, it was found to be 0.222 (Table 4).

Discussion

In the solubility study of lycopene, β -carotene and curcumin, it has been observed that the maximum solubility of these phytoconstituents was found to be in sesame oil, span 80 to tween 80 (1:1) and isopropyl alcohol. Based on these results of this solubility study, sesame oil, span 80 to tween 80 (1:1) and isopropyl alcohol were selected for the preparation of microemulsion. Results of the solubility study are presented in Fig. 3.

From results of the pseudo-ternary phase diagrams, 2:1 ratio of surfactant to co-surfactant and oil to Smix (2:8) was found to be the best for the development of microemulsion since the maximum microemulsion boundary area was observed as shown in Fig. 4. The maximum microemulsion boundary area represents the formation of microemulsion with micron-sized globules at the interface of oil, water and Smix. This area represents clear, transparent and stable microemulsion with no phase separation up to 72 h when kept on standing in the sealed glass container. Finally, these ratios of components were considered to make an optimized microemulsion system, and microemulsion-containing phytoconstituents were formulated successfully. This optimized microemulsion was characterized for various physiochemical parameters for the confirmation of quality.



The spreadability of the prepared sunscreen formulation was studied on the CT-3 texture analyser. The area under positive curve is a measure of energy required to deform the sample to a defined depth grade in order of its stability. Higher peak load and work done indicate lower spreadability. Lower peak load value coupled with a lower work done value indicates that the sample is more spreadable. In the case of sunscreen cream formulation, the texture analysis data represents the spreadability of cream (17 ± 5 g cm/s) as shown in Figs. 5 and 6. The negative peak indicates the work done by the probe which was lower than the positive curve which proves that the test formulation possesses good spreadability.

From the above data, it is concluded that the PII (Primary Irritation Index) of both microemulsion and sunscreen cream in the range of 0.0–0.4 and indicating irritancy was negligible.

Conclusion

Prevention from harmful effects of ultraviolet radiation of the sun is on prime importance to everyone by considering cosmeceutical intension and personal external appearance of the individuals. The use of many available synthetic components such as sun protection may be harmful due to various serious issues as discussed in this manuscript. Considering many beneficial effects of phytoconstituents like antioxidant activity and excellent sun protection effect, the present study has focused on the development of microemulsion-based sunscreen cream formulation with excellent SPF values. From the findings of the present research, it has been concluded that stable microemulsion system containing lycopene, β -carotene and curcumin as an important phytoconstituents possessing both antioxidant and ultraviolet radiation protection properties can be formulated successfully as a sunscreen cream formulation.

Abbreviations

UV: Ultraviolet; ROS: Reactive oxygen species; MPKV: Mahatma Phule Krushi Vidyapith; TLC: Thin-layer chromatography; IR: Infrared; IPM: Isopropyl myristate; IPA: Isopropyl alcohol; PEG: Polyethylene glycol; SPF: Sun protecting factor; CF: Correction factor; RH: Relative humidity; ICH: International Conference on Harmonisation

Acknowledgements

The authors are thankful to the Institute of Sanjivani College of Pharmaceutical Education and Research, Kopargaon, for providing the necessary facilities to carry out our research work in the current format. The authors are very thankful to the Principal and all the supporting members of the institution for providing all the facilities to conduct this research study. The authors are also grateful to the Institutional Animal Ethical Committee (IAEC) for approving the protocol and permission for the animal study. Finally, the authors are thankful to everyone for providing direct or indirect support to conduct this study.

Authors' contributions

RDB has given her contribution for constructing the idea for the manuscript. SSK has given her contribution for collecting the data and material for this

work. PNK has given his contribution for taking responsibility in the construction of the entire part of the manuscript. VVP has given his contribution for making planning as well as organizing and supervising of the course of the article and taking responsibility. MAG has given contribution for guiding the entire team as well as taking effort before submission of the article. All authors have read and approved the final manuscript.

Funding

The research work is of routing major dissertation work of the students, and it is carried through college funding.

Availability of data and materials

All data and materials are available upon request

Ethics approval and consent to participate

Institutional Animal Ethics Committee for Animal Experiments of Sanjivani College of Pharmaceutical Education and Research, Kopargaon, approved the study under the protocol SCPER/CPCSEA/IAEC/2016-17/04 and all experiments were conducted in accordance with guidelines of Committee for the Purpose of Control and Supervision of Experiments on Animals (CPCSEA).

Consent for publication

Not applicable.

Competing interests

The authors declare that they have no competing interests

Author details

¹Department of Pharmacognosy, Sanjivani College of Pharmaceutical Education and Research, Pune University, Kopargaon, India. ²Department of Pharmaceutics, Rajarshi Shahu College of Pharmacy, Sant Gadgebaba Amravati University, Buldhana, India. ³Department of Pharmaceutics, N. N. Saththa College of Pharmacy, BAT University, Ahmednagar, India.

Received: 5 May 2020 Accepted: 12 August 2020

Published online: 05 November 2020

References

1. Valachovic E, Zurbenko I (2014) Skin cancer, irradiation, and sunspots: The solar cycle effect. *Biomed Res Int* 11:734–748. <https://doi.org/10.1155/2014/538574>
2. Rancan F, Rosan S, Boehm K, Fernández E, Hidalgo ME, Quihot W et al (2002) Protection against UVB irradiation by natural filters extracted from lichens. *J Photochem Photobiol B Biol* 68(2–3):133–139
3. Kohlhardt-Floehr C, Boehm F, Troppens S, Lademann J, Truscott TG (2010) Prooxidant and antioxidant behaviour of usnic acid from lichens under UVB-light irradiation - Studies on human cells. *J Photochem Photobiol B Biol* 101(1):97–102
4. Millot M, Di Meo F, Tomasi S, Boustie J, Trouillas P (2012) Photoprotective capacities of lichen metabolites: a joint theoretical and experimental study. *J Photochem Photobiol B Biol* 111:17–26
5. Lohezic-Le Devehat F, Legouin B, Couteau C, Boustie J, Coiffard L (2013) Lichenic extracts and metabolites as UV filters. *J Photochem Photobiol B Biol* 120:17–28
6. Boehm F, Clarke K, Edge R, Fernandez E, Navaratnam S, Quihot W et al (2009) Lichens - Photophysical studies of potential new sunscreens. *J Photochem Photobiol B Biol* 95(1):40–45
7. Rojas JL, Diaz-Santos M, Valencia-Islas NA (2015) Metabolites with antioxidant and photo-protective properties from *Usnea roccellina* Motyka, a lichen from Colombian Andes. *UK J Pharm Biosci* 3(4):18
8. Baker LA, Marchetti B, Karsili TNV, Stavros VG, Ashfold MNR (2017) Photoprotection: extending lessons learned from studying natural sunscreens to the design of artificial sunscreen constituents. *Chemical Society Reviews*. Royal Society of Chemistry 46:3770–3791
9. Radice M, Manfredini S, Ziosi P, Dissette V, Buso P, Fallacara A et al (2016) Herbal extracts, lichens and biomolecules as natural photo-protection alternatives to synthetic UV filters. A systematic review. *FitoTerapia* 114:144–162

10. Cefali LC, Ataide JA, Moriel P, Foglio MA, Mazzola PG (2016) Plant-based active photoprotectants for sunscreens. *Int J Cosmet Sci* 38(4):346–353
11. Saraf S, Kaur C (2010) Phytoconstituents as photoprotective novel cosmetic formulations. *Pharmacognosy Reviews* 4:1–11
12. Offord EA, Gautier JC, Avanti O, Scaletta C, Runge F, Krämer K et al (2002) Photoprotective potential of lycopene, β -carotene, vitamin E, vitamin C and carnosic acid in UVA-irradiated human skin fibroblasts. *Free Radic Biol Med* 32(12):1293–1303
13. Köpcke W, Krutmann J (2008) Protection from sunburn with β -carotene—a meta-analysis. *Photochem Photobiol* 84(2):284 <http://doi.wiley.com/10.1111/j.1751-1097.2007.00253.x>
14. Kawakami K, Yoshikawa T, Hayashi T, Nishihara Y, Masuda K (2002) Microemulsion formulation for enhanced absorption of poorly soluble drugs. II. In vivo study. *J Control Release* 81(1–2):75–82
15. Kogan A, Garti N (2006) Microemulsions as transdermal drug delivery vehicles. Vols. 123–126. *Advances in Colloid and Interface Science* 123–126: 369–385
16. Boonme P (2007) Applications of microemulsions in cosmetics [Internet]. Vol. 6, *Journal of Cosmetic Dermatology*. *J Cosmet Dermatol* 6:223–228
17. Lawrence MJ, Rees GD (2000) Microemulsion-based media as novel drug delivery systems. *Adv Drug Deliv Rev* 45(1):89–121
18. Sabale V, Vora S (2012) Formulation and evaluation of microemulsion-based hydrogel for topical delivery. *Int J Pharm Investig* 2(3):140
19. Kulkarni S, Bhalke R, Pande V, Kendre P, Kulkarni SS (2014) *Indo American Journal of Pharmaceutical Research*. Herbal plants in photo protection and sun screening action: an overview. *Indo Am. J Pharm Res* 4(02):1104–1113
20. Fikselová M, Šilhár S, Mareček J, Frančáková H (2008) Extraction of carrot (*Daucus carota* L.) carotenes under different conditions. *Czech J Food Sci* 26(4):268–274
21. Revathy S, Elumalai S, Benny M, Antony B (2011) Isolation, purification and identification of curcuminoids from turmeric (*Curcuma longa* L.) by column chromatography. *J Exp Sci* 2(7):21–25
22. Kendre PN, Chaudhari PD (2017) Effect of polyvinyl caprolactam–polyvinyl acetate–polyethylene glycol graft copolymer on bioadhesion and release rate property of eplerenone pellets. *Drug Dev Ind Pharm* 43(5):751–761
23. Karathanos VT, Mourtzinou I, Yannakopoulou K, Andrikopoulos NK (2007) Study of the solubility, antioxidant activity and structure of inclusion complex of vanillin with β -cyclodextrin. *Food Chem* 101(2):652–658
24. Kendre PN, Chaudhari PD (2018) Effect of amphiphilic graft co-polymer-carrier on physical stability of bosentan nanocomposite: assessment of solubility, dissolution and bioavailability. *Eur J Pharm Biopharm* 126:177–186
25. Chandra A, Sharma K, Irchhiya R (2009) Microemulsion-based hydrogel formulation for transdermal delivery of dexamethasone. *Asian J Pharm* 3(1):30–36
26. Hussain A, Luckham PF, Tadros TF (1997) Phase behaviour of PH dependent microemulsions at high temperatures and high salinities. *Rev l'Institute Fr du Pet* 52(2):228–231
27. Smaoui S, Ben Hlima H, Ben Chobba I, Kadri A (2017) Development and stability studies of sunscreen cream formulations containing three photoprotective filters. *Arab J Chem*:S1216–S1222. <https://doi.org/10.1016/j.arabjc.2013.02>
28. Derle DV, Sagar BSH, Pimpale R (2006) Microemulsion as a vehicle for transdermal permeation of nimesulide. *Indian J Pharm Sci* 68(5):622–625
29. Nesseem D (2011) Formulation of sunscreens with enhancement sun protection factor response based on solid lipid nanoparticles. *Int J Cosmet Sci* 33(1):70–79
30. Dutra EA, Da Costa E, Oliveira DAG, Kedor-Hackmann ERM, Miritello Santoro MIR (2004) Determination of sun protection factor (SPF) of sunscreens by ultraviolet spectrophotometry. *Rev Bras Ciencias Farm J Pharm Sci* 40(3): 381–385

Publisher's Note

Springer Nature remains neutral with regard to jurisdictional claims in published maps and institutional affiliations.

Submit your manuscript to a SpringerOpen[®] journal and benefit from:

- Convenient online submission
- Rigorous peer review
- Open access: articles freely available online
- High visibility within the field
- Retaining the copyright to your article

Submit your next manuscript at ► springeropen.com

Evaluation of the diuretic activity of ethanolic and aqueous extracts of *Tabernaemontana divaricata* in rats

Short Title: Diuretic potential of *Tabernaemontana divaricata* plant extracts

Chanchal Raj^{1*}, Shailesh Kewatkar², A. Balasubramaniam³, Ashish Jain¹, Prakash Turiya⁴,
Sandeep Dhull⁵, Nadeem Sayyed⁵

¹ Department of Pharmacognosy, Shri D. D. Vispute College of Pharmacy and Research Center,
New Panvel, Navi Mumbai, Maharashtra, India

² Departments of Pharmacognosy, Rajarshi Shahu College of Pharmacy, Buldana, Maharashtra,

India

³ Dean, School of Pharmacy, ITM University, Gwalior, Madhya Pradesh, India

⁴ Consultant Medical Writer, Indore, Madhya Pradesh, India

⁵ Department of Clinical Research, Meril Life Sciences Pvt. Ltd, Vapi, Gujarat, India

***Corresponding Author**

Chanchal Navin Raj

Shri D. D. Vispute College of Pharmacy and Research Center,

New Panvel, Navi Mumbai 410206,

Maharashtra, India

Email- pharma_chanchal@rediffmail.com

Mob-+91 9826668034

Conflicts of interest: There are no conflicts of interest

Abstract

Tabernaemontana divaricata an evergreen plant belonging to the family Apocynaceae exhibited its application in the ailment called strangury as per traditional literature. Thus, considering the above facts, the objective of the present study was decided to contribute something new via evaluating the diuretic potential of this plant by administering ethanolic and aqueous extracts to healthy rats. Male Wistar rats were administered with different doses of the ethanolic extract (TDEE), and aqueous extracts (TDAE) of *T. divaricata* leaves each at 100, 200 and 400 mg/kg p.o. in normal saline solution (25 ml/kg p.o.), also a normal saline solution (25 ml/kg oral administration) used as control and Furosemide 10 mg/kg p.o. Administration of TDEE at 100, 200 and 400 mg/kg resulted in a significant increase in urine volume and electrolyte excretion, although less than that found with furosemide. TDAE at a test dose level of 100, 200 mg/kg was found to be insignificant when compared to the standard drug. Instead, at 400 mg/kg, TDAE showed enhanced electrolyte excretion. TDEE at test doses are more effective in increasing electrolyte excretion than TDAE in a dose-dependent manner. The results of the study confirmed and supported the traditional use of *T. divaricata* as diuretics.

Keywords: Diuretics, Electrolytes excretion, Furosemide, Strangury, *Tabernaemontana divaricata*

Introduction

Diuretics are the agents that potentiate the urine excretion from the body. The use of diuretics becomes mandatory for specific diseases or disorders, where it becomes important to maintain the water and electrolytes balance in the body [1]. Failing which may lead to severe manifestations causing life-threatening problems. Congestive heart failure (CHF), situations of fluid overload like acute and chronic renal failure, nephritis, cirrhosis, hypertension, and pregnancy-induced toxemia [2-3] are some of the disorders where diuretics proved to be life-saving therapy.

Among the various disorders, hypertension is much of concern as it has implicated in the main etiology for cardiac and renal failure, ischemic heart disease and cerebrovascular disease. The worldwide premature death caused by hypertension has reckoned at 7.1 million, and the burden of disease at 4.5% (WHO, 2003). Many diuretic drugs in practice are Furosemide, thiazides, Acetazolamide, Mannitol, and Ethacrynic acid [4].

Diuretics give relief from pulmonary congestion and peripheral edema. This in turn, decreases the cardiac workload, plasma volume, and oxygen demand, which eventually lower blood pressure [5]. Diuretics with different sites of action and mechanisms of action are prescribed based on the type of therapy needed in various disorders. Carbonic anhydrase inhibitors e.g., Acetazolamide. Osmotic diuretics e.g., Mannitol and Urea. Mannitol and other osmotic diuretics restrict the tubular reabsorption of water and electrolytes. Loop diuretics, high-ceiling diuretics, or Inhibitors of $\text{Na}^+\text{-K}^+\text{-2Cl}^-$ symport, e.g., Furosemide, Bumetanide, Ethacrynic acid, Torsemide.

Loop diuretics inhibit the activity of the $\text{Na}^+\text{-K}^+\text{-2Cl}^-$ symport in the thick ascending limb of Henle's loop. Inhibitors of $\text{Na}^+\text{-K}^+\text{-2Cl}^-$ symport in the thick ascending limb are immensely efficient due to an amalgamation of two factors: first, near about 25% of the filtered Na^+ load is generally reabsorbed by the thick ascending limb, and second lack of reabsorption capacity of nephron segments past the thick ascending limb. Thiazide diuretics and related agents or Inhibitors of Na^+Cl^- symport e.g., Chlorothiazide, Hydrochlorothiazide, Chlorthalidone, Indapamide, and Metolazone. Thiazide and thiazide related diuretics generally act as an inhibitor of Na^+Cl^- cotransporter protein. This action curbs on the reabsorption of Na^+ and Cl^- ions into the distal convoluted tubule, making the tubular fluid hyperosmotic, resulting in diuresis. Potassium-sparing diuretics: these comprise of inhibitors of renal epithelial Na^+ channels e.g., Amiloride and Triamterene. Amiloride and Triamterene block the Na^+ channels and stop $\text{Na}^+\text{-K}^+$ exchange. Antagonists of mineralocorticoid receptors, i.e., aldosterone antagonists, e.g., Spironolactone. It combines with the aldosterone-receptor in the collecting duct and thus prevents the binding of aldosterone with its receptors, thus preventing Na^+ reabsorption and K^+ secretion in the collecting duct.

Carbonic anhydrase inhibitors, a loop diuretic, and thiazide diuretics increase the delivery of Na^+ to the late distal tubule and collecting duct, a situation that often is associated with increased K^+ and H^+ excretion. Thus, there is a natriuresis, diuresis, and potassium accumulation [6-8]. Drug-induced diuresis is favorable for the treatment of many disorders, as mentioned above. However, in current clinical practice, many of the diuretics have been associated with many adverse effects, metabolic alterations, including electrolyte imbalance, activation of the renin-angiotensin and neuroendocrine systems, impairment of sexual function, onset of diabetes, etc. [3, 9]. Hence, it is important to consider alternatives that have greater effectiveness and fewer

side effects. Furthermore, many of the herbs used in folk medicine have yet to be scientifically evaluated for their efficacy and safety [10]. Scores of investigators demonstrated that studies of herbs used in traditional medicine as diuretics were in progressive elevation in the last two decades [11] and might be a promising way for human pathology treatment. Naturally occurring diuretics in coffee and tea like theobromine, caffeine, and theophylline may validate the traditional use of the plant as a diuretic [12]. Some plants show diuretic effects comparable to the loop diuretics e.g., Furosemide [13]. The Indian Ayurvedic system of medicine is rich in treating renal problems. *Abelmoschus esculentus* (Bhindaka), *Bacopa monnieri* (Brahmi), *Barbarea vulgaris* (Cress), *Boerhavia diffusa* (Punarnava), *Emblica officinalis* (Amla) etc. are some of the examples [14].

Chahndani, *Tabernaemontana divaricata* (TD, Family: Apocynaceae) in traditional medicine is used to treat various diseases like ulceration, epilepsy, abdominal tumors, eye infections, inflammation, mania, oedema, leprosy, diarrhea. It has also been used as anthelmintic, aphrodisiac, antihypertensive, emmenagogue, purgative, remedy against poisons and tonic to the brain, liver, and spleen vermicide, odontalgia, biliousness, paralysis, arthralgia, and melalgia and blood disorders. TD also exhibited its application in the ailment called strangury, i.e., painful discharge of urine as per traditional literature [15].

In the present study, we tested the diuretic activity of TD by evaluating the total urine volume and urinary electrolyte excretion against Furosemide (10 mg/kg, p.o.) in rats.

Materials and methods

Plant material

The leaves of TD were collected in January 2010 from the Bhopal, Madhya Pradesh, India. The plant was authenticated and identified by Dr. D. V. Amla, Deputy Director, National Botanical Research Institute, Lucknow, Uttar Pradesh, India, and a voucher specimen no. Tit/NBRI/CIF/141/2009 was deposited.

Preparation of extract

The leaves were dried in the shade, stored at 25°C, powdered and passed through sieve no.40. The dried powdered leaves of TD (500g) were first defatted with Petroleum Ether (60- 80°C) and later extracted with ethanol and distilled water separately by maceration for 5 days. After completion of the extraction, the solvent was removed by distillation and concentrated in vacuo (40°C) to yield ethanolic and aqueous extract, respectively.

Preliminary phytochemical screening of TD

The preliminary phytochemical investigation was carried out with ethanolic and aqueous extracts of leaves of TD for the qualitative identification of phytochemical constituents. Phytochemical tests were carried out by standard methods [16-17].

Animals

Male Wistar rats weighing 150- 200 g were provided by the animal house. Animals were made available with the standard animal feed and water supply *ad libitum* before the experiments. The animal studies were approved by the Institutional Animal Ethics Committee (Reg. no. 831/bc/04/CPCSEA), New Delhi, India. For each experimental study rats were starved for 18 h with access to water only.

Drugs and chemicals

Furosemide (Lasix, SANOFIAVENTIS), potassium chromate, silver nitrate, etc. were used in the present study.

Acute toxicity study

An acute toxicity study was carried out for the extracts of TD following the Organization of economic co-operation and development (OECD) guidelines [18]. The extract was dissolved in distilled water in a dose of 2 g/kg body weight and orally administered to overnight-fasted, healthy rats (n = 6). The animals were observed continuously for 24 h for mortality.

Evaluation of diuretic activity

Animals were maintained under standard conditions of temperature and humidity and underwent an adaptation period of three days. The animals were divided into eight groups (n= 6). Group I served as the control and received normal saline solution (25 ml/kg oral administration); group II received the reference diuretic, Furosemide 10 mg/kg p.o.; groups III, IV and V received the ethanolic extract of TD (TDEE) at 100, 200 and 400 mg/kg p.o., respectively, in normal saline solution (25 ml/kg p.o.) and groups VI, VII, and VIII received the aqueous extract of TD (TDAE) at 100, 200 and 400 mg/kg p.o., respectively, also in normal saline solution (25 ml/kg p.o.). The diuretic activity was assessed based on the method of Lipschitz *et al.* (1943) [19].

Immediately after the administration of all the doses; animals were placed individually in metabolic cages that were specially designed to separate urine and feces and kept at a controlled temperature of 20-25 °C. At the end of 12 h [20] the volume of urine was collected and

measured. The animals were deprived of food and water during the period of experimentation. The parameters viz. body weight before and after the test period, total urine volume, and concentration of Na^+ , K^+ , and Cl^- were measured. The concentration of Na^+ and K^+ cations was determined by a flame photometric method while that of Cl^- was determined by titration with silver nitrate solution (N/50) using three drops of 5% potassium chromate solution as an indicator [21-22].

Statistical analysis

Results are expressed as the mean \pm SEM. Data was analyzed by one-way analysis of variance (ANOVA) followed by Dunnett's multiple comparison tests. A value of $P < 0.05$ was considered statistically significant.

Results

Preliminary phytochemical screening of TD

Phytochemical screening of TD revealed the presence of resins, alkaloids, tannins, amino acids, proteins, flavonoids, saponins, phenols, steroids, glycosides and tri-terpenoids.

Effect on urine volume

The animals were observed for 12 h and showed no signs of dehydration. Group II animals that were dosed with the reference diuretic (furosemide) significantly increased urine output as compared to the control group ($P < 0.001$), with a diuretic index of 2.75 (**Table 1**). Administration of the test drug i.e., TDEE at 100, 200 and 400 mg/kg, also resulted in a significant increase in urine volume, although less than that found with the reference drug. In the case of TDAE, at a test dose level of 100, 200 and 400 mg/kg the diuretic indices obtained were 1.88, 1.92 and 2.05, respectively, with a significant result at the test dose of 400 mg/kg, p.o. Thus

TDEE at test doses is more effective in enhancing the urine excretion as compared to TDAE in a dose-dependent manner.

Effect on urinary electrolyte excretion

Immediately after the administration of all the doses, animals were placed individually in metabolic cages. The volume of urine was collected and measured, and the concentration of electrolytes was determined, which is mentioned in **Table 2**. It was found that TDEE showed a significant increase in the excretion of sodium, potassium, and chloride ions in a dose-dependent manner. The increase in electrolyte excretion with the ethanolic extract (at all doses) was less than that found with furosemide. TDAE at a test dose level of 100, 200 were found to be insignificant when compared to the standard drug, while at 400 mg/kg, it showed increased electrolyte excretion. Thus TDEE at test doses is more effective in enhancing the electrolyte excretion compared to TDAE and that in a dose-dependent manner.

Discussion

The diuretic effect of the orally administered ethanolic and aqueous extracts of TD has been evaluated in normal rats, and compared with that produced by furosemide, a loop diuretic widely used in clinical practice. The results obtained in the study are immensely helpful in establishing the scientific evidence for the traditionally claimed diuretic efficiency of TD. An encyclopedia of world medicinal plants has demonstrated the use of decoction of leaves of TD as an anti-hypertensive and diuretic. Also, TD exhibited its application in the ailment called strangury, i.e., a painful discharge of urine as per traditional literature [23].

Diuresis is associated with an increase in urine volume i.e., water excretion and a net loss of electrolytes in the urine. The acute treatment of rats with TDEE and TDAE exhibited a significant diuretic activity in a dose-dependent manner. Urine volume and cation excretion were

measured and found to be increasing with increased dose. Administration of TDEE at 100, 200, and 400 mg/kg resulted in a significant increase in urine volume, although less than that found with furosemide. Similar is the case with TDEE regarding electrolyte excretion. TDAE at a test dose level of 100 and 200 mg/kg was found to be insignificant when compared to the standard drug. Instead, at 400 mg/kg, TDAE showed enhanced electrolyte excretion. Thus TDEE at test doses is more effective in increasing electrolyte excretion than TDAE in a dose-dependent manner. Furosemide is well known for its potential saluretic and diuretic effects and from the study, it was observed that TD extracts were acting similarly as furosemide. Furosemide is categorized under loop diuretics or high ceiling diuretics, acts by inhibiting NKCC2, the luminal Na-K- 2Cl symport in the thick ascending limb of the loop of Henle. It also annihilates the cortico-medullary osmotic gradient and obstructs the negative as well as positive free water clearance [24-25]. By inhibiting the transporter, the loop diuretic declines the reabsorption of NaCl in the kidney and also diminishes the lumen-positive potential that derives from K recycling. This electrical potential normally propels divalent cation reabsorption in the loop. Thus, by reducing this loop potential, diuretics induce an increase in Mg and Ca [26].

Conclusion

Active principles of plants such as flavonoids, saponins, and organic acids are found to be responsible for the diuretic effect. These natural products might be acting synergistically or individually. The preliminary phytochemical analysis of TD revealed the presence of these constituents. The present study with reference to the excretion of Na⁺, K⁺, and Cl⁻, showed a more significant natriuretic effect than kaluretic one. The results of the study confirmed and supported the traditional use of TD as diuretics.

References

1. Wang DJ, Gottlieb SS. Diuretics: still the mainstay of treatment. Crit Care Med. 2008 Jan;36(1 Suppl): S89-94.
2. Agunu A., E.M. Abdurahamn, G.O. Andrew and Z. Muhammed, 2005. Diuretic activity of stem bark extracts of *Steganotaenia araliaceae* Hochst [Apiaceae]. J. Ethnopharmacol., 96:471-475.
3. Sivakumar B, Malta D, Mak S, Dash S, Newton GE, Arcand J. Evaluating the confounding effects of medical therapies on potassium intake assessment in patients with heart failure. Nutr Metab Cardiovasc Dis. 2020 Feb 24. pii: S0939-4753(20)30058-2.
4. Singh R.G., R.P. Singh and K.P. Usha, 1991. Experimental evaluation of diuretic action of herbal drug (*Tribulus terrestris* Linn) on albino rats. J. Res. Edu. Ind. Med., 3: 19-21.
5. Jain D.L., A.M. Baheti, S.R. Prakash and P.L. Ingale, 2007. Study of antacid and diuretic activity of ash and extracts of *Musa sapientum* L. fruit peel. Pharmacog. Mag., 3:116-119.
6. Tripathi, S.K., 2003. Traditional knowledge: Its significance and implications, Indian J. Traditional Knowledge, 2(2): 99-106.
7. Chaudhuri, S.K., 2005. Quintence of medical pharmacology, 3rd ed., New central book agency (P) Ltd., Kolkata, 378-380, 221-228.
8. Pasricha, P.J. and E.K. Jackson, 2006. Treatment Of Disorders Of Bowel Motility And Water Flux; Antiemetics; Agents Used In Biliary And Pancreatic Disease, Diuretics, In: Goodman and Gilman's The Pharmacological Basis Of Therapeutics (Eds. L.L. Brunton,

- J.S. Lazo and K.L. Parker), 11thed., McGraw-Hill Medical Publishing Division, New York, 995-98,737-767.
9. Wile, D., 2012. Diuretics: a review. *Ann. Clin. Biochem.*, 49(5):419-431.
 10. Bent, S., 2008. Herbal medicine in the United States: review of efficacy, safety, and regulation: grand rounds at University of California, San Francisco Medical Center. *J. Gen. Intern. Med.*, 23(6):854-859.
 11. Martin N., C. Pantoja, L. Chiang, L. Bardisa, C. Araya and R. Roman, 1991. Hemodynamic effects of a boiling water dialysate of maize silk in normotensive anaesthetised dogs. *J. Ethnopharmacol.*, 31:259–262.
 12. Devi P., R. Meera, P. Muthumani, R. Chilakalapudi, V.K. Thota, D.V.D. Murthy and K. Jeyasundari, 2010. *Inter. J. Pharm. and Bio. Arch.*, 1(4): 331-334.
 13. Geetha G., A.K. Chandrasekharan, P. Brindha and G. Shyamala, 2006. Preliminary phytochemical and pharmacognostical studies of *Achyranthus rubrofuscus* Linn. *Hamdad Medicus.*, V. 49 (4) : 115-120.
 14. Khare, C.P., 2007. *Indian Medicinal Plants*, Springer-Verlag Berlin/Heidelberg.
 15. Dixit PK and Mittal S: A Comprehensive review on herbal remedies of diuretics. *International Journal of Research in Pharmacy and Science* 2013; 3(1): 29-31.
 16. Kokate, C.K., 1994. *Practical Pharmacognosy*, 4thed., Vallabh Prakashan, Delhi, 107-111.
 17. Khandelwal, K.R., June 2004. *Practical Pharmacognosy Techniques and Experiments*, 11thed., Nirali Prakashan, Pune, 157-159.

18. OECD Guidelines—“Guidance document on acute oral toxicity testing” (2001) series on testing and assessment no. 24, Organization for economic co-operation and development, OECD environment, health and safety publications, Paris. (www.oecd.org/ehs) accessed on 12th January 2007.
19. Lipschitz W.L., Z. Haddian and A. Kerpskar, 1943. Bioassay of diuretics. *Pharmacol. Exp. Ther.*, 79:97-110.
20. Montejano-Rodriguez J.R., G. Almaguer-Vargas, J.A. Gayosso-De-Lucio, M.E. Ocharan Hernandez, R.E.M. Martinez, M.E. Hernandez Caballero, J.J.M. Torres-Valencia, J.A.S. Ramirez, 2013. Evaluation of the diuretic activity of the ethanolic extract of *Geranium seemannii* Peyr. in Wistar rats. *J. Pharm. Res.*, 6:709 -713.
21. Indian Pharmacopoeia, Vol II, Publications and Information Directorate (CSIR), New Delhi, India. 1996. p. 689.
22. Neuman, M., 2002. Metabolic effects and drug interactions provoked by certain vegetables: grapefruit, St. John’s wort and garlic. *Press. Med.*, 31:1416-1422.
23. Kumari S, Mazumder A and Bhattacharya S: Evaluation of anti-diarrheal and diuretic activity of *Tabernaemontana divaricata* Linn. leaves. *Int J Pharmacognosy* 2018; 5(7): 409-13.
24. Hannaert P., M. Alvarez, D. Pirot, 2002. Rat NKCC2/NKCC1 cotransporter selectivity for loop diuretic drugs. *Naunyn- Schmiedeberg’s Arch. Pharmacol.*, 365(3):193-199.
25. Castrop H., J.N. Lorenz, B. Hansen, 2005. Contribution of the basolateral isoform of the Na-K-2Cl - cotransporter (NKCC1/ BSC2) to renin secretion. *Am. J. Physiol. Renal Physiol.*, 289:1185-1192.

26. Ares G.R., P.S. Caceres and P.A. Ortiz, 2011. Molecular regulation of NKCC2 in the thick ascending limb. *Am. J. Physiol. Renal Physiol.*, 301(6):1143-1159.

Table Legends:

Table 1: Effect of *T. divaricata* extracts and Furosemide on urine volume

Table2: Effect of *T. divaricata* extracts and Furosemide on electrolyte excretion

Table 1: Effect of *T. divaricata* extracts and Furosemide on urine volume

Treatment	Dose (mg/kg)	Urine volume (ml/100 g/12 h)	Diuretic index
Control	-	5.3 ± 0.6	-
Furosemide	10	14.6 ± 2.6 ^{***}	2.75
TDEE	100	11.1 ± 0.3 [*]	2.09
TDEE	200	11.9 ± 0.7 [*]	2.24
TDEE	400	13.4 ± 1.2 ^{**}	2.52
TDAE	100	10.0 ± 1.0 ^{ns}	1.88
TDAE	200	10.2 ± 1.0 ^{ns}	1.92
TDAE	400	10.9 ± 0.7 [*]	2.05

TDEE: Ethanolic extract of *T. divaricata*; **TDAE:** Aqueous extract of *T. divaricata*
 Values are expressed as the mean \pm SEM; * $P < 0.001$ compared to the control group, ** $P < 0.01$ compared to Furosemide group (ANOVA followed by Dunnett's test).

Diuretic Index = Volume of test group/Volume of control group.

Table2: Effect of *T. divaricata* extracts and Furosemide on electrolyte excretion

Treatment	Dose (mg/kg)	Total Na ⁺ (μmoles/kg)	Total K ⁺ (μmoles/kg)	Total Cl ⁻ (μmoles/kg)
Control	-	1680 \pm 1.0	665.8 \pm 4.0	637.0 \pm 52.4
Furosemide	10	3654 \pm 1.6 ^{***}	1429 \pm 5.9 ^{***}	1836 \pm 61.1 ^{***}
TDEE	100	2275 \pm 1.0 [*]	859.5 \pm 1.7 [*]	1174 \pm 85.7 ^{**}
TDEE	200	2365 \pm 1.1 ^{**}	929.5 \pm 2.8 ^{**}	1334 \pm 97.9 ^{***}
TDEE	400	2726 \pm 1.1 ^{***}	1176 \pm 4.8 ^{***}	1678 \pm 52.5 ^{***}
TDAE	100	1870 \pm 1.0 ^{ns}	834.5 \pm 2.6 [*]	932.3 \pm 56.7 [*]
TDAE	200	1980 \pm 1.0 ^{ns}	856.5 \pm 4.7 [*]	941.5 \pm 88.8 [*]
TDAE	400	2203 \pm 1.9 [*]	863.5 \pm 2.4 [*]	1007 \pm 77.9 ^{**}

TDEE: Ethanolic extract of *T. divaricata*; **TDAE:** Aqueous extract of *T. divaricata*.

Values are expressed as the mean \pm SEM; * $P < 0.001$ compared to the control group, ** $P < 0.01$, *** $P < 0.001$, compared to Furosemide group (ANOVA followed by Dunnett's test).



Anti-inflammatory, Anti-oxidant and Anti-microbial Properties of Polyherbal Formulation in Acne Treatment

Rakesh S. Shivatare*¹, Dr. Shailesh M. Kewatkar², Priya Lohakare¹, Nitin Bhutale¹, Ramesh Musale¹, Durga Choudhary³, Gayatri Ganu⁴, Dr. Dheeraj H. Nagore⁵

¹ Research scholar, JJT University, Jhunjhunu, Rajasthan, India.

² Rajarshi Shahu College of Pharmacy, Buldana, Maharashtra, India.

³ Research associate, Mprex Healthcare, Pune, India.

⁴ Vice president Clinical Research, Mprex Healthcare, Pune, India.

⁵ Research Guide, JJT University, Jhunjhunu, Rajasthan, India.

*Corresponding author's E-mail: rakeshshivatare@gmail.com

Received: 05-02-2020; Revised: 24-04-2020; Accepted: 30-04-2020.

ABSTRACT

Nowadays, individual herbs are insufficient to achieve a desired therapeutic effect. When it is optimized as multiple herbs composition in a particular ratio it will give a therapeutic effect in a better way with reduced toxicity. In order to develop such an intervention, the present study was intended to develop a polyherbal cream from extracts of *Santalum album*, *Rubia cordifolia*, *Ocimum sanctum*, *Emblica officinalis*, *Glycyrrhiza glabra*, *Persea americana*, *Simmondsia chinensis*, *Vitis vinifera*. The present study emphasizes on screening of polyherbalism as anti-inflammatory, antioxidant and anti-microbial in Acne treatment. The polyherbal cream showed significant activity against *P. acnes* and *S. aureus* with diameter of 10 mm and 15 mm inhibition zone respectively. The polyherbal cream exhibited moderate antioxidant activity with IC50 value of 8.9 mg/ml. Topical anti-inflammatory activity was assessed by carrageenan induced paw oedema compared with Diclofenac. The percentages of edema inhibition were 79.9 % (p < 0.01) after five hours. The outcome of the study suggested that polyherbal cream could be possible to use as the natural anti-acne formulations.

Keywords: Polyherbal cream, Anti-acne, Anti-inflammatory, Anti-microbial, antioxidant.

INTRODUCTION

Herbal treatments applied topically have gained considerable attention due to their widespread use and ill-defined benefit/risk ratio¹. Topical application of cream and ointment at pathological sites offer great advantages in a faster release of a drug directly to site of action². The concept of polyherbalism has mentioned in "Sarangdhar Samhita". This stated that products with combined extracts of plants are considered more effective rather than individual ones. The active phytoconstituents of individual plants have been recognized but are generally present in small quantities, which is not enough to produce the desired therapeutic action for curing acne. Medicinal plants with antimicrobial, antioxidant and anti-inflammatory properties used in the treatment of acne. Polyherbalism results in cheaper medication by reducing the duration of therapy or individual cost for anti-acne medications³.

Acne vulgaris (acne) is one of the most commonly encountered skin diseases and usually affects nearly everybody during their lifetime⁴. Pathophysiology of acne is attributed to different notable factors such as androgen-mediated stimulation of sebaceous gland activity, follicular hyper keratinization, hormonal imbalance, inflammation and external bacterial infection. Propionibacterium acnes and Staphylococcus epidermidis are the major bacteria found on skin causes acne^{5,6}. A number of topical and systematic therapies are available

for acne; various antibiotics, comedolytic agents, and anti-inflammatory drugs are available as a topical therapy, whereas modern systematic cure includes antibiotics, hormones, zinc and laser treatment⁷. However, an excessive use of these drugs over a long time can lead to the rising resistance of bacteria. These drugs have limitations with respect to toxicity and side effects also such as skin drying, headache, nausea etc. To overcome these limitations, there is an imperative need for the development of effective, safe and low-cost anti-acne drugs. Exploration of herbal resources may provide valuable leads that can be further developed as anti-acne drugs⁸.

Santalum album seed exhibited significant antioxidant and antimicrobial activity due to rich and diverse presence of saturated fatty acid⁹. The plant bioactives of *Rubia cordifolia* exhibited antioxidant and anti-microbial activities and has been found to have efficacy, traditionally in treatment of acne¹⁰. *Ocimum sanctum* contains fixed oil and linolenic acid having the ability to block cyclooxygenase and lipoxygenase pathways of arachidonic acid metabolism. Therefore, they show anti-inflammatory activities¹¹. *Emblica Officinalis* contains two hydrolysable tannins Emblicanin A and B which have antioxidant properties along with anti-microbial activities¹². *Glycyrrhiza glabra* L. showed existence of numerous useful metabolites such as: flavonoids, saponins, alkaloids and so on. Because of these



constituents they exhibited effective antioxidant and anti-bacterial activities. β -glycyhrritinic acid has anti-inflammatory properties in different animal models¹³. *Persea Americana* which constitute a drug known as piasclidine, has inhibited the release and activity of metalloproteinases and pro-inflammatory cytokines which play a major role in the development of osteoarthritis¹⁴. *Simmondsia Chinensis* extracts shown to possess antimicrobial and antifungal activities against several pathogens. The researchers isolated 10 flavonoids and four lignans from *Simmondsia Chinensis* extracts. They reported that flavonoidglycosides showed stronger antioxidant and lipoxygenase inhibitory effects than their glycoside counterparts¹⁵. *Vitis vinifera* has its own significance in traditional medicine system. It has been used for decades for the treatment of various ailments like antioxidant, Antibacterial effects¹⁶.

The selected herbs for this study aimed different pharmacological targets involved in the acne treatment like suppression of the production of inflammatory cytokines and inflammatory transduction cascades, reduction of oxidative factors, enhancement of anti-oxidative enzymes. The development of polyherbal formulation for the treatment of acne having antimicrobial, antioxidant and anti-inflammatory properties is the need of present times.

MATERIALS AND METHODS

Chemicals

Analytical grade chemicals were used for the study. The media and broth used for microbial culture were procured from Hi-Media Pvt. Limited, Bombay, India. The chemi-cals used for the experimental work included Carbopol 940(Merck Ltd), propylene glycol-400 (SD Fine Chemical Ltd), ethanol (Merck Ltd), methylparaben (Supreme Chemicals), propylparaben (Supreme Chemicals), triethanolamine (SD Fine Chemical Ltd), EDTA (S. D Fine lab India).

Plant Material

The dried extract of *Santalum album seed*, *Rubia cordifolia*, *Ocimum sanctum*, *Embllica Officinalis*, *Glycyrrhiza glabra*, *Persea Americana*, *Simmondsia Chinensis*, *Vitis vinifera* was purchased from local market, India.

Anti-inflammatory activities of polyherbal cream

Carrageenan induced paw edema in rats

The anti-inflammatory activities of the PR/HC/1718/013 Cream under study were evaluated by using the carrageenan-induced edema model. The in50 mg, 100mg, 200mg polyherbal cream and standard diclofenac cream was applied to the plantar surface of the left hind paw of negative control, standard and test drug treated group respectively by gently rubbing 50 times with the index finger. Three hours after the dose, 0.1 ml of 1% carrageenan solution in normal saline was injected via

sub-plantar route in the left hind paw of each animal. The right hind paw however received 0.1 ml of saline. Paw edema was measured every 60 min up to 4 h after the injection of carrageenan. A digital Vernier calliper (Digi calliper) was used to measure the difference in footpad thickness between the right and left foot. Mean values of treated groups and control group were compared and analyzed using statistical methods¹⁷.

Antioxidant activities of polyherbal cream

DPPH Radical Scavenging Activity

Antioxidant activities of extracts were measured spectrophotometrically by using 1, 1- diphenyl 2-picryl hydrazyl (DPPH). 0.1 mM DPPH solution was prepared in methanol. 1 ml of DPPH stock solution was mixed with 1 ml of PR/HC/1718/013 Cream solution of different concentrations (50, 100, 200 μ g/ml). The mixer of 1 ml methanol and 1 ml DPPH stock solution was used as a control. Ascorbic acid was used as the standard reference compound with the same concentration. The reactions were carried out in triplicate and allowed to stand at room temperature for 30 min. Reduction in the absorbance was measured by UV-Vis spectrophotometer at 517 nm. The inhibition percentage was calculated using the following formula¹⁸.

$$\% \text{ Reduction} = (\text{Abs DPPH} - \text{Abs Dil.}) / \text{Abs DPPH} \times 100$$

Whereby:

Abs DPPH = Average absorption of the DPPH solution

Abs Dil. = Average absorption of the three absorption values of each dilution

Antimicrobial activity of polyherbal cream

Procedure for *Propionibacterium acne* activity

The dried surface of a blood agar plate was inoculated by spreading culture suspension of *Propionibacterium acne* (100 μ l) on agar surface. The wells were bored into the surface of the inoculated agar plate and the known concentration of sample (100 μ l) was added to the wells. Plates were kept in the freeze for pre-diffusion for 30 minutes and then placed under anaerobic conditions, in an incubator set to 37°C for 48 hours. All the samples were dissolved in methanol: water (50: 50) to obtain different concentrations. The cups were bored in agar medium spread with the test organism, using a sterile cork borer with 8 mm inner diameter. These cups were filled with 100 μ l sample solutions and the plates were incubated at 37°C for 48 hours under anaerobic conditions. The assessment of the antimicrobial activity was based on the measurement of the diameter of the zone of inhibition. Simultaneously zone of inhibition of diluent was also considered in the calculation¹⁹.

Procedure for *Staphylococcus aureus* activity

Inoculation of Test Plates: The dried surface of a Mueller-Hinton agar plate was inoculated by spreading culture suspension (100 μ l) on agar surface. The wells were bored



into the surface of the inoculated agar plate and the known concentration of sample (100 μ l) was added to the wells in triplicates. Plates were kept in the freeze for pre-diffusion for 30 minutes and then placed in an incubator set to 37°C for 24 hours. Samples were dissolved in methanol: water (50:50) to obtain different concentrations. Muller Hinton agar as used for antibacterial test. The cups were bored in agar medium spread with the test organism, using a sterile cork borer with 8 mm inner diameter. These cups were filled with 100 μ l sample solutions and the plates were incubated at 37°C. The assessment of the antimicrobial activity was based on the measurement of the diameter of the zone of inhibition. Simultaneously zone of inhibition of diluent was also considered in the calculation²⁰.

RESULT AND DISCUSSION

Anti-inflammatory activities of polyherbal cream

Carrageenan induced paw edema in rats

Carrageenan-induced inflammation is useful in detecting orally active anti-inflammatory agents; therefore, it has significant predictive value for anti-inflammatory agents acting through mediators of acute inflammation. The development of edema induced by carrageenan injection causes an acute and local inflammatory response. In past studies, anti-inflammatory effects by plethysmometric measurement of formalin-induced paw edema on herbal cream formulation. The result indicates that the extracts inhibited the paw edema size and shows inhibition of the inflammation.

The herbal cream formulation has significantly inhibited edema at higher dose. The positive control group was compared with standard i.e. Diclofenac Tablet, Marketed product 1, 2, 3 and cream formulation of PR/HC/1718/013. As per statistical analysis, the herbal test cream has been shown highly significant effect after 3 Hr of drug administration and the standard cream has shown highly significant effect after 2 Hr of drug administration shown in Table 1 and Figure 1.

Table 1: Effect of Herbal cream on carrageenan-induced paw edema in rats

	% inhibition					
	30 min	1 HR	2 HR	3 HR	4HR	5HR
Diclofenac Tablet	8.56±1.56	5.23±0.07	36.59±1.31	56.91±0.06	72.69±0.43	85.63±1.23***
PR/HC/1718/013	1.23±0.29	4.60±1.21	19.63±0.35	34.09±0.09	59.76±1.04	79.90±0.09**
Marketed Product 1	0.96±2.98	1.90±1.13	12.07±2.01	29.80±1.63	41.06±0.08	52.80±0.82
Marketed Product 2	0.73±1.67	1.53±0.83	13.42±1.10	25.30±1.09	42.08±0.78	53.07±1.01
Marketed Product 3	1.78±0.05	2.27±0.81	16.78±0.85	31.03±0.56	46.75±0.89	59.98±0.94*

Results are expressed as mean \pm S.E.M (n=6), one-way ANNOVA followed by Tukey multiple comparison test. *P<0.05, **P<0.01, ***P<0.001, When compared with control groups.

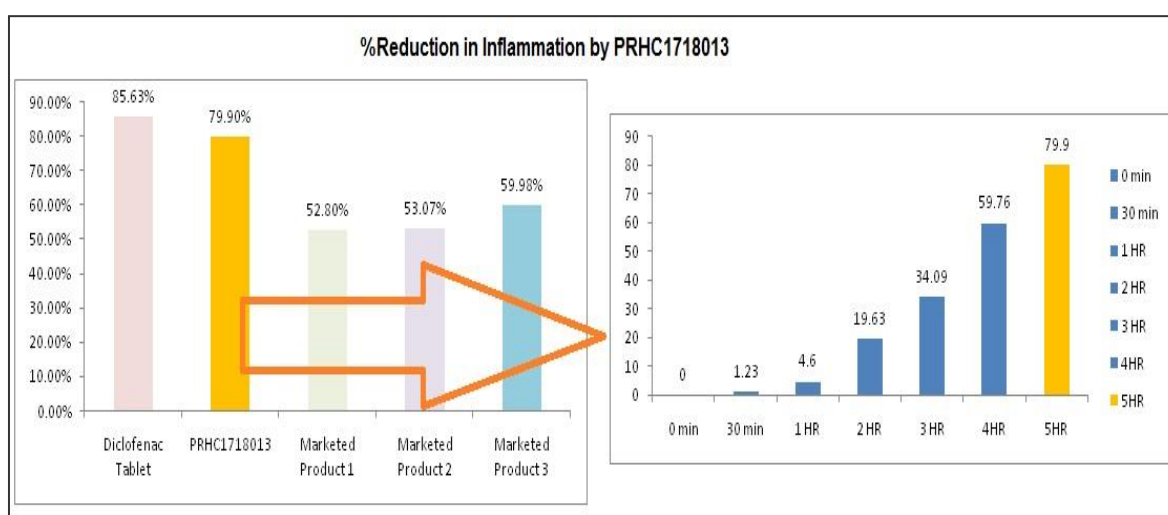


Figure 1: %Reduction in Inflammation by PR/HC/1718/013 cream

Antioxidant assay

DPPH-Free radical scavenging activity

DPPH is a stable free radical and accepts an electron or hydrogen radical to become a stable diamagnetic molecule. In the DPPH assay, the antioxidants are able to reduce the stable radical DPPH to non-radical form,

DPPH-H. The purple colored alcoholic solution of DPPH radical changes to yellow in the presence of hydrogen-donating antioxidant which could be measured at 517nm, the activity is expressed as effective concentration EC50, which is the concentration of the sample leading to 50% reduction of the initial DPPH concentration. Effectiveness of antioxidant properties is inversely correlated with



EC50 values. If the EC50 value of a cream less than 10mg/ml, that's mean the extract is an effective antioxidant. In this study, the EC50 value of cream was

8.9 mg/ml less than 10mg/ml this indicates that the samples have effective antioxidant activity (Table 2).

Table 2: Antioxidant properties of PR/HC/1718/013 cream

Sr. No.	Sample Name	DPPH free radical scavenging capacities (mg/ml)
1	PR/HC/1718/013	8.9
2	Marketed Product 1	4.6
3	Marketed Product 2	7.5
4	Marketed Product 3	1.8

Note: Data were expressed as mean ± (n = 3)

Antimicrobial activity of polyherbal cream

To determine antibacterial effects of PR/HC/1718/013 Cream against skin bacteria *Propionibacterium acne* and *Staphylococcus aureus* were chosen for the test. As listed in Table 3, PR/HC/1718/013 showed antimicrobial

activities against the tested both strains. Tetracycline, Doxycycline and clindamycin, were active against both strains (Figure 2). PR/HC/1718/013 showed anti-acne activity by inhibiting *Propionibacterium acne* and *Staphylococcus aureus* micro-organisms.

Table 3: Antimicrobial activity of polyherbal cream

SN	Name of compound	<i>Propionibacterium acne</i> activity		<i>Staphylococcus aureus</i> activity	
		MIC (µg/mL)	Zone of Inhibition in mm	MIC (µg/mL)	Zone of Inhibition in mm
1	PR/HC/1718/013	75 (µg/mL)	10	140 (µg/mL)	15
2	Tetracycline	2 (µg/mL)	15	7.5 (µg/mL)	16
3	Doxycycline	3 (µg/mL)	14	7.5 (µg/mL)	14
4	Clindamycin	10 (µg/mL)	15	5 (µg/mL)	20

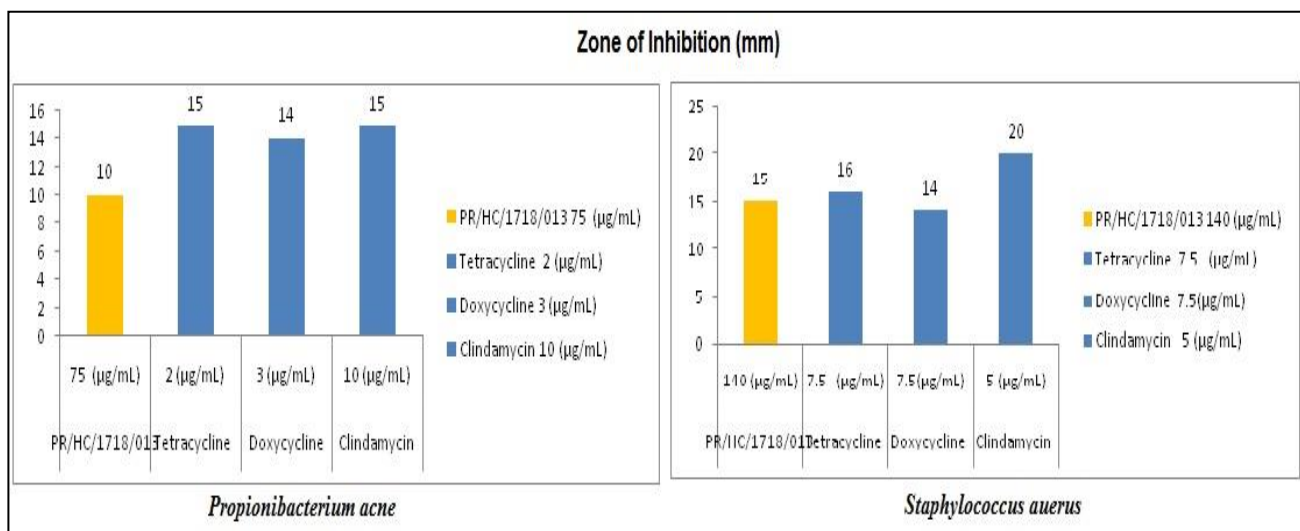


Figure 2: Zone of Inhibition in mm by *Propionibacterium acne* and *Staphylococcus aureus*

CONCLUSION

The results of this study indicate that PR/HC/1718/013 Cream show antibacterial activity with less MIC against acne causing bacteria. Additionally, PR/HC/1718/013 Cream also showed good antioxidant activity along with anti-inflammatory activity. The antioxidant, anti-inflammatory and antimicrobial activities of polyherbal composition might be among the contributing factors that showed remarkable improvement in collagen synthesis

and reduced microbial load that could be involved in the healing process of acne. As these are the natural Cream, so they have no or less side effects. These can also be an alternative and better option for resistant acne causing bacteria. The topical anti-acne formulations can be developed using these plant extracts individually or in combination.



REFERENCES

1. Aburjai T, Natsheh FM. Plants used in cosmetics. *Phytotherapy Research: An International Journal Devoted to Pharmacological and Toxicological Evaluation of Natural Product Derivatives*. 17(9), 2003 Nov, 987-1000.
2. Avinash S, Gowda DV, Suresh J, Ram AS, Srivastava A, Osmani RM. Formulation and evaluation of topical gel using *Eupatorium glandulosum* Michx for wound healing activity. *Scholars Research Library*. 8(8), 2016, 255-66.
3. Dev SK, Choudhury PK, Srivastava R, Sharma M. Antimicrobial, anti-inflammatory and wound healing activity of polyherbal formulation. *Biomedicine & Pharmacotherapy*. 111, 2019 Mar 1, 555-67.
4. Friedlander SF, Baldwin HE, Mancini AJ, Yan AC, Eichenfield LF. The acne continuum: an age-based approach to therapy. *In Seminars in cutaneous medicine and surgery* (Vol. 30, No. 3 Suppl, 2011 Sep, pp. S6-11).
5. Coenye T, Peeters E, Nelis HJ. Biofilm formation by *Propionibacterium acnes* is associated with increased resistance to antimicrobial agents and increased production of putative virulence factors. *Research in microbiology*. 158(4), 2007 May 1, 386-92.
6. Williams HC, Dellavalle RP, Garner S. *Acne vulgaris*. *The Lancet*. 379(9813), 2012 Jan 28, 361-72.
7. Vora J, Srivastava A, Modi H. Antibacterial and antioxidant strategies for acne treatment through plant extracts. *Informatics in Medicine Unlocked*. 13, 2018 Jan 1, 128-32.
8. Kumar A, Baboota S, Agarwal SP, Ali J, Ahuja A. Treatment of acne with special emphasis on herbal remedies. *Expert Review of Dermatology*. 3(1), 2008 Feb 1, 111-22.
9. Gautam PV, Usman MR, Lodhi S, Patil V. Phytochemical Investigation And In Vitro Antimicrobial Screening of *Santalum Album* Seeds Extracts. *Int J Pharm Pharmsci*. 9(11), 2017, 117-124.
10. Bhat BA, Shergojri FA, Gaur M, Shammi QJ. A Comprehensive Review on *Rubia cardifolia* (Manjistha). *International journal of advance research in science and engineering*. 07(07), 2018, 127-141.
11. Kulkarni KV, Adavirao BV. A review on, Indian traditional shrub Tulsi (*Ocimum sanctum*): the unique medicinal plant. *J Med Plants Studies*. 6(2), 2018, 106-110.
12. Dasaroju S, Gottumukkala KM. Current trends in the research of *Emblca officinalis* (Amla): A pharmacological perspective. *Int J Pharm Sci Rev Res*. 24(2), 2014, 150-9.
13. Parvaiz M, Hussain K, Khalid S, Hussain N, Iram N, Hussain Z, Ali MA. A review: Medicinal importance of *Glycyrrhiza glabra* L. (Fabaceae family). *Global J Pharmacol*. 8(1), 2014, 8-13.
14. Ranade SS, Thiagarajan P. A review on *Persea americana* Mill. (avocado)-its fruits and oil. *Int. J. PharmTech Res*. 8(6), 2015, 72-7.
15. Al-Obaidi JR, Halabi MF, AlKhalifah NS, Asanar S, Al-Soqeer AA, Attia MF. A review on plant importance, biotechnological aspects, and cultivation challenges of jojoba plant. *Biological research*. 50 (25), 2017, 1-9.
16. Nassiri-Asl M, Hosseinzadeh H. Review of the pharmacological effects of *Vitis vinifera* (Grape) and its bioactive constituents: an update. *Phytotherapy Research*. 30(9), 2016 Sep, 1392-403.
17. Oliveira RB, Chagas-Paula DA, Secatto A, Gasparoto TH, Faccioli LH, Campanelli AP, Da Costa FB. Topical anti-inflammatory activity of yacon leaf extracts. *Revista Brasileira de Farmacognosia*. 23(3), 2013 May 1, 497-505.
18. Lee YL, Jian SY, Lian PY, Mau JL. Antioxidant properties of extracts from a white mutant of the mushroom *Hypsizygus marmoreus*. *Journal of Food Composition and Analysis*. 21(2), 2008 Mar 1, 116-24.
19. Ankita Y, Richa B, Sharma RA. Isolation, quantification and antimicrobial activities of phytosterols from different parts of *Cassia pumila* Lamk. *Int. J. Pharm*. 4, 2014, 86-92.
20. Jahan F, Lawrence R, Kumar V, Junaid M. Evaluation of antimicrobial activity of plant extracts on antibiotic susceptible and resistant *Staphylococcus aureus* strains. *J Chem Pharm Res*. 3(4), 2011, 777-89.

Source of Support: Nil, Conflict of Interest: None.



INTERNATIONAL JOURNAL OF RESEARCH IN PHARMACEUTICAL SCIENCES

Published by JK Welfare & Pharmascope Foundation

Journal Home Page: www.pharmascope.org/ijrps

Isolation, Identification and Characterization of Ximenynic Acid with Anti-Aging Activity from *Santalum Album*


Rakesh S Shivatare^{*1}, Ramesh Musale¹, Priya Lohakare¹, Dipika Patil¹, Durga Choudhary², Gayatri Ganu², Dheeraj H Nagore³, Shailesh M Kewatkar⁴

¹JJT University, Jhunjhunu, Rajasthan, India

²Mprex Healthcare, Pune, India

³Department of Research and Development, Mprex healthcare, Pune, India

⁴Rajarshi Shahu College of Pharmacy, Buldana, Maharashtra, India

Article History:	ABSTRACT	
Received on: 02.08.2019 Revised on: 08.11.2019 Accepted on: 15.11.2019	<p>Medicinal plants and its products have been used as a remedial agent in most irising countries for treating diseases. Furthermore, an increasing reliance on the use of medicinal plants in industrialized societies has been traced for the extraction and development of several drugs and chemotherapeutics from these herbal plants. Novel acetylenic fatty acids named Ximenynic acid (XMA) were successfully isolated from the seeds of <i>Santalum album</i> L by N-Hexane extraction. Ximenynic acid (or Santalbic acid) is one of the few acetylenic fatty acids occurring at higher levels in plant seed oils. Ximenynic acid predominantly exists in the seed oil of <i>Santalaceae</i>, <i>Olacaceae</i>, and <i>Opiliaceae</i> families. The structure of XMA was characterized by UV-visible spectroscopy, Infrared Spectrum (IR), NMR Spectroscopy, Differential scanning calorimetry (DSC), Thermal Gravimetric Analysis (TGA), X-ray diffraction (XRD), Fourier Transform Infrared Spectroscopy (FT-IR), LCMS spectral analysis. The antiaging activities were assessed by anti-collagenase enzyme assay. Structural analysis revealed that XMA was a crystalline material with a melting point of 38.25°C and an average molecular weight of 278 kDa. Which is composed of carboxylic acid, butylenic acid, methylene, allylic in their structure. The antiaging assay showed that XMA exhibited significant collagenase inhibition activity as compared with Catechin. These findings suggested that the acetylenic fatty acids XMA could be served as a novel antiaging in Pharmaceutical as well as the cosmetic industry.</p>	
<p>Keywords:</p> <p>Ximenynic acid, Santalum album, isolation, Characterization, Antiaging assay</p>		

1 *Corresponding Author

2 Name: Rakesh S Shivatare

3 Phone: +919890250523

4 Email: rakeshshivatare@gmail.com

5

6 ISSN: 0975-7538

7 DOI: <https://doi.org/10.26452/ijrps.v10i3>.

8

9 Production and Hosted by

10 Pharmascope.org

11 © 2019 | All rights reserved.

12

INTRODUCTION

Plants are considered an essential source of medicines for humans. Plant parts like leaves, flowers, roots, stems, seeds, and fruit are used as food resources for human as well as a safe medicine for the treatment of different diseases. Plant-derived herbal medicine is used as the main source for the treatment of diseases since ancient times (Hussain *et al.*, 2013). Ethnopharmacology of natural products isolated from herbal plants possesses pharmacological and therapeutic efficacy for treating diseases (Pan *et al.*, 2013). Aging is a natural process in all living organisms. Anti-aging has always been an interest in mankind. After much

13

14

15

16

17

18

19

20

21

22

23

24

25

26

research being done in the field, it is now widely accepted that aging is a multifarious event resulting from the collective effects of genetic variation, environmental risk factors, nutritional factors and lifestyle (Harman, 1998; Chang *et al.*, 2010). In recent years, the study of herbal medicine has received increasing attention in aging research. It is suggested that some traditional herbs have anti-aging properties and they are potential candidates for the treatment of chronic and aging-associated diseases. (Harman, 1998; Christensen, 2001).

Santalum album L., namely Sandalwood, given great respect as "Green Gold," is a traditional hemiparasitic tree and has an extensive record in Indian religious rituals and traditional Chinese medicine (Agnihotri and Tamrakar, 2017; Kim *et al.*, 2006). Their essential oil (sandalwood oil) is broadly used in the cosmetic, perfumery, and aromatherapy industries. It has been reported to have diverse biological properties such as antiviral, anti-carcinogenesis, and antitumor effects (Howes *et al.*, 2004). The herb is stated to have α -santalol, β -santalol, α -santalene, β -santalene, α -santalal, β -santalal, α -curcumene, tricycloekasantal (Guo *et al.*, 2014; Bapat and Rao, 1988). The seed oil of the *Santalum album* is shadowy red viscid fixed oil containing santalbic acid (or ximenynic acid) and stearolic acid (9-octadecenoic acid) (Pasha and Ahmad, 1993; Aitzetmüller *et al.*, 2003). Ximenynic acid, octadeca-11-trans-en-9-ynoic acid, is one of the few acetylenic fatty acids taking place at higher levels in plant seed oils (Carballeira, 2008). In universal, ximenynic acid exhibits many biological activities and pharmacological effects, including antibacterial, antifungal, anti-inflammatory activities (Konczak *et al.*, 2010).

Since the demand for ximenynic acid has an increasing trend, it is important to synthesized new methods of this ximenynic acid. The aim of this article is to syntheses ximenynic acid with extraction, identification and purification of ximenynic acid, as well as the recent findings regarding its pharmacological activities and the different approaches carried out to increase the use of ximenynic acid in different formulation.

MATERIALS AND METHODS

Plant materials

Santalum album L. Seed was collected from a local Shop in Pune. Their identity and Authentication were confirmed by the Department of Pharmacognosy Dr. D. Y. Patil Institute of Pharmaceutical Research and sciences, Pimpri, India, by correlating their morphological and microscopical characters

with those given in the literature. The remaining seed samples were dried in the shade. Coarse powder (60 #) of dried leaves of plants was stored for their microscopical study and phytochemical investigations.

Extraction, isolation and purification of XMA

Santalum album L. Seed samples were ground with a pestle and mortar and extracted N-hexane in a Soxhlet apparatus for 2 hr. The solution was dried to yield a viscous, pale yellow oil. The oil was refluxed with a solution of potassium hydroxide in 95% ethanol for 1 hr. The mixture was cooled and acidified with HCl to pH 1. The Free Fatty Acid as viscous oil was obtained by drying the solution over anhydrous sodium sulfate. Ximenynic acid was obtained by crystallization from N-hexane at 25°C. Recrystallization gave trans-ximenynic acid as white flakes, melting point 39°C.

Acetylenic fatty acids characterizations and structural analysis of XMA

FT-IR spectra analysis

The FT-IR spectrum of the XMA was determined using a Fourier transform infrared spectrophotometer (FT-IR) (Spectrum one FT-IR, Perkin Elmer Co., USA 1600 apparatus). XMA samples were ground with KBr powder and then pressed into pellets for FT-IR determination in the frequency range of 4000–400 cm^{-1} .

XRD analysis

The XRPD analysis of isolated XMA was carried out in an XRD 6000 diffractometer (Shimadzu) with adopted scanning from 10 to 70 (2θ scale and $\text{Cu}(K\alpha 1)$ radiation). The equipment was operated on 40.0 kV and 30.0 mA. The data were plotted by means of the software Origin version 8.1.

DSC analysis

The DSC curves were obtained on a TA Instruments Calorimeter; model DSC Q20, using aluminum crucibles with about 2 ± 0.1 mg of samples under the nitrogen atmosphere, at the flow of 50 mL min^{-1} . Rising temperature experiments were conducted at the temperature range from 25 to 400°C and heating rate of 10°C min^{-1} .

TGA analysis

Thermogravimetric analyses were performed in a TG apparatus (Shimadzu, Japan). Sample (2.0 mg) was heated at a rate of 10°C/min from ambient temperature to 200°C. Nitrogen was used as the purge gas at a flow rate of 20 ml/min.

LCMS analysis

The LC-MS analysis was carried out at Sai Life-sciences Pune, Maharashtra, India. 20 μL of compound (in methanol) was injected into the LC-MS and the mass spectra of the XMA was recorded. A mobile phase of methanol: water (40:60), at a flow rate of 0.2 mL min^{-1} for 60 min, was used for the separation on a BDS HYPERSIL C-18 (4.6×250 mm, 50 μm) 97 HPLC column. Mass spectra were obtained using ESI-Mass Spectrometer equipped with an electrospray ionization source, in positive ion mode under the flow of Helium gas at 1 mL min^{-1}

162 NMR analysis

163 XMA dried in a vacuum over P_2O_5 for 3 days, and then 20 mg of the sample was dissolved in 2.0 mL of D_2O . ^1H NMR and ^{13}C NMR spectrum recorded by AVANCE III 400MHz NMR spectrometer (Bruker Corporation, Switzerland). Chemical shifts were given in ppm.

169 In vitro antiaging activities analysis of XMA

169 Anti-collagenase enzyme assay

170 The assay employed was based on a spectrophotometric method with some modifications for use in a microplate reader. 50 μL trisine buffer solution (pH 7.5), 50 μL of samples with different concentrations and 50 μL of the enzyme (125 U/ml ChC) were added into 96-well microplate. To start the reaction 50 μL of 0.5 mM N-(3-[2-Furyl]-acryloyl)LeuGly-Pro-Ala (FALGPA) was added. The solution was then incubated for 20 minutes after the reaction started. The decrease of FALGPA absorbance was monitored at 340 nm in the microplate reader at a constant temperature of 25°C. Standard Catechin was used for comparison. Negative controls were performed with water.

165 Enzyme inhibition activity(%)

$$166 = \frac{[\text{Absorbance of negative control} - \text{Absorbance of sample}]}{\text{Absorbance of negative control}} \times 100$$

167 RESULTS AND DISCUSSION

168 Acetylenic fatty acids characterizations and structural analysis of XMAFT- IR spectra analysis

170 The IR spectrum is shown in Figure 1. The characteristic absorptions were performed in the range of 400– 4000 cm^{-1} by FT-IR spectra. The broad and intense absorption peak around 3458.48 cm^{-1} was attributed to the Bonded -OH stretching, and the weak band near 3107.43 cm^{-1} was due to the -C=CH. That also shown Absorbance at 2908.75 cm^{-1} for the Alkane-CH, 2222.07 cm^{-1} for -C \equiv C-, 1695.49 cm^{-1} for Acetic carbonyl-C=O. One stretching peaks at 1437.02 cm^{-1} were due to the presence

of -C=C-Aliphatic bond. The Absorbance at 1257.63 cm^{-1} was the indication of -C=O hetero atom. The band at 943.22 cm^{-1} could be assigned to the presence of -C=C-di-substituted olefinic. These absorption bands belonged to the characteristic functional groups of Acetylenic fatty acids.

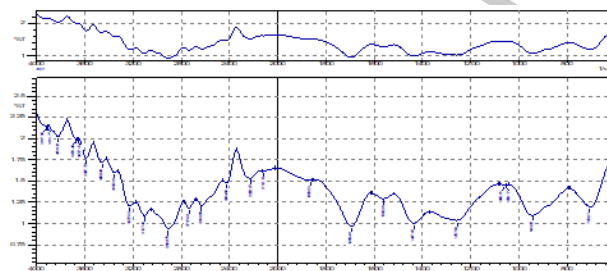


Figure 1: IR spectrum of XMA

186 XRD analysis

187 The X-ray diffractogram of XMA is shown in Figure 2. The interplanar spacing has been calculated using Bragg's equation given as; $n\lambda = 2d \sin\theta$, where θ is one half the angle read from the diffractogram. As presented in Figure 2, the sample shows strong peaks at approximately 8°, 11°, 14°, and 24° 2θ . However, other peaks between 18° and 19° 2θ , are very weak and unresolved or are shoulders on more intense peaks. The result of the XPRD corroborates that of XMA is present as a crystalline material.

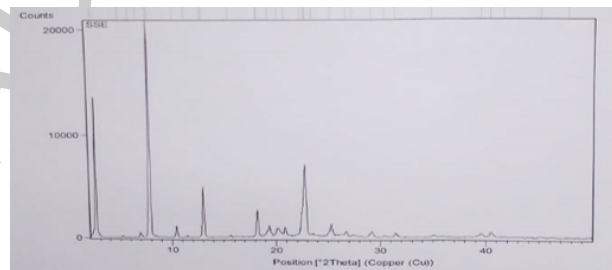


Figure 2: X-ray diffractogram of XMA

197 DSC analysis

198 Differential scanning calorimetry (DSC) was used to measure the occurrence of exothermal or endothermal changes with an increase in temperature. DSC, because of its sensitivity and accuracy, has been extensively used to study the phase transitions of polymers. The thermogram for XMA is shown in Figure 3. It shows that the XMA has both amorphous and crystalline portions. Glass transition (T_g) temperature occurred at 38.25°C while a melting peak was observed at about 39°C. One endothermic peak is exhibited by the sample corresponding to its melting point. The continuous (broad) endothermic transition that followed the glass transition is indicative of crystallite melting occurring over the glass transition range. The glass transi-

213 tion temperature (Tg) was also observed to be very
 214 high, indicating a high degree of crystallinity of the
 215 XMA. The knowledge of Tg is essential in produc-
 216 tion processes and storage as Tg is affected by mois-
 217 ture and other additives, facilitating conversion to
 218 the rubbery state and hence facilitating crystalliza-
 219 tion through molecular rearrangement. No decom-
 220 position of the sample was visible after melting, as
 221 there was no other exothermic event after 38.25°C,
 222 thus, indicating the absence of impurities.

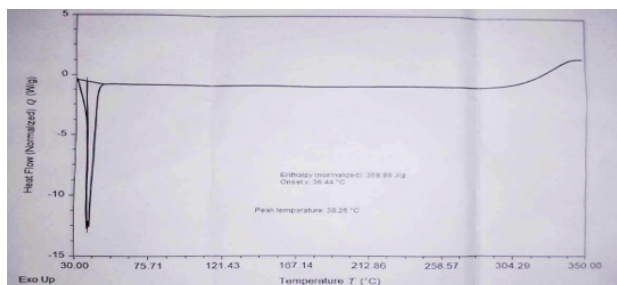


Figure 3: XRD thermogram for XMA

223 **TGA analysis**

224 The thermogravimetric analysis (TGA) was used to
 225 determine the weight loss of the material on heating.
 226 Transitions involving mass changes are detected by
 227 TGA as a function of temperature and time. The
 228 TG curve for the XMA shown in Figure 4, showed
 229 a thermal degradation occurs in three steps. The
 230 first step occurs between 150°C-250°C, a fast pro-
 231 cess with a mass loss of 54.17% was probably due
 232 to thermal decomposition of the compound with
 233 breaking of carboxylic acid linkage. The second step
 234 occurred between 250°C-300°C, where the mass
 235 loss of 8.319% was observed and the loss of 1.369%
 236 indicates the occurrence of the third step of degra-
 237 dation.

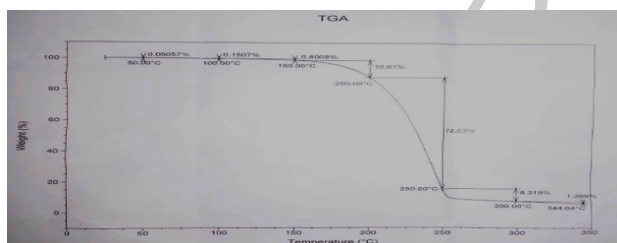


Figure 4: The thermogravimetric curve for the XMA

238 **LCMS analysis**

239 A mass spectrum is a plot of the relative abundance
 240 of a fragmented ion against the ratio of mass/charge
 241 of these ions. Using mass spectrometry, relative
 242 molecular mass (molecular weight) can be deter-
 243 mined with high accuracy and an exact molecu-
 244 lar formula can be determined with knowledge of
 245 places where the molecule has been fragmented. A

molecular formula shows data. It is a single charged
 246 compound. The molecular weight of the structure
 247 mentioned is 278. So M/Z for the assigned molecu-
 248 lar structure is 278 as charged on it is 1 shown in
 249 Figure 5. When LCMS did with an ESI source and sin-
 250 gle quadrupole analyzer, it is clearly shown M/Z is
 251 277, which is negative ionization mode i.e., M-H.
 252

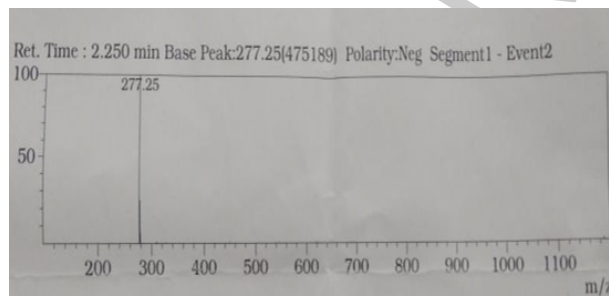


Figure 5: LCMS Spectra for XMA

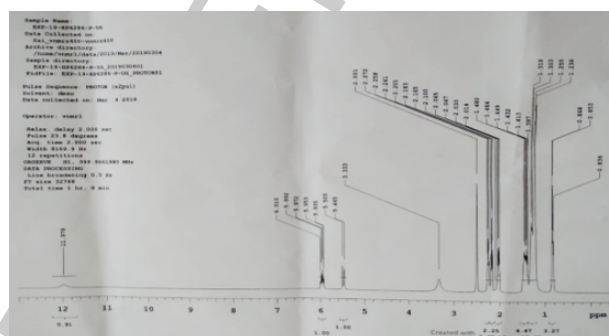
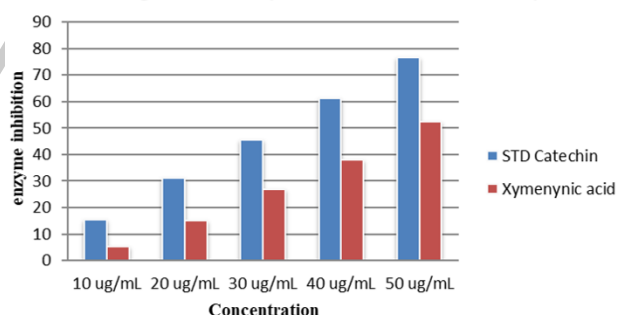


Figure 6: In vitro antiaging activities analysis of XMA

Collagenase enzyme inhibition activity



Graph 1: Graph of Collagenase enzyme inhibition activity of XMA

238 **NMR analysis**

239 NMR is primarily related to the magnetic proper-
 240 ties of certain atomic nuclei, notably the nucleus of
 241 the hydrogen atom, the proton, the carbon, and an
 242 isotope of carbon. NMR spectroscopy has enabled
 243 many researchers to study molecules by recording
 244 the differences between the various magnetic nuclei
 245 and thereby giving a clear picture of what the posi-
 246

Table 1: Collagenase enzyme inhibition activity of XMA

Collagenase enzyme inhibition activity (Percentage %)			
Concentration	Negative Control	STD Catechin	Xymenynic acid
10 ug/mL	NA	15.42	5.19
20 ug/mL	NA	30.99	15.11
30 ug/mL	NA	45.50	27.02
40 ug/mL	NA	61.22	37.86
50 ug/mL	NA	76.79	52.37

tions of these nuclei are in the molecule. Moreover, it will demonstrate which atoms are present in neighboring groups. Proton NMR spectrum is shown in Figure 6 indicates the presence of carboxylic acid proton atom at 11.978ppm. The NMR spectrum also indicates unsaturation at 6.010ppm and 5.505 ppm due to butylenic and methylene proton atom, respectively. Presence alkynyl proton atoms at chemical shift (δ) value of 2.501 ppm and 3.333ppm while 1.413ppm-2.272ppm chemical shift value indicates the presence of allylic proton atoms. The δ value of 0.836ppm-1.319ppm shows the presence of alkyl primary proton atoms in the molecule.

275 **Anti-collagenase enzyme assay**

276 Collagen, the major component of the skin, is
277 degraded by the enzyme collagenase. Inhibition of
278 collagenase activity delays the process of forming
279 pre-collagen fibers and, subsequently, the wrinkling
280 process. Isolated XMA inhibited the enzyme by more
281 than 50%, at a concentration of 50 ug/ml (Table 1
282 and Graph 1).

283 **CONCLUSIONS**

284 In the present research, the XMA was successfully
285 isolated and purified from *Santalum album* seed.
286 Chemical characterization and structural elucidation
287 were done by FTIR, NMR and LCMS. The isolated
288 XMA was pure crystalline powder and relatively
289 stable below 150°C checked through DSC,
290 XRD and TGA. XMA was successfully isolated in a
291 pure crystal form and that isolated crystals were
292 characterized by FTIR, DSC and TGA, indicating no
293 impurities and were used for further phytochemical
294 screening. While determining Structural properties,
295 the XRD pattern of the isolated compound matched
296 with the standard pattern of XMA and structure of
297 XMA was confirmed as that of Xymenynic acid by
298 1D and 2D-NMR spectroscopic methods. Analysis
299 of isolated XMA revealed its purity 99.1%, with a
300 good yield value of 2% - 5% and considering the
301 purity that was the acceptable range of the yield
302 value of the isolated Xymenynic acid to be claimed

as API. In addition, the results of antiaging activities suggested XMA had stronger antiaging activities in a concentration-dependent manner, which indicated that XMA had the potential as a novel natural antiaging in functional food. In future research, the detailed structure of XMA needs further study.

309 **Authors' contribution**

Rakesh Shivatare, Ramesh Musale, Priya Lohakare and Dipika Patil's contribution included collecting samples, designing and performing laboratory work, whereas the Durga Choudhary, Dr. Gayatri Ganu analyzing the results, and preparing the paper. Dr. Dheeraj Nagore, Dr. Shailesh Kewatkar's contribution included data interpretation and identification of the compounds. All the authors have read the final manuscript and approved the submission.

319 **Conflicts of interest**

The authors declare no conflicts of interest.

321 **ACKNOWLEDGEMENT**

322 The authors gratefully acknowledge the financial
323 support provided by Sai Lifesciences. We thank Dr.
324 D. Y. Patil Institute of Pharmaceutical Research and
325 sciences, Pimpri, India for discussion and identification
326 of plant materials. We also acknowledge Sai
327 Lifesciences Pune for the analysis of isolated samples.
328

329 **REFERENCES**

- 330 Agnihotri, S., Tamrakar, K. 2017. Phytochemical
331 Investigation of Santalum album Leaves and
332 Fruits. International Journal of Scientific and
333 Research Publications, 7(7):529–533.
- 334 Aitzetmüller, K., Matthäus, B., Friedrich, H. 2003.
335 A new database for seed oil fatty acids - The
336 database SOFA. European Journal of Lipid Science
337 and Technology, 105:123–127.
- 338 Bapat, V. A., Rao, P. S. 1988. Sandalwood plantlets
339 from "Synthetic seeds". Plant Cell Reports,
340 7(6):434–436.

- 341 Carballeira, N. M. 2008. New advances in fatty acids
342 as antimalarial, antimycobacterial and antifungal
343 agents. *Progress in Lipid Research*, 47(1):50–61.
- 344 Chang, R. C., So, K. F., Y-S, H., . C. 2010. Anti-aging
345 herbal medicine-How and why can they be used
346 in aging-associated neurodegenerative diseases?
347 *Ageing Research Reviews*, 9(3):354–362.
- 348 Christensen, H. 2001. What Cognitive Changes can
349 be Expected with Normal Ageing? *Australian
350 & New Zealand Journal of Psychiatry*, 35(6):768–
351 775.
- 352 Guo, H., Zhang, J., Gao, W., Qu, Z., Liu, C. 2014. The
353 anti-diarrhoeal activity of methanol extract of *San-
354 talum album* L. in mice and gastrointestinal effect
355 on the contraction of isolated jejunum in rats. *Jour-
356 nal of Ethnopharmacology*, 154(3):704–710.
- 357 Harman, D. 1998. Aging: phenomena and theo-
358 ries. *Annals of the New York Academy of Sciences*,
359 854(1):1–7.
- 360 Howes, M.-J. R., Simmonds, M. S. J., Kite, G. C. 2004.
361 Evaluation of the quality of sandalwood essential
362 oils by gas chromatography-mass spectrometry.
363 *Journal of Chromatography A*, 1028(2):307–312.
- 364 Hussain, J., Rehman, N. U., Al-Harrasi, A., Ali, L., Khan,
365 A. L., Albroumi, M. A. 2013. Essential oil compo-
366 sition and nutrient analysis of selected medicinal
367 plants in the Sultanate of Oman. *Asian Pacific Jour-
368 nal of Tropical Disease*, 3(6):421–428.
- 369 Kim, T. H., Ito, H., Hatano, T., Takayasu, J., Tokuda,
370 H., Nishino, H., Yoshida 2006. New antitumor
371 sesquiterpenoids from *Santalum album* of Indian
372 origin. *Tetrahedron*, 62(29):6981–6989.
- 373 Konczak, I., Zabarar, D., Dunstan, M., Aguas, P.
374 2010. Antioxidant capacity and hydrophilic phy-
375 tochemicals in commercially grown native Aus-
376 tralian fruits. *Food Chemistry*, 123(4):1048–1054.
- 377 Pan, S. Y., Zhou, S. F., Gao, S. H., Yu, Z. L., Zhang,
378 S. F., Tang, M. K., Ko, K. M. 2013. New Perspectives
379 on How to Discover Drugs from Herbal Medicines:
380 CAM's Outstanding Contribution to Modern Ther-
381 apeutics. *Evidence-Based Complementary and
382 Alternative Medicine*, pages 1–25.
- 383 Pasha, M. K., Ahmad, F. 1993. Synthesis of oxy-
384 genated fatty acid esters from santalbic acid ester.
385 *Lipids*, 28(11):1027–1031.

In vitro Antioxidant Activity and Stability Indicating High-performance Thin-layer Chromatographic Method for Ximenynic Acid in *Santalum album* Seed Extract

Rakesh S. Shivatare¹, Ramesh Musale¹, Priya Lohakare¹, Dipika Patil¹, Durga Choudhary², Gayatri Ganu³, Dheeraj H. Nagore^{3,4}, Sohan Chitlange⁵, Shailesh M. kewatkar⁶

¹Research Scholar, Department of Pharmaceutical Sciences, JJT University, Jhunjhunu, Rajasthan, India,

²Research Associate, Department of Regulatory, Mprex Healthcare, Pune, Maharashtra, India, ³Vice President Clinical Research, Mprex Healthcare, Maharashtra, Pune, India, ⁴Research Guide, JJT University, Jhunjhunu, Rajasthan, India, ⁵Principal, Dr. D. Y. Patil Institute of Pharmaceutical Research and Sciences, Pune, Maharashtra, India, ⁶Department of Pharmacognosy, Rajarshi Shahu College of Pharmacy, Buldana, Maharashtra, India

Abstract

Introduction: Due to emergent concern about the unhealthy consequences of chemicals in the health industry, the interest toward natural and herbal substances have been growing every day; though, regrettably they possess several quality control issues. In this study, the antioxidant effect of *Santalum album* seed extract was evaluated. Furthermore, discover effortless, accurate, responsive, and stability-indicating high-performance thin-layer chromatographic (HPTLC) assay method for the detection and quantification of ximenynic acid in *S. album* seed extract. **Materials and Methods:** Antioxidant activity was evaluated by 2, 2-diphenyl-1, 1-picrylhydrazyl (DPPH) radical scavenging method. The HPTLC method contains aluminum plates precoated with silica gel 60 F254 as a stationary phase. The mobile phase was a combination of toluene: chloroform:methanol: formic acid (2:5:0.3:0.3 v/v/v/v). Densitometric analysis of ximenynic acid was carried out in the absorbance mode at 550 nm using Camag thin-layer chromatography scanner-3. **Results:** Antioxidant potential was observed in DPPH scavenging assay ($EC = 4.0 \pm 0.02$ mg/mL) and by *S. album* seed extract. The HPTLC method was validated as per the ICH guidelines for specificity, precision, linearity, robustness, and accuracy. The method was established to give dense and symmetrical band for ximenynic acid at retention factor 0.45 ± 0.02 . The repeatability of the method was found to be 1.25 relative standard deviations and recovery values from 99.94 to 100.10% for ximenynic acid. **Conclusion:** These findings indicate that *S. album* seed extract may have antioxidant potential. Statistical analysis confirmed that the projected method is repeatable, selective, and accurate for estimating the content of ximenynic acid. Since the projected mobile phase successfully resolves the ximenynic acid, this HPTLC method can be useful for identification and quantitation of these phytochemicals in herbal extracts and pharmaceutical dosage form.

Key words: Antioxidant activity, high-performance thin-layer chromatographic, *Santalum album*, ximenynic acid

INTRODUCTION

Herbal medicine plays an important role in the health care of many urbanized, developing countries. The use of herbal products is increasing worldwide due to the distinct advantages.^[1] Nearly 80% of African and Asian population depend on traditional medicines for their primary health care.^[2] These medicines are readily available in the market from health food stores without prescriptions.^[3]

In general, it is believed that the risk associated with herbal drugs is very less, but reports on serious reactions are

Address for correspondence:

Rakesh S. Shivatare, Research Scholar, JJT University, Jhunjhunu, Rajasthan, India. Phone: +91-9890250523.
E-mail: rakeshshivatare@gmail.com

Received: 07-08-2019

Revised: 28-10-2019

Accepted: 08-11-2019

indicating the need for development of effective marker systems for identification of the individual components.^[4] Consistency, stability and quality control for herbal drugs is possible, but difficult to achieve. Further, the guideline of these drugs is not standardized across all countries. There is variation in the methods used transverse medicine systems and countries in achieving stability and quality control.^[5,6]

Santalum album L. (*Santalaceae*), namely Sandalwood, given great respect as “Green Gold,” is a traditional hemiparasitic tree and has an extensive record in Indian religious rituals and traditional Chinese medicine.^[7] Their essential oil (sandalwood oil) is broadly used in the cosmetic, perfumery, and aromatherapy industries and has been reported to have diverse biological properties such as antiviral, anticarcinogenesis, and antitumor effects.^[8] The herb is stated to have α -santalol, β -santalol, α -santalone, β -santalone, α -santalalene, β -santalalene, α -curcumene, and tricycloekasantal.^[9,10] The seed oil of *S. album* is shadowy red viscid fixed oil containing santalbic acid (or ximenynic acid) and stearolic acid (9-octadecynoic acid).^[7,11,12] Ximenynic acid, octadeca-11-trans-en-9-ynoic acid, is one of the few acetylenic fatty acids taking place at higher levels in plant seed oils.^[13] In universal, ximenynic acid exhibits many biological activities and pharmacological effects, including antibacterial, antifungal, and anti-inflammatory activities.^[14,15]

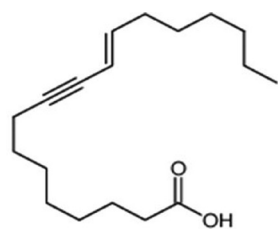
In a present study, the quality assessment *S. album* seed extract was carried out by doing *in vitro* antioxidant activity with their fingerprinting using thin-layer chromatography (TLC). However, in the current literature antioxidant potential and high-performance TLC (HPTLC) method were not stated. Looking at the advantages of HPTLC method, such as, is an inexpensive analytical apparatus because of its less operating price, high sample throughput, and need for minimum sample clean-up. It was thought, needful to develop HPTLC method for analysis of ximenynic acid in formulations.

MATERIALS AND METHODS

Chemicals and reagents

Standard ximenynic acid was purchased from Sami Lab India and used without additional purification, due to its high purity, at least 99.12%. The molecular structure of the ximenynic acid is given in Table 1. 2,2-diphenyl-1-picrylhydrazyl (DPPH), butylated hydroxyl toluene (BHT), and Vitamin C were purchased from Merck Co. (Mumbai, India). Purified water (Millipore Equipment, France) was used to prepare the stock solution. Analytical-reagent grade solvents such as toluene, chloroform, formic acid, anisaldehyde reagent, and methanol were obtained from Merck Ltd., India. As stationary phases, the following plate (Merck) was used: HPTLC aluminum

Table 1: Chemical properties of ximenynic acid^[16]

Molecule	Ximenynic acid
CAS number	557-58-4
Chemical formula	C ₁₈ H ₃₀ O ₂
IUPAC name	(E)-octadec-11-en-9-ynoic acid
Representation	
Molecular weight	278.43
Appearance	White powder

plates precoated with silica gel 60F₂₅₄ (20 cm × 20 cm, 0.2 mm thickness).

Plant material

The seed extract of *S. album* (Batch number: C182203) was obtained from Sami Lab India. Which are manufactured in November 2018 and expired in October 2019.

DPPH radical scavenging activity

The free radical scavenging capacity of seed extract of *S. album* was determined using the established DPPH method. To obtain an indication of the antioxidant activity of *S. album* seed extraction, 5 mL of a freshly prepared 0.004% of DPPH in methanol was mixed with 50 μ L of different concentration 5, 10, 15, 25, 35, and 50 mg/mL of each sample and the absorbance of each dilution after 30 min was measured at 517 nm. BHT and Vitamin C were the antioxidant used as a positive control.^[17]

All tests were performed in triplicate and the methanol was used as a blank solution. The percentage DPPH reduction (or DPPH radical scavenging capacity) was calculated as:

$$\% \text{ Reduction} = (\text{Abs DPPH} - \text{Abs Dil.}) / \text{Abs DPPH} \times 100$$

Whereby:

Abs DPPH = Average absorption of the DPPH solution,

Abs Dil. = Average absorption of the three absorption values of each dilution.

Statistical analysis

The statistical analyses were performed using the Prism software. Values were compared to control using analysis of variance (ANOVA) followed by Tukey multiple comparison test.

Simultaneous quantification of ximenynic acid using HPTLC

Preparation of standard solution of ximenynic acid

Standard stock solution was prepared by dissolving 30 mg of ximenynic acid into 100 mL volumetric flask. Added 70 mL of methanol and sonicated to dissolve. Make up the volume to 100 mL with methanol and mixed well, which yields a solution of concentration 300 ppm and was used as working standard for the analysis.

Preparation of test solution for analysis

Weighed and dissolved *S. album* seed extract equivalent to 30 mg of ximenynic acid into 100 mL volumetric flask. Added 70 mL of methanol and sonicated to dissolve. Make up the volume to 100 mL with methanol and mixed well.

Chromatographic conditions and instrumentation

A Camag HPTLC system consisting of Linomat V automatic sample applicator with Camag TLC Scanner 3 and Camag WinCAT software was used for the detection and quantification of ximenynic acid in the formulations. The samples were speckled in the form of band of width 6 mm with CAMAG 100 μ L syringe on precoated silica gel 60F₂₅₄ aluminum plate (20 cm \times 10 cm or 10 cm \times 10 cm with 0.2 mm thickness) using Linomat 5 applicator CAMAG (Switzerland) built-in with a CAMAG 100 μ L syringe. The volume applied on each track was 5 μ L. The ascending development was carried out in the mobile phase toluene:chloroform:methanol:formic acid (2:5:0.3:0.3 v/v/v/v) in a CAMAG twin trough chamber (20 cm \times 10 cm). The optimized chamber saturation time for the mobile phase was 15 min at room temperature (25 \pm 2°C). The length of the chromatogram run was just about 80 mm. After development, plates were dried by dryer and sprayed with anisaldehyde reagent as derivatization reagent. Again the plates were air-dried after development in a current of air. The densitometric scanning was performed using CAMAG TLC scanner-3 (Switzerland) operated by win CATS software V 1.4.3.6336 at 550 nm after derivatization. The slit dimension was 5 mm \times 0.45 mm with a scanning speed of 20 mm/s. The HPTLC chromatographic condition are shown in Table 2. The amount of ximenynic acid present in the samples was evaluated by peak area with linear regression.

Calibration curve and linearity

The acceptability of linearity data is often evaluated by examining the correlation coefficient and intercept of the linear regression line for the response versus concentration plot. The stock solution of ximenynic acid was diluted to five different concentrations between 50% and 150% of working concentration. The plate was developed and analyzed to engender the calibration equation for quantification of ximenynic acid in samples. The curves demonstrated coefficient of correlation (r^2) \geq 0.9996.

Table 2: Chromatographic condition

Chromatographic condition	Details
Saturation time	15 min
Plate activation	At 105°C for 5 min
Mobile phase chamber	Twin through chamber (10 \times 10 and 20 \times 10)
Wavelength detection	550 nm after derivatization
Derivatization reagent	Anisaldehyde reagent
Photo documentation	At white R light
Application volume	5 μ L
Retention factor	0.45
Type of application	Band type
Room temperature	22°C at the time of experimentation
Storage conditions of sample and STD	At 2–8°C and in dark chamber
Diluent	Methanol

Method validations^[18-21]

Validation of the analytical method was done according to the International Conference on Harmonization guideline. The method was validated for specificity, solution stability, recovery, robustness, and precision.

Specificity

Specificity was ascertained by applying 5 μ L band of standard, blank, and sample solutions on the HPTLC plates. The bands for ximenynic acid from sample solutions were authenticated by comparing the retention factor (Rf) and spectra of the bands to those of the standards. The peak purity of ximenynic acid was analyzed by comparing the spectra at three different levels, i.e., at peak start, peak apex, and peak end positions of the spot. The sensitivity of measurement was anticipated in terms of the limit of quantification (LOQ) and the limit of detection (LOD). The LOQ and LOD were calculated by the use of equations $LOD = 3 \times N/B$ and $LOQ = 10 \times N/B$ where N is the standard deviation of the peak area of the drug ($n = 3$), taken as a measure of noise and B is the slope of the corresponding calibration plot.

Precision

The precision of the developed method was studied by performing system, method, and intermediate precision studies. The sample application and measurement of peak area were resolute by performing six replicate measurements of the same band using a sample solution containing 300 ppm of ximenynic acid.

Solution stability

The sample solution and standard solution were prepared as per the proposed method and subjected to stability study at room temperature for 6 h. The change in response of ximenynic acid in sample solution with respect to time is calculated as an absolute percent difference against initial response.

Robustness

The volume of the mobile phase, polar solvent volume, and saturation time was involved in this study. The effect of these changes on both the R_f values and peak areas was evaluated by calculating the relative standard deviations (RSD) for each parameter.

Table 3: DPPH scavenging activity of extract

Samples	% EC50 (mg/mL)		
	Seed extract (50 mg/mL)	Vitamin C	BHT
1	4.1*	2.2**	2.0**
2	3.8*	2.1**	1.9***
3	3.9*	1.9***	1.9***
Mean	4.0*	2.0***	2.0***

Results are expressed as mean standard error of mean ($n=6$), one-way analysis of variance followed by Tukey multiple comparison test. * $P<0.05$, ** $P<0.01$, *** $P<0.001$. When compared with control groups. DPPH: 2,2-diphenyl-1-picrylhydrazyl, BHT: Butylated hydroxyl toluene

Table 4: Result of linearity of xymenynic acid

Conc. of xymenynic acid (ppm)	Average peak area of xymenynic acid
150	3254
200	4282
300	6245
350	7365
450	9456

Table 5: Result of method precision and intermediate precision study

S. No.	Peak area of xymenynic acid	Assay (% W/W, method precision)	Assay (% W/W, intermediate precision)
1.	6155	100.91	101.10
2.	6258	98.29	100.17
3.	6139	101.09	98.96
4.	6287	98.53	100.23
5.	6123	98.71	100.50
6.	NA	99.09	101.75
Average	6192.4	99.44	100.45
% RSD	1.21	1.25	0.94
Overall % RSD	NA		1.17

RSD: Relative standard deviations

Accuracy (recovery)

Accuracy of the method was ascertained by spiking the preanalyzed samples with a known amount of ximenynic acid (80, 100, and 120%). The average percentage recovery was estimated by applying values of peak area to the regression equations of the calibration graph.

RESULTS AND DISCUSSION**DPPH radical scavenging activity**

DPPH is a stable free radical and accepts an electron or hydrogen radical to become a stable diamagnetic molecule. In the DPPH assay, the antioxidants are able to reduce the stable radical DPPH to non-radical form, DPPH-H. The purple-colored alcoholic solution of DPPH radical changes to yellow in the presence of hydrogen-donating antioxidant which could be measured at 517 nm, the activity is expressed as effective concentration EC₅₀, which is the concentration of the sample leading to 50% reduction of the initial DPPH concentration.^[17] Table 3 shows the DPPH scavenging activity of *S. album* seed extract, BHT and Vitamin C at different concentrations, as assayed by DPPH (EC₅₀ mg/mL). The effectiveness of antioxidant properties is inversely correlated with EC₅₀ values. If the EC₅₀ value of an extract <10 mg/mL, that is, mean the extract is an effective antioxidant.^[22] In this study, the EC₅₀ value of *S. album* seed extract was 5 mg/mL <50 mg/mL this indicates that the samples have effective antioxidant activity.

Method optimization for the HPTLC-densitometric measurements

Like so many other unusual fatty acids, ximenynic acid is a distinguishing constituent of the seed oils of only a few closely related plant families. It comes about in the order *Santalales*, i.e., in the traditional “Santalalean” plant families *Santalaceae*, *Olacaceae*, and *Opiliaceae* and has never been found outside the *Santalales*.^[23-25]

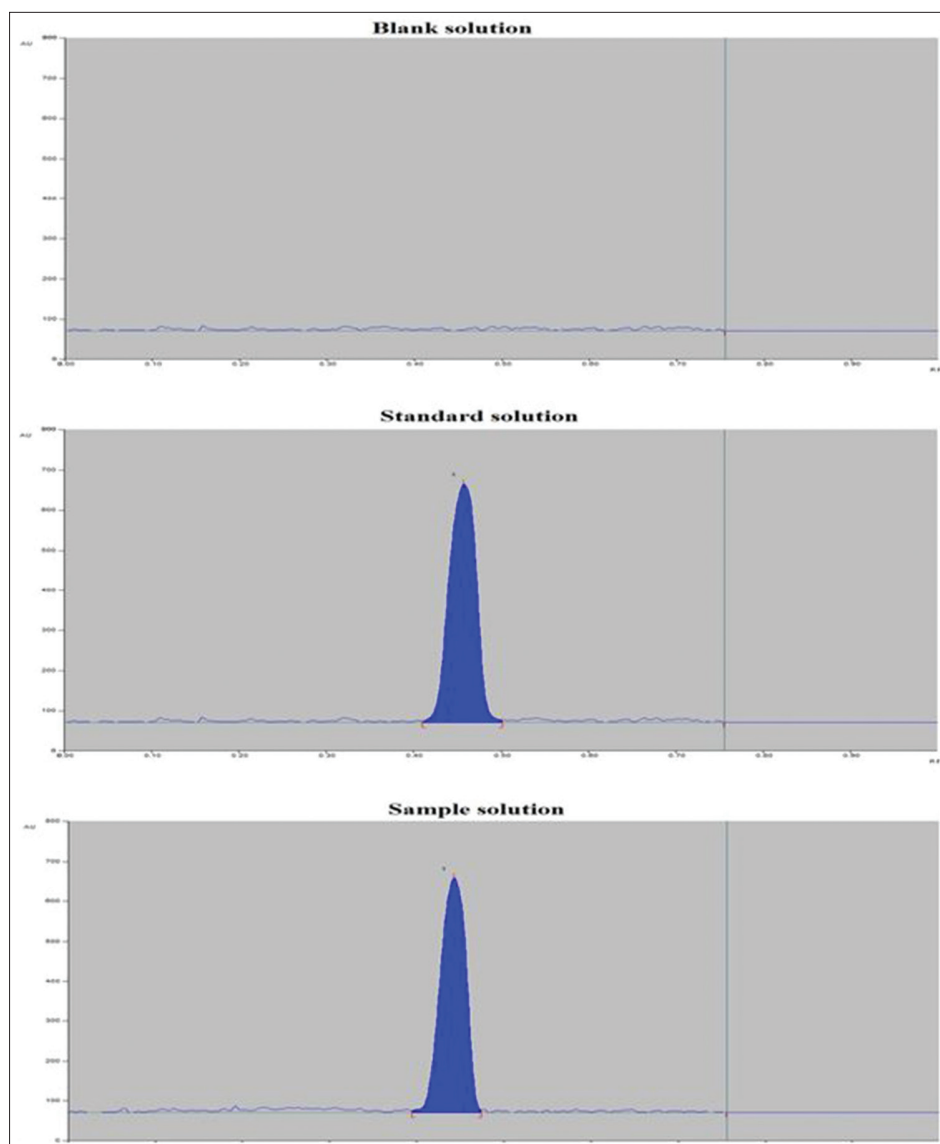


Figure 1: High-performance thin-layer chromatography of blank solution, standard solution, and sample solution

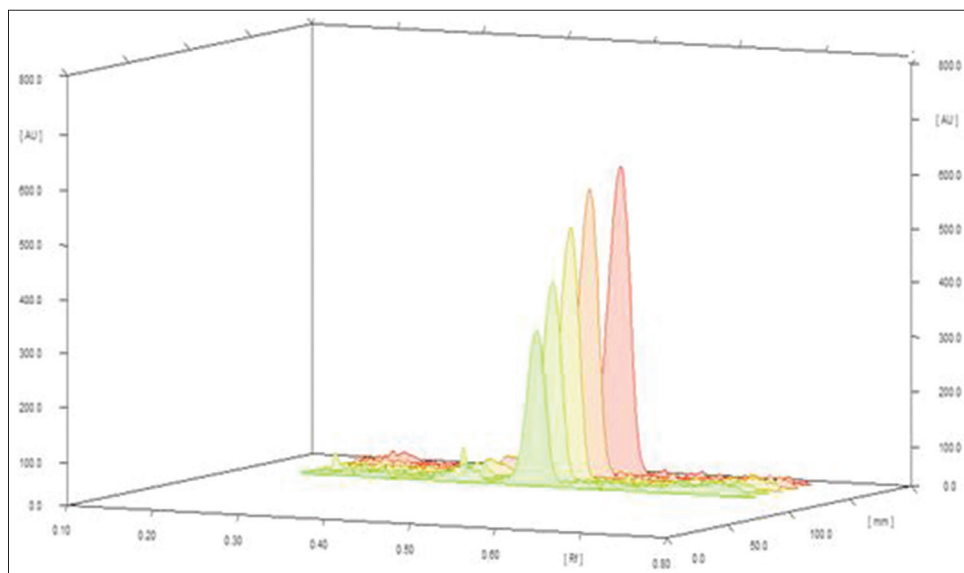


Figure 2: Three-dimensional linearity graph for ximenynic acid

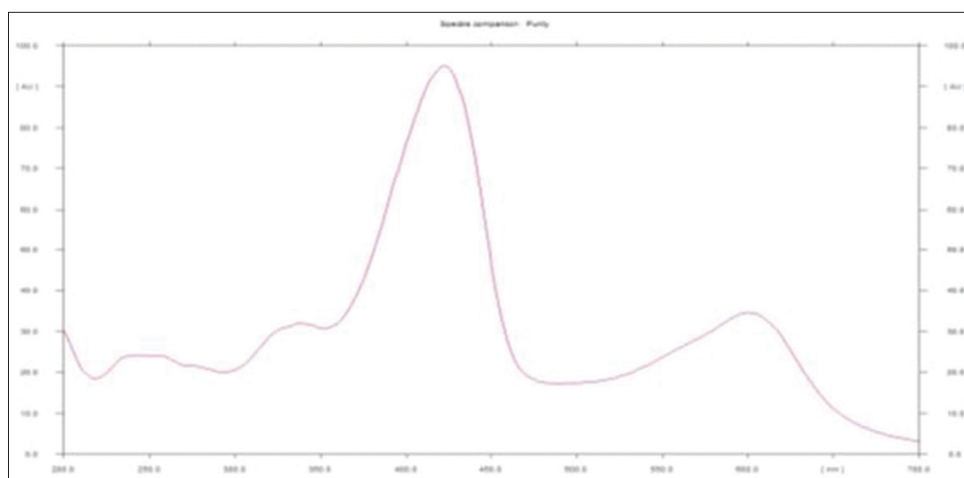


Figure 3: Spectra of xymenynic acid from STD

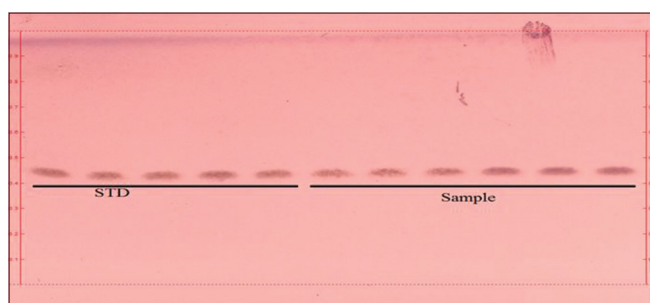


Figure 4: Three-dimensional chromatographs of method precision and intermediate precision study

The HPTLC method was optimized with a sight to develop a stability-indicating assay method. Different composition of the mobile phase for reversed-phase-HPTLC analysis was experimented with a goal to obtain high resolution and reproducible peaks. The required objective was achieved using toluene:chloroform:methanol:formic acid (2:5:0.3:0.3 v/v/v/v) mobile phase. It gave impenetrable, compact, and well-alienated spots of the drug. This mobile phase showed good resolution of ximenynic acid peak from the extract of *S. album*. The wavelength of 550 nm after derivatization was found to be optimal for the highest sensitivity. Sharp and well-defined peaks for the ximenynic acid were obtained at $R_f 0.45 \pm 0.02$. The present method is faster as the time needed for development of plate is reduced considerably to $< \frac{1}{2}$ h for chamber saturation. At this wavelength, the ximenynic acid showed optimum response [Figure 1].

Method validation

Calibration curve and linearity

A calibration curve was constructed by plotting peak area against the concentration of ximenynic acid (ppm). The results of linearity are shown in Table 4. They confirm the linearity of the standard curves over the range studied (150–450 ppm). Linear regression of concentration

Table 6: Result of robustness study for xymenynic acid

Robustness parameter	% RSD	Rt	Peak purity
Saturation time (minute)			
14	1.25	0.45	Pass
15	1.36	0.45	Pass
16	1.75	0.45	Pass
Polar solvent volume (Formic acid)			
0.4	1.96	0.44	Pass
0.5	1.25	0.45	Pass
0.6	1.25	0.46	Pass
Mobile phase volume			
9	1.63		Pass
10	1.27		Pass
11	1.96		Pass

RSD: Relative standard deviations

versus peak area plots resulted in an average coefficient of determination (r^2) > 0.999 . The average equation for calibration curves was $y = 20.63x + 135.3$. The 3-D chromatographs of all calibration concentrations are shown in Figure 2, respectively.

Specificity and sensitivity

The outcome of spectral comparison for ximenynic acid was found to be specific at peak start (S), peak apex (M), and peak-end (E), respectively. The ultraviolet spectra of the standards are presented in Figure 3. The intimacy of peak purity values to one indicates that the spots were only attributed to a single compound. By comparing the photos and chromatograms of the blank solution, standard solution, and sample solution, it was observed that no peak was coeluted with the analyte band from bank solution. LOD and LOQ were found to be 8 ppm and 25 ppm, respectively. Hence, the method was found to be highly sensitive for determination of MIL.

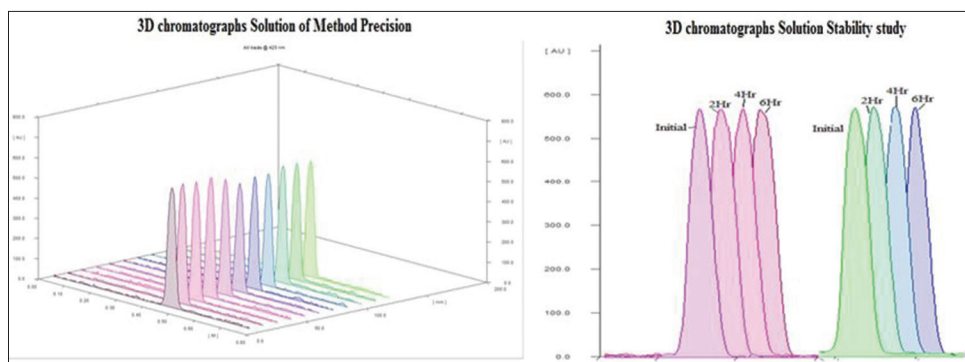


Figure 5: Three-dimensional chromatographs of method precision and solution stability study

Table 7: Result of accuracy study for xymenynic acid

Band	Sample	Recovery levels (%)	STD wt. (spiked)	Amount recover	% recovery	Average % recovery
1.	Sample 1	80	24.13	24.06	99.71	99.94
2.	Sample 2	80	24.06	24.05	99.96	
3.	Sample 3	80	24.05	24.09	100.17	
4.	Sample 1	100	30.14	30.16	100.07	100.11
5.	Sample 2	100	30.02	30.18	100.53	
6.	Sample 3	100	30.13	30.05	99.73	
7.	Sample 1	120	36.12	36.13	100.03	100.10
8.	Sample 2	120	36.05	36.17	100.33	
9.	Sample 3	120	36.05	36.03	99.94	

Precision

System, method, and intermediate precision of the developed method were articulated in terms of RSD of the peak area [Figure 4]. The consequences showed that the system, method, and intermediate variations of the results at concentration of 300 ppm for ximenynic acid were within the acceptable range [Figure 5]. The coefficients of variation for system, method, and intermediate precision of the method were found to be <1.21%. The ximenynic acid was also analyzed by two different analysts within the same day, and the results revealed that there is good intermediate precision between analysts [Table 5].

Solution stability

There was no significant divergence in peak area of ximenynic acid (RSD <1.5%) observed on analysis up to 6 h. No decomposition of the drug was observed during chromatogram development. These observations suggest that the drug is stable under the typical processing and storage conditions of the analytical procedure [Figure 5].

Robustness

The results obtained in the new conditions (variation in composition mobile phase, polar solvent volume, and saturation time) were in accordance with the original results, as shown in Table 6, though the R_f varied very slightly (0.45 ± 0.1). The % RSD values for peak area were <1.0

indicating the highly robust nature of the developed method. The low RSD values indicate the robustness of the method [Table 6].

Accuracy (recovery)

The developed method showed high and reliable recoveries at all studied levels. The percentage recovery of ximenynic acid at all three levels was found to be satisfactory [Table 7]. For ximenynic acid, the % recovery was found between 99.94% and 100.10%.

CONCLUSION

The seed extract of *S. album* exhibited antioxidant activity as manifested through DPPH radical scavenging. An extensive literature assessment revealed that the xymenynic acid is currently available for the treatment of skin. In this research HPTLC method for determination of xymenynic acid was developed, as there is no official HPTLC method reported in major pharmacopeias such as USP, EP, JP, BP, and IP. A stability-indicating HPTLC method was developed and validated for the determination of xymenynic acid in seed extract on pre-coated silica gel HPTLC plates using toluene:chloroform:methanol:formic acid (2:5:0.3:0.3 v/v/v/v) as the mobile phase with densitometric detection at 550 nm after derivatization. With virtue of the results obtained, the present method is precise, specific,

accurate stability-indicating assay method. The method can reduce the cost of reagents and time for analysis. It also utilized the advantage of applying numerous sample spots on HPTLC plate, which may be more beneficial for regulatory quality control laboratories particularly to facilitate the post-marketing surveillance program. In addition, the method is economical and not requires certain types of stationary phases.

REFERENCES

- Sahoo N, Manchikanti P, Dey SH. Herbal drug patenting in India: IP potential. *J Ethnopharmacol* 2011;137:289-97.
- Sahoo N, Manchikanti P, Dey SH. Herbal drugs: Standards and regulation. *Fitoterapia* 2010;81:462-71.
- Wal P, Wal A, Gupta S, Sharma G, Rai AK. Pharmacovigilance of herbal products in India. *J Young Pharm* 2011;3:256-8.
- Farah MH, Olsson S, Bate J, Lindquist M, Edwards R, Simmonds MS, *et al.* Botanical nomenclature in pharmacovigilance and a recommendation for standardization. *Drug Saf* 2006;29:1023-9.
- Kirtikar KR, Basu BD. *Indian Medicinal Plants*. 2nd ed., Vol. 1. Delhi: Periodical Expert Book Agency; 1984. p. 293.
- Hazra AK, Chakraborty B, Mitra A, Sur TK. A rapid HPTLC method to estimate piperine in C formulations containing plant ingredients of Piperaceae family. *J Ayurveda Integr Med* 2018;2018:1-7
- Agnihotri S, Tamrakar K. Phytochemical investigation of *Santalum album* leaves and fruits. *Int J Sci Res Pub* 2017;7:529-33.
- Kim TH, Ito H, Hatano T, Takayasu J, Tokuda H, Nishino H, *et al.* New antitumor sesquiterpenoids from *Santalum album* of Indian origin. *Tet* 2006;62:6981-9.
- Howes MJ, Simmonds MS, Kite GC. Evaluation of the quality of sandalwood essential oils by gas chromatography-mass spectrometry. *J Chromatogr A* 2004;1028:307-12.
- Guo H, Zhang J, Gao W, Qu Z, Liu C. Anti-diarrhoeal activity of methanol extract of *Santalum album* L. In mice and gastro intestinal effect on the contraction of isolated jejunum in rats. *J Ethnopharmacol* 2014;154:704-10.
- Jha N. *Santalum album*: Sandalwood. Poland: Phytopharm; 2008. p. 3-12.
- Pasha MK, Ahmad F. Synthesis of the oxygenated fatty acid ester from santalbic acid ester. *Lipids* 1993;28:1027-31.
- Aitzetmuller K, Matthus B, Friedrichc H. Potential uses of the seed oil fatty acids database SOFA. *Eur J Lipid Sci Technol* 2003;105:92-103.
- Carballeira NM. New advances in fatty acids as antimalarial, antimycobacterial and antifungal agents. *Prog Lipid Res* 2008;47:50-61.
- Konczak I, Zabarás D, Dunstan M, Aguas P. Antioxidant capacity and hydrophilic phytochemicals in commercially grown native Australian fruits. *Food Chem* 2010;123:1048-54.
- Ximenynic Acid; 2019. Available from: https://www.pubchem.ncbi.nlm.nih.gov/compound/Ximenynic_acid. [Last accessed on 2019 Jan 05].
- Lee YL, Jian SY, Lian PY, Man JI. Antioxidant properties of extracts from a white mutant of the mushroom *Hypsizygus marmoreus*. *J Food Compos Anal* 2008;21:116-24.
- IFPMA. International Conference on Harmonization (ICH) of Technical Requirements for Registration of Pharmaceuticals for Human use, Harmonized Tripartite Guideline on Validation of Analytical Procedures: Text and Methodology Q2 (R1), Complementary Guideline on Methodology incorporated. Geneva: ICH Steering Committee, IFPMA; 2005.
- Shewiyo DH, Kaaleb E, Rishab PG, Dejaegherc B, Verbekec JS, Heydenc YV. HPTLC methods to assay active ingredients in pharmaceutical formulations: A review of the method development and validation steps. *J Pharm Biomed Anal* 2012;66:11-23.
- Thomas AB, Patil SD, Nanda RK, Kothapalli LP, Bhosle SS, Deshpande AD. Stability-indicating HPTLC method for simultaneous determination of nateglinide and metformin hydrochloride in pharmaceutical dosage form. *Saudi Pharm J* 2011;19:221-31.
- Kasaye L, Hymete A, Mohamed AI. HPTLC-densitometric method for simultaneous determination of salmeterol xinafoate and fluticasone propionate in dry powder inhalers. *Saudi Pharm J* 2010;18:153-9.
- Stoilova I, Krastanov A, Stoyanova A, Denev P, Gargova S. Antioxidant activity of a ginger extracts (*Zingiber officinale*). *Food Chem* 2007;102:764-70.
- Angiosperm Phylogeny Group. An update of the angiosperm phylogeny group classification for the orders and families of flowering plants: APG II. *Bot J Linn Soc* 2003;141:399-436.
- Angiosperm Phylogeny Group. An update of the angiosperm phylogeny group classification for the orders and families of flowering plants: APG III. *Bot J Linn Soc* 2009;161:105-21.
- Nickrent DL, Malecot V, Vidal-Russell R, Der JP. A revised classification of *Santalales*. *Taxon* 2010; 59:538-58.

Source of Support: Nil. **Conflict of Interest:** None declared.

**IN VIVO AND IN VITRO INVESTIGATIONS OF PHARMACOLOGICAL POTENTIALS OF CASSIA
OBTUSIFOLIA PLANT**KEWATKAR SM^{1*}, PAITHANKAR VV², BHUJBAL SS³, JAIN SP¹, NAGORE DH⁴

¹Department of Pharmacognosy, Rajarshi Shahu College of Pharmacy, Buldana, Maharashtra, India. ²Department of Pharmacology, Vidyabharti College of Pharmacy, Amravati, Maharashtra, India. ³Dr. D.Y. Patil Institute of Pharmaceutical Sciences and Research, Pimpri-Chinchwad, Maharashtra, India. ⁴Department of Pharmacy, Shri Jagdishprasad Jhabarmal Tibrewala University, Jhunjhunu, Rajasthan, India.
Email: kewatkar.shailesh@gmail.com

Received: 14 December 2019, Revised and Accepted: 11 January 2020

ABSTRACT

Objectives: *Cassia obtusifolia* L. belonging to the Family Caesalpiniaceae, proposed to have abundant pharmacological potential and widely consumed as laxative, diuretic, and stomachic. The aim of the present research was to study the anti-inflammatory, analgesic, antipyretic, and antioxidant potentials of *C. obtusifolia* plant.

Methods: Various acute and chronic animal models such as Carrageenan-induced paw edema, tail immersion method, acetic acid-induced writhing, and *in vitro* methods were used to study the profound pharmacological and antioxidant potentials.

Results: The results for pharmacological study were statistically analyzed by one-way ANOVA followed by Dunnett's multiple comparisons using INTA software.

Conclusion: The present study reveals that *C. obtusifolia* possesses comparable anti-inflammatory, analgesic, antipyretic, and antioxidant potential.

Keywords: *Cassia obtusifolia*, Anti-inflammatory, Antioxidant, Carrageenan, Antipyretic.

© 2020 The Authors. Published by Innovare Academic Sciences Pvt Ltd. This is an open access article under the CC BY license (<http://creativecommons.org/licenses/by/4.0/>) DOI: <http://dx.doi.org/10.22159/ajpcr.2020.v13i3.36623>

INTRODUCTION

Drugs presently used for the management of pain and inflammatory conditions are either narcotics, for example, opioids or non-narcotics, for example, salicylates and corticosteroids, and for example, hydrocortisone. Being synthetically designed these drugs possess well-recognized side and toxic effects. On the contrary, many medicines from plant origin had been used for long time. Exploring the healing power of plants, people from centuries have been trying to alleviate and treat diseases with different plant extracts and formulations [1]. Plants represent a large intact source of structurally novel compounds that might serve as the basis for the development of novel drugs. Screening of the plants for their biological activity merely depends on their chemotaxonomic investigation or ethnobotanical knowledge for a particular disease. Identification of a specific compound against a specific disease is a challenging extensive process [2]. Literature research for several medicinal plants possesses active constituents with significant anti-inflammatory and analgesic activities.

Cassia obtusifolia L. belonging to Caesalpiniaceae family, also known as sicklepod is extensively used as a traditional medicine [3]. The foremost active components of *C. obtusifolia* include anthraquinones, naphthopyrones, and lactones which are assumed to possess various medicinal potentials. The plant is also widely consumed as laxative, diuretic, stomachic, and digestive aid [4].

Hence, an attempt has been made to conduct studies for ascertaining anti-inflammatory, antipyretic, and analgesic potential of the medicinal plant *C. obtusifolia* using different animal models. Different *in vitro* methods were also used to study the antioxidant potential of *C. obtusifolia* plant.

METHODS**Chemicals**

All AR grade solvents such as ethanol, ethyl acetate, sodium carbonate, sodium phosphate, hydrogen peroxide, and trichloroacetic acid were procured from Merck Life Science Private Ltd, Vikhroli (East), Mumbai, India. Gallic acid, Folin-Ciocalteu reagent;1, and 1-diphenyl-2-picrylhydrazyl (DPPH) were procured from SD-Fine Chem Ltd., Fischer Scientific Pvt. Ltd, Pune, India, and HiMedia Lab. Ltd., Mumbai, respectively. Marketed tablet formulations of indomethacin, pentazocine, and paracetamol were used as standard drugs that were procured from the local market.

Procurement and authentication of plant

The leaves of the plant were collected from fields of Sant Tukaram Nagar, Pimpri, Pune, and authenticated by the Botanical Survey of India, Pune, and were given the voucher specimen number SMK-1.

Extraction procedure

Leaves of *C. obtusifolia* Linn. (2 kg) were dried under shade and grinded to get the coarse powdered material. The extraction of the powdered leaves was carried out by the maceration (water) process. Then, the solution was filtered and to this filtrate, alcohol was added to get precipitate of the polysaccharides. Then, the resulting solution was filtered and the filtrate was evaporated to 1/4th of the total volume. After evaporating 1/4th of the total volume of the solution, it was successively extracted with ethyl acetate. The ethyl acetate extract was evaporated to get the brownish-yellow colored flavonoid-rich fraction of *C. obtusifolia* Linn. (FRCO) (1% w/w) which gave a positive response to the Shinoda test for the flavonoids [5-7].

Pharmacological screening

The pharmacological screening was performed on Swiss albino mice of either sex weighing 18–25 g and Wistar rats of either sex weighing 150–200 g at Padm. Dr. D.Y. Patil Institute of Pharmaceutical Sciences and Research, Pimpri, Pune. The animals were kept in the departmental animal house in well cross-ventilated room at $27\pm 2^\circ\text{C}$, light and dark cycles of 12 h, respectively, for 1 week before and during the experiments. All the animals of either sex were housed in groups of five under standard laboratory conditions with free access to a standard pellet diet and water *ad libitum*. All experiments were conducted in accordance with the guidelines of the local animal ethical committee (Registration no. 198/CPCSEA).

Preparation of test solutions

FRCO was accurately weighed and suspended in distilled water using 1% gum acacia. Other standard solutions such as indomethacin, pentazocine, and paracetamol were suspended in normal saline solution.

Acute toxicity study

Acute toxicity study was carried out on Swiss albino mice which were divided into three groups, each containing six animals. Group I animals were treated with vehicle (1% gum acacia) and were served as control group, while the Groups II and III animals were administered with aqueous extract of *C. obtusifolia* and flavonoid-rich FRCO orally in varying doses of 0.50, 0.75, 1.00, 1.25, 1.50, 1.75, 2.00, and 2.50g/kg, respectively. The animals were continuously observed for 72 h to detect changes in the autonomic or behavioral responses such as alertness, spontaneous activity, irritability, and urination. Any mortality during experimentation and in the following 7 days was also recorded [8].

Anti-inflammatory activity

Anti-inflammatory activity was studied using acute and chronic anti-inflammatory models such as carrageenan-induced paw edema, acetic acid-induced vascular permeability, and cotton pellet-induced granuloma.

Carrageenan-induced paw edema

The acute hind paw edema was produced by injecting 0.1 ml of carrageenan (1% suspension in saline) locally into the subplantar aponeurosis of the right hind paw of rats. Animals were divided into five groups, six rats per group. FRCO was administered orally at different doses (50, 100, and 200 mg/kg) along with the standard drug indomethacin (10 mg/kg, p.o.) and 1% acacia solution (p.o.). FRCO and indomethacin were administered 1 h before injection of carrageenan in the right hind paw subplantar of each rat. The rat pedal volume up to the ankle joint was measured using plethysmometer (Ugo Basile, 7140, Italy) at 0, 1, 2, 3, 4, 5, 6, and 24 h after the injection of carrageenan and the percent inhibition was calculated using the formula;

$$\text{Percent inhibition} = \frac{V_c - V_t}{V_c} \times 100$$

Where V_c and V_t represent the mean increase in paw volume in control and treated groups, respectively [9].

Acetic acid-induced vascular permeability

The mice were intravenously injected with 10 ml/kg of 1% Evans Blue dye solution in saline, followed by intraperitoneal injection of 10 ml/kg of 0.7% acetic acid. The FRCO (50 mg/kg, 100 mg/kg, and 200 mg/kg), indomethacin (10 mg/kg), and 1% acacia solution (p.o.) were administered orally 1 h before the injection of Evans blue. Twenty minutes after the injection of acetic acid, the mice were sacrificed by cervical dislocation. Peritoneal fluids were collected by washing with 5 ml of normal saline and then centrifuged at 3000 rpm for 15 min. The absorbance of the supernatant was read at 590 nm using a spectrophotometer (Shimadzu 7140) [10-12].

Cotton pellet-induced granuloma

The test samples, indomethacin, and 1% acacia solution in distilled water were administered orally once daily for 7 days. Sterilized cotton

pellet weighing 20 mg were put subcutaneously into the groin region of rats on the 1st day. The animals were sacrificed on the 8th day. The pellets, which by then were surrounded by granuloma tissue, and the thymus were dissected out carefully and dried at 600°C to a constant weight. The wet weight and dry weight were determined. The percentage of inhibition was expressed by comparing the mean weight in the test groups with that in the control group.

Analgesic activity

Analgesic activity was studied using four different models, such as acetic acid-induced writhing, hot plate method, formalin test, and tail immersion test [11,13].

Acetic acid-induced writhing test

In the writhing test, male mice were divided into five groups. The mice were treated with 0.6% acetic acid solution in normal saline injected intraperitoneally at a dose of 10 ml/kg. The numbers of writhes were counted starting from 5 min after injection that lasted for 15 min. The response consisted of abdominal wall contractions, pelvic rotation, followed by hind limb stretches. The test samples, indomethacin, and 1% acacia solution (p.o.) were administered orally 1 h before acetic acid injection. The percentage of analgesic activity was calculated as follows:

$$\text{Percentage analgesic activity} = \frac{N_c - N_t}{N_c} \times 100$$

Where, N_c is the average number of stretches of the control group, N_t is the average number of stretches of the test drug group [11,14].

Hot plate method

The hot plate test was carried out at a fixed temperature of $55\pm 5^\circ\text{C}$. The reaction consisted of paw licking and jumping. The time in seconds between the platform and reaction was recorded as the response latency. The mice exhibiting latency time >30 s or <5 s were excluded from the study. The latency time was determined at 0 min, 30 min, 60 min, 90 min, and 120 min after administration of the test samples, pentazocine (10 mg/kg i.p.), and 1% acacia solution (p.o.) [10,14,15].

Formalin test

Albino mice of either sex were divided into five groups. Group I considered as normal control received orally with the vehicle 1% gum acacia, Group II with standard indomethacin (5 mg/kg, i.p.), Groups III, IV, and V were given orally with different doses, i.e., 50 mg/kg, 100 mg/kg, and 200 mg/kg of FRCO. One hour after the above treatment, 20 μl of 2.5% formalin was injected into the subplantar region of each animal. Duration of paw lickings was monitored for 0–5 min (Early phase) and at 20–25 min (Late phase) after formalin challenge [16].

Tail immersion test

The basal reaction time of each mouse was determined using tail-withdrawal response when one-third of the tail was immersed in a water bath at $51\pm 1^\circ\text{C}$. Mice with basal reaction time between 5 and 10 s were selected 24 h before the test. The animals were treated with gum acacia 1%, pentazocine (10 mg/kg, i.p.), and FRCO (50, 100 and 200 mg/kg p.o.) and 30, 60, 90, and 120 min later the reaction time was evaluated. The cutoff time for immersion was 180 s [17].

Antipyretic activity

The antipyretic property of FRCO was tested in rats in which hyperthermia was introduced. Initial rectal temperature was recorded using Digital Tele Thermometer (Model No. 461E, INCO, Ambala, India). Rats were made hyperthermic by subcutaneous injection of 20% yeast suspension at the dose of 1 ml/100 g of body weight. When rectal temperature was at peak (16 h after injection of yeast suspension), the rectal temperature was again recorded. Test and control drug was given orally. After 1 h, temperature was recorded followed by 1 h interval for consecutive 5 h.

In vitro antioxidant activity

In vitro antioxidant activity was studied by total phenolic content, DPPH free radical scavenging activity, hydrogen peroxide assay, and reducing power assay.

Total phenolic content

2 ml sample solution, 10 ml water, and 2 ml Folin-Ciocalteu reagent were mixed up and volume was made up to 25 ml by adding sodium carbonate solution. After incubation, the absorbance of the solution was measured at 750 nm. Instead of sample solution, gallic acid was added and same procedure was repeated for the standard gallic acid solution. From the stock solution of gallic acid, different concentrations were prepared 250, 500, 750, 1000, and 1250 μ l and calibration curve was plotted. Line equation obtains from the calibration curve was used for determining % of total polyphenols with that of gallic acid [18,19].

DPPH free radical scavenging activity

1 ml of different concentrations of extract solution were taken in different vials. To this, 5 ml of methanolic solution of DPPH was added, shaken well and mixture was incubated at 37°C for 20 min. Absorbance was measured against methanol as a blank at 517 nm and absorbance of DPPH was taken as control. Percent antiradical activity was calculated using the following formula [20]:

$$\% \text{ Scavenging activity} = \frac{\text{OD}_{\text{Control}} - \text{OD}_{\text{Test sample}}}{\text{OD}_{\text{Control}}} \times 100$$

Hydrogen peroxide assay

1 ml different concentrations of extract solution were taken in different vials. Different concentrations (25–200 μ g/ml) of FRCO were added

to 0.6 ml of H_2O_2 (40 mM). The absorbance of the solution was read at 230 nm after 10 min against a blank containing FRCO in phosphate-buffered without H_2O_2 . The concentration of H_2O_2 was determined spectrophotometrically at 230 nm. The percent scavenging of H_2O_2 by FRCO was calculated using the formula [21]:

$$\% \text{ Scavenging} = \frac{\text{Absorbance of control} - \text{Absorbance of sample}}{\text{Absorbance of control}} \times 100$$

Reducing power assay

1 ml of FRCO (dilution) was mixed with 1 ml of 0.2 M sodium phosphate-buffered (pH 6.6) and 1 ml of 1% potassium ferricyanide. The reaction mixtures were incubated 50 OC for 20 min. Then, 1 ml of 10% trichloroacetic acid was added into the reaction mixture. The mixtures were then centrifuged for 10 min at room temperature. The supernatant obtained (1 ml) was added with 1 ml of distilled water and 200 μ l of 0.1% FeCl_3 . The blank was prepared in the same manner as the samples except that 1% potassium ferricyanide was replaced by distilled water. The absorbance of the reaction mixture was measured at 700 nm. The reducing power was expressed using the following formula [22].

$$\% \text{ Scavenging} = \frac{A_0 - A_1}{A_0} \times 100$$

Where A_0 is the absorbance of the blank and A_1 is the absorbance of test.

Statistical analysis

Values were presented as mean \pm SEM. Statistical analysis was performed by one-way ANOVA followed by Dunnett's multiple comparison using INTA software. The level of significance was set as $p < 0.05$ and $p < 0.01$.

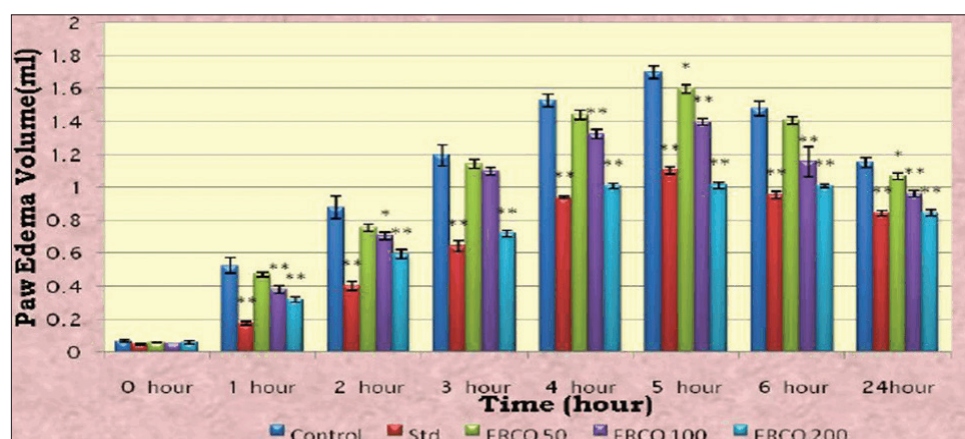


Fig. 1: Effects of FRCO on carrageenan-induced hind paw edema. * $p < 0.05$, ** $p < 0.01$, compared with the control group (ANOVA followed by Dunnett's test). Where, $N = 5$ Mean \pm SEM = Mean \pm Standard error of mean

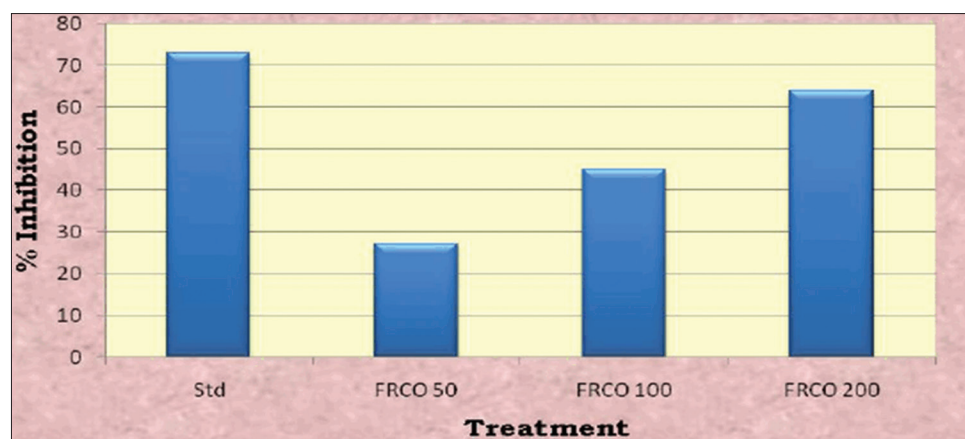


Fig. 2: Effect of FRCO on acetic acid-induced vascular permeability in mice. Where, $N = 5$ Mean \pm SEM = Mean \pm Standard error of mean

RESULTS AND DISCUSSION

Acute toxicity study

There was no toxic reaction or mortality observed. Flavonoid-rich fraction was found to be safe up to 2000 mg/kg p.o. Thus, based on the results of preliminary toxicity testing of the doses of 50, 100, and 200 mg/kg p.o. were chosen for further experiments.

Anti-inflammatory activity

Effect of FRCO on carrageenan-induced hind paw edema in rats

In carrageenan-induced hind paw edema, FRCO (50, 100, and 200 mg/kg, p.o.) reduced carrageenan-induced edema formation significantly at 1st, 2nd, 5th, and 6th h. A significant inhibition in edema formation was observed by both FRCO and indomethacin at 24th h (Fig. 1).

Effects of FRCO on acetic acid-induced vascular permeability

The FRCO treatment inhibited acetic acid-induced vascular permeability, and the same was reflected in increased leakage of dye. The amount of dye leakage was significantly ($p < 0.01$) reduced by all the doses (50, 100, and 200 mg/kg, p.o.) of extract. The dose of indomethacin (10 mg/kg p.o.) prevented significantly dye leakage and the effect was greater than the FRCO (Table 1 and Fig. 2).

Effects of FRCO on cotton pellet-induced granuloma

In cotton pellet-induced granuloma in rats, the FRCO treatment orally inhibited the inflammatory effect on both the phases of inflammation

and effect was found to be dose-related. Indomethacin (10 mg/kg p.o.) treatment also elicited inhibitory effects on both exudate and granulation phases of inflammation. The indomethacin effect was greater than the FRCO (Fig. 3).

Analgesic activity

Effects of FRCO on acetic acid-induced writhing test

The FRCO at the dose 50, 100, and 200 mg/kg, p.o. inhibited acetic acid-induced writhing in mice. Indomethacin showed greater inhibition in acetic acid-induced writhing as compared to FRCO (Table 2 and Fig. 4).

Effects of FRCO on hot plate method

The FRCO at the dose 50, 100, and 200 mg/kg, p.o. significantly inhibited the latency period. Pentazocine showed greater inhibition in the hot plate method model of analgesic as compared to FRCO (Table 3).

Effects of FRCO on the formalin test method

In the formalin test method, the FRCO treatment orally inhibited both phases, i.e., early and late phase and effect was found to be dose related. Indomethacin 5 mg/kg i.p shows an inhibitory reaction greater than the FRCO (Fig. 5).

Effects of FRCO on tail-flick test

The ability of FRCO to induce the central analgesia was evaluated by temperature-based tests. As per the results, in tail-flick test the FRCO treatment orally increase the time duration of flicking of tail when

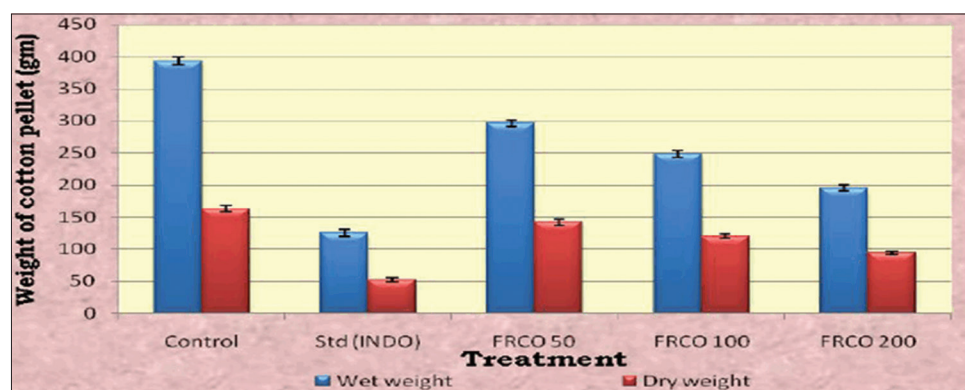


Fig. 3: Effect of FRCO on cotton pellet-induced granuloma in rats. Where, N = 5 Mean \pm SEM = Mean \pm Standard error of mean

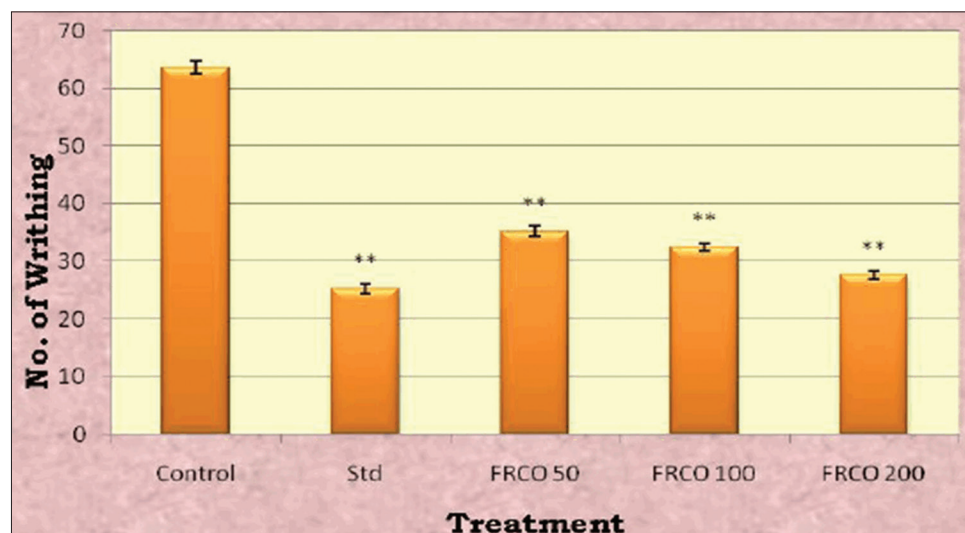


Fig. 4: Effect of FRCO on acetic acid-induced writhing test. * $p < 0.05$, ** $p < 0.01$, compared with the control group (ANOVA followed by Dunnett's test). Where, N = 5 Mean \pm SEM = Mean \pm Standard error of mean

Table 1: Effect of FRCO on acetic acid-induced vascular permeability in mice

Name of groups	OD	Amount of dye leakage	% Inhibition
Control	0.1101±0.001	26.25 µg/ml	-
Std. (INDO)	0.0321±0.007	07.75 µg/ml	73
FRCO 50	0.0835±0.001	20.12 µg/ml	27
FRCO 100	0.0605±0.002	14.62 µg/ml	45
FRCO 200	0.0450±0.003	10.87 µg/ml	64

OD: Optical density, FRCO: Flavonoid-rich fraction of *C. obtusifolia* Linn. Where, N=5 Mean±SEM=Mean±Standard error of mean

Table 2: % Inhibition of FRCO on acetic acid-induced writhing test

S. No.	Group	Dose (mg/kg)	Number of writhing	% inhibition
1.	Control	--	63.6±1.030	--
2.	Std. (INDO)	10	25.2±0.860 **	60
3.	FRCO 50	50	35.2±0.969 **	44
4.	FRCO 100	100	32.4±0.678 **	49
5.	FRCO 200	200	27.6±0.748 **	56

*p<0.05, **p<0.01, compared with control group (ANOVA followed by Dunnett's test). Where, N=5, Mean±SEM=Mean±Standard error of mean

Table 3: Effect of FRCO in hot plate method

Group	Dose mg/kg	Time (h)				
		0 h	0.5 h	1 h	1.5 h	2 h
Control	-	6.56±0.060	6.42±0.037	6.7±0.044	6.62±0.048	6.7±0.044
Std(PENT)	10	6.62±0.048	14.08±0.080**	15.98±0.058**	16.74±0.067**	15.96±0.050**
FRCO 50	50	6.7±0.044	8.68±0.058**	9.4±0.063**	11.8±0.054**	11.12±0.066**
FRCO 100	100	6.18±0.048	9.2±0.044**	11.2±0.054**	12.7±0.083**	12.2±0.044**
FRCO 200	200	6.44±0.040	9.74±0.074**	12.04±0.081**	13.16±0.074**	12.38±0.086**

*p<0.05, **p<0.01, compared with control group (ANOVA followed by Dunnett's test). Where, N=5 Mean±SEM=Mean±Standard error of mean

Table 4: Effect of FRCO on pyrexia-induced by brewer's yeast in rats

Group	Dose mg/kg	Temperature (°C) (Mean ± SEM)					
		1 h	2 h	3 h	4 h	5 h	6 h
Vehicle	-	37.34±0.097	37.42±0.058	37.48±0.073	37.40±0.054	37.52±0.086	37.5±0.031
Control	-	39.42±0.073	39.6±0.044	39.44±0.067	39.28±0.066	38.06±0.050	39.08±0.050
Std. (PARA)	150	39.2±0.077	38.9±0.070	38.68±0.037	38.34±0.050	38.10±0.044	37.52±0.086
FRCO 50	50	39.34±0.060	39.3±0.083	39.24±0.067	38.92±0.037	38.92±0.048	38.60±0.070
FRCO 100	100	39.4±0.034	39.36±0.067	39.36±0.040	38.98±0.058	38.62±0.020	38.46±0.040
FRCO 200	200	39.28±0.058	39.22±0.131	38.78±0.058	38.52±0.177	38.50±0.063	38.38±0.058

*p<0.05, **p<0.01, compared with control group (ANOVA followed by Dunnett's test). Where, N = 5 Mean ± SEM = Mean ± Standard error of mean

Table 5: Effect of FRCO on pyrexia-induced by brewer's yeast in rats

Group	Dose mg/kg	Difference in temperature (°C) (Mean ± SEM)					
		1 h	2 h	3 h	4 h	5 h	6 h
Vehicle	-	0.46±0.04	0.54±0.024	0.6±0.04	0.6±0.031	0.54±0.050	0.62±0.037
Control	-	2.32±0.106	2.5±0.083	2.36±0.050	2.18±0.02	1.96±0.074	2.00±0.070
Std. (PARA)	150	2.22±0.142	1.62±0.058**	1.52±0.080**	0.98±0.080**	0.94±0.060**	40.52±0.050**
FRCO 50	50	2.24±0.040	2.36±0.02	1.76±0.024	1.82±0.037	1.74±0.037 *	1.5±0.031**
FRCO 100	100	2.18±0.037	2.3±0.031	2.16±0.024	2.14±0.024*	1.4±0.031**	1.22±0.037**
FRCO 200	200	2.26±0.040	2.3±0.031	1.5±0.158*	1.76±0.024**	1.46±0.024**	0.76±0.024**

*p<0.05, **p<0.01, compared with control group (ANOVA followed by Dunnett's test). Where, N = 5 Mean ± SEM = Mean ± Standard error of mean. FRCO: Flavonoid-rich fraction of *C. obtusifolia* Linn.

deep into the water bath. The pretreated animals increased the basal reaction time. At high doses (200 mg/kg) of FRCO and pentazocine (10 mg/kg i.p) increase the percentage reaction time effectively. Pentazocine (10 mg/kg i.p) shows an inhibitory reaction greater than the FRCO (Fig. 6).

Antipyretic activity

Effect of FRCO on pyrexia-induced by brewer's yeast in rats

In the antipyretic activity, FRCO at the dose level of 50, 100, and 200 mg/kg significantly reduced the fever induced by the brewer's yeast in rats. FRCO reduced the fever particularly at 5th and 6th h in dose-dependent manner, whereas paracetamol reduced the fever right from the 2nd to the 6th h (Tables 4 and 5).

In vitro antioxidant activity

Total phenolic content

Total polyphenolic content was observed to be 31.50 mg/g of gallic acid. It was observed that gallic acid being the major component of ethanolic extract and was mainly responsible for antioxidant activity.

DPPH free radical scavenging activity

In DPPH radical scavenging activity, FRCO and ascorbic acid showed significant DPPH free radical scavenging activity at different concentrations (50, 100, 150, 200, and 250 µg/ml) in dose-dependent manner. IC₅₀ value was found to be 137 and 200 µg/ml for ascorbic acid and FRCO, respectively (Table 6 and Fig. 7).

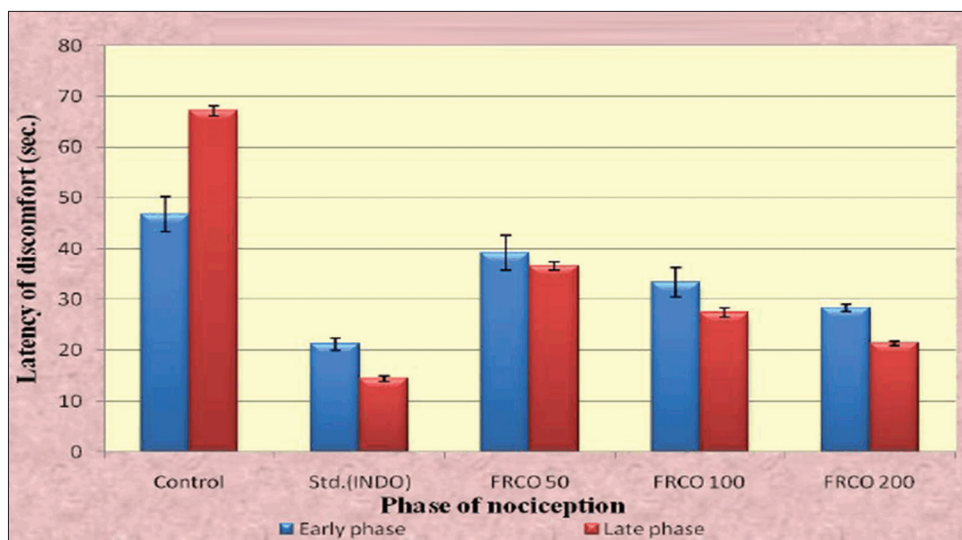


Fig. 5: Effects of FRCO on formalin test method. * $p < 0.05$, ** $p < 0.01$, compared with the control group (ANOVA followed by Dunnett's test). Where, $N = 5$ Mean \pm SEM = Mean \pm Standard error of mean

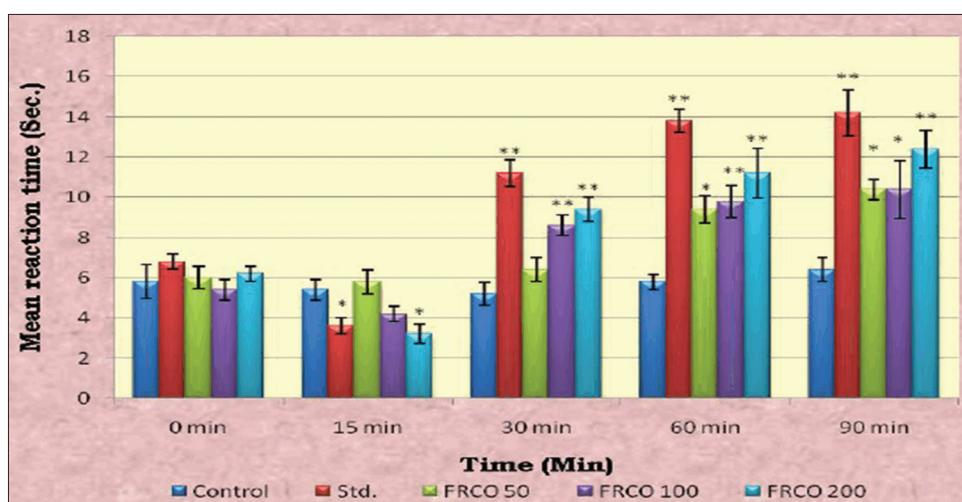


Fig. 6: Effect of FRCO on tail-flick test. * $p < 0.05$, ** $p < 0.01$, compared with the control group (ANOVA followed by Dunnett's test). Where, $N = 5$ Mean \pm SEM = Mean \pm Standard error of mean

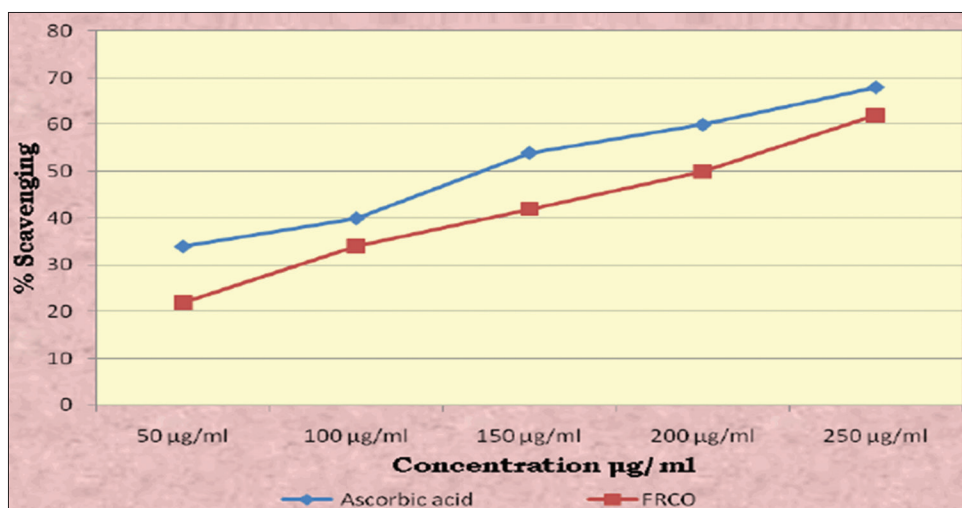


Fig. 7: Effect of FRCO in DPPH free radical scavenging assay

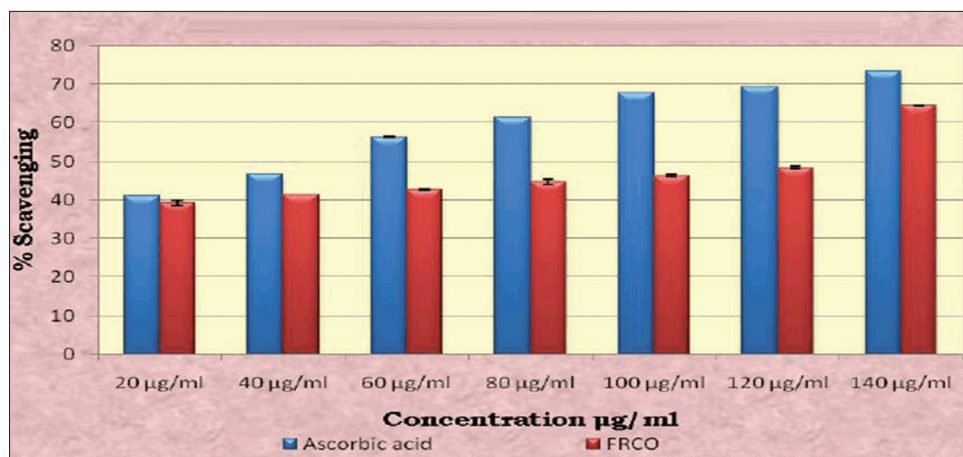


Fig. 8: Effect of FRCO in hydrogen peroxide assay

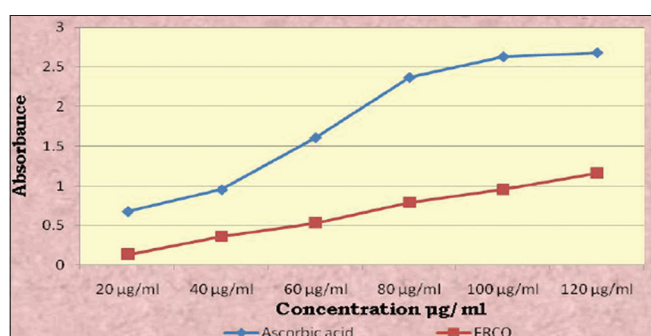


Fig. 9: Effect of FRCO in reducing power assay

Table 6: Effect of FRCO in DPPH free radical scavenging assay

Concentration µg/ml	% Scavenging ascorbic acid	IC ₅₀ value	% Scavenging FRCO	IC ₅₀ value
50 µg/ml	34±2.000	137	22±2.000	200
100 µg/ml	40±2.000		34±2.000	
150 µg/ml	54±3.464		42±3.464	
200 µg/ml	60±3.464		50±4.000	
250 µg/ml	68±2.000		62±3.464	

Table 7: Effect of FRCO in hydrogen peroxide assay

Concentration µg/ml	Ascorbic acid		FRCO	
	% Scavenging	IC ₅₀ value	% Scavenging	IC ₅₀ value
20	41.04±0.006	48	39.33±0.667	127
40	46.66±0.004		41.33±0.002	
60	56.33±0.002		42.66±0.333	
80	61.33±0.002		44.66±0.666	
100	67.66 ± 0.0007		46.33±0.333	
120	69.33±0.006		48.33±0.333	
140	73.32±0.002		54.49±0.130	

FRCO: Flavonoid-rich fraction of *C. obtusifolia* Linn.

Table 8: Effect of FRCO in reducing power assay

Concentration (µg/ml)	Absorbance of Ascorbic acid	Absorbance of FRCO
20	0.674±0.0117	0.1341±0.0020
40	0.9495±0.0038	0.3632±0.0170
60	1.6078±0.0083	0.5342±0.0021
80	2.3690±0.0248	0.7930±0.0010
100	2.6314±0.0040	0.9544±0.0010
120	2.6817±0.0014	1.1616±0.0500

Effect of FRCO in hydrogen peroxide assay

In hydrogen peroxide assay, FRCO and ascorbic acid, showed significant radical scavenging activity at different concentrations (20, 40, 60, 80, 100, 120, and 140 µg/ml) in dose-dependent manner. IC₅₀ value was found to be 48 and 127 g/ml for ascorbic acid and FRCO, respectively (Table 7 and Fig. 8).

Reducing power assay

In reducing power assay, FRCO and ascorbic acid showed significant radical power ability at different concentrations (20, 40, 60, 80, 100, and 120 µg/ml) in dose-dependent manner (Table 8 and Fig. 9).

CONCLUSION

The *C. obtusifolia* plant belonging to Caesalpiniaceae family consisted of flavonoids as the major chemical constituents. These flavonoid-rich fractions were profound to have certain pharmacological potential. Thus, the present study reveals the anti-inflammatory, analgesic, antipyretic, and antioxidant potential of flavonoid-rich fractions of *C. obtusifolia* plant. The results of the *in vitro* assays and animal models conclude that *C. obtusifolia* has comparable pharmacological potentials.

ACKNOWLEDGMENTS

The authors gratefully acknowledge the support provided by Rajarshi Shahu College of Pharmacy, Buldana, Maharashtra, India.

AUTHORS' CONTRIBUTIONS

Dr. S.M Kewatkar and Dr. Vivek Paithankar contribution included designing and performing laboratory work, analyzing the results, and preparing the paper. Dr. Santosh Bhujbal, Dr. S.P. Jain, and Dr. D.H. Nagore contribution included data interpretation and identification of the compounds. All the authors have read the final manuscript and approved the submission.

CONFLICTS OF INTEREST

The authors declare that they have no conflicts of interest.

AUTHORS FUNDING

None.

REFERENCES

- Steinmeyer J. Pharmacological basis for the therapy of pain and inflammation with nonsteroidal anti-inflammatory drugs. *Arthritis Res* 2000;2:379-85.
- Chandrika M, Chellaram C. Efficacy of antioxidation and anti-inflammation of the leaf extracts of *Borreria hispida*. *Int J Pharm Pharm Sci* 2016;8:369-72.
- Sakat S, Juvekar AR, Gambhire MN. *In vitro* antioxidant and anti-

- inflammatory activity of methanol extract of *Oxalis corniculata* Linn. Int J Pharm Pharm Sci 2010;2:146-55.
4. Hatano T, Uebayashi H, Ito H, Shiota S, Tsuchiya T, Yoshida T. Phenolic constituents of Cassia seeds and antibacterial effect of some naphthalenes and anthraquinones on methicillin-resistant *Staphylococcus aureus*. Chem Pharm Bull (Tokyo) 1999;47:1121-7.
 5. Al-Meshal IA, Tariq M, Parmar NS, Ageel AM. Anti-inflammatory activity of the flavonoid fraction of khat (*Catha edulis* Forsk). Agents Actions 1986;17:379-80.
 6. Cibir TR, Srinivas G, Devi DG, Srinivas P, Lija Y, Abraham A. Antioxidant and antiproliferative effects of flavonoids from *Emilia sonchifolia* Linn on human cancer cells. Int J Pharm 2006;2:520-4.
 7. Castardo JC, Prudente AS, Ferreira J, Guimarães CL, Monache FD, Filho VC, et al. Anti-inflammatory effects of hydroalcoholic extract and two biflavonoids from *Garcinia gardneriana* leaves in mouse paw oedema. J Ethnopharmacol 2008;118:405-11.
 8. Organisation for Economic Co-operation and Development. OECD Guideline for Testing Of Chemicals. Acute Oral Toxicity-acute Toxic Class Method Adopted. France: Organisation for Economic Co-operation and Development; 2001;1:1-14.
 9. Zeashan H, Amresh G, Rao CV, Singh S. Antinociceptive activity of *Amaranthus spinosus* in experimental animals. J Ethnopharmacol 2009;122:492-6.
 10. Xie F, Zhang M, Zhang CF, Wang ZT, Yu BY, Kou JP. Anti-inflammatory and analgesic activities of ethanolic extract and two limonoids from *Melia toosendan* fruit. J Ethnopharmacol 2008;117:463-6.
 11. Zhang L, Hu JJ, Lin JW, Fang WS, Du GH. Anti-inflammatory and analgesic effects of ethanol and aqueous extracts of *Pterocarpus hookeri* (CB Clarke) Hoeck. J Ethnopharm 2009;123:510-4.
 12. Whittle BA. The use of changes in capillary permeability in mice to distinguish between narcotic and nonnarcotic analgesics. Br J Pharmacol 1964;22:246-53.
 13. Arumugam P, Priya NG, Subathra M, Ramesh A. Anti-inflammatory activity of four solvent fractions of ethanol extract of *Mentha spicata* L. investigated on acute and chronic inflammation induced rats. Environ Toxicol Pharmacol 2008;26:92-5.
 14. Mahmoudi M, Morteza-Semnani K, Mojra E. Anti-inflammatory and antinociceptive activity of *Thymus pubescens* extract. Fitoterapia 2008;79:361-5.
 15. Singh A, Malhotra S, Subban R. Anti-inflammatory and analgesic agents from Indian medicinal plants. Int J Integr Bio 2008;3:57-72.
 16. Jyothi G, Carey WM, Kumar RB, Mohan KG. Antinociceptive and anti-inflammatory activity of methanolic extract of leaves of *Shorea busta*. Pharmacologyonline 2008;1:9-19.
 17. Roldão Ede F, Witaicenis A, Seito LN, Hiruma-Lima CA, Di Stasi LC. Evaluation of the antiulcerogenic and analgesic activities of *Cordia verbenacea* DC. (Boraginaceae). J Ethnopharmacol 2008;119:94-8.
 18. Lompo M, Guissou I, Dubois J, Dehaye JP, Ouédraogo A, Traore A, et al. Mechanism of the anti-inflammatory activity of *Khaya senegalensis* A. Juss. (Meliaceae). Int J Pharmacol 2007;3:137-42.
 19. Devi BP, Boominathan R, Mandal SC. Evaluation of antipyretic potential of *Cleome viscosa* Linn. (Capparidaceae) extract in rats. J Ethnopharmacol 2003;87:11-3.
 20. Panovska TK, Kulevanova S. Effect of some *Teucrium* species (Lamiaceae) on lipid peroxidation in rat liver microsomes. Fresenius Environ Bull 2005;14:957-9.
 21. Shabrina RI, Elya BE, Noviani AR. Antioxidant activities of fractions from ethyl acetate extracts of *Garcinia fruticosa* lauterb leaves. Int J Appl Pharm 2018;10:44-50.
 22. Usha B, Pushpalatha KC. *In vitro* antioxidant activity and phytochemical screening of leaf extracts of *Grewia heterotricha* mast. Int J Curr Pharm Res 2016;8:68-72.



Discovery of Naturally Occurring Flavonoids as Human Cytochrome P450 (CYP3A4) Inhibitors with the Aid of Computational Chemistry

Sharuk L. Khan ^{1*}, Gajanan M. Sonwane ¹, Falak A. Siddiqui ¹, Shirish P. Jain ¹, Mayura A. Kale ²,
Vijay S. Borkar ¹

¹ Rajarshi Shahu College of Pharmacy, Buldana, Maharashtra, India 443001.

² Government College of Pharmacy, Aurangabad, Maharashtra, India 431005

Address for Correspondence: Sharuk L.Khan, sharique.4u4@gmail.com

Received:

13.07.2019

Accepted:

11.04.2020

Published:

20.12.2020

Keywords

Human
Cytochrome
P450 (CYP3A4);
Flavonoids;
Doxorubicin;
Molecular
docking; PyRx
Virtual Screening
Tool.

ABSTRACT: Purpose: The human cytochrome P450 3A4 (CYP3A4) is the biggest individual from the CYP3A subfamily and records for 30–60% of the total for CYP450 adult liver. Hereditary varieties in CYP3A4 are a noteworthy hotspot for inter-patient changeability in plasma concentration, adverse effects and pharmacological response to medications. This research was done to discover naturally occurring novel CYP3A4 inhibitors from flavonoids. Methods: The molecular docking method was used to optimize the inhibiting activity of flavonoids against CYP3A4. PyRx Virtual Screening Tool 0.8 and BIOVIA Discovery Studio 2019 was used for simulation. Results: Flavonoids like Pongamoside A, Pongamoside B, and Pongamoside D have more binding affinity (kcal/mol) i.e. -11.6, -10.9, -10.8 respectively than Doxorubicin which have -10.7 against CYP3A4. Although, Daidzein, Genistein, and Luteolin form more hydrogen bonds than doxorubicin. Conclusion: The rational synthesis of natural analogues in reference to synthetic drugs, could generate drugs with improved therapeutic effect for chemoprevention. CYP3A4 plays a major role in the metabolism of various drugs; by the help of flavonoids, we can control the selective drug metabolism by inhibiting CYP3A4. Despite this, these molecules are not marketed for cancer treatment because of high polarity. If we could overcome this problem, these molecules can acts as effective anticancer agents in the future. Still, if we want to use these compounds clinically, there is a need to generate more scientific evidence and quality data by using *in vivo* and *in vitro* models. © 2020 iGlobal Research and Publishing Foundation. All rights reserved.

Cite this article as: Khan, S.L.; Sonwane, G.M.; Siddiqui, F.A.; Jain, S.P.; Kale, M.A.; Borkar, V.S. Discovery of naturally occurring flavonoids as human cytochrome P450 (CYP3A4) inhibitors with the aid of computational chemistry. Indo Global J. Pharm. Sci., 2020; 10(4): 58-69. DOI: <http://doi.org/10.35652/IGJPS.2020.10409> .

INTRODUCTION

Flavonoids are a well-known category of polyphenolic compounds. These are the regular dietary materials of the human, as many of the plants contains flavonoids. There are plenty of plants that exerts good pharmacological properties including anticancer activity just because of the presence of flavonoids. Flavonoids are the essential plant shades that act as chemical messengers, physiological controllers, and cell cycle inhibitors [1]. Flavonoids stand out amongst the most tried and broadly distributed substances of plant sources. They are found in natural products, vegetables, leguminous plants and even a few sorts of greenery. The skeleton of flavonoids

comprises of 1-benzopyran. It is a C6-C3-C6 framework, in which sweet-smelling rings are associated, shaping a focal pyran or pyron cycle. Contingent upon the position to which ring is associated with the chromane, flavonoids are grouped into isoflavonoids and neoflavonoids [2].

Amongst the different other natural substances, flavonoids hold much consideration because of their noteworthy range of pharmacological activities, such as cell reinforcement, antimutagenic, antibacterial, antiangiogenic, anti-

inflammatory, anti-allergic, modulators of enzymatic activities and anti-cancer activity [3]. Apigenin, luteolin, quercetin and kaempferol, the hydroxylated flavonoids are the main constituents of various dietary products and beverages and have been the focus of extensive research over the last years. Apigenin exerts anticancer effects through the modulation of various pathways namely, apoptosis, Reactive oxygen species (ROS) and DNA damage and repair [4].

Malignant growth is one of the terrible illnesses caused by unusual cell growth and can attack different tissues. They shape a subset of neoplasms. It speaks of the greatest social insurance issues for humankind and requests a proactive system for cure [5]. It is accounted for the rate of malignancy that has been expanding in developing nations and has turned into the fourth driving reason for death around the world. Chemoprevention by phytoconstituents has advanced as a powerful procedure to control the prevalence of malignant growth. The journey of anticancer agents from plant sources began in the 1950s with the discovery of the vinca alkaloids, vincristine, vinblastine, combretastatin, and colchicine. These Phytochemicals act explicitly on tumor cells without influencing non-cancerous cells. Carcinogenesis is a mind-boggling marvel that includes many signaling cascades. Phytochemicals are viewed as reasonable candidates for anticancer medication advancement due to their pleiotropic activities on target. The examination is in advancement for creating potential competitors (those can square or back off the development of disease cells without any side effects) from these phytochemicals. Numerous phytochemicals and their determined analogs have been distinguished as potential candidates for anticancer treatment. Plants serve as a source of novel compound elements and give a promising line to investigate on malignant growth. The plant and plant metabolites are the reforming sources as these are simple, more secure, easy, quick, and less dangerous as contrasted to traditional treatment methods. There is a positive relationship set up by the epidemiological examinations between expanded utilization of common items with diminished danger of disease. The mechanism responsible for chemoprevention remains essentially unidentified, however, it is likely identified with the closeness of phytochemicals related to plants. Consequently, the search for powerful and more secure natural anticancer agents have attracted the researchers throughout the world. [6,7].

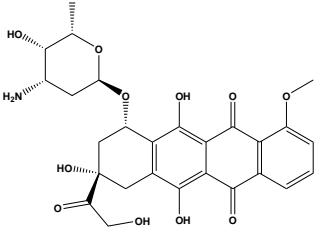
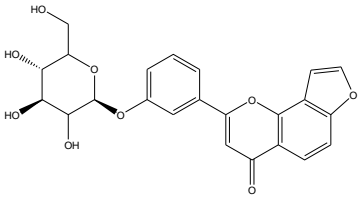
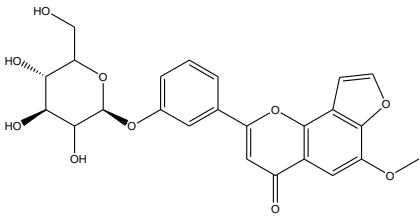
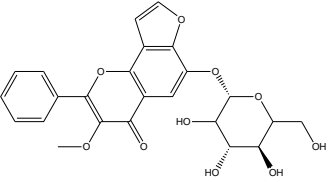
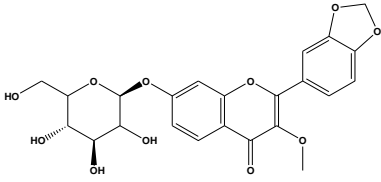
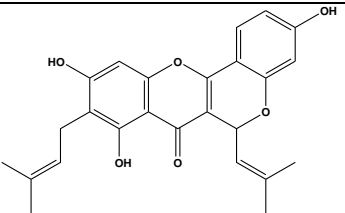
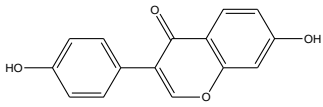
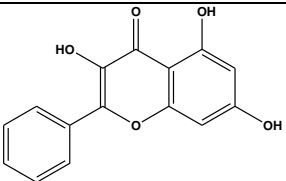
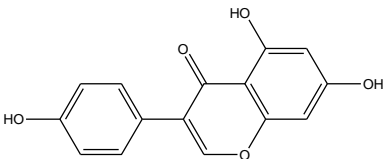
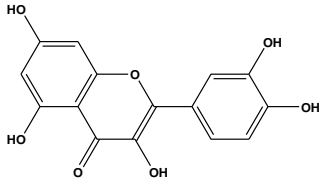
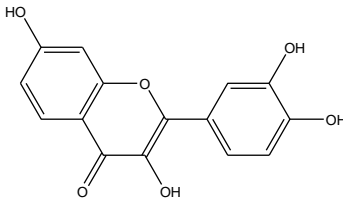
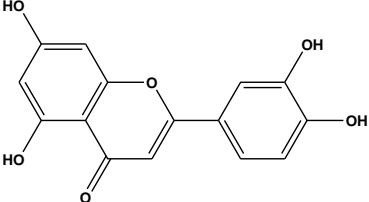
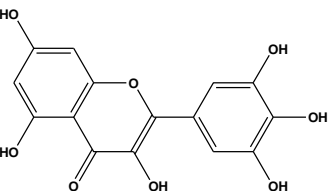
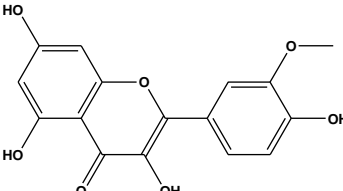
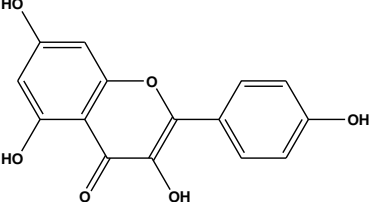
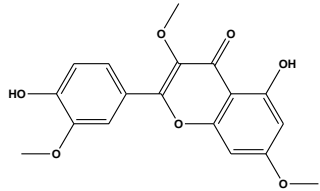
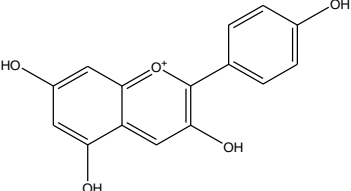
The human cytochrome P450 3A4 (CYP3A4) is the biggest individual from the CYP3A subfamily and records for 30–60% of the total for CYP450 adult liver. The CYP3A4 gene is limited on chromosome 7q21 and up to now, 41 CYP3A4 alleles have been recognized. The human CYP3A locus

contains the three CYP3A gene (CYP3A4, CYP3A5, and CYP3A7), three pseudogenes, and a novel CYP3A gene named CYP3A43. Hereditary varieties in CYP3A4 are a noteworthy hotspot for inter-patient changeability in plasma concentration, adverse effects and pharmacological response to medications, for example, paclitaxel, fentanyl, tamoxifen, tacrolimus, and statins. Moreover, existing investigations have announced the role of CYP3A4 inadequate alleles in the disease susceptibility to prostate malignant growth, estrogen receptor-negative breast cancer, and type-2 diabetes [8,9].

Protein-ligand docking is a fundamental part of computer-aided drug design, and it distinguishes the coupling pattern of proteins and ligands by computer simulation. Molecular docking results decide a general binding mode of a ligand. Varieties of compounds from plant sources have been accounted to have significant anticancer properties; in any case, their modes of activity have not been characterized. Molecular docking studies were performed on some flavonoids by using Autodock vina 1.1.2 in PyRx 0.8. [10]. The docking was performed utilizing receptor proteins required with cell cycle, cell development, and DNA replication, i.e., cyclin-subordinate protein kinase 2 (CDK-2), CDK-6, DNA topoisomerases I and II, B-cell lymphoma 2 (Bcl-2), vascular endothelial development factor receptor 2 (VEGFR-2), and the telomere: G-quadruplexes. By molecular docking, the bound confirmations and the coupling attachment among flavonoid and CYP3A4 as the target could be anticipated [11]. Doxorubicin, sold under the brand names adriamycin, used to treat breast malignant growth, bladder cancer, lymphoma, and intense lymphocytic leukemia was utilized for docking studies whose binding interactions were compared with the flavonoids [12].

Docking of the small molecule into the binding site of a receptor and guessing the binding interaction of the complex is a noteworthy part of the structure-based drug design process. By molecular docking, the bound conformations and the binding affinity between Flavonoids and human cytochrome P450 3A4 as the target could be predicted [13]. **Table 1** represents the names and structures of doxorubicin and the flavonoids used for molecular docking. The structures of all the compounds were generated by using ChemDraw Ultra 8.0 with the help of IUPAC name took from the official website of U.S. National Library of Medicine PubChem (<https://pubchem.ncbi.nlm.nih.gov/>).

Table 1. Name and Structures of compounds used for molecular docking

Doxorubicin 	Pongamoside A 	Pongamoside B 
Pongamoside C 	Pongamoside D 	Cyclocommunin 
Daidzein 	Galangin 	Genistein 
Quercetin 	Fisetin 	Luteolin 
Myricetin 	Isorhamnetin 	Kaempferol 
Pachypodol 	Pelargonidin 	

MATERIALS AND METHODS

System used for Molecular docking

Molecular docking was performed on Lenovo ThinkPad with 64-bit operating system, Processor: Intel(R) Core(TM) i5-4300M CPU @2.60 GHz 2.59 GHz, RAM: 4GB by using PyRx-Virtual Screening Tool.

Ligand Preparation

The Structures of all the compounds (SDF File) were downloaded from the official website of the U.S. National Library of Medicine PubChem (<https://pubchem.ncbi.nlm.nih.gov/>). Structures then imported into PyRx 0.8 using open bable tool and energy minimization

(optimization) was performed by considering fundamental parameters based on the element, its hybridization, and connectivity i.e. by Universal Force Field (UFF)[16]. These ligands were then converted to AutoDock Ligand format (PDBQT).

Macromolecule Preparation

Autodock vina 1.1.2 in PyRx 0.8 was used to perform the docking studies of all the compounds against the crystal structure of human cytochrome P450 3A4 (CYP3A4). The crystal structure of CYP3A4 was obtained from the RCSB Protein Data Bank (PDB) with PDB ID-4K9T (<http://www.rcsb.org/structure/4K9T>) with Homo sapiens organism and Escherichia coli expression system. The CYP3A4 crystal structure was optimized, purified and prepared for docking with the help of Discovery Studio Visualizer 2019 by removing unwanted water molecules, bound ligands from protein structure and saved again in PDB file format to the same folder[17].

Molecular Docking Procedure

The purified CYP3A4 crystal structure file was loaded to docking software PyRx 0.8 using a load molecule option from the File toolbar. Chain-A was used to perform the docking, as it contains the active site which confirmed by checking interactions of native ligand present in the crystal structure (<http://www.rcsb.org/3d-view/4K9T?preset=ligandInteraction&sele=1RD>). The CYP3A4 crystal structure was then converted to Autodock macromolecule (pdbqt format) by using the right-click option. Binding affinity studies were performed by using Vina Wizard Tool in PyRx 0.8. All the ligand molecules (PDBQT Files), and target (CYP3A4) were selected for docking study. For molecular docking simulation, the three-dimensional grid box (size_x = 18.5286782874Ao; size_y = 26.047226475Ao; size_z = -9.59195798998Ao) was designed using Autodock tool 1.5.6 with exhaustiveness value of 8. After selecting molecules, the active amino acid residues were selected to define the cavity with the help of Toggle Selection Spheres

option given in PyRx[18]. To occupy all the active binding sites and essential residues, the grid box was aligned properly. All the ligands and CYP3A4 then subjected for docking to get the finding affinities.

Identification of Cavity and Active Amino Acid Residues

The active amino acid residues in the protein were identified and noted using BIOVIA Discovery Studio Visualizer (version-19.1.0.18287)[17]. The selection of the amino acids in the active site was used to analyze the grid box and to define the cavity. All the docking poses, ligand and protein interactions were studied by importing output files into Discovery Studio which enables us to identify the types of interactions. Discovery Studio is an offline life sciences software that offers tools to study drug-receptor interaction, docking poses visualization and macromolecule preparations. The chosen cavity was the binding site of the native ligand in PDB 4K9T.

RESULTS AND DISCUSSION

All the flavonoids and doxorubicin successfully docked on CYP3A4. Binding energy is released when a drug molecule associates with a target, leading to a lowering of the overall energy of the complex [14]. Molecular formula, Lipinski’s rule of five, binding affinity (kcal/mol), and active amino acid residues are presented in Table 1. Lipinski’s rule of five plays an important role in molecule screening and validation. Here, Pongamosides i.e. Pongamoside A, Pongamoside B, and Pongamoside D have shown better binding affinity than doxorubicin.

Table 2 represents 3D- & 2D-images of docking poses along with no. of hydrogen bonds involved in the interaction. The 2D-docking pose also shows the chemical structure of the ligands which enables us to predict groups and/or atoms involved in the bond formation with CYP3A4.

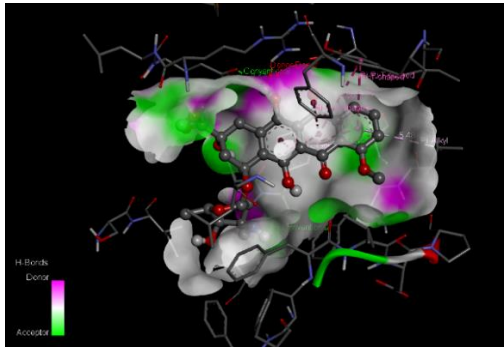
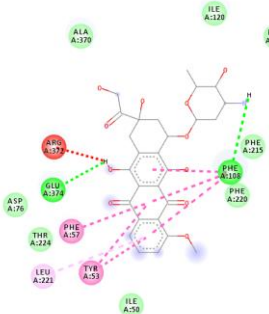
Table 2. Properties, Lipinski’s rule of five, binding affinity and active amino acid residues.

Name of Compound	Molecular Formula	Lipinski’s rule of five		Binding affinity (kcal/mol)	Active amino acid residues
Doxorubicin	C ₂₇ H ₂₉ NO ₁₁	Molecular weight (<500 DA)	543.5	-10.7	Ala370, Ile120, Phe241, Phe213, Val240, Phe215, Phe108, Phe220, Ile50, Tyr53, Leu221, Phe57, Thr224, Asp76, Glu374 (Forms unfavourable bond with Arg372)
		XLogP (<5)	1.3		
		H-Bond donor (5)	6		
		H-bond acceptor (<10)	12		
Pongamoside A	C ₂₃ H ₂₀ O ₉	Molecular weight (<500 DA)	440.4	-11.6	Leu373, Ala370, Arg372,

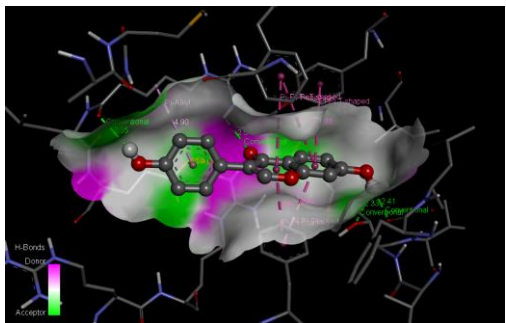
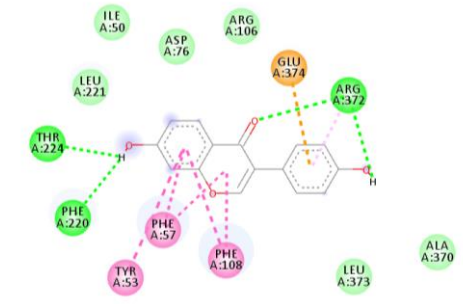
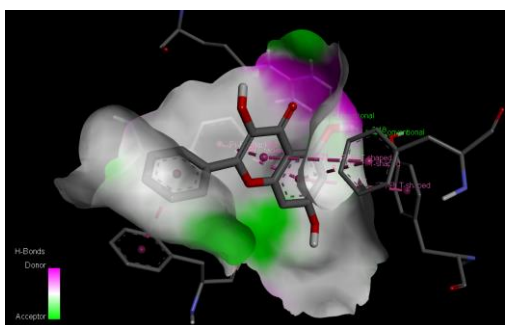
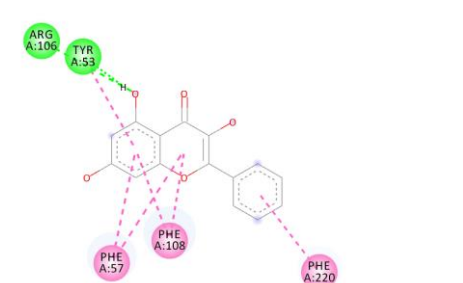
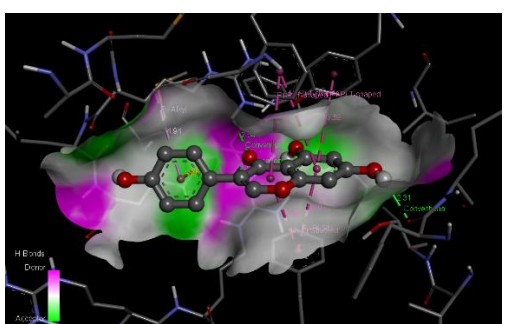
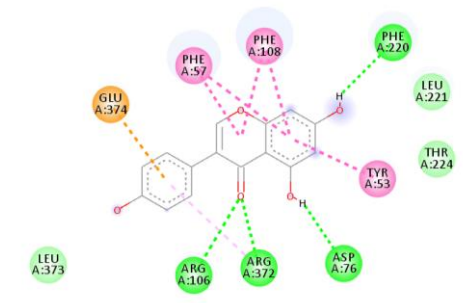
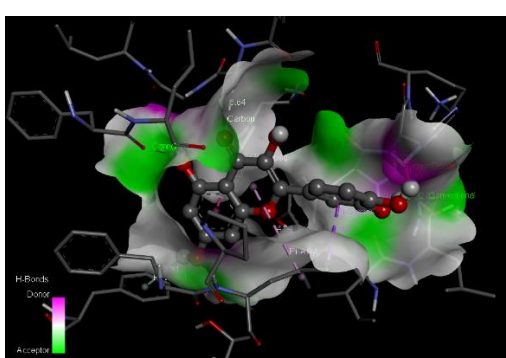
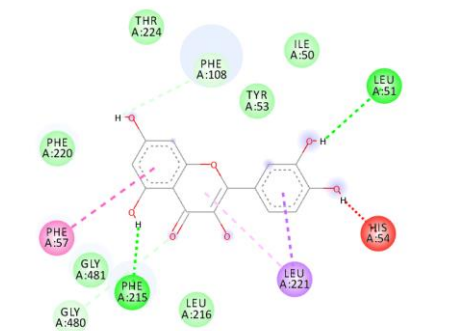

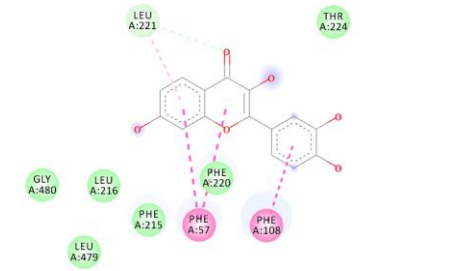
		XLogP (<5)	1.4		Met371, Gly481, Asp76, Leu482, Ile50, Leu221, Pro218, Leu216, Tyr53, Phe57, Phe220, Phe108, Arg105, Glu374
		H-Bond donor (5)	4		
		H-bond acceptor (<10)	9		
<u>Pongamoside B</u>	C ₂₄ H ₂₂ O ₁₀	Molecular weight (<500 DA)	470.4	-10.9	Arg372, Ala370, Met371, Leu216, Gly480, His54, Tyr53, Leu221, Thr224, Phe57, Arg106, Glu374, Arg105 (Forms unfavourable bond with Gly481)
		XLogP (<5)	1.4		
		H-Bond donor (5)	4		
		H-bond acceptor (<10)	10		
<u>Pongamoside D</u>	C ₂₃ H ₂₂ O ₁₁	Molecular weight (<500 DA)	474.4	-10.8	Phe57, Leu216, Tyr53, Gly480, Gly56, Leu479, His54, Leu221, Ile50, Asp76, Thr224, Phe220, Phe108
		XLogP (<5)	1		
		H-Bond donor (5)	4		
		H-bond acceptor (<10)	11		
<u>Pongamoside C</u>	C ₂₄ H ₂₂ O ₁₀	Molecular weight (<500 DA)	470.4	-10.6	Leu221, Pro218, Leu216, Asp217, Phe57, Phe108, Ile369, Gly481, Met371, Arg372, Glu374, Arg106, Phe215, Thr224, Ile50, Tyr53, Phe220
		XLogP (<5)	1.6		
		H-Bond donor (5)	2		
		H-bond acceptor (<10)	10		
<u>Cyclocommunin</u>	C ₂₅ H ₂₄ O ₆	Molecular weight (<500 DA)	420.4	-10.1	Phe215, Val240, Phe108, Thr224, Glu374, Arg372, Phe220, Phe213, Phe241, Phe304, Ile301
		XLogP (<5)	4.1		
		H-Bond donor (5)	3		
		H-bond acceptor (<10)	3		
<u>Daidzein</u>	C ₁₅ H ₁₀ O ₄	Molecular weight (<500 DA)	254.2	-9.3	Leu221, Ile50, Asp76, Arg106, Glu374, Arg372, Ala370, Leu373, Phe108, Phe57, Tyr53, Phe220, Thr224
		XLogP (<5)	2.5		
		H-Bond donor (5)	2		
		H-bond acceptor (<10)	4		
<u>Galangin</u>	C ₁₅ H ₁₀ O ₅	Molecular weight (<500 DA)	270.2	-9.3	Arg106, Tyr53, Phe220, Phe108, Phe57
		XLogP (<5)	2.3		
		H-Bond donor (5)	3		
		H-bond acceptor (<10)	5		
<u>Genistein</u>	C ₁₅ H ₁₀ O ₅	Molecular weight (<500 DA)	270.2	-9.1	Glu374, Phe57, Phe108, Phe220, Leu221, Thr224, Tyr53, Asp76, Arg372, Arg106, Leu373
		XLogP (<5)	2.7		
		H-Bond donor (5)	3		
		H-bond acceptor (<10)	5		
<u>Quercetin</u>	C ₁₅ H ₁₀ O ₇	Molecular weight (<500 DA)	302.2	-8.7	Thr224, Phe108, Tyr53, Ile50, Leu51, Leu221, Leu216, Phe215, Gly481, Gly480, Phe57, Phe220 (Forms unfavourable bond with His54)
		XLogP (<5)	1.5		
		H-Bond donor (5)	5		
		H-bond acceptor (<10)	7		
<u>Fisetin</u>	C ₁₅ H ₁₀ O ₆	Molecular weight (<500 DA)	286.2	-8.7	Leu221, Thr224, Phe108, Phe220, Phe57, Phe215, Leu479, Leu216, Gly480
		XLogP (<5)	2		
		H-Bond donor (5)	4		
		H-bond acceptor (<10)	6		
<u>Luteolin</u>	C ₁₅ H ₁₀ O ₆	Molecular weight (<500 DA)	286.2	-8.6	Phe215, Leu221, Phe57, Leu479, Gly56, His54, Ile50, Phe108, Thr225, Phe220
		XLogP (<5)	1.4		
		H-Bond donor (5)	4		
		H-bond acceptor (<10)	6		

Myricetin	C ₁₅ H ₁₀ O ₈	Molecular weight (<500 DA)	318.2	-8.6	Leu221, Phe57, Thr224, Phe215, Gly480, Leu216, Leu479, Ile50, Leu51, His54
		XLogP (<5)	1.2		
		H-Bond donor (5)	6		
		H-bond acceptor (<10)	8		
Isorhamnetin	C ₁₆ H ₁₂ O ₇	Molecular weight (<500 DA)	316.2	-8.4	Leu221, Pro218, Phe57, Thr224, Phe220, Phe215, Leu216, Gly480, Leu479, Tyr53, Ile50, Leu51, His54 (Forms unfavourable bond with Gly481)
		XLogP (<5)	1.9		
		H-Bond donor (5)	4		
		H-bond acceptor (<10)	7		
Kaempferol	C ₁₅ H ₁₀ O ₆	Molecular weight (<500 DA)	286.2	-8.4	Phe108, Phe215, Phe57, Gly481, Gly480, Leu216, Tyr53, Phe220, Thr224
		XLogP (<5)	9.8		
		H-Bond donor (5)	1		
		H-bond acceptor (<10)	1		
Pachypodol	C ₁₈ H ₁₆ O ₇	Molecular weight (<500 DA)	344.3	-8.3	Leu221, Pro218, Leu479, Gly480, Phe215, Leu216, Phe220, Thr224, Phe108, Phe57, Tyr53, His54, Ile50, Leu51
		XLogP (<5)	3.1		
		H-Bond donor (5)	2		
		H-bond acceptor (<10)	7		
Pelargonidin	C ₁₅ H ₁₁ O ₅ ⁺	Molecular weight (<500 DA)	271.2	-8.2	Tyr53, Phe215, Gly481, Phe220, Phe108, Leu221, Phe57, Thr224, Ile50
		XLogP (<5)	2.1		
		H-Bond donor (5)	4		
		H-bond acceptor (<10)	1		

Table 3. 3D- & 2D-images of docking poses along with no. of hydrogen bonds involved.

Name of Compound	3D-docking pose	2D-docking pose	No. of hydrogen bonds involved
Doxorubicin			02
Pongamoside A			00

<p>Pongamoside B</p>			<p>02</p>
<p>Pongamoside D</p>			<p>02</p>
<p>Pongamoside C</p>			<p>02</p>
<p>Cyclocommunin</p>			<p>00</p>

<p>Daidzein</p>			<p>04</p>
<p>Galangin</p>			<p>02</p>
<p>Genistein</p>			<p>04</p>
<p>Quercetin</p>			<p>02</p>
<p>Fisetin</p>			<p>00</p>

<p>Luteolin</p>			<p>03</p>
<p>Myricetin</p>			<p>01</p>
<p>Isorhamnetin</p>			<p>02</p>
<p>Kaempferol</p>			<p>00</p>

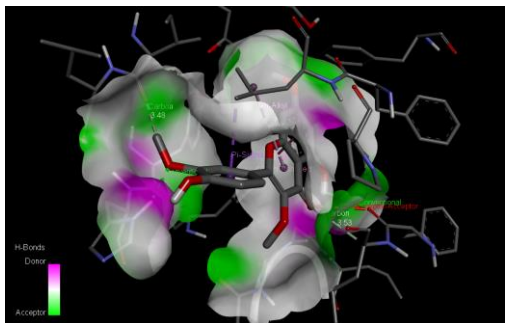
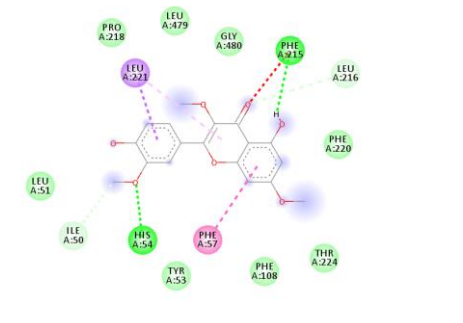
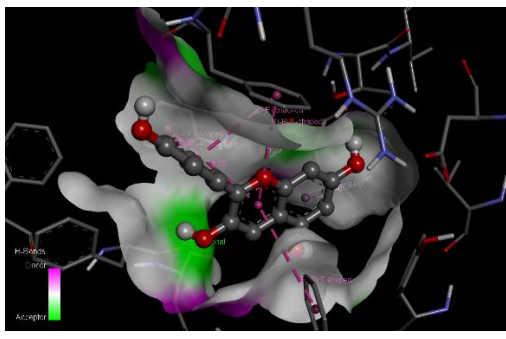
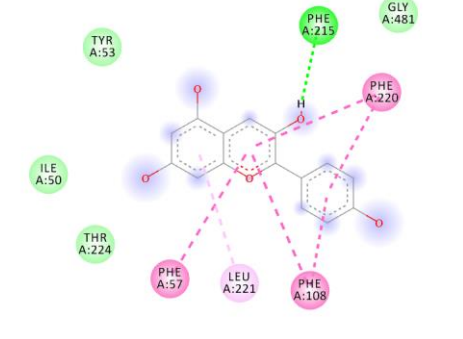
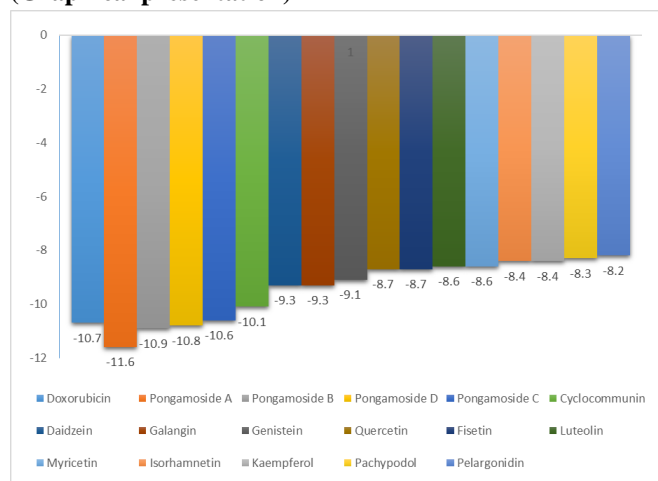
<p>Pachypodol</p>			<p>02</p>
<p>Pelargonidin</p>			<p>01</p>

Figure 1 represents the comparative binding affinities (kcal/mol) of doxorubicin and flavonoids. Many of the flavonoids have shown better binding affinity than doxorubicin.

Figure 1. Comparative binding affinities of the compounds (Graphical presentation)



As we have represented docking data along with 2D- & 3D-docking poses including no. hydrogen bonds involved in the interactions in Table 2. The formation of a hydrogen bond with the target molecule always results in inhibition of the receptor. Sadhna Sinha et al reported the Molecular docking of flavones at the colchicines binding pocket which revealed that the compounds bind at a-b interfacial site of tubulin,

correlating binding interactions with probable inhibition mechanism. The study reveals important observations to generate improved flavonoids that leads to cell apoptosis [15]. In case of Pongamoside A, it forms zero hydrogen bonds but still its binding affinity i.e. -11.6 kcal/mol is best because Pongamoside A forms van der Waals force attraction, Pi-Pi Stacked bonds, Pi-Pi T-shaped bonds, Amide-Pi stacked bonds and Pi alkyl bonds with more amino acid residues than doxorubicin i.e. -10.7 kcal/mol which forms two hydrogen bonds with CYP3A4. Pongamoside B and Pongamoside D have binding affinities (kcal/mol) -10.9 and -10.8 with the formation of 2-2 hydrogen bonds each with CYP3A4. This can be sufficient scientific evidence showing more potency of these flavonoids in terms of inhibition of CYP3A4 than the approved drug, doxorubicin. Although, Pongamoside C, Galangin, Quercetin, Isorhamnetin, Pachypodol forms 2-2 hydrogen bonds each with binding affinities -10.6, -9.3, -8.7, -8.4 and -8.3 kcal/mol respectively. Surprisingly Daidzein and Genistein formed 4 hydrogen bonds each with CYP3A4 with a docking score of -9.3 and -9.1 kcal/mol respectively which is much enough to inhibit the activity of CYP3A4. Luteolin has formed 3 hydrogen bonds with -8.6 kcal/mol binding affinity. The amino acid residues in the cavity involved in the interactions are represented in **Table 1**.

CONCLUSION

It is well known that natural compounds have proven to have a safe biological window as compared to molecules from a synthetic source. In present work, molecular docking studies disclosed, that flavonoids Pongamoside A, Pongamoside B,

and Pongamoside D have a better binding affinity towards CYP3A4 than doxorubicin. Although, if we talk about the formation of hydrogen bonds with target macromolecule, Daidzein, Genistein, and Luteolin form more hydrogen bonds than doxorubicin. In conclusion, the above docking study disclosed that rational synthesis of natural analogues in reference to synthetic drugs could generate drugs with improved therapeutic effects for chemoprevention. CYP3A4 plays a major role in the metabolism of various drugs; by the help of flavonoids, we can control the selective drug metabolism by inhibiting CYP3A4. Despite this, these molecules are not marketed for cancer treatment because of their high polarity. If we could overcome this problem, these molecules can act as effective anticancer agents in the future. Still, if we want to use these compounds clinically, there is a need to generate more scientific evidence and quality data by using *in vivo* and *in vitro* models.

ACKNOWLEDGEMENT

None

CONFLICTS OF INTEREST

None.

DATA AVAILABILITY

Not declared.

FUNDING SOURCE

Not declared

REFERENCES

[1] Grigalius I, Petrikaite V. Relationship between antioxidant and anticancer activity of trihydroxyflavones. *Molecules.*, 2017;22. <https://doi.org/10.3390/molecules22122169>.

[2] Ravishankar D, Rajora AK, Greco F, Osborn HMI. Flavonoids as prospective compounds for anti - cancer therapy. *Int J Biochem Cell Biol.*, 2016:1–5. <https://doi.org/10.1016/j.biocel.2013.10.004>.

[3] Mehranfar F, Bordbar AK, Parastar H. A combined spectroscopic, molecular docking and molecular dynamic simulation study on the interaction of quercetin with β -casein nanoparticles. *J Photochem Photobiol B Biol.*, 2013;127:100–7. <https://doi.org/10.1016/j.jphotobiol.2013.07.019>.

[4] Iqbal J, Abbasi BA, Mahmood T, Kanwal S, Ali B, Shah SA, et al. Plant-derived anticancer agents: A green anticancer approach. *Asian Pac J Trop Biomed.*, 2017;7:1129–50. <https://doi.org/10.1016/j.apjtb.2017.10.016>.

[5] Balachandran C, Sangeetha B, Duraipandiyan V, Raj MK, Ignacimuthu S, Al-Dhabi NA, et al. A flavonoid isolated from *Streptomyces* sp. (ERINLG-4) induces apoptosis in

human lung cancer A549 cells through p53 and cytochrome c release caspase dependant pathway. *Chem Biol Interact.*, 2014;224:24–35. <https://doi.org/10.1016/j.cbi.2014.09.019>.

[6] Iqbal J, Abbasi BA, Mahmood T, Kanwal S, Ali B, Khalil AT. Plant-derived anticancer agents : A green anticancer approach. *Asian Pac J Trop Biomed.*, 2017:1–23. <https://doi.org/10.1016/j.apjtb.2017.10.016>.

[7] Kumar P. PLANT DERIVED ANTICANCER AGENTS AND THEIR STRUCTURE: A REVIEW. *Int Res J Pharm.*, 2018;9:43–9. <https://doi.org/10.7897/2230-8407.09687>.

[8] Cacabelos R, Cacabelos P, Torrellas C. Personalized Medicine of Alzheimer ' s Disease. Elsevier Inc.; 2014. <https://doi.org/10.1016/B978-0-12-386882-4.00027-X>.

[9] Gurusamy U, Shewade DG. Pharmacogenomics in India. Elsevier Inc.; 2014. <https://doi.org/10.1016/B978-0-12-386882-4.00046-3>.

[10] Hejazi II, Khanam R, Mehdi SH, Bhat AR, Rizvi MMA, Thakur SC, et al. Antioxidative and anti-proliferative potential of *Curculigo orchoides* Gaertn in oxidative stress induced cytotoxicity: In vitro, ex vivo and in silico studies. *Food Chem Toxicol.*, 2018;115:244–59. <https://doi.org/10.1016/j.fct.2018.03.013>.

[11] Rasouli H, Farzaei MH, Mansouri K, Mohammadzadeh S, Khodarahmi R. Plant cell cancer: May natural phenolic compounds prevent onset and development of plant cell malignancy? A literature review. *Molecules.*, 2016;21:14–21. <https://doi.org/10.3390/molecules21091104>.

[12] Phosrithong N, Ungwitayatorn J. Molecular docking study on anticancer activity of plant-derived natural products. *Med Chem Res.*, 2010;19:817–35. <https://doi.org/10.1007/s00044-009-9233-5>.

[13] Saeed M, Kadioglu O, Khalid H, Sugimoto Y, Efferth T. Activity of the dietary flavonoid, apigenin, against multidrug-resistant tumor cells as determined by pharmacogenomics and molecular docking. *J Nutr Biochem.*, 2015;26:44–56. <https://doi.org/10.1016/j.jnutbio.2014.09.008>.

[14] Mokale SN, Begum A, Sakle NS, Shelke VR, Bhavale SA. Design , synthesis and anticancer screening of 3- (3- (substituted phenyl) acryloyl) -2H-chromen-2ones as selective anti-breast cancer agent. *Biomed Pharmacother.*, 2017;89:966–72. <https://doi.org/10.1016/j.biopha.2017.02.089>.

[15] Sinha S, Amin H, Nayak D, Bhatnagar M, Kacker P, Chakraborty S, et al. Assessment of microtubule depolymerization property of flavonoids isolated from *Tanacetum gracile* in breast cancer cells by biochemical and molecular docking approach. *Chem Biol Interact.*, 2015;239:1–11. <https://doi.org/10.1016/j.cbi.2015.06.034>.

[16] Skiff, A. K. Rappe, C. J. Casewit, K. S. Colwell, W. A. Goddard III WMS. UFF, a Full Periodic Table Force Field for Molecular Mechanics and Molecular Dynamics Simulations. *J Am Chem Soc.*, 2009;114:10024–35. <https://doi.org/https://doi.org/10.1021/ja00051a040>.

[17] Dassault Systèmes BIOVIA, Discovery Studio Modeling Environment, Release 2017, San Diego: Dassault Systèmes., 2016.

- [18] Dallakyan S, Olson AJ. Small-molecule library screening by docking with PyRx. *Methods Mol Biol.*, 2015;1263:243–50. https://doi.org/10.1007/978-1-4939-2269-7_19.

Indo Global Journal of Pharmaceutical Sciences(ISSN 2249 1023; CODEN- IGJPAI; NLM ID: 101610675) indexed and abstracted in CrossRef (DOI Enabling), CNKI, UGC CARE Journal List, EMBASE (Elsevier), National Library of Medicine (NLM) Catalog (NCBI), ResearchGate, Publons (Clarivate Analytics), CAS (ACS), Index Copernicus, Google Scholar and many more. For further details, visit <http://iglobaljournal.com>



Discovery of Naturally Occurring Flavonoids as Human Cytochrome P450 (CYP3A4) Inhibitors with the Aid of Computational Chemistry

Sharuk L. Khan ^{1*}, Gajanan M. Sonwane ¹, Falak A. Siddiqui ¹, Shirish P. Jain ¹, Mayura A. Kale ²,
Vijay S. Borkar ¹

¹ Rajarshi Shahu College of Pharmacy, Buldana, Maharashtra, India 443001.

² Government College of Pharmacy, Aurangabad, Maharashtra, India 431005

Address for Correspondence: Sharuk L.Khan, sharique.4u4@gmail.com

Received:

13.07.2019

Accepted:

11.04.2020

Published:

20.12.2020

Keywords

Human
Cytochrome
P450 (CYP3A4);
Flavonoids;
Doxorubicin;
Molecular
docking; PyRx
Virtual Screening
Tool.

ABSTRACT: Purpose: The human cytochrome P450 3A4 (CYP3A4) is the biggest individual from the CYP3A subfamily and records for 30–60% of the total for CYP450 adult liver. Hereditary varieties in CYP3A4 are a noteworthy hotspot for inter-patient changeability in plasma concentration, adverse effects and pharmacological response to medications. This research was done to discover naturally occurring novel CYP3A4 inhibitors from flavonoids. Methods: The molecular docking method was used to optimize the inhibiting activity of flavonoids against CYP3A4. PyRx Virtual Screening Tool 0.8 and BIOVIA Discovery Studio 2019 was used for simulation. Results: Flavonoids like Pongamoside A, Pongamoside B, and Pongamoside D have more binding affinity (kcal/mol) i.e. -11.6, -10.9, -10.8 respectively than Doxorubicin which have -10.7 against CYP3A4. Although, Daidzein, Genistein, and Luteolin form more hydrogen bonds than doxorubicin. Conclusion: The rational synthesis of natural analogues in reference to synthetic drugs, could generate drugs with improved therapeutic effect for chemoprevention. CYP3A4 plays a major role in the metabolism of various drugs; by the help of flavonoids, we can control the selective drug metabolism by inhibiting CYP3A4. Despite this, these molecules are not marketed for cancer treatment because of high polarity. If we could overcome this problem, these molecules can acts as effective anticancer agents in the future. Still, if we want to use these compounds clinically, there is a need to generate more scientific evidence and quality data by using *in vivo* and *in vitro* models. © 2020 iGlobal Research and Publishing Foundation. All rights reserved.

Cite this article as: Khan, S.L.; Sonwane, G.M.; Siddiqui, F.A.; Jain, S.P.; Kale, M.A.; Borkar, V.S. Discovery of naturally occurring flavonoids as human cytochrome P450 (CYP3A4) inhibitors with the aid of computational chemistry. Indo Global J. Pharm. Sci., 2020; 10(4): 58-69. DOI: <http://doi.org/10.35652/IGJPS.2020.10409> .

INTRODUCTION

Flavonoids are a well-known category of polyphenolic compounds. These are the regular dietary materials of the human, as many of the plants contains flavonoids. There are plenty of plants that exerts good pharmacological properties including anticancer activity just because of the presence of flavonoids. Flavonoids are the essential plant shades that act as chemical messengers, physiological controllers, and cell cycle inhibitors [1]. Flavonoids stand out amongst the most tried and broadly distributed substances of plant sources. They are found in natural products, vegetables, leguminous plants and even a few sorts of greenery. The skeleton of flavonoids

comprises of 1-benzopyran. It is a C6-C3-C6 framework, in which sweet-smelling rings are associated, shaping a focal pyran or pyron cycle. Contingent upon the position to which ring is associated with the chromane, flavonoids are grouped into isoflavonoids and neoflavonoids [2].

Amongst the different other natural substances, flavonoids hold much consideration because of their noteworthy range of pharmacological activities, such as cell reinforcement, antimutagenic, antibacterial, antiangiogenic, anti-

inflammatory, anti-allergic, modulators of enzymatic activities and anti-cancer activity [3]. Apigenin, luteolin, quercetin and kaempferol, the hydroxylated flavonoids are the main constituents of various dietary products and beverages and have been the focus of extensive research over the last years. Apigenin exerts anticancer effects through the modulation of various pathways namely, apoptosis, Reactive oxygen species (ROS) and DNA damage and repair [4].

Malignant growth is one of the terrible illnesses caused by unusual cell growth and can attack different tissues. They shape a subset of neoplasms. It speaks of the greatest social insurance issues for humankind and requests a proactive system for cure [5]. It is accounted for the rate of malignancy that has been expanding in developing nations and has turned into the fourth driving reason for death around the world. Chemoprevention by phytoconstituents has advanced as a powerful procedure to control the prevalence of malignant growth. The journey of anticancer agents from plant sources began in the 1950s with the discovery of the vinca alkaloids, vincristine, vinblastine, combretastatin, and colchicine. These Phytochemicals act explicitly on tumor cells without influencing non-cancerous cells. Carcinogenesis is a mind-boggling marvel that includes many signaling cascades. Phytochemicals are viewed as reasonable candidates for anticancer medication advancement due to their pleiotropic activities on target. The examination is in advancement for creating potential competitors (those can square or back off the development of disease cells without any side effects) from these phytochemicals. Numerous phytochemicals and their determined analogs have been distinguished as potential candidates for anticancer treatment. Plants serve as a source of novel compound elements and give a promising line to investigate on malignant growth. The plant and plant metabolites are the reforming sources as these are simple, more secure, easy, quick, and less dangerous as contrasted to traditional treatment methods. There is a positive relationship set up by the epidemiological examinations between expanded utilization of common items with diminished danger of disease. The mechanism responsible for chemoprevention remains essentially unidentified, however, it is likely identified with the closeness of phytochemicals related to plants. Consequently, the search for powerful and more secure natural anticancer agents have attracted the researchers throughout the world. [6,7].

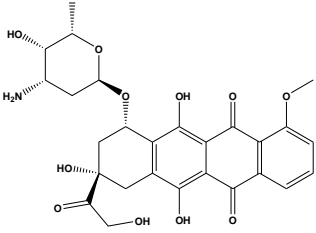
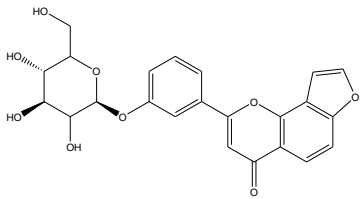
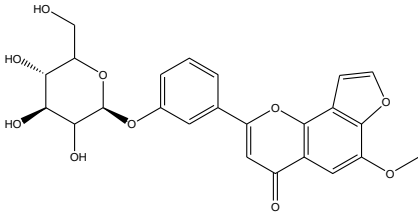
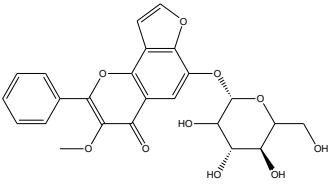
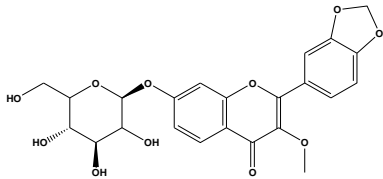
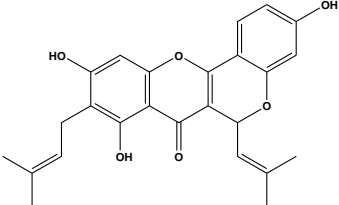
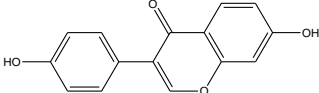
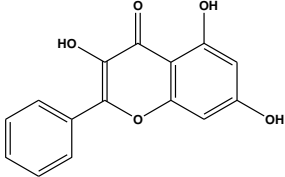
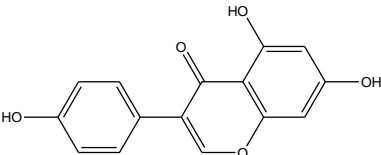
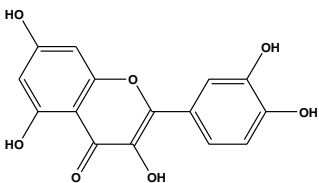
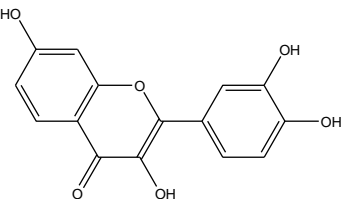
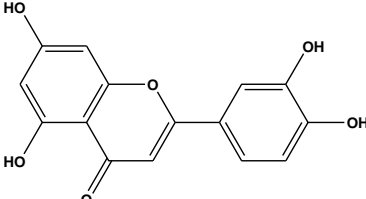
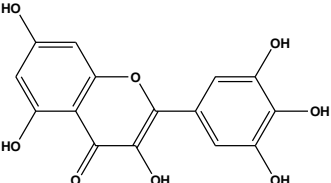
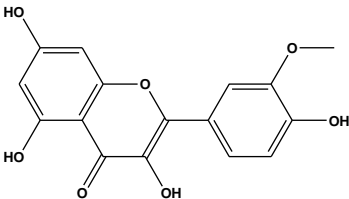
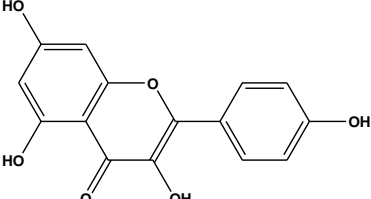
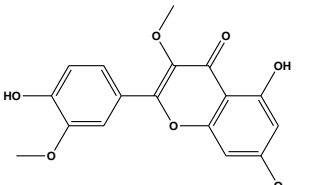
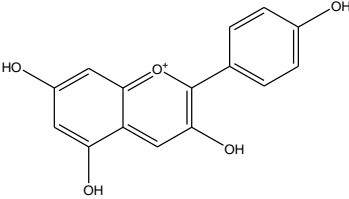
The human cytochrome P450 3A4 (CYP3A4) is the biggest individual from the CYP3A subfamily and records for 30–60% of the total for CYP450 adult liver. The CYP3A4 gene is limited on chromosome 7q21 and up to now, 41 CYP3A4 alleles have been recognized. The human CYP3A locus

contains the three CYP3A gene (CYP3A4, CYP3A5, and CYP3A7), three pseudogenes, and a novel CYP3A gene named CYP3A43. Hereditary varieties in CYP3A4 are a noteworthy hotspot for inter-patient changeability in plasma concentration, adverse effects and pharmacological response to medications, for example, paclitaxel, fentanyl, tamoxifen, tacrolimus, and statins. Moreover, existing investigations have announced the role of CYP3A4 inadequate alleles in the disease susceptibility to prostate malignant growth, estrogen receptor-negative breast cancer, and type-2 diabetes [8,9].

Protein-ligand docking is a fundamental part of computer-aided drug design, and it distinguishes the coupling pattern of proteins and ligands by computer simulation. Molecular docking results decide a general binding mode of a ligand. Varieties of compounds from plant sources have been accounted to have significant anticancer properties; in any case, their modes of activity have not been characterized. Molecular docking studies were performed on some flavonoids by using Autodock vina 1.1.2 in PyRx 0.8. [10]. The docking was performed utilizing receptor proteins required with cell cycle, cell development, and DNA replication, i.e., cyclin-subordinate protein kinase 2 (CDK-2), CDK-6, DNA topoisomerases I and II, B-cell lymphoma 2 (Bcl-2), vascular endothelial development factor receptor 2 (VEGFR-2), and the telomere: G-quadruplexes. By molecular docking, the bound confirmations and the coupling attachment among flavonoid and CYP3A4 as the target could be anticipated [11]. Doxorubicin, sold under the brand names adriamycin, used to treat breast malignant growth, bladder cancer, lymphoma, and intense lymphocytic leukemia was utilized for docking studies whose binding interactions were compared with the flavonoids [12].

Docking of the small molecule into the binding site of a receptor and guessing the binding interaction of the complex is a noteworthy part of the structure-based drug design process. By molecular docking, the bound conformations and the binding affinity between Flavonoids and human cytochrome P450 3A4 as the target could be predicted [13]. **Table 1** represents the names and structures of doxorubicin and the flavonoids used for molecular docking. The structures of all the compounds were generated by using ChemDraw Ultra 8.0 with the help of IUPAC name took from the official website of U.S. National Library of Medicine PubChem (<https://pubchem.ncbi.nlm.nih.gov/>).

Table 1. Name and Structures of compounds used for molecular docking

Doxorubicin	Pongamoside A	Pongamoside B
		
Pongamoside C	Pongamoside D	Cyclocommunin
		
Daidzein	Galangin	Genistein
		
Quercetin	Fisetin	Luteolin
		
Myricetin	Isorhamnetin	Kaempferol
		
Pachypodol	Pelargonidin	
		

MATERIALS AND METHODS

System used for Molecular docking

Molecular docking was performed on Lenovo ThinkPad with 64-bit operating system, Processor: Intel(R) Core(TM) i5-4300M CPU @2.60 GHz 2.59 GHz, RAM: 4GB by using PyRx-Virtual Screening Tool.

Ligand Preparation

The Structures of all the compounds (SDF File) were downloaded from the official website of the U.S. National Library of Medicine PubChem (<https://pubchem.ncbi.nlm.nih.gov/>). Structures then imported into PyRx 0.8 using open bable tool and energy minimization

(optimization) was performed by considering fundamental parameters based on the element, its hybridization, and connectivity i.e. by Universal Force Field (UFF)[16]. These ligands were then converted to AutoDock Ligand format (PDBQT).

Macromolecule Preparation

Autodock vina 1.1.2 in PyRx 0.8 was used to perform the docking studies of all the compounds against the crystal structure of human cytochrome P450 3A4 (CYP3A4). The crystal structure of CYP3A4 was obtained from the RCSB Protein Data Bank (PDB) with PDB ID-4K9T (<http://www.rcsb.org/structure/4K9T>) with Homo sapiens organism and Escherichia coli expression system. The CYP3A4 crystal structure was optimized, purified and prepared for docking with the help of Discovery Studio Visualizer 2019 by removing unwanted water molecules, bound ligands from protein structure and saved again in PDB file format to the same folder[17].

Molecular Docking Procedure

The purified CYP3A4 crystal structure file was loaded to docking software PyRx 0.8 using a load molecule option from the File toolbar. Chain-A was used to perform the docking, as it contains the active site which confirmed by checking interactions of native ligand present in the crystal structure (<http://www.rcsb.org/3d-view/4K9T?preset=ligandInteraction&sele=1RD>). The CYP3A4 crystal structure was then converted to Autodock macromolecule (pdbqt format) by using the right-click option. Binding affinity studies were performed by using Vina Wizard Tool in PyRx 0.8. All the ligand molecules (PDBQT Files), and target (CYP3A4) were selected for docking study. For molecular docking simulation, the three-dimensional grid box (size_x = 18.5286782874Ao; size_y = 26.047226475Ao; size_z = -9.59195798998Ao) was designed using Autodock tool 1.5.6 with exhaustiveness value of 8. After selecting molecules, the active amino acid residues were selected to define the cavity with the help of Toggle Selection Spheres

option given in PyRx[18]. To occupy all the active binding sites and essential residues, the grid box was aligned properly. All the ligands and CYP3A4 then subjected for docking to get the finding affinities.

Identification of Cavity and Active Amino Acid Residues

The active amino acid residues in the protein were identified and noted using BIOVIA Discovery Studio Visualizer (version-19.1.0.18287)[17]. The selection of the amino acids in the active site was used to analyze the grid box and to define the cavity. All the docking poses, ligand and protein interactions were studied by importing output files into Discovery Studio which enables us to identify the types of interactions. Discovery Studio is an offline life sciences software that offers tools to study drug-receptor interaction, docking poses visualization and macromolecule preparations. The chosen cavity was the binding site of the native ligand in PDB 4K9T.

RESULTS AND DISCUSSION

All the flavonoids and doxorubicin successfully docked on CYP3A4. Binding energy is released when a drug molecule associates with a target, leading to a lowering of the overall energy of the complex [14]. Molecular formula, Lipinski’s rule of five, binding affinity (kcal/mol), and active amino acid residues are presented in Table 1. Lipinski’s rule of five plays an important role in molecule screening and validation. Here, Pongamosides i.e. Pongamoside A, Pongamoside B, and Pongamoside D have shown better binding affinity than doxorubicin.

Table 2 represents 3D- & 2D-images of docking poses along with no. of hydrogen bonds involved in the interaction. The 2D-docking pose also shows the chemical structure of the ligands which enables us to predict groups and/or atoms involved in the bond formation with CYP3A4.

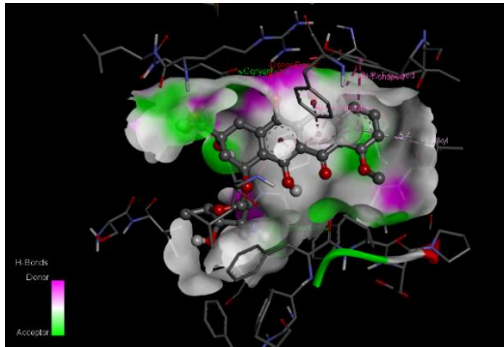
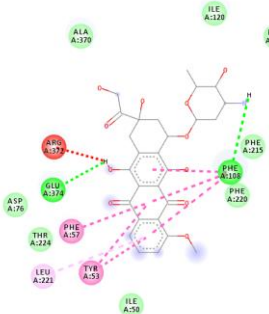
Table 2. Properties, Lipinski’s rule of five, binding affinity and active amino acid residues.

Name of Compound	Molecular Formula	Lipinski’s rule of five		Binding affinity (kcal/mol)	Active amino acid residues
Doxorubicin	C ₂₇ H ₂₉ NO ₁₁	Molecular weight (<500 DA)	543.5	-10.7	Ala370, Ile120, Phe241, Phe213, Val240, Phe215, Phe108, Phe220, Ile50, Tyr53, Leu221, Phe57, Thr224, Asp76, Glu374 (Forms unfavourable bond with Arg372)
		XLogP (<5)	1.3		
		H-Bond donor (5)	6		
		H-bond acceptor (<10)	12		
Pongamoside A	C ₂₃ H ₂₀ O ₉	Molecular weight (<500 DA)	440.4	-11.6	Leu373, Ala370, Arg372,

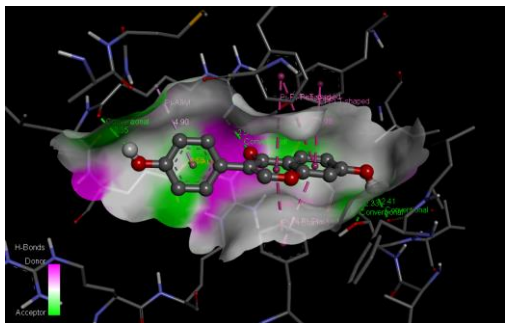
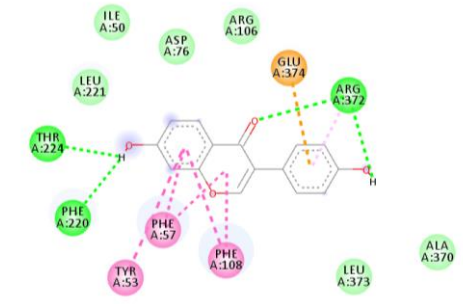
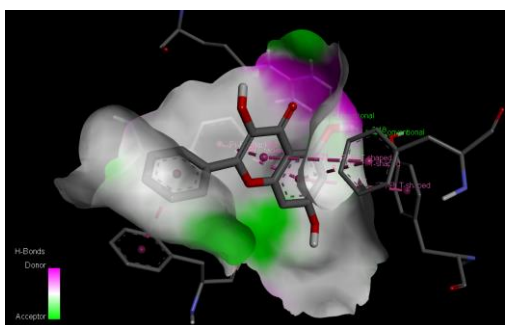
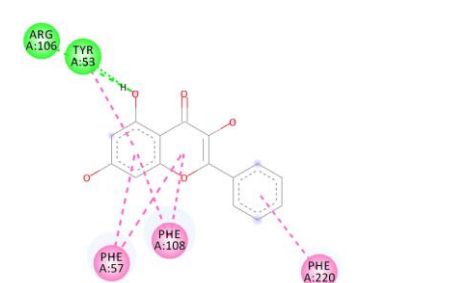
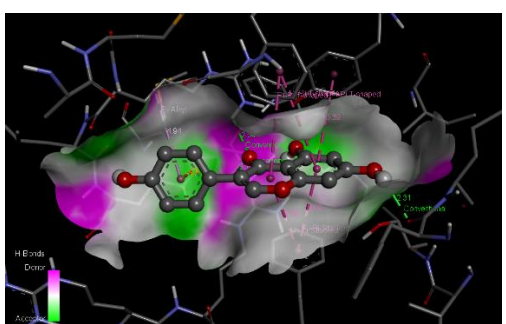
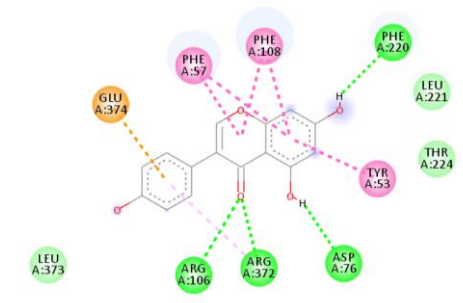
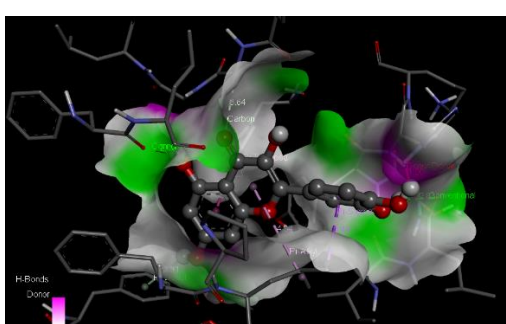
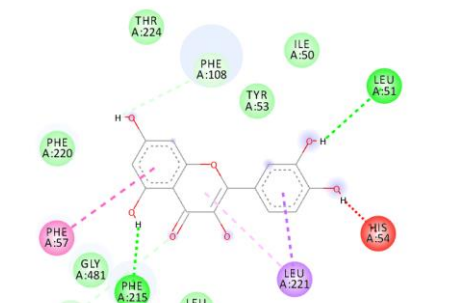
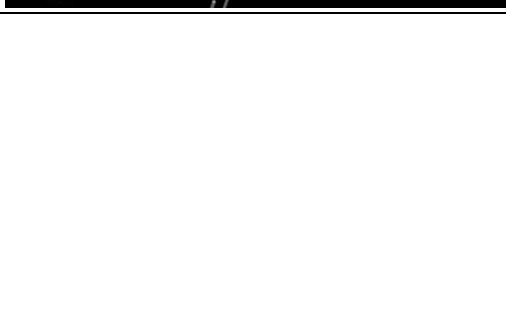
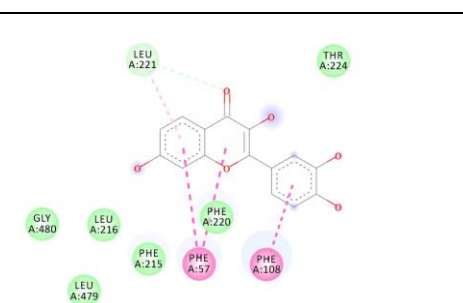
		XLogP (<5)	1.4		Met371, Gly481, Asp76, Leu482, Ile50, Leu221, Pro218, Leu216, Tyr53, Phe57, Phe220, Phe108, Arg105, Glu374
		H-Bond donor (5)	4		
		H-bond acceptor (<10)	9		
<u>Pongamoside B</u>	C ₂₄ H ₂₂ O ₁₀	Molecular weight (<500 DA)	470.4	-10.9	Arg372, Ala370, Met371, Leu216, Gly480, His54, Tyr53, Leu221, Thr224, Phe57, Arg106, Glu374, Arg105 (Forms unfavourable bond with Gly481)
		XLogP (<5)	1.4		
		H-Bond donor (5)	4		
		H-bond acceptor (<10)	10		
<u>Pongamoside D</u>	C ₂₃ H ₂₂ O ₁₁	Molecular weight (<500 DA)	474.4	-10.8	Phe57, Leu216, Tyr53, Gly480, Gly56, Leu479, His54, Leu221, Ile50, Asp76, Thr224, Phe220, Phe108
		XLogP (<5)	1		
		H-Bond donor (5)	4		
		H-bond acceptor (<10)	11		
<u>Pongamoside C</u>	C ₂₄ H ₂₂ O ₁₀	Molecular weight (<500 DA)	470.4	-10.6	Leu221, Pro218, Leu216, Asp217, Phe57, Phe108, Ile369, Gly481, Met371, Arg372, Glu374, Arg106, Phe215, Thr224, Ile50, Tyr53, Phe220
		XLogP (<5)	1.6		
		H-Bond donor (5)	2		
		H-bond acceptor (<10)	10		
<u>Cyclocommunin</u>	C ₂₅ H ₂₄ O ₆	Molecular weight (<500 DA)	420.4	-10.1	Phe215, Val240, Phe108, Thr224, Glu374, Arg372, Phe220, Phe213, Phe241, Phe304, Ile301
		XLogP (<5)	4.1		
		H-Bond donor (5)	3		
		H-bond acceptor (<10)	3		
<u>Daidzein</u>	C ₁₅ H ₁₀ O ₄	Molecular weight (<500 DA)	254.2	-9.3	Leu221, Ile50, Asp76, Arg106, Glu374, Arg372, Ala370, Leu373, Phe108, Phe57, Tyr53, Phe220, Thr224
		XLogP (<5)	2.5		
		H-Bond donor (5)	2		
		H-bond acceptor (<10)	4		
<u>Galangin</u>	C ₁₅ H ₁₀ O ₅	Molecular weight (<500 DA)	270.2	-9.3	Arg106, Tyr53, Phe220, Phe108, Phe57
		XLogP (<5)	2.3		
		H-Bond donor (5)	3		
		H-bond acceptor (<10)	5		
<u>Genistein</u>	C ₁₅ H ₁₀ O ₅	Molecular weight (<500 DA)	270.2	-9.1	Glu374, Phe57, Phe108, Phe220, Leu221, Thr224, Tyr53, Asp76, Arg372, Arg106, Leu373
		XLogP (<5)	2.7		
		H-Bond donor (5)	3		
		H-bond acceptor (<10)	5		
<u>Quercetin</u>	C ₁₅ H ₁₀ O ₇	Molecular weight (<500 DA)	302.2	-8.7	Thr224, Phe108, Tyr53, Ile50, Leu51, Leu221, Leu216, Phe215, Gly481, Gly480, Phe57, Phe220 (Forms unfavourable bond with His54)
		XLogP (<5)	1.5		
		H-Bond donor (5)	5		
		H-bond acceptor (<10)	7		
<u>Fisetin</u>	C ₁₅ H ₁₀ O ₆	Molecular weight (<500 DA)	286.2	-8.7	Leu221, Thr224, Phe108, Phe220, Phe57, Phe215, Leu479, Leu216, Gly480
		XLogP (<5)	2		
		H-Bond donor (5)	4		
		H-bond acceptor (<10)	6		
<u>Luteolin</u>	C ₁₅ H ₁₀ O ₆	Molecular weight (<500 DA)	286.2	-8.6	Phe215, Leu221, Phe57, Leu479, Gly56, His54, Ile50, Phe108, Thr225, Phe220
		XLogP (<5)	1.4		
		H-Bond donor (5)	4		
		H-bond acceptor (<10)	6		

Myricetin	C ₁₅ H ₁₀ O ₈	Molecular weight (<500 DA)	318.2	-8.6	Leu221, Phe57, Thr224, Phe215, Gly480, Leu216, Leu479, Ile50, Leu51, His54
		XLogP (<5)	1.2		
		H-Bond donor (5)	6		
		H-bond acceptor (<10)	8		
Isorhamnetin	C ₁₆ H ₁₂ O ₇	Molecular weight (<500 DA)	316.2	-8.4	Leu221, Pro218, Phe57, Thr224, Phe220, Phe215, Leu216, Gly480, Leu479, Tyr53, Ile50, Leu51, His54 (Forms unfavourable bond with Gly481)
		XLogP (<5)	1.9		
		H-Bond donor (5)	4		
		H-bond acceptor (<10)	7		
Kaempferol	C ₁₅ H ₁₀ O ₆	Molecular weight (<500 DA)	286.2	-8.4	Phe108, Phe215, Phe57, Gly481, Gly480, Leu216, Tyr53, Phe220, Thr224
		XLogP (<5)	9.8		
		H-Bond donor (5)	1		
		H-bond acceptor (<10)	1		
Pachypodol	C ₁₈ H ₁₆ O ₇	Molecular weight (<500 DA)	344.3	-8.3	Leu221, Pro218, Leu479, Gly480, Phe215, Leu216, Phe220, Thr224, Phe108, Phe57, Tyr53, His54, Ile50, Leu51
		XLogP (<5)	3.1		
		H-Bond donor (5)	2		
		H-bond acceptor (<10)	7		
Pelargonidin	C ₁₅ H ₁₁ O ₅ ⁺	Molecular weight (<500 DA)	271.2	-8.2	Tyr53, Phe215, Gly481, Phe220, Phe108, Leu221, Phe57, Thr224, Ile50
		XLogP (<5)	2.1		
		H-Bond donor (5)	4		
		H-bond acceptor (<10)	1		

Table 3. 3D- & 2D-images of docking poses along with no. of hydrogen bonds involved.

Name of Compound	3D-docking pose	2D-docking pose	No. of hydrogen bonds involved
Doxorubicin			02
Pongamoside A			00

<p>Pongamoside B</p>			<p>02</p>
<p>Pongamoside D</p>			<p>02</p>
<p>Pongamoside C</p>			<p>02</p>
<p>Cyclocommunin</p>			<p>00</p>

<p>Daidzein</p>			<p>04</p>
<p>Galangin</p>			<p>02</p>
<p>Genistein</p>			<p>04</p>
<p>Quercetin</p>			<p>02</p>
<p>Fisetin</p>			<p>00</p>

	<p>H-Bonds Donor Acceptor</p>		
<p>Luteolin</p>	<p>H-Bonds Donor Acceptor</p>		<p>03</p>
<p>Myricetin</p>	<p>H-Bonds Donor Acceptor</p>		<p>01</p>
<p>Isorhamnetin</p>	<p>H-Bonds Donor Acceptor</p>		<p>02</p>
<p>Kaempferol</p>	<p>H-Bonds Donor Acceptor</p>		<p>00</p>

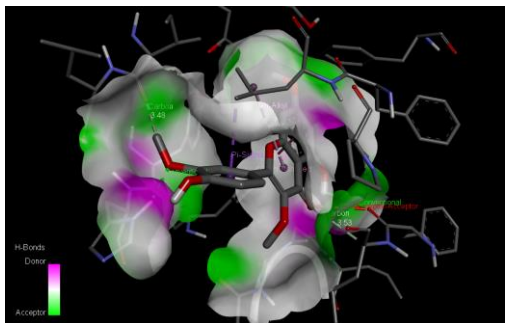
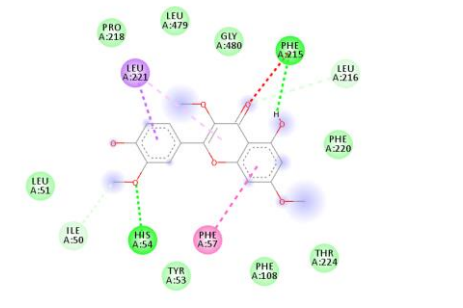
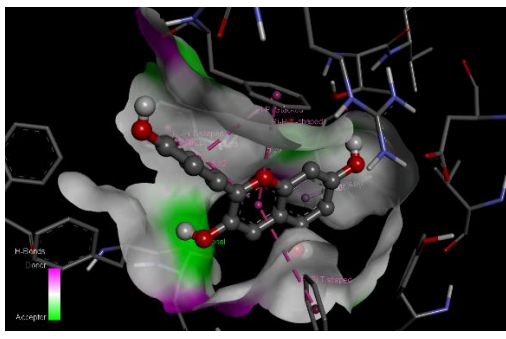
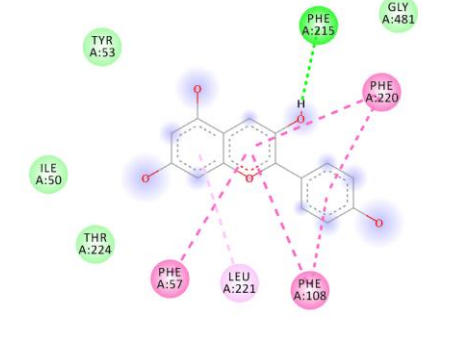
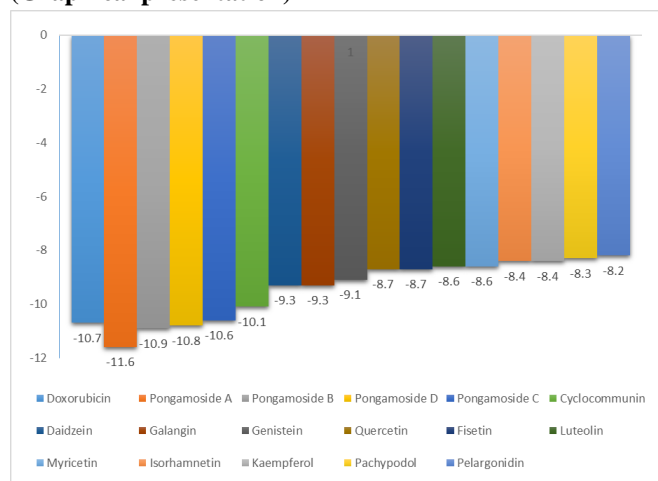
<p>Pachypodol</p>			<p>02</p>
<p>Pelargonidin</p>			<p>01</p>

Figure 1 represents the comparative binding affinities (kcal/mol) of doxorubicin and flavonoids. Many of the flavonoids have shown better binding affinity than doxorubicin.

Figure 1. Comparative binding affinities of the compounds (Graphical presentation)



As we have represented docking data along with 2D- & 3D-docking poses including no. hydrogen bonds involved in the interactions in Table 2. The formation of a hydrogen bond with the target molecule always results in inhibition of the receptor. Sadhna Sinha et al reported the Molecular docking of flavones at the colchicines binding pocket which revealed that the compounds bind at a-b interfacial site of tubulin,

correlating binding interactions with probable inhibition mechanism. The study reveals important observations to generate improved flavonoids that leads to cell apoptosis [15]. In case of Pongamoside A, it forms zero hydrogen bonds but still its binding affinity i.e. -11.6 kcal/mol is best because Pongamoside A forms van der Waals force attraction, Pi-Pi Stacked bonds, Pi-Pi T-shaped bonds, Amide-Pi stacked bonds and Pi alkyl bonds with more amino acid residues than doxorubicin i.e. -10.7 kcal/mol which forms two hydrogen bonds with CYP3A4. Pongamoside B and Pongamoside D have binding affinities (kcal/mol) -10.9 and -10.8 with the formation of 2-2 hydrogen bonds each with CYP3A4. This can be sufficient scientific evidence showing more potency of these flavonoids in terms of inhibition of CYP3A4 than the approved drug, doxorubicin. Although, Pongamoside C, Galangin, Quercetin, Isorhamnetin, Pachypodol forms 2-2 hydrogen bonds each with binding affinities -10.6, -9.3, -8.7, -8.4 and -8.3 kcal/mol respectively. Surprisingly Daidzein and Genistein formed 4 hydrogen bonds each with CYP3A4 with a docking score of -9.3 and -9.1 kcal/mol respectively which is much enough to inhibit the activity of CYP3A4. Luteolin has formed 3 hydrogen bonds with -8.6 kcal/mol binding affinity. The amino acid residues in the cavity involved in the interactions are represented in **Table 1**.

CONCLUSION

It is well known that natural compounds have proven to have a safe biological window as compared to molecules from a synthetic source. In present work, molecular docking studies disclosed, that flavonoids Pongamoside A, Pongamoside B,

and Pongamoside D have a better binding affinity towards CYP3A4 than doxorubicin. Although, if we talk about the formation of hydrogen bonds with target macromolecule, Daidzein, Genistein, and Luteolin form more hydrogen bonds than doxorubicin. In conclusion, the above docking study disclosed that rational synthesis of natural analogues in reference to synthetic drugs could generate drugs with improved therapeutic effects for chemoprevention. CYP3A4 plays a major role in the metabolism of various drugs; by the help of flavonoids, we can control the selective drug metabolism by inhibiting CYP3A4. Despite this, these molecules are not marketed for cancer treatment because of their high polarity. If we could overcome this problem, these molecules can act as effective anticancer agents in the future. Still, if we want to use these compounds clinically, there is a need to generate more scientific evidence and quality data by using *in vivo* and *in vitro* models.

ACKNOWLEDGEMENT

None

CONFLICTS OF INTEREST

None.

DATA AVAILABILITY

Not declared.

FUNDING SOURCE

Not declared

REFERENCES

- [1] Grigalius I, Petrikaite V. Relationship between antioxidant and anticancer activity of trihydroxyflavones. *Molecules.*, 2017;22. <https://doi.org/10.3390/molecules22122169>.
- [2] Ravishankar D, Rajora AK, Greco F, Osborn HMI. Flavonoids as prospective compounds for anti - cancer therapy. *Int J Biochem Cell Biol.*, 2016:1–5. <https://doi.org/10.1016/j.biocel.2013.10.004>.
- [3] Mehranfar F, Bordbar AK, Parastar H. A combined spectroscopic, molecular docking and molecular dynamic simulation study on the interaction of quercetin with β -casein nanoparticles. *J Photochem Photobiol B Biol.*, 2013;127:100–7. <https://doi.org/10.1016/j.jphotobiol.2013.07.019>.
- [4] Iqbal J, Abbasi BA, Mahmood T, Kanwal S, Ali B, Shah SA, et al. Plant-derived anticancer agents: A green anticancer approach. *Asian Pac J Trop Biomed.*, 2017;7:1129–50. <https://doi.org/10.1016/j.apjtb.2017.10.016>.
- [5] Balachandran C, Sangeetha B, Duraipandiyan V, Raj MK, Ignacimuthu S, Al-Dhabi NA, et al. A flavonoid isolated from *Streptomyces* sp. (ERINLG-4) induces apoptosis in human lung cancer A549 cells through p53 and cytochrome c release caspase dependant pathway. *Chem Biol Interact.*, 2014;224:24–35. <https://doi.org/10.1016/j.cbi.2014.09.019>.
- [6] Iqbal J, Abbasi BA, Mahmood T, Kanwal S, Ali B, Khalil AT. Plant-derived anticancer agents : A green anticancer approach. *Asian Pac J Trop Biomed.*, 2017:1–23. <https://doi.org/10.1016/j.apjtb.2017.10.016>.
- [7] Kumar P. PLANT DERIVED ANTICANCER AGENTS AND THEIR STRUCTURE: A REVIEW. *Int Res J Pharm.*, 2018;9:43–9. <https://doi.org/10.7897/2230-8407.09687>.
- [8] Cacabelos R, Cacabelos P, Torrellas C. Personalized Medicine of Alzheimer ' s Disease. Elsevier Inc.; 2014. <https://doi.org/10.1016/B978-0-12-386882-4.00027-X>.
- [9] Gurusamy U, Shewade DG. Pharmacogenomics in India. Elsevier Inc.; 2014. <https://doi.org/10.1016/B978-0-12-386882-4.00046-3>.
- [10] Hejazi II, Khanam R, Mehdi SH, Bhat AR, Rizvi MMA, Thakur SC, et al. Antioxidative and anti-proliferative potential of *Curculigo orchioides* Gaertn in oxidative stress induced cytotoxicity: In vitro, ex vivo and in silico studies. *Food Chem Toxicol.*, 2018;115:244–59. <https://doi.org/10.1016/j.fct.2018.03.013>.
- [11] Rasouli H, Farzaei MH, Mansouri K, Mohammadzadeh S, Khodarahmi R. Plant cell cancer: May natural phenolic compounds prevent onset and development of plant cell malignancy? A literature review. *Molecules.*, 2016;21:14–21. <https://doi.org/10.3390/molecules21091104>.
- [12] Phosrithong N, Ungwitayatorn J. Molecular docking study on anticancer activity of plant-derived natural products. *Med Chem Res.*, 2010;19:817–35. <https://doi.org/10.1007/s00044-009-9233-5>.
- [13] Saeed M, Kadioglu O, Khalid H, Sugimoto Y, Efferth T. Activity of the dietary flavonoid, apigenin, against multidrug-resistant tumor cells as determined by pharmacogenomics and molecular docking. *J Nutr Biochem.*, 2015;26:44–56. <https://doi.org/10.1016/j.jnutbio.2014.09.008>.
- [14] Mokale SN, Begum A, Sakle NS, Shelke VR, Bhavale SA. Design , synthesis and anticancer screening of 3- (3- (substituted phenyl) acryloyl) -2H-chromen-2ones as selective anti-breast cancer agent. *Biomed Pharmacother.*, 2017;89:966–72. <https://doi.org/10.1016/j.biopha.2017.02.089>.
- [15] Sinha S, Amin H, Nayak D, Bhatnagar M, Kacker P, Chakraborty S, et al. Assessment of microtubule depolymerization property of flavonoids isolated from *Tanacetum gracile* in breast cancer cells by biochemical and molecular docking approach. *Chem Biol Interact.*, 2015;239:1–11. <https://doi.org/10.1016/j.cbi.2015.06.034>.
- [16] Skiff, A. K. Rappe, C. J. Casewit, K. S. Colwell, W. A. Goddard III WMS. UFF, a Full Periodic Table Force Field for Molecular Mechanics and Molecular Dynamics Simulations. *J Am Chem Soc.*, 2009;114:10024–35. <https://doi.org/https://doi.org/10.1021/ja00051a040>.
- [17] Dassault Systèmes BIOVIA, Discovery Studio Modeling Environment, Release 2017, San Diego: Dassault Systèmes., 2016.

- [18] Dallakyan S, Olson AJ. Small-molecule library screening by docking with PyRx. *Methods Mol Biol.*, 2015;1263:243–50. https://doi.org/10.1007/978-1-4939-2269-7_19.

Indo Global Journal of Pharmaceutical Sciences(ISSN 2249 1023; CODEN- IGJPAI; NLM ID: 101610675) indexed and abstracted in CrossRef (DOI Enabling), CNKI, UGC CARE Journal List, EMBASE (Elsevier), National Library of Medicine (NLM) Catalog (NCBI), ResearchGate, Publons (Clarivate Analytics), CAS (ACS), Index Copernicus, Google Scholar and many more. For further details, visit <http://iglobaljournal.com>



Discovery of Naturally Occurring Flavonoids as Human Cytochrome P450 (CYP3A4) Inhibitors with the Aid of Computational Chemistry

Sharuk L. Khan ^{1*}, Gajanan M. Sonwane ¹, Falak A. Siddiqui ¹, Shirish P. Jain ¹, Mayura A. Kale ²,
Vijay S. Borkar ¹

¹ Rajarshi Shahu College of Pharmacy, Buldana, Maharashtra, India 443001.

² Government College of Pharmacy, Aurangabad, Maharashtra, India 431005

Address for Correspondence: Sharuk L.Khan, sharique.4u4@gmail.com

Received:

13.07.2019

Accepted:

11.04.2020

Published:

20.12.2020

Keywords

Human
Cytochrome
P450 (CYP3A4);
Flavonoids;
Doxorubicin;
Molecular
docking; PyRx
Virtual Screening
Tool.

ABSTRACT: Purpose: The human cytochrome P450 3A4 (CYP3A4) is the biggest individual from the CYP3A subfamily and records for 30–60% of the total for CYP450 adult liver. Hereditary varieties in CYP3A4 are a noteworthy hotspot for inter-patient changeability in plasma concentration, adverse effects and pharmacological response to medications. This research was done to discover naturally occurring novel CYP3A4 inhibitors from flavonoids. Methods: The molecular docking method was used to optimize the inhibiting activity of flavonoids against CYP3A4. PyRx Virtual Screening Tool 0.8 and BIOVIA Discovery Studio 2019 was used for simulation. Results: Flavonoids like Pongamoside A, Pongamoside B, and Pongamoside D have more binding affinity (kcal/mol) i.e. -11.6, -10.9, -10.8 respectively than Doxorubicin which have -10.7 against CYP3A4. Although, Daidzein, Genistein, and Luteolin form more hydrogen bonds than doxorubicin. Conclusion: The rational synthesis of natural analogues in reference to synthetic drugs, could generate drugs with improved therapeutic effect for chemoprevention. CYP3A4 plays a major role in the metabolism of various drugs; by the help of flavonoids, we can control the selective drug metabolism by inhibiting CYP3A4. Despite this, these molecules are not marketed for cancer treatment because of high polarity. If we could overcome this problem, these molecules can acts as effective anticancer agents in the future. Still, if we want to use these compounds clinically, there is a need to generate more scientific evidence and quality data by using *in vivo* and *in vitro* models. © 2020 iGlobal Research and Publishing Foundation. All rights reserved.

Cite this article as: Khan, S.L.; Sonwane, G.M.; Siddiqui, F.A.; Jain, S.P.; Kale, M.A.; Borkar, V.S. Discovery of naturally occurring flavonoids as human cytochrome P450 (CYP3A4) inhibitors with the aid of computational chemistry. Indo Global J. Pharm. Sci., 2020; 10(4): 58-69. DOI: <http://doi.org/10.35652/IGJPS.2020.10409> .

INTRODUCTION

Flavonoids are a well-known category of polyphenolic compounds. These are the regular dietary materials of the human, as many of the plants contains flavonoids. There are plenty of plants that exerts good pharmacological properties including anticancer activity just because of the presence of flavonoids. Flavonoids are the essential plant shades that act as chemical messengers, physiological controllers, and cell cycle inhibitors [1]. Flavonoids stand out amongst the most tried and broadly distributed substances of plant sources. They are found in natural products, vegetables, leguminous plants and even a few sorts of greenery. The skeleton of flavonoids

comprises of 1-benzopyran. It is a C6-C3-C6 framework, in which sweet-smelling rings are associated, shaping a focal pyran or pyron cycle. Contingent upon the position to which ring is associated with the chromane, flavonoids are grouped into isoflavonoids and neoflavonoids [2].

Amongst the different other natural substances, flavonoids hold much consideration because of their noteworthy range of pharmacological activities, such as cell reinforcement, antimutagenic, antibacterial, antiangiogenic, anti-

inflammatory, anti-allergic, modulators of enzymatic activities and anti-cancer activity [3]. Apigenin, luteolin, quercetin and kaempferol, the hydroxylated flavonoids are the main constituents of various dietary products and beverages and have been the focus of extensive research over the last years. Apigenin exerts anticancer effects through the modulation of various pathways namely, apoptosis, Reactive oxygen species (ROS) and DNA damage and repair [4].

Malignant growth is one of the terrible illnesses caused by unusual cell growth and can attack different tissues. They shape a subset of neoplasms. It speaks of the greatest social insurance issues for humankind and requests a proactive system for cure [5]. It is accounted for the rate of malignancy that has been expanding in developing nations and has turned into the fourth driving reason for death around the world. Chemoprevention by phytoconstituents has advanced as a powerful procedure to control the prevalence of malignant growth. The journey of anticancer agents from plant sources began in the 1950s with the discovery of the vinca alkaloids, vincristine, vinblastine, combretastatin, and colchicine. These Phytochemicals act explicitly on tumor cells without influencing non-cancerous cells. Carcinogenesis is a mind-boggling marvel that includes many signaling cascades. Phytochemicals are viewed as reasonable candidates for anticancer medication advancement due to their pleiotropic activities on target. The examination is in advancement for creating potential competitors (those can square or back off the development of disease cells without any side effects) from these phytochemicals. Numerous phytochemicals and their determined analogs have been distinguished as potential candidates for anticancer treatment. Plants serve as a source of novel compound elements and give a promising line to investigate on malignant growth. The plant and plant metabolites are the reforming sources as these are simple, more secure, easy, quick, and less dangerous as contrasted to traditional treatment methods. There is a positive relationship set up by the epidemiological examinations between expanded utilization of common items with diminished danger of disease. The mechanism responsible for chemoprevention remains essentially unidentified, however, it is likely identified with the closeness of phytochemicals related to plants. Consequently, the search for powerful and more secure natural anticancer agents have attracted the researchers throughout the world. [6,7].

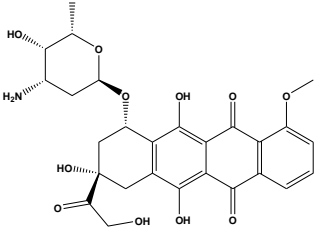
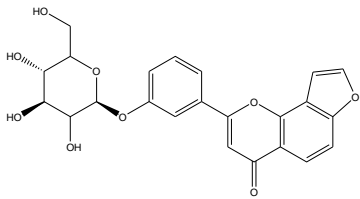
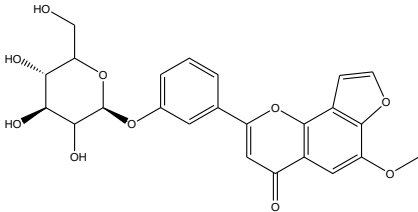
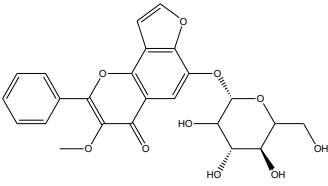
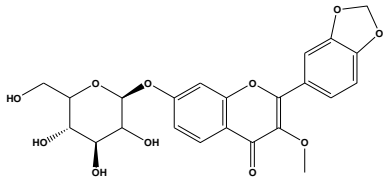
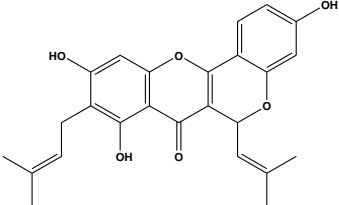
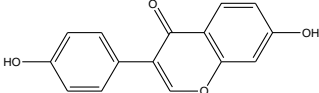
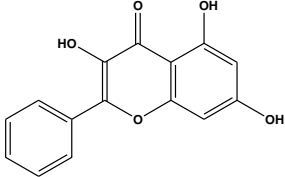
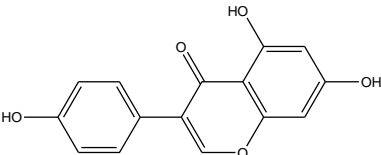
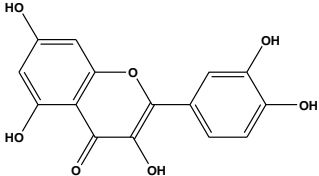
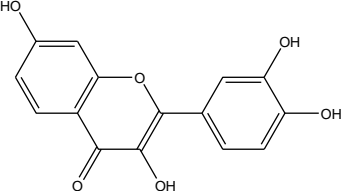
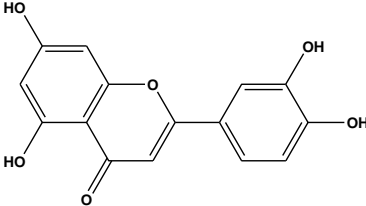
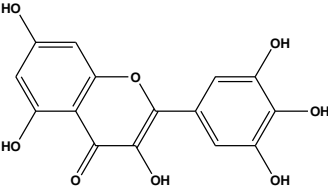
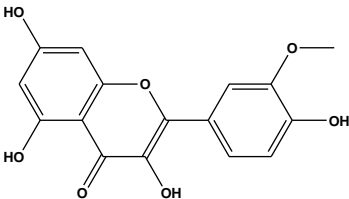
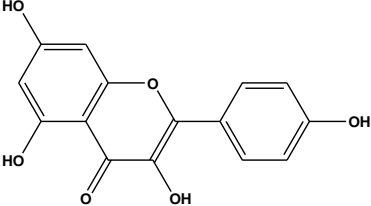
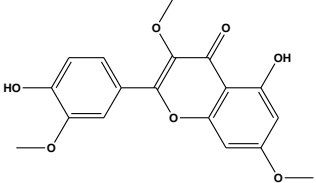
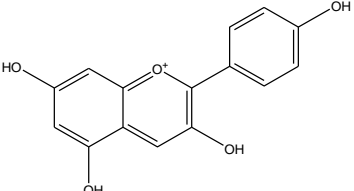
The human cytochrome P450 3A4 (CYP3A4) is the biggest individual from the CYP3A subfamily and records for 30–60% of the total for CYP450 adult liver. The CYP3A4 gene is limited on chromosome 7q21 and up to now, 41 CYP3A4 alleles have been recognized. The human CYP3A locus

contains the three CYP3A gene (CYP3A4, CYP3A5, and CYP3A7), three pseudogenes, and a novel CYP3A gene named CYP3A43. Hereditary varieties in CYP3A4 are a noteworthy hotspot for inter-patient changeability in plasma concentration, adverse effects and pharmacological response to medications, for example, paclitaxel, fentanyl, tamoxifen, tacrolimus, and statins. Moreover, existing investigations have announced the role of CYP3A4 inadequate alleles in the disease susceptibility to prostate malignant growth, estrogen receptor-negative breast cancer, and type-2 diabetes [8,9].

Protein-ligand docking is a fundamental part of computer-aided drug design, and it distinguishes the coupling pattern of proteins and ligands by computer simulation. Molecular docking results decide a general binding mode of a ligand. Varieties of compounds from plant sources have been accounted to have significant anticancer properties; in any case, their modes of activity have not been characterized. Molecular docking studies were performed on some flavonoids by using Autodock vina 1.1.2 in PyRx 0.8. [10]. The docking was performed utilizing receptor proteins required with cell cycle, cell development, and DNA replication, i.e., cyclin-subordinate protein kinase 2 (CDK-2), CDK-6, DNA topoisomerases I and II, B-cell lymphoma 2 (Bcl-2), vascular endothelial development factor receptor 2 (VEGFR-2), and the telomere: G-quadruplexes. By molecular docking, the bound confirmations and the coupling attachment among flavonoid and CYP3A4 as the target could be anticipated [11]. Doxorubicin, sold under the brand names adriamycin, used to treat breast malignant growth, bladder cancer, lymphoma, and intense lymphocytic leukemia was utilized for docking studies whose binding interactions were compared with the flavonoids [12].

Docking of the small molecule into the binding site of a receptor and guessing the binding interaction of the complex is a noteworthy part of the structure-based drug design process. By molecular docking, the bound conformations and the binding affinity between Flavonoids and human cytochrome P450 3A4 as the target could be predicted [13]. **Table 1** represents the names and structures of doxorubicin and the flavonoids used for molecular docking. The structures of all the compounds were generated by using ChemDraw Ultra 8.0 with the help of IUPAC name took from the official website of U.S. National Library of Medicine PubChem (<https://pubchem.ncbi.nlm.nih.gov/>).

Table 1. Name and Structures of compounds used for molecular docking

Doxorubicin	Pongamoside A	Pongamoside B
		
Pongamoside C	Pongamoside D	Cyclocommunin
		
Daidzein	Galangin	Genistein
		
Quercetin	Fisetin	Luteolin
		
Myricetin	Isorhamnetin	Kaempferol
		
Pachypodol	Pelargonidin	
		

MATERIALS AND METHODS

System used for Molecular docking

Molecular docking was performed on Lenovo ThinkPad with 64-bit operating system, Processor: Intel(R) Core(TM) i5-4300M CPU @2.60 GHz 2.59 GHz, RAM: 4GB by using PyRx-Virtual Screening Tool.

Ligand Preparation

The Structures of all the compounds (SDF File) were downloaded from the official website of the U.S. National Library of Medicine PubChem (<https://pubchem.ncbi.nlm.nih.gov/>). Structures then imported into PyRx 0.8 using open bable tool and energy minimization

(optimization) was performed by considering fundamental parameters based on the element, its hybridization, and connectivity i.e. by Universal Force Field (UFF)[16]. These ligands were then converted to AutoDock Ligand format (PDBQT).

Macromolecule Preparation

Autodock vina 1.1.2 in PyRx 0.8 was used to perform the docking studies of all the compounds against the crystal structure of human cytochrome P450 3A4 (CYP3A4). The crystal structure of CYP3A4 was obtained from the RCSB Protein Data Bank (PDB) with PDB ID-4K9T (<http://www.rcsb.org/structure/4K9T>) with Homo sapiens organism and Escherichia coli expression system. The CYP3A4 crystal structure was optimized, purified and prepared for docking with the help of Discovery Studio Visualizer 2019 by removing unwanted water molecules, bound ligands from protein structure and saved again in PDB file format to the same folder[17].

Molecular Docking Procedure

The purified CYP3A4 crystal structure file was loaded to docking software PyRx 0.8 using a load molecule option from the File toolbar. Chain-A was used to perform the docking, as it contains the active site which confirmed by checking interactions of native ligand present in the crystal structure (<http://www.rcsb.org/3d-view/4K9T?preset=ligandInteraction&sele=1RD>). The CYP3A4 crystal structure was then converted to Autodock macromolecule (pdbqt format) by using the right-click option. Binding affinity studies were performed by using Vina Wizard Tool in PyRx 0.8. All the ligand molecules (PDBQT Files), and target (CYP3A4) were selected for docking study. For molecular docking simulation, the three-dimensional grid box (size_x = 18.5286782874Ao; size_y = 26.047226475Ao; size_z = -9.59195798998Ao) was designed using Autodock tool 1.5.6 with exhaustiveness value of 8. After selecting molecules, the active amino acid residues were selected to define the cavity with the help of Toggle Selection Spheres

option given in PyRx[18]. To occupy all the active binding sites and essential residues, the grid box was aligned properly. All the ligands and CYP3A4 then subjected for docking to get the finding affinities.

Identification of Cavity and Active Amino Acid Residues

The active amino acid residues in the protein were identified and noted using BIOVIA Discovery Studio Visualizer (version-19.1.0.18287)[17]. The selection of the amino acids in the active site was used to analyze the grid box and to define the cavity. All the docking poses, ligand and protein interactions were studied by importing output files into Discovery Studio which enables us to identify the types of interactions. Discovery Studio is an offline life sciences software that offers tools to study drug-receptor interaction, docking poses visualization and macromolecule preparations. The chosen cavity was the binding site of the native ligand in PDB 4K9T.

RESULTS AND DISCUSSION

All the flavonoids and doxorubicin successfully docked on CYP3A4. Binding energy is released when a drug molecule associates with a target, leading to a lowering of the overall energy of the complex [14]. Molecular formula, Lipinski’s rule of five, binding affinity (kcal/mol), and active amino acid residues are presented in Table 1. Lipinski’s rule of five plays an important role in molecule screening and validation. Here, Pongamosides i.e. Pongamoside A, Pongamoside B, and Pongamoside D have shown better binding affinity than doxorubicin.

Table 2 represents 3D- & 2D-images of docking poses along with no. of hydrogen bonds involved in the interaction. The 2D-docking pose also shows the chemical structure of the ligands which enables us to predict groups and/or atoms involved in the bond formation with CYP3A4.

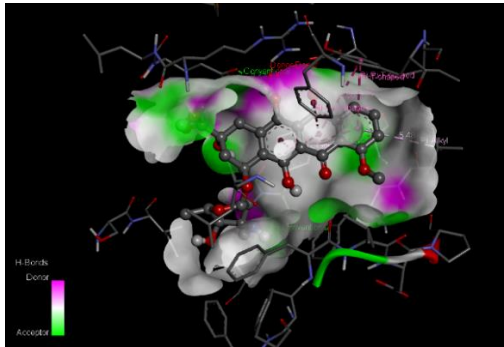
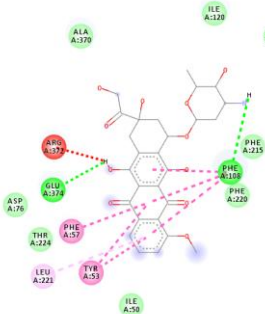
Table 2. Properties, Lipinski’s rule of five, binding affinity and active amino acid residues.

Name of Compound	Molecular Formula	Lipinski’s rule of five		Binding affinity (kcal/mol)	Active amino acid residues
Doxorubicin	C ₂₇ H ₂₉ NO ₁₁	Molecular weight (<500 DA)	543.5	-10.7	Ala370, Ile120, Phe241, Phe213, Val240, Phe215, Phe108, Phe220, Ile50, Tyr53, Leu221, Phe57, Thr224, Asp76, Glu374 (Forms unfavourable bond with Arg372)
		XLogP (<5)	1.3		
		H-Bond donor (5)	6		
		H-bond acceptor (<10)	12		
Pongamoside A	C ₂₃ H ₂₀ O ₉	Molecular weight (<500 DA)	440.4	-11.6	Leu373, Ala370, Arg372,

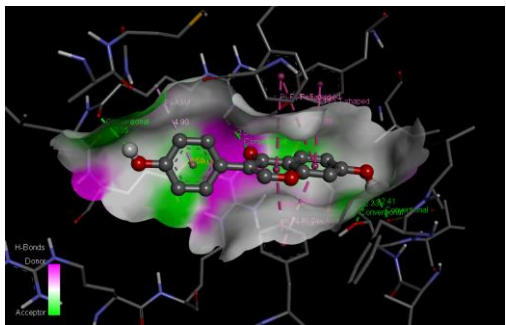
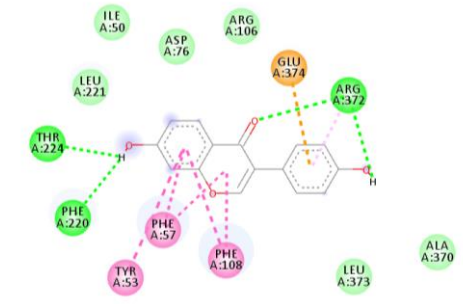
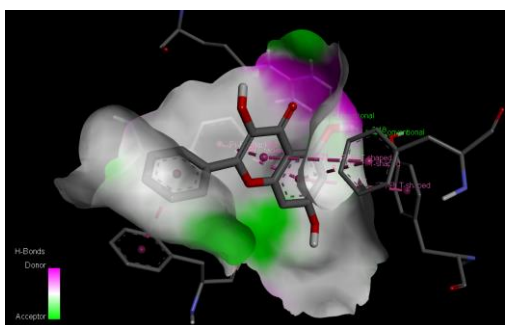
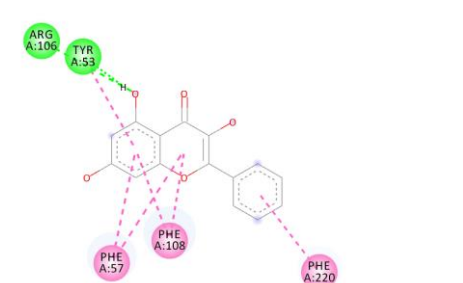
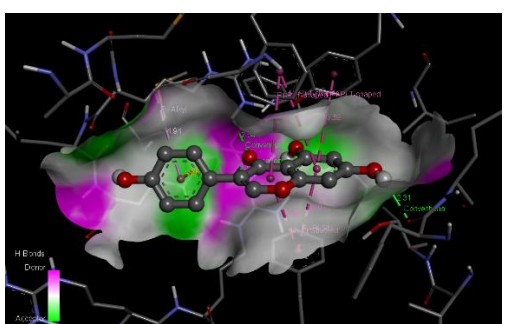
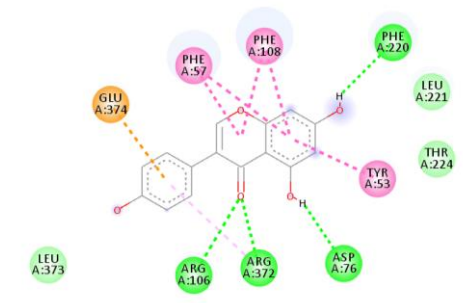
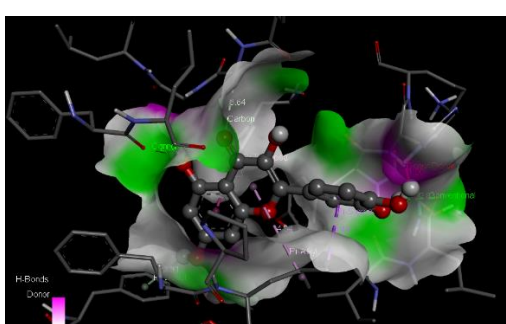
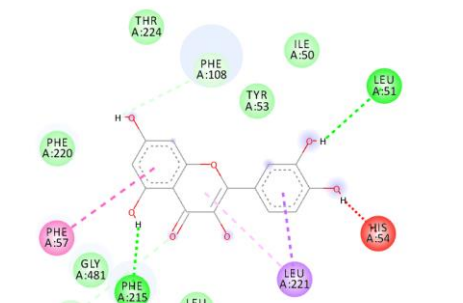
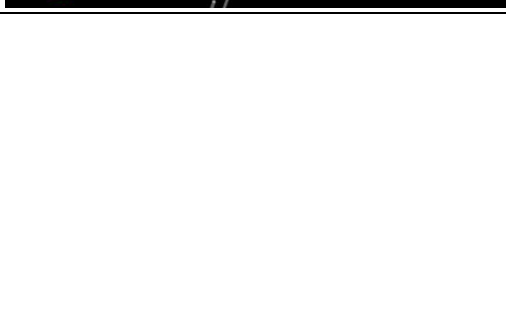
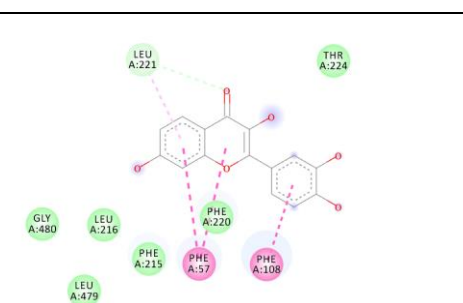
		XLogP (<5)	1.4		Met371, Gly481, Asp76, Leu482, Ile50, Leu221, Pro218, Leu216, Tyr53, Phe57, Phe220, Phe108, Arg105, Glu374
		H-Bond donor (5)	4		
		H-bond acceptor (<10)	9		
<u>Pongamoside B</u>	C ₂₄ H ₂₂ O ₁₀	Molecular weight (<500 DA)	470.4	-10.9	Arg372, Ala370, Met371, Leu216, Gly480, His54, Tyr53, Leu221, Thr224, Phe57, Arg106, Glu374, Arg105 (Forms unfavourable bond with Gly481)
		XLogP (<5)	1.4		
		H-Bond donor (5)	4		
		H-bond acceptor (<10)	10		
<u>Pongamoside D</u>	C ₂₃ H ₂₂ O ₁₁	Molecular weight (<500 DA)	474.4	-10.8	Phe57, Leu216, Tyr53, Gly480, Gly56, Leu479, His54, Leu221, Ile50, Asp76, Thr224, Phe220, Phe108
		XLogP (<5)	1		
		H-Bond donor (5)	4		
		H-bond acceptor (<10)	11		
<u>Pongamoside C</u>	C ₂₄ H ₂₂ O ₁₀	Molecular weight (<500 DA)	470.4	-10.6	Leu221, Pro218, Leu216, Asp217, Phe57, Phe108, Ile369, Gly481, Met371, Arg372, Glu374, Arg106, Phe215, Thr224, Ile50, Tyr53, Phe220
		XLogP (<5)	1.6		
		H-Bond donor (5)	2		
		H-bond acceptor (<10)	10		
<u>Cyclocommunin</u>	C ₂₅ H ₂₄ O ₆	Molecular weight (<500 DA)	420.4	-10.1	Phe215, Val240, Phe108, Thr224, Glu374, Arg372, Phe220, Phe213, Phe241, Phe304, Ile301
		XLogP (<5)	4.1		
		H-Bond donor (5)	3		
		H-bond acceptor (<10)	3		
<u>Daidzein</u>	C ₁₅ H ₁₀ O ₄	Molecular weight (<500 DA)	254.2	-9.3	Leu221, Ile50, Asp76, Arg106, Glu374, Arg372, Ala370, Leu373, Phe108, Phe57, Tyr53, Phe220, Thr224
		XLogP (<5)	2.5		
		H-Bond donor (5)	2		
		H-bond acceptor (<10)	4		
<u>Galangin</u>	C ₁₅ H ₁₀ O ₅	Molecular weight (<500 DA)	270.2	-9.3	Arg106, Tyr53, Phe220, Phe108, Phe57
		XLogP (<5)	2.3		
		H-Bond donor (5)	3		
		H-bond acceptor (<10)	5		
<u>Genistein</u>	C ₁₅ H ₁₀ O ₅	Molecular weight (<500 DA)	270.2	-9.1	Glu374, Phe57, Phe108, Phe220, Leu221, Thr224, Tyr53, Asp76, Arg372, Arg106, Leu373
		XLogP (<5)	2.7		
		H-Bond donor (5)	3		
		H-bond acceptor (<10)	5		
<u>Quercetin</u>	C ₁₅ H ₁₀ O ₇	Molecular weight (<500 DA)	302.2	-8.7	Thr224, Phe108, Tyr53, Ile50, Leu51, Leu221, Leu216, Phe215, Gly481, Gly480, Phe57, Phe220 (Forms unfavourable bond with His54)
		XLogP (<5)	1.5		
		H-Bond donor (5)	5		
		H-bond acceptor (<10)	7		
<u>Fisetin</u>	C ₁₅ H ₁₀ O ₆	Molecular weight (<500 DA)	286.2	-8.7	Leu221, Thr224, Phe108, Phe220, Phe57, Phe215, Leu479, Leu216, Gly480
		XLogP (<5)	2		
		H-Bond donor (5)	4		
		H-bond acceptor (<10)	6		
<u>Luteolin</u>	C ₁₅ H ₁₀ O ₆	Molecular weight (<500 DA)	286.2	-8.6	Phe215, Leu221, Phe57, Leu479, Gly56, His54, Ile50, Phe108, Thr225, Phe220
		XLogP (<5)	1.4		
		H-Bond donor (5)	4		
		H-bond acceptor (<10)	6		

Myricetin	C ₁₅ H ₁₀ O ₈	Molecular weight (<500 DA)	318.2	-8.6	Leu221, Phe57, Thr224, Phe215, Gly480, Leu216, Leu479, Ile50, Leu51, His54
		XLogP (<5)	1.2		
		H-Bond donor (5)	6		
		H-bond acceptor (<10)	8		
Isorhamnetin	C ₁₆ H ₁₂ O ₇	Molecular weight (<500 DA)	316.2	-8.4	Leu221, Pro218, Phe57, Thr224, Phe220, Phe215, Leu216, Gly480, Leu479, Tyr53, Ile50, Leu51, His54 (Forms unfavourable bond with Gly481)
		XLogP (<5)	1.9		
		H-Bond donor (5)	4		
		H-bond acceptor (<10)	7		
Kaempferol	C ₁₅ H ₁₀ O ₆	Molecular weight (<500 DA)	286.2	-8.4	Phe108, Phe215, Phe57, Gly481, Gly480, Leu216, Tyr53, Phe220, Thr224
		XLogP (<5)	9.8		
		H-Bond donor (5)	1		
		H-bond acceptor (<10)	1		
Pachypodol	C ₁₈ H ₁₆ O ₇	Molecular weight (<500 DA)	344.3	-8.3	Leu221, Pro218, Leu479, Gly480, Phe215, Leu216, Phe220, Thr224, Phe108, Phe57, Tyr53, His54, Ile50, Leu51
		XLogP (<5)	3.1		
		H-Bond donor (5)	2		
		H-bond acceptor (<10)	7		
Pelargonidin	C ₁₅ H ₁₁ O ₅ ⁺	Molecular weight (<500 DA)	271.2	-8.2	Tyr53, Phe215, Gly481, Phe220, Phe108, Leu221, Phe57, Thr224, Ile50
		XLogP (<5)	2.1		
		H-Bond donor (5)	4		
		H-bond acceptor (<10)	1		

Table 3. 3D- & 2D-images of docking poses along with no. of hydrogen bonds involved.

Name of Compound	3D-docking pose	2D-docking pose	No. of hydrogen bonds involved
Doxorubicin			02
Pongamoside A			00

<p>Pongamoside B</p>			<p>02</p>
<p>Pongamoside D</p>			<p>02</p>
<p>Pongamoside C</p>			<p>02</p>
<p>Cyclocommunin</p>			<p>00</p>

<p>Daidzein</p>			<p>04</p>
<p>Galangin</p>			<p>02</p>
<p>Genistein</p>			<p>04</p>
<p>Quercetin</p>			<p>02</p>
<p>Fisetin</p>			<p>00</p>

	<p>3D molecular model of a protein-ligand complex. The protein backbone is shown in grey, and the ligand is shown in stick representation. Green and purple surfaces represent electron density maps. A legend indicates 'H-Bonds', 'Donor', and 'Acceptor'.</p>		
<p>Luteolin</p>	<p>3D molecular model of Luteolin bound to a protein. The protein backbone is shown in grey, and Luteolin is shown in stick representation. Green and purple surfaces represent electron density maps. A legend indicates 'H-Bonds', 'Donor', and 'Acceptor'.</p>	<p>2D interaction diagram of Luteolin with amino acid residues. The ligand is shown in stick representation, and residues are shown as colored circles. Residues include PHE A-215, LEU A-221, PHE A-57, LEU A-479, GLY A-56, HIS A-54, ILE A-50, THR A-224, and PHE A-108.</p>	<p>03</p>
<p>Myricetin</p>	<p>3D molecular model of Myricetin bound to a protein. The protein backbone is shown in grey, and Myricetin is shown in stick representation. Green and purple surfaces represent electron density maps. A legend indicates 'H-Bonds', 'Donor', and 'Acceptor'.</p>	<p>2D interaction diagram of Myricetin with amino acid residues. The ligand is shown in stick representation, and residues are shown as colored circles. Residues include THR A-224, LEU A-221, PHE A-57, HIS A-54, LEU A-51, ILE A-50, LEU A-479, LEU A-216, GLY A-480, and PHE A-215.</p>	<p>01</p>
<p>Isorhamnetin</p>	<p>3D molecular model of Isorhamnetin bound to a protein. The protein backbone is shown in grey, and Isorhamnetin is shown in stick representation. Green and purple surfaces represent electron density maps. A legend indicates 'H-Bonds', 'Donor', and 'Acceptor'.</p>	<p>2D interaction diagram of Isorhamnetin with amino acid residues. The ligand is shown in stick representation, and residues are shown as colored circles. Residues include PRO A-218, THR A-224, PHE A-57, PHE A-220, GLY A-480, PHE A-215, LEU A-221, LEU A-51, ILE A-50, TYR A-53, GLY A-480, LEU A-216, and LEU A-479.</p>	<p>02</p>
<p>Kaempferol</p>	<p>3D molecular model of Kaempferol bound to a protein. The protein backbone is shown in grey, and Kaempferol is shown in stick representation. Green and purple surfaces represent electron density maps. A legend indicates 'H-Bonds', 'Donor', and 'Acceptor'.</p>	<p>2D interaction diagram of Kaempferol with amino acid residues. The ligand is shown in stick representation, and residues are shown as colored circles. Residues include GLY A-481, LEU A-216, PHE A-108, PHE A-215, PHE A-57, GLY A-480, TYR A-53, THR A-224, and PHE A-220.</p>	<p>00</p>

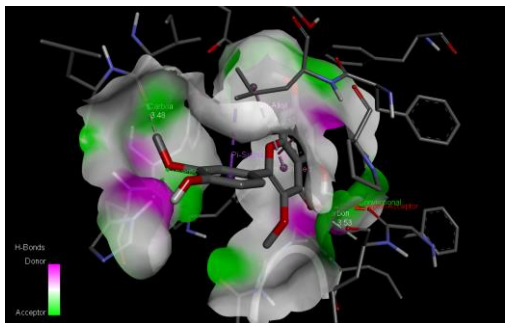
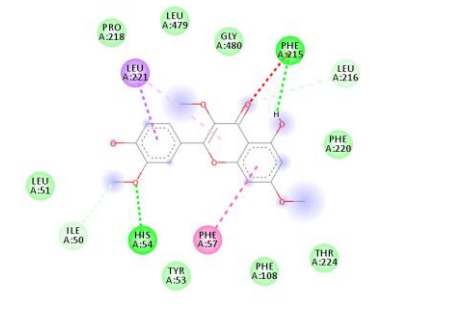
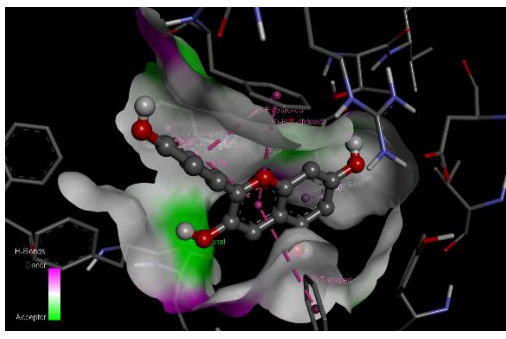
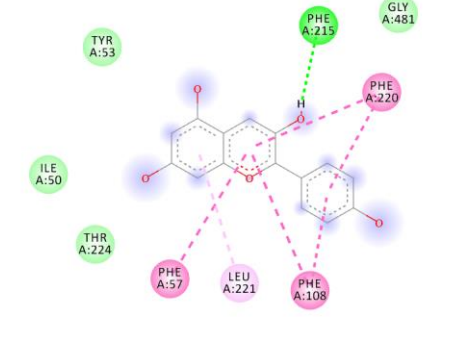
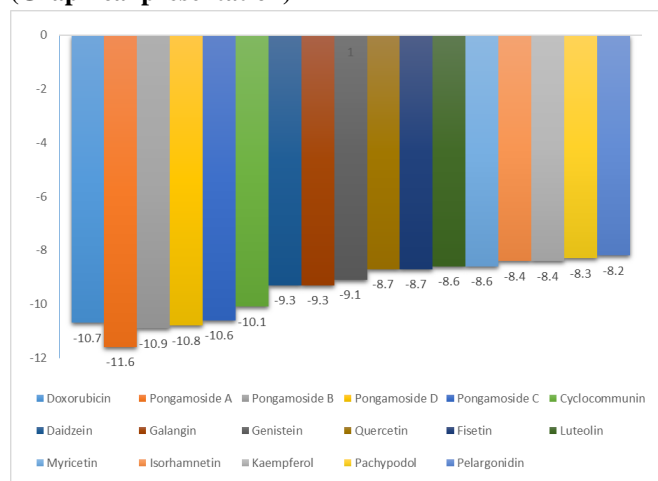
<p>Pachypodol</p>			<p>02</p>
<p>Pelargonidin</p>			<p>01</p>

Figure 1 represents the comparative binding affinities (kcal/mol) of doxorubicin and flavonoids. Many of the flavonoids have shown better binding affinity than doxorubicin.

Figure 1. Comparative binding affinities of the compounds (Graphical presentation)



As we have represented docking data along with 2D- & 3D-docking poses including no. hydrogen bonds involved in the interactions in Table 2. The formation of a hydrogen bond with the target molecule always results in inhibition of the receptor. Sadhna Sinha et al reported the Molecular docking of flavones at the colchicines binding pocket which revealed that the compounds bind at a-b interfacial site of tubulin,

correlating binding interactions with probable inhibition mechanism. The study reveals important observations to generate improved flavonoids that leads to cell apoptosis [15]. In case of Pongamoside A, it forms zero hydrogen bonds but still its binding affinity i.e. -11.6 kcal/mol is best because Pongamoside A forms van der Waals force attraction, Pi-Pi Stacked bonds, Pi-Pi T-shaped bonds, Amide-Pi stacked bonds and Pi alkyl bonds with more amino acid residues than doxorubicin i.e. -10.7 kcal/mol which forms two hydrogen bonds with CYP3A4. Pongamoside B and Pongamoside D have binding affinities (kcal/mol) -10.9 and -10.8 with the formation of 2-2 hydrogen bonds each with CYP3A4. This can be sufficient scientific evidence showing more potency of these flavonoids in terms of inhibition of CYP3A4 than the approved drug, doxorubicin. Although, Pongamoside C, Galangin, Quercetin, Isorhamnetin, Pachypodol forms 2-2 hydrogen bonds each with binding affinities -10.6, -9.3, -8.7, -8.4 and -8.3 kcal/mol respectively. Surprisingly Daidzein and Genistein formed 4 hydrogen bonds each with CYP3A4 with a docking score of -9.3 and -9.1 kcal/mol respectively which is much enough to inhibit the activity of CYP3A4. Luteolin has formed 3 hydrogen bonds with -8.6 kcal/mol binding affinity. The amino acid residues in the cavity involved in the interactions are represented in **Table 1**.

CONCLUSION

It is well known that natural compounds have proven to have a safe biological window as compared to molecules from a synthetic source. In present work, molecular docking studies disclosed, that flavonoids Pongamoside A, Pongamoside B,

and Pongamoside D have a better binding affinity towards CYP3A4 than doxorubicin. Although, if we talk about the formation of hydrogen bonds with target macromolecule, Daidzein, Genistein, and Luteolin form more hydrogen bonds than doxorubicin. In conclusion, the above docking study disclosed that rational synthesis of natural analogues in reference to synthetic drugs could generate drugs with improved therapeutic effects for chemoprevention. CYP3A4 plays a major role in the metabolism of various drugs; by the help of flavonoids, we can control the selective drug metabolism by inhibiting CYP3A4. Despite this, these molecules are not marketed for cancer treatment because of their high polarity. If we could overcome this problem, these molecules can act as effective anticancer agents in the future. Still, if we want to use these compounds clinically, there is a need to generate more scientific evidence and quality data by using *in vivo* and *in vitro* models.

ACKNOWLEDGEMENT

None

CONFLICTS OF INTEREST

None.

DATA AVAILABILITY

Not declared.

FUNDING SOURCE

Not declared

REFERENCES

- [1] Grigalius I, Petrikaite V. Relationship between antioxidant and anticancer activity of trihydroxyflavones. *Molecules.*, 2017;22. <https://doi.org/10.3390/molecules22122169>.
- [2] Ravishankar D, Rajora AK, Greco F, Osborn HMI. Flavonoids as prospective compounds for anti - cancer therapy. *Int J Biochem Cell Biol.*, 2016:1–5. <https://doi.org/10.1016/j.biocel.2013.10.004>.
- [3] Mehranfar F, Bordbar AK, Parastar H. A combined spectroscopic, molecular docking and molecular dynamic simulation study on the interaction of quercetin with β -casein nanoparticles. *J Photochem Photobiol B Biol.*, 2013;127:100–7. <https://doi.org/10.1016/j.jphotobiol.2013.07.019>.
- [4] Iqbal J, Abbasi BA, Mahmood T, Kanwal S, Ali B, Shah SA, et al. Plant-derived anticancer agents: A green anticancer approach. *Asian Pac J Trop Biomed.*, 2017;7:1129–50. <https://doi.org/10.1016/j.apjtb.2017.10.016>.
- [5] Balachandran C, Sangeetha B, Duraipandiyan V, Raj MK, Ignacimuthu S, Al-Dhabi NA, et al. A flavonoid isolated from *Streptomyces* sp. (ERINLG-4) induces apoptosis in human lung cancer A549 cells through p53 and cytochrome c release caspase dependant pathway. *Chem Biol Interact.*, 2014;224:24–35. <https://doi.org/10.1016/j.cbi.2014.09.019>.
- [6] Iqbal J, Abbasi BA, Mahmood T, Kanwal S, Ali B, Khalil AT. Plant-derived anticancer agents : A green anticancer approach. *Asian Pac J Trop Biomed.*, 2017:1–23. <https://doi.org/10.1016/j.apjtb.2017.10.016>.
- [7] Kumar P. PLANT DERIVED ANTICANCER AGENTS AND THEIR STRUCTURE: A REVIEW. *Int Res J Pharm.*, 2018;9:43–9. <https://doi.org/10.7897/2230-8407.09687>.
- [8] Cacabelos R, Cacabelos P, Torrellas C. Personalized Medicine of Alzheimer ' s Disease. Elsevier Inc.; 2014. <https://doi.org/10.1016/B978-0-12-386882-4.00027-X>.
- [9] Gurusamy U, Shewade DG. Pharmacogenomics in India. Elsevier Inc.; 2014. <https://doi.org/10.1016/B978-0-12-386882-4.00046-3>.
- [10] Hejazi II, Khanam R, Mehdi SH, Bhat AR, Rizvi MMA, Thakur SC, et al. Antioxidative and anti-proliferative potential of *Curculigo orchoides* Gaertn in oxidative stress induced cytotoxicity: In vitro, ex vivo and in silico studies. *Food Chem Toxicol.*, 2018;115:244–59. <https://doi.org/10.1016/j.fct.2018.03.013>.
- [11] Rasouli H, Farzaei MH, Mansouri K, Mohammadzadeh S, Khodarahmi R. Plant cell cancer: May natural phenolic compounds prevent onset and development of plant cell malignancy? A literature review. *Molecules.*, 2016;21:14–21. <https://doi.org/10.3390/molecules21091104>.
- [12] Phosrithong N, Ungwitayatorn J. Molecular docking study on anticancer activity of plant-derived natural products. *Med Chem Res.*, 2010;19:817–35. <https://doi.org/10.1007/s00044-009-9233-5>.
- [13] Saeed M, Kadioglu O, Khalid H, Sugimoto Y, Efferth T. Activity of the dietary flavonoid, apigenin, against multidrug-resistant tumor cells as determined by pharmacogenomics and molecular docking. *J Nutr Biochem.*, 2015;26:44–56. <https://doi.org/10.1016/j.jnutbio.2014.09.008>.
- [14] Mokale SN, Begum A, Sakle NS, Shelke VR, Bhavale SA. Design , synthesis and anticancer screening of 3- (3- (substituted phenyl) acryloyl) -2H-chromen-2ones as selective anti-breast cancer agent. *Biomed Pharmacother.*, 2017;89:966–72. <https://doi.org/10.1016/j.biopha.2017.02.089>.
- [15] Sinha S, Amin H, Nayak D, Bhatnagar M, Kacker P, Chakraborty S, et al. Assessment of microtubule depolymerization property of flavonoids isolated from *Tanacetum gracile* in breast cancer cells by biochemical and molecular docking approach. *Chem Biol Interact.*, 2015;239:1–11. <https://doi.org/10.1016/j.cbi.2015.06.034>.
- [16] Skiff, A. K. Rappe, C. J. Casewit, K. S. Colwell, W. A. Goddard III WMS. UFF, a Full Periodic Table Force Field for Molecular Mechanics and Molecular Dynamics Simulations. *J Am Chem Soc.*, 2009;114:10024–35. <https://doi.org/https://doi.org/10.1021/ja00051a040>.
- [17] Dassault Systèmes BIOVIA, Discovery Studio Modeling Environment, Release 2017, San Diego: Dassault Systèmes., 2016.

- [18] Dallakyan S, Olson AJ. Small-molecule library screening by docking with PyRx. *Methods Mol Biol.*, 2015;1263:243–50. https://doi.org/10.1007/978-1-4939-2269-7_19.

Indo Global Journal of Pharmaceutical Sciences(ISSN 2249 1023; CODEN- IGJPAI; NLM ID: 101610675) indexed and abstracted in CrossRef (DOI Enabling), CNKI, UGC CARE Journal List, EMBASE (Elsevier), National Library of Medicine (NLM) Catalog (NCBI), ResearchGate, Publons (Clarivate Analytics), CAS (ACS), Index Copernicus, Google Scholar and many more. For further details, visit <http://iglobaljournal.com>



Discovery of Naturally Occurring Flavonoids as Human Cytochrome P450 (CYP3A4) Inhibitors with the Aid of Computational Chemistry

Sharuk L. Khan ^{1*}, Gajanan M. Sonwane ¹, Falak A. Siddiqui ¹, Shirish P. Jain ¹, Mayura A. Kale ²,
Vijay S. Borkar ¹

¹ Rajarshi Shahu College of Pharmacy, Buldana, Maharashtra, India 443001.

² Government College of Pharmacy, Aurangabad, Maharashtra, India 431005

Address for Correspondence: Sharuk L.Khan, sharique.4u4@gmail.com

Received:

13.07.2019

Accepted:

11.04.2020

Published:

20.12.2020

Keywords

Human
Cytochrome
P450 (CYP3A4);
Flavonoids;
Doxorubicin;
Molecular
docking; PyRx
Virtual Screening
Tool.

ABSTRACT: Purpose: The human cytochrome P450 3A4 (CYP3A4) is the biggest individual from the CYP3A subfamily and records for 30–60% of the total for CYP450 adult liver. Hereditary varieties in CYP3A4 are a noteworthy hotspot for inter-patient changeability in plasma concentration, adverse effects and pharmacological response to medications. This research was done to discover naturally occurring novel CYP3A4 inhibitors from flavonoids. Methods: The molecular docking method was used to optimize the inhibiting activity of flavonoids against CYP3A4. PyRx Virtual Screening Tool 0.8 and BIOVIA Discovery Studio 2019 was used for simulation. Results: Flavonoids like Pongamoside A, Pongamoside B, and Pongamoside D have more binding affinity (kcal/mol) i.e. -11.6, -10.9, -10.8 respectively than Doxorubicin which have -10.7 against CYP3A4. Although, Daidzein, Genistein, and Luteolin form more hydrogen bonds than doxorubicin. Conclusion: The rational synthesis of natural analogues in reference to synthetic drugs, could generate drugs with improved therapeutic effect for chemoprevention. CYP3A4 plays a major role in the metabolism of various drugs; by the help of flavonoids, we can control the selective drug metabolism by inhibiting CYP3A4. Despite this, these molecules are not marketed for cancer treatment because of high polarity. If we could overcome this problem, these molecules can acts as effective anticancer agents in the future. Still, if we want to use these compounds clinically, there is a need to generate more scientific evidence and quality data by using *in vivo* and *in vitro* models. © 2020 iGlobal Research and Publishing Foundation. All rights reserved.

Cite this article as: Khan, S.L.; Sonwane, G.M.; Siddiqui, F.A.; Jain, S.P.; Kale, M.A.; Borkar, V.S. Discovery of naturally occurring flavonoids as human cytochrome P450 (CYP3A4) inhibitors with the aid of computational chemistry. Indo Global J. Pharm. Sci., 2020; 10(4): 58-69. DOI: <http://doi.org/10.35652/IGJPS.2020.10409> .

INTRODUCTION

Flavonoids are a well-known category of polyphenolic compounds. These are the regular dietary materials of the human, as many of the plants contains flavonoids. There are plenty of plants that exerts good pharmacological properties including anticancer activity just because of the presence of flavonoids. Flavonoids are the essential plant shades that act as chemical messengers, physiological controllers, and cell cycle inhibitors [1]. Flavonoids stand out amongst the most tried and broadly distributed substances of plant sources. They are found in natural products, vegetables, leguminous plants and even a few sorts of greenery. The skeleton of flavonoids

comprises of 1-benzopyran. It is a C6-C3-C6 framework, in which sweet-smelling rings are associated, shaping a focal pyran or pyron cycle. Contingent upon the position to which ring is associated with the chromane, flavonoids are grouped into isoflavonoids and neoflavonoids [2].

Amongst the different other natural substances, flavonoids hold much consideration because of their noteworthy range of pharmacological activities, such as cell reinforcement, antimutagenic, antibacterial, antiangiogenic, anti-

inflammatory, anti-allergic, modulators of enzymatic activities and anti-cancer activity [3]. Apigenin, luteolin, quercetin and kaempferol, the hydroxylated flavonoids are the main constituents of various dietary products and beverages and have been the focus of extensive research over the last years. Apigenin exerts anticancer effects through the modulation of various pathways namely, apoptosis, Reactive oxygen species (ROS) and DNA damage and repair [4].

Malignant growth is one of the terrible illnesses caused by unusual cell growth and can attack different tissues. They shape a subset of neoplasms. It speaks of the greatest social insurance issues for humankind and requests a proactive system for cure [5]. It is accounted for the rate of malignancy that has been expanding in developing nations and has turned into the fourth driving reason for death around the world. Chemoprevention by phytoconstituents has advanced as a powerful procedure to control the prevalence of malignant growth. The journey of anticancer agents from plant sources began in the 1950s with the discovery of the vinca alkaloids, vincristine, vinblastine, combretastatin, and colchicine. These Phytochemicals act explicitly on tumor cells without influencing non-cancerous cells. Carcinogenesis is a mind-boggling marvel that includes many signaling cascades. Phytochemicals are viewed as reasonable candidates for anticancer medication advancement due to their pleiotropic activities on target. The examination is in advancement for creating potential competitors (those can square or back off the development of disease cells without any side effects) from these phytochemicals. Numerous phytochemicals and their determined analogs have been distinguished as potential candidates for anticancer treatment. Plants serve as a source of novel compound elements and give a promising line to investigate on malignant growth. The plant and plant metabolites are the reforming sources as these are simple, more secure, easy, quick, and less dangerous as contrasted to traditional treatment methods. There is a positive relationship set up by the epidemiological examinations between expanded utilization of common items with diminished danger of disease. The mechanism responsible for chemoprevention remains essentially unidentified, however, it is likely identified with the closeness of phytochemicals related to plants. Consequently, the search for powerful and more secure natural anticancer agents have attracted the researchers throughout the world. [6,7].

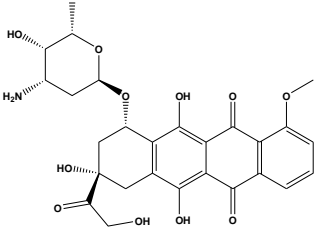
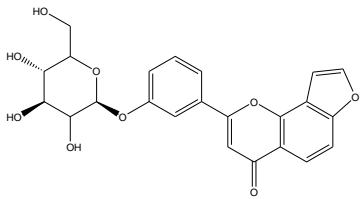
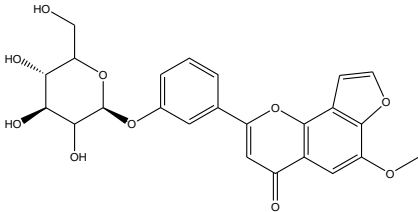
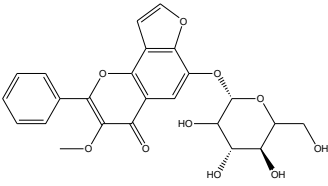
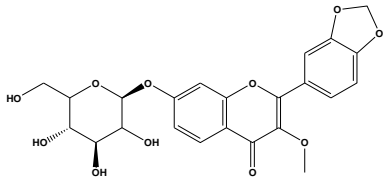
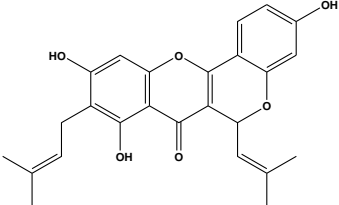
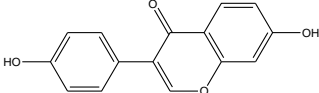
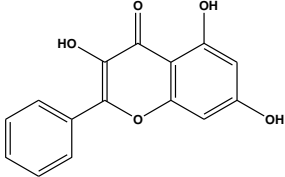
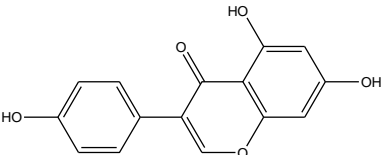
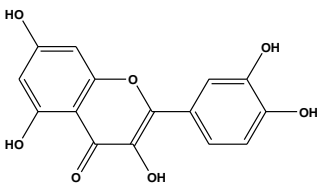
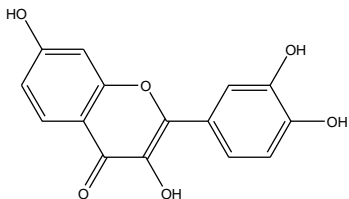
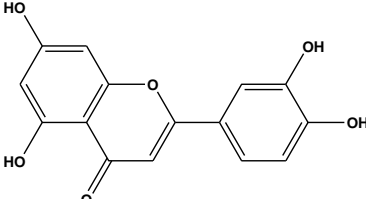
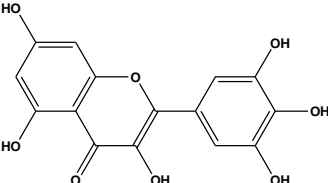
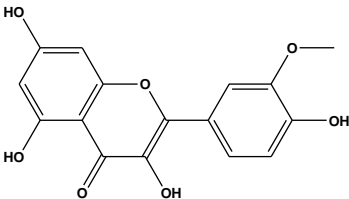
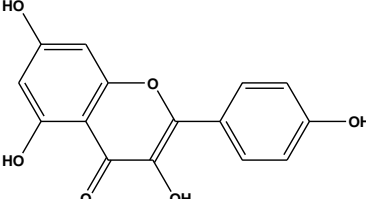
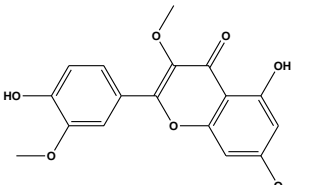
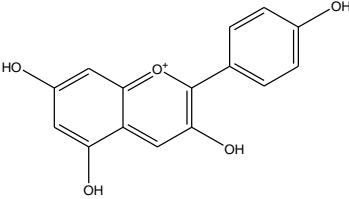
The human cytochrome P450 3A4 (CYP3A4) is the biggest individual from the CYP3A subfamily and records for 30–60% of the total for CYP450 adult liver. The CYP3A4 gene is limited on chromosome 7q21 and up to now, 41 CYP3A4 alleles have been recognized. The human CYP3A locus

contains the three CYP3A gene (CYP3A4, CYP3A5, and CYP3A7), three pseudogenes, and a novel CYP3A gene named CYP3A43. Hereditary varieties in CYP3A4 are a noteworthy hotspot for inter-patient changeability in plasma concentration, adverse effects and pharmacological response to medications, for example, paclitaxel, fentanyl, tamoxifen, tacrolimus, and statins. Moreover, existing investigations have announced the role of CYP3A4 inadequate alleles in the disease susceptibility to prostate malignant growth, estrogen receptor-negative breast cancer, and type-2 diabetes [8,9].

Protein-ligand docking is a fundamental part of computer-aided drug design, and it distinguishes the coupling pattern of proteins and ligands by computer simulation. Molecular docking results decide a general binding mode of a ligand. Varieties of compounds from plant sources have been accounted to have significant anticancer properties; in any case, their modes of activity have not been characterized. Molecular docking studies were performed on some flavonoids by using Autodock vina 1.1.2 in PyRx 0.8. [10]. The docking was performed utilizing receptor proteins required with cell cycle, cell development, and DNA replication, i.e., cyclin-subordinate protein kinase 2 (CDK-2), CDK-6, DNA topoisomerases I and II, B-cell lymphoma 2 (Bcl-2), vascular endothelial development factor receptor 2 (VEGFR-2), and the telomere: G-quadruplexes. By molecular docking, the bound confirmations and the coupling attachment among flavonoid and CYP3A4 as the target could be anticipated [11]. Doxorubicin, sold under the brand names adriamycin, used to treat breast malignant growth, bladder cancer, lymphoma, and intense lymphocytic leukemia was utilized for docking studies whose binding interactions were compared with the flavonoids [12].

Docking of the small molecule into the binding site of a receptor and guessing the binding interaction of the complex is a noteworthy part of the structure-based drug design process. By molecular docking, the bound conformations and the binding affinity between Flavonoids and human cytochrome P450 3A4 as the target could be predicted [13]. **Table 1** represents the names and structures of doxorubicin and the flavonoids used for molecular docking. The structures of all the compounds were generated by using ChemDraw Ultra 8.0 with the help of IUPAC name took from the official website of U.S. National Library of Medicine PubChem (<https://pubchem.ncbi.nlm.nih.gov/>).

Table 1. Name and Structures of compounds used for molecular docking

Doxorubicin	Pongamoside A	Pongamoside B
		
Pongamoside C	Pongamoside D	Cyclocommunin
		
Daidzein	Galangin	Genistein
		
Quercetin	Fisetin	Luteolin
		
Myricetin	Isorhamnetin	Kaempferol
		
Pachypodol	Pelargonidin	
		

MATERIALS AND METHODS

System used for Molecular docking

Molecular docking was performed on Lenovo ThinkPad with 64-bit operating system, Processor: Intel(R) Core(TM) i5-4300M CPU @2.60 GHz 2.59 GHz, RAM: 4GB by using PyRx-Virtual Screening Tool.

Ligand Preparation

The Structures of all the compounds (SDF File) were downloaded from the official website of the U.S. National Library of Medicine PubChem (<https://pubchem.ncbi.nlm.nih.gov/>). Structures then imported into PyRx 0.8 using open bable tool and energy minimization

(optimization) was performed by considering fundamental parameters based on the element, its hybridization, and connectivity i.e. by Universal Force Field (UFF)[16]. These ligands were then converted to AutoDock Ligand format (PDBQT).

Macromolecule Preparation

Autodock vina 1.1.2 in PyRx 0.8 was used to perform the docking studies of all the compounds against the crystal structure of human cytochrome P450 3A4 (CYP3A4). The crystal structure of CYP3A4 was obtained from the RCSB Protein Data Bank (PDB) with PDB ID-4K9T (<http://www.rcsb.org/structure/4K9T>) with Homo sapiens organism and Escherichia coli expression system. The CYP3A4 crystal structure was optimized, purified and prepared for docking with the help of Discovery Studio Visualizer 2019 by removing unwanted water molecules, bound ligands from protein structure and saved again in PDB file format to the same folder[17].

Molecular Docking Procedure

The purified CYP3A4 crystal structure file was loaded to docking software PyRx 0.8 using a load molecule option from the File toolbar. Chain-A was used to perform the docking, as it contains the active site which confirmed by checking interactions of native ligand present in the crystal structure (<http://www.rcsb.org/3d-view/4K9T?preset=ligandInteraction&sele=1RD>). The CYP3A4 crystal structure was then converted to Autodock macromolecule (pdbqt format) by using the right-click option. Binding affinity studies were performed by using Vina Wizard Tool in PyRx 0.8. All the ligand molecules (PDBQT Files), and target (CYP3A4) were selected for docking study. For molecular docking simulation, the three-dimensional grid box (size_x = 18.5286782874Ao; size_y = 26.047226475Ao; size_z = -9.59195798998Ao) was designed using Autodock tool 1.5.6 with exhaustiveness value of 8. After selecting molecules, the active amino acid residues were selected to define the cavity with the help of Toggle Selection Spheres

option given in PyRx[18]. To occupy all the active binding sites and essential residues, the grid box was aligned properly. All the ligands and CYP3A4 then subjected for docking to get the finding affinities.

Identification of Cavity and Active Amino Acid Residues

The active amino acid residues in the protein were identified and noted using BIOVIA Discovery Studio Visualizer (version-19.1.0.18287)[17]. The selection of the amino acids in the active site was used to analyze the grid box and to define the cavity. All the docking poses, ligand and protein interactions were studied by importing output files into Discovery Studio which enables us to identify the types of interactions. Discovery Studio is an offline life sciences software that offers tools to study drug-receptor interaction, docking poses visualization and macromolecule preparations. The chosen cavity was the binding site of the native ligand in PDB 4K9T.

RESULTS AND DISCUSSION

All the flavonoids and doxorubicin successfully docked on CYP3A4. Binding energy is released when a drug molecule associates with a target, leading to a lowering of the overall energy of the complex [14]. Molecular formula, Lipinski’s rule of five, binding affinity (kcal/mol), and active amino acid residues are presented in Table 1. Lipinski’s rule of five plays an important role in molecule screening and validation. Here, Pongamosides i.e. Pongamoside A, Pongamoside B, and Pongamoside D have shown better binding affinity than doxorubicin.

Table 2 represents 3D- & 2D-images of docking poses along with no. of hydrogen bonds involved in the interaction. The 2D-docking pose also shows the chemical structure of the ligands which enables us to predict groups and/or atoms involved in the bond formation with CYP3A4.

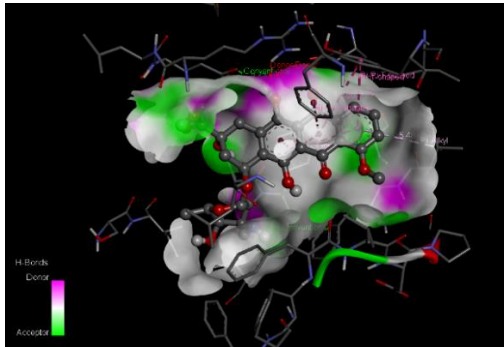
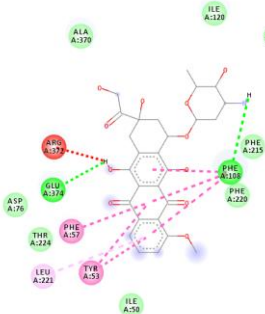
Table 2. Properties, Lipinski’s rule of five, binding affinity and active amino acid residues.

Name of Compound	Molecular Formula	Lipinski’s rule of five		Binding affinity (kcal/mol)	Active amino acid residues
Doxorubicin	C ₂₇ H ₂₉ NO ₁₁	Molecular weight (<500 DA)	543.5	-10.7	Ala370, Ile120, Phe241, Phe213, Val240, Phe215, Phe108, Phe220, Ile50, Tyr53, Leu221, Phe57, Thr224, Asp76, Glu374 (Forms unfavourable bond with Arg372)
		XLogP (<5)	1.3		
		H-Bond donor (5)	6		
		H-bond acceptor (<10)	12		
Pongamoside A	C ₂₃ H ₂₀ O ₉	Molecular weight (<500 DA)	440.4	-11.6	Leu373, Ala370, Arg372,

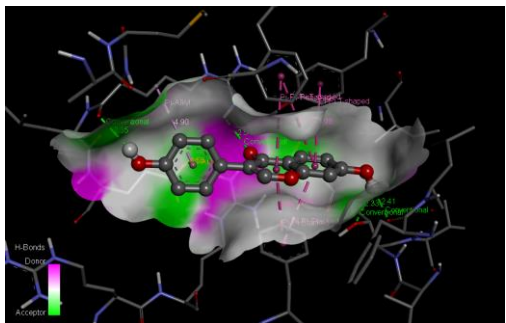
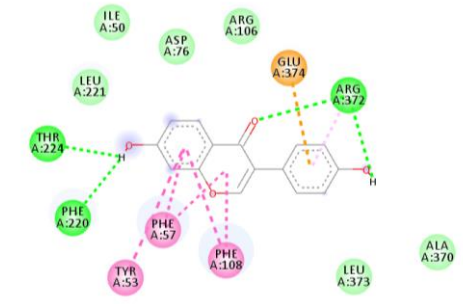
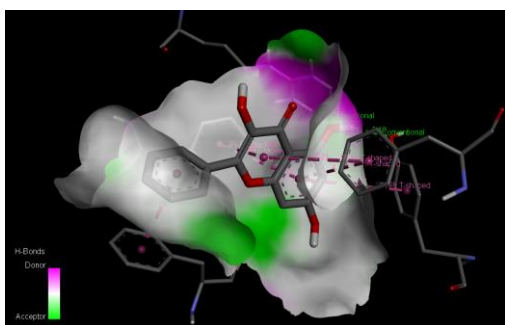
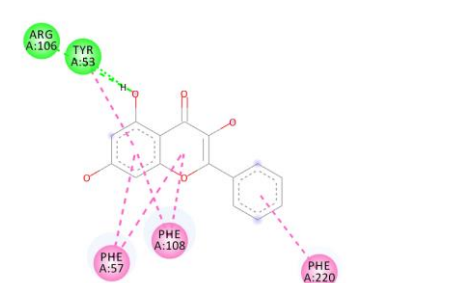
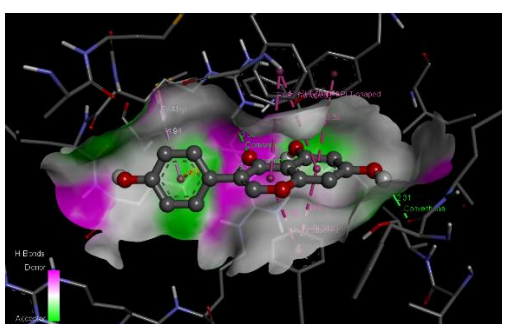
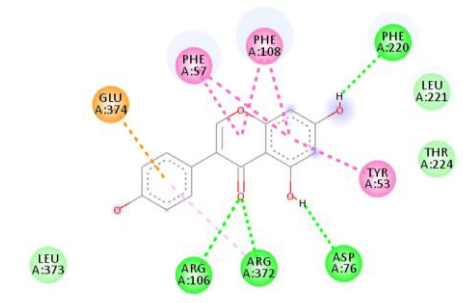
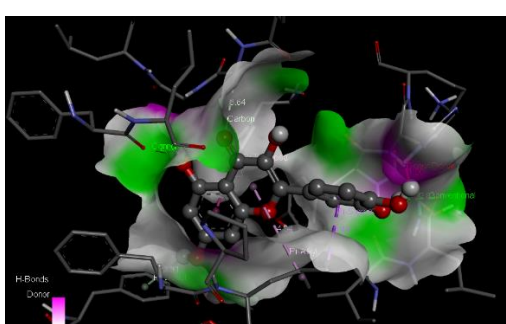
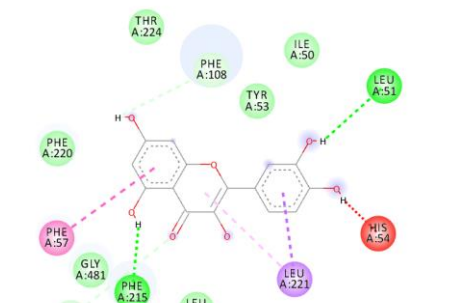
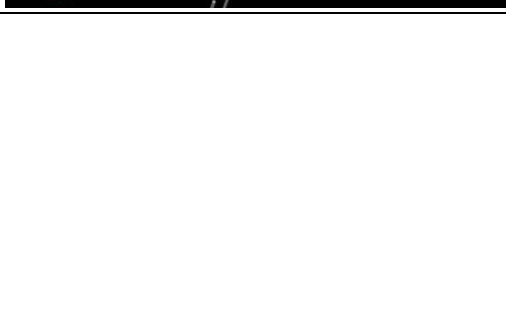
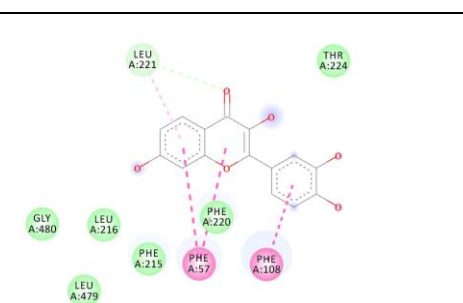
		XLogP (<5)	1.4		Met371, Gly481, Asp76, Leu482, Ile50, Leu221, Pro218, Leu216, Tyr53, Phe57, Phe220, Phe108, Arg105, Glu374
		H-Bond donor (5)	4		
		H-bond acceptor (<10)	9		
<u>Pongamoside B</u>	C ₂₄ H ₂₂ O ₁₀	Molecular weight (<500 DA)	470.4	-10.9	Arg372, Ala370, Met371, Leu216, Gly480, His54, Tyr53, Leu221, Thr224, Phe57, Arg106, Glu374, Arg105 (Forms unfavourable bond with Gly481)
		XLogP (<5)	1.4		
		H-Bond donor (5)	4		
		H-bond acceptor (<10)	10		
<u>Pongamoside D</u>	C ₂₃ H ₂₂ O ₁₁	Molecular weight (<500 DA)	474.4	-10.8	Phe57, Leu216, Tyr53, Gly480, Gly56, Leu479, His54, Leu221, Ile50, Asp76, Thr224, Phe220, Phe108
		XLogP (<5)	1		
		H-Bond donor (5)	4		
		H-bond acceptor (<10)	11		
<u>Pongamoside C</u>	C ₂₄ H ₂₂ O ₁₀	Molecular weight (<500 DA)	470.4	-10.6	Leu221, Pro218, Leu216, Asp217, Phe57, Phe108, Ile369, Gly481, Met371, Arg372, Glu374, Arg106, Phe215, Thr224, Ile50, Tyr53, Phe220
		XLogP (<5)	1.6		
		H-Bond donor (5)	2		
		H-bond acceptor (<10)	10		
<u>Cyclocommunin</u>	C ₂₅ H ₂₄ O ₆	Molecular weight (<500 DA)	420.4	-10.1	Phe215, Val240, Phe108, Thr224, Glu374, Arg372, Phe220, Phe213, Phe241, Phe304, Ile301
		XLogP (<5)	4.1		
		H-Bond donor (5)	3		
		H-bond acceptor (<10)	3		
<u>Daidzein</u>	C ₁₅ H ₁₀ O ₄	Molecular weight (<500 DA)	254.2	-9.3	Leu221, Ile50, Asp76, Arg106, Glu374, Arg372, Ala370, Leu373, Phe108, Phe57, Tyr53, Phe220, Thr224
		XLogP (<5)	2.5		
		H-Bond donor (5)	2		
		H-bond acceptor (<10)	4		
<u>Galangin</u>	C ₁₅ H ₁₀ O ₅	Molecular weight (<500 DA)	270.2	-9.3	Arg106, Tyr53, Phe220, Phe108, Phe57
		XLogP (<5)	2.3		
		H-Bond donor (5)	3		
		H-bond acceptor (<10)	5		
<u>Genistein</u>	C ₁₅ H ₁₀ O ₅	Molecular weight (<500 DA)	270.2	-9.1	Glu374, Phe57, Phe108, Phe220, Leu221, Thr224, Tyr53, Asp76, Arg372, Arg106, Leu373
		XLogP (<5)	2.7		
		H-Bond donor (5)	3		
		H-bond acceptor (<10)	5		
<u>Quercetin</u>	C ₁₅ H ₁₀ O ₇	Molecular weight (<500 DA)	302.2	-8.7	Thr224, Phe108, Tyr53, Ile50, Leu51, Leu221, Leu216, Phe215, Gly481, Gly480, Phe57, Phe220 (Forms unfavourable bond with His54)
		XLogP (<5)	1.5		
		H-Bond donor (5)	5		
		H-bond acceptor (<10)	7		
<u>Fisetin</u>	C ₁₅ H ₁₀ O ₆	Molecular weight (<500 DA)	286.2	-8.7	Leu221, Thr224, Phe108, Phe220, Phe57, Phe215, Leu479, Leu216, Gly480
		XLogP (<5)	2		
		H-Bond donor (5)	4		
		H-bond acceptor (<10)	6		
<u>Luteolin</u>	C ₁₅ H ₁₀ O ₆	Molecular weight (<500 DA)	286.2	-8.6	Phe215, Leu221, Phe57, Leu479, Gly56, His54, Ile50, Phe108, Thr225, Phe220
		XLogP (<5)	1.4		
		H-Bond donor (5)	4		
		H-bond acceptor (<10)	6		

Myricetin	C ₁₅ H ₁₀ O ₈	Molecular weight (<500 DA)	318.2	-8.6	Leu221, Phe57, Thr224, Phe215, Gly480, Leu216, Leu479, Ile50, Leu51, His54
		XLogP (<5)	1.2		
		H-Bond donor (5)	6		
		H-bond acceptor (<10)	8		
Isorhamnetin	C ₁₆ H ₁₂ O ₇	Molecular weight (<500 DA)	316.2	-8.4	Leu221, Pro218, Phe57, Thr224, Phe220, Phe215, Leu216, Gly480, Leu479, Tyr53, Ile50, Leu51, His54 (Forms unfavourable bond with Gly481)
		XLogP (<5)	1.9		
		H-Bond donor (5)	4		
		H-bond acceptor (<10)	7		
Kaempferol	C ₁₅ H ₁₀ O ₆	Molecular weight (<500 DA)	286.2	-8.4	Phe108, Phe215, Phe57, Gly481, Gly480, Leu216, Tyr53, Phe220, Thr224
		XLogP (<5)	9.8		
		H-Bond donor (5)	1		
		H-bond acceptor (<10)	1		
Pachypodol	C ₁₈ H ₁₆ O ₇	Molecular weight (<500 DA)	344.3	-8.3	Leu221, Pro218, Leu479, Gly480, Phe215, Leu216, Phe220, Thr224, Phe108, Phe57, Tyr53, His54, Ile50, Leu51
		XLogP (<5)	3.1		
		H-Bond donor (5)	2		
		H-bond acceptor (<10)	7		
Pelargonidin	C ₁₅ H ₁₁ O ₅ ⁺	Molecular weight (<500 DA)	271.2	-8.2	Tyr53, Phe215, Gly481, Phe220, Phe108, Leu221, Phe57, Thr224, Ile50
		XLogP (<5)	2.1		
		H-Bond donor (5)	4		
		H-bond acceptor (<10)	1		

Table 3. 3D- & 2D-images of docking poses along with no. of hydrogen bonds involved.

Name of Compound	3D-docking pose	2D-docking pose	No. of hydrogen bonds involved
Doxorubicin			02
Pongamoside A			00

Pongamoside B			02
Pongamoside D			02
Pongamoside C			02
Cyclocommunin			00

<p>Daidzein</p>			<p>04</p>
<p>Galangin</p>			<p>02</p>
<p>Genistein</p>			<p>04</p>
<p>Quercetin</p>			<p>02</p>
<p>Fisetin</p>			<p>00</p>

Luteolin			03
Myricetin			01
Isorhamnetin			02
Kaempferol			00

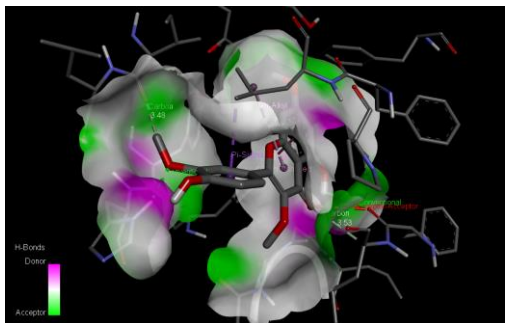
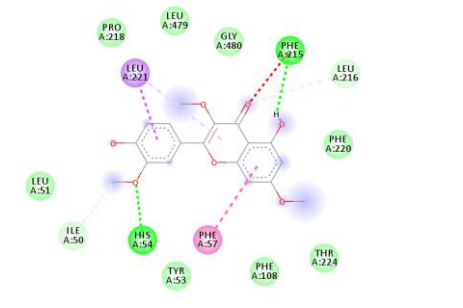
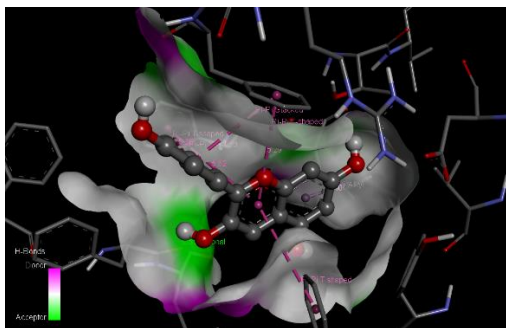
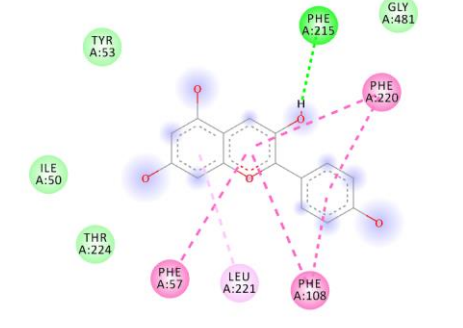
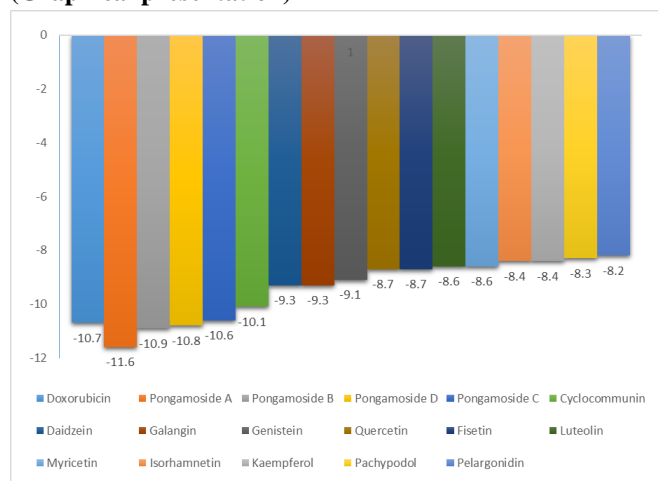
<p>Pachypodol</p>			<p>02</p>
<p>Pelargonidin</p>			<p>01</p>

Figure 1 represents the comparative binding affinities (kcal/mol) of doxorubicin and flavonoids. Many of the flavonoids have shown better binding affinity than doxorubicin.

Figure 1. Comparative binding affinities of the compounds (Graphical presentation)



As we have represented docking data along with 2D- & 3D-docking poses including no. hydrogen bonds involved in the interactions in Table 2. The formation of a hydrogen bond with the target molecule always results in inhibition of the receptor. Sadhna Sinha et al reported the Molecular docking of flavones at the colchicines binding pocket which revealed that the compounds bind at a-b interfacial site of tubulin,

correlating binding interactions with probable inhibition mechanism. The study reveals important observations to generate improved flavonoids that leads to cell apoptosis [15]. In case of Pongamoside A, it forms zero hydrogen bonds but still its binding affinity i.e. -11.6 kcal/mol is best because Pongamoside A forms van der Waals force attraction, Pi-Pi Stacked bonds, Pi-Pi T-shaped bonds, Amide-Pi stacked bonds and Pi alkyl bonds with more amino acid residues than doxorubicin i.e. -10.7 kcal/mol which forms two hydrogen bonds with CYP3A4. Pongamoside B and Pongamoside D have binding affinities (kcal/mol) -10.9 and -10.8 with the formation of 2-2 hydrogen bonds each with CYP3A4. This can be sufficient scientific evidence showing more potency of these flavonoids in terms of inhibition of CYP3A4 than the approved drug, doxorubicin. Although, Pongamoside C, Galangin, Quercetin, Isorhamnetin, Pachypodol forms 2-2 hydrogen bonds each with binding affinities -10.6, -9.3, -8.7, -8.4 and -8.3 kcal/mol respectively. Surprisingly Daidzein and Genistein formed 4 hydrogen bonds each with CYP3A4 with a docking score of -9.3 and -9.1 kcal/mol respectively which is much enough to inhibit the activity of CYP3A4. Luteolin has formed 3 hydrogen bonds with -8.6 kcal/mol binding affinity. The amino acid residues in the cavity involved in the interactions are represented in **Table 1**.

CONCLUSION

It is well known that natural compounds have proven to have a safe biological window as compared to molecules from a synthetic source. In present work, molecular docking studies disclosed, that flavonoids Pongamoside A, Pongamoside B,

and Pongamoside D have a better binding affinity towards CYP3A4 than doxorubicin. Although, if we talk about the formation of hydrogen bonds with target macromolecule, Daidzein, Genistein, and Luteolin form more hydrogen bonds than doxorubicin. In conclusion, the above docking study disclosed that rational synthesis of natural analogues in reference to synthetic drugs could generate drugs with improved therapeutic effects for chemoprevention. CYP3A4 plays a major role in the metabolism of various drugs; by the help of flavonoids, we can control the selective drug metabolism by inhibiting CYP3A4. Despite this, these molecules are not marketed for cancer treatment because of their high polarity. If we could overcome this problem, these molecules can act as effective anticancer agents in the future. Still, if we want to use these compounds clinically, there is a need to generate more scientific evidence and quality data by using *in vivo* and *in vitro* models.

ACKNOWLEDGEMENT

None

CONFLICTS OF INTEREST

None.

DATA AVAILABILITY

Not declared.

FUNDING SOURCE

Not declared

REFERENCES

[1] Grigalius I, Petrikaite V. Relationship between antioxidant and anticancer activity of trihydroxyflavones. *Molecules.*, 2017;22. <https://doi.org/10.3390/molecules22122169>.

[2] Ravishankar D, Rajora AK, Greco F, Osborn HMI. Flavonoids as prospective compounds for anti - cancer therapy. *Int J Biochem Cell Biol.*, 2016:1–5. <https://doi.org/10.1016/j.biocel.2013.10.004>.

[3] Mehranfar F, Bordbar AK, Parastar H. A combined spectroscopic, molecular docking and molecular dynamic simulation study on the interaction of quercetin with β -casein nanoparticles. *J Photochem Photobiol B Biol.*, 2013;127:100–7. <https://doi.org/10.1016/j.jphotobiol.2013.07.019>.

[4] Iqbal J, Abbasi BA, Mahmood T, Kanwal S, Ali B, Shah SA, et al. Plant-derived anticancer agents: A green anticancer approach. *Asian Pac J Trop Biomed.*, 2017;7:1129–50. <https://doi.org/10.1016/j.apjtb.2017.10.016>.

[5] Balachandran C, Sangeetha B, Duraipandiyan V, Raj MK, Ignacimuthu S, Al-Dhabi NA, et al. A flavonoid isolated from *Streptomyces* sp. (ERINLG-4) induces apoptosis in

human lung cancer A549 cells through p53 and cytochrome c release caspase dependant pathway. *Chem Biol Interact.*, 2014;224:24–35. <https://doi.org/10.1016/j.cbi.2014.09.019>.

[6] Iqbal J, Abbasi BA, Mahmood T, Kanwal S, Ali B, Khalil AT. Plant-derived anticancer agents : A green anticancer approach. *Asian Pac J Trop Biomed.*, 2017:1–23. <https://doi.org/10.1016/j.apjtb.2017.10.016>.

[7] Kumar P. PLANT DERIVED ANTICANCER AGENTS AND THEIR STRUCTURE: A REVIEW. *Int Res J Pharm.*, 2018;9:43–9. <https://doi.org/10.7897/2230-8407.09687>.

[8] Cacabelos R, Cacabelos P, Torrellas C. Personalized Medicine of Alzheimer ' s Disease. Elsevier Inc.; 2014. <https://doi.org/10.1016/B978-0-12-386882-4.00027-X>.

[9] Gurusamy U, Shewade DG. Pharmacogenomics in India. Elsevier Inc.; 2014. <https://doi.org/10.1016/B978-0-12-386882-4.00046-3>.

[10] Hejazi II, Khanam R, Mehdi SH, Bhat AR, Rizvi MMA, Thakur SC, et al. Antioxidative and anti-proliferative potential of *Curculigo orchoides* Gaertn in oxidative stress induced cytotoxicity: In vitro, ex vivo and in silico studies. *Food Chem Toxicol.*, 2018;115:244–59. <https://doi.org/10.1016/j.fct.2018.03.013>.

[11] Rasouli H, Farzaei MH, Mansouri K, Mohammadzadeh S, Khodarahmi R. Plant cell cancer: May natural phenolic compounds prevent onset and development of plant cell malignancy? A literature review. *Molecules.*, 2016;21:14–21. <https://doi.org/10.3390/molecules21091104>.

[12] Phosrithong N, Ungwitayatorn J. Molecular docking study on anticancer activity of plant-derived natural products. *Med Chem Res.*, 2010;19:817–35. <https://doi.org/10.1007/s00044-009-9233-5>.

[13] Saeed M, Kadioglu O, Khalid H, Sugimoto Y, Efferth T. Activity of the dietary flavonoid, apigenin, against multidrug-resistant tumor cells as determined by pharmacogenomics and molecular docking. *J Nutr Biochem.*, 2015;26:44–56. <https://doi.org/10.1016/j.jnutbio.2014.09.008>.

[14] Mokale SN, Begum A, Sakle NS, Shelke VR, Bhavale SA. Design , synthesis and anticancer screening of 3- (3- (substituted phenyl) acryloyl) -2H-chromen-2ones as selective anti-breast cancer agent. *Biomed Pharmacother.*, 2017;89:966–72. <https://doi.org/10.1016/j.biopha.2017.02.089>.

[15] Sinha S, Amin H, Nayak D, Bhatnagar M, Kacker P, Chakraborty S, et al. Assessment of microtubule depolymerization property of flavonoids isolated from *Tanacetum gracile* in breast cancer cells by biochemical and molecular docking approach. *Chem Biol Interact.*, 2015;239:1–11. <https://doi.org/10.1016/j.cbi.2015.06.034>.

[16] Skiff, A. K. Rappe, C. J. Casewit, K. S. Colwell, W. A. Goddard III WMS. UFF, a Full Periodic Table Force Field for Molecular Mechanics and Molecular Dynamics Simulations. *J Am Chem Soc.*, 2009;114:10024–35. <https://doi.org/https://doi.org/10.1021/ja00051a040>.


[17] Dassault Systèmes BIOVIA, Discovery Studio Modeling Environment, Release 2017, San Diego: Dassault Systèmes., 2016.

- [18] Dallakyan S, Olson AJ. Small-molecule library screening by docking with PyRx. *Methods Mol Biol.*, 2015;1263:243–50. https://doi.org/10.1007/978-1-4939-2269-7_19.

Indo Global Journal of Pharmaceutical Sciences(ISSN 2249 1023; CODEN- IGJPAI; NLM ID: 101610675) indexed and abstracted in CrossRef (DOI Enabling), CNKI, UGC CARE Journal List, EMBASE (Elsevier), National Library of Medicine (NLM) Catalog (NCBI), ResearchGate, Publons (Clarivate Analytics), CAS (ACS), Index Copernicus, Google Scholar and many more. For further details, visit <http://iglobaljournal.com>

NOTE

Variants in *NIPAL4* and *ALOXE3* cause autosomal recessive congenital ichthyosis in Pakistani families

Abida Akbar^{1,2} | Muneeba Bint-e-Farrakh² | Andrew H. Crosby¹ | Asma Gul²  | Gaurav V. Harlalka^{1,3}

¹RILD Building, Wellcome Wolfson Centre, University of Exeter Medical School, Exeter, UK

²Department of Biological Sciences, International Islamic University, Islamabad, Pakistan

³Rajarshi Shahu College of Pharmacy, Malvihi, Buldana, India

Correspondence

Dr Gaurav V. Harlalka, RILD Building, Wellcome Wolfson Centre, University of Exeter Medical School, Barrack Road, Exeter, UK.

Email: gauravh12@yahoo.co.in

Asma Gul, Department of Biological Sciences, International Islamic University, Islamabad, Pakistan.

Email: gulasma@iiu.edu.pk

Funding information

Higher Education Commission, Grant/Award Number: 1-8/HEC/HRD/2017/7949

Autosomal recessive congenital ichthyosis (ARCI) encompasses clinically diverse and genetically heterogeneous group of cornification disorders, and clinically characterized by generalized scaling, variable erythroderma with a global prevalence of approximately 7:1 million.¹

Patients with ARCI are born as collodion babies or with congenital ichthyosiform erythroderma (CIE) and later develop lamellar ichthyosis (LI) with coarse brown scales or CIE with fine white scales.² To date 12 disease causing genes have been identified in ARCI including *NIPAL4*, *TGM1*, *ALOXE3*, *ALOX12B*, *ABCA12*, *CASP14*, *CERS3*, *PNPLA1*, *SDR9C7*, *LIPN*, *SULT2B1*, and *CYP4F22*.³

NIPAL4 gene is one of the causative genes for autosomal recessive congenital ichthyosis, typically in ARCI type III.⁴ However, the function of *NIPAL4* gene is still unclear, it has been hypothesized that it is a magnesium transporter based on the fact that protein family member *NIPA2* was supposed to be a magnesium transporter.⁵

Mutations in *ALOXE3* gene cause lamellar ichthyosis, congenital ichthyosiform erythroderma (CIE), and pleomorphic ichthyosis. Oxygenation of the linoleate moiety of ceramides catalyzed by *ALOXE3* constitutes an essential step in the formation of the corneocyte lipid envelope.⁶

In this study, two Pakistani families (Family 1 and Family 2) with a history of ARCI were investigated. Written informed consent was obtained from patients or their legal guardians and ethical approval was obtained from the Institutional Ethical Committee of IIUI, Pakistan. Pedigree analysis was indicative of an autosomal recessive mode of inheritance in families 1 and 2 (Figure 1). At the time of clinical examination, the affected individuals IV: 1; IV: 4 in Family 1 were 17 and 9 years old, while affected individuals IV: 5, IV: 6, and V: 4 in Family 2 were 8, 3, and 10 years of ages, respectively. Disease was observed at the age of 3 months in patient IV: 1 and was observed in patient IV: 4 at the time

of birth in Family 1. Both affected members of family 1 (IV: 1, IV: 4) have short stature. Disease symptoms were typically seen at the time of birth in affected individuals (IV: 5, IV: 6, and V: 4) of Family 2. On the basis of basic clinical dermatological assessment, ARCI was the major finding in all affected members of the investigated families.

In order to identify the disease causing mutation, single affected individuals (IV: 1; Family 1 and IV: 5; Family 2) were initially selected to perform whole exome sequence and then validated by Sanger sequencing (details in Supporting Information). This identified a homozygous splice-site variant (NM_001099287.1:c.464-1G>A; Chr5:156894056G>A [GRCh37]) in the intron 2 of *NIPAL4* gene (Figure 1F) in Family 1, and a homozygous nonsense variant (NM-02168.2:C.631C>T; Chr17:80178 51G>A [GRCh37]) in exon 5 of *ALOXE3* gene of family-2 (Figure 1G), as the likely causes of each condition. No other variants were observed in both genes. The *NIPAL4* variant c.464-1G>A is a reported disease causing variant with HGMD accession ID CS075164.⁴ This is a first instance where c.464-1G>A splice-site variant in *NIPAL4* is identified in homozygous form, being present in two affected half-sisters from a Pakistani family (Family 1; Figure 1). III: 4 (father of IV: 4) from Family 1 is also distantly related to III: 3 (mother of IV: 4). The Family 1 is from Azad Kashmir region in Pakistan (Table S3). According to HGMD professional, 18 mutations (Table S1) in *NIPAL4* are known to cause different forms of ichthyosis to date.

In Family 2, a homozygous nonsense variant c.631C>T results in premature termination (p.Arg211*). While the same *ALOXE3* variant is also reported in HGMD (accession ID CM1610944)⁷ this is the first study reporting homozygous *ALOXE3* c.631C>T; (p.Arg211*) nonsense variant. This family is from Multan city in Punjab, Pakistan (Table S3). So far 22 variants (Table S2) in *ALOXE3* have been implicated in various forms of ichthyosis (HGMD Professional 2018.3).

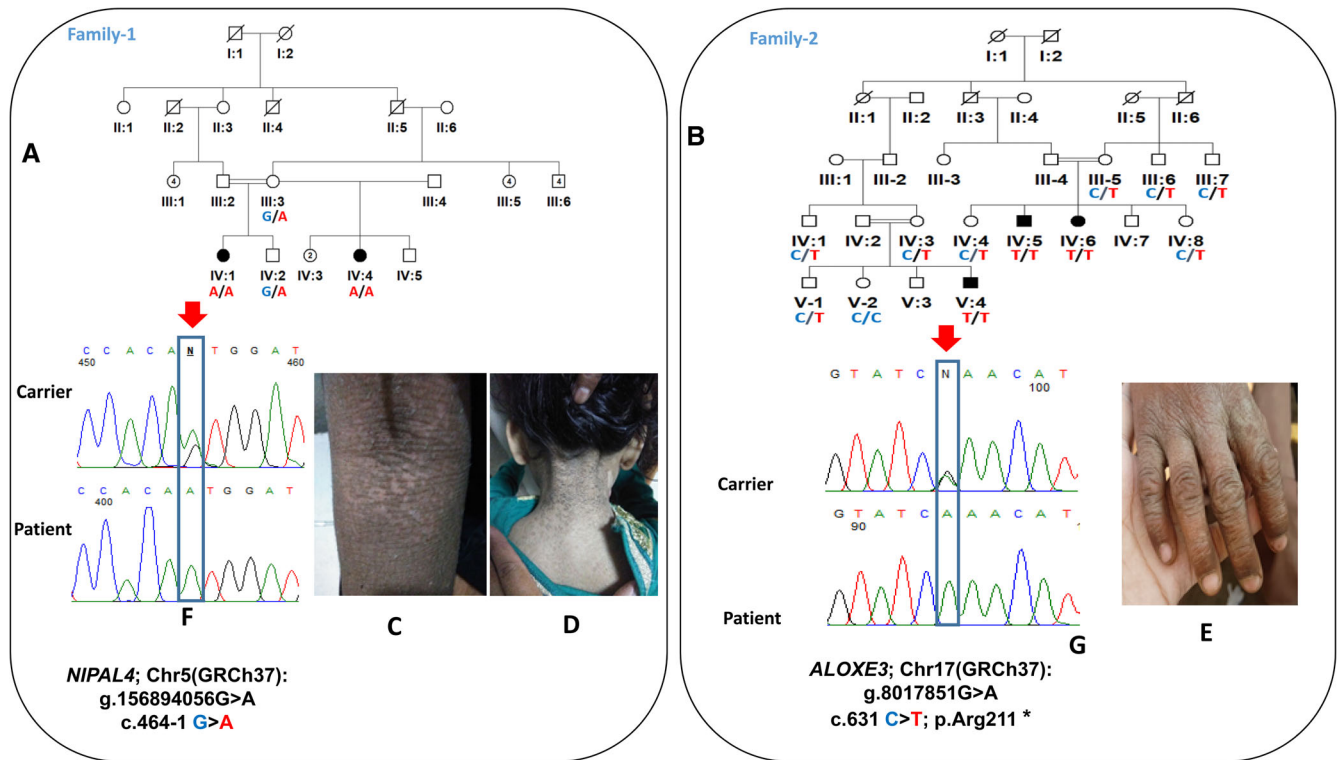


FIGURE 1 A,B, Simplified pedigrees of the extended Pakistani families investigated with genotypes of affected and unaffected individuals. C,D, Clinical presentation of ichthyosis in individuals with *NIPAL4* c.464-1G>A homozygous mutation. E, Clinical presentation of ichthyosis in an individual with *ALOXE3* c.631C>T homozygous variation. F,G, Electropherograms showing DNA sequence at c.464-1 position in *NIPAL4* in individuals (IV: 2; carrier and IV: 4; homozygous) and c.631 position in *ALOXE3* in a heterozygous carrier (III: 5) and homozygous affected individual (V: 4)

Together, the data here provides important information regarding the nature, spectrum and molecular basis of ARCI, enabling early clinical intervention, increased awareness regarding inherited disorders present in a community, and aiding diagnosis and genetic counseling.

ACKNOWLEDGMENTS

We are grateful to all the participating members of both the families. This study was partially supported by the Higher Education Commission (HEC) in Pakistan by awarding IRSIP (Grant No: 1-8/HEC/HRD/2017/7949, PIN: IRSIP 37 BMS 39) to A.A.

CONFLICT OF INTEREST

All authors declare that they have no conflict of interest.

ORCID

Asma Gul <https://orcid.org/0000-0003-0338-3134>

REFERENCES

1. Dreyfus I, Chouquet C, Ezzedine K, et al. Prevalence of inherited ichthyosis in France: a study using capture-recapture method. *Orphanet J Rare Dis.* 2014;9:1.
2. Schmutz M, Martinz V, Janecke AR, et al. Inherited ichthyoses/generalized Mendelian disorders of cornification. *Eur J Hum Genet.* 2013;21:123-133.
3. Cunha L, Dalakloby OM, Gruber R, et al. Unknown mutations and genotype/phenotype correlations of autosomal recessive congenital

ichthyosis in patients from Saudi Arabia and Pakistan. *Mol Genet Genomic Med.* 2019;7:539.

4. Dahlqvist J, Klar J, Hausser I, et al. Congenital ichthyosis: mutations in ichthyin are associated with specific structural abnormalities in the granular layer of epidermis. *J Med Genet.* 2007;44:615-620.
5. Goytain A, Hines RM, Quamme GA. Functional characterization of NIPA2, a selective Mg²⁺ transporter. *Am J Physiol-Cell Physiol.* 2008; 295:944-953.
6. Takeichi T, Okuno Y, Saito C, et al. Congenital Ichthyosis and recurrent eczema associated with a novel *ALOXE3* mutation. *Acta Derm Venereol.* 2017;97:532-533.
7. Pigg MH, Bygum A, Gånemo A, et al. Spectrum of autosomal recessive congenital ichthyosis in Scandinavia: clinical characteristics and novel and recurrent mutations in 132 patients. *Acta Derm Venereol.* 2016;96: 932-938.

SUPPORTING INFORMATION

Additional supporting information may be found online in the Supporting Information section at the end of this article.

How to cite this article: Akbar A, Bint-e-Farrakh M, Crosby AH, Gul A, Harlalka GV. Variants in *NIPAL4* and *ALOXE3* cause autosomal recessive congenital ichthyosis in Pakistani families. *Congenit Anom.* 2020;1-2. <https://doi.org/10.1111/cga.12366>

Supramolecular Complexes of Phospholipids and β -Cyclodextrin with Bioactive β -Carotene: A Comparative Physico-Chemical and Functional Evaluation

Saurabh Gujar¹, Darshan Telange², Anil Pethe^{3*}

¹Shobhaben Pratapbhai Patel School of Pharmacy and Technology Management, SVKM's, NMIMS (Deemed to be University), Mumbai Campus, Mumbai, Maharashtra, INDIA.

²Department of Pharmaceutics and Nanotechnology, Rajarshi Shahu College of Pharmacy, Buldhana, Maharashtra, INDIA.

³School of Pharmacy and Technology Management, SVKM's, NMIMS (Deemed to be University), Hyderabad Campus, Hyderabad, Telangana, INDIA.

ABSTRACT

Background: β -carotene, a chief component of carotenoids family exhibits multiple numbers of pharmacological activities. However, its poor aqueous solubility and low dissolution rate restricts it to become a potential drug candidate. Hence, β -carotene-phospholipids complex (BPLC) and β -carotene- β -cyclodextrin complex (BCDC) were prepared with an objective of enhancing its aqueous solubility and dissolution rate.

Materials and Methods: BPLC and BCDC were synthesized using solvent evaporation and kneading method respectively. BPLC and BCDC, were characterized by particle size and zeta potential analysis, complexation rate, drug loading, Fourier transform infrared spectroscopy and differential scanning calorimetry. Functional characterization of above formulations was performed by solubility and *in vitro* dissolution studies. **Results and Conclusion:** Particle size analysis result of BCDC and BPLC formulations were found to be suitable for oral route of administration. FT- IR and DSC studies supported the formation of BCDC and BPLC formulation. Solubility results displayed that BPLC (1:1) significantly enhanced the aqueous solubility upto (28-fold), compared to BCDC (1:2) (18-fold) and β -carotene. Dissolution studies showed that BPLC (1:1) considerably improved the release rate of β -carotene in PBS (pH 7.4) compared to BCDC (1:2) and β -carotene suspension. Hence, above comparison confirmed that phospholipids could be promising carrier compared to β -cyclodextrin for overall enhancement of aqueous solubility and *in vitro* dissolution rate of β -carotene.

Key words: β -carotene, Phospholipids, β -cyclodextrin, Solubility, *in vitro* dissolution.

Submission Date: 22-11-2019;

Revision Date: 06-02-2020;

Accepted Date: 02-05-2020

DOI: 10.5530/ijper.54.2s.78

Correspondence:

Dr. Anil M. Pethe

School of Pharmacy and Technology Management, SVKM's NMIMS (Deemed to be University), Polepally SEZ, TSIC, Jadcherla, Mehbubnagar-509301, Hyderabad, Telangana, INDIA.

Phone: +91 8879212188

E-mail: anilpethe@gmail.com

INTRODUCTION

β -carotene (β -CTE), a chief component of carotenoids family shows existence in many fruits, vegetables and microalgae such as mangos, cantaloupe, peppers, pumpkin, sweet potatoes, carrots, leaves, fish and sea foods etc. It acts as a great source of vitamin A and hence, it finds application in the maintenance of normal functioning of human eye.¹ Moreover, it is an approved food ingredients and thus, has been employed majorly in countless food, cosmetic and most importantly, in pharmaceutical

products.² Earlier studies have reported a number of clinical benefits of β -CTE such as antioxidant,³ anticancer, cardio-protective and anti-ageing activities.^{4,5} Regardless of therapeutic advantages of β -CTE, its clinical utility is primarily restricted by its poor aqueous solubility ($< 0.6 \mu\text{g/mL}$), low oral bioavailability ($\sim 11 - 30\%$) and easy susceptibility to degradation due to high sensitivity to molecular oxygen, light and temperature. In this situation, overcoming



www.ijper.org

of β -CTE limitations by using suitable carriers and/or methods could be more valuable.

Previously several reports demonstrated the turnaround the above limitations of β -CTE by employing several formulation strategies such as nanodispersion,⁶ nano-emulsion,^{3,7} complexation⁸ and solid dispersion.⁹ However, these formulations reported only the improvement of physical and chemical stability of β -CTE without investigating its aqueous solubility and *in vitro* dissolution rate. Improvement in these two parameters can provide more benefits in the processing of food products. Thus, there is a strong need to develop unique formulation using suitable carrier, which can overcome the observed significant limitations of β -CTE.

Among all existed formulations, complexation system is reported to be a most promising technique for the enhancement of poor aqueous solubility, *in vitro* dissolution rate, oral bioavailability and antioxidant activity of drug molecules.^{10,11} Carriers such as phospholipids and β -cyclodextrin are specifically utilized for the development and preparation of complexation system. Recent studies have evidenced that these carriers on complexation with plant bioactives such as salvianolic acid B,¹² chlorogenic acid,¹³ ferulic acid¹⁴ and idebenone¹⁵ appreciably enhanced the solubility, bioavailability and respective pharmacological activities. Complexation via phospholipids can form stable amorphous phospholipids complex, where bioactive get entrapped within the core of phospholipids and thus, form supramolecular complex by formation of H-bonds, van der Waals and ion-dipole forces between them. Amphiphilic and biocompatible nature of phospholipids can also act as preferable carrier for transportation of hydrophobic drug across biological membrane, which in turn, enhances the bioavailability of drugs.¹⁶ Due to its high amorphous characteristics, it significantly improves the aqueous solubility of hydrophobic drug via reducing its crystalline property and thereby, increases its wetting in aqueous media.¹⁷ Likewise, β -cyclodextrin (β -CD) based complexation system is also called as inclusion complex. Due to its biocompatibility and superficial functionalization, it can freely occupy the varying size of hydrophobic drug within its central cavity (made up of 7-glucopyranose units), which may cause to dehydrate and transfer drug into cavity, form spatial arrangement inclusion complex via non-covalent interactions, resulting to increase the affinity of drug towards aqueous media with random transformation from crystalline to high energy state amorphous powder and finally improves the solubility of drugs. Additionally, the reported

amphiphilic nature of β -CD molecule significantly improves the solubility and dissolution rate of hydrophobic drug via reducing the interfacial tension between the solid particles and dissolution medium.¹⁸ Moreover, both carriers provide multiple advantages to the formulation such as easy preparation process, high drug loading capacity and long term stability etc.

The present research work deals with an enhancement of poor aqueous solubility and dissolution rate of β -CTE by preparing its complex with phospholipids or β -CD and evaluate them comparatively. BCDC and BPLC were prepared by kneading and solvent evaporation method. Prepared complex was physico-chemically and functionally evaluated using particle size analysis, drug loading, FT-IR, DSC, solubility and *in vitro* dissolution rate.

MATERIALS AND METHODS

Materials

Lyophilizer (Model: MSW-137, Macro Scientific Works Pvt. Ltd., New Delhi, India). β -carotene (purity > 99%) was obtained from Natural Remedies Pvt. Ltd., Bangalore, India. Cholesterol was received as gift sample from VAV Life Sciences Pvt. Ltd., Mumbai, India. Phospholipon[®]90H was purchased from Molychem, Mumbai India. Absolute ethanol, ethylenediamine tetraacetic acid (EDTA), disodium hydrogen phosphate, potassium dihydrogen phosphate and sodium chloride were obtained from Loba Chemicals Pvt. Ltd., Mumbai, India. All other chemicals received for the study were of analytical grade reagent.

Preparation of β -carotene – β – cyclodextrin complex (BCDC)

The β -cyclodextrin based complex of β -carotene was prepared in molar ratios of (i.e. 1:1, 1:2 and 1:3) using kneading method reported earlier in literature.¹⁹ Briefly, the β -CTE and β -CD, both were accurately and individually weighed according to their molar ratios and then transferred into a clean and previously air-dried mortar. The weighed mixture was mixed and dissolved using 20 mL of absolute ethanol. The solvent was allowed to evaporate, which in turn, resulting to formation of porous solid mass. The obtained mass was dried using hot air oven at 50°C for 24 hr for removal of entrapped solvent, if any. The dried mass was sieved to get uniform size particles. These particles were then placed in an amber colored glass vials previously flushed with nitrogen and finally stored at RT, till further physico-chemical analysis.

Preparation of β -carotene- phospholipids complex (BPLC)

Thin film hydration technique was employed for the preparation of β -CTE - phospholipids complex with slight modifications.²⁰ Briefly, as per above mentioned molar ratios, the same quantities of β -CTE and Phospholipon[®] 90H were individually weighed and transferred into 250 mL round bottom flask. The powdered samples were co-dissolved in 10 mL of absolute ethanol. The prepared solution was magnetically stirred (at 25 °C for 1 hr) to ensure uniform mixing of both the components. After stirring, the assembly was subjected to rotary vacuum evaporator, leading to evaporation of solvent and formation of film. The obtained film was hydrated using 5 mL of deionized water and then sonicated. The hydrated solution was then lyophilized using a lyophilizer (Model: MSW-137, Macro Scientific Works Pvt. Ltd., New Delhi, India) under the conditions of controlled condenser temperature of -80 °C and vacuum of 10 Pa. The final dried BPLC was preserved in nitrogen flushed and light resistant container and stored at 4 °C for further analysis. Composition of BCDC and BPLC formulation are shown in Table 1.

Estimation of drug loading and extent of complexation rate (% yield)

The inclusion of β -CTE within the prepared BCDC was estimated by well-known spectrophotometric method described earlier in the literature.²¹ Briefly, the prepared BCDC formulations was accurately weighed (equivalent to ~10 mg of pure β -CTE) and mixed with 100 mL of phosphate buffer solution (0.05M, pH 6.8). The prepared solution was then subjected to membrane filtration (0.45 μ) in order to get clear filtrate. From this solution, few aliquots were removed, diluted appropriately, analyzed for absorbance at suitable detection wavelength ($\lambda_{\text{max}} = 450$ nm) on UV-visible

spectrophotometer (Model: V-630, JASCO International Co., Ltd., Tokyo, Japan). The separate carrier solution with same concentration was also prepared to remove any developed interference while performing analysis.

A method previously described by Tan *et al.*²² was used for the determination of extent of β -CTE in the prepared BPLC formulations. Briefly, the chloroform based dispersion was prepared by dissolving BPLC (equivalent to ~50 mg of β -CTE) into 5 mL of chloroform, followed by stirring, resulting to formation of uniform dispersion. In this dispersion, the BPLC and Phospholipon[®] 90H were showed complete solubility, whereas, pure β -CTE was remained undissolved and settled down at the bottom of the beaker. Next, the dispersion was filtered using Whatman[®] filter paper (ashless, Grade 41, Sigma-Aldrich Corporation, St. Louis, MO) and separate the undissolved residue. This residue was dried at room temperature (25 °C). After drying, it was then dissolved in methanol, diluted suitably and analyzed the resulting solution on UV-visible spectrophotometer (Model: V-630, JASCO International Co., Ltd., Tokyo, Japan) at detection wavelength of ($\lambda_{\text{max}} = 450$ nm). The below described equation (1) was used to calculate the extent of complexation rate of pure β -CTE with Phospholipon[®] 90H.

$$\text{Extent of complexation (\%)} = (c_i - c_f) / c_i \times 100 \quad (1)$$

Where, c_i represents the theoretical concentration of β -CTE in BPLC and c_f designates the observed concentration of β -CTE in the filtrate.

Physico-chemical characterization

Particle size and zeta potential

A well established Photon Cross-Correlation Spectroscopy (PCCS) attached with Dynamic Light Scattering (DLS) technology used by our laboratory previously, was utilized for determination of particle size distribution and zeta potential of BCDC and BPLC formulations.²³ Briefly, BCDC and BPLC formulations (equivalent to ~ 5 mg) was weighed, dispersed in 10 mL of deionized water and stirred well. The prepared dispersion was placed into sample holder and examined in the sensitivity range of 1 nm to 10 μ m using particle size analyzer (Model: NANOPHOX Sympatec, GmbH, Clausthal-Zellerfeld, Germany). The analyzer analyzed the particle size distribution of both formulations by optimization of particle count rate via adjusting the sample position. The analysis was carried out at room temperature (25 °C). Obtained results were read by using software accompanying with this instrument.

Table 1: Composition of the prepared BCDC and BPLC formulations.

Formulations	β -carotene (mg)	β -cyclodextrin (mg)
BCDC		
BCDC 1	536.88	1135
BCDC 2	536.88	2270
BCDC 3	536.88	3405
Formulations	β -carotene (mg)	Phospholipon [®] 90H (mg)
BPLC		
BPLC 1	536.88	790
BPLC 2	536.88	1580
BPLC 3	536.88	2370

The aqueous dispersion of BCDC and BPLC as prepared above, was also used for the determination of zeta potential within the sensitivity range of -200 to + 200 mV using Nano Particle Analyzer (Model: NanoPlus™-2, Particulate system, Norcross, GA, USA) attached with Dynamic Light Scattering (DLS) technology. This operational procedure was carried out at RT.

FT-IR study

The molecular level interactions between the samples of β -CTE, β -CD, Phospholipon® 90H, physical mixture (PM) of β -CTE and β -CD, PM of β -CTE and Phospholipon® 90H, BCDC and BPLC formulations were analyzed using FT-IR spectrophotometer (Model: FTIR-8300, Shimadzu, Kyoto, Japan) procedure previously reported by our members.²⁴ Briefly, an approximate amount of each sample (~ 2 mg) and FT-IR grade of potassium bromide (~200 mg) were weighed, transferred and mixed well. The prepared homogenous powder were collected and then compressed into transparent discs using Mini-Hand Press Machine (Model: MHP-1, P/N-200-66747-91, Shimadzu, Kyoto, Japan) at a pressure of 10 ton/Nm². Each sample discs were scanned (32 scans) within the wave number range of (4000 to 400 cm⁻¹) with scanning resolution was fixed at 4 cm⁻¹. After this, the scanned FT-IR absorption peaks for each sample were analyzed and interpreted by software (IR solution, Version 1.10) accompanying with this instrument.

DSC study

A differential scanning calorimeter (Model: DSC-1 821e, Mettler-Taledo AG, Analytical, Schwerzenbach, Switzerland) was employed to understand the thermal characteristics of above mentioned components of BCDC and BPLC formulations. A DSC analysis procedure earlier reported by our group was employed in this study.²⁵ Briefly, the formulation components were individually weighed (~ 2.0 mg \pm 0.2) and transferred to the clean glass vials. Before analysis, the DSC instrument was calibrated by purified standard Indium (In) in order to get uniform heat flow and heat capacity. Sample analyzing area was also cleared with entrapped oxygen by purging liquid N₂ at a flow rate of 50 mL/min. Weighed samples were then subjected to heating within the fixed range of 40 to 400°C or more, if any, at a temperature increment of 10°C/min. The final thermal spectrums of each component were read using the attached software (Universal Analysis 2000, V4.5A, Build 4.5.0.5) accompanying with instrument.

Solubility studies

The solubility performance of β -CTE, PM, BCDC and BPLC formulations in water and/or *n*-octanol were analyzed by following the procedure as described by Singh *et al.*¹⁷ Briefly, the aqueous and/or *n*-octanol dispersion (approximate 5 mL each) with an excess amount of each individual sample was prepared and then agitated on water bath shaker temperature (Model: RSB-12, Remi House, Mumbai, India) for 24 hr, leading to formation of homogenous dispersion. The prepared dispersion was centrifuged at 1500 RPM for 25 min and filtered using 0.45 μ membrane. From the obtained filtrate, the small aliquots was pipette out, diluted suitably and analyzed the resulting solution at maximum wavelength of (λ_{max} = 450 nm) using UV-visible spectrophotometer (Model: V-630, JASCO International Co., Ltd., Tokyo, Japan). This analytical procedure was performed at room temperature (25°C).

Functional characterization

In vitro dissolution studies

In this study, the dialysis membrane dissolution method, earlier described by Maiti *et al.*²⁶ was used to study the comparative *in vitro* dissolution performance of β -CTE, BCDC and BPLC formulations. Briefly, the dialysis membrane with following characteristics such as (LA395, dialysis membrane-110, average diameter ~21.34, average flat width ~32, capacity ~3.63 mL, molecular size cut-off range 12,000 - 14,000 Da, HiMedia Laboratories, Mumbai, India) was employed in the current study. The procured membrane was washed and rinsed as per the suggestions received from the manufacturer. After washing, the small size dialysis bags were prepared, loaded with samples such as β -CTE (~ 2 mg), BCDC (~ 2 mg of pure β -CTE) and BPLC formulations (~ 2 mg of pure β -CTE) and then tied using thread. Moreover, bags loaded with samples were also checked for leakage, if any. Next to this, the bags containing samples were suspended in vertical position into freshly prepared phosphate buffered-saline (PBS, 200 mL, pH 7.4) with Tween® 20 (1%, v/v) solution dissolution media and stirred well at 50 RPM using magnetic stirrer. The small solution was removed at a fixed time intervals, diluted appropriately and assayed at maximum wavelength (λ_{max} = 450 nm) for recording the absorbance on UV-visible spectrophotometer (Model: V-630, JASCO International Co., Ltd., Tokyo, Japan). The measured absorbance gives the information regarding cumulative release of β -CTE from its suspension, BCDC and BPLC over the period of 12 hr.

RESULTS AND DISCUSSION

Formulation of BCDC and BPLC

The oral bioavailability of drug mainly depends upon the numerous physical properties of drug such as low aqueous solubility, permeability, dissolution rate, first-pass metabolism and presystemic metabolism. Among all, the poor aqueous solubility and low permeability are the main properties of drugs which can influence the poor oral bioavailability.²⁷ β -CTE, an investigational drug candidate, also demonstrates poor aqueous solubility and fair solubility in most of the organic solvents.²⁸ According to this physical property, β -CTE was processed into BCDC and BPLC formulations via kneading and thin film hydration method respectively. Many stable formulations of β -CD and phospholipids-based complexes with flavonoids/terpenoids have been successfully developed by authors with the use of dichloromethane,²⁹ water and methanol (1:1),¹⁹ 1, 4-dioxane²³ and tetrahydrofuran (THF).³⁰ In the current study, we have adopted the same formulation strategy as well as solvents for the preparation of flavonoids/terpenoids - β -CD as well as phospholipids complex. However, during processing, the formulation components showed an insolubility and/or poor solubility in these solvents, which in turn, resulting to precipitation of β -CTE, β -CD and phospholipids respectively. Poor solubility problem of these formulation components was solved by employing the new series of solvents. From all these investigated solvents, the absolute ethanol with its semi-polar nature, class III solvents and low toxic nature exhibited a preferable solvent of choice for the rapid dissolution of β -CTE, β -CD and phospholipids respectively. Therefore, the absolute ethanol was chosen as a solvent of choice for the preparation of BCDC and BPLC formulations.

Drug loading and extent of complexation rate (% yield)

Results of drug loading and extent of complexation rate for BCDC and BPLC formulations are discussed below. The values of drug loading and extent of complexation rate for all BCDC and BPLC formulations were found to be in the range of 91 to 94% w/w and 96 to 98% w/w, respectively. The BCDC 2 (ratio 1:2) and BPLC 1 (ratio 1:1) formulation showed higher value around $\sim 97.60 \pm 0.20$ % and $\sim 98.33 \pm 0.18$ % respectively. Moreover, the obtained higher values of BCDC 2 and BPLC 1 formulations were selected as optimized formulations for further characterization. It was found that adopted method used for the estimation of drug loading and complexation rate is robust,

validated and clearly supports the selected and incorporated carrier.

Particle size and zeta potential analysis

The physical stability of sub-micron particles that dispersed in the liquid medium is assessed by estimation of its mean particle size and zeta potential respectively. The analyzed mean particle size distribution of BCDC and BPLC formulations are shown in Figure 1 (a and c). Stavic *et al.* have reported that particle size < 500 nm particularly, used endocytosis pathway for its transportation across the biological membrane.³¹ In this study, BCDC formulation showed mean particle size and polydispersity index (PDI) around ~ 162 nm and $\sim 0.27 \pm 0.09$, whereas, the mean particle size and PDI values for BPLC formulations was found to be ~ 119.12 nm and $\sim 0.35 \pm 0.08$ respectively. Results for BCDC and BPLC indicates that its suitability for oral route of administration with wide range of particle distribution. These findings were in agreement with earlier published reports.³² In addition to particle size, the zeta potential (ζ) is another valuable stability indicator, used for the determination of charges on the surface of the particles and also possibly helps in determination of its performance upon oral administration. The acceptable range of zeta potential values for multiparticulate system is reported to be in between -30 mV to $+30$ mV respectively. Figure 1(b and d) shows the zeta potential values of BCDC and BPLC formulations. The zeta potential values for BCDC and BPLC were found about $\sim -10.7 \pm 0.15$ mV and -6.50 ± 0.10 mV respectively. From the combined results it indicates that BCDC and BPLC, both shows the desirable physical stability and it was attributed to lower particle size, zeta potential and higher PDI value.

FT-IR study

FT-IR spectrum of β -CTE, β -CD, Phospholipon[®] 90H, BCDC and BPLC formulations are shown in Figure 2

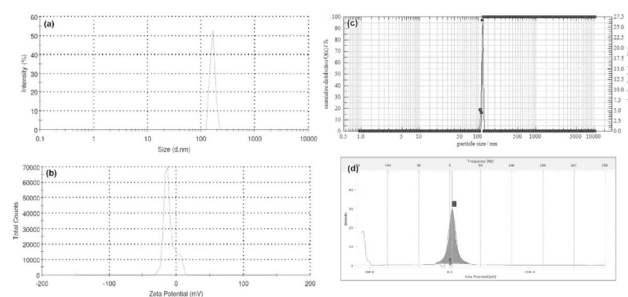


Figure 1: Particle size distribution of (a) BCDC and (c) BPLC, formulations and zeta potential analysis of (b) BCDC and (d) BPLC formulations.

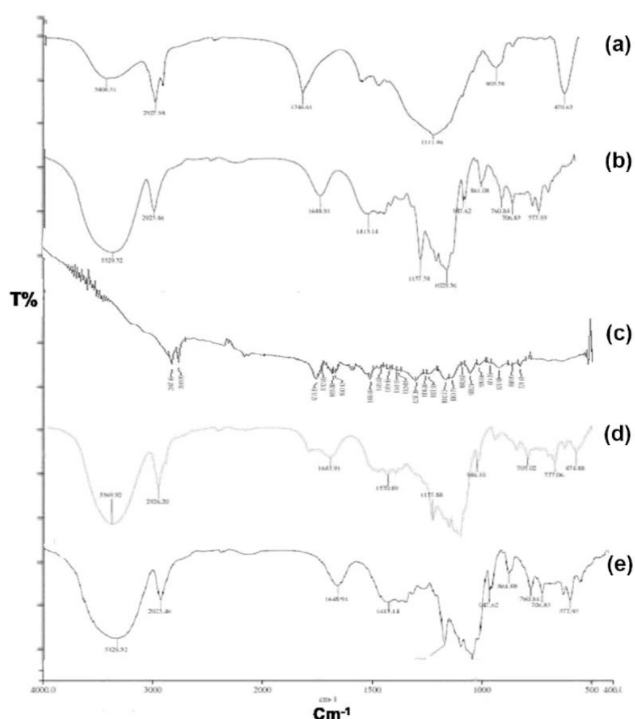


Figure 2: FT-IR spectrum of (a) β -CTE, (b) β -CD, (c) Phospholipon[®]90H, (d) BCDC, (e) BPLC formulations.

(a, b, c, d and e) respectively. The units are shown in cm^{-1} . β -CTE (Figure 2a) showed absorption peak at 2927 for asymmetric (aliphatic C-H stretching) and 2874 for symmetric (aromatic C-H stretching). Absorption peak at 1458 and 1360 shows the presence of aromatic (C-C stretching) and symmetric (C-H stretching) group. Peak observed at 1746 and 803 corresponds to carbonyl group stretching and (= CH group) in alkenes.³³ FT-IR spectrum of β -CD is shown in (Figure 2b). Observed absorption peak at 3329, 2952, 1413 and 1029 indicates the presence of (O-H stretching), aliphatic (C-H₂ bending), (aliphatic C-H stretching) and (C-O stretching) vibration groups respectively. These peaks were found in agreement with earlier reports.²⁹ (Figure 2c) shows the absorption peaks of Phospholipon[®] 90H. Peak found at 2917 and 2849 represents the presence of (C-H stretching) of long fatty acid chain. Additional peaks were observed at 1731, 1237 and 1092 and 970 for (C=O stretching vibration for fatty acid ester), (P=O and P-O-C stretching) and $[-N^+(\text{CH}_2)_3]$.¹⁷ FT-IR spectrum of BCDC in (Figure 2d) exhibited peaks shifted at 3369, 2926 and 1643 compared to that of plain β -CTE and β -CD, whereas, in (Figure 2e), the BPLC also showed peaks shifted at 2925 and 1240 from their original peaks of β -CTE and Phospholipon[®] 90H. Shifting of these peaks in BCDC as well as in BPLC formulation could be ascribed to strong participation of weak intermo-

lecular interaction i.e. H-bonding, ion-dipole and van der Waals forces between polar part of β -CTE and carriers, which further resulting to formation of BCDC and BPLC.

DSC study

Figure 3a, 3b, 3c, 3d and 3e depicts the DSC thermograms of pure β -CTE, β -CD, Phospholipon[®] 90H, BCDC and BPLC formulations. Pure β -CTE (Figure 3a) showed strong and sharp endothermic peak around $\sim 187.17^\circ\text{C}$ indicates its purity and crystalline nature.⁹ A DSC curve of β -CD is shown in (Figure 3b). It exhibits two endothermic peaks; first broad peak appeared around $\sim 100^\circ\text{C}$, indicative to release of water molecules from β -CD. Second broad melting peak with less intensity were appeared above $\sim 300^\circ\text{C}$, corresponds to its degradation peak. These results were found to be consistent with earlier published reports.³⁴ As revealed in (Figure 3c), Phospholipon[®] 90H displays five different peaks around $\sim 83.62^\circ\text{C}$, 105.11°C , 122.00°C , 178.20°C and 238.24°C respectively. First three peaks with small, diffused and mild characteristics were likely due to melting nature of Phospholipon[®] 90H under the influence of increasing temperature. Last two small intensity peaks were ascribed by physical transformation of Phospholipon[®] 90H form gel to liquid crystal state via physico-chemical modification in the carbon-hydrogen segment.³⁵ Two new endothermic peaks at about $\sim 73.26^\circ\text{C}$ and

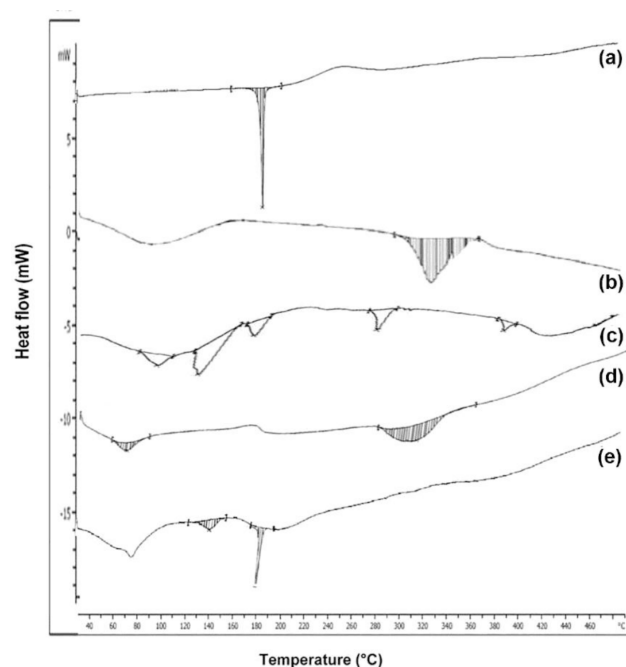


Figure 3: DSC thermograms of (a) β -CTE, (b) β -CD, (c) Phospholipon[®]90H, (d) BCDC, (e) BPLC formulations.

$\sim 318.18^\circ\text{C}$ with different intensities were displayed by BCDC formulations in (Figure 3d). First peak was appeared to be completely new one with disappearance of unusual peaks of β -CTE and β -CD. Moreover, the peak at $\sim 318.18^\circ\text{C}$ represents the same feature as that of original second peak of β -CD indicates that it didn't contribute in the complexation process. BPLC (Figure 3e) exhibited two new melting peaks around $\sim 147.29^\circ\text{C}$ and $\sim 192.17^\circ\text{C}$ respectively. Additionally, β -CTE and Phospholipon[®] 90H peak were absent in this thermograms. Weak forces of interactions such as ion-dipole and van der Waals forces between polar part of β -CTE and carriers could thus be the main reason for BCDC and BPLC synthesis. Findings are well supported by earlier published literature.³⁶

Solubility studies

Solubility results of pure β -CTE, PM of β -CTE and β -CD (1:2), PM of β -CTE and Phospholipon[®] 90H (1:1), BCDC and BPLC formulations in water and/or n-octanol are presented in Table 2. Pure β -CTE shows low aqueous solubility up to $\sim 0.52 \mu\text{g/mL}$, whereas, the same compound exhibited higher solubility in n-octanol i.e. $\sim 714.10 \mu\text{g/mL}$, indicates strong lipophilic and poor hydrophilic nature of β -CTE. PM of β -CTE and β -CD (1:2) as well as β -CTE and Phospholipon[®] 90H (1:1) displays somewhat better aqueous solubility around $\sim 3.11 \mu\text{g/mL}$ (6-fold) and $\sim 4.61 \mu\text{g/mL}$ (9-fold) over to that of β -CD. The significance level was found to be ($p < 0.05$). Formation of a close association of β -CTE with β -CD and Phospholipon[®] 90H is thought to be main reason for slight improvement in the PM aqueous solubility. Both PM did not show any significant improvement in the n-octanol solubility. Compared to pure β -CTE and PM, the BCDC (1:2) offered a significant ($p < 0.05$) higher solubility in water around $\sim 9.21 \mu\text{g/mL}$ and it is enhanced by 18-fold. This finding is well supported by earlier reports, which

suggest that central cavity of β -CD (made up of 7-glucopyranose units) freely accommodates the β -CTE molecules, forms soluble inclusion complex with random transformation from crystalline to amorphous powder, resulting to improve aqueous solubility of β -CTE.³⁷ The n-octanol solubility was also found to be higher ($\sim 872.49 \mu\text{g/mL}$) compared to pure drug and PM. Finally, BPLC (1:1) showed an excellent and more significant ($p < 0.01$) improved aqueous solubility around $\sim 14.61 \mu\text{g/mL}$ (28-fold), compared to drug, PM and BCDC formulations and it was likely due to partial amorphization and amphiphilic nature of BPLC.¹⁷

In vitro dissolution studies

The comparative *in vitro* dissolution performance of β -CTE from β -CTE suspension, BCDC (1:2) and BPLC (1:1) formulations in PBS (pH 7.4) for testing period up to 12 hr are described in Figure 4. The release pattern of β -CTE from its suspension after 5 hr was found to be $\sim 12\%$ and by the end of 12 hr dissolution period, the suspension showed only $\sim 20\%$ of β -CTE released. This lowered amount of release could be attributed by poor aqueous solubility of β -CTE. Compared to suspension, the BCDC (1:2) formulation, after 5 hr of testing period, released β -carotene around $\sim 29\%$, however, after this period, the BCDC demonstrated a continued release performance and thereby, reached to a maximum release about $\sim 68\%$ by the end of dissolution period. Enhancement of dissolution rate of BCDC formulation could be well explained by favorable strong interaction between β -CTE and apolar cavity of β -CD, which may cause to dehydrate and

Table 2: Solubility analysis of pure β -CTE, PM of β -CTE and β -CD and Phospholipon[®]90H, BCDC and BPLC formulations.

Formulations	Aqueous solubility ($\mu\text{g/mL}$)	n-octanol solubility ($\mu\text{g/mL}$)
Pure β -CTE	0.52 ± 0.08	714.10 ± 1.32
PM of β -CTE and β -CD	3.11 ± 0.24	769.21 ± 1.26
PM of β -CTE and Phospholipon [®] 90H	4.61 ± 0.19	802.01 ± 1.12
BCDC 2	9.21 ± 1.41	872.43 ± 1.48
BPLC 1	14.67 ± 1.38	931.22 ± 2.33

All results are expressed as mean \pm Std. Dev., $n=3$

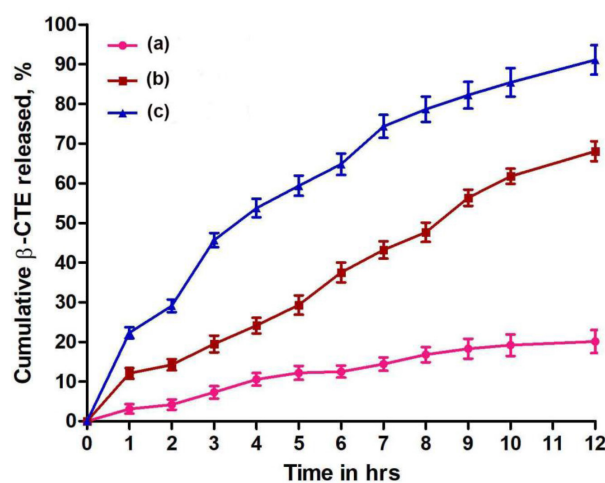


Figure 4: The *in-vitro* dissolution profiles of (a) β -CTE release from β -CTE suspension, (b) BCDC and (c) BPLC formulations. Values are presented as mean \pm Std. Dev. ($n = 3$).

transfer the drug into the cavity, resulting to increase the affinity of hydrophobic drug towards the water and subsequently, increase the dissolution rate. Additionally, the reported amphiphilic nature of β -CD molecule significantly improves the dissolution rate of hydrophobic drug via reducing the interfacial tension between the solid particles and dissolution medium.^{18,38} The rate and extent of dissolution of BPLC (1:1) formulation, after 5 hr of study, was observed to be $\sim 59\%$ and by the end of dissolution period, the same formulation continuously released the β -CTE to a maximum level about $\sim 91\%$. This higher release was likely attributed to solubility and wettability phenomenon, where Phospholipon[®] 90H on complexation with the β -CTE particles can increase its solubility and then wettability in water, forms uniform dispersion and consequently increase the dissolution rate.³⁹ This comparison clearly indicates that BPLC formulation enhanced the dissolution of β -CTE more significantly over to that of plain drug and BCDC. After release study, the kinetic analysis of BCDC and BPLC formulations via examined different release models, exhibited higher correlation coefficient (R^2) about ~ 0.9943 and ~ 0.9889 respectively and thereby, both of these followed the first order and Higuchi as best-fit dissolution mechanism. Moreover, the release exponent value (n) of BCDC and BPLC demonstrated around ~ 0.48 and ~ 0.49 respectively. Based on these values, it was found that, BCDC and BPLC displayed the Fickian diffusion as the principal release mechanism. The improved solubility and dissolution rate of β -CTE using Phospholipon[®] 90H via thin film hydration technique could be helpful in the enhancement of its permeability and thereby improving the *in vivo* antioxidant, biopharmaceutical and most important, the pharmacokinetic potential.

CONCLUSION

The phospholipids and β -cyclodextrin carriers have shown the noteworthy potential for enhancement of aqueous solubility and *in vitro* dissolution rate of β -CTE. This goal was achieved by the preparation of BCDC and BPLC formulation using kneading and solvent evaporation method respectively. Based on lower particle size, zeta potential and PDI values, BCDC and BPLC both were found to show oral route suitability. Physico-chemical characterization by FT-IR and DSC studies showed that BCDC and BPLC, both were formed with the involvement of weak intermolecular forces of interactions such as H-bonding, ion-dipole and van der Waals forces between the polar part of β -CTE and carriers. BPLC (1:1) significantly

enhanced the aqueous solubility around (28-fold), compared to that of BCDC (1:2) (18-fold) and pure β -CTE. Equally, rate and extent of dissolution of BPLC (1:1) was found to be enhanced more significantly over to that of BCDC (1:2) and pure β -CTE for 12hr testing period. In conclusion, the phospholipids carriers-based BPLC formulations could be employed as a promising carrier, compared to β -CD carrier for enhancement of poor aqueous solubility and *in vitro* dissolution rate of β -CTE and similar bioactive compounds. Moreover, the improved solubility and dissolution rate of β -CTE using thin film hydration method could be helpful in the enhancement of its permeability, *in vivo* antioxidant and pharmacokinetic potential.

ACKNOWLEDGEMENT

The corresponding author thanks to Dr. Bala Prabhakar, Dean, School of Pharmacy and Technology Management, SVKM's, NMIMS (Deemed to be University), Mumbai for providing necessary facilities to complete this research work.

CONFLICT OF INTEREST

The author declares no conflict of interest.

ABBREVIATIONS

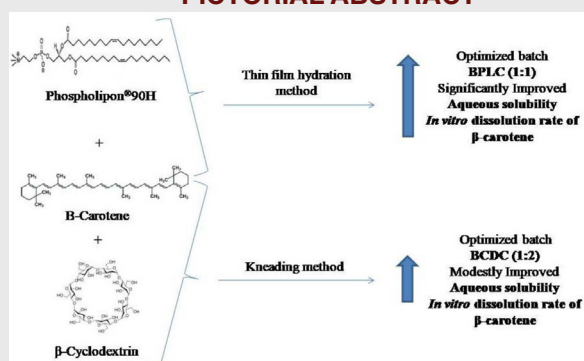
β -carotene: β - CTE; **β -cyclodextrin:** β -CD; **BCDC:** β -carotene- β -cyclodextrin complex; **BPLC:** β -carotene-phospholipids complex; **PM:** Physical mixture; **DSC:** Differential scanning calorimetry; **FT-IR:** Fourier transform infrared spectroscopy.

REFERENCES

- Boon C, McClements D, Weiss J, Decker A. Factors influencing the chemical stability of carotenoids in foods. *Crit Rev Food Sci and Nutr.* 2010;50(6):515-32.
- Martín A, Mattea F, Gutiérrez L, Miguel F, Cocero MJ. Co-precipitation of carotenoids and bio-polymers with the supercritical anti-solvent process. *J of Supercritical Fluids.* 2007;41(1):138-47.
- Mao K, Xu X, Yang J, Yuan F, Gao X, Zhao J. Effects of small and large molecule emulsifiers on the characteristics of β -carotene nanoemulsions prepared by high pressure homogenization. *Food Technol Biotechnol.* 2009;47(3):336-42.
- Gerster H. Anticarcinogenic effect of common carotenoids. *Int J Vitamin and Nutr Res.* 1993;63(2):93-121.
- Lintig JV. Colours with functions: Elucidating the biochemical and molecular basis of carotenoid metabolism. In *Annual Rev of Nutr.* 2010;30:35-56.
- Ribeiroa S, Chua S, Ichikawab S, Nakajimaa M. Preparation of nanodispersions containing β -carotene by solvent displacement method. *Food Hydrocolloids.* 2008;22(1):12-7.
- Liang R, Shoemaker F, Yang X, Zhong F, Huang Q. Stability and bioaccessibility of β -carotene in nanoemulsions stabilized by modified starches. *J Agric Food Chem.* 2013;61(6):1249-57.

8. Deng X, Zhang N, Tang CH. Soy protein isolate as a nano carrier for enhanced water dispersibility, stability and bioaccessibility of β -carotene. *J Sci Food Agric*. 2017;97(7):2230-7.
9. Ishimoto K, Miki S, Ohno A, Nakamura Y, Otani S, Nakamura M, *et al.* β -Carotene solid dispersion prepared by hot-melt technology improves its solubility in water. *J Food Sci Technol*. 2019;56(7):3540-6.
10. Semalty A, Semalty M, Singh D, Rawat MSM. Preparation and characterization of phospholipid complexes of naringenin for effective drug delivery. *J Incl Phenom Macrocycl Chem*. 2010;67(3-4):253-60.
11. Bhattacharyya S, Ahammed SM, Saha BP, Mukherjee PK. The gallic acid-phospholipid complex improved the antioxidant potential of gallic acid by enhancing its bioavailability. *AAPS Pharm Sci Tech*. 2013;14(3):1025-33.
12. Zhang WL, Cui Y, Fan YQ, Yang JK, Liu P, *et al.* Bioavailability and foam cells permeability enhancement of salvianolic acid B pellets based on drug-phospholipids complex technique. *Eur J Pharm Biopharm*. 2012;83(1):76-86.
13. Bhattacharyya S, Majhi S, Saha BP, Mukherjee PK. Chlorogenic acid - phospholipid complex improve protection against UVA induced oxidative stress. *J Photochem Photobiol B Biol*. 2014;130:293-8.
14. Han X, Zhang Z, Shen H, Zheng J, Zhang G. Comparison of structures, physicochemical properties and *in vitro* bioactivity between ferulic acid- β -cyclodextrin conjugate and the corresponding inclusion complex. *Food Res Int*. 2019;125:1-10.
15. Valentina V, Vincenza C, Barbara F, Domenico M, Giuseppe A, Barbara T, *et al.* Physicochemical characterization and antioxidant activity evaluation of idebenone/hydroxypropyl- β -cyclodextrin inclusion complex. *Biomolecules*. 2019;9(531):2-29.
16. Pichot R, Watson RL, Norton IT. Phospholipids at the interface: Current trends and challenges. *Int J Mol Sci*. 2013;14(6):11767-94.
17. Singh D, Rawat MSM, Semalty A, Semalty M. Chrysophanol-phospholipid complex. *J Therm Anal Calorim*. 2012;111(3):2069-77.
18. Lin SY, Kao YH. Solid particulates of β -cyclodextrin inclusion complexes directly prepared by spray-drying technique. *Int J Pharm*. 1989;56(3):249-59.
19. Ghosh A, Biswas S, Ghosh T. Preparation and evaluation of silymarin β -cyclodextrin molecular inclusion complexes. *J Young Pharmacists*. 2011;3(3):205-10.
20. Munyendo WLL, Zhang Z, Abbas S, Waddad AY, Lv H, Baraza LD, *et al.* Micelles of TPGS modified apigenin phospholipid complex for oral administration: Preparation, *in vitro* and *in vivo* evaluation. *J Biomed Nanotech*. 2013;9(12):2034-47.
21. Choudhary A, Rana A, Aggarwal G, Kumar V, Zakir F. Development and characterization of an atorvastatin solid dispersion formulation using skimmed milk for improved oral bioavailability. *Acta Pharmaceutica Sinica B*. 2012;2(4):421-8.
22. Tan Q, Liu S, Chen X, Wu M, Wang H, Yin H, *et al.* Design and evaluation of a novel evodiamine-phospholipid complex for improved oral bioavailability. *AAPS PharmSciTech*. 2012;13(2):534-47.
23. Telange DR, Patil AT, Pethe AM, Anand S, Fegade H, Dave VS. Formulation and characterization of an apigenin-phospholipid phytosome (APLC) for improved solubility, *in vivo* bioavailability and antioxidant potential. *Eur J Pharm Sci*. 2017;108:36-49.
24. Telange DR, Nirgulkar SB, Umekar MJ, Patil AT, Pethe AM, Bali NR. Enhanced transdermal permeation and anti-inflammatory potential of phospholipids complex-loaded matrix film of umbelliferone: Formulation development, physico-chemical and functional characterization. *Eur J Pharm Sci*. 2019;131:23-38.
25. Telange DR, Denge RP, Patil AT, Gupta SV, Dave VS. Pentaerythritol as an excipients/solid dispersion carrier for improved solubility and permeability of ursodeoxycholic acid. *J Excp Food Chem*. 2018;9(3):80-95.
26. Maiti K, Murugan V, Saha BP, Mukherjee K, Mukherjee PK. Exploring the effect of hesperetin-HPSC complex: A novel drug delivery system on the *in vitro* release, therapeutic efficacy and pharmacokinetics. *AAPS Pharm Sci Tech*. 2009;10(3):943-50.
27. Savjani K, Gajjar A, Savjani J. Drug solubility: Importance and enhancement techniques. *ISRN Pharm*. 2012;1-10.
28. DePaz E, Martin A, Bartolome A, Largo M, Cocero MJ. Development of water soluble β -carotene formulations by high temperature, high-pressure emulsification and antisolvent precipitation. *Food Hydrocolloids*. 2014;37:14-24.
29. Semalty A, Tanwar Y, Semalty M. Preparation and characterization of cyclodextrin inclusion complex of naringenin and critical comparison with phospholipid complexation for improving solubility and dissolution. *J Therm Anal Calorim*. 2014;115(3):2471-78.
30. Zhang H, Sun X, Peng Q, Shi S, Gong T, Zhang J. Preparation, characterization and *in vivo* evaluation of a self-nanoemulsifying drug delivery system (SNEDDS) loaded with morin-phospholipid complex. *Int J Nanomedicine*. 2011;6:3405-14.
31. Savic R, Luo L, Eisenberg A, Maysinger D. Micellar nanocontainers distribute to defined cytoplasmic organelles. *Science*. 2003;300(5619):615-8.
32. Hadian Z, Maleki M, Abdi K, Atyabi F, Mohammadi A, Khaksar R. Preparation and characterization of nanoparticle β -cyclodextrin: Geraniol inclusion complexes. *Iranian J Pharm Res*. 2018;17(1):39-51.
33. Kaur P, Ghoshal G, Jain A. Bio-utilization of fruits and vegetables waste to produce β -carotene in solid state fermentation: Characterization and antioxidant activity. *Process Biochem*. 2019;76:155-64.
34. Lira MCB, Ferraz MS, DaSilva C, Cortes ME, Teixeira KI, Caetano NP, *et al.* Inclusion complex of usnic acid with β -cyclodextrin: Characterization and nanoencapsulation into liposomes. *J Incl Phenom Macrocycl Chem*. 2009;64(3-4):215-24.
35. Cai X, Luan Y, Jiang Y, Song A, Shao W, Li Z, *et al.* Huperzine A-phospholipid complex-loaded biodegradable thermosensitive polymer gel for controlled drug release. *Int J Pharm*. 2012;433(1-2):102-11.
36. Lasonder E, Weringa WD. An NMR and DSC study of the interaction of phospholipid vesicles with some anti-inflammatory agents. *J Colloid Interface Sci*. 1990;139(2):469-78.
37. Liu L, Guo QX. The driving forces in the inclusion complexation of cyclodextrins. *J Incl Phenom Macrocycl Chem*. 2002;42(1-2):1-14.
38. Rawat S, Jain SK. Enhancement of intestinal absorption of few cox-2 inhibitors through interaction with β -cyclodextrin. *Indian J Pharm Sci*. 2007;69(4):529-34.
39. Perrut M, Jung J, Leboeuf F. Enhancement of dissolution rate of poorly-soluble active ingredients by supercritical fluid processes Part I: Micronization of neat particles. *Int J Pharm*. 2005;288(1):3-10.

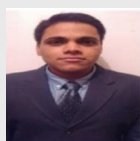
PICTORIAL ABSTRACT



SUMMARY

Antioxidant is an important phytochemicals, substance and/or compound which significantly scavenge the free radicals and thereby, slow down the oxidation of biological macromolecules such as protein, lipids and carbohydrates. This activity is totally depend upon the biopharmaceutical, physico-chemical and functional properties of antioxidant compound. β -carotene, is one them, which is an essential part of carotenoid family and perform the same actions more appreciably. Moreover, it also provides an essential benefit to the human body via converting it into vitamin A. However, the poor aqueous solubility and low *in vitro* dissolution rate confined it become a strong candidate. In this study, the observed limitations of this wonder molecule were improved by preparing its formulations using Phospholipon[®]90H and β -cyclodextrin carriers respectively. The prepared optimized formulations i.e. BPLC (1:1) and BCDC (1:2) were characterized using particle size and zeta potential, drug loading, complexation rate, FT-IR, DSC, solubility study and *in vitro* dissolution rate. Characterization studies demonstrated that optimized BPLC (1:1) were drastically improved an aqueous solubility and *in vitro* dissolution rate over to that of BCDC (1:2) and plain β -carotene. Therefore, the results of this study indicates that Phospholipon[®]90H significantly improved the biopharmaceutical attributes compared to β -cyclodextrin and thus, can be used as promising carrier for the other compound with low aqueous solubility and *in vitro* dissolution rate.

About Authors



Mr. Saurabh Gujar, is working as research student in Shobhaben Pratapbhai Patel School of Pharmacy and Technology management, SVKM's, NMIMS (Deemed to be University), Mumbai Campus, Mumbai, Maharashtra, India. His area interest is development of nanoformulations for BCS class II drugs.



Dr. Darshan R. Telange, is working as Assistant Professor in Rajarshi Shahu College of Pharmacy, Buldhana, Maharashtra, India. According to research area, he is working on solid-state characterization, targeted nanoformulation and phytosomal formulations etc.



Dr. Anil M. Pethe, is working as Associate Dean at School of Pharmacy and Technology Management, SVKM's NMIMS (Deemed to be University), Hyderabad Campus, Telangana, India. His area of interest include development and evaluation of target based nanoformulations, QbD optimization and solubility enhancement etc.

Cite this article: Gujar S, Telange D, Pethe A. Supramolecular Complexes of Phospholipids and β -Cyclodextrin with Bioactive β -Carotene: A Comparative Physico-Chemical and Functional Evaluation. Indian J of Pharmaceutical Education and Research. 2020;54(2s):s220-s229.

Antiparkinsonian and Antioxidant Effects of Hydroalcoholic Extract of *Camellia sinensis*, *Asparagus racemosus*, *Mucuna pruriens* and their Combination

Mahendra Ashok Giri^{1*}, Rasika Dnyandeo Bhalke², K Vanitha Prakash³, Sanjay Bhaskar Kasture⁴

¹Department of Pharmacology, Rajarshi Shahu College of Pharmacy, Buldhana, Maharashtra, INDIA.

²Sanjivani College of Pharmaceutical Education and Research, Pune University, Kopargaon, Maharashtra, INDIA.

³Shri Sai Jyoti College of Pharmacy, Vattinagula Pally, Gandhipeth, Hyderabad, Telangana, INDIA.

⁴Pinnacle Biomedical Research Institute, Bhopal, Madhya Pradesh, INDIA.

ABSTRACT

Objectives: Because of environmental risk factors Parkinson's disease rate doubled in last decades. In upcoming decades rate of Parkinson's disease is expected to be 12 million people in aging population. Present treatments are having huge side effects and requires more combinations. Hence objective of this study is to provide herbal combination for Parkinson's disease with reduced side and adverse effects. **Methods:** The antiparkinsonian activity of HECS, HEAR, HEMP and Mixture was evaluated by using haloperidol induced catalepsy, reserpine induced hypolocomotion, tacrine induced vacuous chewing movements and orofacial brusts. Antioxidant activity was assessed by using DPPH radical and H₂O₂ scavenging assay. The results were analyzed by repeated measure ANOVA followed by Dunnett's test. **Results:** Significant reduction ($P < 0.05$) in haloperidol-induced catalepsy was observed in the all groups at the doses of 30 and 100 mg/kg when given orally. Mixture 30 mg/kg showed extremely significant ($P < 0.001$) reduction in duration of catalepsy. Pretreatment with Mixture at 100mg/kg was significantly ($P < 0.05$) reduces Reserpine induced hypolocomotion which is more significant as compared with other treatments. Similarly, HECS 30 mg/kg and mixture was more effective ($P < 0.05$) than remaining extracts in reducing tacrine induced Vacuous

chewing movements. In tacrine induced orofacial brust Mixture and HEAR 30 mg/kg shows extremely significant ($P < 0.001$) reduction of orofacial brusts. Similarly Mixture and HECS 100 mg/kg is more effective than other treatment in tacrine induced tongue protrusion. In DPPH scavenging assay, all the extracts exhibited free radical scavenging activity. In DPPH assay the IC₅₀ value of ascorbic acid, HECS, HEAR, HEMP and Mixture (1:1:1) was 14.99, 18.44, 26.51, 23.19 and 20.47 µg/ml respectively. **Conclusion:** 1:1:1 mixture show extremely significant antioxidant and anti-parkinsonian activity as compare with individual hydroalcoholic extract. Thus the studied combination possess potent antiparkinsonian effect.

Key words: Antioxidant, Antiparkinsons, *Camellia sinensi*, *Asparagus racemosus*, *Mucuna prurines*, Haloperidol, Reserpine, Tacrine.

Correspondence

Prof. Mahendra Ashok Giri

Rajarshi Shahu College of Pharmacy, Buldhana-443001, Maharashtra, INDIA.

Phone no: +91-9764489091

Email: mahi_jaan83@yahoo.com

DOI: 10.5330/ijpi.2020.4.99

INTRODUCTION

Parkinson's Disease (PD) is a complex multi-framework, neurodegenerative sickness. In spite of the fact that dominantly saw as motor ailment, it likewise has incapacitating non-motor highlights, which are as often as possible missed and not treated. The degeneration of dopaminergic neurons is viewed as the underlying driver of the trademark traditional engine side effects and non-motor indications. Significant treatment objectives are to increase striatal dopamine levels with antecedent replacement and additionally decrease its breakdown. As the ailment advances, a consistent increment in the portion of levodopa is inescapable. Be that as it may, higher dosages cause engine intricacies of dyskinesia and dystonia and bargain clinical treatment. Based on the studies, it is known that mitochondrial dysfunction, Neuronal death in substantial nigra and changed oxidative stress are the two crucial cellular stress parameters playing important role in PD pathogenesis. In parkinsons disease tremors, bradykinesia, stiffness in limbs and torso and postural instability are the four main symptoms. The focal point of the executives is the alleviation of the clinically prevailing motor side effects of PD. In any case, presently, there is an expanding acknowledgment of the non-motor highlights of PD, which additionally need consideration. These highlights are rest aggravations, constipation, psychological decay, melancholy, dread, tension, bladder

issues, weight changes, weakness and loss of vitality, autonomic brokenness/hypotension and sexual issues. These can be predominant and incapacitating in a sizeable number of patients, influencing a mind-blowing nature. PD additionally has pre-malady manifestations like blockage and loss of smell, decreased outward appearances, soft tone, rest changes, wooziness which go before months to decades before clinical determination of PD. The current restorative technique against PD essentially depends on reestablishing the ideal degree of dopamine (DA) and its related flagging pathways, for which Levodopa or L-DOPA (L-3, 4-dihydroxyphenylalanine), a forerunner of dopamine is regulated to the PD patients. L-DOPA gives introductory advantage by hindering the malady movement; be that as it may, long haul benefits are impossible. Additionally, it is likewise directed in blend with carbidopa, a fringe decarboxylase inhibitor. This aides in reducing the reaction of L-DOPA which principally incorporate gastrointestinal and cardiovascular issues. Another procedure for PD treatment is the utilization of monoamine oxidase B (MAO-B) inhibitors. The movement of MAO-B compound is expanded by virtue of DA metabolism which hoists oxidative stress and mitochondrial dysfunctions. Until this point, mitochondrial brokenness and adjusted oxidative stress are viewed as the conceivable system prompting neuronal cell death. Therefore, therapeutic approaches

This is an open access article distributed under the terms of the Creative Commons Attribution-NonCommercial-ShareAlike 4.0 License, which allows others to remix, tweak, and build upon the work non-commercially, as long as the author is credited and the new creations are licensed under the identical terms.

that optimize ROS and enhance mitochondrial function are being thoroughly considered in the current scenario. There is a generous extension to benefit of the modalities of conventional information in the administration for both the non-motor and pre-disease highlights of PD. Exploration during the most recent multi decade has distinguished a few plants that show restorative property against neurodegenerative issues like PD and AD.^{1,2} Therefore, the present study aims to investigate antioxidant and neuroprotective activity of *Mucuna pruriens*, *Camellia sinensis* and *Asparagus racemosus* in combination to get rid from side effects of L-DOPA and also development of novel therapeutic approach against PD to address each cardinal sign of PD by using these herb with different potential.

Mucuna pruriens L. (Family: *Fabaceae*) is a tropical legume plant usually known as velvet beans. *Mucuna pruriens* is generally exploited for the treatment of Parkinsonism and dissimilar sorts of sexual debilities. It also acts as an aphrodisiac, anti-snake venom, antidiabetic, antioxidant and have a strong potential to improve the fertility of sperm. It has immense medicinal properties specifically due to high L-DOPA (L-3,4-dihydroxyphenylalanine) content and its role in parkinsons disease. Besides L-DOPA it also contains glycoside, gallic acid, glutathione, Levodopa. It improves locomotor and behaviour function, alleviate oxidative stress, metal chelation, mitochondrial and synaptic function.^{3,4}

Camellia sinensis is popularly known as Green Tea belonging to Theaceae family. Green tea and its bioactive constituents are most popular for their cell reinforcement properties, prompting clinical examinations in ailments related with responsive oxygen species, for example, malignancy or cardiovascular and neurodegenerative maladies. The most important phytoconstituents of *Camellia sinensis* are polyphenolic compounds known as catechins including Epigallocatechin Gallate (EGCG), Catechin (C), Epicatechin (EC), Gallocatechin (GC), Gallocatechin Gallate (GCG), Epigallocatechin (EGC) and Epicatechin Gallate (ECG). Flavonols add values to the oxidative damage prevention capacities of tea leaves. The aglycones of the fundamental flavonols in tea leaves are quercetin, kaempferol and myricetin. Polyphenols, for example, epigallocatechin gallate, because of their mitigating and antioxidant impacts, are known to introduce neuroprotective properties, what could clarify their advantages in neurodegenerative illnesses.⁵⁻⁷

Asparagus racemosus, otherwise called *shatavari* (family Asparagaceae), is a significant therapeutic plant endemic to tropical India and Thailand. It is notable medication in Ayurvedic rasayana that forestall maturing, increment life span and improve mental capacity. Also, it is suggested in Ayurvedic messages for the avoidance and treatment of gastric ulcers, dyspepsia and as a galactagogue. The significant dynamic mixes in the root are steroidal saponins, for example, asparacoside, shatavarin IV, V and XI and different constituents, for example, racemosol and asparagamine. It indicated high free radical searching just as neurotropic modulatory properties in infections related with neuron cell misfortune. The anti-PD compounds present in *A. racemosus* include racemosol and rhamnose.^{8,9}

The neuroprotective effects of *Mucuna pruriens*, *Camelia sinensis* and *Asparagus racemosus* extract in PD animal model have been reported by many researchers. However, the neuroprotective effect of combination is not reported hence present study aims at studying antiparkinsonian and antioxidant activity of these herbs in order to minimized side effects of available therapies and addressed motor and non-motor symptoms.

MATERIALS AND METHODS

Experimental Animals

Experiments were performed utilizing male Wistar rodents (Rats) weighing 180-200g. Creatures were kept up at 22°C ± 2°C on a

standard pellet diet and tap water *ad libitum*. Institutional Animal Ethics Committee for Animal Experiments of Sanjivani College of Pharmaceutical Education and Research, Kopargaon approved the study under the protocol SCPER/CPCSEA/IAEC/2019-20/01 and all experiments were conducted in accordance with guidelines of Committee for the Purpose of Control and Supervision of Experiments on Animals (CPCSEA). Behavioral tests were performed during the light cycle between 10.00 a.m. and 4.00 p.m.

Drugs and Chemicals

Tacrine and Reserpine were purchased from Sigma, Aldrich, Mumbai. All other chemicals used were of analytical grade and purchased from standard manufacturer.

Plant material and extraction

Dry powder of *Mucuna pruriens* seeds, *Asparagus racemosus* roots and *Camelia sinensis* leaves was purchased from local market and were authenticated from Department of Pharmacognosy, Sanjivani College of Pharmaceutical Education and Research, Kopargaon.

Hydroalcoholic extracts were prepared using Soxhlet's extractor. The extracts were filtered and dried. Extracts were subjected to phytochemical screening.¹⁰ The extracts were administered in doses of 30 and 100 mg/kg (p.o.). Control group was given only vehicle in equivalent volume of plant extract.

Experimental design

Animals were randomly divided into following groups of 5 animals each.

Group I - Control

Group II - Haloperidol (0.5 mg/kg) or Reserpine (1 mg/kg) or Tacrine (5 mg/kg),

Group III - HEMP (30 mg/kg),

Group IV - HEMP (100 mg/kg), Group V - HECS (30 mg/kg),

Group VI - HECS (100 mg/kg),

Group VII - HEAR (30 mg/kg),

Group VIII - HEAR (100 mg/kg),

Group IX - 1:1:1 Mixture (30 mg/kg),

Group X - 1:1:1 Mixture (100 mg/kg).

These groups were used for treatment of Parkinson's symptoms.

Assessment of anti-parkinsonian activity

Haloperidol induced catalepsy

Male Wistar rats (weighing 180–200 g) were divided into ten groups of five each. Rats were pretreated with vehicle, HECS (30 and 100 mg/kg, p.o.), HEAR (30 and 100 mg/kg, p.o.), HEMP (30 and 100 mg/kg, p.o.), 1:1:1 HECS:HEAR:HEMP (30 and 100 mg/kg, p.o.) 30 min before haloperidol (0.5 mg/kg, intra-peritoneally). Post administration of haloperidol duration of catalepsy was measured at 0, 30, 60, 90, 120, 150 and 180 min utilizing bar test. Both the forepaws of the animals were placed on a wooden bar raised above the ground. The cutoff time (time for which animal was placed on elevated bar) was 300 sec.^{11,12}

Tacrine induced jaw movements

The observation chamber consisted of a clear Plexiglas box measuring 28×28×28 cm³, which had a wire mesh floor. The box was elevated 42 cm from the surface of the table, allowing behavioral observation from all angles. Rats were divided into groups and treated with vehicle, HECS (30 and 100 mg/kg, p.o.), HEAR (30 and 100 mg/kg, p.o.), HEMP (30 and 100 mg/kg, p.o.) and 1:1:1 HECS:HEAR:HEMP (30 and 100 mg/kg, p.o.). After 20 min, tacrine (5 mg/kg i.p.) was administered and the

number of chewing movements, orofacial bursts and tongue protrusions were measured every ten min for 60 min.^{13,14}

Reserpine-induced hypolocomotion

Reserpine was injected intraperitoneally at a dose of 1 mg/kg in a suspension with Tween-80, 1 h after the mice were treated with vehicle, HECS (30 and 100 mg/kg, p.o.), HEAR (30 and 100 mg/kg, p.o.), HEMP (30 and 100 mg/kg, p.o.) and 1:1:1 HECS:HEAR:HEMP (30 and 100 mg/kg, p.o.). The effect of the study compounds on reserpine-induced hypolocomotion was assessed using Actophotometer (Dolphine, India). The locomotor activity of the animals was measured for 2 min, at 2 h, 3h and 4h after reserpine had been administered.¹⁵

Antioxidant activity

DPPH scavenging assay

The free radical scavenging activity of the HEMP, HECS and HEAR was measured in terms of hydrogen donating or radical scavenging ability using the stable free radical DPPH. 0.1 mM solution of DPPH in methanol was prepared and 1 ml of this solution was added to 3 ml of HEMP, HECS and HEAR solution in water at various concentrations (2-1000 µg/ml). The mixture was incubated for 45 min at room temperature and the absorbance was measured at 517 nm against the corresponding blank solution. Ascorbic acid was used as reference standard. Percentage inhibition of DPPH free radical was calculated using the following equation:

$$\text{DPPH Scavenged (\%)} = [(Ac - At)/Ac] \times 100$$

Where *Ac*: absorbance of the control and *At*: absorbance of the extract or reference standard. The antioxidant activity was expressed as IC₅₀. The IC₅₀ value was defined as the concentration in µg/ml of the extract that inhibits the formation of DPPH radicals by 50%.¹⁶⁻¹⁸

Statistical analysis

Results were expressed as mean ± SEM. Significant differences between groups were determined by analysis of variance test followed by Dunnett's test.

RESULTS

Haloperidol Induced catalepsy

In haloperidol induced cataleptic animal model mixture 30 mg/kg shows extremely significant reduction in cataleptic phase as shown in Figure 1. Followed by mixture 30 mg/kg, 100 mg/kg also shows extremely significant reduction in catalepsy. Almost all the hydroalcoholic extracts shows significant reduction in catalepsy induced by haloperidol but when combined in 1:1:1 proportion mixture shows extremely significant reduction with reduced dose of individual extract of *Camellia sinensis*, *Asparagus racemosus* and *Mucuna pruriens* as revealed in Figure 1.

Reserpine Induced Hypolocomotion

Hydro alcoholic extract of *Camellia sinensis*, *Asparagus racemosus* and *Mucuna pruriens* are studied for locomotor activity and hypolocomotion was induced with reserpine. In reserpine induced hypolocomotion hydro alcoholic extract shows significant increase in locomotor activity but as compare with low dose of 30 mg/kg, 100 mg/kg of HECS, HEAR and mixture shows more significant increase in locomotor activity. Mixture of 100 mg/kg shows extremely significant increase in locomotion and mixture 30 mg/kg shows very significant effect at first and third hour as exposed in Figure 2.

Tacrine Induced Vacuous Chewing Movement (VCM)

In tacrine induced vacuous chewing movements hydroalcoholic extract of *Camellia sinensis* at dose of 100 mg/kg shows extremely significant reduction in vacuous chewing movements followed by 30 mg/kg. Mixture of 30 mg/kg and 100 mg/kg subsequently shows very significant reduction in tacrine induced vacuous chewing movements followed by significant reduction observed in HEAR and HEMP at 30 and 100 mg/kg dose as presented in Figure 3.

Tacrine Induced Orofacial Brust (OB)

In tacrine induced orofacial brust mixture at 30 mg/kg shows extremely significant reduction as compare to 100 mg/kg. Apart from that HECS 100 mg/kg and HEAR 30 mg/kg individually shows extremely significant reduction in orofacial brust. HECS 30 mg/kg, HEAR 100 mg/kg, HEMP 30 mg/kg and HEMP 100 mg/kg shows significant reduction in tacrine induced orofacial brust individually as shown in Figure 4.

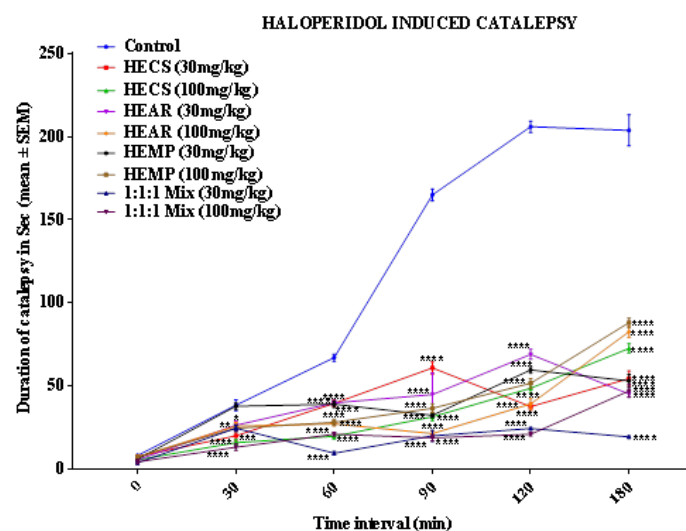


Figure 1: Effect of HECS, HEAR, HEMP and its combination on Haloperidol induced catalepsy. All the values are expressed as mean ± SEM; n=5, **p*<0.05, ***p*<0.01, ****p*<0.001, *****p*<0.0001 significant compared to control (repeated measures ANOVA followed by Dunnett's test).

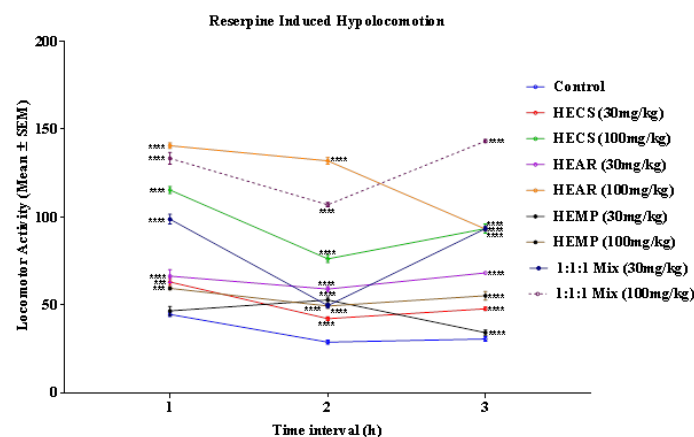


Figure 2: Effect of HECS, HEAR, HEMP and its combination on Reserpine induced Hypolocomotion. All the values are expressed as mean ± SEM; n=5, **p*<0.05, ***p*<0.01, ****p*<0.001, *****p*<0.0001 significant compared to control (repeated measures ANOVA followed by Dunnett's test).

Tacrine Induced Tongue Protrusion (TP)

In tacrine induced tongue protrusion Mixture 30 mg/kg and 100 mg/kg shows extremely significant reduction in tongue protrusion along with individual treatment of HECS 30 mg/kg, HECS 100 mg/kg, HEAR 30 and 100 mg/kg, HEMP 30 and 100 mg/kg shows significantly reduction in tongue protrusion as displayed in Figure 5.

DPPH scavenging assay

HECS shown strong DPPH scavenging activity followed by 1:1:1 mixture. The scavenging effect of HECS, HEAR, HEMP and mixture was comparable to ascorbic acid. The IC₅₀ value of Ascorbic acid, HECS, HEAR, HEMP and mixture was 14.99, 18.44, 26.51, 23.19 and 20.47 µg/ml respectively. As compared with ascorbic acid HECS and mixture shows strong antioxidant effect as revealed in Figure 6.

DISCUSSION

Blocked dopamine D2 receptor shows extrapyramidal side effect as catalepsy,¹⁹ haloperidol blocks D2 receptor and causes development of

cataplepsy in mice. Nishchal et al. (2014) states that antipsychotic drugs such as haloperidol used to treat schizophrenia causes loss of correction in externally imposed posture and development of behavioral state called catalepsy.²⁰ *Camellia sinensis* has epigallocatechine gallate like polyphenols which are an active ingredient shows curation in protective properties of brain against specific diseases and improvement in brain functioning like mental health and boosted mood.²¹ Various active polyphenols present in *Camellia sinensis* plays important role in reduction in catalepsy. Nabavi et al. (2017) proved that catechins present in *Camellia sinensis* reduces depression by means of inhibiting monoamine oxidase (MAO).²² Elsaid et al. (2015) stated that accumulation of reactive oxygen species produces oxidative stress in brain causes neurotoxicity and antioxidant property of *Asparagus officinalis* have potentials to protect neuronal damage caused by reactive oxygen species.²³ As

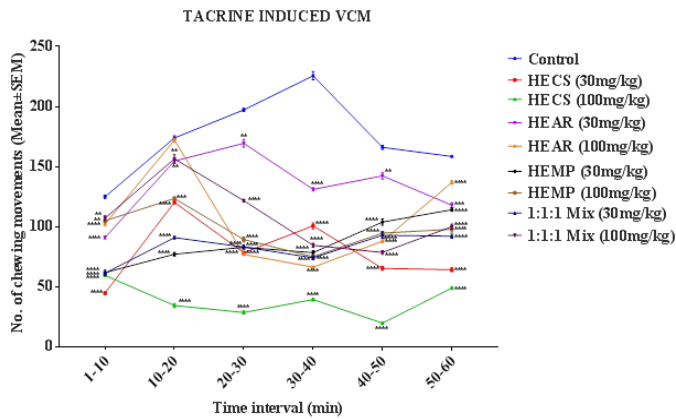


Figure 3: Effect of HECS, HEAR, HEMP and its combination on Tacrine induced VCM. All the values are expressed as mean ± SEM; n=5, *p<0.05, **p<0.01, ***p<0.001, ****p<0.0001 significant compared to control (repeated measures ANOVA followed by Dunnett's test).

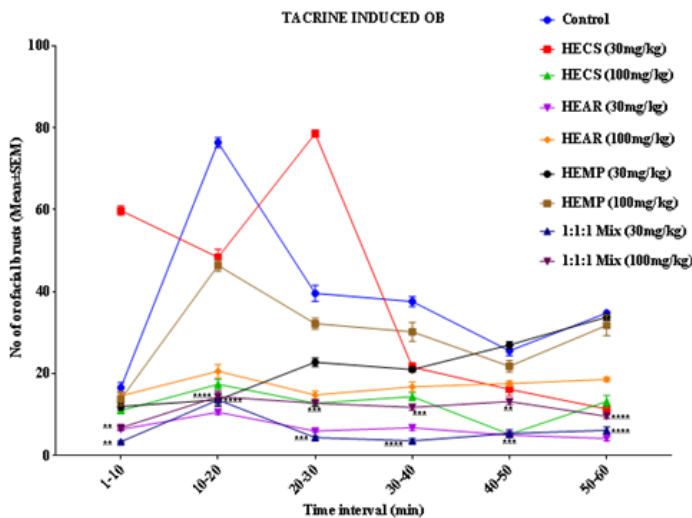


Figure 4: Effect of HECS, HEAR, HEMP and its combination on Tacrine induced OB. All the values are expressed as mean ± SEM; n=5, *p<0.05, **p<0.01, ***p<0.001, ****p<0.0001 significant compared to control (repeated measures ANOVA followed by Dunnett's test).

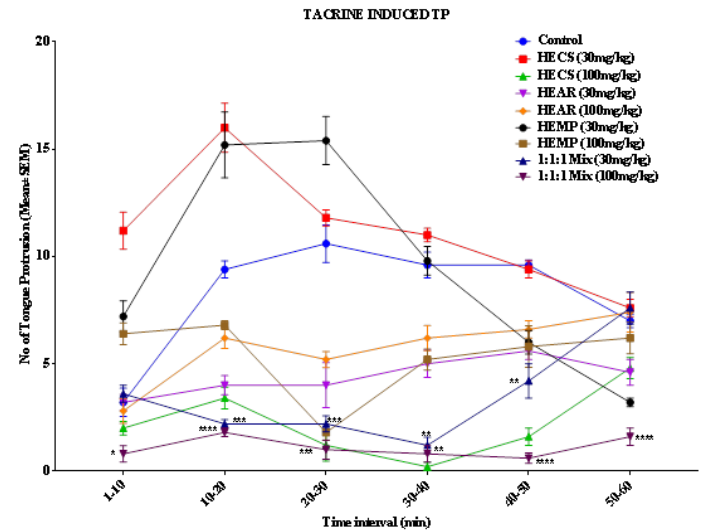


Figure 5: Effect of HECS, HEAR, HEMP and its combination on Tacrine induced TP. All the values are expressed as mean ± SEM; n=5, *p<0.05, **p<0.01, ***p<0.001, ****p<0.0001 significant compared to control (repeated measures ANOVA followed by Dunnett's test).

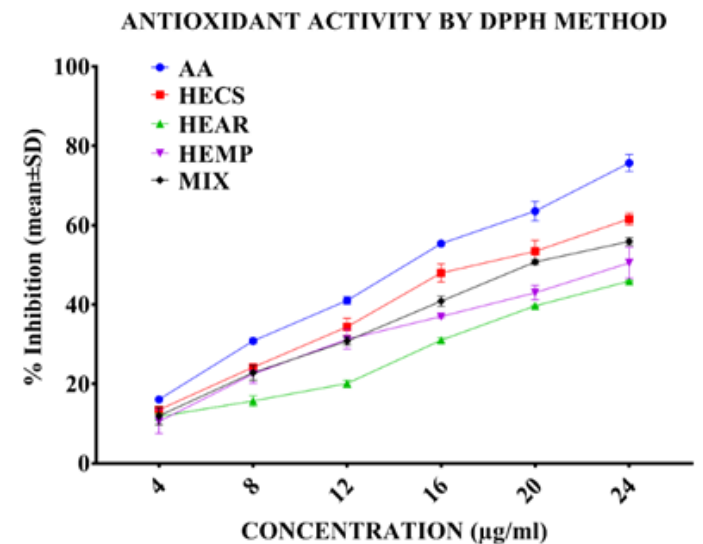


Figure 6: Percent inhibition shown by Ascorbic acid, HECS, HEAR, HEMP and 1:1:1 Mixture in DPPH scavenging assay. All the values are expressed in mean ± SD.

per the study of Periera *et al.* (2020) reduction in striatal dopamine levels and short-term memory impairments are seen after Reserpine administration in rats which mimics the pre-motor phase of Parkinson's disease.²⁴ Dopamine depletion causes hypersensitivity of D2 receptors in corticostriatal terminals hence dopamine metabolism results in reduced dopamine release in synaptic cleft shows early and late impairment in behavior and social recognition tasks (Periera *et al.* 2020).²⁴ Dopamine and 5 hydroxy tryptamine are responsible for regulation of mood in brain, however our study reveals that improved in locomotion activity with *Camellia sinensis* was might be due to its effect on increased levels of 5 hydroxy tryptamine in brain region.²⁵ In present study we observe that the extract of *Camellia sinensis* significantly shows improvements in haloperidol induced catalepsy, reserpine induced hypolocomotion and tacrine induced vacuous chewing movements and are due to the direct or indirect effect of chemical constituents present in extract. Estrogen plays vital role in various parts of brain via estrogen receptors. One of the major function associated with estrogen via estrogen receptor in hippocampus and cerebral cortex region is modulating the function of brain-derived neurotrophic factor levels and improving learning and memory impairments.⁸ Lalert *et al.* (2013) have revealed in previous study that root extract of *Asparagus racemosus* reverses learning and memory impairments in ovariectomized rats.²⁶ The effect of the root extract was due to direct effect on the estrogen receptor without enhancing the estrogen levels.⁸ Various chemical components present in *Asparagus racemosus* root extract such as steroidal saponins (like asparacosides, shatavarin iv, v and xi), racemosal and asparagine are might be shows significant neuroprotection. Present study result reveals that the root extract of *Asparagus racemosus* shows significant improvements in catalepsy, hypolocomotion and vacuous chewing movements are also due to the presence of different chemical constituents. Reserpine by showing effect on vesicular monoamine transporter 2 proteins reduces storage for biogenic amines and causes monoamine oxidase to actively deplete biogenic amines such as serotonin, dopamine and norepinephrines (Hedgcock *et al.* 2019).²⁷ Lebowitz and Khoshbouei (2020) stated that dopamine signaling simplified as neurobiological substrate for salient stimuli and as per the stimuli goal oriented movement.²⁸ As dopamine plays an important role in movement, reserpine induced depletion of dopamine causes movement related disorganization such as hypolocomotion. *Mucuna pruriens* contains main and active chemical constituent as L-dopa which has a dose dependant toxic effect with other chemical constituents present in *Mucuna pruriens* such as hallucinogenic tryptamines and anti-nutritional factors phenols and tannins.^{29,30} Extract of *Mucuna pruriens* seed due to presence of chemical constituent such as L-dopa possess anti-parkinsonian effect at various animal models used for development of parkinsonian symptoms. Tacrine causes increase in acetylcholine levels at cholinergic synapses by blocking enzyme called acetylcholinesterase which is responsible for hydrolysis of acetylcholine. Cousins *et al.* (1997) reported that enhanced concentration of acetylcholine by anticholinesterase tacrine produces parkinsonian side effects such as bradikinesia, rigidity, tremor and in rats it shows purposeless chewing movement.³¹ Hence for study we are using tacrine induced vacuous chewing movement animal model for motor effects. DPPH assay is reliable parameter for measurement of antioxidant activity. All the extracts shown antioxidant potentials due to various chemical constituents present in extract as compared with ascorbic acid but HECS and 1:1:1 mixture shows extremely significant antioxidant potentials as compare with other treatment groups.

CONCLUSION

Present study reveals that hydroalcoholic extracts of *Camellia sinensis*, *Asparagus racemosus* and *Mucuna pruriens* possess significant effect on

haloperidol induced catalepsy, reserpine induced hypolocomotion and tacrine induced vacuous chewing movements individually but when combination was used for the same study shows extremely significant effects in dose related manner because of number of additional chemical constituents and their lower concentrations present in the mixture.

ACKNOWLEDGEMENT

The authors are thankful to the Institute of Sanjivani College of Pharmaceutical Education and Research, Kopergaon, for providing the necessary facilities for carry out our research work in the current format.

CONFLICT OF INTEREST

The authors declare that they have no competing interests.

ABBREVIATIONS

AA: Ascorbic acid; **Ac:** Absorbance of control; **At:** Absorbance of extract; **DPPH:** 2,2 -diphenyl - 1 - picrylhydrazyl; **HEAR:** Hydroalcoholic extract of *Asparagus racemosus*; **HECS:** Hydroalcoholic extract of *Camellia sinensis*; **HEMP:** Hydroalcoholic extract of *Mucuna pruriens*; **MIX:** Mixture; **OB:** Orofacial brush; **VCM:** Vacuous chewing movement.

REFERENCES

1. Srivastav S, Fatima M, Mondal AC. Important medicinal herbs in Parkinson's disease pharmacotherapy. *Biomed Pharmacother.* 2017;92:856-63.
2. Pathak-Gandhi N, Vaidya ADB. Management of Parkinson's disease in Ayurveda: Medicinal plants and adjuvant measures. *J Ethnopharmacol.* 2017;197:46-51.
3. Singh SK, Dhawan SS, Lal RK, Shanker K, Singh M. Biochemical characterization and spatio-temporal analysis of the putative L-DOPA pathway in *Mucuna pruriens*. *Planta.* 2018;248(5):1277-87.
4. Guest J, Grant R. The Benefits of Natural Products for Neurodegenerative Diseases. *Adv Neurobiol.* 2016;12:199-228.
5. Bedrood Z, Rameshrad M, Hosseinzadeh H. Toxicological effects of *Camellia sinensis* (green tea): A review. *Phytotherapy Research.* John Wiley and Sons Ltd. 2018;(7):1163-80.
6. Williams RJ, Spencer JPE. Flavonoids, cognition and dementia: Actions, mechanisms and potential therapeutic utility for Alzheimer disease. *Free Radical Biology and Medicine.* 2012;(1):35-45.
7. Bitu PN, DaSilva AB, Neves KRT, Silva AH, Leal LKAM, Viana GSB. Neuroprotective Properties of the Standardized Extract from *Camellia sinensis* (Green Tea) and Its Main Bioactive Components, Epicatechin and Epigallocatechin Gallate, in the 6-OHDA Model of Parkinson's Disease. *Evidence-based Complement Altern Med.* 2015.
8. Lalert L, Kruevaisayawan H, Amatyakul P, Ingkaninan K, Khongsombat O. Neuroprotective effect of *Asparagus racemosus* root extract via the enhancement of brain-derived neurotrophic factor and estrogen receptor in ovariectomized rats. *J Ethnopharmacol.* 2018;225:336-41.
9. Banjari I, Marček T, Tomić S, Waisundara VY. Forestalling the Epidemics of Parkinson's Disease Through Plant-Based Remedies. *Front Nutr.* 2018;5:1-9.
10. Trease and Evans. Elsevier: Trease and Evans' Pharmacognosy, 16th Edition: Evans. 2009;121-35. Available from: <https://www.elsevier.ca/ca/product.jsp?isbn=9780702029332>.
11. Nair SV, Arjuman A, Dorababu P, Gopalakrishna HN, Rao UC, Mohan L. Effect of NR-ANX-C (a polyherbal formulation) on haloperidol induced catalepsy in albino mice. *Indian J Med Res.* 2007;126(5):480-4.
12. Somani RS, Kasture VS, Kasture SB. Haloperidol inhibits (-) bicuculline-induced seizures and bicuculline potentiates haloperidol-induced catalepsy in mice. *Indian J Pharmacol.* 2020;31(6):434.
13. Naidu PS, Kulkarni SK. Excitatory mechanisms in neuroleptic-induced vacuous chewing movements (VCMs): Possible involvement of calcium and nitric oxide. *Behav Pharmacol.* 2001;12(3):209-16.
14. Crowley JJ, Adkins DE, Pratt AL, Quackenbush CR, DenOord EJV, Moy SS, *et al.* Antipsychotic-induced vacuous chewing movements and extrapyramidal side effects are highly heritable in mice. *Pharmacogenomics J.* 2012;12(2):147-55.
15. Fernandes VS, Santos JR, Leão AHFF, Medeiros AM, Melo TG, Izídio GS, *et al.* Repeated treatment with a low dose of reserpine as a progressive model of Parkinson's disease. *Behav Brain Res.* 2012;231(1):154-63.
16. Farooq S, Sehgal A. Antioxidant activity of different forms of green tea: Loose leaf, bagged and matcha. *Curr Res Nutr Food Sci.* 2018;6(1):35-40.
17. Pal A, Kumar M, Saharan V, Bhushan B. Anti-oxidant and free radical scavenging activity of Ashwagandha (*Withania somnifera* L.) leaves. *J Glob Biosci.*

- 2015;4(1):1127-37.
18. Patil R, Gadakh R, Gound H, Kasture S. Antioxidant and Anticholinergic Activity of *Rubia cordifolia*. *Pharmacologyonline*. 2011;2:272-8.
 19. Wadenberg MLG, Kapur S, Soliman A, Jones C, Vaccarino F. Dopamine D2 receptor occupancy predicts catalepsy and the suppression of conditioned avoidance response behaviour in rats. *Psychopharmacology*. 2000;150(4):422-9.
 20. Nishchal BS, Rai S, Prabhu MN, Ullal SD, Rajeswari S, Gopalakrishna HN. Effect of *Tribulus terrestris* on haloperidol-induced catalepsy in mice. *Indian J Pharm Sci*. 2014;76(6):564-7.
 21. Camfield DA, Stough C, Farrimond J, Scholey AB. Acute effects of tea constituents L-theanine, caffeine and epigallocatechin gallate on cognitive function and mood: A systematic review and meta-analysis. *Nutr Rev*. 2014;72(8):507-22.
 22. Nabavi SM, Daglia M, Braidly N, Nabavi SF. Natural products, micronutrients and nutraceuticals for the treatment of depression: A short review. *Nutritional Neuroscience: Taylor and Francis Ltd*. 2017;20(3):180-94. Available from: <https://www.tandfonline.com/doi/abs/10.1080/1028415X.2015.1103461>.
 23. Elsaid FG, Shati AA, Sarhan MA. Role of *Matricaria recutita* L. and *Asparagus officinalis* L. against the neurotoxicity of diazinon in rats. *J Basic Appl Zool*. 2015;72:26-35.
 24. Pereira AG, Poli A, Matheus FC, DeBortoli DSL, Fadanni GP, Izidio GS, *et al.* Temporal development of neurochemical and cognitive impairments following reserpine administration in rats. *Behav Brain Res*. 2020;383:112517.
 25. Mirza B, Ikram H, Bilgrami S, Haleem DJ, Haleem MA. Neurochemical and behavioral effects of green tea (*Camellia sinensis*): A model study. *Pak J Pharm Sci*. 2013;26(3):511-6.
 26. Lalert L, Kruevaisayawan H, Amatyakul P, Khongsombat O. Neuroprotective effects of *A. racemosus* root extract in ovariectomized rats. *J Physiol Biomed Sci*. 2013;26(1):18-22.
 27. Hedgecock T, Phillips A, Ludrick B, Golden T, Wu N. Molecular Mechanisms and Applications of a Reserpine-Induced Rodent Model. *SSR Inst Int J Life Sci*. 2019;5(1):2160-7.
 28. Lebowitz JJ, Khoshbouei H. Heterogeneity of dopamine release sites in health and degeneration. *Neurobiol Dis*. 2020;134(11):104633. Available from: <https://doi.org/10.1016/j.nbd.2019.104633>.
 29. Lampariello L, Cortelazzo A, Guerranti R, Sticozzi C, Valacchi G. The magic velvet bean of *Mucuna pruriens*. *J Tradit Complement Med*. 2012;2(4):331-9.
 30. Cassani E, Cilia R, Laguna J, Barichella M, Contin M, Cereda E, *et al.* *Mucuna pruriens* for Parkinson's disease: Low-cost preparation method, laboratory measures and pharmacokinetics profile. *J Neurol Sci*. 2016;365:175-80.
 31. Cousins MS, Carriero DL, Salamone JD. Tremulous jaw movements induced by the acetylcholinesterase inhibitor tacrine: Effects of antiparkinsonian drugs. *Eur J Pharmacol*. 1997;322(2-3):137-45.

Article History: Submission Date : 21-08-2020; Revised Date : 18-09-2020; Acceptance Date : 09-11-2020.

Cite this article: Giri MA, Bhalke RD, Prakash KV, Kasture SB. Antiparkinsonian and Antioxidant Effects of Hydroalcoholic Extract of *Camellia sinensis*, *Asparagus racemosus*, *Mucuna pruriens* and their Combination. *Int. J. Pharm. Investigation*, 2020;10(4):569-74.

Evaluation Of *Camellia sinensis*, *Withania somnifera* and their Combination for Antioxidant and Antiparkinsonian Effect

MA Giri ^{1*}, RD Bhalke ², K Vanitha Prakash ³, SB Kasture ⁴

1. Rajarshi Shahu College of Pharmacy, Buldana, Maharashtra, India, 443001
2. Sanjivani College of Pharmaceutical Education and Research, Kopargaon, Maharashtra, India, 423603
3. Shri Sai Jyoti College of Pharmacy, Vattinagula Pally, Gandhipeth, Hyderabad, 500075
4. Pinnacle Biomedical Research Institute, Bhopal, Madhya Pradesh, India, 462003

Abstract:

Aims: *Camellia sinensis* and *Withania somnifera*, well known for antioxidant potentials, in present work hydroalcoholic extract of *Camellia sinensis* (HECS), *withania somnifera* (HEWS) and 1:1 combination mixture has been studied for protective effect against haloperidol, reserpine and tacrine induced neuronal damage.

Methods: Albino Mice either sex were treated with haloperidol (0.5 mg/kg) and wistar rats either sex were treated with reserpine (1 mg/kg) and tacrine (5 mg/kg) intraperitoneally. HECS, HEWS and mixture was administered at different doses of 30 mg/kg and 100 mg/kg (p.o) indifferent groups 30 min prior to haloperidol, reserpine and tacrine. Behavioural changes due to neuronal damage and antioxidant status were analysed. Behavioural changes were observed by using bar test, Actophotometer and Plexiglas chamber.

Results: 1:1 mixture (HECS:HEWS) significantly ($P<0.05$) improved antioxidant status and behavioural activities altered by haloperidol induced catalepsy, reserpine induced hypolocomotion and tacrine induced vacuous chewing movement, orofacial bruits in a dose dependant manner.

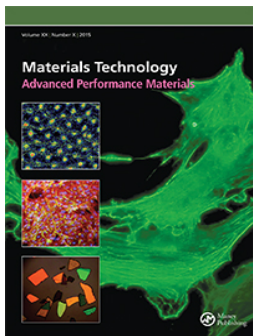
Conclusion: 1:1 mixture possesses antioxidant activity and protects neuronal damage which is more noticeable at dose of 30 mg/kg against haloperidol induced catalepsy, reserpine induced hypolocomotion and tacrine induced vacuous chewing movements and orofacial bruits.

Keywords: Antioxidant, Antiparkinson, *Camellia sinensis*, *Withania somnifera*, Haloperidol, Reserpine, Tacrine

INTRODUCTION:

Neurodegenerative diseases like Alzheimer's, Parkinson's, Huntington's and multiple sclerosis are associated with the process of memory loss and cognitive decline which results from selective degeneration of particular neuronal cells and the deposit of aggregated proteins. Parkinson's disease (PD) is mainly characterized as a movement disorder but non-motor symptoms are also involved. Since dopamine is associated with motor activity, the progressive loss of dopaminergic neurons in PD leads to muscle rigidity, tremors and bradykinesia as well as cognition, mental, sleeping, personality and behaviour disorders including depression and anxiety [1-2]. The mechanisms responsible for dopaminergic neuronal loss in PD are complex and yet unclear. Pathogenic factors such as oxidative and nitrosative stress, mitochondrial dysfunction, apoptosis, inflammatory responses and excitotoxicity have been proposed for the degeneration of dopaminergic neurons. Literature review suggests increased reactive oxygen species (ROS) and oxidative damage in the cascade of events leading to degeneration of dopaminergic neurons. This is mainly due to the observations that increased level of lipid peroxidation, modifications of proteins, and DNA and RNA oxidation products are seen in the brain of Parkinsonian patients [3-4]. Currently, there is no cure for PD and the drugs used for treatment are levodopa, dopamine agonists and monoamine oxidase-B (MAO-B) inhibitors, which provide only symptomatic relief. Levodopa has been considered the gold standard drug therapy for Parkinson's disease but it is limited only to relieving symptoms and its long term use may cause serious side effects that include involuntary movements (dyskinesia), the on-off effect may cause Parkinson's related movement problems to appear and

disappear suddenly and unpredictably. The side effects of allopathic medicines for PD are highly alarming; hence, the current research is now focusing on herbs used in alternative systems of medicine as neuroprotective [5]. In this quest, some herbs have been found to be effective neuroprotectants. Phytoconstituents like polyphenols, flavonoids exhibit antiparkinsonian activity against experimentally induced PD. *Withania somnifera* and *Camellia sinensis* are an important plants used in Ayurveda for the treatment of various disorders of the CNS and are rich in polyphenols, flavonoids, alkaloids and lactones. *Camellia sinensis* is popularly known as Green Tea belonging to Theaceae family. The most important phytoconstituents of *Camellia sinensis* are polyphenolic compounds known as catechins including epigallocatechin gallate (EGCG), catechin (C), epicatechin (EC), gallic acid (GA), gallic acid gallate (GCG), epigallocatechin (EGC), and epicatechin gallate (ECG). Flavonols contribute to the antioxidant capabilities of tea leaves. The aglycones of the main flavonols in tea leaves are quercetin, kaempferol, and myricetin. Pharmacologically active constituents of *Camellia sinensis* have been shown to possess hepatoprotective, cardioprotective, neuroprotective, anticancer, antiobesity, antidiabetic, antibacterial, antiviral and antioxidant effects. Antioxidant property of catechin contributes to protection from neurodegeneration [6-7]. *Withania somnifera* commonly known as Ashwagandha, Asgand, Indian ginseng, and winter cherry belongs to the family Solanaceae is an important medicinal plant that has been used in Ayurvedic and indigenous medicine. The biologically active chemical constituents are alkaloids (isopelletierine, anaferine), steroidal lactones (withanolides, withaferins), saponins containing an





Design & Development of Curcumin Loaded Zinc Oxide Nanoparticles Decorated Mesoporous Silica Liquid Stitches: A Proof of Concept in Animals

Ajinkya Kailas Pote , Vishal Vijay Pande , Vipul Pralhadbhai Patel , Mahendra Ashok Giri , Rasika D Bhalke & Aniket Uttam Pund

To cite this article: Ajinkya Kailas Pote , Vishal Vijay Pande , Vipul Pralhadbhai Patel , Mahendra Ashok Giri , Rasika D Bhalke & Aniket Uttam Pund (2020): Design & Development of Curcumin Loaded Zinc Oxide Nanoparticles Decorated Mesoporous Silica Liquid Stitches: A Proof of Concept in Animals, Materials Technology, DOI: [10.1080/10667857.2020.1863557](https://doi.org/10.1080/10667857.2020.1863557)

To link to this article: <https://doi.org/10.1080/10667857.2020.1863557>

 View supplementary material [↗](#)

 Published online: 30 Dec 2020.

 Submit your article to this journal [↗](#)

 Article views: 38

 View related articles [↗](#)

 View Crossmark data [↗](#)



Design & Development of Curcumin Loaded Zinc Oxide Nanoparticles Decorated Mesoporous Silica Liquid Stitches: A Proof of Concept in Animals

Ajinkya Kailas Pote^a, Vishal Vijay Pande^b, Vipul Pralhadbhai Patel^c, Mahendra Ashok Giri^a, Rasika D Bhalke^c and Aniket Uttam Pund^d

^aDepartment of Pharmaceutics, Rajarshi Shahu College of Pharmacy, Buldana, India; ^bDepartment of Pharmaceutics, RSM's N.N Sattha College of Pharmacy, Ahmednagar, India; ^cDepartment of Pharmaceutics, Sanjivani College of Pharmaceutical Education and Research, Kopargaon, India; ^dResearch Scholar, Department of Pharmaceutics (PG), Sanjivani College of Pharmaceutical Education and Research, Pune University, Kopargaon, India

ABSTRACT

The present research was aimed at synthesising and characterising curcumin-loaded zinc oxide nanoparticle-decorated mesoporous silica as a tissue adhesive (Liquid Stitches). The mesoporous silica nanoparticles facilitate adhesion to tissues through the nanobridging effect. The mesoporous silica was synthesised using a sol-gel methodology, and the drug was incorporated using the wetness impregnation method. The platform that was prepared was characterised using infrared spectroscopy, TEM, DSC, XRD, particle size analysis, BET analysis, a tissue model adhesion test, an antimicrobial assay and a wound model in Sprague Dawley rats. The average particle size was found to be 72.4 nm, while the surface area was found to be 654 m²/g. The tissue model adhesion graphs showed significantly different values for the peak load, work done and deformation at peak load, which reflects a difference between the glue strengths of the mesoporous silica nanoparticles and the Cur-ZnO-MSN and the carrier medium (water). The animal study provided a proof of concept by glueing wounds in less than 1 minute and healing the wound within 5 days.

ARTICLE HISTORY

Received 20 September 2020
Accepted 5 December 2020



KEYWORDS


Tissue glue; mesoporous silica; nanobridging; shear lap adhesion; liquid stitches; zinc oxide nanoparticles

Introduction

Wound healing or surgical incision healing is a complex procedure involving different stages like inflammatory reaction, cell proliferation and synthesis of the elements which make up the extracellular matrix, and the posterior period, called remodelling [1,2]. The minor cuts or wounds may be applied with topical dressings and wound-healing formulations but the major cuts, wounds, surgical incision needs permanent solutions like surgical sutures [3], Cyanoacrylate tissue glue or fibrin glue, etc. [4]. But it has been observed that cyanoacrylates possess toxicity like immunogenicity, local heat production and damage to the tissue or liberation of formaldehyde [5], fibrin glue possess immunogenic reaction as well as cost issue and the sutures may also be risky due to delayed healing and scar tissue formation. So, it was a need of the hour to design and develop an immediate glueing formulation which is safe, give better effect in case of fast wound healing and cost-effective. The unique combination of herbal drug curcumin, zinc oxide and the mesoporous silica platform has been developed in this study for wound healing. The use of Mesoporous silica nanoparticles (MSNs) has been proved to be effective in drug delivery [6], solubility enhancement [7], targeted delivery [8], sustained delivery, bioimaging, sensing, etc. [9]. The

use of these Mesoporous silica nanoparticles (NPs) in tissue glueing and wound healing is being explored because the connection of injured tissues and healing of wounds and trauma is a potential challenge due to the complex nature of healing [10]. It has been proved that the use of mesoporous silica in drug delivery is safe and efficacious. It has been awarded the GRAS status by the USFDA as it is biocompatible and biodegradable in nature [11]. An MSN-based tissue glue can lead to the development of a potential substitute for currently available immunogenic reaction-causing glues such as cyanoacrylates. Its use may prevent the delays in healing and the scar tissue formation that is associated with application of stitches [12]. Moreover, mesoporous silica has a honeycomb-like structure and hence it has ability to acquire drug molecules. The action of a tissue glue is based on the nanobridging effect [11]. The numerous protein chains present in body tissues are adsorbed by the nanoparticles, and a connective bridge is created between them. This bridge facilitates the glueing and healing of the wound. Many nanoparticles, such as titanium dioxide nanoparticles, zinc oxide nanoparticles, silica nanoparticles loaded silver nanoparticles, etc., have been shown to exhibit this effect [13]. Curcumin has multiple effects like antiviral, antibacterial, antifungal, antioxidant mediated anticancer, etc. [14,15]. Even

CONTACT Vishal Vijay Pande  drvishalpande@gmail.com  Rashtriy Shikshan Mandal N.N. Sattha College of Pharmacy, Anand Dham Road, Ahmednagar Tal : Ahmednagar Dist : Ahmednagar (Maharashtra) 414001.

 Supplemental data for this article can be accessed <https://doi.org/10.1080/10667857.2020.1863557> here.

© 2020 Informa UK Limited, trading as Taylor & Francis Group

though these nanoparticles have multiple advantages but it is worthy to note that they have dose-dependant toxicities too. The ZnO nanomaterials release into the aquatic ecosystems through domestic and industrial wastewaters has the potential to induce pernicious effects on fish and other organisms. Increasing concerns on the environmental hazard to aquatic biota have been highlighted by the toxic potential of some metal-based nanomaterials. Several characteristics of ZnO-NPs (e.g. size, shape, surface charge and agglomeration state) play a central role in biological effects such as genotoxic, mutagenic or cytotoxic effects. High doses of curcumin may cause mild side effects in some people. These included an increase in liver size, stained fur, stomach ulcers, inflammation and an increased risk of intestinal or liver cancer. The major disadvantage of porous silica nanoparticles is attributed to the surface density of silanol groups interacting with the surface of the phospholipids of the red blood cell membranes resulting in haemolysis. Another disadvantage is related to metabolic changes induced by porous silica nanoparticles leading to melanoma promotion. The disadvantages of mesoporous silica can be suppressed by different functionalisation to free silanol groups. The nanoparticles investigated in this work are novel in having an elevated tissue bonding strength due to a synergistic effect of MSNs and ZnO NPs. The ZnO NPs not only provides increased tissue bonding strength but also provides antibacterial efficacy. The antibacterial, antifungal and antioxidant efficacy of the product is markedly increased through the use of curcumin, which improves the wound-healing potential considerably. ZnO NPs and curcumin can be easily embedded within MSNs or decorated on MSNs because of the honeycomb-like structure of the MSNs. The resultant curcumin-loaded ZnO NP-containing MSNs can stop the NPs from aggregating and can release them in a controlled manner. This unique combination of MSNs, ZnO NPs and curcumin will provide a multifunctional antimicrobial and antioxidant tissue glue in the future. An NP-based glue can potentially replace the current practice of closing wounds with sutures because it has a quick glueing action and can bring about rapid healing. Most of the side effects associated with the wound closure procedure followed currently can be eliminated by an NP glue. Although NPs have dose-dependent side effects, the dose required for nanobridging is minute and will surely not have any toxic effects associated with it. Due to the nanobridging effect, a mesoporous silica material can be considered a self-healing material as it can glue tissues.

Materials and methods

Materials

Curcumin was obtained as a gift sample from Omniaactive Healthcare. Pluronic F-127 was purchased from Sigma Aldrich. Tetraethylorthosilicate (TEOS)

and 3-aminopropyl triethoxysilane (APTES) were procured from Research-Lab Fine Chem Industries, Mumbai. Zinc nitrate hexahydrate was purchased from Modern Industries, Sinnar. Ethanol and hydrochloric acid were purchased from Loba Chemie, Mumbai.

Methods

Preparation of SBA-15 (sol-gel method)

SBA-15 (Santa Barbara Amorphous-15) was synthesised using the procedure described in Vishal Pande et al. with slight modifications. Tetraethyl orthosilicate (98% TEOS) was used as a silica precursor, and Pluronic F127 (polyoxyethylene – polyoxypropylene block copolymer) was used as a structure-directing agent in a typical hydrothermal synthesis of SBA-15. In brief, 4 g of Pluronic F 127 was dissolved in a mixture of 120 ml 2 M HCl and 30 ml of distilled water. After the Pluronic F 127 was completely dissolved, it was added to 8.5 ml of TEOS. The mixture was stirred using a magnetic stirrer for 22 hours, and later it was subjected to probe sonication for 2 hours to reduce the particle size. In later step, the silica solution was allowed to age at 80°C to form a dry powder. This powder was washed on a filter and dried at 50°C for 24 hours and then calcinated for 6 h at 550°C to remove the triblock-copolymer from the pores. The powder was denoted as MSNs.

Amine functionalisation

One gram of the MSNs was dispersed in 100 ml of ethanol. Then, 1 ml of 3-Aminopropyltriethoxysilane (APTES) was added to the dispersion slowly. The mixture was then stirred for 12 hours and centrifuged at 5000 rpm for 25 minutes. The residue was washed several times with deionised water to remove the unreacted APTES and finally dried in air. It was designated as MSN-NH₂ [6].

Zinc oxide decoration

As in a typical synthesis, 30% w/w zinc nitrate hexahydrate was triturated with the MSN-NH₂ in a mortar and pestle. The temperature of this powder was raised to 540°C for 5 hours in a tube furnace by controlled heating at a rate of 2–3°Cminute⁻¹ in an open atmosphere. This powder was designated as ZnO-MSN [16].

Drug loading

The incipient wetness impregnation method was used to load curcumin in the ZnO-MSNs. Initially, 50 ml of ethanol was added to the drug (500 mg). The drug was dissolved completely in the solvent. Further, the ZnO-MSNs (500 mg) were added to the solution. The mixture was stirred in the dark for 48 hours at 25°C using a magnetic stirrer. After washing with water,

centrifugation and drying at room temperature. The drug-loaded product was obtained, and it was designated as Cur-ZnO-MSN [17].

Characterisation

FT-IR study

The MSNs, MSN-NH₂, ZnO-MSN and Cur-ZnO-MSN were characterised using FT-IR in order to determine the functional groups. The samples were dried well before they were subjected to IR spectroscopy. The dried samples were placed on the diamond, and the FT-IR spectra were recorded. (FT-IR 8400 S, Shimadzu Co Kyoto, Japan) [11].

Transmission electron microscopy (TEM)

A TEM works in a similar way as an SEM, but instead of having electrons ejected from the surface of a sample, an electron beam is sent through the sample. The MSNs and ZnO-MSN were characterised using a Technai G2 20 (Philips, Holland) to confirm that they were nanoparticles and to visualise the pores on the particles. The samples were prepared on a 300-mesh copper grid and scanned with the TEM operated at 200 KV [18].

Scanning electron microscopy (SEM)

SEM is generally used to characterise MSNs in terms of the particle size, particle shape and surface structure. The samples were mounted on a silver sample holder with an adhesive. To make the surfaces of the samples conductive, they were coated with gold metal at a pressure of 10 mm Hg. For recording of micrographs scanning electron microscope was used with an accelerating voltage of 20 KV at different magnification values [19].

Particle size analysis

The glueing action is based on the nanobridging effect, and so it is essential to determine the particle size of the MSNs and Cur-ZnO-MSNs. The particle size was measured using a Horiba Scientific instrument in three runs (30 seconds per run) at room temperature. The size is measured in this system using dynamic light scattering [8].

Nitrogen adsorption/desorption isotherms (BET surface area analysis)

Surface analysis of the MSNs was performed using nitrogen sorption isotherms plotted using a Micromeritics Tristar 3000 sorptometer. The surface

area was calculated using the Brunauer–Emmett–Teller (BET) equation [6].

Powder X-ray diffraction (PXRD)

The MSNs and the ZnO-MSN were characterised using PXRD. An X-ray diffractometer (Model No. 3000, Seifert, Germany) was used to record the powder X-ray diffraction patterns of the samples. Ni-filtered Cu-K radiation, a voltage of 40 kV, a current of 30 mA radiation scattered in the crystalline regions of the sample was measured using a vertical goniometer. The diffraction patterns were obtained using a step width of 0.04°C with a detector resolution 2θ (diffraction angle) value between 10° and 50° at ambient temperature [20].

Differential scanning calorimetry (DSC)

Thermal curves of each sample were recorded using a simultaneous differential scanning calorimeter (TA Instruments Q 1000). A sample of approximately 2.5 mg of the MSNs was scanned in a hermetic pan made of aluminium at a heating rate of 10°C/minute over a range from 50°C to 220°C, with an empty aluminium pan used as a reference. The samples were heated under a nitrogen atmosphere (flow rate of N₂, 50 ml/minute) [6].

Quantification of drug encapsulation efficiency and drug loading efficiency [21]

The amount of Curcumin entrapped in the nanoparticles was determined by Curcumin-loaded nanocomposites from the suspension containing free curcumin by centrifugation, and the amount of free curcumin in the supernatant was measured by ultraviolet (UV) spectrophotometer at 421 nm. The amount of drug entrapped into nanoparticles was calculated as the difference between the drug used for the formulation and the amount of drug in the supernatant. The per cent of entrapment efficiency was calculated by the following formula given in Equation 1 and the loading efficiency was calculated by Equation 2.

$$\begin{aligned} \% \text{Entrapment Efficiency} &= \\ & \frac{\text{Total amount of Drug Added} - \text{Amount of Entrapped Drug}}{\text{Total Amount of Drug Added}} \\ & \times 100 \end{aligned} \quad 1$$

$$\% \text{Loading Efficiency} = \frac{m_2 - m_1}{m_1} \times 100 \quad 2$$

where

*m*₁ = initial weight of MSN template and

*m*₂ = weight of drug-loaded MSNs

In vitro drug release study

Fifty milligrams of the nanocomposite were placed in a dialysis bag (Mw Cut off of 12000 Dalton). The bag was placed in a 50-ml conical flask. Twenty millilitres of phosphate buffer solution (pH 7.4) was used as a dissolution medium and added to a conical flask. The flask was maintained at 37°C using a shaking incubator. The flask was rotated at a speed of 50 rpm. Five millilitres of the medium was withdrawn at various time intervals using a 5.0-mL pipette and replaced by 5.0 ml of the phosphate buffer solution (pH 7.4). The drug content was estimated using a UV spectrophotometer [22].

Shear lap adhesion test

The Shear lap adhesion test was used to determine the glueing efficiency of the nanocomposite and its strength. The shear lap adhesion test was done using goat skin pieces. Two fresh goat skin pieces of length 10 cm, width 5 cm & 1.9 ± 0.04 mm in thickness were obtained from a local slaughterhouse. A 20% w/v sterilised nanocomposite suspension in water was prepared and 20 μ l of the nanocomposite suspension was applied on one goat skin piece. The other piece was made to overlap it over a length of 2 cm and then pressed for 30 seconds. The pressure applied was equivalent to pressure when slightly pressed with the thumb. It was simulated to pressure applied by physician for holding the skin while applying stitches. The strength measurements were conducted on the glued skin using a CT-3 texture analyser (Brookfield Engineering). The peak load required to break the bond, the work done and the deformation at the peak load were determined. The test was performed for MSNs, Cur-ZnO-MSNs and placebo [11].

Sterility testing

Cur-ZnO-MSNs was subjected for the Sterility testing. It was intended for detecting the presence of viable form of microorganisms and performed by using fluid Thioglycolate medium and Soybean casein digest medium, as per the Indian pharmacopoeia. The Cur-ZnO-MSNs were sterilised and was tested in aseptic conditions for viable forms of bacteria, fungi, yeast in both the media by direct inoculation method for 7 & 13 days [23].

Antimicrobial assay

Strains isolated from clinical samples obtained from a pathology lab (Metropolis Lab, Nashik) were first grown on selective media and then utilised for an antimicrobial assay. The antimicrobial assay was performed using the agar well method. Twenty

microlitres of the sterilised Cur-ZnO-MSN formulation (20% w/v nanocomposites in water) was added to a well bored in the centre of an agar plate. The zone of inhibition was tested against resistant *P. aeruginosa* and *S. aureus* [24].

Stability testing

The Cur-ZnO-MSNs were subjected to stability testing. The stability study was conducted according to the ICH guidelines at $40 \pm 2^\circ\text{C}$ and $75 \pm 5\%$ RH for 3 months. Samples were withdrawn at 0, 30, 60 and 90 days and analysed for any physical changes. The shear lap adhesion test & drug content was analysed using the validated UV method described by Warule Pooja et al. in 2017 [25,26].

Animal study: incision model

Rats were divided into two groups (test and control). Each group consisted of six rats. A cutaneous incision of length 1 cm was made on the abdomen of each rat under anaesthesia. Closure sutures were made for the wounds of the control group, and a commercial wound-healing gel was applied on the wounds. Twenty microlitres of the sterilised formulation (20% w/v of Cur-ZnO-MSNs in sterile water for injection) was added to the wound of each rat in the test group using a pipette. The wounds were pressed at the edges from both sides using fingers for 50 seconds, and the excess nano-adhesive was removed. Macroscopic images of the wound site of each rat were taken at 1, 3 and 5 days, and the wound widths were measured [11].

Statistical analysis

The experimental results were analysed with Graph Pad Prism and data are presented as the mean \pm SD. Statistical significance was evaluated using one-way ANOVA, ordinary same followed by Dunnet test when only two groups were compared. If more than two groups were compared, evaluation of significance was performed using one-way ANOVA, repeated measure followed by Dunnet test.

Results

FT-IR study

The FT-IR spectra of the MSNs showed a peak at 3350 cm^{-1} . This band is due to the stretching mode of OH, the Si-O-Si rocking mode at 819 cm^{-1} and the O-Si-O bending mode at $1000\text{--}1300\text{ cm}^{-1}$. Major peaks of MSN-NH₂ were observed at 1638 cm^{-1} , 2991 cm^{-1} , 1066 cm^{-1} and 788.9 cm^{-1} , which reflect NH₂ bending, NH₂ stretching, Si-O-Si stretching and Si-OH stretching, respectively. The FT-IR spectra of ZnO-MSN show

peaks at 1066 cm^{-1} , 797 cm^{-1} , 3339 cm^{-1} , 649 cm^{-1} and 653 cm^{-1} , which are associated with the stretching and bending of the silanol and oxide functions. The Cur-ZnO-MSNs spectra show peaks at 1512 cm^{-1} , due to stretching of the carbonyl bond, at $3200\text{--}3500\text{ cm}^{-1}$, due to stretching of the O-H group, at 670 cm^{-1} , due to C = C bending, and 3742 cm^{-1} , due to stretching of the alcohol group.

TEM study

The TEM analysis shows that the MSNs have distinct interconnected pores in the form of a honeycomb (Figure 1(a)), and the interconnected pores of MSNs are completely occupied by zinc oxide nanoparticles (ZnO-MSN, Figure 1(b)).

SEM study

The SEM study of the MSNs revealed their surface morphology. They have aggregated particles. Figure 2.

Particle size

The particle sizes of the MSNs and Cur-ZnO-MSNs were found to be 129.9 nm (Figure 3(a)) and 72.4 nm

(Figure 3(b)), respectively. The particle size of the Cur-ZnO-MSNs was less than 100 nm , which indicates that the product will exhibit excellent & desirable the nanobridging effect and glue strength there off.

Nitrogen adsorption/desorption isotherms (BET surface area analysis)

The surface area of the MSNs is $654\text{ m}^2/\text{g}$, while the total pore volume was found to be $0.4\text{ cm}^3/\text{g}$.

Powder X-ray diffraction (PXRD)

The spectrum of the MSNs Figure 4(a) silica shows no reflections adjacent to crystalline ordering and so confirms the amorphous nature of the silica although the graph shows a single broad peak with the maximum at a 2θ value of 22° . The spectrum of the ZnO loaded MSNs Figure 4(b) shows the peaks at 17.25° , 14.466° , 18° , 24.52° and 25.53° . This confirms the amorphous nature of the formulation.

Differential scanning calorimetry (DSC)

In the DSC spectrum of MSNs, Figure 5 a blunt exothermic peak at 87°C was observed. It is an indication that the

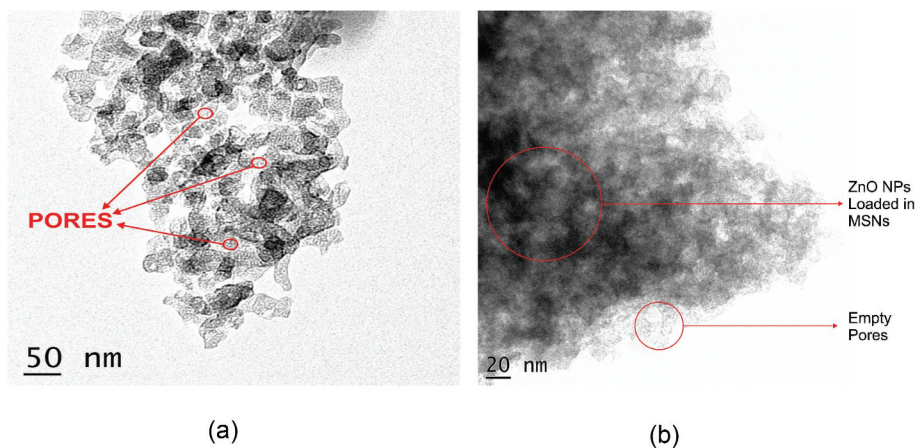


Figure 1. TEM images (a) MSNs (b) ZnO-MSNs.

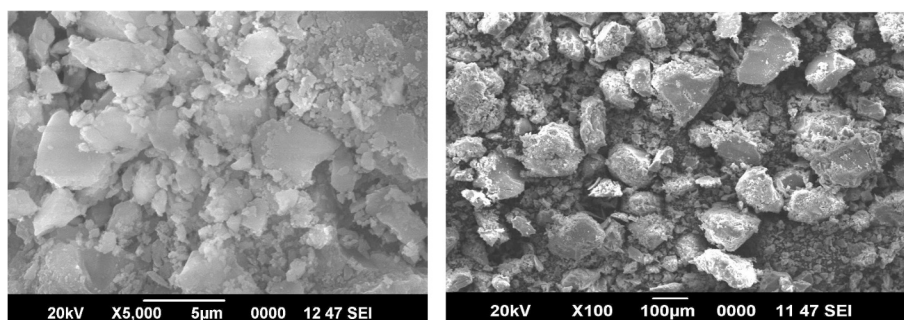


Figure 2. SEM images MSNs.

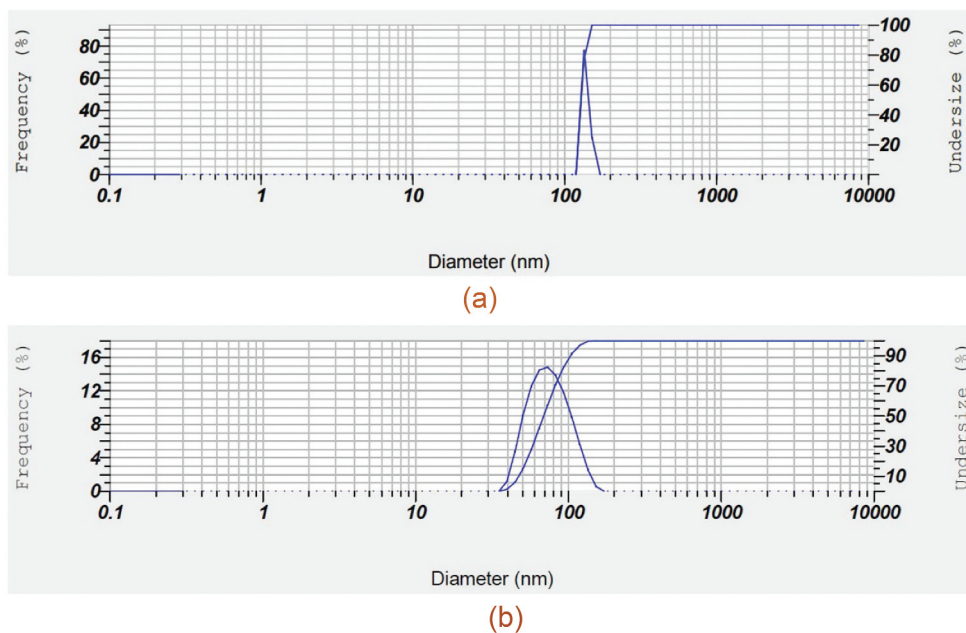


Figure 3. Particle size (a) MSNs (b) Cur-ZnO-MSNs.

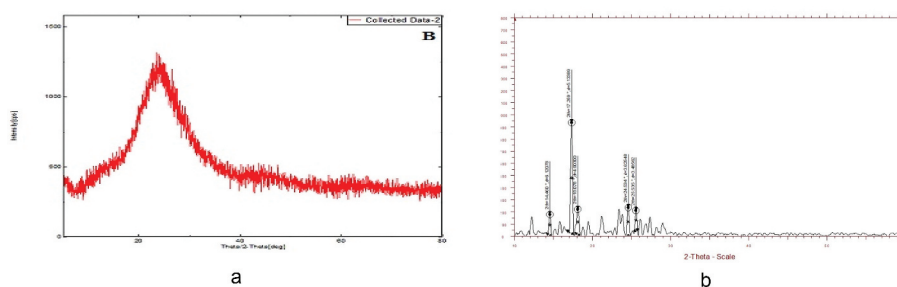


Figure 4. XRD spectra (a) MSNs (b) ZnO-MSNs.

SBA-15 is in an amorphous form, which could be due to the fact that more carrier particles are available for drug adsorption, the onset of melting of amorphous MSNs starts at 60°C, and the end of the peak region was observed at 121°C.

Quantification of drug

The entrapment efficiency of the drug-loaded MSNs was found to be 59%. The loading efficiency was found to be 49.80%.

In vitro drug release study

Up to 49.5% of the drug was released from the formulation within 10 hours and more than 90% was released in 24 hours.

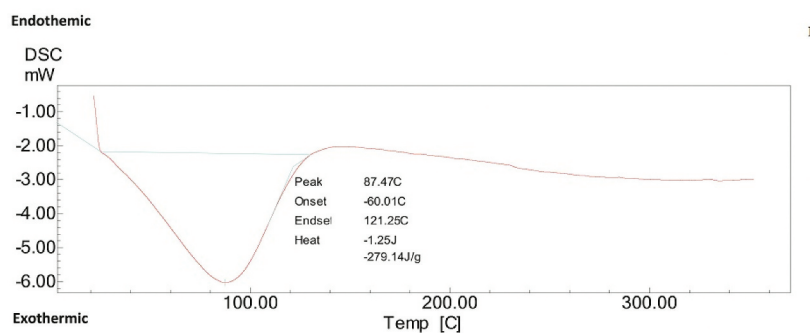


Figure 5. DSC spectra of MSNs.

This sustained release of the drug will provide longer antibacterial and antioxidant action, which will reduce the chances of infection and potentiate wound healing (Figure 6).

Shear lap adhesion test

The shear lap adhesion test was carried out to determine the glue strength. The mean peak loads of the MSNs, Cur-ZnO-MSNs and water were found to be 98.166 g, 781.33 g and 19.16 g, respectively.

Extremely Significant difference was found between the peak loads required to break the bond between two tissues of the MSNs and Cur-ZnO-MSNs.

The deformations at the peak load were calculated for the MSNs, Cur-ZnO-MSNs and water. They were 7.80 ± 0.2196 mm, 15.72 ± 0.411 mm and 4.865 ± 0.4508 mm, respectively.

The work done was also calculated for the MSNs, Cur-ZnO-MSNs and water. It was found to be 11.12 ± 0.5070 mJ, 48.3 ± 1.3567 mJ and 1.77 ± 0.3162 mJ, respectively.

This also shows the better efficacy of the Cur-ZnO-MSNs compared with the MSNs. The mean \pm SD was calculated for the peak load, deformation and work done (Table 1)

The extremely significant results obtained regarding the glue strength of the Cur-ZnO-MSNs indicate that it is a potential tissue glueing formulation. The very high values of peak load suggest that the bond between wounded tissue will not break and lead to re wounding and haemorrhage.

Figure 8(a-c) shows the representative CT3 load distance curves of MSNs, Cur-ZnO-MSNs, water.

Figure 9(a,b) shows glueing of goat skin by MSNs and Cur-ZnO-MSNs, respectively.

Sterility testing

There was no growth in the sterilised Cur-ZnO-MSNs in the fluid thioglycolate medium and the soybean casein digest medium, which indicates that there were no viable forms of bacteria, fungi or yeast in the

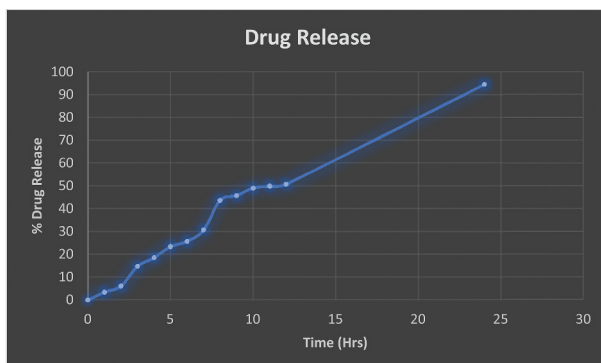


Figure 6. In vitro drug release study.

formulation. It was concluded that the formulation is suitable for use in open wounds.

Antimicrobial assay

The antimicrobial assay was performed against strains that will potentially infect skin wounds. The formulation showed a zone of inhibition at the dose to be used for glueing skin, from which it can be concluded that the dose used for glueing skin will successfully inhibit the growth of microbes. When the experiment was performed thrice, the mean zone of inhibition was calculated to be 18 mm against *S. aureus* and 15 mm against *P. aeruginosa*.

Figure 10 shows the representative zones of inhibition against *S. aureus* and *P. aeruginosa*.

Stability testing

The stability studies indicate that the CUR-ZnO-MSNs are stable. There was no change in physical appearance, and the other parameters are as stated in Table 2. This indicates that formulation was stable.

Animal study

Incision model

The study showed that the rat incision wounds were glued in less than 1 minute. Moreover, they were almost healed within the time period of 5 days. The incision wound widths of the rats treated with tissue glue at days 1, 3 and 5 were 7 mm, 3.5 mm and 1.1 mm, respectively, while those of the rats treated with closure sutures were 13 mm, 11.16 mm and 8 mm, respectively. Table 3 depicts day-wise decrease in wound width by tissue glue (liquid Stitches). Table 4 depicts day-wise decrease in wound width by sutures

Discussion

The present research was aimed to develop an alternative for sutures, cyanoacrylate adhesives, etc. which are currently used to close the wounds or surgical incisions; as these solutions have a drawback of toxicity and delayed healing. Moreover, the sutures lead to the formation of scar tissue as well as the permanent marks on the skin which is not desirable. The cyanoacrylates produce the local heat and liberate the formaldehyde upon application which leads to damage of tissue. To overcome these problems, we have developed liquid stitches. The mesoporous silica has a USFDA GRAS status hence it is safe as compared to the cyanoacrylates. The formulated liquid stitches are available in powder form which can be reconstituted by sterile water for injection and used for glueing the skin. The mechanism involved in glueing the skin by the liquid stitches is the nanobridging effect. The nanoparticles adsorb various tissue chains on its surface and

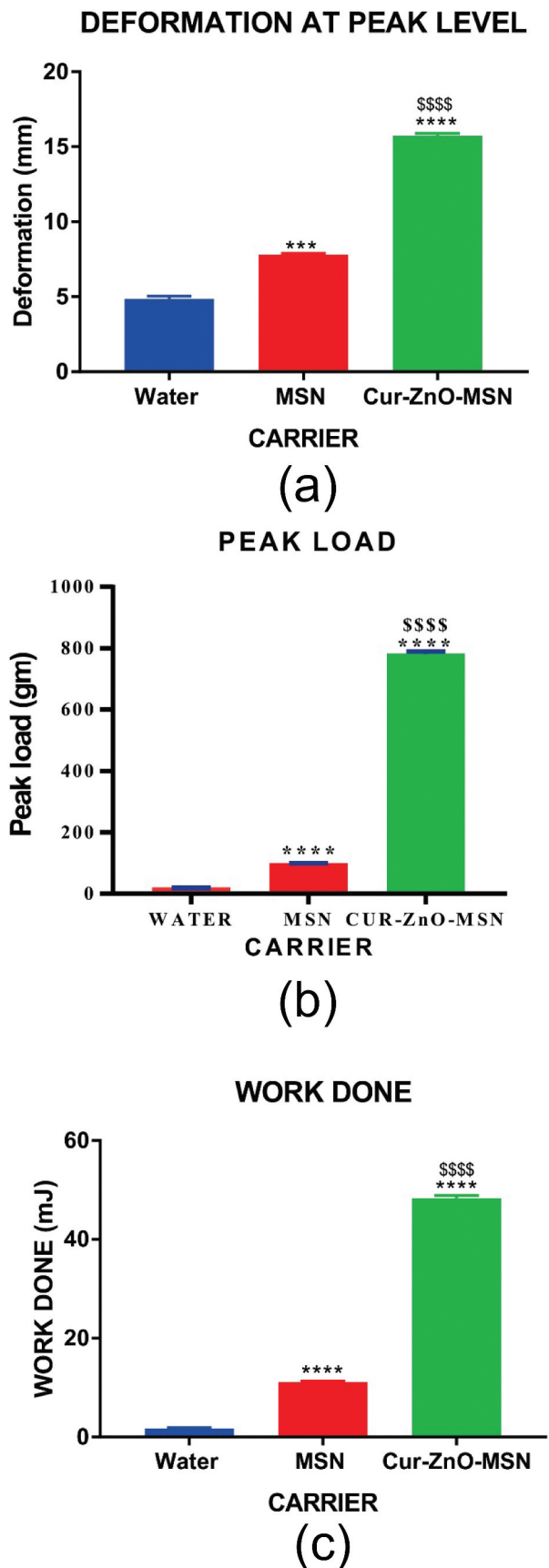


Figure 7. Graphical representation of shear lap adhesion test. (a) Deformation at peak level. (b) Work Done. (c) Peak Load. These data represent six separate experiments and are presented as the mean values \pm SD, * = $P < 0.1$: Significant, ** = $P < 0.01$: Very significant, and *** & more = $P < 0.001$: Extremely Significant **VS Water**; \$ = $P < 0.1$: Significant, \$\$ = $P < 0.01$: Very significant, and \$\$\$ & more = $P < 0.001$: Extremely Significant **VS MSNs**.

Table 1. Shear lap adhesion test.

Sr no	MSN						Cur-ZnO-MSN						Carrier Media (Water)					
	Peak load (gm)	Deformation (mm)	Work done (mJ)	Peak load (gm)	Deformation (mm)	Work done (mJ)	Peak load (gm)	Deformation (mm)	Work done (mJ)	Peak load (gm)	Deformation (mm)	Work done (mJ)	Peak load (gm)	Deformation (mm)	Work done (mJ)	Peak load (gm)	Deformation (mm)	Work done (mJ)
1	94	7.56	10.80	756	15.11	46.10	19	4.67	1.80									
2	100	7.94	11.12	814	16.31	50.14	15	4.45	1.21									
3	98	7.81	10.94	795	15.94	49.17	17	4.53	1.71									
4	95	7.58	10.89	779	15.74	48.34	23	5.49	2.14									
5	105	8.14	12.14	769	15.45	47.84	19	4.67	1.80									
6	97	7.79	10.88	775	15.79	48.21	22	5.38	1.98									
Mean ± S.D	98.166 ± 3.422	7.80 ± 0.2196	11.12 ± 0.5070	781.33 ± 20.46	15.72 ± 0.411	48.3 ± 1.3567	19.16 ± 2.99	4.865 ± 0.4508	1.77 ± 0.3162									

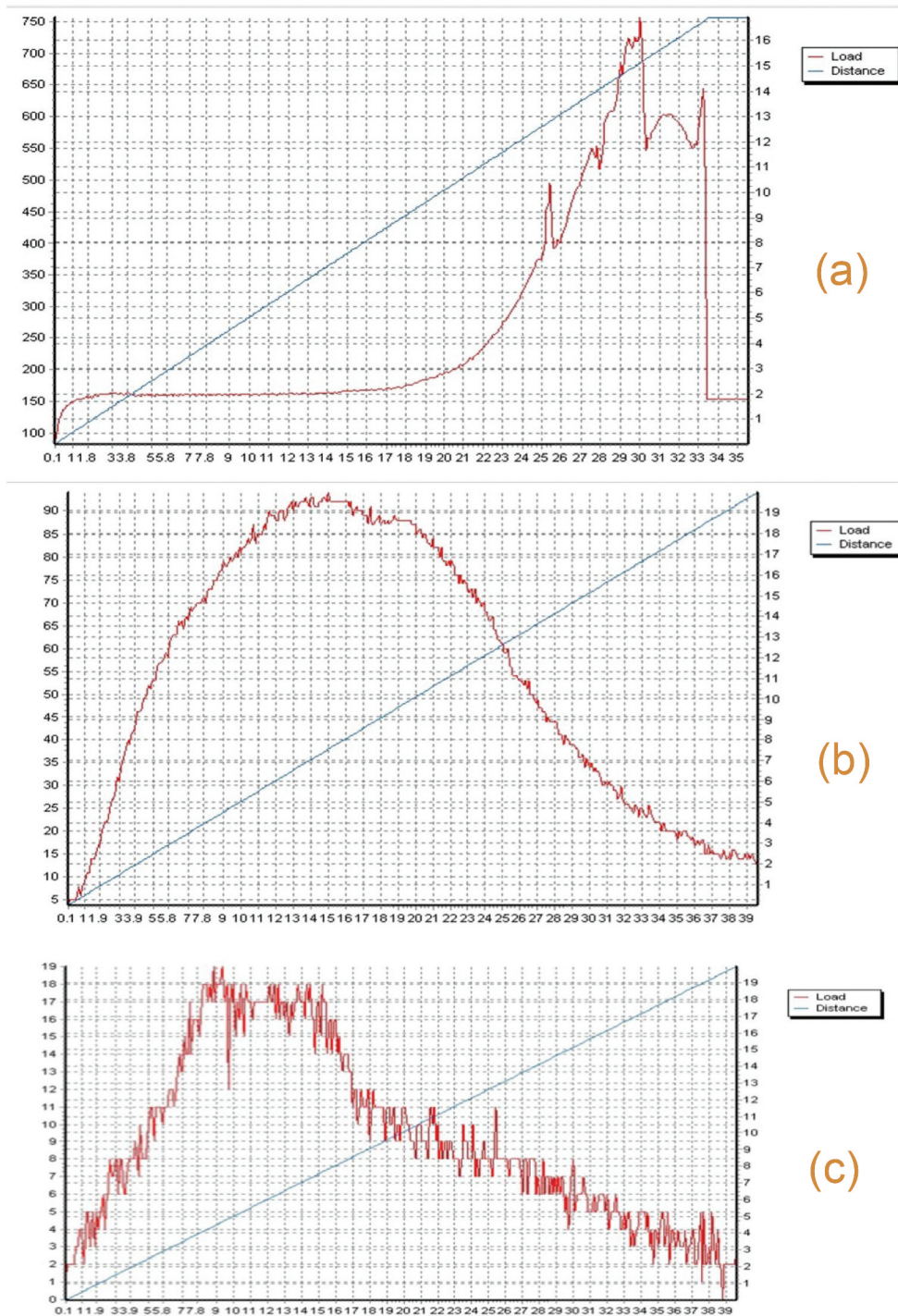


Figure 8. Representative load distance curves. (a) MSNs (b) Cur-ZnO MSNs (c) Water

create a bridge between them which results in immediate glueing of the skin as represented in Figure 13. The formulated liquid stitches have mesoporous silica loaded with zinc oxide nanoparticles and Curcumin. The inorganic mesoporous silica and contribute to the nanobridging effect and is a platform for loading nanoparticles and API curcumin. The zinc oxide nanoparticles played a dual role. Firstly, it added the strength to the adhesive bond created between tissue chains and it also contributed in the antibacterial efficacy of the liquid stitches. The curcumin was used to offer antibacterial activity to the liquid stitches and also the antioxidant nature

contributed to rapid healing of wound. The FTIR study confirmed all the functionalisation and groups required in the platform. The TEM study revealed the porous nature of the platform confirmed the loading of zinc oxide nanoparticles. The SEM study shows the aggregated mesoporous silica nanoparticles. The major requirement for nanoparticles to show excellent nanobridging effect is the particle size of the nanoparticles below 100 nm. The particle size analysis gave the confirmation that liquid stitches have size less than 100 nm and will show the excellent nanobridging effect which will lead to the immediate glueing of skin with desirable

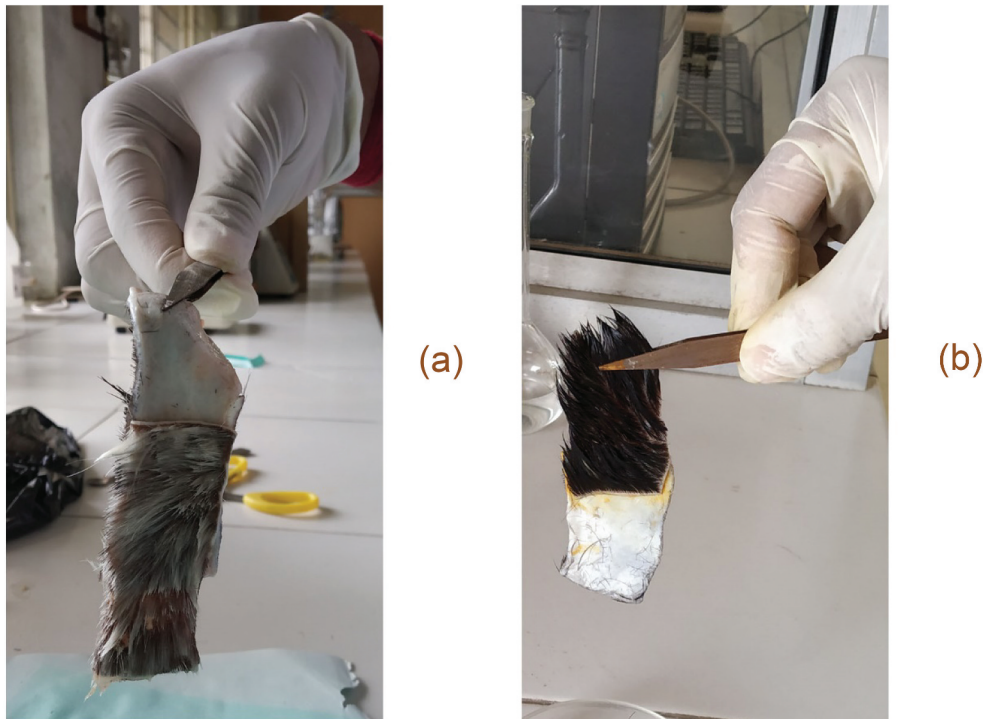


Figure 9. Representative images of glued goat skin (a) MSNs (b) Cur-ZnO-MSNs.

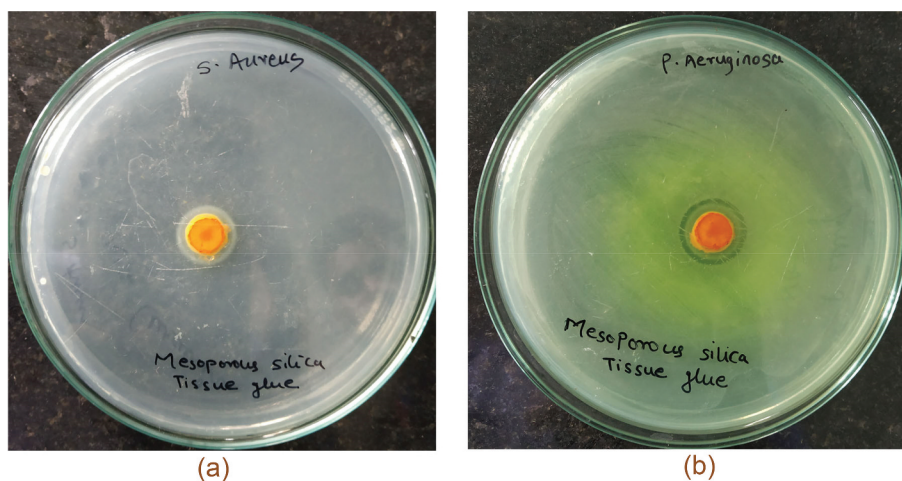


Figure 10. Zone of inhibition against the (a) *S. aureus* & (b) *P. aeruginosa*.

strength. The BET analysis revealed the high surface area and pore volume of the MSNs platform. The sustained release of the drug in the drug release studies suggests that the product display antimicrobial and antioxidant activity longer, which will support the healing mechanisms. The stability study showed no significant decrease in the drug content and the adhesive strength of the formulation. The shear lap adhesion test proved that the nanocomposite exhibited significant tissue glue activity as there were extremely significant differences between the peak-load, deformation and work-done values of the Cur-ZnO-MSNs and the MSNs and the medium (water). The sterility test of the product proved that it can be used in open wounds. The zones of inhibitions at the dose used to glue tissues indicate that the antimicrobial nature of the glue will support the healing. The animal activity

provided proof of the concept that the formulation can glue tissues in less than 1 minute. The formulation healed wounds extremely significantly compared with sutures (one of the remedies generally used in wound closure in India). This indicates that the liquid stitch formulation can potentially replace the sutures which are currently practised to heal the wound or incisions.

Conclusions

The current research involved the design and development of curcumin and ZnO nanoparticle-loaded mesoporous silica as a tissue glue. The nanocomposite of mesoporous silica loaded with ZnO and curcumin was developed in order to glue tissues using the nanobridging

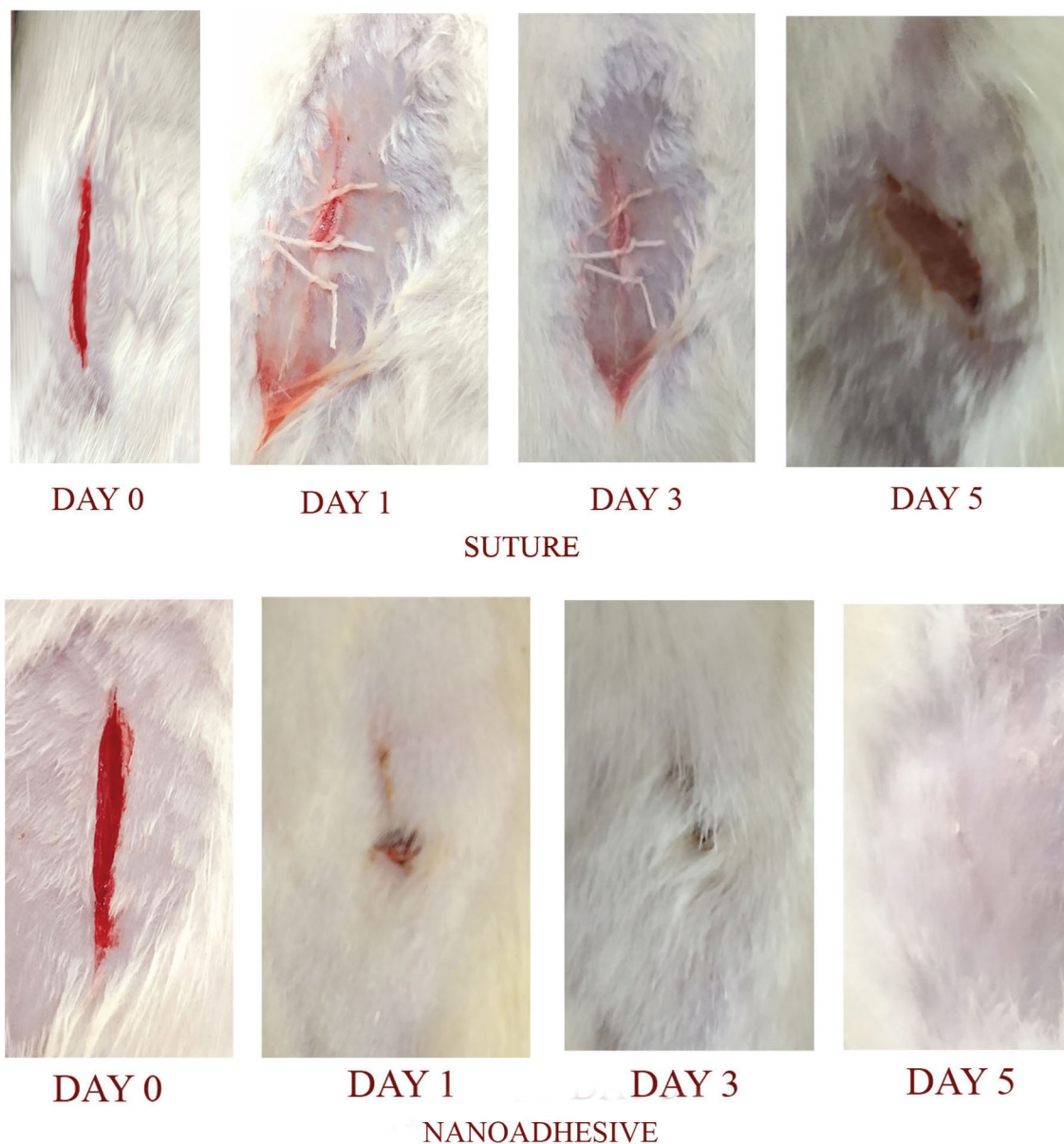


Figure 11. Representative macroscopic images of the wound healing treated by suture and Cur-Zno-MSNs nano-adhesives in a Sprague Dawley rat model for 5 days. * = P < 0.1: Significant, ** = P < 0.01: Very significant, and *** & more = P < 0.001: Extremely Significant.

CONTROL Vs TEST TREATED WOUND WIDTH

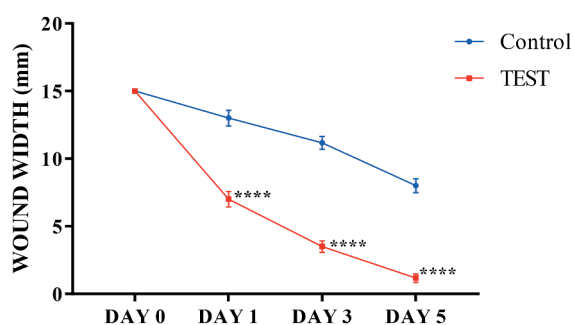


Figure 12. Measurement of the width between the borders of the wound area after 5 days. The values represent the mean values SD, n = 6.

Table 2. Stability studies of formulation.

Month	Drug content	Peak load	Deformation at peak load	Work done
0	98 ± 0.31	754 ± 10.46	14.91 ± 0.510	45.94 ± 1.31
1	96 ± 0.13	750 ± 13.6	14.73 ± 0.101	45.1 ± 1.04
2	95.25 ± 0.23	743 ± 11.29	13.84 ± 0.31	44.8 ± 1.43
3	93 ± 0.14	741 ± 10.17	13.21 ± 0.411	44.1 ± 1.29

effect. The MSN platform has high surface area, pore volume and capacity to load curcumin and zinc oxide nanoparticles. The final formulation has the particle size in the desired range and ability to show the nanobridging efficacy. The shear lap adhesion showed significant difference in adhesive strength of MSNs and final

Table 3. Test rats treated with tissue glue.

Rat no	Wound width (mm) Day 0	Wound width (mm) Day 1	Wound width (mm) Day 3	Wound width (mm) Day 5
1	15	7	4	1
2	15	8	3	2
3	15	9	2	1
4	15	6	4	0
5	15	5	3	1
6	15	7	5	2
Mean ± S.D	15 ± 0.00	7 ± 1.414	3.5 ± 1.048	1.16 ± 0.7527

Table 4. Control rats treated with sutures.

Rat no	Wound width (mm) Day 0	Wound width (mm) Day 1	Wound width (mm) Day 3	Wound width (mm) Day 5
1	15	12	10	9
2	15	13	11	9
3	15	13	11	8
4	15	14	12	7
5	15	15	13	9
6	15	11	10	6
Mean ± S.D	15 ± 0.00	13 ± 1.414	11.16 ± 1.169	8 ± 1.264

formulation which proved that combination of zinc oxide nanoparticles had a synergistic effect on tissue

adhesive activity. The product was stable during accelerated stability studies. The liquid stitch formulation was antibacterial in nature which is desired in any wound-healing product. The liquid stitches glued the skin in less than 1 minute and it had significant glueing and healing potency. It can be concluded that the formulated liquid stitch has the potential to replace the Sutures: A currently available solution for wound healing and can become the potential alternative for wound closure in near future.

Acknowledgments

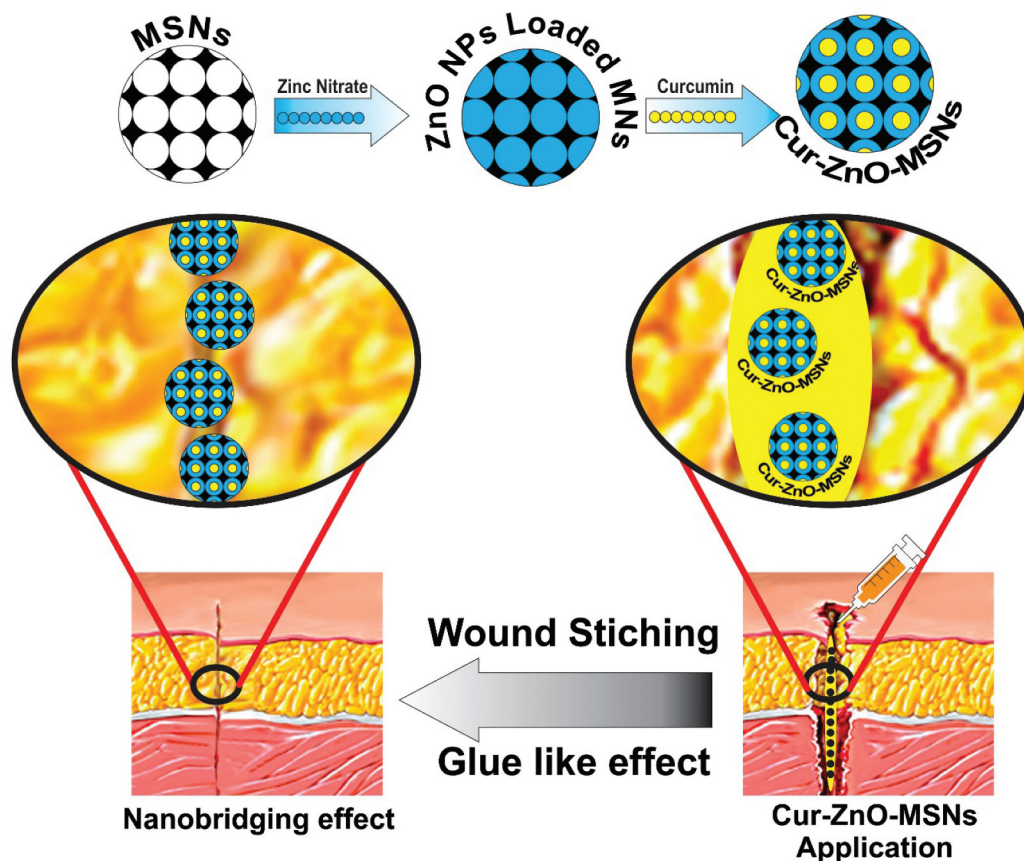
The authors acknowledge AICTE, New Delhi; Department of Microbiology, Sanjivani Arts Commerce and Science College, Kopergaon & Metropolis Lab, Nashik.

Disclosure statement

Authors declare no conflict of interest.

Funding

This work was supported by the All India Council for Technical Education [9-259/IDC/MODROB/Policy-1/2019-20].

**Figure 13.** Mechanism of liquid stitches.

References

- [1] Gonzalez ACDO, Andrade ZDA, Costa TF, et al. Wound healing – a literature review. *An Bras Dermatol*. 2016;91(5):614–620.
- [2] Nayak BS, Sandiford S, Maxwell A. Evaluation of the wound-healing activity of ethanolic extract of *Morinda citrifolia* L. leaf. *Evid Based Complement Altern Med*. 2009;6(3):351–356.
- [3] Byrne M, Aly A. The surgical suture. *Aesthetic Surg J*. 2019;39:S67–72.
- [4] Al-Mubarak L, Al-Haddab M. Cutaneous wound closure materials: an overview and update. *J Cutan Aesthet Surg* [Internet]. 2013;6(4):178. [cited 2020 Jul 17] Available from: [/pmc/articles/PMC3884880/?report=abstract](https://pubmed.ncbi.nlm.nih.gov/PMC3884880/?report=abstract)
- [5] Leggat PA, Smith DR, Kedjarune U. Surgical applications of cyanoacrylate adhesives: a review of toxicity. *ANZ J Surg* [Internet]. 2007;77:209–213. [cited 2020 Jul 17]. Available from: <https://pubmed.ncbi.nlm.nih.gov/17388821/>
- [6] Pande VV, Jadhav KS, Giri MA, et al. Design and development of paliperidone mesoporous silica template as a platform for surge dose drug delivery system. *Mater Technol* [Internet]. 2019;34(3):117–125.
- [7] Şen Karaman D, Patrignani G, Rosqvist E, et al. Mesoporous silica nanoparticles facilitating the dissolution of poorly soluble drugs in orodispersible films. *Eur J Pharm Sci*. 2018;122(March):152–159.
- [8] Pande VV, Borawake DD, Halnor VV. Fabrication and characterization of gemcitabine hydrochloride loaded mesoporous silica nanoparticles as theranostics platform for pancreatic cancer [Internet]. *Mater Technol*. 2018;3313:815–824.
- [9] Zhang XA, Jia HH, Wang XF, et al. Biosensors based on acetylcholinesterase immobilized on mesoporous silica thin films. *Chinese Sci Bull*. 2009;54(17):3023–3028.
- [10] Wu H, Li F, Wang S, et al. Ceria nanocrystals decorated mesoporous silica nanoparticle based ROS-scavenging tissue adhesive for highly efficient regenerative wound healing. *Biomaterials* [Internet]. 2018;151:66–77.
- [11] Lu MM, Bai J, Shao D, et al. Antibacterial and biodegradable tissue nano-adhesives for rapid wound closure. *Int J Nanomedicine*. 2018;13:5849–5863.
- [12] Leggat PA, Smith DR, Kedjarune U. Surgical applications of cyanoacrylate adhesives: a review of toxicity. *ANZ J Surg*. 2007;77(4):209–213.
- [13] Gao Y, Han Y, Cui M, et al. ZnO nanoparticles as an antimicrobial tissue adhesive for skin wound closure. *J Mater Chem B*. 2017;5(23):4535–4541. doi: 10.1039/c7tb00664k.
- [14] Kendre PN, Chaudhari PD. Design and optimization of oral bioadhesive nanocurcumin delivery using novel hydrophilic carrier for cancer treatment: an alternative to parenteral chemotherapy. *Indian Drugs*. 2016;53(8):24–36.
- [15] Moghadamtousi SZ, Kadir HA, Hassandarvish P, et al. Review on antibacterial, antiviral, and antifungal activity of curcumin. *Biomed Res Int* [Internet]. 2014;2014. [cited 2020 Jul 17]. Available from: [/pmc/articles/PMC4022204/?report=abstract](https://pubmed.ncbi.nlm.nih.gov/PMC4022204/?report=abstract)
- [16] Lihitkar PB, Violet S, Shirolkar M, et al. Confinement of zinc oxide nanoparticles in ordered mesoporous silica MCM-41. *Mater Chem Phys* [Internet]. 2012;133(2–3):850–856.
- [17] Elbially NS, Aboushoushah SF, Sofi BF, et al. Multifunctional curcumin-loaded mesoporous silica nanoparticles for cancer chemoprevention and therapy. *Microporous Mesoporous Mater*. 2020 Jan 1;291:109540.
- [18] Panage S, Pande V, Patil S, et al. Design and synthesis of mesoporous silica for inclusion of poorly water soluble drug sertaconazole nitrate as a drug delivery platform. *Der Pharm Lett*. 2014;6(4):159–168.
- [19] Kumar S, Malik MM, Purohit R. Synthesis of high surface area mesoporous silica materials using soft templating approach [Internet]. *Mater Today Proc*. 2018;52:4128–4133.
- [20] Fong SYK, Ibisogly A, Bauer-Brandl A. Solubility enhancement of BCS Class II drug by solid phospholipid dispersions: spray drying versus freeze-drying. *Int J Pharm* [Internet]. 2015 Dec 30;496(2):382–391. [cited 2020 Mar 30]. Available from: <http://www.ncbi.nlm.nih.gov/pubmed/26468038>
- [21] Pande VV, Khedkar PV, Giri MA. Fabrication and characterisation of gemcitabine hydrochloride loaded magnetically responsive mesoporous silica nanocomposites as smart hybrid theranostic platform for treatment of pancreatic cancer. *Mater Technol* [Internet]. 2020;1–8. DOI:10.1080/10667857.2020.1734729.
- [22] Peretti E, Mileto I, Stella B, et al. Strategies to obtain encapsulation and controlled release of pentamidine in mesoporous silica nanoparticles. *Pharmaceutics*. 2018;10(4):11–14.
- [23] Pharmaceutical sterility testing – contract pharma [Internet]. [cited 2020 Mar 30]. Available from: https://www.contractpharma.com/issues/2008-03/view_features/pharmaceutical-sterility-testing/
- [24] Amin T, Naik HR, Hussain SZ, et al. In-vitro antioxidant and antibacterial activities of pumpkin, quince, muskmelon and bottle gourd seeds. *J Food Meas Charact*. 2018;12(1):182–190.
- [25] ICH Official web site. ICH [Internet]. [cited 2020 Mar 30]. Available from: <https://www.ich.org/>
- [26] Warule PPV, et al. Development and validation of UV spectrophotometric method for the estimation of curcumin in an ayurvedic formulation [Internet]. *Int J Pharm Drug Anal*. 2017;93–97. [cited 2020 Mar 30]. Available from: http://www.ijpda.com/view_issue.php?id=MzAO

B-SITOSTEROL: ISOLATION FROM *MUNTINGIA CALABURA* LINN. BARK EXTRACT, STRUCTURAL ELUCIDATION, AND MOLECULAR DOCKING STUDIES AS POTENTIAL INHIBITOR OF SARS-COV-2 M^{PRO} (COVID-19)

RAKESH N CHAUDHARI¹, SHARUK L.KHAN^{2*}, RAVINDRA S CHAUDHARY¹, SHIRISH P JAIN², FALAK A SIDDUQUI²

¹Department of Pharmacognosy, JES's College of Pharmacy, Nandurbar, Maharashtra, India. ²Department of Pharmaceutical Chemistry, Rajarshi Shahu College of Pharmacy, Buldana, Maharashtra, India. Email: sharique.4u4@gmail.com

Received: 18 March 2020, Revised and Accepted: 20 April 2020

ABSTRACT

Objective: A novel human coronavirus, labeled as SARS-CoV-2 (COVID-19), causing pneumonia is spreading around the world. At present, there are no specific treatments for COVID-19. β -sitosterol is well known for its multiple biological actions. This research aims to isolate and study the binding affinity of β -sitosterol for SARS-CoV-2 (COVID-19) main protease (M^{PRO}).

Methods: Extraction and column chromatography was performed to isolate the β -sitosterol from an n-hexane extract of *Muntingia calabura* bark followed by thin-layer chromatography (TLC), high-performance TLC (HPTLC), Fourier-transform infrared (FTIR), and ultraviolet-visible spectroscopy. The molecular docking studies were performed on SARS-CoV-2 M^{PRO} to determine the binding affinity of the β -sitosterol using PyRx Virtual Screening Tool.

Results: In the present study, preliminary phytochemical screening showed the presence of carbohydrate, steroid, terpenoid, and flavonoid compounds. A total of 115 fractions was collected from column chromatography using benzene as a solvent by an isocratic elution technique. HPTLC fingerprinting analysis showed the presence of β -sitosterol under 366 nm. FTIR characterization was performed of the same fraction which gives the absorption peaks which resembles the β -sitosterol structure.

Conclusion: The overall study concludes this method can be considered as a standard method for isolation of β -sitosterol from *M. calabura* bark. Favipiravir has a less binding affinity, i.e. -5.7 kcal/mol than β -sitosterol which has -6.9 kcal/mol. The number of hydrogen bonds formed by the favipiravir is much more, i.e., 4 than β -sitosterol which formed only 01 hydrogen bonds with SARS-CoV-2 M^{PRO}.

Keywords: *Muntingia calabura*, β -sitosterol, SARS-CoV-2 (COVID-19), Molecular docking, High-performance thin-layer chromatography.

© 2020 The Authors. Published by Innovare Academic Sciences Pvt Ltd. This is an open access article under the CC BY license (<http://creativecommons.org/licenses/by/4.0/>) DOI: <http://dx.doi.org/10.22159/ajpcr.2020.v13i5.37909>

INTRODUCTION

Muntingia calabura, also known as cherry, it has been an essential herb in the Ayurvedic and indigenous medical systems for over 4000 years. Belong to genus *Muntingia* which contains about 30 species of tropical fruiting trees in the flowering plant family Tiliaceae. *M. calabura* (Muntingiaceae) grows in the tropical and subtropical regions and its parts are used commonly in folk medicine for a varied variety of conditions. According to Ayurveda, varied medicinal properties are attributed to different parts of the mango tree. Cherry is one of the most popular of all tropical fruits. Various parts of the plant are used as a dentifrice, antiseptic, astringent, diaphoretic, stomachic, vermifuge, tonic, laxative, and diuretic and to treat diarrhea, dysentery, anemia, asthma, bronchitis, cough, hypertension, insomnia, rheumatism, toothache, leucorrhoea, hemorrhage, and piles. All parts are used to treat abscesses, broken horn, rabid dog or jackal bite, tumor, snakebite, stings, Datura poisoning, heatstroke, miscarriage, anthrax, blisters, wounds in the mouth, tympanitis, colic, diarrhea, glossitis, indigestion, bacillosis, bloody dysentery, liver disorders, excessive urination, tetanus and asthma, and hermaphrodite [1-3].

COVID-19 is an infectious disease caused by a coronavirus. A new human coronavirus, which has been labeled SARS-CoV-2, began spreading in December 2019 in Wuhan City, China [4]. As of now until 14 April 2020, there were 1,776,867 confirmed cases, 111,828 confirmed deaths, and 213 countries, areas, or territories with cases around the world (<https://www.who.int/emergencies/diseases/novel-coronavirus-2019>). The World Health Organization declared

this disease pandemic. At present, there are no specific vaccines or treatments for COVID-19. However, many ongoing clinical trials are evaluating potential treatments (https://www.who.int/health-topics/coronavirus#tab=tab_1). Favipiravir has recently been approved for a clinical trial to treat COVID-19. Favipiravir is a purine nucleoside which disturbs viral RNA synthesis, was originally developed by Toyama Chemical of Japan [5]. Therefore, in present work, we have taken favipiravir as a reference molecule for the docking study.

METHODS

Plant material

The plant specimen was collected from Gangapur road, Nashik, Maharashtra, India. Dr. A. Benniamin's, (Scientist-C), (Botanical Survey of India, Koregaon Road, Pune), identified and authenticated the voucher specimen of the plant by comparing morphological features. Voucher specimen no. BBJ-1 (Reference number BSI/WRC/Tech./2013).

Preparation of plant material for extraction

Air-dried bark was processed for size reduction using a cutter mill (portable mixer). The crushed material was passed through #40sieves (coarse powder) for uniform particle size, which gave efficient extraction and yield of extract. The 100 g powder was filled in a Soxhlet apparatus and extracted continuously with n-hexane and methanol. The extraction was conceded until the powder becomes colorless. Then, the content of the round bottom flask was kept for the solvent recovery system which promotes the green chemistry extraction methodology. Approximately 100 ml of n-hexane and methanol were recovered by

this process. Then, the extract was subjected for concentration to get the dry extract powder [6].

Phytochemical screening of extract by chemical tests

The phytochemical investigation of the n-hexane extract of *M. calabura* was done using different standard qualitative tests [7]. The results of phytochemical screening of n-hexane extract of *M. calabura* bark for the presence of alkaloids, carbohydrates, steroids, sterol, glycoside, saponins, flavonoids, phenolic compounds, and triterpenoids are presented in Table 1.

Test for alkaloids

Extracted 0.5 g powdered sample with 2.5 ml methanol and 2.5 ml of 2N hydrochloric acid. Then, the filtrate was treated with Meyer's and Wagner's reagents. The sample was recorded negative based on turbidity and color [8].

Test for flavonoids

0.5 g of powdered extract was heated with 5 ml of ethyl acetate, a water bath (40–50°C) for 5 min. The filtrate was then treated with 0.5 ml dilute ammonia solution. A yellow coloration revealed the presence of flavonoids [8].

Test for saponins

1 g of powdered extract boiled in 10 ml of distilled water and filtered the solution. Then, 5 ml of the filtrate was mixed with 5 ml of distilled water and stirred strongly for stable insistent foam. The foaming was mixed with three drops of olive oil and shakes vigorously which forms emulsion, indicated the presence of saponins [9].

Test for glycosides

Keller–Kiliani test – 1 ml of extract was added in 1ml of glacial acetic acid. Then, 1 ml of ferric chloride was added with 1 ml of concentrated sulfuric acid. The green-blue coloration of the solution specified the presence of glycoside [10].

Test for carbohydrates

1 ml of n-hexane extract was added to 1 ml of Molisch's reagent with stirring. 1 ml of concentrated sulfuric acid was added carefully from the side of the test tube. The development of a red or violet color at the inter-phase of the two layers is symbolic of positive test which concludes the presence of carbohydrates [11].

Test for tannins

About 10% alcoholic ferric chloride solution was added in 2 ml of n-hexane extract (1:1). The development of the dark blue color of the solution indicated the presence of tannins [12].

Test for terpenoids

Salkowski test – to 2.5 ml of n-hexane extract, 2 ml of chloroform was added. Then, 2 ml of concentrated sulfuric acid was added slowly to form a layer. A reddish-brown coloration at boundary directed the presence of terpenoids [9].

Test for steroids

To 1 ml of n-hexane extract, add 2 ml acetic anhydride, and 2 ml of concentrated sulfuric acid, color changes from blue to dark green showed the existence of steroids [9].

Evaluation of extractive values

Extractive values are useful for the evaluation of crude drugs and give an idea about the nature of chemical constituents present in them. The amount of extractive a drug yields to a given solvent is often an approximate measure of a certain constituent or group of related constituents the drug contains. Extractive values after the continuous extraction of bark *M. calabura* given in Table 2.

Isolation of different constituents from extract by column chromatography

A cylinder designed glass column comprising the stationary phase (silica gel) is added slowly from the upper end with a liquid solvent (mobile phase) that runs down the column with the help of gravity. This method is used for the decontamination of compounds from a mixture. Once the column is ready, the sample was encumbered inside the top of the column. The mobile solvent is then permitted to flow down through the column. The compounds in mixture have different interactions aptitude with the stationary phase (silica gel), and the mobile phase, in that way, will flow along with the mobile phase at diverse time intervals or degrees. In this way, the separation of compounds from the mixture was achieved. The individual compounds are collected as fractions and analyzed further for structure elucidation [13].

Column chromatography was performed for the isolation of different phytoconstituents by isocratic elution method. The height of the column was 45 cm and the height of silica gel in the column was 30 cm. Benzene was used as a mobile phase. 15–20 ml of each fraction was collected in a test tube and numbered sequentially for additional analysis on thin-layer chromatography (TLC).

TLC

TLC offers partial separation of both organic and inorganic constituents using thin-layered chromatographic plates, particularly useful for testing

Table 1: The details of SARS-CoV-2 main protease (M^{pro}) used (PDB ID-6LU7)

PDB ID	6LU7
Title	The crystal structure of COVID-19 main protease in complex with an inhibitor N3
DOI	10.2210/pdb6LU7/pdb
Authors	Liu, X.; Zhang, B.; Jin, Z.; Yang, H.; Rao, Z.
Deposited on	2020-01-26
Resolution	2.16 Å (reported)
Classification	Viral protein
Organism(s)	Bat SARS-like coronavirus
Expression system	<i>Escherichia coli</i> BL21 (DE3)
Method	X-ray diffraction

Table 2: Preliminary qualitative phytochemical screening on extract of *Muntingia calabura* bark

Sr. No.	Phytochemicals	Test name	n-Hexane extract
1.	Alkaloids	Mayer's test	–
		Wagner's test	–
		Hager's test	–
		Dragendorff's test	–
2.	Flavonoids	Lead acetate test	+++
		Ferric chloride test	++
		Sodium hydroxide test	+++
		Shinoda test	+++
3.	Saponins	Foam test	–
		Hemolytic test	–
4.	Glycosides	Keller–Kiliani test	+
		Legal's test	+
5.	Carbohydrates	Molisch's test	++
		Fehlings test	++
		Benedict test	++
		d) Dilute KMnO ₄	–
6.	Tannins	Ferric chloride test	–
		Lead acetate test	–
		Potassium dichromate test	–
7.	Terpenoids	Salkowski test	+++
8.	Steroids	Salkowski test	+++
		Liebermann–Burchard reaction	+++

Where; +++: Very positive, ++: Strong positive, +: Fair positive, –: Absent

the purity of portions. Spot of each fraction was applied on activated TLC plates with the help of a capillary tube at a 1/2 inch apart from the bottom of the TLC plate, and the plate was kept in a developing chamber comprising an appropriate solvent system for the precise time until the developing solvent reaches one-fourth of the TLC plate. The plate was taken out from the developing chamber and dried. Compound spots visualized using the iodine chamber for the existence of exact compounds [14,15]. The R_f value of each spot was calculated by the formula: $R_f = \text{distance traveled by the sample (cm)}/\text{distance traveled by the solvent (cm)}$.

High performance TLC (HPTLC)

The HPTLC method is the fastest separation technique which gives better precision and accuracy.

Sample preparation

N-hexane extract was dissolved in 1ml of chromatographic grade methanol, which was used for sample application on pre-coated silica gel 60F254 aluminum sheets.

Developing solvent system

The satisfactory resolution of peaks was obtained in the solvent system toluene:ethyl acetate:formic acid (7:2:1).

Sample application

The sample application of extract was carried out (8 mm in length and 0.2 μ l in concentration for extract) using the spray technique. The sample was applied in duplicate on pre-coated silica gel 60F254 aluminum sheets (5 \times 10 cm) with the help of Linomat 5 applicator attached to the CAMAG HPTLC system.

Development of chromatogram

The chromatogram was established in Twin Trough Glass Chamber 10 \times 10 cm saturated with solvent toluene:ethyl acetate:formic acid (7:2:1) for an extract for 15 min.

Detection of spots

The air-dried plate was viewed in ultraviolet light (Fig. 1). The chromatograms were scanned by a densitometer at 360 nm for extract. The R_f values and fingerprint data were recorded by WIN CATS software.

Fourier-transform infrared (FTIR) spectroscopy

FTIR spectrophotometer is feasibly the commanding device for detecting the types of functional groups existent in the phytochemicals. The wavelength of light absorbed is the significant feature of the functional groups seen in the annotated spectrum. By interpreting the infrared spectrum, the functional groups in a compound can be determined. Dried powder of fractions collected from column chromatography of *M. calabura* bark was used for FTIR analysis. 10 mg of the dried extract powder was compressed in 100mg of KBr pellet, to prepare translucent sample discs [16-18]. The powdered sample of the extract was loaded in FTIR spectrophotometer (Shimadzu, Japan), with a scan range from 400 to 4000 cm^{-1} with a resolution of 4 cm^{-1} .

Ultraviolet (UV) visible spectroscopy

The color of the compounds directly affects the absorption and the electrons present in molecules of colored solution go through electronic transitions

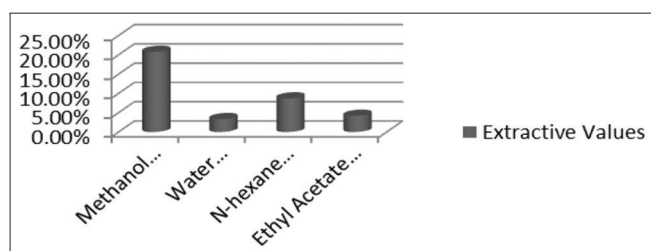


Fig. 1: Graphical presentation of extractive values

invisible ranges of the spectrum. The n-hexane extract was scanned under UV visible spectral analysis. The extract was centrifuged at 3000 rpm for 10 min and filtered through Whatman filter paper no. 1. The sample was diluted to 1:10 with the same solvent [19,20]. The extract was scanned in the wavelength ranging from 200 to 400 nm using UV spectrophotometer (Shimadzu, Japan) and the lambda max value was detected.

Molecular docking

The molecular docking was performed on Lenovo ThinkPad with a 64-bit operating system, Processor: Intel(R) Core(TM) i5-4300M CPU @2.60 GHz 2.59 GHz, RAM: 4GB using PyRx-Virtual Screening Tool.

Ligand preparation

The structures (SDF File) of β -sitosterol and approved drug (Favipiravir) were downloaded from the official website of the U.S. National Library of Medicine PubChem (<https://pubchem.ncbi.nlm.nih.gov/>). The structure then imported into PyRx 0.8 using open babel tool and energy minimization (optimization) was performed by considering fundamental parameters based on the element, its hybridization, and

Table 3: Analysis of extractive values of *Muntingia calabura* bark

Sr. No.	Evaluation parameter	Value (%)
1.	Methanol-soluble extractive value	20.8
2.	Water-soluble extractive value	3.34
3.	N-hexane soluble extractive value	8.7
4.	Ethyl acetate soluble extractive value	4.20

Table 4: Column chromatography and TLC analysis of *Muntingia calabura* bark extract

Fractions No.	Volume (mL)	Number of spots in TLC	Colour identification of spot on TLC	
			Visual	With iodine chamber
1-5	17	3	Colorless	Brown
6-15	17	2	Colorless	Brown
16-27	15	No spot	-	-
28-31	16	2	Colorless	Orange, yellowish
32-41	18	Multiple	Colorless	Orange, yellowish
42-59	20	No spot	-	-
60-75	20	4	Colorless	Yellowish-brown
76-83	18	2	Colorless	Yellowish-brown
84-115	20	1	Colorless	Yellow

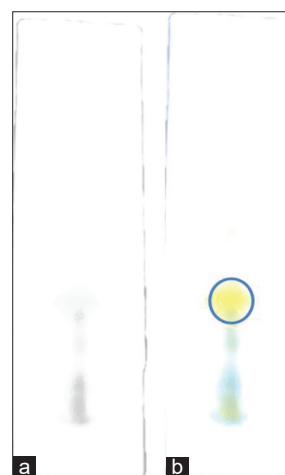


Fig. 2: Thin-layer chromatography of fraction 84-115 (a) daylight, (b) showing single spot after visualizing it in iodine chamber, R_f value=0.53

Table 5: Concern molecular docking details of the molecules

Name of compound	Molecular weight	Binding affinity (kcal/mol)	Ligand energy	No. of hydrogen bonds	Active amino acids
Favipiravir	157.1	-5.7	70.90	4	Gln127, Asp295, Phe08, Asn151, Phe112, Phe294, Thr292, Thr111, Gln110, Ile106
Beta-sitosterol	414.7	-6.9	1658.29	1	Met165, Gln189, Met49, Thr24, Thr26, Thr25, His164, His41, Leu27, Phe140, Leu141, Gly143, Asn142, Ser144, His163, Cys145, His172, Glu166

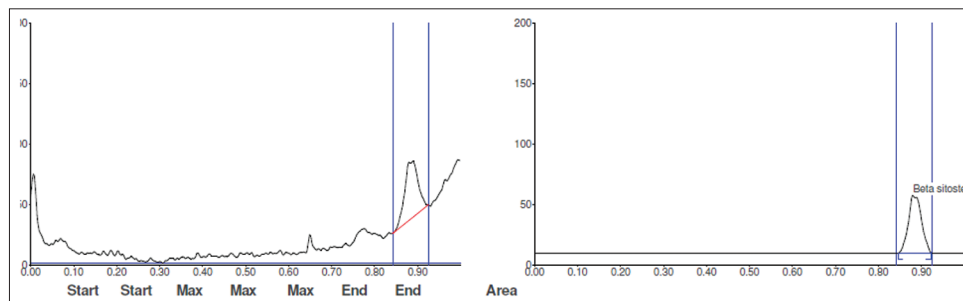
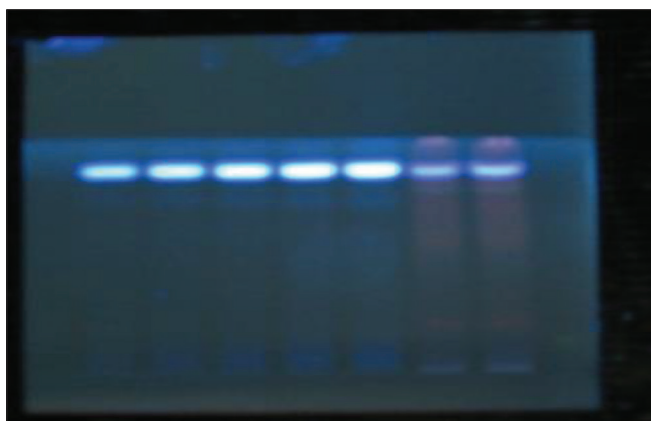


Fig. 3: High-performance thin-layer chromatography fingerprint of fraction 84-115

Fig. 4: Isolated substance: β -sitosterol at 366 nm

connectivity, i.e., by Universal Force Field [21]. This ligand was then converted to AutoDock Ligand format (PDBQT).

Target preparation

The AutoDock Vina 1.1.2 in PyRx 0.8 [22] was used to perform the docking studies of β -sitosterol and approved drug (Favipiravir) against the crystal structure of SARS-CoV-2 M^{pro}. The recently elucidated crystal structure of SARS-CoV-2 M^{pro} was obtained from the RCSB protein data bank (PDB) with PDB ID: 6LU7 (<https://www.rcsb.org/structure/6LU7>). The viral protein structure was optimized, purified, and prepared for docking with the help of Discovery Studio Visualizer 2019 [23] by removing unwanted water molecules, bound ligands from protein structure, and saved again in PDB file format to the same folder.

The details of SARS-CoV-2 main protease (M^{pro}) used (PDB ID-6LU7) are given in Table 1 obtained from PDB X-ray structure validation report which was released on 02 March 2020.

Docking procedure

The purified SARS-CoV-2 M^{pro} file was loaded to docking software PyRx 0.8 using a load molecule option from the File toolbar. Chain-A was used to perform the docking as it contains the active amino acid residues. The receptor structure then converted to AutoDock macromolecule (PDBQT format) using the right-click option. Binding affinity studies

were performed using Vina Wizard Tool in PyRx 0.8. Molecules (PDBQT Files), both ligands (β -sitosterol and favipiravir) as well as the target (SARS-CoV-2 M^{pro}) were selected for docking. For molecular docking simulation, the three-dimensional grid box (size_x=26.3786Ao; size_y=29.0004Ao; size_z=20.8096Ao) was designed using AutoDock tool 1.5.6 with exhaustiveness value of 8. After selecting molecules, the active amino acid residues were selected to define the cavity with the help of the toggle selection spheres option given in PyRx [22]. To occupy all the active binding sites and essential residues, the grid box was aligned properly. The ligands and SARS-CoV-2 M^{pro} then subjected for docking to get the finding affinity with each other.

Identification of cavity and active amino acid residues

The active amino acid residues in the protein were identified and noted using BIOVIA Discovery Studio Visualizer (version-19.1.0.18287). All the docking poses, ligand and protein interactions were studied by importing output files into discovery studio which enables us to identify the types of interactions. The chosen cavity is the binding site of natural inhibitor N3, i.e., native ligand in PDB 7LU7.

RESULTS AND DISCUSSION

Phytochemical screening

The therapeutic effects of this plant are due to the occurrence of bioactive chemical components. The preliminary qualitative phytochemical screening of the n-hexane extract of *M. calabura* bark was done to evaluate the presence of phytoconstituents. The presence of various phytoconstituents such as alkaloid, carbohydrate, glycoside, steroid, tannin, terpenoid, flavonoid, and saponins was determined. The extract showed the presence of flavonoids, carbohydrates, terpenoids, and steroids. Traces of glycosides were also found in the n-hexane extract. The phytochemical screening results are shown in Table 2.

Evaluation of extractive value

Extractive values are useful for the evaluation of crude drugs and give an idea about the nature of chemical constituents present in them. Extractive values are mostly beneficial for the determination of exhausted or adulterated drugs. The extractive value defines superiority as well as the pureness of crude drugs [24]. Thus, alcohol and water-soluble extractive values were determined. Methanol extractive value was found to be 20.8%, the water-soluble extractive value was found to be 3.34%. Fig. 1 represents the graphical data of extractive values.

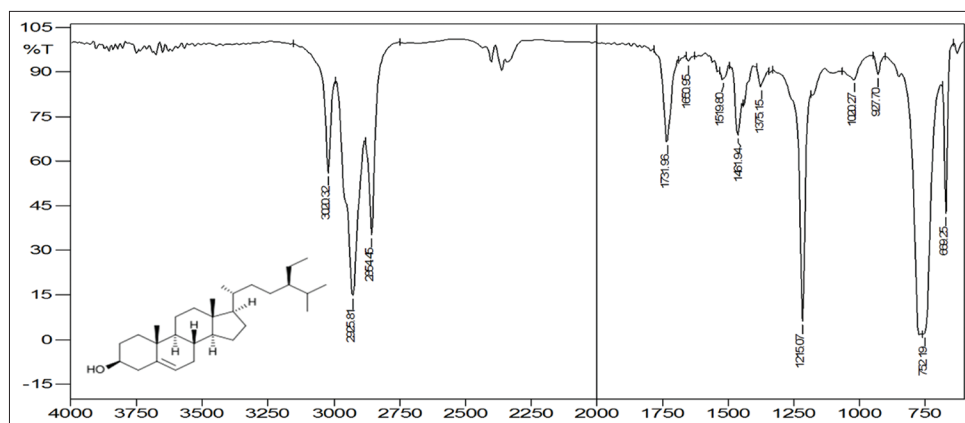


Fig. 5: Fourier-transform infrared spectrum of isolated β -sitosterol

$$\text{Extractive value (\%)} = \frac{\text{Weight of dried extract}}{\text{Weight of plant material}} \times 100$$

Extractive values after continuous extraction of *M. calabura* bark given in Table 3.

Column chromatography and TLC

A total of 115 fractions were collected from column chromatography according to the colors of bands developed in a column and each fraction was 15–20 ml in quantity. TLC was performed for each fraction to check the number of phytoconstituents present in it. TLC can explain the number of compounds present in a particular solution in the form of spots obtained after visualization. The results are presented in Table 4.

From Table 4, it can be concluded that fraction 84–115 showed a single spot on the TLC plate which indicates the presence of a single chemical component in the fraction, so further structural characterization can be done on the fraction 84–115. TLC was taken using the solvent system in a portion of polar and non-polar proportions. The solvent system used was benzene: methanol:ethyl acetate (5:4:1). After the complete run, TLC plates were visualized by iodine chamber. R_f value was found to be 0.53 (Fig. 2). From the qualitative analysis, it has been concluded that extract has steroids as phytoconstituent. After TLC, the same fraction was forwarded for HPTLC analysis and structural elucidation by UV and IR (Fig. 3).

HPTLC fingerprinting profile

The results from HPTLC fingerprint scanned at wavelength 366 nm for fraction 84–115 of *M. calabura* bark represented in Fig. 4. The HPTLC spectral results have resembled with β -sitosterol. The R_f value was found to be 0.88 at 6 μ g which exactly matches the spectral data and peak of standard β -sitosterol. Spectral results are shown in Figs. 2 and 3.

FTIR spectroscopy profile

FTIR spectrum (Fig. 5) showed that the absorption peaks resembles exactly to the functional groups present in β -sitosterol. It showed characteristic bands at 2925.81 cm^{-1} (C-H-stretching, Aliphatic), 3020.32 cm^{-1} (C=C-H-stretching), 1461.94 cm^{-1} (C-H-bending, aliphatic), 1660.96 cm^{-1} (C-C-alkene stretching), 1215.07 cm^{-1} (O-H-bend, Alcoholic), and 1020.27 cm^{-1} (C-O-stretch, alcoholic).

Ultraviolet-visible spectroscopy profile

The qualitative UV-visible profile of fraction 84–115 of *M. calabura* bark, i.e., the isolated β -sitosterol, was taken at the wavelength of 200–400 nm. The lambda max value was observed at 248 nm (Fig. 6).

Molecular docking

The β -sitosterol and favipiravir both successfully docked on SARS-CoV-2 M^{pro} to determine their binding affinity (kcal/mol), i.e., inhibitory potential. Table 5 represents the name of the compounds, molecular

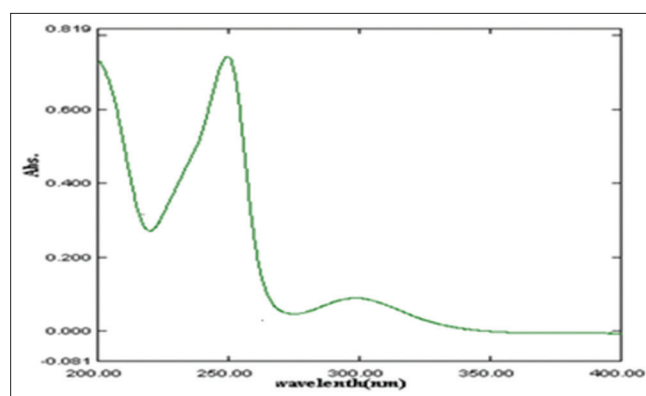


Fig. 6: Ultraviolet spectral maxima of β -sitosterol between 200 and 400 nm

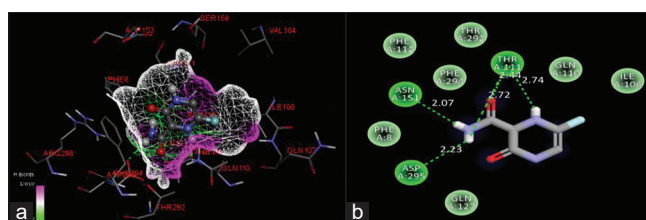


Fig. 7: (a) 3D-docking pose; (b) 2D-docking pose of favipiravir

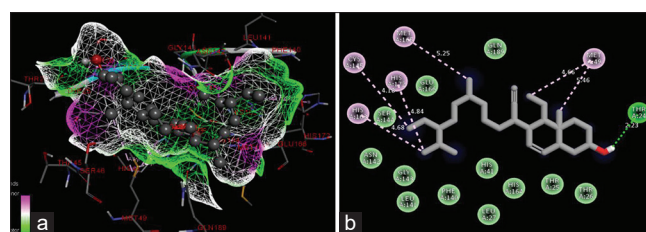


Fig. 8: (a) 3D-docking pose; (b) 2D-docking pose of β -sitosterol

weight, binding affinity (kcal/mol), ligand energy, number of hydrogen bonds formed, and active amino acid residues involved in the interaction.

From molecular docking studies, it has been observed that favipiravir has a less binding affinity, i.e., -5.7 kcal/mol than β -sitosterol which has -6.9 kcal/mol. The number of hydrogen bonds formed by the favipiravir is much more, i.e., 4 than β -sitosterol which formed only 1 hydrogen bonds with SARS-CoV-2 M^{pro} . The binding affinity of β -sitosterol may be more because it interacts with a greater number of amino acids, as shown in Table 5 and forms more van der Waals forces with the target molecule.

Figs. 7a and 8a represent the 3D-docking poses of the molecules favipiravir and β -sitosterol, respectively. Similarly, Figs. 7b and 8b represent the 2D-docking poses of the favipiravir and β -sitosterol, respectively. Favipiravir interacts with amino acids; Gln127, Asp295, Phe08, Asn151, Phe112, Phe294, Thr292, Thr111, Gln110, and Ile106. Whereas, β -sitosterol interacts with Met165, Gln189, Met49, Thr24, Thr26, Thr25, His164, His41, Leu27, Phe140, Leu141, Gly143, Asn142, Ser144, His163, Cys145, His172, and Glu166. Favipiravir forms hydrogen bonds with Asn151 (bond length=2.07Å), Asp295 (bond length=2.23Å), and two hydrogen bonds with Thr111 (bond length=2.72Å, and 2.74Å). β -sitosterol forms only one hydrogen bond with Thr24 (bond length=2.23Å). Bond length plays a very important role in the inhibition of the target enzyme or receptor. Although, more the no of hydrogen bonds formed more will be inhibition. While discussing the inhibitory activity, we have considered both binding affinity as well as the number of hydrogen bonds formed.

CONCLUSION

The results of the phytochemical analysis presented that the n-hexane extract of the *M. calabura* bark contains a variety of chemical compounds. The extract showed the presence of flavonoids, carbohydrates, terpenoids, and steroids. Traces of glycosides were also found in the n-hexane extract. The phytochemical analysis of the extract, the identification of liable biological active compounds, and quality standards are essential for the upcoming study.

This present work visualized the successful application of column chromatographic techniques for the isolation of bioactive constituents from medicinal plants. A total of 115 fractions were collected from column chromatography according to the colors of bands developed in a column and each fraction was 15–20 ml in quantity. Fraction 84–115 showed a single spot on the TLC plate which indicates the presence of a single chemical component in the fraction, so further structural characterization can be done on the fraction 84–115. HPTLC studies suggested that isolated compound was β -sitosterol which gave a characteristic peak in HPTLC profile with R_f value 0.88 at 6 μ g. Structural elucidation of isolated β -sitosterol was done using FTIR and UV-visible spectroscopy which can be set as a marker for the structural characterization of β -sitosterol, but in the future study, the advanced spectroscopic or chromatographic technique can be used to characterize the β -sitosterol. β -sitosterol is an almost non-polar compound. Therefore, n-hexane can be a better solvent to extract β -sitosterol from the plant by extraction. The overall study concludes that this method can be considered as a standard method for isolation of β -sitosterol from *M. calabura* bark.

From molecular docking studies, it has been concluded that favipiravir has a less binding affinity, i.e. -5.7 kcal/mol than β -sitosterol which has -6.9 kcal/mol. The number of hydrogen bonds formed by the favipiravir is much more, i.e. 4 than β -sitosterol which formed only 1 hydrogen bonds with SARS-CoV-2 M^{pro} . There is an alarming situation created by COVID-19 around the world. The discovery of drugs from a natural source or from repurposing drugs can be great hope in the area of this pandemic. If we develop more optimized models for β -sitosterol, it can create a potential lead to generate inhibitors of SARS-CoV-2 M^{pro} in the future. There is a need to generate more clinical quality data to use it clinically.

ACKNOWLEDGMENT

We wish to express our sincere gratitude to Principal, JES's College of Pharmacy, Nandurbar, for providing us an opportunity to do our research work.

CONTRIBUTION OF AUTHORS'

1. Rakesh N. Chaudhari: Performed all the experimental work related to Pharmacognostic study
2. Sharuk L. Khan: Performed molecular docking studies and manuscript writing
3. Ravindra S. Chaudhary: Provided all the necessary facility required to performed lab work
4. Shirish P. Jain: Final review and validation of the data

5. Falak A. Siddiqui: Compiled the Literature source and data analysis related to Molecular docking.

CONFLICTS OF INTEREST

The authors have no conflicts of interest.

FUNDING

There was no funding source.

REFERENCES

1. Singh R, Iye S, Prasad S, Deshmukh N, Gupta U, Zanje A, et al. Phytochemical analysis of muntingia calabura extracts possessing antimicrobial and anti-fouling activities. *Int J Pharmacogn Phytochem Res*2017;9:826-32.
2. Mahmood ND. *Muntingia calabura*: A review of its traditional uses, chemical properties, and pharmacological observations. *Pharm Biol*2014;52:1598-623.
3. Sibi G, Naveen R, Dhananjaya K, Ravikumar KR, Mallesha H. Potential use of *Muntingia calabura* L. Extracts against human and plant pathogens. *Pharmacogn J*2012;4:44-7.
4. Wang LS, Wang YR, Ye DW, Liu QQ. A review of the 2019 novel coronavirus (COVID-19) based on current evidence. *Int J Antimicrob Agents*2020; DOI: 10.1016/j.ijantimicag.2020.105948.
5. Liu C, Zhou Q, Li Y, Garner LV, Watkins SP, Carter LJ, et al. Research and development on therapeutic agents and vaccines for COVID-19 and related human coronavirus diseases. *ACS Cent Sci*2020;6:315-31.
6. Tambe R, Kulkarni M, Bhise K. Preliminary phytochemical screening and HPTLC fingerprinting of bark extracts of *Symplocos racemosa*. *J Pharmacogn Phytochem*2013;2:45-9.
7. World Health Organization. *Quality Control Methods for Medicinal Plant Materials*. Geneva: World Health Organization; 1989. p. 1-15.
8. Harborne JB. *Phytochemical Methods: A Guide to Modern Techniques of Plant Analysis*. Berlin, Germany: Springer; 1973.
9. Edeoga HO, Okwu DE, Mbaebie BO. Phytochemical constituents of some Nigerian medicinal plants. *Afr J Biotechnol*2005;4:685-8.
10. Parekh J, Chanda SV. *In vitro* antimicrobial activity and phytochemical analysis of some Indian medicinal plants. *Turk J Biol*2007;31:53-8.
11. Sofowora A. Research on medicinal plants and traditional medicine in Africa. *J Altern Complement Med*1996;2:365-72.
12. Kumar GS, Jayaveera KN, Kumar CK, Umachigi P, Swamy BM, Kumar DV. Antimicrobial effects of Indian medicinal plants against acne-inducing *Bacteria*. *Trop J Pharm Res*2007;6:717-23.
13. Bajpai VK, Majumder R, Park JG. Isolation and purification of plant secondary metabolites using column-chromatographic technique. *Bangladesh J Pharmacol*2016;11:844-8.
14. Jaber BM, Jasim SF. Phytochemical study of stigmaterol and β -sitosterol in *Viola odorata* plant cultivated in Iraq. *Iraqi J Biotechnol*2014;13:86-94.
15. Ahmad H, Sehgal S, Mishra A, Gupta R, Saraf SA. TLC detection of β -sitosterol in *Michelia champaca* L. Leaves and stem bark and its determination by HPTLC. *Pharmacogn J*2012;4:45-55.
16. Visveshwari M, Subbaiyan B, Thangapandian V. Phytochemical analysis, antibacterial activity, FTIR and GCMS analysis of *Ceropegia juncea* Roxb. *Int J Pharmacogn Phytochem Res*2017;9:914-20.
17. Rajiv P, Deepa A, Vanathi P, Vidhya D. Screening for phytochemicals and ftr analysis of *Myristica dactyloids* fruit extracts. *Int J Pharm Pharm Sci*2017;9:1-4.
18. Dharmalingam V. Phytochemical screening by FTIR spectroscopic analysis of leaf and stem extracts of *Wedelia biflora*. *Int J Nano Corros Sci Eng*2015;2:322-34.
19. Article O, Dhivya SM, Kalaichelvi K. UV-visible spectroscopic and ftr analysis of *Sarcostemma brevistigma*. *Int J Curr Pharm Res*2017;9:46-9.
20. Jain PK, Soni A, Jain P, Bhawsar J. Phytochemical analysis of *Mentha spicata* plant extract using UV-VIS, FTIR and GC/MS technique. *J Chem Pharm Res*2016;8:1-6.
21. SkiffAK, RappeCJ, CasewitKS, ColwellWA. Goddard III WMS. UFF, a full periodic table force field for molecular mechanics and molecular dynamics simulations. *J Am Chem Soc*2009;114:10024-35.
22. Dallakyan S, Olson AJ. Small-molecule library screening by docking with PyRx. *Methods Mol Biol*2015;1263:243-50.
23. Dassault Systèmes BIOVIA. *Discovery Studio Modeling Environment*. San Diego: Dassault SystèmesBIOVIA; 2016.
24. Chaudhari RK, Girase NO. Determination of soluble extractives and physico-chemical studies of bark of *Sesbania sesban* (L) Merr. *J Chem Pharm Res*2015;7:657-60.

B-SITOSTEROL: ISOLATION FROM *MUNTINGIA CALABURA* LINN. BARK EXTRACT, STRUCTURAL ELUCIDATION, AND MOLECULAR DOCKING STUDIES AS POTENTIAL INHIBITOR OF SARS-COV-2 M^{PRO} (COVID-19)

RAKESH N CHAUDHARI¹, SHARUK L.KHAN^{2*}, RAVINDRA S CHAUDHARY¹, SHIRISH P JAIN², FALAK A SIDDUQUI²

¹Department of Pharmacognosy, JES's College of Pharmacy, Nandurbar, Maharashtra, India. ²Department of Pharmaceutical Chemistry, Rajarshi Shahu College of Pharmacy, Buldana, Maharashtra, India. Email: sharique.4u4@gmail.com

Received: 18 March 2020, Revised and Accepted: 20 April 2020

ABSTRACT

Objective: A novel human coronavirus, labeled as SARS-CoV-2 (COVID-19), causing pneumonia is spreading around the world. At present, there are no specific treatments for COVID-19. β -sitosterol is well known for its multiple biological actions. This research aims to isolate and study the binding affinity of β -sitosterol for SARS-CoV-2 (COVID-19) main protease (M^{PRO}).

Methods: Extraction and column chromatography was performed to isolate the β -sitosterol from an n-hexane extract of *Muntingia calabura* bark followed by thin-layer chromatography (TLC), high-performance TLC (HPTLC), Fourier-transform infrared (FTIR), and ultraviolet-visible spectroscopy. The molecular docking studies were performed on SARS-CoV-2 M^{PRO} to determine the binding affinity of the β -sitosterol using PyRx Virtual Screening Tool.

Results: In the present study, preliminary phytochemical screening showed the presence of carbohydrate, steroid, terpenoid, and flavonoid compounds. A total of 115 fractions was collected from column chromatography using benzene as a solvent by an isocratic elution technique. HPTLC fingerprinting analysis showed the presence of β -sitosterol under 366 nm. FTIR characterization was performed of the same fraction which gives the absorption peaks which resembles the β -sitosterol structure.

Conclusion: The overall study concludes this method can be considered as a standard method for isolation of β -sitosterol from *M. calabura* bark. Favipiravir has a less binding affinity, i.e. -5.7 kcal/mol than β -sitosterol which has -6.9 kcal/mol. The number of hydrogen bonds formed by the favipiravir is much more, i.e., 4 than β -sitosterol which formed only 01 hydrogen bonds with SARS-CoV-2 M^{PRO}.

Keywords: *Muntingia calabura*, β -sitosterol, SARS-CoV-2 (COVID-19), Molecular docking, High-performance thin-layer chromatography.

© 2020 The Authors. Published by Innovare Academic Sciences Pvt Ltd. This is an open access article under the CC BY license (<http://creativecommons.org/licenses/by/4.0/>) DOI: <http://dx.doi.org/10.22159/ajpcr.2020.v13i5.37909>

INTRODUCTION

Muntingia calabura, also known as cherry, it has been an essential herb in the Ayurvedic and indigenous medical systems for over 4000 years. Belong to genus *Muntingia* which contains about 30 species of tropical fruiting trees in the flowering plant family Tiliaceae. *M. calabura* (Muntingiaceae) grows in the tropical and subtropical regions and its parts are used commonly in folk medicine for a varied variety of conditions. According to Ayurveda, varied medicinal properties are attributed to different parts of the mango tree. Cherry is one of the most popular of all tropical fruits. Various parts of the plant are used as a dentifrice, antiseptic, astringent, diaphoretic, stomachic, vermifuge, tonic, laxative, and diuretic and to treat diarrhea, dysentery, anemia, asthma, bronchitis, cough, hypertension, insomnia, rheumatism, toothache, leucorrhoea, hemorrhage, and piles. All parts are used to treat abscesses, broken horn, rabid dog or jackal bite, tumor, snakebite, stings, Datura poisoning, heatstroke, miscarriage, anthrax, blisters, wounds in the mouth, tympanitis, colic, diarrhea, glossitis, indigestion, bacillosis, bloody dysentery, liver disorders, excessive urination, tetanus and asthma, and hermaphrodite [1-3].

COVID-19 is an infectious disease caused by a coronavirus. A new human coronavirus, which has been labeled SARS-CoV-2, began spreading in December 2019 in Wuhan City, China [4]. As of now until 14 April 2020, there were 1,776,867 confirmed cases, 111,828 confirmed deaths, and 213 countries, areas, or territories with cases around the world (<https://www.who.int/emergencies/diseases/novel-coronavirus-2019>). The World Health Organization declared

this disease pandemic. At present, there are no specific vaccines or treatments for COVID-19. However, many ongoing clinical trials are evaluating potential treatments (https://www.who.int/health-topics/coronavirus#tab=tab_1). Favipiravir has recently been approved for a clinical trial to treat COVID-19. Favipiravir is a purine nucleoside which disturbs viral RNA synthesis, was originally developed by Toyama Chemical of Japan [5]. Therefore, in present work, we have taken favipiravir as a reference molecule for the docking study.

METHODS

Plant material

The plant specimen was collected from Gangapur road, Nashik, Maharashtra, India. Dr. A. Benniamin's, (Scientist-C), (Botanical Survey of India, Koregaon Road, Pune), identified and authenticated the voucher specimen of the plant by comparing morphological features. Voucher specimen no. BBJ-1 (Reference number BSI/WRC/Tech./2013).

Preparation of plant material for extraction

Air-dried bark was processed for size reduction using a cutter mill (portable mixer). The crushed material was passed through #40 sieves (coarse powder) for uniform particle size, which gave efficient extraction and yield of extract. The 100 g powder was filled in a Soxhlet apparatus and extracted continuously with n-hexane and methanol. The extraction was conceded until the powder becomes colorless. Then, the content of the round bottom flask was kept for the solvent recovery system which promotes the green chemistry extraction methodology. Approximately 100 ml of n-hexane and methanol were recovered by

this process. Then, the extract was subjected for concentration to get the dry extract powder [6].

Phytochemical screening of extract by chemical tests

The phytochemical investigation of the n-hexane extract of *M. calabura* was done using different standard qualitative tests [7]. The results of phytochemical screening of n-hexane extract of *M. calabura* bark for the presence of alkaloids, carbohydrates, steroids, sterol, glycoside, saponins, flavonoids, phenolic compounds, and triterpenoids are presented in Table 1.

Test for alkaloids

Extracted 0.5 g powdered sample with 2.5 ml methanol and 2.5 ml of 2N hydrochloric acid. Then, the filtrate was treated with Meyer's and Wagner's reagents. The sample was recorded negative based on turbidity and color [8].

Test for flavonoids

0.5 g of powdered extract was heated with 5 ml of ethyl acetate, a water bath (40–50°C) for 5 min. The filtrate was then treated with 0.5 ml dilute ammonia solution. A yellow coloration revealed the presence of flavonoids [8].

Test for saponins

1 g of powdered extract boiled in 10 ml of distilled water and filtered the solution. Then, 5 ml of the filtrate was mixed with 5 ml of distilled water and stirred strongly for stable insistent foam. The foaming was mixed with three drops of olive oil and shakes vigorously which forms emulsion, indicated the presence of saponins [9].

Test for glycosides

Keller–Kiliani test – 1 ml of extract was added in 1ml of glacial acetic acid. Then, 1 ml of ferric chloride was added with 1 ml of concentrated sulfuric acid. The green-blue coloration of the solution specified the presence of glycoside [10].

Test for carbohydrates

1 ml of n-hexane extract was added to 1 ml of Molisch's reagent with stirring. 1 ml of concentrated sulfuric acid was added carefully from the side of the test tube. The development of a red or violet color at the inter-phase of the two layers is symbolic of positive test which concludes the presence of carbohydrates [11].

Test for tannins

About 10% alcoholic ferric chloride solution was added in 2 ml of n-hexane extract (1:1). The development of the dark blue color of the solution indicated the presence of tannins [12].

Test for terpenoids

Salkowski test – to 2.5 ml of n-hexane extract, 2 ml of chloroform was added. Then, 2 ml of concentrated sulfuric acid was added slowly to form a layer. A reddish-brown coloration at boundary directed the presence of terpenoids [9].

Test for steroids

To 1 ml of n-hexane extract, add 2 ml acetic anhydride, and 2 ml of concentrated sulfuric acid, color changes from blue to dark green showed the existence of steroids [9].

Evaluation of extractive values

Extractive values are useful for the evaluation of crude drugs and give an idea about the nature of chemical constituents present in them. The amount of extractive a drug yields to a given solvent is often an approximate measure of a certain constituent or group of related constituents the drug contains. Extractive values after the continuous extraction of bark *M. calabura* given in Table 2.

Isolation of different constituents from extract by column chromatography

A cylinder designed glass column comprising the stationary phase (silica gel) is added slowly from the upper end with a liquid solvent (mobile phase) that runs down the column with the help of gravity. This method is used for the decontamination of compounds from a mixture. Once the column is ready, the sample was encumbered inside the top of the column. The mobile solvent is then permitted to flow down through the column. The compounds in mixture have different interactions aptitude with the stationary phase (silica gel), and the mobile phase, in that way, will flow along with the mobile phase at diverse time intervals or degrees. In this way, the separation of compounds from the mixture was achieved. The individual compounds are collected as fractions and analyzed further for structure elucidation [13].

Column chromatography was performed for the isolation of different phytoconstituents by isocratic elution method. The height of the column was 45 cm and the height of silica gel in the column was 30 cm. Benzene was used as a mobile phase. 15–20 ml of each fraction was collected in a test tube and numbered sequentially for additional analysis on thin-layer chromatography (TLC).

TLC

TLC offers partial separation of both organic and inorganic constituents using thin-layered chromatographic plates, particularly useful for testing

Table 1: The details of SARS-CoV-2 main protease (M^{pro}) used (PDB ID-6LU7)

PDB ID	6LU7
Title	The crystal structure of COVID-19 main protease in complex with an inhibitor N3
DOI	10.2210/pdb6LU7/pdb
Authors	Liu, X.; Zhang, B.; Jin, Z.; Yang, H.; Rao, Z.
Deposited on	2020-01-26
Resolution	2.16 Å (reported)
Classification	Viral protein
Organism(s)	Bat SARS-like coronavirus
Expression system	<i>Escherichia coli</i> BL21 (DE3)
Method	X-ray diffraction

Table 2: Preliminary qualitative phytochemical screening on extract of *Muntingia calabura* bark

Sr. No.	Phytochemicals	Test name	n-Hexane extract
1.	Alkaloids	Mayer's test	–
		Wagner's test	–
		Hager's test	–
		Dragendorff's test	–
2.	Flavonoids	Lead acetate test	+++
		Ferric chloride test	++
		Sodium hydroxide test	+++
		Shinoda test	+++
3.	Saponins	Foam test	–
		Hemolytic test	–
4.	Glycosides	Keller–Kiliani test	+
		Legal's test	+
5.	Carbohydrates	Molisch's test	++
		Fehlings test	++
		Benedict test	++
		d) Dilute KMnO ₄	–
6.	Tannins	Ferric chloride test	–
		Lead acetate test	–
		Potassium dichromate test	–
7.	Terpenoids	Salkowski test	+++
		Liebermann–Burchard reaction	+++

Where; +++: Very positive, ++: Strong positive, +: Fair positive, –: Absent

the purity of portions. Spot of each fraction was applied on activated TLC plates with the help of a capillary tube at a 1/2 inch apart from the bottom of the TLC plate, and the plate was kept in a developing chamber comprising an appropriate solvent system for the precise time until the developing solvent reaches one-fourth of the TLC plate. The plate was taken out from the developing chamber and dried. Compound spots visualized using the iodine chamber for the existence of exact compounds [14,15]. The R_f value of each spot was calculated by the formula: $R_f = \text{distance traveled by the sample (cm)}/\text{distance traveled by the solvent (cm)}$.

High performance TLC (HPTLC)

The HPTLC method is the fastest separation technique which gives better precision and accuracy.

Sample preparation

N-hexane extract was dissolved in 1ml of chromatographic grade methanol, which was used for sample application on pre-coated silica gel 60F254 aluminum sheets.

Developing solvent system

The satisfactory resolution of peaks was obtained in the solvent system toluene:ethyl acetate:formic acid (7:2:1).

Sample application

The sample application of extract was carried out (8 mm in length and 0.2 μ l in concentration for extract) using the spray technique. The sample was applied in duplicate on pre-coated silica gel 60F254 aluminum sheets (5 \times 10 cm) with the help of Linomat 5 applicator attached to the CAMAG HPTLC system.

Development of chromatogram

The chromatogram was established in Twin Trough Glass Chamber 10 \times 10 cm saturated with solvent toluene:ethyl acetate:formic acid (7:2:1) for an extract for 15 min.

Detection of spots

The air-dried plate was viewed in ultraviolet light (Fig. 1). The chromatograms were scanned by a densitometer at 360 nm for extract. The R_f values and fingerprint data were recorded by WIN CATS software.

Fourier-transform infrared (FTIR) spectroscopy

FTIR spectrophotometer is feasibly the commanding device for detecting the types of functional groups existent in the phytochemicals. The wavelength of light absorbed is the significant feature of the functional groups seen in the annotated spectrum. By interpreting the infrared spectrum, the functional groups in a compound can be determined. Dried powder of fractions collected from column chromatography of *M. calabura* bark was used for FTIR analysis. 10 mg of the dried extract powder was compressed in 100mg of KBr pellet, to prepare translucent sample discs [16-18]. The powdered sample of the extract was loaded in FTIR spectrophotometer (Shimadzu, Japan), with a scan range from 400 to 4000 cm^{-1} with a resolution of 4 cm^{-1} .

Ultraviolet (UV) visible spectroscopy

The color of the compounds directly affects the absorption and the electrons present in molecules of colored solution go through electronic transitions

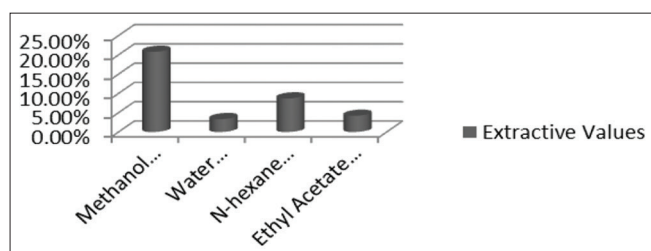


Fig. 1: Graphical presentation of extractive values

invisible ranges of the spectrum. The n-hexane extract was scanned under UV visible spectral analysis. The extract was centrifuged at 3000 rpm for 10 min and filtered through Whatman filter paper no. 1. The sample was diluted to 1:10 with the same solvent [19,20]. The extract was scanned in the wavelength ranging from 200 to 400 nm using UV spectrophotometer (Shimadzu, Japan) and the lambda max value was detected.

Molecular docking

The molecular docking was performed on Lenovo ThinkPad with a 64-bit operating system, Processor: Intel(R) Core(TM) i5-4300M CPU @2.60 GHz 2.59 GHz, RAM: 4GB using PyRx-Virtual Screening Tool.

Ligand preparation

The structures (SDF File) of β -sitosterol and approved drug (Favipiravir) were downloaded from the official website of the U.S. National Library of Medicine PubChem (<https://pubchem.ncbi.nlm.nih.gov/>). The structure then imported into PyRx 0.8 using open babel tool and energy minimization (optimization) was performed by considering fundamental parameters based on the element, its hybridization, and

Table 3: Analysis of extractive values of *Muntingia calabura* bark

Sr. No.	Evaluation parameter	Value (%)
1.	Methanol-soluble extractive value	20.8
2.	Water-soluble extractive value	3.34
3.	N-hexane soluble extractive value	8.7
4.	Ethyl acetate soluble extractive value	4.20

Table 4: Column chromatography and TLC analysis of *Muntingia calabura* bark extract

Fractions No.	Volume (mL)	Number of spots in TLC	Colour identification of spot on TLC	
			Visual	With iodine chamber
1-5	17	3	Colorless	Brown
6-15	17	2	Colorless	Brown
16-27	15	No spot	-	-
28-31	16	2	Colorless	Orange, yellowish
32-41	18	Multiple	Colorless	Orange, yellowish
42-59	20	No spot	-	-
60-75	20	4	Colorless	Yellowish-brown
76-83	18	2	Colorless	Yellowish-brown
84-115	20	1	Colorless	Yellow

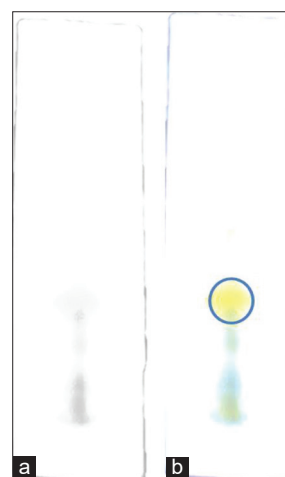


Fig. 2: Thin-layer chromatography of fraction 84-115 (a) daylight, (b) showing single spot after visualizing it in iodine chamber, R_f value=0.53

Table 5: Concern molecular docking details of the molecules

Name of compound	Molecular weight	Binding affinity (kcal/mol)	Ligand energy	No. of hydrogen bonds	Active amino acids
Favipiravir	157.1	-5.7	70.90	4	Gln127, Asp295, Phe08, Asn151, Phe112, Phe294, Thr292, Thr111, Gln110, Ile106
Beta-sitosterol	414.7	-6.9	1658.29	1	Met165, Gln189, Met49, Thr24, Thr26, Thr25, His164, His41, Leu27, Phe140, Leu141, Gly143, Asn142, Ser144, His163, Cys145, His172, Glu166

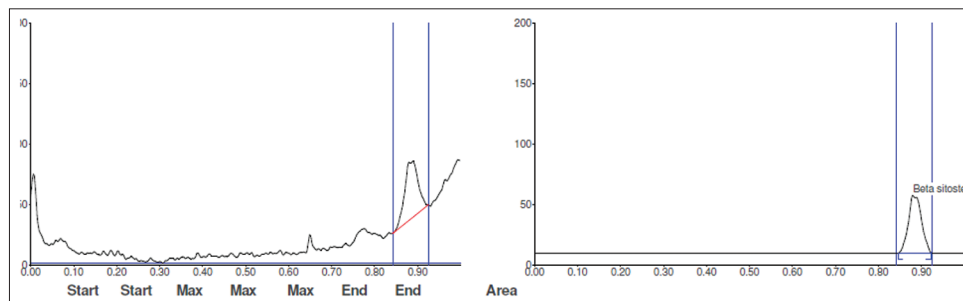
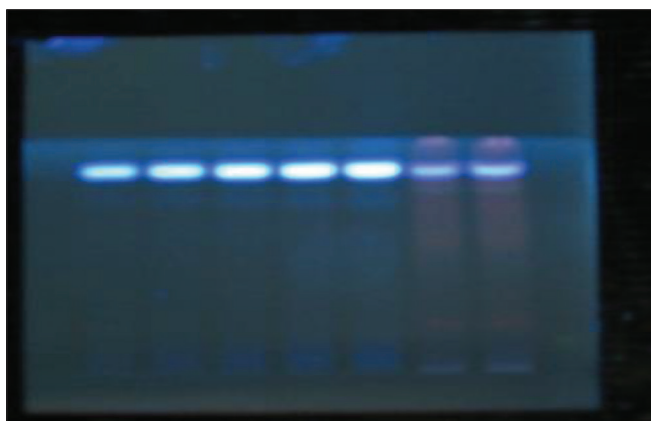


Fig. 3: High-performance thin-layer chromatography fingerprint of fraction 84-115

Fig. 4: Isolated substance: β -sitosterol at 366 nm

connectivity, i.e., by Universal Force Field [21]. This ligand was then converted to AutoDock Ligand format (PDBQT).

Target preparation

The AutoDock Vina 1.1.2 in PyRx 0.8 [22] was used to perform the docking studies of β -sitosterol and approved drug (Favipiravir) against the crystal structure of SARS-CoV-2 M^{pro}. The recently elucidated crystal structure of SARS-CoV-2 M^{pro} was obtained from the RCSB protein data bank (PDB) with PDB ID: 6LU7 (<https://www.rcsb.org/structure/6LU7>). The viral protein structure was optimized, purified, and prepared for docking with the help of Discovery Studio Visualizer 2019 [23] by removing unwanted water molecules, bound ligands from protein structure, and saved again in PDB file format to the same folder.

The details of SARS-CoV-2 main protease (M^{pro}) used (PDB ID-6LU7) are given in Table 1 obtained from PDB X-ray structure validation report which was released on 02 March 2020.

Docking procedure

The purified SARS-CoV-2 M^{pro} file was loaded to docking software PyRx 0.8 using a load molecule option from the File toolbar. Chain-A was used to perform the docking as it contains the active amino acid residues. The receptor structure then converted to AutoDock macromolecule (PDBQT format) using the right-click option. Binding affinity studies

were performed using Vina Wizard Tool in PyRx 0.8. Molecules (PDBQT Files), both ligands (β -sitosterol and favipiravir) as well as the target (SARS-CoV-2 M^{pro}) were selected for docking. For molecular docking simulation, the three-dimensional grid box (size_x=26.3786Ao; size_y=29.0004Ao; size_z=20.8096Ao) was designed using AutoDock tool 1.5.6 with exhaustiveness value of 8. After selecting molecules, the active amino acid residues were selected to define the cavity with the help of the toggle selection spheres option given in PyRx [22]. To occupy all the active binding sites and essential residues, the grid box was aligned properly. The ligands and SARS-CoV-2 M^{pro} then subjected for docking to get the finding affinity with each other.

Identification of cavity and active amino acid residues

The active amino acid residues in the protein were identified and noted using BIOVIA Discovery Studio Visualizer (version-19.1.0.18287). All the docking poses, ligand and protein interactions were studied by importing output files into discovery studio which enables us to identify the types of interactions. The chosen cavity is the binding site of natural inhibitor N3, i.e., native ligand in PDB 7LU7.

RESULTS AND DISCUSSION

Phytochemical screening

The therapeutic effects of this plant are due to the occurrence of bioactive chemical components. The preliminary qualitative phytochemical screening of the n-hexane extract of *M. calabura* bark was done to evaluate the presence of phytoconstituents. The presence of various phytoconstituents such as alkaloid, carbohydrate, glycoside, steroid, tannin, terpenoid, flavonoid, and saponins was determined. The extract showed the presence of flavonoids, carbohydrates, terpenoids, and steroids. Traces of glycosides were also found in the n-hexane extract. The phytochemical screening results are shown in Table 2.

Evaluation of extractive value

Extractive values are useful for the evaluation of crude drugs and give an idea about the nature of chemical constituents present in them. Extractive values are mostly beneficial for the determination of exhausted or adulterated drugs. The extractive value defines superiority as well as the pureness of crude drugs [24]. Thus, alcohol and water-soluble extractive values were determined. Methanol extractive value was found to be 20.8%, the water-soluble extractive value was found to be 3.34%. Fig. 1 represents the graphical data of extractive values.

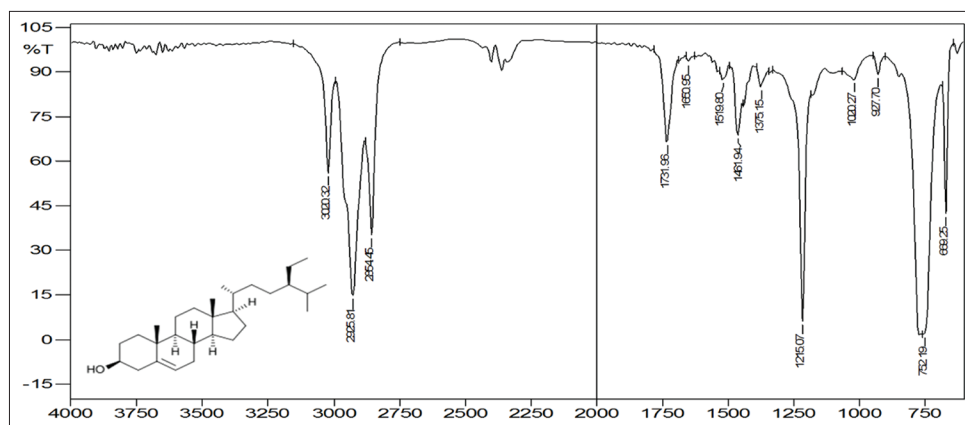


Fig. 5: Fourier-transform infrared spectrum of isolated β -sitosterol

$$\text{Extractive value (\%)} = \frac{\text{Weight of dried extract}}{\text{Weight of plant material}} \times 100$$

Extractive values after continuous extraction of *M. calabura* bark given in Table 3.

Column chromatography and TLC

A total of 115 fractions were collected from column chromatography according to the colors of bands developed in a column and each fraction was 15–20 ml in quantity. TLC was performed for each fraction to check the number of phytoconstituents present in it. TLC can explain the number of compounds present in a particular solution in the form of spots obtained after visualization. The results are presented in Table 4.

From Table 4, it can be concluded that fraction 84–115 showed a single spot on the TLC plate which indicates the presence of a single chemical component in the fraction, so further structural characterization can be done on the fraction 84–115. TLC was taken using the solvent system in a portion of polar and non-polar proportions. The solvent system used was benzene: methanol:ethyl acetate (5:4:1). After the complete run, TLC plates were visualized by iodine chamber. R_f value was found to be 0.53 (Fig. 2). From the qualitative analysis, it has been concluded that extract has steroids as phytoconstituent. After TLC, the same fraction was forwarded for HPTLC analysis and structural elucidation by UV and IR (Fig. 3).

HPTLC fingerprinting profile

The results from HPTLC fingerprint scanned at wavelength 366 nm for fraction 84–115 of *M. calabura* bark represented in Fig. 4. The HPTLC spectral results have resembled with β -sitosterol. The R_f value was found to be 0.88 at 6 μ g which exactly matches the spectral data and peak of standard β -sitosterol. Spectral results are shown in Figs. 2 and 3.

FTIR spectroscopy profile

FTIR spectrum (Fig. 5) showed that the absorption peaks resembles exactly to the functional groups present in β -sitosterol. It showed characteristic bands at 2925.81 cm^{-1} (C-H-stretching, Aliphatic), 3020.32 cm^{-1} (C=C-H-stretching), 1461.94 cm^{-1} (C-H-bending, aliphatic), 1660.96 cm^{-1} (C-C-alkene stretching), 1215.07 cm^{-1} (O-H-bend, Alcoholic), and 1020.27 cm^{-1} (C-O-stretch, alcoholic).

Ultraviolet-visible spectroscopy profile

The qualitative UV-visible profile of fraction 84–115 of *M. calabura* bark, i.e., the isolated β -sitosterol, was taken at the wavelength of 200–400 nm. The lambda max value was observed at 248 nm (Fig. 6).

Molecular docking

The β -sitosterol and favipiravir both successfully docked on SARS-CoV-2 M^{pro} to determine their binding affinity (kcal/mol), i.e., inhibitory potential. Table 5 represents the name of the compounds, molecular

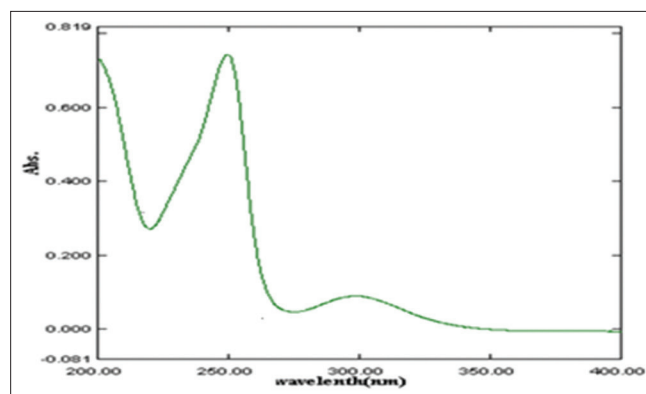


Fig. 6: Ultraviolet spectral maxima of β -sitosterol between 200 and 400 nm

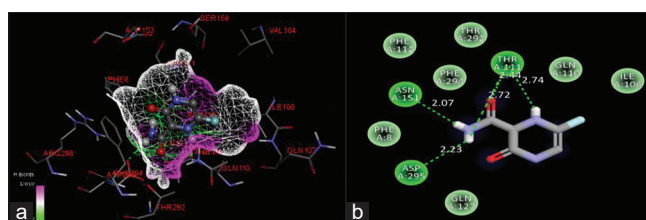


Fig. 7: (a) 3D-docking pose; (b) 2D-docking pose of favipiravir

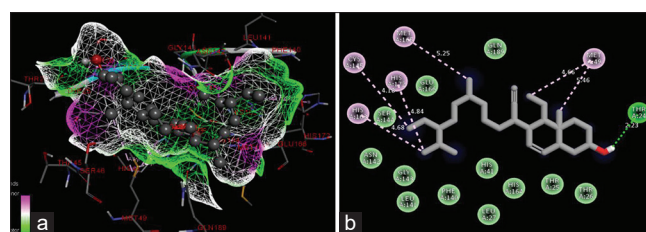


Fig. 8: (a) 3D-docking pose; (b) 2D-docking pose of β -sitosterol

weight, binding affinity (kcal/mol), ligand energy, number of hydrogen bonds formed, and active amino acid residues involved in the interaction.

From molecular docking studies, it has been observed that favipiravir has a less binding affinity, i.e., -5.7 kcal/mol than β -sitosterol which has -6.9 kcal/mol. The number of hydrogen bonds formed by the favipiravir is much more, i.e., 4 than β -sitosterol which formed only 1 hydrogen bonds with SARS-CoV-2 M^{pro} . The binding affinity of β -sitosterol may be more because it interacts with a greater number of amino acids, as shown in Table 5 and forms more van der Waals forces with the target molecule.

Figs. 7a and 8a represent the 3D-docking poses of the molecules favipiravir and β -sitosterol, respectively. Similarly, Figs. 7b and 8b represent the 2D-docking poses of the favipiravir and β -sitosterol, respectively. Favipiravir interacts with amino acids; Gln127, Asp295, Phe08, Asn151, Phe112, Phe294, Thr292, Thr111, Gln110, and Ile106. Whereas, β -sitosterol interacts with Met165, Gln189, Met49, Thr24, Thr26, Thr25, His164, His41, Leu27, Phe140, Leu141, Gly143, Asn142, Ser144, His163, Cys145, His172, and Glu166. Favipiravir forms hydrogen bonds with Asn151 (bond length=2.07Å), Asp295 (bond length=2.23Å), and two hydrogen bonds with Thr111 (bond length=2.72Å, and 2.74Å). β -sitosterol forms only one hydrogen bond with Thr24 (bond length=2.23Å). Bond length plays a very important role in the inhibition of the target enzyme or receptor. Although, more the no of hydrogen bonds formed more will be inhibition. While discussing the inhibitory activity, we have considered both binding affinity as well as the number of hydrogen bonds formed.

CONCLUSION

The results of the phytochemical analysis presented that the n-hexane extract of the *M. calabura* bark contains a variety of chemical compounds. The extract showed the presence of flavonoids, carbohydrates, terpenoids, and steroids. Traces of glycosides were also found in the n-hexane extract. The phytochemical analysis of the extract, the identification of liable biological active compounds, and quality standards are essential for the upcoming study.

This present work visualized the successful application of column chromatographic techniques for the isolation of bioactive constituents from medicinal plants. A total of 115 fractions were collected from column chromatography according to the colors of bands developed in a column and each fraction was 15–20 ml in quantity. Fraction 84–115 showed a single spot on the TLC plate which indicates the presence of a single chemical component in the fraction, so further structural characterization can be done on the fraction 84–115. HPTLC studies suggested that isolated compound was β -sitosterol which gave a characteristic peak in HPTLC profile with R_f value 0.88 at 6 μ g. Structural elucidation of isolated β -sitosterol was done using FTIR and UV-visible spectroscopy which can be set as a marker for the structural characterization of β -sitosterol, but in the future study, the advanced spectroscopic or chromatographic technique can be used to characterize the β -sitosterol. β -sitosterol is an almost non-polar compound. Therefore, n-hexane can be a better solvent to extract β -sitosterol from the plant by extraction. The overall study concludes that this method can be considered as a standard method for isolation of β -sitosterol from *M. calabura* bark.

From molecular docking studies, it has been concluded that favipiravir has a less binding affinity, i.e. -5.7 kcal/mol than β -sitosterol which has -6.9 kcal/mol. The number of hydrogen bonds formed by the favipiravir is much more, i.e. 4 than β -sitosterol which formed only 1 hydrogen bonds with SARS-CoV-2 M^{pro} . There is an alarming situation created by COVID-19 around the world. The discovery of drugs from a natural source or from repurposing drugs can be great hope in the area of this pandemic. If we develop more optimized models for β -sitosterol, it can create a potential lead to generate inhibitors of SARS-CoV-2 M^{pro} in the future. There is a need to generate more clinical quality data to use it clinically.

ACKNOWLEDGMENT

We wish to express our sincere gratitude to Principal, JES's College of Pharmacy, Nandurbar, for providing us an opportunity to do our research work.

CONTRIBUTION OF AUTHORS'

1. Rakesh N. Chaudhari: Performed all the experimental work related to Pharmacognostic study
2. Sharuk L. Khan: Performed molecular docking studies and manuscript writing
3. Ravindra S. Chaudhary: Provided all the necessary facility required to performed lab work
4. Shirish P. Jain: Final review and validation of the data

5. Falak A. Siddiqui: Compiled the Literature source and data analysis related to Molecular docking.

CONFLICTS OF INTEREST

The authors have no conflicts of interest.

FUNDING

There was no funding source.

REFERENCES

1. Singh R, Iye S, Prasad S, Deshmukh N, Gupta U, Zanje A, et al. Phytochemical analysis of muntingia calabura extracts possessing antimicrobial and anti-fouling activities. Int J Pharmacogn Phytochem Res2017;9:826-32.
2. Mahmood ND. *Muntingia calabura*: A review of its traditional uses, chemical properties, and pharmacological observations. Pharm Biol2014;52:1598-623.
3. Sibi G, Naveen R, Dhananjaya K, Ravikumar KR, Mallesha H. Potential use of *Muntingia calabura* L. Extracts against human and plant pathogens. Pharmacogn J2012;4:44-7.
4. Wang LS, Wang YR, Ye DW, Liu QQ. A review of the 2019 novel coronavirus (COVID-19) based on current evidence. Int J Antimicrob Agents2020; DOI: 10.1016/j.ijantimicag.2020.105948.
5. Liu C, Zhou Q, Li Y, Garner LV, Watkins SP, Carter LJ, et al. Research and development on therapeutic agents and vaccines for COVID-19 and related human coronavirus diseases. ACS Cent Sci2020;6:315-31.
6. Tambe R, Kulkarni M, Bhise K. Preliminary phytochemical screening and HPTLC fingerprinting of bark extracts of *Symplocos racemosa*. J Pharmacogn Phytochem2013;2:45-9.
7. World Health Organization. Quality Control Methods for Medicinal Plant Materials. Geneva: World Health Organization; 1989. p. 1-15.
8. Harborne JB. Phytochemical Methods: A Guide to Modern Techniques of Plant Analysis. Berlin, Germany: Springer; 1973.
9. Edeoga HO, Okwu DE, Mbaebie BO. Phytochemical constituents of some Nigerian medicinal plants. Afr J Biotechnol2005;4:685-8.
10. Parekh J, Chanda SV. *In vitro* antimicrobial activity and phytochemical analysis of some Indian medicinal plants. Turk J Biol2007;31:53-8.
11. Sofowora A. Research on medicinal plants and traditional medicine in Africa. J Altern Complement Med1996;2:365-72.
12. Kumar GS, Jayaveera KN, Kumar CK, Umachigi P, Swamy BM, Kumar DV. Antimicrobial effects of Indian medicinal plants against acne-inducing *Bacteria*. Trop J Pharm Res2007;6:717-23.
13. Bajpai VK, Majumder R, Park JG. Isolation and purification of plant secondary metabolites using column-chromatographic technique. Bangladesh J Pharmacol2016;11:844-8.
14. Jaber BM, Jasim SF. Phytochemical study of stigmaterol and β -sitosterol in *Viola odorata* plant cultivated in Iraq. Iraqi J Biotechnol2014;13:86-94.
15. Ahmad H, Sehgal S, Mishra A, Gupta R, Saraf SA. TLC detection of β -sitosterol in *Michelia champaca* L. Leaves and stem bark and its determination by HPTLC. Pharmacogn J2012;4:45-55.
16. Visveshwari M, Subbaiyan B, Thangapandian V. Phytochemical analysis, antibacterial activity, FTIR and GCMS analysis of *Ceropegia juncea* Roxb. Int J Pharmacogn Phytochem Res2017;9:914-20.
17. Rajiv P, Deepa A, Vanathi P, Vidhya D. Screening for phytochemicals and ftr analysis of *Myristica dactyloids* fruit extracts. Int J Pharm Pharm Sci2017;9:1-4.
18. Dharmalingam V. Phytochemical screening by FTIR spectroscopic analysis of leaf and stem extracts of *Wedelia biflora*. Int J Nano Corros Sci Eng2015;2:322-34.
19. Article O, Dhivya SM, Kalaichelvi K. UV-visible spectroscopic and ftr analysis of *Sarcostemma brevistigma*. Int J Curr Pharm Res2017;9:46-9.
20. Jain PK, Soni A, Jain P, Bhawsar J. Phytochemical analysis of *Mentha spicata* plant extract using UV-VIS, FTIR and GC/MS technique. J Chem Pharm Res2016;8:1-6.
21. SkiffAK, RappeCJ, CasewitKS, ColwellWA. Goddard III WMS. UFF, a full periodic table force field for molecular mechanics and molecular dynamics simulations. J Am Chem Soc2009;114:10024-35.
22. Dallakyan S, Olson AJ. Small-molecule library screening by docking with PyRx. Methods Mol Biol2015;1263:243-50.
23. Dassault Systèmes BIOVIA. Discovery Studio Modeling Environment. San Diego: Dassault SystèmesBIOVIA; 2016.
24. Chaudhari RK, Girase NO. Determination of soluble extractives and physico-chemical studies of bark of *Sesbania sesban* (L) Merr. J Chem Pharm Res2015;7:657-60.



Pharmacological Activity Investigation of Alkaline Water – A Review

Gajanan Sonwane^{1*}, Sujat Bhagat¹, Vijay Borkar¹, Shirish Jain¹, Sharuk Khan¹, Mayura Kale²

¹Department of Pharmaceutical Chemistry, Rajarshi Shahu College of Pharmacy, Buldana, India.

²Departments of Pharmaceutical Chemistry, Government College of Pharmacy, Aurangabad, India.

*Corresponding author's E-mail: sonwane.gajanan@rediffmail.com

Received: 12-06-2020; Revised: 21-08-2020; Accepted: 28-08-2020.

DOI: 10.47583/ijpsrr.2020.v64i01.017

ABSTRACT

In present study various pharmacological investigation of alkaline water compiled, now days due to fast life acidity become a huge problem in metro cities which is origin for various diseases such as GERD, hypertension, skin diseases, hyperthyroidism, hyperlipidemia, cancer, diabetes etc. Various researches worked on activity of alkaline water and various clinical trials are in tunnel. Compile date elucidate the importance of alkaline water in various diseases treatments and future prospectus in clinical trials of various cancer and related diseases.

Keywords: Alkaline water, acidity, Cancer, Pharmacological investigation.

INTRODUCTION

Acidity is most important and ignored reason in development of different diseases like hypertension¹, skin diseases², hyperthyroidism³, hyperlipidemia⁴, cancer⁵, diabetes⁶ and related diseases etc. In allopathy physician only work on sign and symptoms

of the diseases after performing various expensive diagnosis test like ECG, Kidney function, Blood test etc., but the root of this disease condition is completely ignored. The Natural alkaline water is one the solution to cure root of this diseases. In this article would like explore the various researches done on alkaline water and futuristic research possibilities.



Figure 1: Root cause of various life-threatening diseases

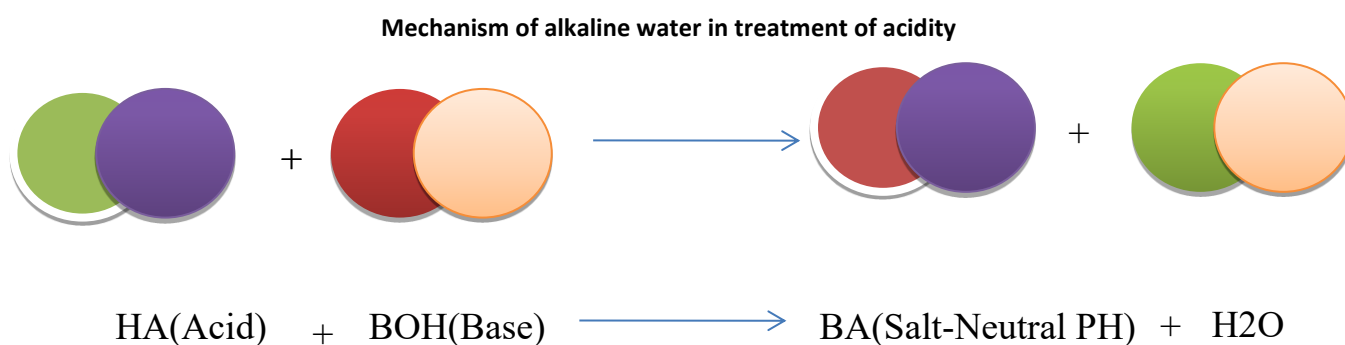


Figure 2: Mechanism of alkaline water

Research performed by American institute for cancer research claimed that acidity can alter the body's pH balance and promote cancer. The unproven theory is based on lab studies that advise cancer cells thrive in an acidic (low pH) environment, but cannot survive in alkaline (high pH) surroundings. The Research proven that the cells in an isolated lab setting. Altering the cell environment of the human body to create a less-acidic, less-cancer-friendly environment is virtually impossible. Even slight changes to your body's pH are life-threatening events. Patients with kidney disease and pulmonary dysfunction. To avoid even small disruption of acid-base balance we can focus on root cause that is the acidity, which can prevent further diseases consequences.⁷

Alkaline water

The "basic" in alkaline water alludes to its pH level. A pH level is a number that estimates how acidic or soluble a substance is on a size of 0 to 14. For instance, something with a pH of 1 would be acidic and something with a pH of 13 would be basic. Basic water has a higher pH level than standard drinking water. Along these lines, a few backers of antacid water trust it can kill the corrosive in your body. Typical drinking water, for the most part, has an unbiased pH of 7. Antacid water regularly has a pH of 8 or 9. In any case, pH alone isn't sufficient to bestow considerable alkalinity to water. Basic water should likewise contain alkaline minerals and negative oxidation decrease potential (ORP). ORP is the capacity of water to go about as a cancer prevention agent. The more negative the ORP esteem, the more anti-oxidizing it is.

AN OVERVIEW OF THERAPEUTIC POTENTIAL OF ALKALINE WATER

Alkaline water as a treatment of reflux disease.

Koufman JA et al (2012)⁸ performed clinical trial on human volunteer they proven the effect of alkaline water in treatment on human reflux diseases specially the natural alkaline water leads to denature human pepsin and its acts like buffering agents. Researcher proven the effective denaturation of pepsin at pH 8.8 exactly.

Alkaline water as an antioxidant activity

Lucas Pellegrina et al (2019)⁹ has carried out growth response biological investigation by using different alkaline

PH water on pacu juveniles. In this experiment Pacu fish were investigated to the different PH such as 5.5, 6.5, 7.5 and 8.5 for 45 days. In that experiment they were found that the fish at water PH of 8.5 were developed at significantly higher than another PH. And in acidic PH it reduces the muscle antioxidant capacity against peroxy radicles and glutathione s transferase. It was also observed by investigator that the Change PH did not affects on other factors like blood glucose, Hematocrit, Plasma, muscle content of protein thiols and thiobarbituric acid reactivity substances.

Yoshinori Tanaka et al (2018)¹⁰ used AEW (alkaline electrolyzed water) for investigation on abdominal complaints under the guidance of ethical committee. Researcher selected a group of objects without any complained of gastrointestinal problem for which AEW used in Japan. Researcher demonstrated a double blind randomized controlled trial for four weeks. Before control trial preliminary investigation was performed like blood tests, physical fitness. and questionnaire evaluation. In this study they concluded no significant side effect on intestinal integrity. Additionally, they stated the improvised sleeping state and felt good when awakening due to reduction in oxidative stress which opened up the novel research area alkaline water as antioxidant agents

Alkaline water as an anti-aging property

Massimiliano Magro et al (2016)¹¹ has performed the survival study on 150 mice for 3-years and by using accelerated failure time (AFT) model proved that the survival rate of mice watered with alkaline water is more than the control mice. It was also observed that alkaline watered mice have decline aging factor as compare to control group. Again, investigator performed toxicity assessment study by using histopathological examination on kidney, intestine heart liver and brain which resulted in no significant pathology

Alkaline water as an anti-bacterial activity

Ahn, Seon-Mi et al (2010)¹² presented pharmacological investigation study of AIW (Alkaline ionized water), PW (purified water and DW (drinking water) in which they performed. In which PH and ORP (oxidation- reduction potential) of water was 9.5 and 120mV, 7.2 and 144 mV and 7.3 and 564mV, respectively. Research proven no

significant antioxidant activity of any of water used in experiment quoted above. Only the power of standard substance used in DPPH ((1,1-diphenyl-2-picryl hydrazyl) assay that is vitamin C found to be stable in AIW and PW as compare to DW. Similarly, the standard used in antithrombosis activity that is aspirin shown improved biological absorbance in AIW and PW as compare to DW. Research also investigate the cell growth analysis and viable cell count of *Escherichia coli* in above 3 motioned water as a result again AIW and PW showed antibacterial activity and DW not.

Alkaline water as a power booster for sports men

Jakub Chycki et al (2018)¹³ worked on problem faced by sports men due to water restriction for quick weight loss before tournaments they proven the effect of alkaline water as prevention for exercise-induced metabolic acidosis. Researcher performed the double randomized clinical trials on sixteen well trained sports athletes by keeping control with normal tap water for three weeks. Anaerobic performance was evaluated by two double 30 s Wingate tests for lower and upper limbs, respectively, with a passive rest interval of 3 minutes between the bouts of exercise. The results indicate that drinking alkalized water enhances hydration, improves acid-base balance and anaerobic exercise performance. Significant increase in mean power when comparing the values (7.98 J/kg to 9.38 J/kg with $p = 0.001$) at baseline vs. at the conclusion of the study in the experimental group supplemented with alkaline water. In contrast, the control group which received table water did not reveal any statistically significant results.

Joseph Weidman et al (2016)¹⁴ studied the fluid replacement beverages ingested on healthy adults after exercise showed hydration biomarkers like effects researcher carried out randomized, double-blind, parallel-arm trial assessed the effect of high-pH water on blood viscosity. After exercise-induced dehydration as a results high-pH water reduced high-shear viscosity by an average of 6.30% compared to 3.36% with standard purified water ($p = 0.03$) significant difference in whole blood viscosity was detected in this study when assessing a high-pH, electrolyte water versus an acceptable standard purified water during the recovery phase following strenuous exercise-induced dehydration.

Jr, Senay LC et al (1996)¹⁵ collected various clinical trials data on human sports volunteers in japan in which fluid replacement promotes optimal physical performance, reduced water scavenges active oxygen & protects DNA from oxidative damage, The mechanism of the enhanced antioxidant effects of reduced water produced by electrolysis, Antimicrobial interventions to reduce Salmonella species on poultry, Treatment of *Escherichia coli* inoculated alfalfa sprouts with electrolyzed oxidizing water, Inactivation of *E. coli* & *Listeria* on plastic kitchen cutting boards by electrolyzed oxidizing water, Effect of electrolyzed water on wound healing, The bactericidal effects of electrolyzed oxidizing water on bacterial strains

in hospital infections, Effect of electrolyzed oxidizing water on excised burn-wounds, Decomposition of ethylene, a flower-senescence hormone, with electrolyzed anode water, Use of Ionized water in hypochlorhydria, achlorhydria, reduction of high blood pressure, Use of Ionized water for gynecological conditions, Clinical Improvements obtained from the uptake of Ionized Water, Alkaline ionized water for abdominal complaints: Placebo controlled double blind tests, Physiological effects of alkaline ionized water: intestinal fermentation, Effects of calcium alkaline ionized water on formation and maintenance of osseous tissues, Reduced Water for Prevention of Disease, Use of Ionized water in heart disease and toxins, Use of Ionized water in skin disease, Use of Ionized water in allergies, Use of Ionized water in diabetes treatment, Use of Ionized water in treating Acidosis, Environmental electrochemistry of water clinical study on volunteer researcher recommended that individuals consume a alkaline water especially during the period that includes the meal prior to exercise, to promote proper hydration before exercise or competition. It is recommended that individuals drink about 500 ml (about 17 ounces) of alkaline water about 2 hours before exercise to promote adequate hydration and allow time for excretion of excess ingested water.

CONCLUSION

Various researchers signify the importance of alkaline PH water in growth factor by using randomized human and *in vivo* trials for. Researcher opens up the novel hypothesis for human trial on ageing factor investigation. The importance of alkaline water for drug stability and antibacterial properties will be a blockbuster area for drug absorbance enhancement and various pharmacological investigations. Regardless of the advancement of the alkaline water by the media and sales representatives, there is no genuine research to either encourage or discredit these facts and figures. This methodical survey of the writing uncovered an absence of proof possibly in support of alkaline water for the inception or treatment of malignancy. Advancement of alkaline water to people in general for cancer and another acid related diseases treatment isn't legitimized.

REFERENCES

1. Monteiro C.:Acidity Theory of Atherosclerosis: History, Pathophysiology, Therapeutics and Risk Factors - A Mini Review. Position Heal, 2015, 1.
2. Campbell KL: Fatty Acid Supplementation and Skin Disease. The Veterinary, clinics of North America. Small animal practice. 20(6), 1990, 1475–1486.
3. Thompson DM:Gastric Acidity in Hyperthyroidism. J. Bowman Gray Scholer Medicine Wake. For. Coll. 7(1), 1949, 8–16.
4. Sulyok E: Metabolic Acidosis, Nitrogen Balance and Weight Gain in Preterm Infants. Acta Paediatr. Academic Science Hunger. 17(4), 1976, 267–276.
5. Andreev OA: Wei, D.; Engelman, D.; Reshetnyak, Y.



- Acidity at the Surfaces of Cancer Cells. *Biophysical Journal*. 114(3), 2018, 359a.
6. Grant, A. E. Alkaline Water in Diabetes. *British Medical Journal*. 2, 1902, 1621–1622.
 7. WCRF, American Institute for Cancer Research: World Cancer Research Fund, Food, Nutrition and the Prevention of Cancer (WCRF): A Global Perspective. *Nutrition*, 16, 1997, 523–526.
 8. Koufman JA; Johnston, N. Potential Benefits of PH 8.8 Alkaline Drinking Water as an Adjunct in the Treatment of Reflux Disease. *Annals of Otolaryngology, Rhinology & Laryngology*. 121(7), 2012, 431-434.
 9. Pellegrin L; Nitz, L. F.; Maltez, L. C.; Copatti, C. E.; Garcia, L. Alkaline Water Improves the Growth and Antioxidant Responses of Pacu Juveniles (*Piaractus Mesopotamicus*). *Aquaculture*, 519, 2019, 713-734.
 10. Higashimura Y; Baba, Y.; Inoue, R.; Takagi, T.; Uchiyama, K.; Mizushima, K.; Hirai, Y.; Ushiroda, C.; Tanaka, Y.; Naito, Y. Effects of Molecular Hydrogen-Dissolved Alkaline Electrolyzed Water on Intestinal Environment in Mice. *Medical Gas Research*, 8(1), 2018, 6–11.
 11. Magro, M, Corain L, Ferro S, Baratella D, Bonaiuto E, Terzo M: Alkaline Water and Longevity: A Murine Study. *Evidence-based Complement. Alternative. Medicine*, 1, 2016, 1–6.
 12. Ahn S, Kang M, Kim MI, Sohn H: Effect of Alkaline Ionized Water on Stabilization of Antioxidation, Antithrombosis and Antibacterial Activities. *Journal of Life Sciences*. 20(7), 2010, 1107–1112.
 13. Chycki J, Kurylas A, Maszczyk A, Golas A, Zajac A: Alkaline Water Improves Exercise-Induced Metabolic Acidosis and Enhances Anaerobic Exercise Performance in Combat Sport Athletes. *PLoS One*, 13(11), 2018, 1-10.
 14. Weidman J, Holsworth RE, Brossman B, Cho DJ, St Cyr J, Fridman G: Effect of Electrolyzed High-PH Alkaline Water on Blood Viscosity in Healthy Adults. *Journal of the International Society of Sports Nutrition*. 13(1), 2016, 45.
 15. Jr s, clinical studies of alkaline water. *Medicine & Science in Sports & Exercise*, 28(1), 1996, 1-10.

Source of Support: None declared.

Conflict of Interest: None declared.

For any question relates to this article, please reach us at: editor@globalresearchonline.net

New manuscripts for publication can be submitted at: submit@globalresearchonline.net and submit_ijpsrr@rediffmail.com





Pharmacological Activity Investigation of Alkaline Water – A Review

Gajanan Sonwane^{1*}, Sujat Bhagat¹, Vijay Borkar¹, Shirish Jain¹, Sharuk khan¹, Mayura Kale²

¹Department of Pharmaceutical Chemistry, Rajarshi Shahu College of Pharmacy, Buldana, India.

² Departments of Pharmaceutical Chemistry, Government College of Pharmacy, Aurangabad, India.

*Corresponding author's E-mail: sonwane.gajanan@rediffmail.com

Received: 12-06-2020; Revised: 21-08-2020; Accepted: 28-08-2020.

DOI: 10.47583/ijpsrr.2020.v64i01.017

ABSTRACT

In present study various pharmacological investigation of alkaline water compiled, now days due to fast life acidity become a huge problem in metro cities which is origin for various diseases such as GERD, hypertension, skin diseases, hyperthyroidism, hyperlipidemia, cancer, diabetes etc. Various researches worked on activity of alkaline water and various clinical trials are in tunnel. Compile date elucidate the importance of alkaline water in various diseases treatments and future prospectus in clinical trials of various cancer and related diseases.

Keywords: Alkaline water, acidity, Cancer, Pharmacological investigation.

INTRODUCTION

Acidity is most important and ignored reason in development of different diseases like hypertension¹, skin diseases², hyperthyroidism³, hyperlipidemia⁴, cancer⁵, diabetes⁶ and related diseases etc. In allopathy physician only work on sign and symptoms

of the diseases after performing various expensive diagnosis test like ECG, Kidney function, Blood test etc., but the root of this disease condition is completely ignored. The Natural alkaline water is one the solution to cure root of this diseases. In this article would like explore the various researches done on alkaline water and futuristic research possibilities.



Figure 1: Root cause of various life-threatening diseases

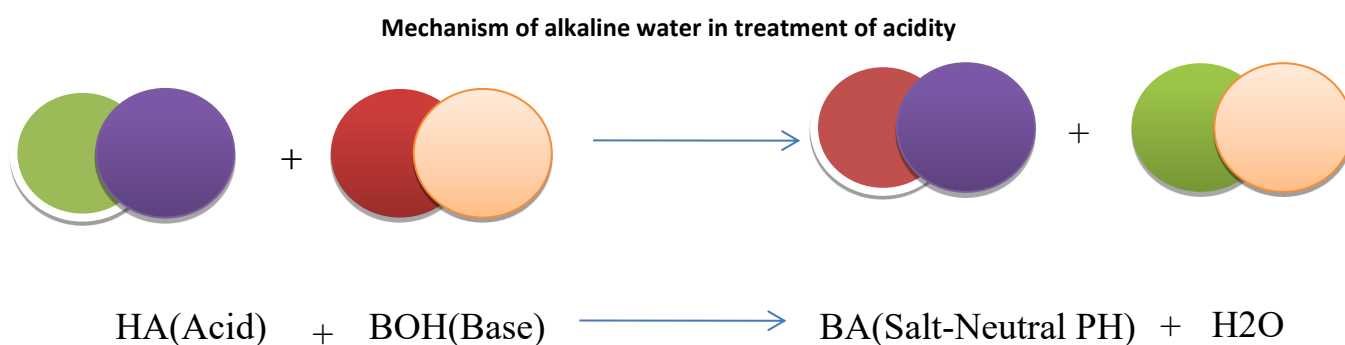


Figure 2: Mechanism of alkaline water

Research performed by American institute for cancer research claimed that acidity can alter the body's pH balance and promote cancer. The unproven theory is based on lab studies that advise cancer cells thrive in an acidic (low pH) environment, but cannot survive in alkaline (high pH) surroundings. The Research proven that the cells in an isolated lab setting. Altering the cell environment of the human body to create a less-acidic, less-cancer-friendly environment is virtually impossible. Even slight changes to your body's pH are life-threatening events. Patients with kidney disease and pulmonary dysfunction. To avoid even small disruption of acid-base balance we can focus on root cause that is the acidity, which can prevent further diseases consequences.⁷

Alkaline water

The "basic" in alkaline water alludes to its pH level. A pH level is a number that estimates how acidic or soluble a substance is on a size of 0 to 14. For instance, something with a pH of 1 would be acidic and something with a pH of 13 would be basic. Basic water has a higher pH level than standard drinking water. Along these lines, a few backers of antacid water trust it can kill the corrosive in your body. Typical drinking water, for the most part, has an unbiased pH of 7. Antacid water regularly has a pH of 8 or 9. In any case, pH alone isn't sufficient to bestow considerable alkalinity to water. Basic water should likewise contain alkaline minerals and negative oxidation decrease potential (ORP). ORP is the capacity of water to go about as a cancer prevention agent. The more negative the ORP esteem, the more anti-oxidizing it is.

AN OVERVIEW OF THERAPEUTIC POTENTIAL OF ALKALINE WATER

Alkaline water as a treatment of reflux disease.

Koufman JA et al (2012)⁸ performed clinical trial on human volunteer they proven the effect of alkaline water in treatment on human reflux diseases specially the natural alkaline water leads to denature human pepsin and its acts like buffering agents. Researcher proven the effective denaturation of pepsin at pH 8.8 exactly.

Alkaline water as an antioxidant activity

Lucas Pellegrina et al (2019)⁹ has carried out growth response biological investigation by using different alkaline

PH water on pacu juveniles. In this experiment Pecu fish were investigated to the different PH such as 5.5, 6.5, 7.5 and 8.5 for 45 days. In that experiment they were found that the fish at water PH of 8.5 were developed at significantly higher than another PH. And in acidic PH it reduces the muscle antioxidant capacity against peroxy radicles and glutathione s transferase. It was also observed by investigator that the Change PH did not affects on other factors like blood glucose, Hematocrit, Plasma, muscle content of protein thiols and thiobarbituric acid reactivity substances.

Yoshinori Tanaka et al (2018)¹⁰ used AEW (alkaline electrolyzed water) for investigation on abdominal complaints under the guidance of ethical committee. Researcher selected a group of objects without any complained of gastrointestinal problem for which AEW used in Japan. Researcher demonstrated a double blind randomized controlled trial for four weeks. Before control trial preliminary investigation was performed like blood tests, physical fitness. and questionnaire evaluation. In this study they concluded no significant side effect on intestinal integrity. Additionally, they stated the improvised sleeping state and felt good when awakening due to reduction in oxidative stress which opened up the novel research area alkaline water as antioxidant agents

Alkaline water as an anti-aging property

Massimiliano Magro et al (2016)¹¹ has performed the survival study on 150 mice for 3-years and by using accelerated failure time (AFT) model proved that the survival rate of mice watered with alkaline water is more than the control mice. It was also observed that alkaline watered mice have decline aging factor as compare to control group. Again, investigator performed toxicity assessment study by using histopathological examination on kidney, intestine heart liver and brain which resulted in no significant pathology

Alkaline water as an anti-bacterial activity

Ahn, Seon-Mi et al (2010)¹² presented pharmacological investigation study of AIW (Alkaline ionized water), PW (purified water and DW (drinking water) in which they performed. In which PH and ORP (oxidation- reduction potential) of water was 9.5 and 120mV, 7.2 and 144 mV and 7.3 and 564mV, respectively. Research proven no

significant antioxidant activity of any of water used in experiment quoted above. Only the power of standard substance used in DPPH ((1,1-diphenyl-2-picryl hydrazyl) assay that is vitamin C found to be stable in AIW and PW as compare to DW. Similarly, the standard used in antithrombosis activity that is aspirin shown improved biological absorbance in AIW and PW as compare to DW. Research also investigate the cell growth analysis and viable cell count of *Escherichia coli* in above 3 motioned water as a result again AIW and PW showed antibacterial activity and DW not.

Alkaline water as a power booster for sports men

Jakub Chycki et al (2018)¹³ worked on problem faced by sports men due to water restriction for quick weight loss before tournaments they proven the effect of alkaline water as prevention for exercise-induced metabolic acidosis. Researcher performed the double randomized clinical trials on sixteen well trained sports athletes by keeping control with normal tap water for three weeks. Anaerobic performance was evaluated by two double 30 s Wingate tests for lower and upper limbs, respectively, with a passive rest interval of 3 minutes between the bouts of exercise. The results indicate that drinking alkalized water enhances hydration, improves acid-base balance and anaerobic exercise performance. Significant increase in mean power when comparing the values (7.98 J/kg to 9.38 J/kg with $p = 0.001$) at baseline vs. at the conclusion of the study in the experimental group supplemented with alkaline water. In contrast, the control group which received table water did not reveal any statistically significant results.

Joseph Weidman et al (2016)¹⁴ studied the fluid replacement beverages ingested on healthy adults after exercise showed hydration biomarkers like effects researcher carried out randomized, double-blind, parallel-arm trial assessed the effect of high-pH water on blood viscosity. After exercise-induced dehydration as a results high-pH water reduced high-shear viscosity by an average of 6.30% compared to 3.36% with standard purified water ($p = 0.03$) significant difference in whole blood viscosity was detected in this study when assessing a high-pH, electrolyte water versus an acceptable standard purified water during the recovery phase following strenuous exercise-induced dehydration.

Jr, Senay LC et al (1996)¹⁵ collected various clinical trials data on human sports volunteers in japan in which fluid replacement promotes optimal physical performance, reduced water scavenges active oxygen & protects DNA from oxidative damage, The mechanism of the enhanced antioxidant effects of reduced water produced by electrolysis, Antimicrobial interventions to reduce Salmonella species on poultry, Treatment of *Escherichia coli* inoculated alfalfa sprouts with electrolyzed oxidizing water, Inactivation of *E. coli* & *Listeria* on plastic kitchen cutting boards by electrolyzed oxidizing water, Effect of electrolyzed water on wound healing, The bactericidal effects of electrolyzed oxidizing water on bacterial strains

in hospital infections, Effect of electrolyzed oxidizing water on excised burn-wounds, Decomposition of ethylene, a flower-senescence hormone, with electrolyzed anode water, Use of Ionized water in hypochlorhydria, achlorhydria, reduction of high blood pressure, Use of Ionized water for gynecological conditions, Clinical Improvements obtained from the uptake of Ionized Water, Alkaline ionized water for abdominal complaints: Placebo controlled double blind tests, Physiological effects of alkaline ionized water: intestinal fermentation, Effects of calcium alkaline ionized water on formation and maintenance of osseous tissues, Reduced Water for Prevention of Disease, Use of Ionized water in heart disease and toxins, Use of Ionized water in skin disease, Use of Ionized water in allergies, Use of Ionized water in diabetes treatment, Use of Ionized water in treating Acidosis, Environmental electrochemistry of water clinical study on volunteer researcher recommended that individuals consume a alkaline water especially during the period that includes the meal prior to exercise, to promote proper hydration before exercise or competition. It is recommended that individuals drink about 500 ml (about 17 ounces) of alkaline water about 2 hours before exercise to promote adequate hydration and allow time for excretion of excess ingested water.

CONCLUSION

Various researchers signify the importance of alkaline PH water in growth factor by using randomized human and *in vivo* trials for. Researcher opens up the novel hypothesis for human trial on ageing factor investigation. The importance of alkaline water for drug stability and antibacterial properties will be a blockbuster area for drug absorbance enhancement and various pharmacological investigations. Regardless of the advancement of the alkaline water by the media and sales representatives, there is no genuine research to either encourage or discredit these facts and figures. This methodical survey of the writing uncovered an absence of proof possibly in support of alkaline water for the inception or treatment of malignancy. Advancement of alkaline water to people in general for cancer and another acid related diseases treatment isn't legitimized.

REFERENCES

1. Monteiro C.:Acidity Theory of Atherosclerosis: History, Pathophysiology, Therapeutics and Risk Factors - A Mini Review. Position Heal, 2015, 1.
2. Campbell KL: Fatty Acid Supplementation and Skin Disease. The Veterinary, clinics of North America. Small animal practice. 20(6), 1990, 1475–1486.
3. Thompson DM:Gastric Acidity in Hyperthyroidism. J. Bowman Gray Scholer Medicine Wake. For. Coll. 7(1), 1949, 8–16.
4. Sulyok E: Metabolic Acidosis, Nitrogen Balance and Weight Gain in Preterm Infants. Acta Paediatr. Academic Science Hunger. 17(4), 1976, 267–276.
5. Andreev OA: Wei, D.; Engelman, D.; Reshetnyak, Y.



- Acidity at the Surfaces of Cancer Cells. *Biophysical Journal*. 114(3), 2018, 359a.
6. Grant, A. E. Alkaline Water in Diabetes. *British Medical Journal*. 2, 1902, 1621–1622.
 7. WCRF, American Institute for Cancer Research: World Cancer Research Fund, Food, Nutrition and the Prevention of Cancer (WCRF): A Global Perspective. *Nutrition*, 16, 1997, 523–526.
 8. Koufman JA; Johnston, N. Potential Benefits of PH 8.8 Alkaline Drinking Water as an Adjunct in the Treatment of Reflux Disease. *Annals of Otolaryngology, Rhinology & Laryngology*. 121(7), 2012, 431-434.
 9. Pellegrin L; Nitz, L. F.; Maltez, L. C.; Copatti, C. E.; Garcia, L. Alkaline Water Improves the Growth and Antioxidant Responses of Pacu Juveniles (*Piaractus Mesopotamicus*). *Aquaculture*, 519, 2019, 713-734.
 10. Higashimura Y; Baba, Y.; Inoue, R.; Takagi, T.; Uchiyama, K.; Mizushima, K.; Hirai, Y.; Ushiroda, C.; Tanaka, Y.; Naito, Y. Effects of Molecular Hydrogen-Dissolved Alkaline Electrolyzed Water on Intestinal Environment in Mice. *Medical Gas Research*, 8(1), 2018, 6–11.
 11. Magro, M, Corain L, Ferro S, Baratella D, Bonaiuto E, Terzo M: Alkaline Water and Longevity: A Murine Study. *Evidence-based Complement. Alternative. Medicine*, 1, 2016, 1–6.
 12. Ahn S, Kang M, Kim MI, Sohn H: Effect of Alkaline Ionized Water on Stabilization of Antioxidation, Antithrombosis and Antibacterial Activities. *Journal of Life Sciences*. 20(7), 2010, 1107–1112.
 13. Chycki J, Kurylas A, Maszczyk A, Golas A, Zajac A: Alkaline Water Improves Exercise-Induced Metabolic Acidosis and Enhances Anaerobic Exercise Performance in Combat Sport Athletes. *PLoS One*, 13(11), 2018, 1-10.
 14. Weidman J, Holsworth RE, Brossman B, Cho DJ, St Cyr J, Fridman G: Effect of Electrolyzed High-PH Alkaline Water on Blood Viscosity in Healthy Adults. *Journal of the International Society of Sports Nutrition*. 13(1), 2016, 45.
 15. Jr s, clinical studies of alkaline water. *Medicine & Science in Sports & Exercise*, 28(1), 1996, 1-10.

Source of Support: None declared.

Conflict of Interest: None declared.

For any question relates to this article, please reach us at: editor@globalresearchonline.net

New manuscripts for publication can be submitted at: submit@globalresearchonline.net and submit_ijpsrr@rediffmail.com





Pharmacological Activity Investigation of Alkaline Water – A Review

Gajanan Sonwane^{1*}, Sujat Bhagat¹, Vijay Borkar¹, Shirish Jain¹, Sharuk Khan¹, Mayura Kale²

¹Department of Pharmaceutical Chemistry, Rajarshi Shahu College of Pharmacy, Buldana, India.

² Departments of Pharmaceutical Chemistry, Government College of Pharmacy, Aurangabad, India.

*Corresponding author's E-mail: sonwane.gajanan@rediffmail.com

Received: 12-06-2020; Revised: 21-08-2020; Accepted: 28-08-2020.

DOI: 10.47583/ijpsrr.2020.v64i01.017

ABSTRACT

In present study various pharmacological investigation of alkaline water compiled, now days due to fast life acidity become a huge problem in metro cities which is origin for various diseases such as GERD, hypertension, skin diseases, hyperthyroidism, hyperlipidemia, cancer, diabetes etc. Various researches worked on activity of alkaline water and various clinical trials are in tunnel. Compile date elucidate the importance of alkaline water in various diseases treatments and future prospectus in clinical trials of various cancer and related diseases.

Keywords: Alkaline water, acidity, Cancer, Pharmacological investigation.

INTRODUCTION

Acidity is most important and ignored reason in development of different diseases like hypertension¹, skin diseases², hyperthyroidism³, hyperlipidemia⁴, cancer⁵, diabetes⁶ and related diseases etc. In allopathy physician only work on sign and symptoms

of the diseases after performing various expensive diagnosis test like ECG, Kidney function, Blood test etc., but the root of this disease condition is completely ignored. The Natural alkaline water is one the solution to cure root of this diseases. In this article would like explore the various researches done on alkaline water and futuristic research possibilities.



Figure 1: Root cause of various life-threatening diseases

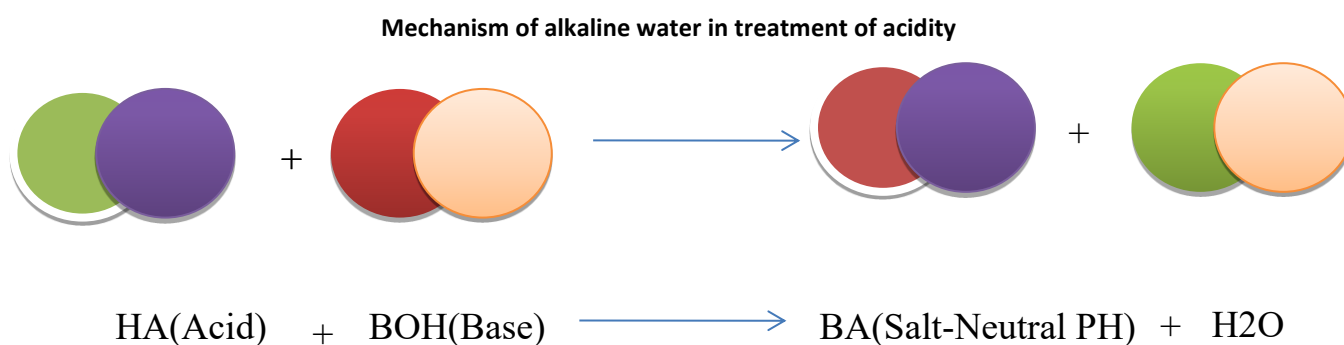


Figure 2: Mechanism of alkaline water

Research performed by American institute for cancer research claimed that acidity can alter the body's pH balance and promote cancer. The unproven theory is based on lab studies that advise cancer cells thrive in an acidic (low pH) environment, but cannot survive in alkaline (high pH) surroundings. The Research proven that the cells in an isolated lab setting. Altering the cell environment of the human body to create a less-acidic, less-cancer-friendly environment is virtually impossible. Even slight changes to your body's pH are life-threatening events. Patients with kidney disease and pulmonary dysfunction. To avoid even small disruption of acid-base balance we can focus on root cause that is the acidity, which can prevent further diseases consequences.⁷

Alkaline water

The "basic" in alkaline water alludes to its pH level. A pH level is a number that estimates how acidic or soluble a substance is on a size of 0 to 14. For instance, something with a pH of 1 would be acidic and something with a pH of 13 would be basic. Basic water has a higher pH level than standard drinking water. Along these lines, a few backers of antacid water trust it can kill the corrosive in your body. Typical drinking water, for the most part, has an unbiased pH of 7. Antacid water regularly has a pH of 8 or 9. In any case, pH alone isn't sufficient to bestow considerable alkalinity to water. Basic water should likewise contain alkaline minerals and negative oxidation decrease potential (ORP). ORP is the capacity of water to go about as a cancer prevention agent. The more negative the ORP esteem, the more anti-oxidizing it is.

AN OVERVIEW OF THERAPEUTIC POTENTIAL OF ALKALINE WATER

Alkaline water as a treatment of reflux disease.

Koufman JA et al (2012)⁸ performed clinical trial on human volunteer they proven the effect of alkaline water in treatment on human reflux diseases specially the natural alkaline water leads to denature human pepsin and its acts like buffering agents. Researcher proven the effective denaturation of pepsin at pH 8.8 exactly.

Alkaline water as an antioxidant activity

Lucas Pellegrina et al (2019)⁹ has carried out growth response biological investigation by using different alkaline

PH water on pacu juveniles. In this experiment Pecu fish were investigated to the different PH such as 5.5, 6.5, 7.5 and 8.5 for 45 days. In that experiment they were found that the fish at water PH of 8.5 were developed at significantly higher than another PH. And in acidic PH it reduces the muscle antioxidant capacity against peroxy radicles and glutathione s transferase. It was also observed by investigator that the Change PH did not affects on other factors like blood glucose, Hematocrit, Plasma, muscle content of protein thiols and thiobarbituric acid reactivity substances.

Yoshinori Tanaka et al (2018)¹⁰ used AEW (alkaline electrolyzed water) for investigation on abdominal complaints under the guidance of ethical committee. Researcher selected a group of objects without any complained of gastrointestinal problem for which AEW used in Japan. Researcher demonstrated a double blind randomized controlled trial for four weeks. Before control trial preliminary investigation was performed like blood tests, physical fitness. and questionnaire evaluation. In this study they concluded no significant side effect on intestinal integrity. Additionally, they stated the improvised sleeping state and felt good when awakening due to reduction in oxidative stress which opened up the novel research area alkaline water as antioxidant agents

Alkaline water as an anti-aging property

Massimiliano Magro et al (2016)¹¹ has performed the survival study on 150 mice for 3-years and by using accelerated failure time (AFT) model proved that the survival rate of mice watered with alkaline water is more than the control mice. It was also observed that alkaline watered mice have decline aging factor as compare to control group. Again, investigator performed toxicity assessment study by using histopathological examination on kidney, intestine heart liver and brain which resulted in no significant pathology

Alkaline water as an anti-bacterial activity

Ahn, Seon-Mi et al (2010)¹² presented pharmacological investigation study of AIW (Alkaline ionized water), PW (purified water and DW (drinking water) in which they performed. In which PH and ORP (oxidation- reduction potential) of water was 9.5 and 120mV, 7.2 and 144 mV and 7.3 and 564mV, respectively. Research proven no

significant antioxidant activity of any of water used in experiment quoted above. Only the power of standard substance used in DPPH ((1,1-diphenyl-2-picryl hydrazyl) assay that is vitamin C found to be stable in AIW and PW as compare to DW. Similarly, the standard used in antithrombosis activity that is aspirin shown improved biological absorbance in AIW and PW as compare to DW. Research also investigate the cell growth analysis and viable cell count of *Escherichia coli* in above 3 motioned water as a result again AIW and PW showed antibacterial activity and DW not.

Alkaline water as a power booster for sports men

Jakub Chycki et al (2018)¹³ worked on problem faced by sports men due to water restriction for quick weight loss before tournaments they proven the effect of alkaline water as prevention for exercise-induced metabolic acidosis. Researcher performed the double randomized clinical trials on sixteen well trained sports athletes by keeping control with normal tap water for three weeks. Anaerobic performance was evaluated by two double 30 s Wingate tests for lower and upper limbs, respectively, with a passive rest interval of 3 minutes between the bouts of exercise. The results indicate that drinking alkalinized water enhances hydration, improves acid-base balance and anaerobic exercise performance. Significant increase in mean power when comparing the values (7.98 J/kg to 9.38 J/kg with $p = 0.001$) at baseline vs. at the conclusion of the study in the experimental group supplemented with alkaline water. In contrast, the control group which received table water did not reveal any statistically significant results.

Joseph Weidman et al (2016)¹⁴ studied the fluid replacement beverages ingested on healthy adults after exercise showed hydration biomarkers like effects researcher carried out randomized, double-blind, parallel-arm trial assessed the effect of high-pH water on blood viscosity. After exercise-induced dehydration as a results high-pH water reduced high-shear viscosity by an average of 6.30% compared to 3.36% with standard purified water ($p = 0.03$) significant difference in whole blood viscosity was detected in this study when assessing a high-pH, electrolyte water versus an acceptable standard purified water during the recovery phase following strenuous exercise-induced dehydration.

Jr, Senay LC et al (1996)¹⁵ collected various clinical trials data on human sports volunteers in japan in which fluid replacement promotes optimal physical performance, reduced water scavenges active oxygen & protects DNA from oxidative damage, The mechanism of the enhanced antioxidant effects of reduced water produced by electrolysis, Antimicrobial interventions to reduce Salmonella species on poultry, Treatment of *Escherichia coli* inoculated alfalfa sprouts with electrolyzed oxidizing water, Inactivation of *E. coli* & *Listeria* on plastic kitchen cutting boards by electrolyzed oxidizing water, Effect of electrolyzed water on wound healing, The bactericidal effects of electrolyzed oxidizing water on bacterial strains

in hospital infections, Effect of electrolyzed oxidizing water on excised burn-wounds, Decomposition of ethylene, a flower-senescence hormone, with electrolyzed anode water, Use of Ionized water in hypochlorhydria, achlorhydria, reduction of high blood pressure, Use of Ionized water for gynecological conditions, Clinical Improvements obtained from the uptake of Ionized Water, Alkaline ionized water for abdominal complaints: Placebo controlled double blind tests, Physiological effects of alkaline ionized water: intestinal fermentation, Effects of calcium alkaline ionized water on formation and maintenance of osseous tissues, Reduced Water for Prevention of Disease, Use of Ionized water in heart disease and toxins, Use of Ionized water in skin disease, Use of Ionized water in allergies, Use of Ionized water in diabetes treatment, Use of Ionized water in treating Acidosis, Environmental electrochemistry of water clinical study on volunteer researcher recommended that individuals consume a alkaline water especially during the period that includes the meal prior to exercise, to promote proper hydration before exercise or competition. It is recommended that individuals drink about 500 ml (about 17 ounces) of alkaline water about 2 hours before exercise to promote adequate hydration and allow time for excretion of excess ingested water.

CONCLUSION

Various researchers signify the importance of alkaline PH water in growth factor by using randomized human and *in vivo* trials for. Researcher opens up the novel hypothesis for human trial on ageing factor investigation. The importance of alkaline water for drug stability and antibacterial properties will be a blockbuster area for drug absorbance enhancement and various pharmacological investigations. Regardless of the advancement of the alkaline water by the media and sales representatives, there is no genuine research to either encourage or discredit these facts and figures. This methodical survey of the writing uncovered an absence of proof possibly in support of alkaline water for the inception or treatment of malignancy. Advancement of alkaline water to people in general for cancer and another acid related diseases treatment isn't legitimized.

REFERENCES

1. Monteiro C.:Acidity Theory of Atherosclerosis: History, Pathophysiology, Therapeutics and Risk Factors - A Mini Review. Position Heal, 2015, 1.
2. Campbell KL: Fatty Acid Supplementation and Skin Disease. The Veterinary, clinics of North America. Small animal practice. 20(6), 1990, 1475–1486.
3. Thompson DM:Gastric Acidity in Hyperthyroidism. J. Bowman Gray Scholer Medicine Wake. For. Coll. 7(1), 1949, 8–16.
4. Sulyok E: Metabolic Acidosis, Nitrogen Balance and Weight Gain in Preterm Infants. Acta Paediatr. Academic Science Hunger. 17(4), 1976, 267–276.
5. Andreev OA: Wei, D.; Engelman, D.; Reshetnyak, Y.



- Acidity at the Surfaces of Cancer Cells. *Biophysical Journal*. 114(3), 2018, 359a.
6. Grant, A. E. Alkaline Water in Diabetes. *British Medical Journal*. 2, 1902, 1621–1622.
 7. WCRF, American Institute for Cancer Research: World Cancer Research Fund, Food, Nutrition and the Prevention of Cancer (WCRF): A Global Perspective. *Nutrition*, 16, 1997, 523–526.
 8. Koufman JA; Johnston, N. Potential Benefits of PH 8.8 Alkaline Drinking Water as an Adjunct in the Treatment of Reflux Disease. *Annals of Otolaryngology, Rhinology & Laryngology*. 121(7), 2012, 431-434.
 9. Pellegrin L; Nitz, L. F.; Maltez, L. C.; Copatti, C. E.; Garcia, L. Alkaline Water Improves the Growth and Antioxidant Responses of Pacu Juveniles (*Piaractus Mesopotamicus*). *Aquaculture*, 519, 2019, 713-734.
 10. Higashimura Y; Baba, Y.; Inoue, R.; Takagi, T.; Uchiyama, K.; Mizushima, K.; Hirai, Y.; Ushiroda, C.; Tanaka, Y.; Naito, Y. Effects of Molecular Hydrogen-Dissolved Alkaline Electrolyzed Water on Intestinal Environment in Mice. *Medical Gas Research*, 8(1), 2018, 6–11.
 11. Magro, M, Corain L, Ferro S, Baratella D, Bonaiuto E, Terzo M: Alkaline Water and Longevity: A Murine Study. *Evidence-based Complement. Alternative. Medicine*, 1, 2016, 1–6.
 12. Ahn S, Kang M, Kim MI, Sohn H: Effect of Alkaline Ionized Water on Stabilization of Antioxidation, Antithrombosis and Antibacterial Activities. *Journal of Life Sciences*. 20(7), 2010, 1107–1112.
 13. Chycki J, Kurylas A, Maszczyk A, Golas A, Zajac A: Alkaline Water Improves Exercise-Induced Metabolic Acidosis and Enhances Anaerobic Exercise Performance in Combat Sport Athletes. *PLoS One*, 13(11), 2018, 1-10.
 14. Weidman J, Holsworth RE, Brossman B, Cho DJ, St Cyr J, Fridman G: Effect of Electrolyzed High-PH Alkaline Water on Blood Viscosity in Healthy Adults. *Journal of the International Society of Sports Nutrition*. 13(1), 2016, 45.
 15. Jr s, clinical studies of alkaline water. *Medicine & Science in Sports & Exercise*, 28(1), 1996, 1-10.

Source of Support: None declared.

Conflict of Interest: None declared.

For any question relates to this article, please reach us at: editor@globalresearchonline.net

New manuscripts for publication can be submitted at: submit@globalresearchonline.net and submit_ijpsrr@rediffmail.com





Pharmacological Activity Investigation of Alkaline Water – A Review

Gajanan Sonwane^{1*}, Sujat Bhagat¹, Vijay Borkar¹, Shirish Jain¹, Sharuk Khan¹, Mayura Kale²

¹Department of Pharmaceutical Chemistry, Rajarshi Shahu College of Pharmacy, Buldana, India.

²Departments of Pharmaceutical Chemistry, Government College of Pharmacy, Aurangabad, India.

*Corresponding author's E-mail: sonwane.gajanan@rediffmail.com

Received: 12-06-2020; Revised: 21-08-2020; Accepted: 28-08-2020.

DOI: 10.47583/ijpsrr.2020.v64i01.017

ABSTRACT

In present study various pharmacological investigation of alkaline water compiled, now days due to fast life acidity become a huge problem in metro cities which is origin for various diseases such as GERD, hypertension, skin diseases, hyperthyroidism, hyperlipidemia, cancer, diabetes etc. Various researches worked on activity of alkaline water and various clinical trials are in tunnel. Compile date elucidate the importance of alkaline water in various diseases treatments and future prospectus in clinical trials of various cancer and related diseases.

Keywords: Alkaline water, acidity, Cancer, Pharmacological investigation.

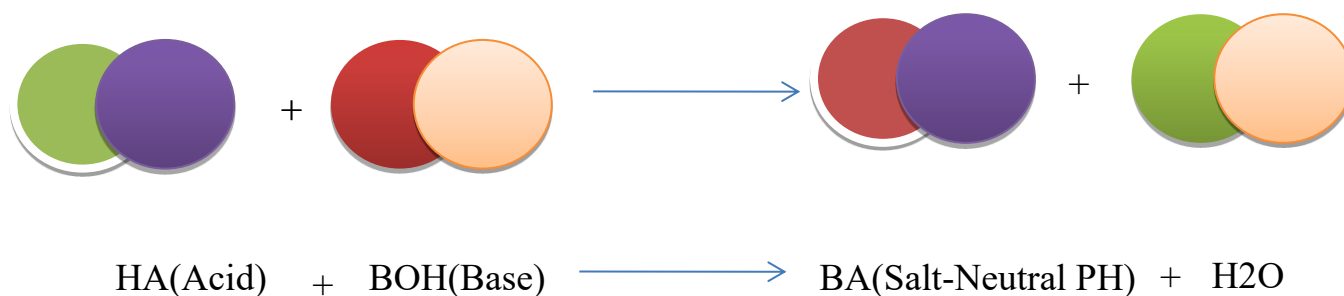
INTRODUCTION

Acidity is most important and ignored reason in development of different diseases like hypertension¹, skin diseases², hyperthyroidism³, hyperlipidemia⁴, cancer⁵, diabetes⁶ and related diseases etc. In allopathy physician only work on sign and symptoms

of the diseases after performing various expensive diagnosis test like ECG, Kidney function, Blood test etc., but the root of this disease condition is completely ignored. The Natural alkaline water is one the solution to cure root of this diseases. In this article would like explore the various researches done on alkaline water and futuristic research possibilities.



Figure 1: Root cause of various life-threatening diseases

Mechanism of alkaline water in treatment of acidity**Figure 2:** Mechanism of alkaline water

Research performed by American institute for cancer research claimed that acidity can alter the body's pH balance and promote cancer. The unproven theory is based on lab studies that advise cancer cells thrive in an acidic (low pH) environment, but cannot survive in alkaline (high pH) surroundings. The Research proven that the cells in an isolated lab setting. Altering the cell environment of the human body to create a less-acidic, less-cancer-friendly environment is virtually impossible. Even slight changes to your body's pH are life-threatening events. Patients with kidney disease and pulmonary dysfunction. To avoid even small disruption of acid-base balance we can focus on root cause that is the acidity, which can prevent further diseases consequences.⁷

Alkaline water

The "basic" in alkaline water alludes to its pH level. A pH level is a number that estimates how acidic or soluble a substance is on a size of 0 to 14. For instance, something with a pH of 1 would be acidic and something with a pH of 13 would be basic. Basic water has a higher pH level than standard drinking water. Along these lines, a few backers of antacid water trust it can kill the corrosive in your body. Typical drinking water, for the most part, has an unbiased pH of 7. Antacid water regularly has a pH of 8 or 9. In any case, pH alone isn't sufficient to bestow considerable alkalinity to water. Basic water should likewise contain alkaline minerals and negative oxidation decrease potential (ORP). ORP is the capacity of water to go about as a cancer prevention agent. The more negative the ORP esteem, the more anti-oxidizing it is.

AN OVERVIEW OF THERAPEUTIC POTENTIAL OF ALKALINE WATER**Alkaline water as a treatment of reflux disease.**

Koufman JA et al (2012)⁸ performed clinical trial on human volunteer they proven the effect of alkaline water in treatment on human reflux diseases specially the natural alkaline water leads to denature human pepsin and its acts like buffering agents. Researcher proven the effective denaturation of pepsin at pH 8.8 exactly.

Alkaline water as an antioxidant activity

Lucas Pellegrina et al (2019)⁹ has carried out growth response biological investigation by using different alkaline

PH water on pacu juveniles. In this experiment Pacu fish were investigated to the different PH such as 5.5, 6.5, 7.5 and 8.5 for 45 days. In that experiment they were found that the fish at water PH of 8.5 were developed at significantly higher than another PH. And in acidic PH it reduces the muscle antioxidant capacity against peroxy radicals and glutathione s transferase. It was also observed by investigator that the Change PH did not affects on other factors like blood glucose, Hematocrit, Plasma, muscle content of protein thiols and thiobarbituric acid reactivity substances.

Yoshinori Tanaka et al (2018)¹⁰ used AEW (alkaline electrolyzed water) for investigation on abdominal complaints under the guidance of ethical committee. Researcher selected a group of objects without any complained of gastrointestinal problem for which AEW used in Japan. Researcher demonstrated a double blind randomized controlled trial for four weeks. Before control trial preliminary investigation was performed like blood tests, physical fitness. and questionnaire evaluation. In this study they concluded no significant side effect on intestinal integrity. Additionally, they stated the improvised sleeping state and felt good when awakening due to reduction in oxidative stress which opened up the novel research area alkaline water as antioxidant agents

Alkaline water as an anti-aging property

Massimiliano Magro et al (2016)¹¹ has performed the survival study on 150 mice for 3-years and by using accelerated failure time (AFT) model proved that the survival rate of mice watered with alkaline water is more than the control mice. It was also observed that alkaline watered mice have decline aging factor as compare to control group. Again, investigator performed toxicity assessment study by using histopathological examination on kidney, intestine heart liver and brain which resulted in no significant pathology

Alkaline water as an anti-bacterial activity

Ahn, Seon-Mi et al (2010)¹² presented pharmacological investigation study of AIW (Alkaline ionized water), PW (purified water and DW (drinking water) in which they performed. In which PH and ORP (oxidation- reduction potential) of water was 9.5 and 120mV, 7.2 and 144 mV and 7.3 and 564mV, respectively. Research proven no

significant antioxidant activity of any of water used in experiment quoted above. Only the power of standard substance used in DPPH ((1,1-diphenyl-2-picryl hydrazyl) assay that is vitamin C found to be stable in AIW and PW as compare to DW. Similarly, the standard used in antithrombosis activity that is aspirin shown improved biological absorbance in AIW and PW as compare to DW. Research also investigate the cell growth analysis and viable cell count of *Escherichia coli* in above 3 motioned water as a result again AIW and PW showed antibacterial activity and DW not.

Alkaline water as a power booster for sports men

Jakub Chycki et al (2018)¹³ worked on problem faced by sports men due to water restriction for quick weight loss before tournaments they proven the effect of alkaline water as prevention for exercise-induced metabolic acidosis. Researcher performed the double randomized clinical trials on sixteen well trained sports athletes by keeping control with normal tap water for three weeks. Anaerobic performance was evaluated by two double 30 s Wingate tests for lower and upper limbs, respectively, with a passive rest interval of 3 minutes between the bouts of exercise. The results indicate that drinking alkalized water enhances hydration, improves acid-base balance and anaerobic exercise performance. Significant increase in mean power when comparing the values (7.98 J/kg to 9.38 J/kg with $p = 0.001$) at baseline vs. at the conclusion of the study in the experimental group supplemented with alkaline water. In contrast, the control group which received table water did not reveal any statistically significant results.

Joseph Weidman et al (2016)¹⁴ studied the fluid replacement beverages ingested on healthy adults after exercise showed hydration biomarkers like effects researcher carried out randomized, double-blind, parallel-arm trial assessed the effect of high-pH water on blood viscosity. After exercise-induced dehydration as a results high-pH water reduced high-shear viscosity by an average of 6.30% compared to 3.36% with standard purified water ($p = 0.03$) significant difference in whole blood viscosity was detected in this study when assessing a high-pH, electrolyte water versus an acceptable standard purified water during the recovery phase following strenuous exercise-induced dehydration.

Jr, Senay LC et al (1996)¹⁵ collected various clinical trials data on human sports volunteers in japan in which fluid replacement promotes optimal physical performance, reduced water scavenges active oxygen & protects DNA from oxidative damage, The mechanism of the enhanced antioxidant effects of reduced water produced by electrolysis, Antimicrobial interventions to reduce Salmonella species on poultry, Treatment of *Escherichia coli* inoculated alfalfa sprouts with electrolyzed oxidizing water, Inactivation of *E. coli* & *Listeria* on plastic kitchen cutting boards by electrolyzed oxidizing water, Effect of electrolyzed water on wound healing, The bactericidal effects of electrolyzed oxidizing water on bacterial strains

in hospital infections, Effect of electrolyzed oxidizing water on excised burn-wounds, Decomposition of ethylene, a flower-senescence hormone, with electrolyzed anode water, Use of Ionized water in hypochlorhydria, achlorhydria, reduction of high blood pressure, Use of Ionized water for gynecological conditions, Clinical Improvements obtained from the uptake of Ionized Water, Alkaline ionized water for abdominal complaints: Placebo controlled double blind tests, Physiological effects of alkaline ionized water: intestinal fermentation, Effects of calcium alkaline ionized water on formation and maintenance of osseous tissues, Reduced Water for Prevention of Disease, Use of Ionized water in heart disease and toxins, Use of Ionized water in skin disease, Use of Ionized water in allergies, Use of Ionized water in diabetes treatment, Use of Ionized water in treating Acidosis, Environmental electrochemistry of water clinical study on volunteer researcher recommended that individuals consume a alkaline water especially during the period that includes the meal prior to exercise, to promote proper hydration before exercise or competition. It is recommended that individuals drink about 500 ml (about 17 ounces) of alkaline water about 2 hours before exercise to promote adequate hydration and allow time for excretion of excess ingested water.

CONCLUSION

Various researchers signify the importance of alkaline PH water in growth factor by using randomized human and *in vivo* trials for. Researcher opens up the novel hypothesis for human trial on ageing factor investigation. The importance of alkaline water for drug stability and antibacterial properties will be a blockbuster area for drug absorbance enhancement and various pharmacological investigations. Regardless of the advancement of the alkaline water by the media and sales representatives, there is no genuine research to either encourage or discredit these facts and figures. This methodical survey of the writing uncovered an absence of proof possibly in support of alkaline water for the inception or treatment of malignancy. Advancement of alkaline water to people in general for cancer and another acid related diseases treatment isn't legitimized.

REFERENCES

1. Monteiro C.:Acidity Theory of Atherosclerosis: History, Pathophysiology, Therapeutics and Risk Factors - A Mini Review. Position Heal, 2015, 1.
2. Campbell KL: Fatty Acid Supplementation and Skin Disease. The Veterinary, clinics of North America. Small animal practice. 20(6), 1990, 1475–1486.
3. Thompson DM:Gastric Acidity in Hyperthyroidism. J. Bowman Gray Scholer Medicine Wake. For. Coll. 7(1), 1949, 8–16.
4. Sulyok E: Metabolic Acidosis, Nitrogen Balance and Weight Gain in Preterm Infants. Acta Paediatr. Academic Science Hunger. 17(4), 1976, 267–276.
5. Andreev OA: Wei, D.; Engelman, D.; Reshetnyak, Y.



- Acidity at the Surfaces of Cancer Cells. *Biophysical Journal*. 114(3), 2018, 359a.
6. Grant, A. E. Alkaline Water in Diabetes. *British Medical Journal*. 2, 1902, 1621–1622.
 7. WCRF, American Institute for Cancer Research: World Cancer Research Fund, Food, Nutrition and the Prevention of Cancer (WCRF): A Global Perspective. *Nutrition*, 16, 1997, 523–526.
 8. Koufman JA; Johnston, N. Potential Benefits of PH 8.8 Alkaline Drinking Water as an Adjunct in the Treatment of Reflux Disease. *Annals of Otolaryngology, Rhinology & Laryngology*. 121(7), 2012, 431-434.
 9. Pellegrin L; Nitz, L. F.; Maltez, L. C.; Copatti, C. E.; Garcia, L. Alkaline Water Improves the Growth and Antioxidant Responses of Pacu Juveniles (*Piaractus Mesopotamicus*). *Aquaculture*, 519, 2019, 713-734.
 10. Higashimura Y; Baba, Y.; Inoue, R.; Takagi, T.; Uchiyama, K.; Mizushima, K.; Hirai, Y.; Ushiroda, C.; Tanaka, Y.; Naito, Y. Effects of Molecular Hydrogen-Dissolved Alkaline Electrolyzed Water on Intestinal Environment in Mice. *Medical Gas Research*, 8(1), 2018, 6–11.
 11. Magro, M, Corain L, Ferro S, Baratella D, Bonaiuto E, Terzo M: Alkaline Water and Longevity: A Murine Study. *Evidence-based Complement. Alternative. Medicine*, 1, 2016, 1–6.
 12. Ahn S, Kang M, Kim MI, Sohn H: Effect of Alkaline Ionized Water on Stabilization of Antioxidation, Antithrombosis and Antibacterial Activities. *Journal of Life Sciences*. 20(7), 2010, 1107–1112.
 13. Chycki J, Kurylas A, Maszczyk A, Golas A, Zajac A: Alkaline Water Improves Exercise-Induced Metabolic Acidosis and Enhances Anaerobic Exercise Performance in Combat Sport Athletes. *PLoS One*, 13(11), 2018, 1-10.
 14. Weidman J, Holsworth RE, Brossman B, Cho DJ, St Cyr J, Fridman G: Effect of Electrolyzed High-PH Alkaline Water on Blood Viscosity in Healthy Adults. *Journal of the International Society of Sports Nutrition*. 13(1), 2016, 45.
 15. Jr s, clinical studies of alkaline water. *Medicine & Science in Sports & Exercise*, 28(1), 1996, 1-10.

Source of Support: None declared.

Conflict of Interest: None declared.

For any question relates to this article, please reach us at: editor@globalresearchonline.net

New manuscripts for publication can be submitted at: submit@globalresearchonline.net and submit_ijpsrr@rediffmail.com






Synthesis of 2,5-disubstituted-1,3,4-thiadiazole derivatives from (2S)-3-(benzyloxy)-2-[(*tert*-butoxycarbonyl) amino] propanoic acid and evaluation of anti-microbial activity

Amit A. Pund , Shweta S. Saboo , Gajanan M. Sonawane , Amol C. Dukale & Baban K. Magare


To cite this article: Amit A. Pund , Shweta S. Saboo , Gajanan M. Sonawane , Amol C. Dukale & Baban K. Magare (2020): Synthesis of 2,5-disubstituted-1,3,4-thiadiazole derivatives from (2S)-3-(benzyloxy)-2-[(*tert*-butoxycarbonyl) amino] propanoic acid and evaluation of anti-microbial activity, Synthetic Communications, DOI: [10.1080/00397911.2020.1817488](https://doi.org/10.1080/00397911.2020.1817488)

To link to this article: <https://doi.org/10.1080/00397911.2020.1817488>

 View supplementary material 

 Published online: 11 Sep 2020.



 Submit your article to this journal 

 View related articles 

 View Crossmark data 



Synthesis of 2,5-disubstituted-1,3,4-thiadiazole derivatives from (2S)-3-(benzyloxy)-2-[(*tert*-butoxycarbonyl) amino] propanoic acid and evaluation of anti-microbial activity

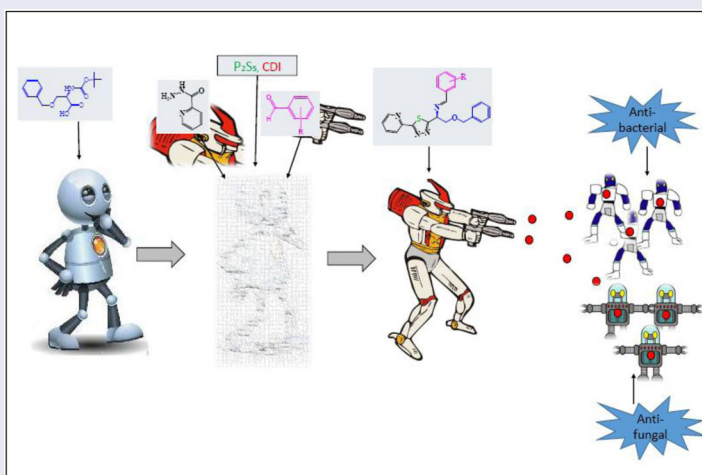
Amit A. Pund^a , Shweta S. Saboo^b, Gajanan M. Sonawane^c, Amol C. Dukale^d, and Baban K. Magare^a 

^aUG, PG and Research Centre, Department of Chemistry, Shivaji Arts Commerce and Science College, Aurangabad, Maharashtra, India; ^bGovernment College of Pharmacy, Aurangabad, Maharashtra, India; ^cRajarshi Shahu College of Pharmacy, Buldhana, Maharashtra, India; ^dSwami Muktanand College of Science Yeola, District Nashik, Maharashtra, India

ABSTRACT

The new compounds **AP-1** to **AP-10** were synthesized from starting material (2S)-3-(benzyloxy)-2-[(*tert*-butoxycarbonyl) amino]propanoic acid (**1**). The intermediate 2,5-disubstituted-1,3,4-thiadiazole amine (**5**) was prepared by coupling of (2S)-3-(Benzyloxy)-2-[(*tert*-butoxycarbonyl) amino]propanoic acid (**1**) with pyridine-2-carboxylic acid hydrazide (**2**) in the presence of carbonyldiimidazole (CDI) followed by 1,3,4-thiadiazole ring formation via diacylhydrazines derivative (**3**) and deprotection with shorter reaction time and excellent yield. The structures of new compounds were confirmed by spectral analysis. The series of new synthesized compounds **AP-1** to **AP-10** were evaluated for their anti-microbial activities *in vitro* and compounds **AP-1**, **AP-3**, **AP-4**, and **AP-10** showed strong activities against all tested microorganisms.

GRAPHICAL ABSTRACT




ARTICLE HISTORY

Received 3 July 2020

KEYWORDS

Anti-microbial; carbonyldiimidazole; evaluation; pyridine-2-carboxylic acid hydrazide; 1,3,4-thiadiazole

CONTACT Baban K. Magare  magrebk75@gmail.com  UG, PG and Research Centre, Department of Chemistry, Shivaji Arts, Commerce and Science College, Kannad. Dist. Aurangabad, Maharashtra, India.

 Supplemental data for this article can be accessed on the [publisher's website](#).

© 2020 Taylor & Francis Group, LLC

Introduction

Thiadiazole and their derivatives have great importance in medicinal and pharmaceutical chemistry due to their diverse biological activity such as anti-convulsant,^[1] antioxidant,^[2] antidiabetic,^[3] anti-bacterial,^[4] anti-fungal,^[5,6] anti-depressant,^[7] anti-inflammatory,^[8] and anti-tubercular activities.^[9] Moreover, there are many thiadiazole containing drugs in the market, such as carbonic anhydrase inhibitors, acetazolamide, and methazolamide as diuretic drugs, cefazolin as the first generation cephalosporin, sulfamethizole as an anti-microbial sulfonamide, and the antiparasitic drug, megalol drug were effectively treated with many diseases.^[10] Imine derivative have significant role in medicinal and pharmaceutical chemistry due to a broad spectrum of biological activities like anti-microbial,^[11] anti-convulsant,^[12] anti-tubercular,^[13] anti-cancer,^[14] anti-inflammatory,^[15] analgesic,^[16] antioxidant,^[17] and anthelmintic.^[18] The imine group (azomethine) of Schiff bases may be involved in the formation of a hydrogen bond with the active centers of cell constituents and interferes in normal cell metabolism.^[19] The synthesis of 2,5-disubstituted-1,3,4-thiadiazole-based heterocyclic compounds attracted much attention due to broad spectrum in biological activities and which was used in synthetic chemistry. An imine derivatives containing thiadiazole moiety gained the remarkable importance due to their widespread biological activities and used in synthetic chemistry. In addition, the presence of sulfur atom in thiadiazole ring causes high liposolubility as well as improves pharmacokinetic properties. Imine and thiadiazole containing compounds showed anti-bacterial,^[20,21] anti-fungal,^[22] anti-viral,^[23,24] anti-HIV,^[25] anti-convulsant,^[26] anti-tubercular,^[27] and anti-cancer activity.^[28] Mousa^[29] synthesized new imine and 1, 3, 4-thiadiazole containing compounds and evaluated for anti-microbial activities. Naveen Kumar et al.^[30] have reported the synthesis and characterization of a series of imine derivatives by the condensation of 5-ethyl-1,3,4-thiadiazol-2-amine with different aromatic aldehydes. These compounds were screened for microbial activity *in vitro* and reported to exhibit potent anti-bacterial and anti-fungal activities. Pandey et al.^[31] described the synthesis and evaluated anti-microbial activity, analgesic activity, and anti-inflammatory activities of new imine derivatives of 2-amino-5-aryl-1,3,4-thiadiazole. Chandraprakash Gharu^[32] was discussed anti-bacterial and antioxidant activities of new imine derivatives and hydroxyl derivatives of 1,3,4-thiadiazole containing N-phenyl piperazine moiety. Hassan et al.^[33] synthesized 5-(4-aminophenyl)-2-amino-1,3,4-thiadiazole derivatives and evaluated anti-cancer activity against breast cancer (MCF7) and human prostate cancer (DU 145). The anti-cancer results revealed that thiadiazole derivative exhibited more effect in breast cancer than in prostate cell line. The schiff base 5-[4-aminophenyl]-2-[4-(dimethylamino) benzylideneamino]-1,3,4-thiadiazole was synthesized by reflux conditions and screened for anti-cancer activity. Efficient one-pot synthesis of 3,5-disubstituted 1,3,4-thiadiazole from dithioesters under mild condition was reported by Kemparajegowda et al.^[34] Helena Lundberg et al.^[35] studied selective catalytic amide formation from non-activated carboxylic acids and amines. This strategy was implemented for the formation of diacylhydrazines from non-activated carboxylic acids and hydrazide. The synthesis of 1,3,4-thiadiazole derivatives from diacylhydrazines in the presence of Lowessons reagent and phosphorus pentasulfide.^[36,37] The 2-substituted phenyl-5-(5-substituted phenyl-2-furoyl)-[1,3,4]-thiadiazoles is synthesized by using Lawesson's reagent under microwave irradiation and showed fungicidal biological activities.^[38] The one-pot

synthesis of 1,3,4-thiadiazoles derivatives were reported by using carboxylic acids and hydrazine in the presence of Vilsmeier reagent and Lawesson's reagent.^[39] The synthesis and evaluation of imine derivative, 4-(((5-Mercapto-1,3,4-thiadiazol-2-yl) imino) methyl)-2-methoxyphenol containing 1,3,4-thiadiazole ring was showed tyrosine inhibitory activities.^[40] The 5-(3-indolyl)-2-substituted-[1,3,4-] thiadiazoles derivatives were screened against prostate (PC3, DU145, and LnCaP), breast (MCF7 and MDA-MB-231), pancreatic (PaCa2) cancer cell lines and resolved moderate activities.^[41] The 1,3,4-thiadiazole containing derivatives of 2-amino-1,3,4-thiadiazole, that is, 2-(5-(4-chlorophenylamino)-[1,3,4]-thiadiazol-2-yl)-4-aminophenol were showed significant anti-bacterial activity against *S. aureus* and *Escherichia coli* strains and anti-fungal activity against *Aspergillus niger* with MIC values of 25 µg/mL.^[42]

Though the literature survey revealed that the several methods had been reported for the synthesis of 2,5-disubstituted-1,3,4-thiadiazole derivatives. In search of new class of anti-microbial compounds, a new series of 2,5-disubstituted-1,3,4-thiadiazole derivatives (AP-1 to AP-10) were synthesized, characterized by spectral analysis and evaluated their anti-microbial activities.

Results and discussion

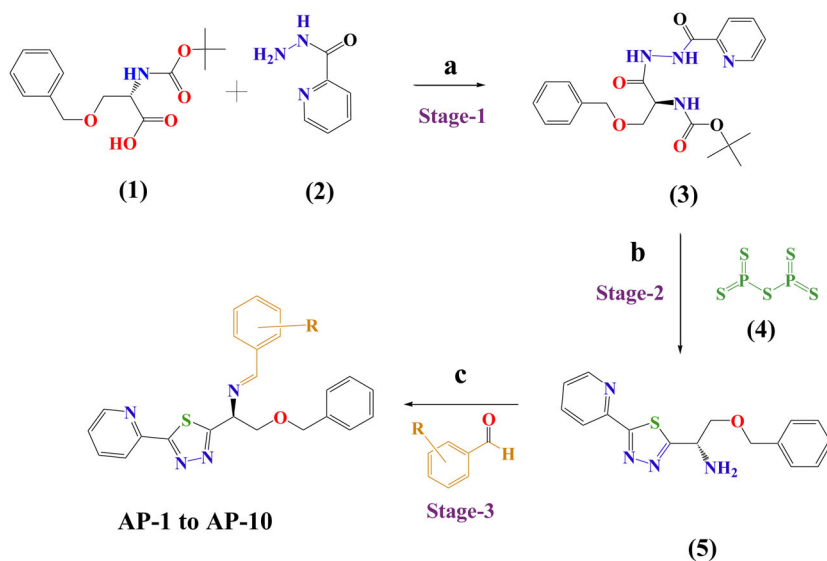
The starting material diacylhydrazine derivative (3) was synthesized from *N*-*boc*-*O*-benzyl-*L*-serine amino acid (1) and pyridine-2-carboxylic acid hydrazide (2) in presence of carbonyldiimidazole (CDI) as coupling reagent, reported by Dr H. A. Staab.^[43] The solution of *N*-*boc*-*O*-benzyl-*L*-serine amino acid (1) was prepared in DCM containing CDI and the solution of pyridine-2-carboxylic acid hydrazide (2) was prepared in DCM. After clear solution, they were mixed slowly together with constant stirring. The reaction was monitored by TLC (DCM:MeOH: 9:1), after complete reaction, the reaction mixture was quenched with water and product extracted with DCM. The organic layer was concentrated under vacuum, and crystalized in MTBE to get white solid diacylhydrazine (3). The structure of compound (3) confirmed by FTIR, mass, ¹H and ¹³C NMR. The absorption bands for C–N and C=O functional groups in compound (3) were observed at 1242.16 and 1695.43 cm⁻¹, respectively. ¹H NMR spectrum of compound (3) revealed the presence of two singlet remarked for the NH at δ = 10.12 and 9.16 ppm and confirmed by D₂O ex-change. In addition to multiple signals, doublet and triplet for aromatic nine proton observed at δ = 8.59 to 7.29 ppm. The δ = 5.43 ppm shows singlet for the *boc*-protected NH group. The two protons of the CH₂-*ph* group shows singlet at δ = 4.60 ppm. The δ = 1.47 ppm shows singlet for nine protons of *boc*-compound. ¹³C NMR spectrum for carbonyl carbon of compound (3) at δ = 167.3 and δ = 160.6 ppm. The 11 aromatic carbon shows δ = 148.5–122.4 ppm value. The CH₂-*ph* carbon confirmed by δ = 73.6 ppm. The ESMS result shows (M + 1) = 415.2.

In the next step, thiadiazole ring was formed by cyclization of diacylhydrazine (3) in the presence of sodium carbonate and phosphorus pentasulfide by heating in THF at 45–55 °C. After completion of reaction, it is treated with aqueous sodium bicarbonate solution and product so formed, extracted with toluene. Then 35% aqueous hydrochloric acid solution was added in organic layer and heated at 50–75 °C temperature. The two layers were formed at room temperature, separated, filtered and pH of aqueous

layer was adjusted at 8.5–9.5 by using aqueous sodium hydroxide solution. The product thus obtained and was extracted in DCM and concentrated and obtained residue was purified by silica gel chromatography to get compound (5). The structure of compound (5) confirmed by FTIR, mass, ^1H and ^{13}C NMR. The FTIR spectrum of compound (5) indicated the existence of broad absorption band of NH and C–N functional group at 3376.11 cm^{-1} and 1245.53 cm^{-1} , respectively. The ^1H NMR of aromatic compounds shows $\delta = 8.64\text{--}7.28\text{ ppm}$. The two protons of the $\text{CH}_2\text{-ph}$ group shows singlet at $\delta = 4.60\text{ ppm}$. The $\delta = 2.23\text{ ppm}$ confirmed the singlet for two protons of NH_2 compound and confirmed NH_2 proton by D_2O ex-change. The ^{13}C NMR spectrum for 1,3,4-thiadiazole compound shows $\delta = 175.6$ and 170.7 ppm for two carbon atoms. The $\delta = 52.1\text{ ppm}$ value confirmed CH-NH_2 carbon. The ESMS result shows $(M + 1) = 313$.

Finally a series of schiff's bases containing 1,3,4-thiadiazole ring (**AP-1** to **AP-10**) compounds were synthesized by condensation of compound (5) as amine with various aromatic aldehydes. After completion of reaction, the reaction mixture was extracted in DCM. The organic layer was concentrated under vacuum and residue so obtained was suspended in MTBE, it was then filtered and recrystallized in IPA to obtain pure compounds (**AP-1** to **AP-10**) (**Stage-3**). The structures of new compounds (**AP-1** to **AP-10**) were confirmed by spectral analysis. In FTIR the diagnostic band of 1,3,4-thiadiazole ring at $683.23\text{--}700.98\text{ cm}^{-1}$ and $1583.34\text{--}1695.80\text{ cm}^{-1}$ were assigned to C–S and C=N stretch, respectively. The structure of **AP-1**, **AP-3**, and **AP-6** compounds clearly showed the absorption band for the NO_2 group at $1521.84\text{--}1527.62\text{ cm}^{-1}$ and $1342.46\text{--}1350.17\text{ cm}^{-1}$ and compounds **AP-2**, **AP-7**, and **AP-8**, assured the absorption bands at $1276.88\text{--}1309.98\text{ cm}^{-1}$ for the OH functional group. Similarly the compounds **AP-5** and **AP-10** showed the FTIR bands at 827.46 and 1010.31 cm^{-1} for Cl and F functional groups, respectively. The ^1H NMR spectra of **AP-1** compound confirmed the structure. The $\delta = 8.65\text{--}7.26\text{ ppm}$ shows aromatic protons. The singlet of CH=N (imine group) proton confirmed by $\delta = 8.36\text{ ppm}$. ^{13}C NMR spectrum for two tertiary carbons of 1,3,4-thiadiazole ring in **AP-1** compound shows at $\delta = 171.9$ and 171.1 ppm for two tertiary carbons and confirmed by DEPT. The imine group shows $\delta = 162.1\text{ ppm}$. The tertiary carbon attached to nitro group shows $\delta = 149.8\text{ ppm}$. The ESMS $(M + 1) = 447.1$ confirmed the molecular weight of **AP-1** compound. The ^1H NMR spectra of **AP-2** compound confirmed the structure. The $\delta = 8.65\text{--}6.88\text{ ppm}$ shows aromatic protons. The broad singlet for the OH- group shows $\delta = 6.33\text{ ppm}$ value. The singlet of CH=N (imine group) proton confirmed by $\delta = 8.36\text{ ppm}$. ^{13}C NMR spectrum for two tertiary carbons of 1,3,4-thiadiazole ring in **AP-2** compound shows at $\delta = 173.6$ and 170.8 ppm for two tertiary carbons and confirmed by DEPT. The imine group and tertiary carbon attached to hydroxy group shows $\delta = 163.9\text{ ppm}$. The ESMS $(M + 1) = 417.1$ confirmed the molecular weight of **AP-2** compound. The **AP-3** compound shows ^1H NMR spectra at $\delta = 8.65\text{--}7.26\text{ ppm}$ shows aromatic protons. The CH=N (imine group) proton confirmed by singlet at $\delta = 8.36\text{ ppm}$. ^{13}C NMR spectrum 1,3,4-thiadiazole ring containing two tertiary carbon in **AP-3** compound shows $\delta = 171.9$ and 171.1 ppm and confirmed by DEPT. The imine group carbon atom shows $\delta = 163.9\text{ ppm}$. The ESMS $(M + 1) = 447.2$ confirmed the molecular weight of **AP-3** compound. The **AP-4** compound confirmed by ^1H NMR spectra at $\delta = 8.64\text{--}6.90\text{ ppm}$ shows aromatic protons. The CH=N

(imine group) proton confirmed by singlet at $\delta = 8.37$ ppm. The methoxy compound shows singlet $\delta = 3.98$ ppm. ^{13}C NMR spectrum of **AP-4** compound having 1,3,4-thiadiazole ring containing two tertiary carbons shows $\delta = 173.3$ and 170.1 ppm and confirmed by DEPT. The imine group carbon atom shows $\delta = 163.9$ ppm. The methoxy carbon shows $\delta = 69.4$ ppm. The ESMS ($M + 1$) = 461.1 confirmed the molecular weight of **AP-4** compound. The ^1H NMR spectra for **AP-5** shows at $\delta = 8.65$ – 7.26 ppm shows aromatic protons. The $\text{CH}=\text{N}$ (imine group) confirmed by singlet at $\delta = 8.37$ ppm. ^{13}C NMR spectrum 1,3,4-thiadiazole ring containing two tertiary carbon in **AP-5** shows $\delta = 172.7$ and 170.9 ppm and confirmed by DEPT. The imine group carbon atom shows $\delta = 163.0$ ppm. The ESMS ($M + 1$) = 435.1 confirmed the molecular weight of **AP-5** compound. The ^1H NMR spectra of **AP-6** compound confirmed the structure. The $\delta = 8.65$ – 7.27 ppm shows aromatic protons. The singlet of $\text{CH}=\text{N}$ (imine group) proton confirmed by $\delta = 8.37$ ppm. ^{13}C NMR spectrum for two tertiary carbon of 1,3,4-thiadiazole ring in **AP-6** compound shows at $\delta = 171.9$ and 171.1 ppm for two tertiary carbons and confirmed by DEPT. The imine group shows $\delta = 162.1$ ppm. The ESMS ($M + 1$) = 447.1 confirmed the molecular weight of **AP-6** compound. The ^1H NMR spectra of **AP-7** compound confirmed the structure. The $\delta = 8.65$ – 6.28 ppm shows aromatic protons. The singlet of $\text{CH}=\text{N}$ (imine group) proton confirmed by $\delta = 8.36$ ppm. The OH group shows broad singlet at $\delta = 6.03$ ppm and methoxy group shows singlet at $\delta = 4.01$ ppm. ^{13}C NMR spectrum for two tertiary carbons of 1,3,4-thiadiazole ring in **AP-7** compound shows at $\delta = 173.3$ and 170.9 ppm for two tertiary carbons and confirmed by DEPT. The imine group shows $\delta = 163.9$ ppm. The methoxy group shows $\delta = 69.5$ ppm value. The ESMS ($M + 1$) = 445.1 confirmed the molecular weight of **AP-7** compound. The ^1H NMR spectra of **AP-8** compound confirmed the structure. The $\delta = 8.65$ – 6.88 ppm shows aromatic protons. The singlet of $\text{CH}=\text{N}$ (imine group) proton confirmed by $\delta = 8.36$ ppm. The OH group shows broad singlet at $\delta = 6.33$ ppm. ^{13}C NMR spectrum for two tertiary carbon of 1,3,4-thiadiazole ring in **AP-8** compound shows at $\delta = 173.7$ and 170.8 ppm for two tertiary carbon and confirmed by DEPT. The imine group shows $\delta = 163.9$ ppm. The ESMS ($M + 1$) = 417.1 confirmed the molecular weight of **AP-8** compound. The ^1H NMR spectra of **AP-9** compound confirmed the structure. The $\delta = 8.65$ – 6.90 ppm shows aromatic protons. The singlet of $\text{CH}=\text{N}$ (imine group) proton confirmed by $\delta = 8.37$ ppm. The value $\delta = 3.99$ ppm indicated that the presence of methoxy proton. ^{13}C NMR spectrum for two tertiary carbon of 1,3,4-thiadiazole ring in **AP-9** compound shows at $\delta = 172.8$ and 170.2 ppm for two tertiary carbon and confirmed by DEPT. The imine group shows $\delta = 161.0$ ppm. The $\delta = 69.5$ ppm confirmed the presence of methoxy carbon. The ESMS ($M + 1$) = 431.1 confirmed the molecular weight of **AP-9** compound. The ^1H NMR spectra of **AP-10** compound confirmed the structure. The $\delta = 8.65$ – 6.92 ppm shows aromatic protons. The singlet of $\text{CH}=\text{N}$ (imine group) proton confirmed by $\delta = 8.36$ ppm. ^{13}C NMR spectrum for two tertiary carbon of 1,3,4-thiadiazole ring in **AP-10** compound shows at $\delta = 173.3$ and 170.9 ppm for two tertiary carbons and confirmed by DEPT. The imine group shows $\delta = 163.9$ ppm. The ESMS ($M + 1$) = 419.1 confirmed the molecular weight of **AP-10** compound. Schematic representation of synthetic route for synthesis of compounds **AP-1** to **AP-10** showed in [Scheme 1](#). Structural representations of compounds (**AP-1** to **AP-10**) are enlisted in [Figure 1](#).



Reagents: **a:** CDI, DCM, RT **b:** Phosphorous pentasulfide (P_2S_5), THF, 45-55°C, $NaHCO_3$; $Conc.HCl$, MeOH, $NaCO_3$ 45-55°C **c:** IPA, reflux

Scheme 1. Schematic representation of synthesis route for compounds AP-1 to AP-10.

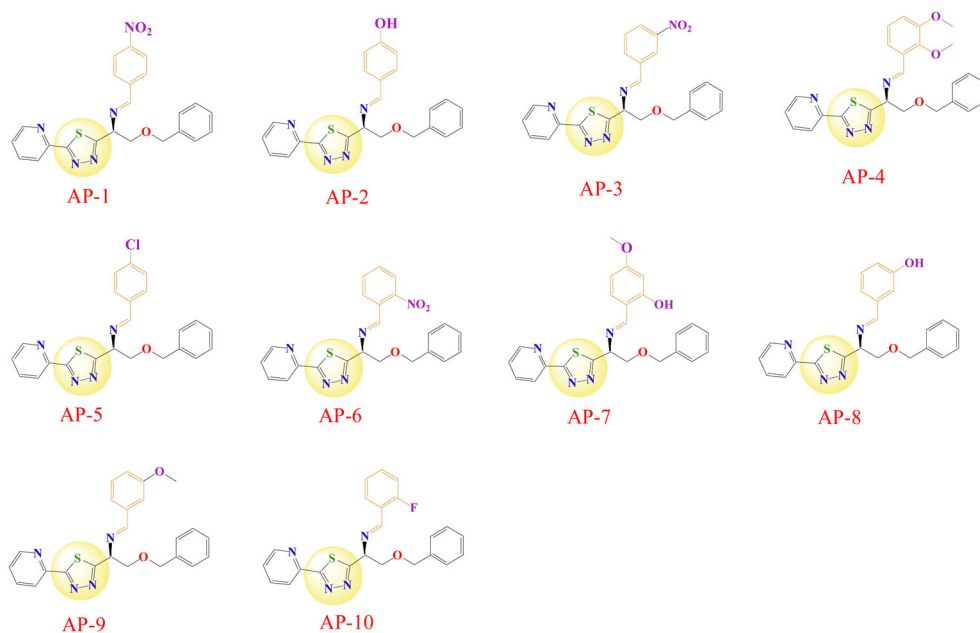


Figure 1. Structural representation of compounds (AP-1 to AP-10). 3, 4-thiadiazole is a well-known five member ring heterocyclic chromosphere, containing one sulfur atom and two nitrogen atoms. It is excessively

Conclusion

Series of new schiff base on 2,5-disubstituted 1,3,4-thiadiazole had been successfully synthesized and characterized by IR, Mass, ^1H NMR and ^{13}C NMR spectroscopic methods. The synthesized compounds **AP-1** to **AP-10** were screened against various microbial strains and compared with different drugs. It observed that compounds **AP-3** and **AP-4** incorporating nitro or methoxy group exhibited the highest inhibitory activity against Gram-negative bacteria strain and appeared to be more than reference drugs. Compounds **AP-2**, **AP-3**, **AP-4**, and **AP-6** containing nitro, methoxy, or hydroxyl group(s) showed excellent zone inhibitory activity against Gram-positive bacteria strains which appeared to be equivalent to standard reference drugs. The compound **AP-10** found to be most potent among all the fungal strains and exhibited the highest inhibitory values than reference drugs. This may be attributed to the presence of fluorine atom incorporated with thiadiazole ring and imine functional group in the structure. The compounds **AP-1**, **AP-3**, **AP-4**, **AP-7**, and **AP-10** exhibited excellent anti-microbial and anti-fungal activities.

Experimental

The melting points of synthesized compounds were recorded on melting point apparatus (Veego, Model-VMP-AD). The IR spectra were recorded on Shimadzu FTIR-8400S spectrometer. The ^1H NMR and ^{13}C NMR spectra were run on a Bruker spectrophotometer at 500 MHz and 125 MHz respectively. The elemental (C, H, and N) analyses were measured on Perkin-Elmer 2400.

General procedure for the synthesis of (S)-{1-Benzyloxymethyl-2-oxo-2-[N'-(pyridine-2-carbonyl)-hydrazino]-ethyl}-carbamic acid tert-butyl ester (compound-3) (AP-diamide or diacylhydrazine derivative)

To a solution of (2S)-3-(benzyloxy)-2-[(*tert*-butoxycarbonyl) amino] propanoic acid (**1**) (49.6 g, 0.1603 mol), carbonyldiimidazole (26.0 g, 0.1603 mol) in DCM was added in solution of pyridine-2-carboxylic acid hydrazide (**2**) (20.0 g, 0.1458 mol) in DCM and whole reaction was stirred for 1.0 h. The reaction was monitored by TLC (DCM:MeOH: 9:1), after reaction completion, the reaction was quenched with water and product extracted with DCM. The organic layer was washed with 10% brine solution (400 mL) and after layer separation organic layer was concentrated at 45 °C under vacuum, the obtained residue was suspended in MTBE. It was then filtrated and dried to get white compound (**3**) as white solid, yield = 58.02 g (96%), m.p. = 187–189 °C. IR spectrum, ν , cm^{-1} : 1242.16 (C–N), 1421.54 (C=C), 699.91(C–S), 2980.02 (C–H), 1695.43 (C=O), 1070.49 (C–O). ^1H NMR spectrum, δ , ppm (J, Hz): 10.12 (1H, s, NH), 9.16 (1H, s, NH), 8.59–8.58 (1H, d, $J=4$, H-2 pyridine), 8.16–8.15 (1H, d, $J=4$, H-5 pyridine), 7.88–7.85 (1H, t, H-4 pyridine), 7.48–7.46 (1H, t, H-3 pyridine), 7.35–7.29 (5H, m, ph), 5.43 (1H, s, NH-Boc), 4.60 (2H, s, $\text{CH}_2\text{-Ph}$), 4.51–4.49 (1H, t, CH-N-Boc), 3.97–3.96 (1H, d, $J=4$, CH = N), 3.67–3.66 (1H, d, $J=4$, CH), 1.47 (9H, s, H-Boc) and NH proton confirmed by D_2O exchange. ^{13}C -NMR (125 MHz, CDCl_3 , 25 °C, TMS): $\delta=167.3$, 160.6, 148.5, 148.1, 137.4, 137.2, 128.5, 128.0, 127.9, 126.8, 122.5, 73.6, 69.3, 28.3. ESMS

(M + 1): 415.2. Anal. calcd for $C_{21}H_{26}N_4O_5$: C = 60.86%, H = 6.32%, N = 13.52%, O = 19.30%, found: C = 60.85, H = 6.33%, N = 13.52%.

Step 2: General procedure for the synthesis (S)-2-benzyloxy-1-(5-pyridin-2-yl-[1, 3, 4] thiadiazol-2-yl)-ethylamine (compound-5) (AP-amine)

To a solution of diacylhydrazine derivative (AP-diamide) (**3**) (50.0 g, 0.1208 mol), sodium carbonate (12.8 g, 0.1207 mol) and phosphorus pentasulfide (P_2S_5) (13.4 g, 0.060 mol), in THF (200 mL) were stirred at 45–55 °C for 8 h. The reaction was monitored by TLC (DCM:MeOH: 9:1) after completion of reaction, quenched with 5% sodium bicarbonate solution (300 mL) and product so obtained was extracted in toluene (500 mL). After aqueous workup the toluene layer mixed with 35% aqueous hydrochloric acid solution (100 mL) and warmed 50–75 °C temperature for 8 h. After reaction completion by TLC (DCM:MeOH: 9:1) and it was cooled to room temperature and added water (500 mL). The two layers were separated, aqueous layer was collected in round bottom flask and pH 8.5–9.5 adjusts by using 10% aqueous sodium hydroxide solution. The product thus obtained and was extracted in DCM and the DCM layer washed with water and concentrated and obtained residue was purified by silica gel chromatography to get compound (**5**) as dark brown color solid, yield = 25.6 g (68%), m.p.=160–162 °C. IR spectrum, ν , cm^{-1} : 1245.53 (C–N), 1431.14 (C=C), 700.98 (C–S), 3061.86 (C–H), 3376.11 (N–H). 1H NMR spectrum, δ , ppm (J, Hz): 8.64–8.63 (1H, d, $J = 4$, H-2 pyridine), 8.33–8.31 (1H, d, $J = 8$ H-5 pyridine), 7.84–7.81 (1H, t, H-4 pyridine), 7.37–7.28 (6H, m, ph and H-3 pyridine), 4.67–4.66 (1H, t, CH–N), 4.60 (2H, s, CH_2 –Ph), 3.92–3.90 (1H, d, $J = 8$, CH=N), 3.76–3.73 (1H, d, $J = 12$, CH), 2.23 (2H, s, NH_2), and NH proton confirmed by D_2O exchange. ^{13}C -NMR (125 MHz, $CDCl_3$, 25 °C, TMS): δ =175.7, 170.7, 149.7, 149.3, 137.5, 137.0, 128.4, 127.8, 127.7, 125.1, 120.7, 73.8, 73.4, 52.2. ESMS (M + 1): 313. Anal. calcd for $C_{16}H_{16}N_4OS$: C = 61.52%, H = 5.16%, N = 17.93%, S = 10.26%, found: C = 61.53%, H = 5.16%, N = 17.92%, S = 10.27%.

Biological activity procedure, Biological Activity, General experiment details, 1H , ^{13}C NMR, ES-MS, and FTIR spectra. This material can be found via the “[Supplementary Content](#)” section of this article’s web page.

Acknowledgments

The authors gratefully acknowledge the Director, UGC, WRO Pune for providing financial assistance and thankful to Principal, Shivaji Arts, Commerce and Science College Kannad, District Aurangabad (M.S.) for providing research laboratory facilities. The authors are grateful to Dr. Arvind Merwade, AVP of Wockhardt Research Centre, Aurangabad and Dr. Dinanath Deoram Patil, Principal, Sahakar Maharshi Bhausaheb Santuji Thorat Arts, Science and Commerce College, Sangamner for motivation and kind support during work.

Disclosure statement

No potential conflict of interest was reported by the author(s).

ORCID

Amit A. Pund  <http://orcid.org/0000-0002-3406-6783>

Baban K. Magare  <http://orcid.org/0000-0001-6719-0441>

References

- [1] Ashraf, S. H.; Gaber, O. M.; Ahmed, A. A.; Ahmed, M. N.; Mohamed, A. A. Synthesis and anti-Bacterial Evaluation of Fused Pyrazoles and Schiff Bases. *Synth. Commun.* **2018**, *48*, 2761–2772. DOI: [10.1080/00397911.2018.1524492](https://doi.org/10.1080/00397911.2018.1524492).
- [2] Khan, I.; Ali, S.; Hameed, S.; Rama, N. H.; Hussain, M. T.; Wadood, A.; Uddin, R.; Ul-Haq, Z.; Khan, A.; Ali, S.; Choudhary, M. I. Synthesis, Antioxidant Activities and Urease Inhibition of Some New 1,2,4-Triazole and 1,3,4-Thiadiazole Derivatives. *Eur. J. Med. Chem.* **2010**, *45*, 5200–5207. DOI: [10.1016/j.ejmech.2010.08.034](https://doi.org/10.1016/j.ejmech.2010.08.034).
- [3] Lee, J.; Lee, H.; Seo, H.; Son, E.; Lee, S.; Jung, M.; Lee, M.; Han, H.; Kim, J.; Kang, J.; et al. Novel C-Aryl Glucoside SGLT2 Inhibitors as Potential Antidiabetic Agents: 1,3,4-Thiadiazolymethylphenyl Glucoside Congeners. *Bioorg. Med. Chem.* **2010**, *18*, 2178–2194. DOI: [10.1016/j.bmc.2010.01.073](https://doi.org/10.1016/j.bmc.2010.01.073).
- [4] Li, P.; Shi, L.; Yang, X.; Yang, L.; Chen, X.; Wu, F.; Shi, Q.; Xu, W.; He, M.; Hu, Y.; et al. Design, Synthesis, and Antibacterial Activity Against Rice Bacterial Leaf Blight and Leaf Streak of 2,5-Substituted-1,3,4-Oxadiazole/Thiadiazole Sulfone Derivative. *Bioorg. Med. Chem. Lett.* **2014**, *24*, 1677–1680. DOI: [10.1016/j.bmcl.2014.02.060](https://doi.org/10.1016/j.bmcl.2014.02.060).
- [5] Liu, F.; Luo, X.; Song, B.; Bhadury, P.; Yang, S.; Jin, L.; Xue, W.; Hu, D. Synthesis and Antifungal Activity of Novel Sulfoxide Derivatives Containing Trimethoxyphenyl Substituted 1,3,4-Thiadiazole and 1,3,4-Oxadiazole Moiety. *Bioorg. Med. Chem.* **2008**, *16*, 3632–3640. DOI: [10.1016/j.bmc.2008.02.006](https://doi.org/10.1016/j.bmc.2008.02.006).
- [6] Xu, W.; Li, S.; He, S.; Yang, S.; Li, X.; Li, P. Synthesis and Bioactivities of Novel Thioether/Sulfone Derivatives Containing 1,2,3-Thiadiazole and 1,3,4-Oxadiazole/Thiadiazole Moiety. *Bioorg. Med. Chem. Lett.* **2013**, *23*, 5821–5824. DOI: [10.1016/j.bmcl.2013.08.107](https://doi.org/10.1016/j.bmcl.2013.08.107).
- [7] Yusuf, M.; Khan, R.; Ahmed, B. Syntheses and Anti-Depressant Activity of 5-Amino-1, 3, 4-Thiadiazole-2-Thiol Imines and Thiobenzyl Derivatives. *Bioorg. Med. Chem.* **2008**, *16*, 8029–8034. DOI: [10.1016/j.bmc.2008.07.056](https://doi.org/10.1016/j.bmc.2008.07.056).
- [8] Amir, M.; Kumar, H.; Javed, S. Non-carboxylic Analogues of Naproxen: Design, Synthesis, and Pharmacological Evaluation of some 1,3,4-Oxadiazole/Thiadiazole and 1,2,4-Triazole Derivatives. *Arch. Pharm.* **2007**, *340*, 577–585. DOI: [10.1002/ardp.200700065](https://doi.org/10.1002/ardp.200700065).
- [9] Zhang, K.; Wang, P.; Xuan, L.; Fu, X.; Jing, F.; Li, S.; Liu, Y.; Chen, B. Synthesis and Antitumor Activities of Novel Hybrid Molecules Containing 1,3,4-Oxadiazole and 1,3,4-Thiadiazole Bearing Schiff Base Moiety. *Bioorg. Med. Chem. Lett.* **2014**, *24*, 5154–5156. DOI: [10.1016/j.bmcl.2014.09.086](https://doi.org/10.1016/j.bmcl.2014.09.086).
- [10] Tahghighi, A.; Babalouei, F. Thiadiazoles: The Appropriate Pharmacological Scaffolds with Leishmanicidal and Antimalarial Activities: A Review. *Iran. J. Basic Med. Sci.* **2017**, *20*, 613–622. DOI: [10.22038/IJBMS.2017.8828](https://doi.org/10.22038/IJBMS.2017.8828).
- [11] Mounika, K.; Anupama, B.; Pragathi, J.; Gyanakumari, C. Synthesis, Characterization and Biological Activity of a Schiff Base Derived from 3-Ethoxy Salicylaldehyde and 2-Amino Benzoic Acid and Its Transition Metal Complexes. *J. Sci. Res.* **2010**, *2*, 513–524. DOI: [10.3329/jsr.v2i3.4899](https://doi.org/10.3329/jsr.v2i3.4899).
- [12] Chaubey, A.; Pandeya, S. Synthesis & Anticonvulsant Activity (Chemo Shock) of Schiff and Mannich Bases of Isatin Derivatives with 2-Amino Pyridine (Mechanism of Action*). *Int. J. PharmTech Res.* **2012**, *4*, 590–598.
- [13] Aboul-Fadl, T.; Mohammed, F.; Hassan, E. Synthesis, Antitubercular Activity and Pharmacokinetic Studies of Some Schiff Bases Derived from 1-Alkylisatin and Isonicotinic Acid Hydrazide (INH). *Arch. Pharm. Res.* **2003**, *26*, 778–784. DOI: [10.1007/BF02980020](https://doi.org/10.1007/BF02980020).

- [14] Miri, R.; Razzaghi-Asl, N.; Mohammad, M. QM Study and Conformational Analysis of an Isatin Schiff Base as a Potential Cytotoxic Agent. *J. Mol. Model.* **2013**, *19*, 727–735. DOI: [10.1007/s00894-012-1586-x](https://doi.org/10.1007/s00894-012-1586-x).
- [15] Sondhi, S.; Singh, N.; Kumar, A.; Lozach, O.; Meijer, L. Synthesis, Anti-inflammatory, Analgesic and Kinase (CDK-1, CDK-5 and GSK-3) Inhibition Activity Evaluation of Benzimidazole/Benzoxazole Derivatives and Some Schiff's Bases. *Bioorg. Med. Chem.* **2006**, *14*, 3758–3765. DOI: [10.1016/j.bmc.2006.01.054](https://doi.org/10.1016/j.bmc.2006.01.054).
- [16] Chinnasamy, R.; Sundararajan, R.; Govindaraj, S. Synthesis, Characterization, and Analgesic Activity of Novel Schiff Base of Isatin Derivatives. *J. Adv. Pharm. Technol. Res.* **2010**, *1*, 342–347. DOI: [10.4103/01110-5558.72428](https://doi.org/10.4103/01110-5558.72428).
- [17] Wei, D.; Li, N.; Lu, G.; Yao, K. Synthesis, Catalytic and Biological Activity of Novel Dinuclear Copper Complex with Schiff Base. *Sci. China Ser. B.* **2006**, *49*, 225–229. DOI: [10.1007/s11426-006-0225-8](https://doi.org/10.1007/s11426-006-0225-8).
- [18] Avaji, P.; Kumar, C.; Patil, S.; Shivananda, K.; Nagaraju, C. Synthesis, Spectral Characterization, *In-vitro* Microbiological Evaluation and Cytotoxic Activities of Novel Macrocylic bis Hydrazone. *Eur. J. Med. Chem.* **2009**, *44*, 3552–3559. DOI: [10.1016/j.ejmech.2009.03.032](https://doi.org/10.1016/j.ejmech.2009.03.032).
- [19] Venugopala, K.; Jayashree, B. Synthesis of Carboxamides of 2'-Amino-4'-(6-Bromo-3-Coumarinyl)Thiazole as Analgesic and Anti-Inflammatory Agents. *Indian J. Heterocycl. Chem.* **2003**, *12*, 307–310.
- [20] Foroumadi, A.; Rineh, A.; Emami, S.; Siavoshi, F.; Massarrat, S.; Safari, F.; Rajabalian, S.; Falahati, M.; Lotfali, E.; Shafiee, A. Synthesis and Anti-*Helicobacter pylori* Activity of 5-(Nitroaryl)-1,3,4-Thiadiazoles with Certain Sulfur Containing Alkyl Side Chain. *Bioorg. Med. Chem. Lett.* **2008**, *18*, 3315–3320. DOI: [10.1016/j.bmcl.2008.04.033](https://doi.org/10.1016/j.bmcl.2008.04.033).
- [21] Talath, S.; Gadad, A. Synthesis, Antibacterial and Antitubercular Activities of Some 7-[4-(5-Amino-[1,3,4]Thiadiazole-2-Sulfonyl)-Piperazin-1-yl] Fluoroquinolonic Derivatives. *Eur. J. Med. Chem.* **2006**, *41*, 918–924. DOI: [10.1016/j.ejmech.2006.03.027](https://doi.org/10.1016/j.ejmech.2006.03.027).
- [22] Mentese, E.; Ülker, S.; Kahveci, B. Synthesis and Study of α -Glucosidase Inhibitory, *anti-Microbial and Antioxidant Activities of Some Benzimidazole Derivatives Containing Triazole, Thiadiazole, Oxadiazole, and Morpholine Rings. *Chem. Heterocycl. Comp.* **2015**, *50*, 1671–1682. DOI: [10.1007/s10593-015-1637-1](https://doi.org/10.1007/s10593-015-1637-1).
- [23] Bagihalli, G.; Avaji, P.; Patil, S.; Badami, P. Synthesis, Spectral Characterization, **in Vitro* Antibacterial, Antifungal and Cytotoxic Activities of Co(II), Ni(II) and Cu(II) Complexes with 1,2,4-Triazole Schiff Bases. *Eur. J. Med. Chem.* **2008**, *43*, 2639–2649. DOI: [10.1016/j.ejmech.2008.02.013](https://doi.org/10.1016/j.ejmech.2008.02.013).
- [24] Jarrahpour, A.; Khalili, D.; Clercq, E.; Salmi, C.; Brunel, J. Synthesis, Antibacterial, Antifungal and Antiviral Activity Evaluation of Some New bis-Schiff Bases of Isatin and their Derivatives. *Molecules.* **2007**, *12*, 1720–1730. DOI: [10.3390/12081720](https://doi.org/10.3390/12081720).
- [25] Asati, K.; Srivastava, S. Synthesis of 5-Arylidene-2-Aryl-3-(Benzotriazolacetamidyl)-1, 3-Thiazolidin-4-Ones as Analgesic and Anti-Microbial Agents. *Indian J. Chem.* **2006**, *45*, 526–531.
- [26] Sharma, R.; Misra, G. P.; Sainy, J.; Chaturvedi, S. C. Synthesis and Biological Evaluation of 2-Amino-5-Sulfanyl-1, 3, 4-Thiadiazole Derivatives as Antidepressant, Anxiolytics and Anticonvulsant Agents. *Med. Chem. Res.* **2011**, *20*, 245–253. DOI: [10.1007/s00044-010-9308-3](https://doi.org/10.1007/s00044-010-9308-3).
- [27] Sonwane, S.; Srivastava, S. Synthesis and Biological Significance of 2-Amino-4-Phenyl-1, 3-Thiazole Derivatives. *Proc. Natl. Acad. Sci.* **2008**, *78A*, 129–136.
- [28] Jalhan, S.; Jindal, A.; Gupta, A.; Hemraj, H. Synthesis, Biological Activities and Chemistry of Thiadiazole Derivatives and Schiff Bases. *Asian J. Pharm. Clin. Res.* **2012**, *5*, 199–208.
- [29] Mousa, M. Synthesis, Characterization and Evaluation of Anti-Bacterial Activity of 1, 3, 4-Thiadiazole Derivatives Containing Schiff Bases. *J. Chem. Pharm. Res.* **2017**, *9*, 196–200.
- [30] Naveen, M.; Shiva, K.; Chandan, S.; Prasad, N. Synthesis and Characterization of Thiadiazole Containing Schiff Base: Anti-Microbial Activity. *Der Pharma Chemica* **2014**, *6*, 10–14.

- [31] Pandey, A.; Rajavel, R.; Chandraker, R.; Dash, D. Synthesis of Schiff Bases of 2-Amino-5-Aryl-1, 3, 4-Thiadiazole and Its Analgesic, Anti-Inflammatory and Anti-Bacterial Activity. *E-J. Chem.* **2012**, *9*, 2524–2531. DOI: [10.1155/2012/145028](https://doi.org/10.1155/2012/145028).
- [32] Gharu, C. Green and Efficient Protocol for Synthesis of Schiff Bases and Hydroxyl Derivatives of 1, 3, 4-Thiadiazole Containing n-Phenyl Piperazine Moiety and Their Anti-Microbial and Antioxidant Potential. *Res. J. Chem. Sci.* **2014**, *4*, 43–47.
- [33] Hassan, F.; Hairunisa, N.; Mohammed, S.; Yousif, E. A Study on Antitumor Effect of 1, 3, 4-Thiadiazole Derivatives in Prostate and Breast Cancer Cell Lines (*In Vitro*). *Preprints* **2017**, 2017030053. DOI: [10.20944/preprints201703.0053.v1](https://doi.org/10.20944/preprints201703.0053.v1).
- [34] Kemparajegowda; Hassan, A.; Nagarakere, C.; Rangappa, S.; Kempegowda, M.; Kanchugarakoppal, S. Efficient One-Pot Synthesis of 3, 5-Disubstituted 1, 3, 4-Thiadiazole from Dithioesters under Mild Condition. *Chem. Select.* **2019**, *4*, 4611–4614. DOI: [10.1002/slct.201900630](https://doi.org/10.1002/slct.201900630).
- [35] Lundberg, H.; Tinnis, F.; Selander, N.; Adolfsson, H. Catalytic Amide Formation from Non-*Activated Carboxylic Acids and Amines. *Chem. Soc. Rev.* **2014**, *43*, 2714–2742. DOI: [10.1039/c3cs60345h](https://doi.org/10.1039/c3cs60345h).
- [36] Hu, Y.; Li, C.; Wang, M.; Yang, H.; Zhu, L. 1,3,4-Thiadiazole: Synthesis, Reactions, and Applications in Medicinal, Agricultural, and Materials Chemistry. *Chem. Rev.* **2014**, *114*, 5572–5610. DOI: [10.1021/cr400131u](https://doi.org/10.1021/cr400131u).
- [37] Nagendra, G.; Lamani, R.; Narendra, N.; Sureshababu, V. A Convenient Synthesis of 1, 3, 4-Thiadiazole and 1, 3, 4-Oxadiazole Based Peptidomimetics Employing Diacylhydrazines Derived from Amino Acids. *Tetrahedron Lett.* **2010**, *51*, 6338–6341. DOI: [10.1016/j.tetlet.2010.09.122](https://doi.org/10.1016/j.tetlet.2010.09.122).
- [38] Cui, N.; Li, S.; Hu, K.; Tian, H.; Jiang, Z.; Wang, Y.; Yan, J. Synthesis and Fungicidal Activity of Novel 2, 5-Disubstituted-1, 3, 4-Thiadiazole Derivatives Containing 5-Phenyl-2-Furan. *Sci. Rep.* **2016**, *6*, 20204. DOI: [10.1038/srep20204](https://doi.org/10.1038/srep20204).
- [39] Zarei, M. One-Pot Synthesis of 1, 3, 4-Thiadiazoles Using Vilsmeier Reagent as a Versatile Cyclodehydration Agent. *Tetrahedron.* **2017**, *73*, 1867–1872. DOI: [10.1016/j.tet.2017.02.042](https://doi.org/10.1016/j.tet.2017.02.042).
- [40] Li, J.; Chen, S. Y.; Tao, S.; Wang, H.; Li, J. J.; Swartz, S.; Musial, C.; Hernandez, A. A.; Flynn, N.; Murphy, B. J.; et al. Design and Synthesis of Tetrazole-Based Growth Hormone Secretagogue: The SAR Studies of the O-Benzyl Serine Side Chain. *Bioorg. Med. Chem. Lett.* **2008**, *18*, 1825–1829. DOI: [10.1016/j.bmcl.2008.02.021](https://doi.org/10.1016/j.bmcl.2008.02.021).
- [41] Tang, J.; Liu, J.; Wu, F. Molecular Docking Studies and Biological Evaluation of 1,3,4-Thiadiazole Derivatives Bearing Schiff Base Moieties as Tyrosinase Inhibitors. *Bioorg. Chem.* **2016**, *69*, 29–36. DOI: [10.1016/j.bioorg.2016.09.007](https://doi.org/10.1016/j.bioorg.2016.09.007).
- [42] Kumar, N.; Kumar, M.; Chang, K.; Shah, K. Synthesis and Anticancer Activity of 5-(3-Indolyl)-1,3,4-Thiadiazoles. *Eur. J. Med. Chem.* **2010**, *45*, 4664–4668. DOI: [10.1016/j.ejmech.2010.07.023](https://doi.org/10.1016/j.ejmech.2010.07.023).
- [43] Staab, H. New Methods of Preparative Organic Chemistry IV. Syntheses Using Heterocyclic Amides (Azolides). *Angew. Chem. Int. Ed. Engl.* **1962**, *1*, 351–367. DOI: [10.1002/anie.196203511](https://doi.org/10.1002/anie.196203511).



Pharmacognostical Standardisation of *Ailanthus Excelsa* Leaves and *Randia Dumetorum* Fruit Along with Antioxidant Activity and Free Radical Scavenging Capacity of Its Fractions

Vivek V Paithankar^{*1}, Shailesh M Kewatkar², Trupti A Nimburkar³, Supriya S Deshpande⁴

¹Department of Pharmacology, Vidya Bharti College of Pharmacy, Amravati, Maharashtra, India

²Rajarshi Shahu College of Pharmacy, Buldana, Maharashtra, India

³Dr Rajendra Gode College of Pharmacy, Amravati, Maharashtra, India

⁴Dr Panjabrao Deshmukh Medical College, Amravati, Maharashtra, India

Article History:

Received on: 21 Jul 2020
Revised on: 28 Aug 2020
Accepted on: 07 Sep 2020

Keywords:

Standardisation,
Antioxidant Activity,
Ailanthus Excelsa,
Randia Dumetorum

ABSTRACT

The world is observing an unprecedented development in the usage of herbal product at national as well as international levels. This requires the improvement of current and aimed standards for estimating the quality, safety and efficacy of these drugs. The leaves of *Ailanthus excelsa* and the fruits of *Randia Dumetorum* are medicinal plants that are used for many diseases around the world. We then collected the flavonoids and saponin fraction extracted from the leaves of *Ailanthus excelsa* and the fruits of *Randia dumetorum*. To determine the reliability, quality and purity of these particles, we provide a crucial pharmacological profile along with the antioxidant activity. Pharmacological studies, such as morphological, physicochemical, TLC, and phytochemical analysis of all fractions containing total phenol and flavonoids, were performed according to specific methods. DPPH tests estimated the antioxidant action of all fractions, Hydrogen peroxide scavenging assay, and reducing power assay method. Previous phytochemical studies discovered the occurrence of saponins, flavonoids, tannins, and especially phenolic chemicals. All fractions have antioxidant effects, depending on the existence of a phenolic compound. The above parameters are vital to establishing pharmacological rules for the authentication of *Ailanthus excelsa* leaves and *Randia Dumetorum* fruits.



*Corresponding Author

Name: Vivek V Paithankar
Phone: +919890250523
Email: rakeshshivatare@gmail.com

ISSN: 0975-7538

DOI: <https://doi.org/10.26452/ijrps.v11iSPL4.4268>

Production and Hosted by

Pharmascope.org
© 2020 | All rights reserved.

INTRODUCTION

Presently there is an enormous deal of awareness in herbal medicine today. This interest is mainly

because medicinal plants do not have adverse effects. A quarter of the world's population or 1.42 trillion people are not expected to rely on traditional medicines to treat various diseases (Kadam *et al.*, 2012). Traditional medical systems such as Ayurveda play an essential role in today's health field, especially in the treatment of malignant diseases (Shivatare *et al.*, 2014). However, the most significant barriers to the use of alternative drugs in industrialised countries are the lack of documentation and strict quality control. Research on traditional medicines needs to be documented. In this context, it is vital to try to standardise the plant substance that will be utilised as a remedy (Modi *et al.*, 2010; Shruthi *et al.*, 2010). Normalisation can be done through pharmacological and phyto-

chemical studies. These studies help to define and standardise plant substance. Appropriate detection with a quality guarantee of preliminary materials is essential requirements for the quality of phytotherapy reproduction, which contributes to improving its protection and usefulness (Sharma *et al.*, 2015; Kadam *et al.*, 2011).

Ailanthus excelsa (family- *Simaroubaceae*) is called "Mahanimba" as it resembles a neem plant (*Azadirachta indica*). The statement *Ailanthus* is resulting as of *Ailanthus*, and it means procession plant (Lavhale and Mishra, 2007). The name of one of the species of Moluccas, in Latin, means high excelsa. Recent research has shown that it contains six flavonoids secluded from the leaves of *A. excelsa* (Loizzo *et al.*, 2007). The bark of the leaves and the alcohol extracted from the stem show excellent anti-implantation activity and early abortion (Dhanasekaran *et al.*, 1993). *Randia Dumetorum* (*Xeromphis Spinosa*) belonging to family *Rubiaceae* is a vital medicine and is called deciduous (Movalia and Gajera, 2009).

A review of the literature shows that the results are bitter and sweet; warming, aphrodisiac, emetic, vaginal, carminative, antipyretic; It treats abscesses, ulcers, inflammation, wounds, tumours, skin diseases and has an antibacterial effect (Satpute *et al.*, 2012). Many experts believe that fruit fibres have anthelmintic properties and are also used in abortion as a folk medicine (Satpute *et al.*, 2009). Recently, the antioxidant properties of their components, usually polyphenol compounds, have been attributed to the function of medicinal plants in the manage or prevention of the disease. The intake of natural antioxidants while minimising the risk of cancer, diabetes, cardiovascular problems, and other age-related diseases (Subba and Mandal, 2015).

No information has been provided on pharmacological studies on the fruiting bodies of the leaves of *Ailanthus excelsa* and *Randia Dumetorum*. No data are provided on antioxidant activity. Therefore, this research focused on the standardisation of two plant fractions, measuring several aspects: morphology, physicochemistry, and TLC analysis. The content of qualitative and quantitative phytochemicals was also combined with antioxidant activities to investigate the presence of phytoactive ingredients.

MATERIALS AND METHODS

Reagent and Chemicals

The entire reagents and chemicals required for the evaluation of pharmacognostic, phytochemical

screening, TLC and antioxidant activity were analytical grade obtained from J.T. Baker, Merck and Rankem.

Procurement, authentication and extraction of sample

The leaves of plant *Ailanthus excelsa* and Fruit of *Randia Dumetorum* were collected from fields of Bhopal (Madhya Pradesh) and validated by Safia College of Science, Bhopal. (Madhya Pradesh) were specified the specimen number 157/Bot/Safia/2010 (*Ailanthus excelsa*) and 158/Bot/Safia/2010 (*Randia Dumetorum*).

The leaves of plant *Ailanthus excelsa* and Fruit of *Randia Dumetorum* were clean and dehydrated below the shade. The desiccated samples were then ground into powdered form. All parts of the plant were crushed and extracted with water, using the method of decoration. This aqueous extract was then filtered, and alcohol (ethanol) was slowly added to this extracted liquid water to make polysaccharides. The solution was then filtered, and the filtered evaporated 1/4 of the total volume.

The same amount of ethyl acetate was then added using a separatory funnel to obtain a separate fraction of constituents of the roots in ethyl acetate. The ethyl acetate extract was acidified with 0.1 N HCl to increase the amount of the extract. The ethyl acetate fraction was evaporated to give the residue; it was then dissolved in methanol and evaporated to give a crystalline powder. Finally, the obtained powder was also analysed to determine the presence of phytoactive ingredients. In this study, it was seen that Shinoda responded positively to the flavonoid test. Besides, TLC confirmed the positivity of flavonoids in the appropriate solvent system (EAFW).

Same plant materials were used for getting saponins rich fraction. Pulverised plant materials were treated with ethanol: water (70:30) for maceration till seven days after defatting with petroleum ether (40:60). The blend was agitated at a normal interval in this stage. Obtained extract after filtration through muslin cloth followed by filter paper was concentrated using rotary vacuum evaporator (40°C), taking precaution that extract does not get powdered.

The concentrated extract was further treated with n-butanol to get an n-butanol soluble fraction. N-butanol soluble fraction was further treated with chilled diethyl ether. After treating with chilled diethyl ether, the precipitate was formed. This mixture with precipitate was kept at -20°C for 24 hrs. Precipitates were further separated by centrifugation. This precipitate was further dissolved

in methanol and methanol was evaporated slowly, to get crystalline powder.

Pharmacognostic Study

Macroscopical characters

External features, dimensions and organoleptic properties of leaves and fruits were studied.

Physicochemical Evaluation

The physicochemical properties of the component were evaluated to estimate the superiority and purity of the powder form. On physical evaluation, they were ash value viz., total ash value with acid insoluble ash value and water-soluble ash value were evaluated. The value of the residue indicates that the drug contains inorganic salts. Values for the extraction of water and soluble alcohol were established. The information obtained from these tests is useful for standardising and maintaining quality standards. These chemical-physical constants are determined according to the procedures mentioned under WHO guidelines (Ibrahim et al., 2012; Baravalia et al., 2011).

Phytochemical Investigations

The leaves of the fruits of *Ailanthus excelsa* and *Randia Dumetorum* were subjected to phytochemical studies before extraction. A preliminary phytochemical test was performed to confirm that the occurrence of different pharmacologically active phytochemicals in the crude powered drug. The tests were performed by a regular procedure (Kokate, 1994; Khandelwal, 2005).

TLC characterisation

TLC is generally utilised for the quick investigation of drugs and drug preparations. Fractions were put forwarded for the characterisation through thin layer chromatography (TLC; silica gel 60 F254, Merck). Chromatograms are estimated beneath U.V. light at 254 and 365 nm to identify the existence of flavonoids plus saponin, respectively. To verify the existence of flavonoids, TLC is furthermore sprayed by an Ammonia vapour. Saponin was identified by Anisaldehyde-sulphuric acid reagent along with Vanillin-phosphoric acid reagent.

Total phenolics Content

The Folin-Ciocalteu technique was applied to find out the entire phenolic content of the plant extract. Gallic acid is utilised as the standard to compare with fractions, and whole phenolic acid was articulated as mg / g gallic acid equivalent (GAE). 10, 20, 30, 40 and 50 (μg / ml) gallic acid concentrations be made in methanol. Sample of 1 mg / mL of plant extract in methanol was prepared, and 0.5 ml of every above-prepared sample was added for

analysis and diluted with 2.5ml of a Ciocalteu-Folin reagent (10 times dilute) and mixed with 2 ml of 7.5 per cent sodium carbonate. The tubes are covered with paraffin and set aside at room temperature for 30 mins previous to the absorbance was read at 760 nm spectrometrically. All determination is finished three times. Folin-Ciocalteu reagent is responsive to reducing agents, as well as polyphenols. After the reaction, it turns blue. This blue colour was measured spectrophotometrically (Chang et al., 2002).

Total flavonoid content

The colourimetric technique of aluminium chloride evaluated the total flavonoids contained inside the plant extract. Briefly, part of the sample was diluted (1 mg / ml) or standard solution (10, 20, 30, 40 and 50 μg / ml) to 75 μl . A solution of NaNO_2 was added, and 0.15 ml of AlCl_3 was mixed 6 min earlier. Following 5 min, 1/2 ml of NaOH be added. The last amount was changed to 2.5 ml with purified water and mixed well.

The absorption of the combination is set at 510 nm compared to the similar combination, without the addition of the sample, as a blank. The entire flavonoid content was articulated as mg / g dry weight (mg / g D.W.) using the normal calibration curve. Every sample is scrutinised three times (Villano et al., 2007).

Studies of Antioxidant Activities

In vitro antioxidant activity of the different fractions at different concentration (Table 1) was studied by three procedures: with free radical scavenging by DPPH, Hydrogen peroxide assay and reducing power assay procedures.

Sample preparation

AEFF: *Ailanthus excelsa* Flavonoid Fraction

AESF: *Ailanthus excelsa* Saponin Fraction

RDF: *Randia Dumetorum* Flavonoid Fraction

RDSF: *Randia Dumetorum* Saponin Fraction

DPPH free radical scavenging activity

To measure the DPPH radical scavenging activity, Barros et al. (2007) was carried out to the method. The drop of DPPH radicals was measured by determining the absorption at 517 nm. The radical scavenging activity was measured as a percentage of DPPH strains by the following equation,

DPPH radical scavenging %

$$= [(A_0 - A_1) / A_0] \times 100$$

Where A_0 is the absorbance of the DPPH solution and A_1 is the absorbance of the sample (Barros et al., 2007).

Hydrogen peroxide radical inhibition assay (H_2O_2)

Ruch *et al.* (1989) were used the method to determine the H_2O_2 scavenging ability of extracts. The H_2O_2 scavenging capacities of the extracts were calculated using formula, (Ruch *et al.*, 1989).

H_2O_2 radical scavenging %

$$= [(A_{Blank} - A_{Sample})/A_{Blank}] \times 100$$

Reducing power assay

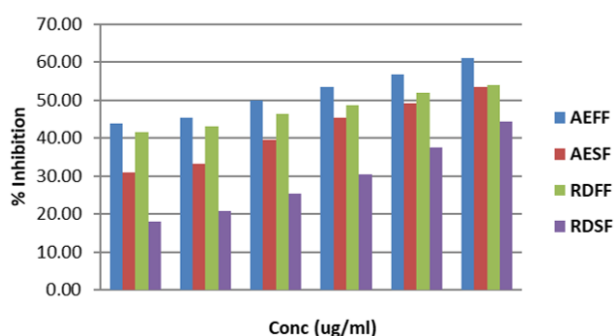
The extracts were prepared in different concentrations. Phosphate buffer (2.5 ml, 2 M, pH 6.6) and potassium ferricyanide were mixed with 1 ml of each in distilled water. The blend was incubated at 50°C for 20 min. A portion of trichloroacetic acid (TCA) was added to the combination which was then centrifuged at 2000 RPM for 20 min. The superior layer of the solution was mixed with water and $FeCl_3$ (0.5ml), and the absorbance was calculated at 700 nm. Increased reducing power was indicated by increased in absorbance of the reaction mixture (Yildirim *et al.*, 2001).

RESULTS AND DISCUSSION

Pharmacognostical studies

Physical Evaluation

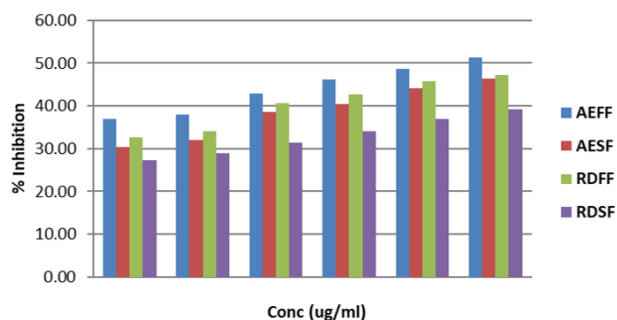
The correct identity of the leaves of *Ailanthus excelsa* and the fruits of *Randia Dumetorum* is determined by pharmacological research. Morphological research of drugs includes evaluation of drugs by colour, odour, taste, size, shape and unique features, like touch, texture etc. It evaluates special features, among others. It is a qualitative assessment technique based on an analysis of the morphological and sensory profiles of each drug (Table 2).



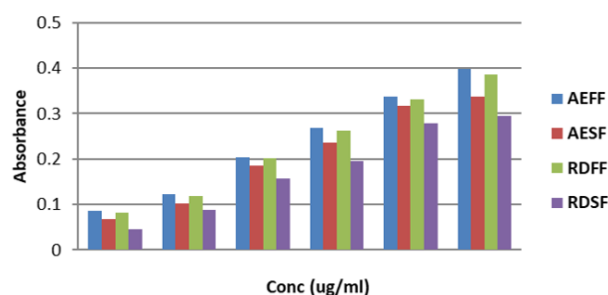
Graph 1: Effect of Fractions in DPPH free radical scavenging assay

Physicochemical Evaluation

When raw materials are burned, ash residues are formed consisting of inorganic materials (metal



Graph 2: Effect of Fractions in Hydrogen peroxide scavenging assay



Graph 3: Effect of Fractions in Hydrogen peroxide scavenging assay

salts and silica). This value is within a reasonably wide range and is, therefore, an essential parameter for evaluating raw materials. The value of the ash identifies more direct dirt, such as sand or dirt (Table 3).

Phytochemical Investigations

Phytochemical screening of crude extracts of leaves of *A. excelsa* and fruit of *R. Dumetorum* by using chemical method revealed the presence of bioactive constituents such as Alkaloids, Carbohydrates, Flavonoids, Saponins, Tannins and Phenolic compounds, Glycosides (Table 4 and Table 5).

TLC characterisation

TLC is primary; easy to use an analytical method, and the solvent used are not hazardous and do not require advanced tools. Depending on the solvent fraction compounds, the solvent system was chosen. TLC examined all fragments of *A. excelsa* and *R. Dumetorum*, and the results of this study are, flavonoids and saponins are present in fractions (Table 6).

Yield Percentage, Total Phenolics and Total Flavonoids

The fraction yield percentage, total phenolics and flavonoid contents of the extracts obtained from the aqueous extract of *A. excelsa* leaves and fruit of *R. Dumetorum* are presented in Table 7. Among the

Table 1: Concentration of different extracts for Antioxidant activity

AEFF ($\mu\text{g/ml}$)	AESF ($\mu\text{g/ml}$)	RDFE ($\mu\text{g/ml}$)	RDSF ($\mu\text{g/ml}$)
10	100	10	100
20	200	20	200
40	400	40	400
60	600	60	600
80	800	80	800
100	1000	100	1000

Table 2: Morphological characters

Sr. No.	Particulars	<i>Ailanthus excelsa</i> Leaves	<i>Randia Dumetorum</i> Fruit
1.	Colour	Greyish green	yellowish-brown
2.	Odour	Pleasant	Unpleasant
3.	Taste	Slightly Bitter	Bitter
4.	Length	40–100 cm	1.8 – 4.5 cm
5.	Surface	soft and velvety	Smooth
6.	Shape	Pinnate	Ovoid

Table 3: Determination of Ash values of crude drugs

Sr. No.	Particulars	<i>A. excelsa</i> Leaf (% w/w)	<i>R. Dumetorum</i> Fruit (% w/w)
1.	Total ash	9.00	10.50
2.	Acid-insoluble ash	1.92	0.5
3.	Water-insoluble ash	6.10	4.65

different fractions, the maximum yield was obtained for the Flavonoid fraction of *R. Dumetorum* (4%) followed by *A. excelsa* (3%). For total flavonoid content (TFC) estimation standard curve of Rutin was used, and content was estimated as Rutin equivalent (RE). For total phenol content estimation (TPC) standard curve of Gallic acid was used and estimated as Gallic acid equivalent (GAE). TFC in *Ailanthus excelsa* and *Randia Dumetorum* were found to be 26 and 19 $\mu\text{g/mg}$ RE respectively. Total Phenol Content in *Ailanthus excelsa* and *Randia Dumetorum* were found to be 65.14 and 62.44 $\mu\text{g/mg}$ GAE, respectively.

Studies of Antioxidant Activities

Due to the complexity of phytochemicals, the antioxidant activity of plant extracts cannot be evaluated using a single method. Therefore, it is vital to use generally accepted tests to evaluate the antioxidant activity of plant extracts. Many methods of antioxidants have been developed to evaluate antioxidant activity and explain how antioxidants work.

DPPH free radical scavenging activity

The DPPH oxidation test used in this document to measure the capacity of radical-scavenging capacity (RSC) is used worldwide. The ability of radical bio-

logical agents to remove DPPH can be expressed as a unit capable of producing antioxidants. The DPPH alcohol solution has a bright purple colour, with an absorption peak at 517 nm when one of the radical scavengers disappears in the reaction system and only one electron of nitrogen is attached to the DPPH. The reaction rate and potential of the radical promoter depend on the rate and maximum value of the DPPH event (Sharma and Gupta, 2008; Gupta and Sharma, 2010).

Compared to other methods, the DPPH test has many advantages, such as good stability, reliable accuracy, simplicity, and feasibility. The results of the DPPH process are presented in several ways. Most studies indicate an IC₅₀ value that is defined as the amount of antioxidant needed to reduce the initial DPPH concentration by 50%. This value is measured by plotting inhibition proportion against Fractions concentration. However, for plant extracts or pure compounds, the IC₅₀ Value changes according to the final concentration of the DPPH used. AEFF showed IC₅₀ of 42.63 $\mu\text{g/ml}$, AESF showed IC₅₀ of 83.42 $\mu\text{g/ml}$, RDFE showed IC₅₀ of 68.92 $\mu\text{g/ml}$, and RDSF showed IC₅₀ of 123.22 $\mu\text{g/ml}$ against DPPH radical (Table 8 and Graph 1).

Table 4: Preliminary Phytochemical testing of parent Ethanolic extract

Sr. No	Test	Observation	A. excelsa Leaf	R. Dumetorum Fruit
A. Alkaloids				
1	Hager's test	Yellow ppt	(+)	(+)
2	Mayer's test	White ppt	(+)	(+)
3	Wagner's test	Reddish brown ppt	(+)	(+)
B. Carbohydrates				
1	Molish's Test	Violet ring formed	(+)	(+)
2	Fehling's test	Brick red ppt	(-)	(+)
3	Barfoed's test	No change	(-)	(-)
C. Cardiac glycosides				
1	Legal test	No red color	(-)	(-)
2	Keller Killiani test	No change	(-)	(+)
D. Flavonoids				
1	Shinoda test	Pink color	(+)	(+)
2	Lead acetate test	Yellow color	(+)	(+)
E. Protein and amino acids				
1	Biuret test	No change	(-)	(+)
2	Millon's test	No change	(+)	(-)
3	Ninhydrin test	No change	(+)	(-)
F. Saponins				
1	Foam test	No foam formation	(+)	(+)
G. Steroids				
1	Salkowski reaction	Yellow fluorescence	(+)	(-)
2	Liebermann – Burchard reaction	Green color	(+)	(+)
H. Tannins and Phenolic compounds				
1	Ferric chloride test	Deep blue-black color	(+)	(-)
2	Gelatin test	White ppt	(-)	(+)
3	Lead acetate test	White ppt	(+)	(+)
4	Potassium dichromate test	Red ppt	(+)	(+)
5	Acetic acid test	Red color	(+)	(-)
6	Iodine test	Red color	(+)	(+)
I. Glycosides				
1	Borntrager's Test	NA	(+)	(+)
J. Mucilage				
1	Ruthenium red	NA	(-)	(+)
K. Cyanogenetic glycoside				
1	Sodium picrate test	NA	(-)	(-)

Table 5: Chemical test for rich fractions

Sr.no.	Test	AAFF	RDFD	Inference
Flavonoid rich fraction of crude drugs				
1.	Shinoda test	+	+	Flavonoids present
2.	Acid base test	+	+	Flavonoids present
Saponin rich fraction of crude drugs				
Sr.no.	Test	AASF	RDSF	Inference
1.	Foam test	+	+	Saponins present

Table 6: TLC characterization of Fractions

Sr. No	Mobile Phase	Spraying Reagent	No. of Spots		Rf Value		Inference
			AEFF	RDFD	AEFF	RDFD	
1	Chloroform: Methanol	Ammonia vapour/ VS reagent	2	1	0.25, 0.80	0.65	Flavonoids
2	Ethyl acetate: Formic acid: Glacial acetic acid: Water	Ammonia vapour/ VS reagent	2	3	0.34, 0.50	0.25, 0.45, 0.75	Flavonoids
			AESF	RDSF	AESF	RDSF	
1	Chloroform: Gallic acid: Methanol: Water	Anisaldehyde-sulphuric acid reagent	1	2	0.25	0.45, 0.70	Saponins
2	Chloroform: Methanol: Water	Vanillin-phosphoric acid reagent	2	2	0.15, 0.19	0.55, 0.60	Saponins

Table 7: Extract yield percentage, total phenolics and total flavonoid content in *A.excelsa* and *R. Dumetorum*

S. No.	Extract	% Yield	Total Phenolic Content	Total flavonoid content
1.	AEFF	3	65.14	26
2.	AESF	2.3	NA	NA
3.	RDFD	4	62.44	19
4	RDSF	2.6	NA	NA

Table 8: Effect of Fractions in DPPH free radical scavenging assay (% Inhibition)

S. No	Conc. (ug/ml)	AEFF	AESF	RDFD	RDSF
1	10	43.91	30.99	41.51	17.89
2	20	45.38	33.21	43.17	20.84
3	40	49.81	39.66	46.49	25.46
4	60	53.50	45.38	48.71	30.44
5	80	56.82	49.07	51.85	37.45
6	100	61.07	53.50	54.06	44.28
	IC ₅₀	42.63	83.42	68.92	123.22

Table 9: Effect of Fractions in Hydrogen peroxide scavenging assay (% Inhibition)

S. No	Conc. (ug/ml)	AEFF	AESF	RDFD	RDSF
1	10	36.95	30.40	32.51	27.24
2	20	38.00	31.90	34.01	28.97
3	40	42.89	38.53	40.63	31.30
4	60	46.12	40.33	42.74	34.01
5	80	48.68	44.02	45.67	37.02
6	100	51.32	46.28	47.18	39.13
	IC ₅₀	88.47	115.75	108.4	181.13

Table 10: Effect of Fractions in Hydrogen peroxide scavenging assay (Absorbance)

S. No	Conc. (ug/ml)	AEFF	AESF	RDFE	RDSF
1	10	0.087	0.068	0.082	0.046
2	20	0.122	0.103	0.118	0.088
3	40	0.204	0.186	0.201	0.157
4	60	0.269	0.236	0.263	0.195
5	80	0.337	0.317	0.332	0.278
6	100	0.398	0.338	0.386	0.294

Hydrogen peroxide scavenging

Hydrogen peroxide itself is not very reactive, but it sometimes becomes toxic to cells because it can carry hydroxyl radicals into the cells. Therefore, the elimination of H₂O₂ is essential to protect antioxidants in cell or food systems. It was noted that all of the samples tested in this study had the effect of removing hydrogen peroxide (Pietta, 2000). IC₅₀ values are 88.47, 115.75, 108.4, and 181.13 for AEFF, AESF, RDFE, and RDSF respectively (Table 9 and Graph 2)

Reducing power assay

All test samples were also found to be having better-reducing power with good goodness of fit ($R^2 > 0.9$) for all test samples. Substances with reduced potency react with potassium ferricyanide (Fe³⁺) to form potassium ferrioxalate (Fe²⁺) and then react with iron chloride with the absorption of up to 700 nm to form a ferric, ferrous complex iron (Table 10 and Graph 3). With an increase in concentration, absorbance increased for all test samples (Wenli et al., 2004).

CONCLUSION

Pharmacological standardisation of the two plants includes physicochemical assessment, identification, verification, and detection of adulteration and quality control of the crude drug. Hot aqueous extract from the leaves of *Ailanthus excelsa* and the fruits of *Randia Dumetorum*, which have the most significant value for extraction. Therefore, we come to the breakdown of the aqueous extract. Analysis of the ash value shows that inorganic substances are present in very normal quantities. If physical and chemical methods are not sufficient, a phytochemical test can be used identified from their impurities. Phytochemical tests are helpful to detect various phyto components. Over the past two decades, the TLC method has been an essential tool for qualitative and quantitative phytochemical analysis of herbal products and preparations. The results of this study show that the leaves of

Ailanthus excelsa and the fruits of *Randia Dumetorum* showed free radical scavenging, Hydrogen peroxide scavenging and reducing power activity. The antioxidant activity of each fraction of the two plants can be attributed to the polyphenol content and phytochemical components. The results of this study suggest that fractions of both plants could be a natural source of antioxidants as a therapeutic agent for a biological system that is sensitive to free-reaction intermediates.

ACKNOWLEDGEMENT

The authors thank Rajarshi Shahu college of pharmacy, Buldana for providing facilities to conduct the research.

Conflict of Interest

There are no conflicts of interest among all the authors with the publication of the manuscript.

Funding Support

The authors declare that they have no funding support for this study.

REFERENCES

- Baravalia, Y., Nagani, K., Chanda, S. 2011. Evaluation of pharmacognostic and physicochemical parameters of *Woodfordia fruticosa* Kurz. Flowers. *Pharmacognosy Journal*, 2(18):13-18.
- Barros, L., Baptista, P., Ferreira, I. C. 2007. Effect of *Lactarius piperatus* fruiting body maturity stage on antioxidant activity measured by several biochemical assays. *Food and Chemical Toxicology*, 45(9):1731-1737.
- Chang, C. C., Yang, M. H., Wen, H. M., Chern, J. C. 2002. Estimation of total flavonoid content in propolis by two complementary colorimetric methods. *Journal of food and drug analysis*, 10(3):178-182.
- Dhanasekaran, S., Suresh, B., Sethuraman, M., Rajan, S., Dubey, R. 1993. Antifertility activity of *Ailanthus excelsa* Linn. in female albino rats. *Indian journal of experimental biology*, 31(4):384-385.

- Gupta, V. K., Sharma, S. K. 2010. In vitro antioxidant activities of aqueous extract of *Ficus bangalensis* Linn. root. *International Journal of Biological Chemistry*, 4(3):134-140.
- Ibrahim, J. A., Makinde, O., Ibekwe, N. N. 2012. Pharmacognostic, physicochemical standardization and phytochemical analysis of leaves of cultivated *Crotalaria lachnosema* Stapf. *Journal of Applied Pharmaceutical Science*, 2(9):67-70.
- Kadam, P. V., Deoda, R. S., Shivatare, R. S., Yadav, K. N., Patil, M. J. 2012. Pharmacognostic, phytochemical and physicochemical studies of *Mimusops Elengi* Linn stem bark (Sapotaceae). *Der Pharmacia Lettre*, 4(2):607-613.
- Kadam, P. V., Yadav, K. N., Narappanawar, N. S., Shivatare, R. S., Bhusnar, H. U., Patil, M. J. 2011. Development of Quality Standards of *Terminalia catappa* Leaves. *Pharmacognosy Journal*, 3(26):19-24.
- Khandelwal, K. R. 2005. A text book of Practical Pharmacognosy. *Nirali Praskashan, Pune*, 12(13):15-163.
- Kokate, C. K. 1994. Practical pharmacognosy, 4th edition. . pages 179-181, New Delhi. Vallabh-Prakan. New Delhi.
- Lavhale, M. S., Mishra, S. H. 2007. Nutritional and therapeutic potential of *Ailanthus excelsa*-A Review. *Pharmacognosy Reviews*, 1(1):105-113.
- Loizzo, M. R., Said, A., Tundis, R., Rashed, K., Statti, G. A., Hufner, A., Menichini, F. 2007. Inhibition of angiotensin converting enzyme (ACE) by flavonoids isolated from *Ailanthus excelsa* (Roxb) (Simaroubaceae). *Phytotherapy Research*, 21(1):32-36.
- Modi, D. C., Patel, J. K., Shah, B. N., Nayak, B. S. 2010. Pharmacognostic studies of the seed of *Syzygium cumini* Linn. *Pharma Science Monitor*, 1(1):20-26.
- Moivalia, D., Gajera, F. 2009. Antibacterial activity of methanolic fruit extract of *Randia dumetorum* Lamk. *International Journal of PharmTech Research*, 1(3):679-681.
- Pietta, P-G. 2000. Flavonoids as Antioxidants. *Journal of Natural Products*, 63(7):1035-1042.
- Ruch, R. J., jun Cheng, S., Klaunig, J. E. 1989. Prevention of cytotoxicity and inhibition of intercellular communication by antioxidant catechins isolated from Chinese green tea. *Carcinogenesis*, 10(6):1003-1008.
- Satpute, K. L., Jadhav, M. M., Karodi, R. S., Katare, Y. S., Patil, M. J., Rub, R., Bafna, A. R. 2009. Immunomodulatory activity of fruits of *Randia dumetorum* Lamk. *Journal of pharmacognosy and phytotherapy*, 1(3):36-40.
- Satpute, K. L., Sonvane, S. M., Bodas, K. S., Sheth, N. S. 2012. Antibacterial activity of fruits of *Randia dumetorum* Lamk. *Journal of Natural Product and Plant Resources*, 2(3):381-384.
- Sharma, R., Joshi, A., Pandey, D., Hemalatha, S. 2015. Pharmacognostical Standardization, Antioxidant Activity, and Phytochemical Analysis of Leaves from *Enicostemma verticillatum*. *Journal of Herbs, Spices & Medicinal Plants*, 21(2):182-192.
- Sharma, S., Gupta, V. 2008. In vitro antioxidant studies of *Ficus racemosa* Linn. root. *Pharmacognosy Magazine*, 4(13):70-74.
- Shivatare, R., Kadam, P., Bhusnar, H., Bhilwade, S., Patil, M. 2014. Immunostimulatory effect of *Mimusops elengi* Linn stem bark in mice. *International Journal of Green Pharmacy*, 8(3):1-7.
- Shruthi, S. D., Ramachandra, Y. L., Rai, S. P., Jha, P. K. 2010. Pharmacognostic evaluation of the leaves of *Kirganelia reticulata* Baill.(Euphorbiaceae). *Asian and Australasian Journal of Plant Science and Biotechnology*, 4(1):62-65.
- Subba, A., Mandal, P. 2015. Pharmacognostic Studies and In Vitro Antioxidant Potential of Traditional Polyherbal Formulation of West Sikkim with *Asparagus* Spp. *Pharmacognosy Journal*, 7(6):348-355.
- Villaño, D., Fernández-Pachón, M. S., Moyá, M. L., Troncoso, A. M., García-Parrilla, M. C. 2007. Radical scavenging ability of polyphenolic compounds towards DPPH free radical. *Talanta*, 71(1):230-235.
- Wenli, Y., Yaping, Z., Bo, S. 2004. The radical scavenging activities of radix *puerariae* isoflavonoids: A chemiluminescence study. *Food Chemistry*, 86(4):525-529.
- Yıldırım, A., Mavi, A., Kara, A. A. 2001. Determination of Antioxidant and Antimicrobial Activities of *Rumex crispus* L. Extracts. *Journal of Agricultural and Food Chemistry*, 49(8):4083-4089.